

---

## Volumes in This Set

**Volume 11 / Bioinorganic and Bioorganic Chemistry**

**Volume 12 / The Iron and Cobalt Pigments: Biosynthesis, Structure, and Degradation**

**Volume 13 / Chlorophylls and Bilins: Biosynthesis, Synthesis, and Degradation**

**Volume 14 / Medical Aspects of Porphyrins**

**Volume 15 / Phthalocyanines: Synthesis**

**Volume 16 / Phthalocyanines: Spectroscopic and Electrochemical Characterization**

**Volume 17 / Phthalocyanines: Properties and Materials**

**Volume 18 / Multiporphyrins, Multiphthalocyanines, and Arrays**

**Volume 19 / Applications of Phthalocyanines**

**Volume 20 / Phthalocyanines: Structural Characterization**

---

# The Porphyrin Handbook

Volume 11 / Bioinorganic and Bioorganic  
Chemistry

## Editors

**Karl M. Kadish**

Department of Chemistry  
University of Houston  
Houston, Texas

**Kevin M. Smith**

Department of Chemistry  
Louisiana State University  
Baton Rouge, Louisiana

**Roger Guilard**

Faculté des Sciences Gabriel  
Université de Bourgogne  
Dijon, France



**ACADEMIC PRESS**

An imprint of Elsevier Science

Amsterdam · Boston · London · New York · Oxford · Paris  
San Diego · San Francisco · Singapore · Sydney · Tokyo

---

Academic Press  
*An imprint of Elsevier Science*  
525 B Street, Suite 1900  
San Diego, California 92101-4495  
USA

© 2003 Elsevier Science (USA) All rights reserved.

This work is protected under copyright by Elsevier Science, and the following terms and conditions apply to its use:

#### Photocopying

Single photocopies of single chapters may be made for personal use as allowed by national copyright laws. Permission of the Publisher and payment of a fee is required for all other photocopying, including multiple or systematic copying, copying for advertising or promotional purposes, resale, and all forms of document delivery. Special rates are available for educational institutions that wish to make photocopies for non-profit educational classroom use.

Permissions may be sought directly from Elsevier's Science & Technology Rights Department in Oxford, UK: phone: (+44) 1865 843830, fax: (+44) 1865 853333, e-mail: [permissions@elsevier.com](mailto:permissions@elsevier.com). You may also complete your request on-line via the Elsevier Science homepage (<http://www.elsevier.com>), by selecting 'Customer Support' and then 'Obtaining Permissions'.

In the USA, users may clear permissions and make payments through the Copyright Clearance Center, Inc., 222 Rosewood Drive, Danvers, MA 01923, USA; phone: (+1) (978) 7508400, fax: (+1) (978) 7504744, and in the UK through the Copyright Licensing Agency Rapid Clearance Service (CLARCS), 90 Tottenham Court Road, London W1P 0LP, UK; phone: (+44) 207 631 5555; fax: (+44) 207 631 5500. Other countries may have a local reprographic rights agency for payments.

#### Derivative Works

Tables of contents may be reproduced for internal circulation, but permission of Elsevier Science is required for external resale or distribution of such material. Permission of the Publisher is required for all other derivative works, including compilations and translations.

#### Electronic Storage or Usage

Permission of the Publisher is required to store or use electronically any material contained in this work, including any chapter or part of a chapter.

Except as outlined above, no part of this work may be reproduced, stored in a retrieval system or transmitted in any form or by any means, electronic, mechanical, photocopying, recording or otherwise, without prior written permission of the Publisher. Address permissions requests to: Elsevier's Science & Technology Rights Department, at the phone, fax and e-mail addresses noted above.

#### Notice

No responsibility is assumed by the Publisher for any injury and/or damage to persons or property as a matter of products liability, negligence or otherwise, or from any use or operation of any methods, products, instructions or ideas contained in the material herein. Because of rapid advances in the medical sciences, in particular, independent verification of diagnoses and drug dosages should be made.

First edition 2003

ISBN: **0-12-393220-3 (Set of Volumes 11–20)**

0-12-393221-1 (Volume 11)  
0-12-393222-X (Volume 12)  
0-12-393223-8 (Volume 13)  
0-12-393224-6 (Volume 14)  
0-12-393225-4 (Volume 15)  
0-12-393226-2 (Volume 16)  
0-12-393227-0 (Volume 17)  
0-12-393228-9 (Volume 18)  
0-12-393229-7 (Volume 19)  
0-12-393230-0 (Volume 20)

∞ The paper used in this publication meets the requirements of ANSI/NISO Z39.48-1992 (Permanence of Paper).

Transferred to Digital Printing 2011

# Preface

Volumes 1–10 of *The Porphyrin Handbook* were first published in late 1999 and met with resounding international acclaim. After only two months on the shelves, our publisher, Academic Press, was awarded the 1999 Chemistry award by the Professional and Scholarly Publishing Division of the American Association of Publishers, Inc.; this honor recognized *The Porphyrin Handbook* as the “best chemistry book of the year.” At that time we, the three editors, began receiving calls and requests from our colleagues and our Academic Press publisher to “expand the work and fill in the gaps” so as to assemble the best ever up-to-date compendium of every possible aspect of the field of porphyrins, other tetrapyrroles, and related macrocycles.

Shortly after publication of the first ten volumes of *The Porphyrin Handbook*, the First International Conference on Porphyrins and Phthalocyanines (ICPP-1) took place in Dijon, France (June 2000), hosted by one of the three editors of the Handbook. At that major international event, the Society of Porphyrins and Phthalocyanines (SPP) was created, and in early 2002 our fledgling SPP took over publication of the *Journal of Porphyrins and Phthalocyanines* (JPP) from John Wiley & Sons, with one of the three Handbook editors serving as Editor-in-Chief. At ICPP-2 in Kyoto, Japan (July 2002), it became abundantly clear that *The Porphyrin Handbook*, Volumes 1–10, was serving well our community of research scientists. This applied equally to our society (SPP) and journal (JPP), which are incrementally enhancing the international visibility of our field. Our new series of Handbook volumes (11–20) and the continuation of our popular international conference series (ICPP-3, to be held in New Orleans, USA, in 2004) each in their own way will contribute further to the scientific enrichment of the porphyrin and phthalocyanine research areas.

However, even before publication of Volumes 1–10, we were becoming aware of the great interest and excitement about the treatise from our real audience, the scientists, clinicians, and engineers working in our field – “you won’t be covering biology or biosynthesis, let’s have Volume 11 soon” – “what about phthalocyanines? They’re (tetraazatetra benzo)porphyrins too!” So, in very short order the three of us met, put together a plan for continuation, and obtained the publisher’s approval and blessings for ten more volumes; this last action was no mean accomplishment since con-

solidations were taking place in the publishing sector, and the new set of volumes would be published by Elsevier.

Our sequel, in ten more volumes (11–20), builds upon the first published set of works by extending its authoritative treatise of the tetrapyrroles. We have moved on from synthesis, chemistry, spectroscopy and applications of porphyrins to address, in depth, many of the sub-fields not covered in the first treatise (Volumes 1–10). To be sure, there were still some loose ends, but we believe that our plan was fairly comprehensive. New topics this time include biology and medical implications of porphyrin systems, the biosynthesis of porphyrins, chlorophylls and vitamin B<sub>12</sub>. Other areas covered include clinical and biochemical aspects of genetically transmitted or drug induced diseases associated with errors in heme metabolism, as well as the transformation of hemes into bile pigments, the organic synthesis of bilins, recent work on phytochrome and the pathways of degradation of chlorophyll in senescent plants. In addition, Volumes 11–20 address every aspect of the synthesis, chemistry, structure and spectroscopy of phthalocyanines.

Our 61 chapters (coincidentally the same number of chapters as in the 1–10 set of volumes) are once again written by internationally recognized experts and we were particularly gratified by two organizational aspects; firstly, we received almost no rejections of our requests for chapters, and secondly, almost all of our contracted authors provided us with chapters in a timely manner which, we believe, are as good in quality, or even better, than those in the first ten volumes. Indeed, once again we believe that our contributors have produced research articles that will be dominant in their specific areas for another fifteen years.

We sincerely hope that our readers will appreciate this new treatise as much as they liked our first venture. The tetrapyrrole field continues to expand into new areas and to gather new recruits and converts. We think that having the research field available at ones’ fingertips (even if it comprises twenty volumes) is a wonderful thing, and this can only serve to facilitate future expansion while at the same time recording our field’s rich history.

Karl M. Kadish, *Houston*  
Kevin M. Smith, *Baton Rouge*  
Roger Guilard, *Dijon*

---

# Contributors to Volumes 1–20

## **Takuzo Aida**

Department of Chemistry and Biotechnology  
Graduate School of Engineering  
The University of Tokyo  
Hongo, Bunkyo-ku, Tokyo 113-8656, Japan  
aida@macro.t.u-tokyo.ac.jp

*Chapters 23, 42*

## **Muhammad Akhtar**

School of Biological Sciences  
University of Southampton  
Bassett Crescent East  
Southampton SO16 7PX, UK  
m.akhtar@soton.ac.uk

*Chapter 71*

## **Karl E. Anderson**

Departments of Preventive Medicine and  
Community Health Internal Medicine,  
and Pharmacology and Toxicology  
The University of Texas Medical Branch at Galveston  
Texas 77555-1109, USA  
kanderso@utmb.edu

*Chapter 94*

## **John Arnold**

Department of Chemistry  
University of California, Berkeley  
Berkeley, California 94720-1460, USA  
arnold@socrates.Berkeley.edu

*Chapter 17*

## **Karine Auclair**

Department of Chemistry  
McGill University  
801 Sherbrooke Street West  
Montréal, Québec, Canada H3A 2K6  
karine.auclair@mcgill.ca

*Chapter 75*

## **Nick Bampos**

University Chemical Laboratory  
Cambridge University  
Cambridge, CB2 1EW, UK

*Chapter 15*

## **Lucia Banci**

CERM and Department of Chemistry  
University of Florence  
50019 Sesto Fiorentino (Florence), Italy  
banci@cerm.unifi.it

*Chapter 39*

## **Jean-Michel Barbe**

Laboratoire d'Ingénierie Moléculaire  
pour la Séparation et les Applications des Gaz  
LIMSAG (UMR 5633)  
Université de Bourgogne  
Faculté des Sciences "Gabriel"  
6, Bd Gabriel 21000 Dijon, France  
jean-michel.barbe@u-bourgogne.fr

*Chapters 19, 116*

## **Pierrette Battioni**

Université René Descartes  
Laboratoire de Chimie et Biochimie  
Pharmacologiques et Toxicologiques UMR 8061  
75270 Paris, France  
battioni@biomedicale.univ-paris5.fr

*Chapter 26*

**Carl E. Bauer**

Department of Biology  
Indiana University  
Bloomington, Indiana 47405, USA  
cbauer@bio.indiana.edu  
*Chapter 80*

**Marc Bénard**

Laboratoire de Chimie Quantique UMR 7551  
Université Louis Pasteur  
67000 Strasbourg, France  
benard@quantix.u-strasbg.fr  
*Chapter 48*

**Ehud Ben-Hur**

Consultant in Photomedicine  
160 West End Avenue # 24P, New York, NY 10023, USA  
ehudbenhur@yahoo.com  
*Chapter 117*

**Jean Bernadou**

Laboratoire de Chimie de Coordination du CNRS  
31077 Toulouse, France  
bernadou@lcc-toulouse.fr  
*Chapter 31*

**Ivano Bertini**

CERM and Department of Chemistry  
University of Florence  
50019 Sesto Fiorentino (Florence), Italy  
bertini@cerm.unifl.it  
*Chapter 39*

**David W. Bollivar**

Department of Biology  
Illinois Wesleyan University  
P.O. Box 2900, Bloomington, Illinois 61702-2900, USA  
dbolliva@iwu.edu  
*Chapter 78*

**Arnaud Bondon**

UMR 6509, Organométallique et Catalyse,  
Chimie et Électrochimie Moléculaires  
Université de Rennes I  
35042 Rennes, France  
arnaud.bondon@univ.rennes1.fr  
*Chapter 38*

**Sylvia S. Bottomley**

Department of Medicine  
University of Oklahoma College of Medicine and  
Department of Veterans Affairs Medical Center  
Hematology-Oncology Section (111J)  
921 N.E. 13th Street  
Oklahoma City  
Oklahoma 73104-5007, USA  
sylvia-bottomley@ouhsc.edu  
*Chapter 85*

**Roman Boulatov**

Department of Chemistry  
Stanford University  
Stanford, California 94305-5080, USA  
boulatov@stanford.edu  
*Chapter 62*

**Marcel Bouvet**

Laboratoire de Chimie Inorganique et Matériaux Moléculaires  
CNRS – UMR7071  
Université Pierre et Marie Curie  
4, place Jussieu, Case Courrier 42  
75252 Paris cedex 05, France  
marcel.bouvet@cspci.fr  
*Chapter 118*

**Johann W. Buchler**

Institut für Anorganische Chemie  
Darmstadt University of Technology  
D-64287 Darmstadt, Germany  
dg7m@hrzpub.tu-darmstadt.de  
jwbuchler@t-online.de  
*Chapter 20*

**Henry J. Callot**

Faculté de Chimie  
Université Louis Pasteur  
F-67000 Strasbourg, France  
callot@chimie.u-strasbg.fr  
*Chapter 7*

**Isabelle Chambrier**

Wolfson Materials & Catalysis Centre  
School of Chemical Sciences and Pharmacy  
University of East Anglia  
Norwich NR4 7TJ, UK  
i.fernandes@uea.ac.uk  
*Chapter 108*

**Jean-Claude Chambron**

Laboratoire de Chimie Organo-Minérale  
Université Louis Pasteur  
Institut Le Bel  
67070 Strasbourg, France  
jean-claude.chambron@u-bourgogne.fr

*Chapter 40*

**Wai-Shun Chan**

Progenitor Cell Therapy, L.L.C.  
Park 80 West, Plaza II, Suite 200  
Saddle Brook, New Jersey 07663, USA  
wschan@progenitorcell.net

*Chapter 117*

**Jennifer Cheek**

School of Medicine  
University of South Carolina  
Columbia, South Carolina 29208, USA

*Chapter 53*

**Lin Cheng**

Department of Chemistry and Biochemistry  
University of Oklahoma  
Norman, Oklahoma 73019, USA

*Chapter 33*

**Jun-Hong Chou**

School of Chemical Sciences  
University of Illinois at Urbana-Champaign  
Urbana, Illinois 61801, USA

*Chapter 41*

**Zöe Clyde-Watson**

University Chemical Laboratory  
Cambridge University  
Cambridge, CB2 1EW, UK

*Chapter 15*

**James P. Collman**

Department of Chemistry  
Stanford University  
Stanford, California 94305-5080, USA  
jpc@stanford.edu

*Chapter 62*

**Michael J. Cook**

Wolfson Materials & Catalysis Centre  
School of Chemical Sciences and Pharmacy  
University of East Anglia  
Norwich NR4 7TJ, UK  
m.cook@uea.ac.uk

*Chapter 108*

**Anne Corrigan**

Lennox Eales Porphyria Laboratories  
Department of Medicine  
University of Cape Town Medical School  
Observatory, South Africa 7925  
anne@uctgsh1.uct.ac.za

*Chapter 89*

**Timothy M. Cox**

Department of Medicine  
University of Cambridge, Box 157  
Addenbrooke's Hospital, Cambridge CB2 2QQ, UK  
jbg20@medschl.cam.ac.uk

*Chapter 90*

**Claudia Crestini**

Dipartimento di Scienze e Tecnologie Chimiche  
Tor Vergata University  
Via Della Ricerca scientifica  
00133, Rome, Italy  
crestini@uniroma2.it

*Chapter 66*

**Roman S. Czernuszewicz**

Department of Chemistry  
University of Houston  
Houston, Texas 77204-5003, USA  
roman@uh.edu

*Chapter 52*

**Harry A. Dailey**

Biomedical and Health Sciences Institute  
Department of Microbiology, and  
Department of Biochemistry & Molecular Biology  
A220 Life Sciences Building  
University of Georgia  
Athens, Georgia 30602-7229, USA  
hdailey@uga.edu

*Chapter 72*

**Tamara A. Dailey**

Biomedical and Health Sciences Institute  
Department of Microbiology, and  
Department of Biochemistry & Molecular Biology  
A220 Life Sciences Building  
University of Georgia  
Athens, Georgia 30602-7229, USA  
tdailey@uga.edu

*Chapter 72*

**Scott L. Darling**

University Chemical Laboratory  
Cambridge University  
Cambridge, CB2 1EW, UK  
*Chapter 15*

**John Dawson**

Department of Chemistry and Biochemistry  
University of South Carolina  
Columbia, South Carolina 29208, USA  
dawson@psc.sc.edu  
*Chapter 53*

**Gema de la Torre**

Departamento de Química Orgánica  
Universidad Autónoma de Madrid  
28049 Cantoblanco, Madrid, Spain  
gema.delatorre@uam.es  
*Chapter 99*

**Felix W. M. de Rooij**

Department of Internal Medicine, Erasmus MC  
University Medical Center Rotterdam  
P.B. 2040, 3000 CA Rotterdam  
The Netherlands  
f.derooij@erasmusmc.nl  
*Chapters 93, 95*

**Jeffery S. de Ropp**

NMR Facility  
University of California, Davis  
Davis, California 95616, USA  
jsderopp@ucdavis.edu  
*Chapter 37*

**Hubert de Verneuil**

Laboratoire de Pathologie  
Moléculaire et Thérapie Génique, INSERM E0217  
Université V Segalen Bordeaux 2  
146 rue Léo Saignat  
33076 Bordeaux cédex, France  
verneuil@u-bordeaux2.fr  
*Chapter 87*

**Jean-Charles Deybach**

Centre Français des Porphyrines, INSERM U409  
178 rue des Renouillers  
92701 Colombes Cedex, France;  
and Faculté de Médecine Xavier Bichat  
Université Paris VII  
16 rue Henri Huchard  
BP416, 75870 Paris Cedex 18, France  
jc.deybach@wanadoo.fr  
*Chapter 86*

**Danilo Dini**

Institut für Organische Chemie  
Universität Tübingen  
72076 Tübingen, Germany  
danilo.dini@uni-tuebingen.de  
*Chapters 107, 114*

**Maria Pia Donzello**

Dipartimento di Chimica  
Università degli Studi di Roma "La Sapienza"  
P. le Aldo Moro 5, I-00185 Roma, Italy  
mariapia.donzello@uniroma1.it  
*Chapter 112*

**Annie Edixhoven**

Department of Internal Medicine, Erasmus MC  
University Medical Center Rotterdam  
P.B. 2040, 3000 CA Rotterdam  
The Netherlands  
a.edixhoven@erasmusmc.nl  
*Chapter 93*

**G. H. Elder**

Department of Medical Biochemistry  
University of Wales College of Medicine  
Heath Park, Cardiff CF14 4XN, UK  
elder@cardiff.ac.uk  
*Chapter 88*

**Michael Klaus Engel**

Dainippon Ink and Chemicals, Inc.  
Central Research Laboratories  
631 Sakado, Sakura-shi  
Chiba-ken 285-8668, Japan  
michael-engel@ma.dic.co.jp  
*Chapter 122*



**Christoph Erben**

Lucent Technologies—Bell Laboratories  
Murray Hill, New Jersey 07974, USA  
chris\_erben@hotmail.com  
*Chapter 12*

**Claudio Ercolani**

Dipartimento di Chimica  
Università degli Studi di Roma “La Sapienza”  
P. le Aldo Moro 5, I-00185 Roma, Italy  
claudio.ercolani@uniroma1.it  
*Chapters 101, 112*

**Peter Erk**

Performance Chemicals Research  
GVP/C – J 550, BASF AG  
67056 Ludwigshafen/Rh, Germany  
peter.erk@basf-ag.de  
*Chapter 119*

**Jean Fischer**

Laboratoire de Chimie Organométallique et de Catalyse  
Institut le Bel  
Université Louis Pasteur de Strasbourg  
4, rue Blaise Pascal, 67070 Strasbourg, France  
fischer@chimie.u-strasb.fr  
*Chapter 105*

**Steven R. Flom**

Code 5613, Naval Research Laboratory  
Washington, DC 20375-5338, USA  
flom@nrl.navy.mil  
*Chapter 121*

**Carlo Floriani**

Institut de Chimie Minérale et Analytique, BCH  
Université de Lausanne  
Lausanne CH-1015, Switzerland  
*Chapters 24, 25*

**Rita Floriani-Moro**

Institut de Chimie Minérale et Analytique, BCH  
Université de Lausanne  
Lausanne CH-1015, Switzerland  
*Chapters 24, 25*

**Barbara Floris**

Dipartimento di Scienze e Tecnologie Chimiche  
Università di Roma “Tor Vergata”  
Via della Ricerca Scientifica  
I-00133, Roma, Italy  
floris@uniroma2.it  
*Chapter 112*

**Nicole Frankenberg**

Section of Molecular and Cellular Biology  
University of California, Davis  
One Shields Avenue  
Davis, California 95616, USA  
nfrankenberg@tu-bs.de  
*Chapter 83*

**Yuichi Fujita**

Graduate School of Bioagricultural Sciences  
Nagoya University  
Nagoya 464-8601, Japan  
fujita@nuagr1.agr.nagoya-u.ac.jp  
*Chapter 80*

**Shunichi Fukuzumi**

Department of Material and Life Sciences  
Graduate School of Engineering  
Osaka University  
Suita, Osaka 565-0871, Japan  
fukuzumi@chem.eng.osaka-u.ac.jp  
*Chapter 56*

**Philip A. Gale**

Department of Chemistry  
University of Southampton  
Southampton, S017 1BJ, UK  
philip.gale@soton.ac.uk  
*Chapter 45*

**Andreas Gebauer**

Department of Chemistry  
University of California at Berkeley  
Berkeley, California 94720, USA  
andreas@socrates.berkeley.edu  
*Chapters 8, 9*

**Cécile Ged**

Laboratoire de Pathologie  
Moléculaire et Thérapie Génique  
INSERM E0217  
Université V Segalen Bordeaux 2  
146 rue Léo Saignat  
33076 Bordeaux cédex, France  
cecile.ged@u-bordeaux2.fr  
*Chapter 87*

**Abhik Ghosh**

Institute of Chemistry, Faculty of Science  
University of Trømsø  
Trømsø, Norway;  
and San Diego Supercomputer Center  
University of California at San Diego  
La Jolla, California 92093-0505, USA  
Abhik@chem.iut.no  
*Chapter 47*

**Avram Gold**

Department of Environmental Science and Engineering  
The University of North Carolina at Chapel Hill  
Chapel Hill, North Carolina 27599-7400, USA  
agold@sophia.sph.unc.edu  
*Chapter 29*

**Albert Gossauer**

Department of Chemistry  
University of Fribourg  
Route du Musée 9  
CH-1700 Fribourg, Switzerland  
albert.gossauer@unifr.ch  
*Chapter 84*

**Vincent Gotte**

European Synchrotron Radiation Facility  
F-38043 Grenoble, France  
*Chapter 49*

**José Goulon**

European Synchrotron Radiation Facility  
F-38043 Grenoble, France  
goulon@esrf.fr  
*Chapter 49*

**Chantal Goulon-Ginet**

European Synchrotron Radiation Facility  
F-38043 Grenoble, France; and  
Faculté de Pharmacie, Université de Grenoble I  
F-38700 La Tronche, France  
cgoulon@esrf.fr  
*Chapter 49*

**Harry B. Gray**

Beckman Institute, MC 139-74  
California Institute of Technology  
Pasadena, California 91125, USA  
hbgray@caltech.edu  
*Chapter 63*

**Bernhard Grimm**

Institute of Biology/Plant Physiology  
Humboldt University  
Unter den Linden 6  
D 10099 Berlin, Germany  
bernhard.grimm@rz.hu.berlin.de  
*Chapter 69*

**John T. Groves**

Department of Chemistry  
Princeton University  
Princeton, New Jersey 08544-1009, USA  
jtgroves@princeton.edu  
*Chapter 27*

**Lena Gueletti**

Department of Chemistry  
University of Houston  
Houston, Texas 77204-5003, USA  
*Chapter 59*

**Roger Guillard**

Laboratoire d'Ingénierie Moléculaire  
pour la Séparation et les Applications des Gaz  
LIMSAG (UMR 5633)  
Université de Bourgogne  
Faculté des Sciences "Gabriel"  
6, Bd Gabriel 21000 Dijon, France  
roger.guillard@u-bourgogne.fr  
*Chapters 19, 21, 116*

**Devens Gust**

Department of Chemistry and Biochemistry  
Arizona State University  
Tempe, Arizona 85287-1604, USA  
gust@asu.edu  
*Chapter 57*

**Peter Hambright**

Department of Chemistry  
Howard University  
Washington, D.C. 20059, USA  
whambright@howard.edu  
*Chapter 18*

**Michael Hanack**

Institut für Organische Chemie  
Universität Tübingen  
72076 Tübingen, Germany  
hanack@uni-tuebingen.de  
*Chapters 107, 114*

**Mats Hansson**

Department of Biochemistry  
Lund University  
S-22100 Lund, Sweden  
mats.hansson@biokem.lu.se  
*Chapter 77*

**Pierre D. Harvey**

Département de Chimie  
Université de Sherbrooke  
Sherbrooke, P.Q., Canada, J1K 2R1  
pierre.harvey@USherbrooke.ca  
*Chapter 113*

**Fred M. Hawkrige**

Department of Chemistry  
Virginia Commonwealth University  
Richmond, Virginia 23284, USA  
fmhawkri@vcu.edu  
*Chapter 58*

**Joanne C. Hawley**

University Chemical Laboratory  
Cambridge University  
Cambridge, CB2 1EW, UK  
*Chapter 15*

**Takashi Hayashi**

Department of Chemistry and Biochemistry  
Graduate School of Engineering  
Kyushu University  
Higashi-ku Fukuoka 812-8581, Japan  
thayatcm@mbox.nc.kyushu-u.ac.jp  
*Chapter 46*

**Valérie Heitz**

Laboratoire de Chimie Organo-Minérale  
Université Louis Pasteur  
Institut Le Bel  
67070 Strasbourg, France  
heitz@chimie.u-strasbg.fr  
*Chapter 40*

**Heidi Hengelsberg**

Marketing Pigments  
EVP/M – J 550, BASF AG  
67056 Ludwigshafen/Rh, Germany  
heidi.hengelsberg@basf-ag.de  
*Chapter 119*

**Richard J. Hift**

Lennox Eales Porphyria Laboratories  
Department of Medicine  
University of Cape Town Medical School  
Observatory, South Africa 7925  
rjh@uctgsh1.uct.ac.za  
*Chapters 89, 91, 96*

**Shohei Inoue**

Department of Industrial Chemistry  
Faculty of Engineering  
Science University of Tokyo  
Kagurazaka, Shinjuku-ku  
Tokyo 162-8601, Japan  
*Chapter 42*

**Kazuyuki Ishii**

Department of Chemistry  
Graduate School of Science  
Tohoku University  
Sendai 980-8578, Japan  
k-ishii@mail.cc.tohoku.ac.jp  
*Chapter 102*

**N. I. Jaeger**

Institut für Angewandte und Physikalische Chemie  
Fachbereich 2 (Biologie/Chemie)  
Universität Bremen  
Postfach 33 04 40  
D-28334 Bremen, Germany  
jse@uni-bremen.de  
*Chapter 106*

**Laurent Jaquinod**

Department of Chemistry  
University of California, Davis  
Davis, California 95616, USA  
jaquinod@indigo.ucdavis.edu  
*Chapter 5*

**Dong-Lin Jiang**

Department of Chemistry and Biotechnology  
Graduate School of Engineering  
The University of Tokyo  
Hongo, Bunkyo, Tokyo 113-8656, Japan  
jiang@macro.t.u-tokyo.ac.jp  
*Chapter 23*

**Karl M. Kadish**

Department of Chemistry  
University of Houston  
Houston, Texas 77204-5003, USA  
kkadish@uh.edu  
*Chapters 12, 21, 55, 59, 116*

**Hee-Joon Kim**

University Chemical Laboratory  
Cambridge University  
Cambridge, CB2 1EW, UK  
*Chapter 15*

**Mutsumi Kimura**

Department of Functional Polymer Science  
Faculty of Textile Science and Technology  
Shinshu University  
Ueda 386-8567, Japan  
mkimura@giptc.shinshu-u.ac.jp  
*Chapter 120*

**James R. Kincaid**

Chemistry Department  
Marquette University  
Milwaukee, Wisconsin 53233, USA  
kincaid@vms.csd.mu.edu  
*Chapter 51*

**Nagao Kobayashi**

Department of Chemistry, Graduate School of Science  
Tohoku University  
Sendai 980-8578, Japan  
nagaok@mail.cc.tohoku.ac.jp  
*Chapters 13, 100, 102*

**Margaret E. Kosal**

School of Chemical Sciences  
University of Illinois at Urbana-Champaign  
Urbana, Illinois 61801, USA  
*Chapter 41*

**Bernhard Kräutler**

Institute of Organic Chemistry  
University of Innsbruck  
Innrain 52a, A-6020 Innsbruck, Austria  
bernhard.kraeutler@uibk.ac.at  
*Chapters 68, 82*

**Yasuhisa Kuroda**

Department of Polymer Science  
Kyoto Institute of Technology  
Matsugasaki, Kyoto 606 0962, Japan  
ykuroda@ipc.kit.ac.jp  
*Chapter 46*

**J. Clark Lagarias**

Section of Molecular and Cellular Biology  
University of California, Davis  
One Shields Avenue  
Davis, California 95616, USA  
jclagarias@ucdavis.edu  
*Chapter 83*

**Gerd N. La Mar**

Department of Chemistry  
University of California, Davis  
Davis, California 95616, USA  
lamar@indigo.ucdavis.edu  
*Chapter 37*

**Timothy D. Lash**

Department of Chemistry  
Illinois State University  
Normal, Illinois 61794-4160, USA  
tdlash@ilstu.edu  
*Chapter 10*

**Lechosław Latos-Grażyński**

Department of Chemistry  
University of Wrocław  
Wrocław 50 383, Poland  
llg@wchuwr.chem.uni.wroc.pl  
*Chapter 14*

**Claude Lecomte**

Laboratoire de Cristallographie et Modélisation des  
Matériaux Minéraux et Biologiques URA CNRS 809  
Université Henri Poincaré-Nancy 1  
54506 Vandoeuvre-lés-Nancy, France  
lecomte@lcm3b.u-nancy.fr  
*Chapter 48*

**Jinbo Lee**

Department of Chemistry  
Princeton University  
Princeton, New Jersey 08544-1009, USA  
*Chapter 27*

**Paul Le Maux**

Laboratoire de Chimie Organométallique et Biologique  
UMR CNRS 6509, Institut de Chimie  
Université de Rennes 1  
35042 Rennes cedex, France  
paul.lemaux@univ-rennes1.fr  
*Chapter 65*

**Maurice L'Her**

Université de Bretagne Occidentale  
6521/Faculté des Sciences  
B.P. 809, 29285 Brest Cedex, France  
maurice.lher@univ-brest.fr  
*Chapter 104*

**Jonathan S. Lindsey**

Department of Chemistry  
North Carolina State University  
Raleigh, North Carolina 27695-8204, USA  
jlindsey@ncsu.edu  
*Chapter 2*

**Claudio Luchinat**

CERM and Department of Soil Science and Plant Nutrition  
University of Florence  
50019 Sesto Fiorentino (Florence), Italy  
luchinat@cerm.unifi.it  
*Chapter 39*

**John Mack**

Department of Chemistry  
University of Western Ontario, London  
Ontario, Canada, N6A 5B7  
mack@uwo.ca  
*Chapter 103*

**Estelle M. Maes**

Department of Chemistry  
University of Houston  
Houston, Texas 77204-5003, USA  
emaes@uh.edu  
*Chapter 52*

**Chi Ching Mak**

University Chemical Laboratory  
Cambridge University  
Cambridge, CB2 1EW, UK  
*Chapter 15*

**Tadeusz Malinski**

Department of Chemistry and Biochemistry  
Ohio University  
Athens, Ohio 45701, USA  
malinski@ohio.edu  
*Chapter 44*

**Daniel Mansuy**

Université René Descartes  
Laboratoire de Chimie et Biochimie  
Pharmacologiques et Toxicologiques  
UMR 8061, 75270 Paris, France  
daniel.mansuy@biomedicale.univ-paris5.fr  
*Chapter 26*

**Jean-Claude Marchon**

Laboratoire de Chimie Inorganique et Biologique  
Département de Recherche Fondamentale sur la Matière  
Condensée  
CEA-Grenoble, 38054 Grenoble, France  
jcmarchon@cea.fr  
*Chapter 64*

**Pavel Martíásek**

Department of Pediatrics, First Faculty of Medicine  
Charles University  
12109 Prague, Czech Republic  
martasek@egap.cz  
*Chapter 34*

**Bettie Sue S. Masters**

Department of Biochemistry  
The University of Texas Health Science  
Center at San Antonio  
San Antonio, Texas 78284-7760, USA  
masters@uthscsa.edu

*Chapter 34*

**Neil B. McKeown**

Department of Chemistry  
University of Manchester  
Manchester M13 9PL, UK  
neil.mckeown@man.ac.uk

*Chapter 98*

**Craig J. Medforth**

Department of Chemistry  
University of California, Davis  
Davis, California 95616, USA  
medforth@indigo.ucdavis.edu

*Chapter 35*

**Peter N. Meissner**

Lennox Eales Porphyria Laboratories  
Department of Medicine  
University of Cape Town Medical School  
Observatory, South Africa 7925  
pete@uctgsh1.uct.ac.za

*Chapters 89, 91, 96*

**Bernard Meunier**

Laboratoire de Chimie de Coordination du CNRS  
31077 Toulouse, France  
bmeunier@lcc.toulouse.fr

*Chapter 31*

**Tadashi Mizutani**

Department of Synthetic Chemistry  
and Biological Chemistry  
Graduate School of Engineering  
Kyoto University  
Yoshida, Sakyo-ku, Kyoto 606 8501, Japan  
mizutani@sbchem.kyoto-u.ac.jp

*Chapter 46*

**Tatsushi Mogi**

Yoshida ATP System Project, ERATO  
Japan Science and Technology Corporation  
Green Hills Suzukakedai 1F, 5800-3 Nagatsuta, Midori-ku  
Yokohama 226-0026;

*and* Department of Biological Sciences

Graduate School of Science

University of Tokyo

7-3-1 Hongo, Bunkyo-ku, Tokyo 113-0033, Japan

tmogi@res.titech.ac.jp

*Chapter 74*

**Michael R. Moore**

National Research Centre for Environmental Toxicology  
(EnTox), The University of Queensland and  
Queensland Health Scientific Services

39 Kessels Road, Coopers Plains, Brisbane 4108

Queensland, Australia

m.moore@uq.edu.au

*Chapter 96*

**Thomas A. Moore**

Department of Chemistry and Biochemistry  
Arizona State University

Tempe, Arizona 85287-1604, USA

Tom.Moore@asu.edu

*Chapter 57*

**François Moreau-Gaudry**

Laboratoire de Pathologie Moléculaire  
et Thérapie Génique

INSERM E0217

Université V Segalen Bordeaux 2

146 rue Léo Saignat, 33076 Bordeaux cédex

France

francois.moreau-gaudry@u-bordeaux2.fr

*Chapter 87*

**Hari Singh Nalwa**

Hitachi Research Laboratory

Hitachi Ltd.

Hitachi City, Ibaraki 319 1292, Japan

*Chapter 41*

**Dennis K.P. Ng**

Department of Chemistry

The Chinese University of Hong Kong

Shatin, N.T., Hong Kong

dkpn@cuhk.edu.hk

*Chapter 20*

**Jun Nishimoto**

Analytical Research Center for Experimental Sciences  
Saga University  
Saga 840-8502, Japan  
nishimoj@cc.saga-u.ac.jp  
*Chapter 60*

**Roeland J. M. Nolte**

Department of Organic Chemistry, NSR Center  
The University of Nijmegen  
Toernooiveld 1  
NL-6525 ED Nijmegen, The Netherlands  
nolte@sci.kun.nl  
*Chapter 115*

**Rubén Ocampo**

Faculté de Chimie  
Université Louis Pasteur  
67008 Strasbourg, France  
ocampo@chimie.u-strasbg.fr  
*Chapter 7*

**T. Oekermann**

Graduate School of Engineering  
Environmental and Renewable Energy Systems (ERES) Division  
Gifu University  
Yanagido 1-1, Gifu 501-1193, Japan  
torsten@apchem.gifu-u.ac.jp  
*Chapter 106*

**Hisanobu Ogoshi**

Fukui National College of Technology  
Geshi, Sabae  
Fukui 916 8507, Japan  
ogoshi@fukui-nct.ac.jp  
*Chapter 46*

**Paul R. Ortiz de Montellano**

Department of Pharmaceutical Chemistry  
School of Pharmacy  
University of California  
San Francisco, California 94143-0446, USA  
ortiz@cgl.ucsf.edu  
*Chapter 75*

**Sigrid Ostermann**

Institute of Organic Chemistry  
University of Innsbruck, Innrain 52a  
A-6020 Innsbruck, Austria  
sigrid.ostermann@uibk.ac.at  
*Chapter 68*

**Ravindra K. Pandey**

Photodynamic Therapy Center and  
Department of Nuclear Medicine  
Roswell Park Cancer Institute  
Buffalo, New York 14263-0001, USA  
ravindra.pandey@roswellpark.org  
*Chapter 43*

**Roberto Paolesse**

Dipartimento di Scienze e Tecnologie Chimiche  
Università di Roma "Tor Vergata"  
00133 Roma, Italy  
roberto.paolesse@uniroma2.it  
*Chapter 11*

**Annig Pondaven**

Université de Bretagne Occidentale  
6521/Faculté des Sciences  
B.P. 809, 29285 Brest Cedex, France  
annig.pondaven@univ-brest.fr  
*Chapter 104*

**Thomas L. Poulos**

Department of Molecular Biology and Biochemistry  
University of California, Irvine  
Irvine, California 92697-3900, USA  
poulos@uci.edu  
*Chapter 32*

**Geneviève Pratviel**

Laboratoire de Chimie de Coordination du CNRS  
31077 Toulouse, France  
pratviel@lcc-toulouse.fr  
*Chapter 31*

**Hervé Puy**

Centre Français des Porphyries, INSERM U409  
178 rue des Renouillers  
92701 Colombes Cedex, France;  
and Faculté de Médecine  
Paris Ile de France Ouest  
104 boulevard Raymond Poincaré, 92380 Garches, France  
herve.puy@apr.ap-hop-paris.fr  
*Chapter 86*

**J. Martin E. Quirke**

Department of Chemistry  
Florida International University  
Miami, Florida 33199, USA  
quirke@servms.fiu.edu  
*Chapter 54*

**Stephen W. Ragsdale**

Department of Biochemistry  
Beadle Center, 19th and Vine Streets  
University of Nebraska  
Lincoln, Nebraska 68588-0664, USA  
sragdale1@unl.edu

*Chapter 67*

**Neal A. Rakow**

School of Chemical Sciences  
University of Illinois at Urbana-Champaign  
Urbana, Illinois 61801, USA

*Chapter 41*

**C. S. Raman**

Department of Molecular Biology and Biochemistry  
University of California, Irvine 92697-3900  
Irvine, California, USA  
raman@bragg.bio.uct.edu

*Chapter 34*

**René Ramasseul**

Laboratoire de Chimie Inorganique et Biologique  
Département de Recherche Fondamentale sur la Matière  
Condensée  
CEA-Grenoble  
38054 Grenoble, France  
ramasse@drfmc.ceng.cea.fr

*Chapter 64*

**J. Graham Rankin**

Department of Chemistry  
Marshall University  
Huntington, West Virginia 25701, USA  
rankin@mu.edu

*Chapter 52*

**George B. Richter-Addo**

Department of Chemistry and Biochemistry  
University of Oklahoma  
Norman, Oklahoma 73019, USA  
grichteraddo@ou.edu

*Chapter 33*

**Anne Robert**

Laboratoire de Chimie de Coordination du CNRS  
31077 Toulouse, France  
arobert@lcc-toulouse.fr

*Chapter 31*

**M. Salomé Rodríguez-Morgade**

Departamento de Química Orgánica  
Universidad Autónoma de Madrid  
28049 Cantoblanco, Madrid, Spain  
salome.rodriguez@uam.es

*Chapter 99*

**Charles A. Roessner**

Center for Biological NMR, Department of Chemistry  
Texas A&M University  
College Station, Texas 77843, USA  
c-roessner@tamu.edu

*Chapter 76*

**Marie-Madeleine Rohmer**

Laboratoire de Chimie Quantique UMR 7551  
Université Louis Pasteur  
67000 Strasbourg, France  
rohmer@quantix.u-strasbg.fr

*Chapter 48*

**Alan E. Rowan**

Department of Organic Chemistry, NSR Center  
The University of Nijmegen  
Toernooiveld 1  
NL-6525 ED Nijmegen, The Netherlands  
rowan@sci.kun.nl

*Chapter 115*

**Guy Royal**

Department of Chemistry  
University of Houston  
Houston, Texas 77204-5003, USA  
guy.royal@ujf-grenoble.fr

*Chapter 55, 59*

**W. Rüdiger**

Department Biologie I, Botanik  
Universität München  
Menzingerstrasse 67  
D-80638, München, Germany  
ruediger@botanik.biologie.uni-muenchen.de

*Chapter 79*

**Jeremy K. M. Sanders**

University Chemical Laboratory  
Cambridge University  
Cambridge, CB2 1EW, UK

*Chapters 15, 22*



**Patricio J. Santander**

Center for Biological NMR, Department of Chemistry  
Texas A&M University  
College Station, Texas 77843, USA  
santander@tamu.edu  
*Chapter 76*

**James D. Satterlee**

Department of Chemistry  
Washington State University  
Pullman, Washington 99164, USA  
hemeteam@wsu.edu  
*Chapter 37*

**Jean-Pierre Sauvage**

Laboratoire de Chimie Organo-Minérale  
Université Louis Pasteur  
Institut Le Bel  
67070 Strasbourg, France  
sauvage@chimie.u-strasbg.fr  
*Chapter 40*

**W. Robert Scheidt**

Department of Chemistry and Biochemistry  
University of Notre Dame  
Notre Dame, Indiana 46556-5670, USA  
scheidt.1@nd.edu  
*Chapter 16*

**D. Schlettwein**

Physikalische Chemie 1, Fachbereich 9 (Chemie)  
Universität Oldenburg  
Postfach 2503  
D-26111 Oldenburg, Germany  
derck.schlettwein@uni-oldenburg.de  
*Chapter 106*

**Günter Schnurpfeil**

Universität Bremen  
Institut für Organische und Makromolekulare Chemie  
P.O. Box 33 04 40  
28334 Bremen, Germany  
gschnur@chemie.uni-bremen.de  
*Chapter 110*

**A. Ian Scott**

Center for Biological NMR, Department of Chemistry  
Texas A&M University  
College Station, Texas 77843, USA  
aiscott@tamu.edu  
*Chapter 76*

**Mathias O. Senge**

Institut für Chemie, Organische Chemie  
Freie Universität Berlin  
D-14195 Berlin, Germany  
mosenge@chemie.fu-berlin.de  
*Chapters 6, 61*

**Jonathan L. Sessler**

Department of Chemistry and Biochemistry  
Institute for Cellular and Molecular Biology  
The University of Texas at Austin  
Austin, Texas 78712-0165, USA  
sessler@mail.utexas.edu  
*Chapters 8, 9, 45*

**Kirill Shalyaev**

Department of Chemistry  
Princeton University  
Princeton, New Jersey 08544-1009, USA  
*Chapter 27*

**Wesley M. Sharman**

CIHR Group in the Radiation Sciences  
Faculty of Medicine  
Université de Sherbrooke  
Sherbrooke, Québec, Canada, J1H 5N4  
wesleysharman@hotmail.com  
*Chapter 97*

**John A. Shelnutt**

Biomolecular Materials and Interfaces Department  
Sandia National Laboratories  
1001 University Boulevard SE, Albuquerque  
New Mexico 87106, USA; and  
Department of Chemistry  
University of Georgia  
Athens, Georgia 30602-2556, USA  
jasheln@unm.edu  
*Chapter 50*

**Hirofusa Shirai**

Department of Functional Polymer Science  
Faculty of Textile Science and Technology  
Shinshu University  
Ueda 386-8567, Japan  
hshirai@giptc.shinshu-u.ac.jp  
*Chapter 120*

**Peter M. Shoolingin-Jordan**

School of Biological Sciences  
University of Southampton  
Bassett Crescent East  
Southampton, SO16 7PX, UK  
pmsj@soton.ac.uk

*Chapter 70*

**G rard Simonneaux**

Organom tallique et Catalyse, Chimie et  
 lectrochimie Mol culaires  
Universit  de Rennes I  
35042 Rennes, France  
gerard.simonneaux@univ-rennes1.fr

*Chapters 38, 65*

**Andrew G. Smith**

MRC Toxicology Unit, Hodgkin Building  
University of Leicester  
Lancaster Road, Leicester LE1 9HN, UK  
ags5@le.ac.uk

*Chapter 92*

**Kevin M. Smith**

Department of Chemistry  
Louisiana State University  
130 David Boyd Hall  
Baton Rouge, Louisiana 70803-2755, USA  
kmsmith@lsu.edu

*Chapters 1, 3, 81*

**Arthur W. Snow**

Chemistry Division, Code 6123  
Naval Research Laboratory  
4555 Overlook Avenue, SW  
Washington, DC 20375, USA  
snow@ccf.nrl.navy.mil

*Chapter 109*

**Christine Stern**

Laboratoire d'Ing nierie Mol culaire  
pour la S paration et les Applications des Gaz  
LIMSAG (UMR 5633)  
Universit  de Bourgogne  
Facult  des Sciences "Gabriel"  
6, Bd Gabriel 21000 Dijon, France  
christine.stern@u-bourgogne.fr

*Chapter 116*

**Martin J. Stillman**

Department of Chemistry  
University of Western Ontario, London  
Ontario, Canada, N6A 5B7  
martin.stillman@uwo.ca

*Chapter 103*

**Pavel A. Stuzhin**

Department of Organic Chemistry  
Ivanovo State University of Chemistry and Technology  
153460 Ivanovo, Russian Federation  
stuzhin@isuct.ru

*Chapter 101*

**Christopher J. Sunderland**

Department of Chemistry  
Stanford University  
Stanford, California 94305-5080, USA  
sunland@stanford.edu

*Chapter 62*

**Kenneth S. Suslick**

School of Chemical Sciences  
University of Illinois at Urbana-Champaign  
Urbana, Illinois 61801, USA  
ksuslick@uiuc.edu

*Chapters 28, 41*

**Alain Tabard**

Laboratoire d'Ing nierie Mol culaire  
pour la S paration et les Applications des Gaz  
LIMSAG (UMR 5633)  
Universit  de Bourgogne  
Facult  des Sciences "Gabriel"  
6, Bd Gabriel 21000 Dijon, France  
atabard@u-bourgogne.fr

*Chapter 21*

**Masaaki Tabata**

Department of Chemistry  
Faculty of Science and Engineering  
Saga University  
Saga 890-8502, Japan  
tabatam@cc.saga-u.ac.jp

*Chapter 60*

**Pietro Tagliatesta**

Dipartimento di Scienze e Tecnologie Chimiche  
Tor Vergata University  
Via Della Ricerca scientifica  
00133, Rome, Italy  
pietro.tagliatesta@uniroma2.it

*Chapter 66*

**Isao Taniguchi**

Department of Applied Chemistry  
Kumamoto University  
Kumamoto 860, Japan  
taniguch@gpo.kumamoto-u.ac.jp

*Chapter 58*

**James Turner**

Department of Chemistry  
Virginia Commonwealth University  
Richmond, Virginia 23284-2006, USA  
jturner@saturn.vcu.edu

*Chapter 29*

**Pall Thordarson**

Department of Organic Chemistry, NSR Center  
The University of Nijmegen  
Toernooiveld 1  
NL-6525 ED Nijmegen, The Netherlands  
pall@sci.kun.nl

*Chapter 115*

**Russell Timkovich**

Department of Chemistry  
University of Alabama  
Tuscaloosa, Alabama 35487-0336, USA  
rtimkovi@bama.ua.edu

*Chapter 73*

**Tomás Torres**

Departamento de Química Orgánica  
Universidad Autónoma de Madrid  
28049 Cantoblanco, Madrid, Spain  
tomas.torres@uam.es

*Chapter 99*

**Alfred X. Trautwein**

Institut für Physik  
Universität zu Lübeck  
D-23538 Lübeck, Germany  
trautwein@physik.uni-luebeck.de

*Chapter 29*

**Paola Turano**

CERM and Department of Chemistry  
University of Florence  
50019 Sesto Fiorentino (Florence), Italy  
turano@cerm.unifi.it

*Chapter 39*

**Eric Van Caemelbecke**

Department of Chemistry  
University of Houston  
Houston, Texas 77204-5003, USA

*Chapters 21, 55, 59*

**Johan E. van Lier**

CIHR Group in the Radiation Sciences  
Faculty of Medicine  
Université de Sherbrooke  
Sherbrooke, Québec, Canada, J1H 5N4  
jvanlier@courrier.usherb.ca

*Chapter 97*

**Maria da Graça H. Vicente**

Department of Chemistry  
Louisiana State University  
Baton Rouge, Louisiana 70803-2755, USA  
vicente@isu.edu

*Chapter 4*

**Emanuel Vogel**

Institut für Organische Chemie  
Universität zu Köln  
50939 Köln, Germany

*Chapter 8*

**F. Ann Walker**

Department of Chemistry  
University of Arizona  
Tucson, Arizona 85721-0041, USA  
awalker@u.arizona.edu

*Chapter 36*

**Michael Wark**

Institute for Physical Chemistry and Electrochemistry  
University Hanover  
Callin Str. 3-3A  
D-30167 Hanover, Germany  
michael.wark@pci.uni-hannover.de

*Chapter 111*

**Yoshihito Watanabe**

Institute for Molecular Science  
Myodaiji, Okazaki 444-8585, Japan  
yoshi@ims.ac.jp  
*Chapter 30*

**Simon J. Webb**

University Chemical Laboratory  
Cambridge University  
Cambridge, CB2 1EW, UK  
*Chapter 15*

**Steven J. Weghorn**

Tonah Products, Inc.  
Milton, Wisconsin 53563, USA  
sweg@jvl.net.com  
*Chapter 9*

**Raymond Weiss**

Laboratoire de Cristallographie et de Chimie Structurale  
UMR 7513  
Institut Le Bel  
Université Louis Pasteur  
67070 Strasbourg, France  
weiss@chimie.u-strasbg.fr  
*Chapter 29*  
*and*  
Laboratoire de Chimie Supramoléculaire  
Institut de Science et d'Ingénierie Supramoléculaires  
Université Louis Pasteur de Strasbourg  
8, rue Gaspard Monge, F-67000 Strasbourg, France  
weiss@chimie.u-strasbg.fr  
*Chapter 105*

**Stefan Will**

Institut für Organische Chemie  
Universität zu Köln  
50939 Köln, Germany  
*Chapter 12*

**Robert D. Willows**

Department of Biological Sciences  
Macquarie University  
North Ryde, 2109 Australia  
rwillows@rna.bio.mq.edu.au  
*Chapter 77*

**J. H. P. Wilson**

Department of Internal Medicine  
Erasmus MC  
University Medical Center Rotterdam  
P.B. 2040, 3000 CA Rotterdam  
The Netherlands  
j.wilson@erasmusmc.nl  
*Chapters 93, 95*

**Jay R. Winkler**

Beckman Institute, MC 139-74  
California Institute of Technology  
Pasadena, California 91125, USA  
winklerj@caltech.edu  
*Chapter 63*

**Dieter Wöhrle**

Universität Bremen  
Institut für Organische und Makromolekulare Chemie  
P.O. Box 33 04 40  
28334 Bremen, Germany  
woehrle@chemie.uni-bremen.de  
*Chapter 110*

**Gang Zheng**

Department of Nuclear Medicine  
Roswell Park Cancer Institute  
Buffalo, New York 14263-001, USA  
pdtctr@sc3101.med.buffalo.edu  
*Chapter 43*

---

# Contents of Volumes 1–20

## **Volume 1 / Synthesis and Organic Chemistry**

1. Strategies for the Synthesis of Octaalkylporphyrin Systems  
*Kevin M. Smith*
2. Synthesis of *meso*-Substituted Porphyrins  
*Jonathan S. Lindsey*
3. Cyclizations of *a,c*-Biladiene Salts to Give Porphyrins and Their Derivatives  
*Kevin M. Smith*
4. Reactivity and Functionalization of  $\beta$ -Substituted Porphyrins and Chlorins  
*Maria da Graça H. Vicente*
5. Functionalization of 5,10,15,20-Tetra-Substituted Porphyrins  
*Laurent Jaquinod*
6. Highly Substituted Porphyrins  
*Mathias O. Senge*
7. Geochemistry of Porphyrins  
*Henry J. Callot*  
*Rubén Ocampo*

## **Volume 2 / Heteroporphyrins, Expanded Porphyrins and Related Macrocycles**

8. Porphyrin Isomers  
*Jonathan L. Sessler*  
*Andreas Gebauer*  
*Emanuel Vogel*
9. Expanded Porphyrins  
*Jonathan L. Sessler*  
*Andreas Gebauer*  
*Steven J. Weghorn*
10. Syntheses of Novel Porphyrinoid Chromophores  
*Timothy D. Lash*
11. Syntheses of Corroles  
*Roberto Paolesse*

12. Metalloporphyrins: Molecular Structure, Spectroscopy and Electronic States  
*Christoph Erben*  
*Stefan Will*  
*Karl M. Kadish*
13. *meso*-Azaporphyrins and Their Analogues  
*Nagao Kobayashi*
14. Core-Modified Heteroanalogues of Porphyrins and Metalloporphyrins  
*Lechosław Latos-Grażyński*

### **Volume 3 / Inorganic, Organometallic and Coordination Chemistry**

15. Axial Coordination Chemistry of Metalloporphyrins  
*Jeremy K. M. Sanders*  
*Nick Bampos*  
*Zöe Clyde-Watson*  
*Scott L. Darling*  
*Joanne C. Hawley*  
*Hee-Joon Kim*  
*Chi Ching Mak*  
*Simon J. Webb*
16. Systematics of the Stereochemistry of Porphyrins and Metalloporphyrins  
*W. Robert Scheidt*
17. Alkali Metal Porphyrins  
*John Arnold*
18. Chemistry of Water Soluble Porphyrins  
*Peter Hambright*
19. Synthesis, Spectroscopic and Structural Studies of Metal–Metal-Bonded Metalloporphyrins  
*Jean-Michel Barbe*  
*Roger Guilard*
20. Metal Tetrapyrrole Double- and Triple-Deckers with Special Emphasis on Porphyrin Systems  
*Johann W. Buchler*  
*Dennis K.P. Ng*
21. Synthesis, Spectroscopy and Electrochemical Properties of Porphyrins with Metal–Carbon Bonds  
*Roger Guilard*  
*Eric Van Caemelbecke*  
*Alain Tabard*  
*Karl M. Kadish*
22. Coordination Chemistry of Oligoporphyrins  
*Jeremy K. M. Sanders*
23. Dendrimer Porphyrins and Metalloporphyrins: Syntheses, Structures and Functions  
*Takuzo Aida*  
*Dong-Lin Jiang*
24. Metalation and Metal-Assisted Modifications of the Porphyrinogen Skeleton Using *meso*-Octaalkylporphyrinogen  
*Carlo Floriani*  
*Rita Floriani-Moro*

25. Redox Chemistry of the Porphyrinogen Skeleton: Pathways to Artificial Porphyrins and Porphodimethenes  
*Carlo Floriani*  
*Rita Floriani-Moro*

**Volume 4 / Biochemistry and Binding: Activation of Small Molecules**

26. Diversity of Reactions Catalyzed by Heme-Thiolate Proteins  
*Daniel Mansuy*  
*Pierrette Battioni*
27. Oxometalloporphyrins in Oxidative Catalysis  
*John T. Groves*  
*Kirill Shalyaev*  
*Jinbo Lee*
28. Shape-Selective Oxidation by Metalloporphyrins  
*Kenneth S. Suslick*
29. High-Valent Iron and Manganese Complexes of Porphyrins and Related Macrocycles  
*Raymond Weiss*  
*Avram Gold*  
*Alfred X. Trautwein*  
*James Turner*
30. High-Valent Intermediates  
*Yoshihito Watanabe*
31. Metalloporphyrins in Catalytic Oxidations and Oxidative DNA Cleavage  
*Bernard Meunier*  
*Anne Robert*  
*Geneviève Pratviel*  
*Jean Bernadou*
32. Peroxidase and Cytochrome P450 Structures  
*Thomas L. Poulos*
33. Binding and Activation of Nitric Oxide by Metalloporphyrins and Heme  
*Lin Cheng*  
*George B. Richter-Addo*
34. Structural Themes Determining Function in Nitric Oxide Synthases  
*C. S. Raman*  
*Pavel Martásek*  
*Bettie Sue S. Masters*

**Volume 5 / NMR and EPR**

35. NMR Spectroscopy of Diamagnetic Porphyrins  
*Craig J. Medforth*
36. Proton NMR and EPR Spectroscopy of Paramagnetic Metalloporphyrins  
*F. Ann Walker*
37. Nuclear Magnetic Resonance of Hemoproteins  
*Gerd N. La Mar*  
*James D. Satterlee*  
*Jeffery S. De Ropp*

38. Isocyanides and Phosphines as Axial Ligands in Heme Proteins and Iron Porphyrin Models  
*G rard Simonneaux*  
*Arnaud Bondon*
39. Solution Structures of Hemoproteins  
*Lucia Banci*  
*Ivano Bertini*  
*Claudio Luchinat*  
*Paola Turano*

**Volume 6 / Applications: Past, Present and Future**

40. Noncovalent Multiporphyrin Assemblies  
*Jean-Claude Chambron*  
*Val rie Heitz*  
*Jean-Pierre Sauvage*
41. Applications of Porphyrins and Metalloporphyrins to Materials Chemistry  
*Jun-Hong Chou*  
*Hari Singh Nalwa*  
*Margaret E. Kosal*  
*Neal A. Rakow*  
*Kenneth S. Suslick*
42. Metalloporphyrins as Catalysts for Precision Macromolecular Synthesis  
*Takuzo Aida*  
*Shohei Inoue*
43. Porphyrins as Photosensitizers in Photodynamic Therapy  
*Ravindra K. Pandey*  
*Gang Zheng*
44. Porphyrin-Based Electrochemical Sensors  
*Tadeusz Malinski*
45. Calixpyrroles: Novel Anion and Neutral Substrate Receptors  
*Jonathan L. Sessler*  
*Philip A. Gale*
46. Porphyrins and Metalloporphyrins as Receptor Models in Molecular Recognition  
*Hisanobu Ogoshi*  
*Tadashi Mizutani*  
*Takashi Hayashi*  
*Yasuhisa Kuroda*

**Volume 7 / Theoretical and Physical Characterization**

47. Quantum Chemical Studies of Molecular Structures and Potential Energy Surfaces of Porphyrins and Hemes  
*Abhik Ghosh*
48. Models for the Electronic Structure of Metalloporphyrins from High-Resolution X-ray Diffraction and Ab Initio Calculations  
*Claude Lecomte*  
*Marie-Madeleine Rohmer*  
*Marc B nard*



49. X-ray Absorption Spectroscopy Applied to Porphyrin Chemistry  
*José Goulon*  
*Chantal Goulon-Ginet*  
*Vincent Gotte*
50. Molecular Simulations and Normal-Coordinate Structural Analysis of Porphyrins and Heme Proteins  
*John A. Shelnut*
51. Resonance Raman Spectra of Heme Proteins and Model Compounds  
*James R. Kincaid*
52. Resonance Raman Spectroscopy of Petroporphyrins  
*Roman S. Czernuszewicz*  
*Estelle M. Maes*  
*J. Graham Rankin*
53. Magnetic Circular Dichroism Spectroscopy of Heme Proteins and Model Systems  
*Jennifer Cheek*  
*John Dawson*
54. Mass Spectrometry of Porphyrins and Metalloporphyrins  
*J. Martin E. Quirke*

**Volume 8 / Electron Transfer**

55. Electrochemistry of Metalloporphyrins in Nonaqueous Media  
*Karl M. Kadish*  
*Eric Van Caemelbecke*  
*Guy Royal*
56. Electron Transfer Chemistry of Porphyrins and Metalloporphyrins  
*Shunichi Fukuzumi*
57. Intramolecular Photoinduced Electron-Transfer Reactions of Porphyrins  
*Devens Gust*  
*Thomas A. Moore*
58. Electrochemistry of Heme Proteins  
*Fred M. Hawkrige*  
*Isao Taniguchi*

**Volume 9 / Database of Redox Potentials and Binding Constants**

59. Metalloporphyrins in Nonaqueous Media: Database of Redox Potentials  
*Karl M. Kadish*  
*Guy Royal*  
*Eric Van Caemelbecke*  
*Lena Gueletti*
60. Equilibrium Data of Porphyrins and Metalloporphyrins  
*Masaaki Tabata*  
*Jun Nishimoto*

**Volume 10 / Database of Tetrapyrrole Crystal Structure Determination**

61. Database of Tetrapyrrole Crystal Structure Determinations  
*Mathias O. Senge*
- Cumulative Index

**Volume 11 / Bioinorganic and Bioorganic Chemistry**

62. Functional and Structural Analogs of the Dioxygen Reduction Site in Terminal Oxidases  
*James P. Collman*  
*Roman Boulatov*  
*Christopher J. Sunderland*
63. Heme Protein Dynamics: Electron Tunneling and Redox Triggered Folding  
*Harry B. Gray*  
*Jay R. Winkler*
64. Chiral Metalloporphyrins and Their Use in Enantiocontrol  
*Jean-Claude Marchon*  
*René Ramasseul*
65. Carbene Complexes of Metalloporphyrins and Heme Proteins  
*G rard Simonneaux*  
*Paul Le Maux*
66. Metalloporphyrins in the Biomimetic Oxidation of Lignin and Lignin Model Compounds: Development of Alternative Delignification Strategies  
*Claudia Crestini*  
*Pietro Tagliatesta*
67. Biochemistry of Methyl-CoM Reductase and Coenzyme F<sub>430</sub>  
*Stephen W. Ragsdale*
68. Structure, Reactions, and Functions of B<sub>12</sub> and B<sub>12</sub>-Proteins  
*Bernhard Kr utler*  
*Sigrid Ostermann*

**Volume 12 / The Iron and Cobalt Pigments: Biosynthesis, Structure, and Degradation**

69. Regulatory Mechanisms of Eukaryotic Tetrapyrrole Biosynthesis  
*Bernhard Grimm*
70. The Biosynthesis of Coproporphyrinogen III  
*Peter M. Shoolingin-Jordan*
71. Coproporphyrinogen III and Protoporphyrinogen IX Oxidases  
*Muhammad Akhtar*
72. Ferrochelatase  
*Harry A. Dailey*  
*Tamara A. Dailey*
73. The Family of d-Type Hemes: Tetrapyrroles with Unusual Substituents  
*Russell Timkovich*
74. Biosynthesis and Role of Heme O and Heme A  
*Tatsushi Mogi*
75. Heme Oxygenase Structure and Mechanism  
*Paul R. Ortiz de Montellano*  
*Karine Auclair*

76. Genetic and Mechanistic Exploration of the Two Pathways of Vitamin B<sub>12</sub> Biosynthesis

*A. Ian Scott*

*Charles A. Roessner*

*Patricio J. Santander*

### **Volume 13/Chlorophylls and Bilins: Biosynthesis, Synthesis, and Degradation**

77. Mechanism, Structure, and Regulation of Magnesium Chelatase

*Robert D. Willows*

*Mats Hansson*

78. Intermediate Steps in Chlorophyll Biosynthesis: Methylation and Cyclization

*David W. Bollivar*

79. The Last Steps of Chlorophyll Synthesis

*W. Rüdiger*

80. The Light-Independent Protochlorophyllide Reductase: A Nitrogenase-Like Enzyme Catalyzing a Key Reaction for Greening in the Dark

*Yuichi Fujita*

*Carl E. Bauer*

81. Chlorosome Chlorophylls (Bacteriochlorophylls *c*, *d*, and *e*): Structures, Partial Syntheses, and Biosynthetic Proposals

*Kevin M. Smith*

82. Chlorophyll Breakdown and Chlorophyll Catabolites

*Bernhard Kräutler*

83. Biosynthesis and Biological Functions of Bilins

*Nicole Frankenberg*

*J. Clark Lagarias*

84. Synthesis of Bilins

*Albert Gossauer*

### **Volume 14/Medical Aspects of Porphyrins**

85. Erythropoietic Disorders Involving Heme Biosynthesis

*Sylvia S. Bottomley*

86. Acute Intermittent Porphyria: From Clinical to Molecular Aspects

*Jean-Charles Deybach*

*Hervé Puy*

87. Congenital Erythropoietic Porphyria

*Hubert de Verneuil*

*Cécile Ged*

*François Moreau-Gaudry*

88. Porphyria Cutanea Tarda and Related Disorders

*G. H. Elder*

89. Variegated Porphyria

*Peter Meissner*

*Richard Hift*

*Anne Corrigall*

90. Protoporphyrin  
*Timothy M. Cox*
91. Miscellaneous Abnormalities in Porphyrin Production and Disposal  
*Richard Hift*  
*Peter Meissner*
92. Porphyria Caused by Chlorinated AH Receptor Ligands and Associated Mechanisms of Liver Injury and Cancer  
*Andrew G. Smith*
93. Porphyria: A Diagnostic Approach  
*Felix W. M. de Rooij*  
*Annie Edixhoven*  
*J. H. Paul Wilson*
94. Approaches to Treatment and Prevention of Human Porphyrias  
*Karl E. Anderson*
95. Management and Treatment of the Porphyrias  
*J. H. P. Wilson*  
*F. W. M. de Rooij*
96. Porphyria: A Toxicogenetic Disease  
*Richard J. Hift*  
*Peter N. Meissner*  
*Michael R. Moore*

**Volume 15 / Phthalocyanines: Synthesis**

97. Synthesis of Phthalocyanine Precursors  
*Wesley M. Sharman*  
*Johan E. van Lier*
98. The Synthesis of Symmetrical Phthalocyanines  
*Neil B. McKeown*
99. Design and Synthesis of Low-Symmetry Phthalocyanines and Related Systems  
*M. Salomé Rodríguez-Morgade*  
*Gema de la Torre*  
*Tomás Torres*
100. Synthesis and Spectroscopic Properties of Phthalocyanine Analogs  
*Nagao Kobayashi*
101. Porphyrazines with Annulated Heterocycles  
*Pavel A. Stuzhin*  
*Claudio Ercolani*

**Volume 16 / Phthalocyanines: Spectroscopic and Electrochemical Characterization**

102. The Photophysical Properties of Phthalocyanines and Related Compounds  
*Kazuyuki Ishii*  
*Nagao Kobayashi*

103. Electronic Structures of Metal Phthalocyanine and Porphyrin Complexes from Analysis of the UV–Visible Absorption and Magnetic Circular Dichroism Spectra and Molecular Orbital Calculations  
*John Mack*  
*Martin J. Stillman*
104. Electrochemistry of Phthalocyanines  
*Maurice L'Her*  
*Annig Pondaven*
105. Lanthanide Phthalocyanine Complexes  
*Raymond Weiss*  
*Jean Fischer*
106. Photoelectrochemical Reactions at Phthalocyanine Electrodes  
*D. Schlettwein*  
*N. I. Jaeger*  
*T. Oekermann*

**Volume 17 / Phthalocyanines: Properties and Materials**

107. Physical Properties of Phthalocyanine-based Materials  
*Danilo Dini*  
*Michael Hanack*
108. Phthalocyanine Thin Films: Deposition and Structural Studies  
*Michael J. Cook*  
*Isabelle Chambrier*
109. Phthalocyanine Aggregation  
*Arthur W. Snow*
110. Porphyrins and Phthalocyanines in Macromolecules  
*Dieter Wöhrle*  
*Günter Schnurpfeil*
111. Porphyrins and Phthalocyanines Encapsulated in Inorganic Host Materials  
*Michael Wark*

**Volume 18 / Multiporphyrins, Multiphthalocyanines, and Arrays**

112. Single-Atom Bridged Dinuclear Metal Complexes with Emphasis on Phthalocyanine Systems  
*Barbara Floris*  
*Maria Pia Donzello*  
*Claudio Ercolani*
113. Recent Advances in Free and Metalated Multiporphyrin Assemblies and Arrays; A Photophysical Behavior and Energy Transfer Perspective  
*Pierre D. Harvey*
114. Stacked Polymeric Phthalocyanines: Synthesis and Structure-Related Properties  
*Michael Hanack*  
*Danilo Dini*

115. Self-Assembly of Chiral Phthalocyanines and Chiral Crown Ether Phthalocyanines  
*Pall Thordarson*  
*Roeland J. M. Nolte*  
*Alan E. Rowan*
116. New Developments in Corrole Chemistry: Special Emphasis on Face-to-Face Bismacrocycles  
*Roger Guilard*  
*Jean-Michel Barbe*  
*Christine Stern*  
*Karl M. Kadish*

**Volume 19/Applications of Phthalocyanines**

117. Phthalocyanines in Photobiology and Their Medical Applications  
*Ehud Ben-Hur*  
*Wai-Shun Chan*
118. Radical Phthalocyanines and Intrinsic Semiconduction  
*Marcel Bouvet*
119. Phthalocyanine Dyes and Pigments  
*Peter Erk*  
*Heidi Hengelsberg*
120. Enzyme-Like Catalytic Reactions of Metallophthalocyanines and Polymeric Metallophthalocyanines  
*Mutsumi Kimura*  
*Hirofusa Shirai*
121. Nonlinear Optical Properties of Phthalocyanines  
*Steven R. Flom*

**Volume 20/Phthalocyanines: Structural Characterization**

122. Single-Crystal Structures of Phthalocyanine Complexes and Related Macrocycles  
*Michael Klaus Engel*

Cumulative Index

# Functional and Structural Analogs of the Dioxygen Reduction Site in Terminal Oxidases

62

JAMES P. COLLMAN, ROMAN BOULATOV, and CHRISTOPHER J. SUNDERLAND

Department of Chemistry, Stanford University, Stanford, California 94305-5080, USA

I. Introduction: Heme/Cu Terminal Oxidases . . . . .	1
II. Structural and Spectroscopic Models of the Heme $a_3/Cu_B$ Site. . . . .	5
A. General Synthetic Methodologies. . . . .	5
B. Oxo and Hydroxo Bridged Systems . . . . .	11
1. Synthesis. . . . .	11
2. Solid State Structural Studies. . . . .	11
3. Chemical and Electronic Properties. . . . .	12
C. Cyanide Bridged Systems . . . . .	13
1. Synthesis. . . . .	13
2. Solid State Structural Studies. . . . .	14
3. Chemical and Electronic Properties. . . . .	14
D. Carboxylate Bridged Systems. . . . .	16
1. Synthesis. . . . .	16
2. Solid State Structural Studies. . . . .	17
3. Chemical and Electronic Properties. . . . .	17
E. Carbon Monoxide Adducts of (por)Fe <sup>II</sup> /Cu <sup>I</sup> Systems . . . . .	17
1. Synthesis. . . . .	17
2. Chemical and Spectroscopic Properties. . . . .	17
III. Reactivity of Heme $a_3/Cu_B$ Analogs Toward O <sub>2</sub> Under Noncatalytic and Single Turnover Conditions . . . . .	18
A. Characterization of Peroxide Bridged Intermediates . . . . .	19
B. Reaction of Fe <sup>II</sup> /Cu <sup>I</sup> Centers with O <sub>2</sub> . . . . .	22
IV. Functional Analogs of the Dioxygen Reduction Site in Heme/Cu Terminal Oxidases . . . . .	23
A. Methodologies . . . . .	23
B. General Mechanism of Electrocatalytic O <sub>2</sub> (H <sub>2</sub> O <sub>2</sub> ) Reduction at an Iron Porphyrin . . . . .	28
C. Electrocatalytic O <sub>2</sub> Reduction by Simple Fe Porphyrins . . . . .	29
D. Functional Heme $a_3/Cu_B$ Analogs. . . . .	32
V. Cofacial Diporphyrins . . . . .	35
A. Molecular Structure and Physicochemical Properties . . . . .	36
B. Nonaqueous Dioxygen Chemistry of Group 2 Biscobaltdiporphyrins. . . . .	38
C. Electrocatalytic O <sub>2</sub> Reduction . . . . .	40
D. Catalytic Properties of Monocobaltdiporphyrins Containing a Nonredox Active Cation with Strong Lewis Acidity . . . . .	43
E. Summary. . . . .	44
VI. Summary and Outlook . . . . .	44
References . . . . .	45

## I. Introduction: Heme/Cu Terminal Oxidases

Heme/copper terminal oxidases are a superfamily of multisubunit membrane enzymes<sup>1,2</sup> catalyzing the reduction of dioxygen to water as a means of clearing

the electron transport system of electrons derived from oxidative catabolism.<sup>3,4</sup> The electron transport chain takes reducing equivalents from NAD(P)H through a series of steps in which protons are pumped across a mitochondrial or bacterial membrane to generate

a transmembrane potential gradient used to drive ATP synthesis. These reducing equivalents, either at a ubiquinol or cytochrome *c* potential level, are transferred to the terminal oxidase (ubiquinol or cytochrome *c* oxidase, respectively) for the reduction of dioxygen and further translocation of protons (“proton pump”). Cytochrome *c* oxidase (CcO) is present in both the mitochondria of eukaryotic cells and in many prokaryotes, whereas ubiquinol oxidase is found only in some prokaryotes. The CcO-based respiration is more efficient, as it allows for an additional proton-translocating electron transport step in the preceding cytochrome *bc*<sub>1</sub> complex. Both types of heme/copper oxidases possess significant structural similarity of the catalytic subunit (subunit I), which contains an electron transfer heme in addition to the binuclear heme/Cu<sub>B</sub> O<sub>2</sub> reduction site (Figure 1). A major difference between cytochrome *c* and ubiquinol oxidases lies in the presence of an additional electron transfer group, typically the binuclear Cu<sub>A</sub> site in subunit II of CcOs (Figure 2), a center absent in ubiquinol oxidases. As might be expected of such a phylogenetically widely distributed class of enzymes, numerous variations of the system exist with different heme types, proton-pumping efficiencies and mechanisms.<sup>5</sup> There are also a limited number of non heme/Cu terminal oxidases, such as cytochrome *bd*,<sup>6</sup> which possesses a binuclear heme/heme site for dioxygen reduction, and also functions as a proton pump. This

review focuses mainly on biomimetic studies of heme/copper terminal oxidases but cofacial diporphyrins, that can be considered as biomimetic analogs of the O<sub>2</sub> reduction site in alternative oxidases, are discussed in Section V below.

The realization of single crystal X-ray diffraction structures for the fully oxidized thirteen subunit bovine CcO (BOX)<sup>7-9</sup> and four subunit *P. denitrificans* CcO (POX)<sup>10,11</sup> are hallmark achievements in protein crystallography. The primary catalytic subunits, I and II, demonstrate a high degree of structural similarity in both BOX and POX.<sup>12</sup> Subunit I of both structures consists of 12 transmembrane helices in which the low-spin *bis*histidine-coordinated heme *a* and binuclear heme *a*<sub>3</sub>/Cu<sub>B</sub> are found, while subunit II, nestled at the side of subunit I, consists of two transmembrane helices with the Cu<sub>A</sub> domain held aloft of the membrane level (Figure 1). For the purposes of modeling the active site of heme/copper terminal oxidases, it is of particular note that the heme *a*<sub>3</sub>/Cu<sub>B</sub> sites of both POX and BOX are essentially identical (Figure 3). A covalent link between one of the Cu-ligating imidazoles and a conserved tyrosine residue at the *ortho*-phenol position is observed in both enzymes. The Fe<sub>a3</sub>···Cu<sub>B</sub> separations are 4.9, 5.2, 5.3, and 5.3 Å in the fully oxidized, fully reduced, CO- and azide-inhibited BOX,<sup>8</sup> 5.2 Å in both the fully reduced and the fully oxidized four-subunit POX,<sup>13</sup> and 4.5 Å in the fully oxidized

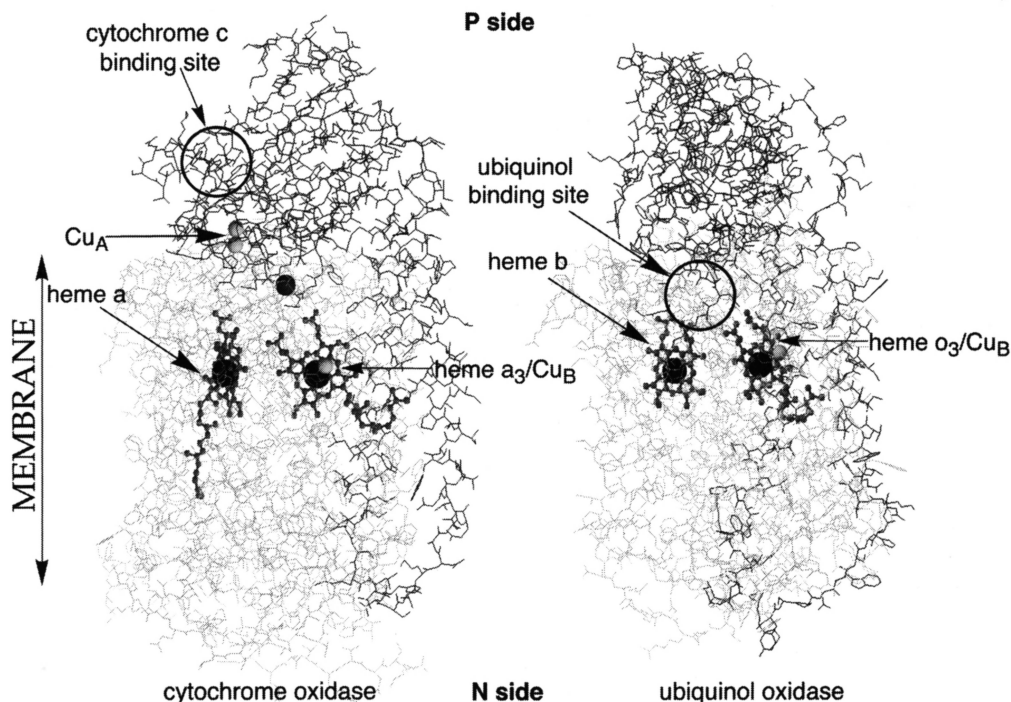
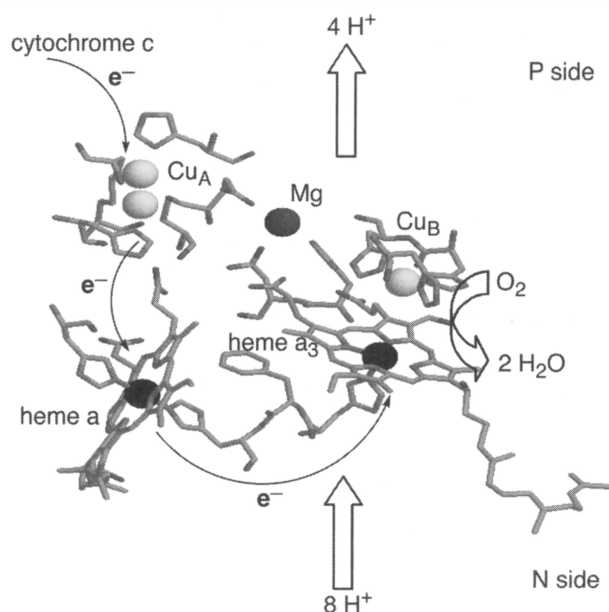
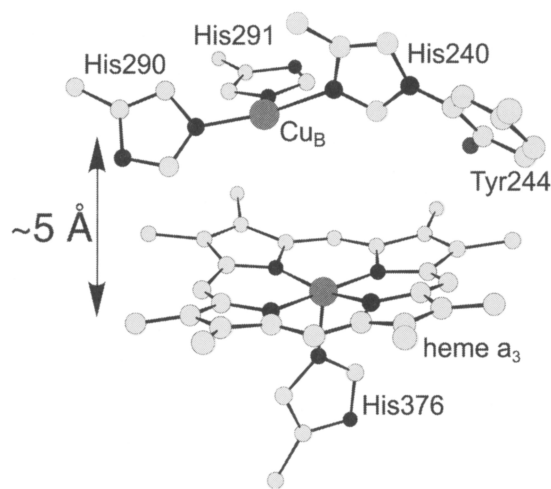


Figure 1. Schematic representation of bovine heart cytochrome *c* oxidase<sup>9</sup> and ubiquinol oxidase.<sup>17</sup>





**Figure 2.** Metal sites in bovine heart cytochrome oxidase (BOX,  $\text{Na}^+$  and  $\text{Zn}^{2+}$  are omitted).<sup>9</sup> Electrons are transferred from ferrocyanochrome c to the binuclear  $\text{Cu}_A$  site, to heme a and finally to the heme  $a_3/\text{Cu}_B$  site where  $\text{O}_2$  is reduced.  $\text{O}_2$  reduction is coupled to translocation of  $4 \text{H}^+$  from the N side to the P side of the membrane.



**Figure 3.** The heme  $a_3/\text{Cu}_B$  site in bovine heart cytochrome oxidase.<sup>9</sup>

two-subunit POX.<sup>11</sup> The variations in the intermetallic separation is most likely due to different ligation of the binuclear site. With the exception of azide and CO-inhibited BOX, the resolution of the existing crystallographic structures (2.3–2.7 Å) is insufficient to determine with confidence the nature of the ligand(s) at the heme  $a_3/\text{Cu}_B$  site. In the fully oxidized two-subunit POX, it appeared to be ligated by water/hydroxide donors within H-bonding distance to each other, for which some spectroscopic evidence exists.<sup>14</sup> In the fully oxidized BOX, the electron density at this site was best fit to a bridging peroxide,  $\text{FeOOCu}$ , with redox titrations used as supporting evidence for this

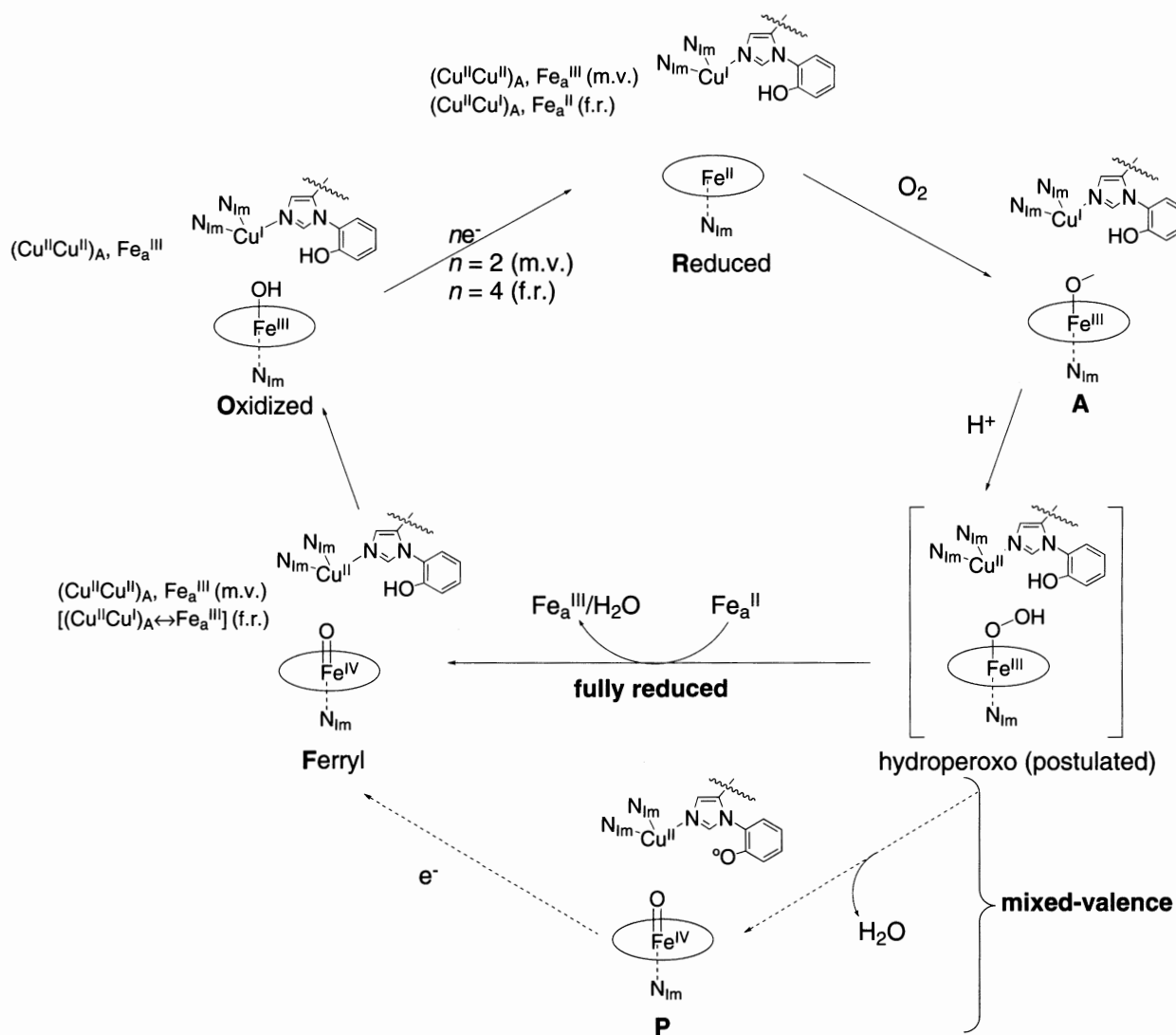
unexpected result.<sup>15</sup> The structures of the two subunit *T. thermophilus*,  $\text{ba}_3$ -cytochrome *c* oxidase (TOX)<sup>16</sup> and the four subunit *E. coli*  $\text{bo}_3$ -ubiquinol oxidase (EOX)<sup>17</sup> have also been determined recently. As for BOX and POX, TOX and EOX possess similar placement of prosthetic groups (Figure 1), although only TOX has been determined at sufficient resolution for detailed structural comparison. The  $\text{Fe}_{a_3}/\text{Cu}_B$  core of TOX (intermetallic distance 4.5 Å) was determined to be bridged by an oxo/hydroxo group with Fe–O and Cu–O bonds of  $\sim 2.3$  Å each. It has long been recognized that the “as isolated” form of terminal oxidases varies in composition and reactivity depending on the isolation

methodology. Thus, the crystal structures may not reflect the ligation state of the binuclear site in catalytically relevant forms of the enzyme.

In mitochondrial CcO electron transfer from external reductants (cytochrome *c in vivo*) to the heme  $a_3$ /Cu<sub>B</sub> site proceeds via Cu<sub>A</sub> and heme a (Figure 2). Among its metal sites, the enzyme can store up to four reducing equivalents above the aerobically stable fully oxidized state ( $\text{Fe}_a^{\text{III}}$ ,  $(\text{Cu}^{\text{II}}\text{Cu}^{\text{II}})_A$ ,  $\text{Fe}_{a_3}^{\text{III}}$ ,  $\text{Cu}_B^{\text{II}}$ ). Although the population of various redox states *in vivo* is unknown, Wikstrom argued that a substantial fraction of cytochrome oxidase is present in the fully reduced ( $\text{Fe}_a^{\text{II}}$ ,  $(\text{Cu}^{\text{II}}\text{Cu}^{\text{I}})_A$ ,  $\text{Fe}_{a_3}^{\text{II}}$ ,  $\text{Cu}_B^{\text{I}}$ ) state even in normoxic tissues.<sup>18</sup> At least two-electron (2e) reduction above the fully oxidized level is required for enzyme to react

with  $\text{O}_2$ . Because the potentials of the redox cofactors depend on the redox state of the enzyme, singly reduced cytochrome oxidase contains ferriheme  $a_3$ , and is thus inert toward  $\text{O}_2$ . In contrast, in the 2e-reduced state (mixed-valence) both electrons localize preferentially at the heme  $a_3$ /Cu<sub>B</sub> site ( $\text{Fe}_{a_3}^{\text{II}}/\text{Cu}_B^{\text{I}}$ ).

The plausible mechanism of steady-state  $\text{O}_2$  reduction by cytochrome oxidase (Figure 4) is a pastiche drawn from studies of  $\text{O}_2$  reduction by fully and partly reduced CcO under single turnover conditions. The identification and time-dependence of intermediates in such studies have been outlined in a number of excellent reviews.<sup>3,19–23</sup> Time-resolved spectroscopic studies are typically initiated by flash photolysis from the CO bound ( $\text{Fe}_{a_3}^{\text{II}}\text{-CO}$ ) state. Coherent transfer<sup>24</sup> of CO from Fe to



**Figure 4.** A probable mechanism of  $\text{O}_2$  reduction at the catalytic site of heme/Cu terminal oxidases in the mixed-valence (m.v.) and fully reduced (f.r.) redox states. The Cu<sub>A</sub> and heme a cofactors are shown explicitly only in steps which involve changes in their oxidation states. In various intermediates Cu<sub>B</sub> may coordinate an exogenous ligand ( $\text{OH}^-$  or  $\text{H}_2\text{O}$ ), which is not shown as its nature remains controversial.

Cu<sub>B</sub> prior to loss from the active site has been followed by IR spectroscopy for a number of terminal oxidases.<sup>25–28</sup> Following loss of CO from the catalytic site, rapid buildup of compound A, the dioxygen adduct Fe<sub>a3</sub>O<sub>2</sub>,<sup>29</sup> is observed (Figure 4). The access of dioxygen to the fully reduced active site is believed to be mediated by Cu<sub>B</sub>, based on kinetics of wild-type enzymes<sup>29–32</sup> and by changes in reactivity of Cu-free mutants.<sup>33</sup> However, no intermediates in the postulated O<sub>2</sub> transfer via Cu have been observed spectroscopically. This heme/O<sub>2</sub> adduct is analogous to that in oxyhemoglobin and oxymyoglobin, and can be considered as an Fe<sup>III</sup>-superoxide species, wherein dioxygen formally underwent one electron reduction. The next observable intermediate is compound P, a species initially believed to possess a Peroxo, O<sub>2</sub><sup>2-</sup> moiety, which is now firmly established to be an O–O bond cleaved ferryl species.<sup>34,35</sup> Thus, at this point, O<sub>2</sub> has been reduced by 4e, with two electrons coming from heme a<sub>3</sub> and Cu<sub>B</sub> ((O<sub>2</sub><sup>-</sup>)Fe<sub>a3</sub><sup>III</sup> → O=Fe<sub>a3</sub><sup>IV</sup> and Cu<sub>B</sub><sup>I</sup> → Cu<sub>B</sub><sup>II</sup>), and the source of the additional electron depending on the initial redox state of the enzyme. In mixed-valence CcO, the final electron is believed to originate from the conserved active site tyrosine (TyrOH → TyrO<sup>•</sup>) to give P<sub>M</sub>.<sup>11,35–37</sup> In fully reduced CcO, the reduction of O<sub>2</sub> in compound A is thought to be concerted with oxidation of ferroheme a to yield compound P<sub>R</sub> without formation of organic radicals.<sup>38,39</sup> The intermediates P<sub>R</sub> and P<sub>M</sub> are thought to be structurally similar, differing mainly in the location of the oxidizing equivalent (Tyr or Fe<sub>a</sub>).<sup>40–42</sup> Although no intermediates have been observed between compounds A and P, the transformation likely proceeds via a ferric-hydroperoxo intermediate,<sup>43</sup> similar to that postulated in O<sub>2</sub> reduction cycles of monometallic heme enzymes.<sup>44</sup> With no further source of electrons within the CcO, P<sub>M</sub> is stable until reducing equivalents enter the enzyme. The P<sub>R</sub> intermediate evolves into a second ferryl species, F, which is proposed to differ from P<sub>R</sub> by protonation of the Cu bound O<sub>2</sub>-derived hydroxide and internal equilibration of the remaining electron between Cu<sub>A</sub> and Fe<sub>a</sub>.<sup>18</sup> Further electron transfer from the Cu<sub>A</sub>/Fe<sub>a</sub> pair reduces the ferryl species to ferriheme a<sub>3</sub> which is recognized as compound O, the stable oxidized state. Convincing evidence for another intermediate between F and O has been reported,<sup>23,39,45</sup> and assigned as a third ferryl-level oxidation state species with altered geometry from that of F. Since this species does not build up, and is spectroscopically similar to F, it is more difficult to define.

While many details are known about the O<sub>2</sub> reduction mechanism in heme/Cu oxidases, important

questions remain unanswered. There are a number of catalytic intermediates that have not been studied in sufficient detail to be assured of their nature and significance. The relevance of some intermediates found in single-turnover experiments to steady-state O<sub>2</sub> reduction *in vivo* is unclear. The molecular origin of heterogeneity of “as isolated” enzyme is not established.

Biomimetic studies of terminal oxidases can be a productive strategy to address some of these controversial issues. For example, synthetic analogs of the heme a<sub>3</sub>/Cu<sub>B</sub> site can be prepared in more clearly defined chemical and metric states. The basic reactivity of the Fe/Cu core in a stereoelectronic environment similar to that of the heme a<sub>3</sub>/Cu<sub>B</sub> site can be probed more easily by studying the interactions of model compounds with small molecules, such as CO, NO, CN<sup>-</sup>, N<sub>3</sub><sup>-</sup>. The latter are endogenous or exogenous inhibitors of the enzyme and are used extensively as spectroscopic probes. Comparing spectroscopic properties of the resulting adducts with those of various forms of terminal oxidases helps understand the possible ligation state(s) of, and the mode of ligand binding to, the catalytic site. Of particular interest to biological function of terminal oxidases is realization within synthetic systems of 4e dioxygen reduction without leakage of highly toxic, partially reduced oxygen intermediates (H<sub>2</sub>O<sub>2</sub> and free oxygen-based radicals, HO<sup>•</sup>, for instance) under physiologically relevant conditions. The chemical circumstances that can lead to such an efficient reduction, and the exploitation of this knowledge are of great fundamental as well as practical interest.

The O<sub>2</sub> reduction cycle of terminal oxidases must be intimately coupled to proton translocation, but the mechanism of this process is poorly understood.<sup>21,46–49</sup> No attempts have been made to create synthetic models of the “proton pump” and this aspect of the terminal oxidases’ chemistry will not be discussed further.

## II. Structural and Spectroscopic Models of the Heme a<sub>3</sub>/Cu<sub>B</sub> Site

### A. GENERAL SYNTHETIC METHODOLOGIES

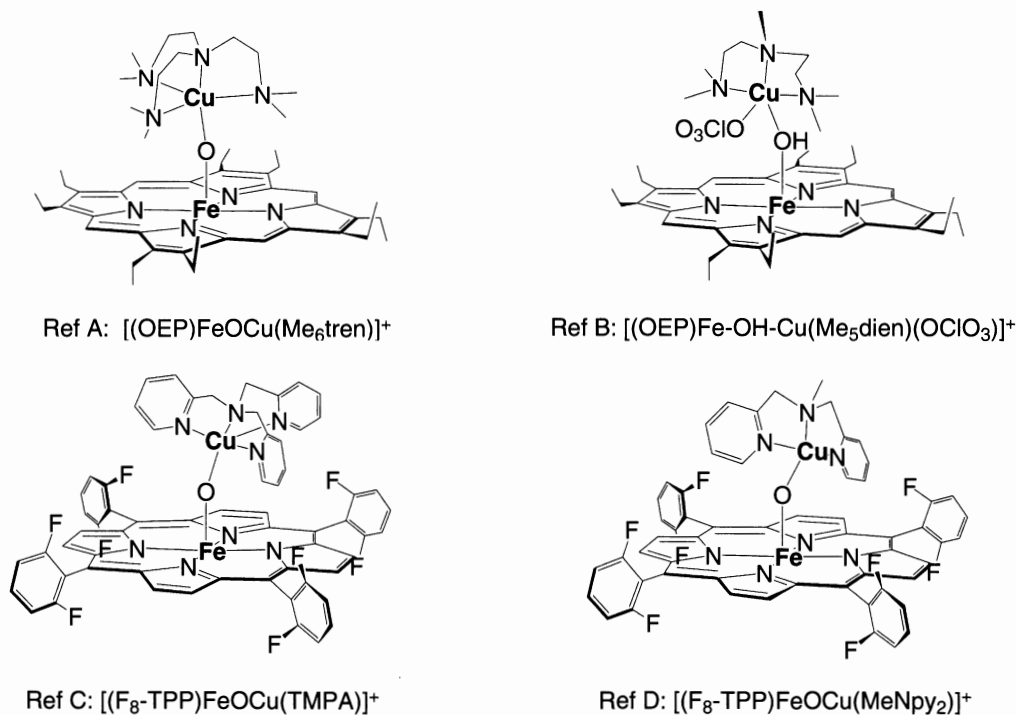
Cytochrome *c* oxidase models can be divided into two classes, those involving noncovalently linked analogs of the metal-binding substructures of the heme a<sub>3</sub>/Cu<sub>B</sub> site and those in which the representative substructures are covalently linked. Noncovalently linked systems are generally comprised of well-known metal–ligand systems, utilized for the convenience of bulk availability without lengthy synthetic procedures. The bimetallic

systems resulting from the reaction of independent porphyrin and copper-site ligands are frequently denoted as *self-assembled*. Typical porphyrins used in self-assembled systems include octaethylporphyrin, (H<sub>2</sub>OEP), tetraphenylporphyrin (H<sub>2</sub>TPP) and *ortho*-octafluorotetraphenylporphyrin (H<sub>2</sub>F<sub>8</sub>TPP). A plethora of Cu complexes have been used (Figures 5–7).<sup>50–60</sup>

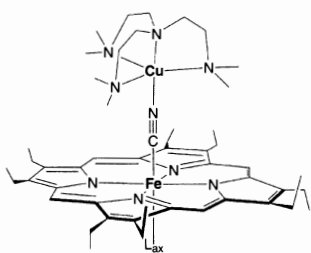
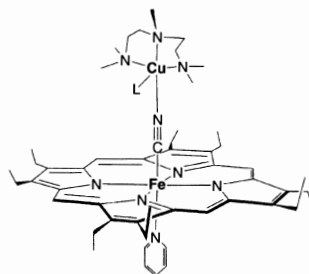
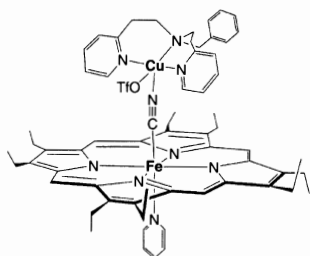
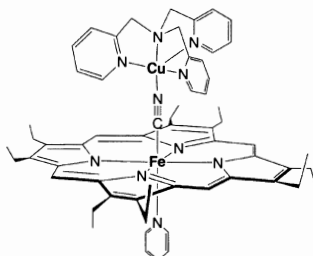
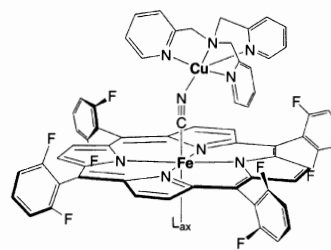
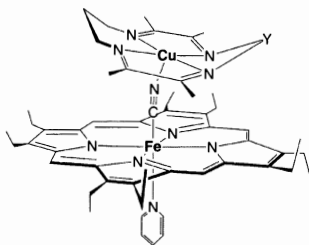
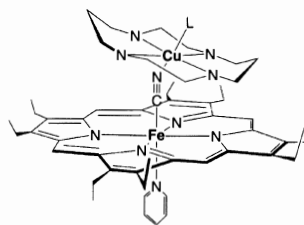
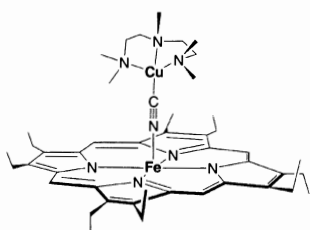
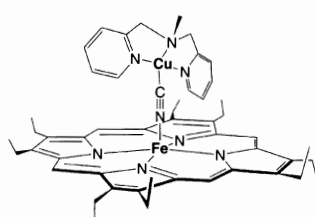
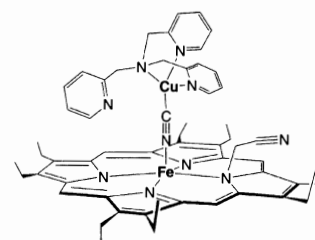
The denotation of a ligand system as *binuclear*, indicates a covalently appended distal metal binding site. Examples pertaining to this section of the review are in Figure 8<sup>61–71</sup> with further examples concerning electrochemical studies presented in Section IV below. Compared to self-assembled systems, covalently linked ligands frequently require lengthier, specialized synthetic procedures. In a well-designed system, the covalent linkage of porphyrin to a distal binding site affords the opportunity not only to kinetically and thermodynamically favor intramolecular heteronuclear, rather than intermolecular homonuclear (Fe/Fe or Cu/Cu) chemistry, but also to fine tune structural constraints so as to examine structure/function trends. With the exception of one research program, all porphyrins used in the synthesis of binuclear CcO models are based on TPP derivatives. This is due to advantages in the synthesis and stability of *meso*-phenyl substituted porphyrins, as well as the availability of *ortho*-phenyl substitution sites for appropriate positioning of appended functional groups over the porphyrin

ring. Nitrogen based distal site ligands have varied from the sp<sup>3</sup> amine triazacyclononane (TACN), 1,4,8,11-tetra-azacyclododecane (cyclam) and *tris*-(2-ethylamine)amine (TREN) based systems, to mixed amine/pyridine *tris*-pyridyl amine caps (e.g., TMPA), quinoline pickets and in the closest structural models, to imidazole pickets (Figures 8 and 12).

Tetraphenylporphyrin platforms can be delineated by the position and means of distal and/or proximal ligand attachment. Systems with a single *ortho*-phenyl substitution<sup>61,72–74</sup> possess the advantage of simpler synthesis and arm attachment, but only allow connecting of the poly-N cap at single, rather than multiple points. Furthermore, they lack the possibility to include a covalently tethered proximal base for coordination as an axial ligand to the metalloporphyrin, leading to consequent attenuation of the porphyrin based dioxygen chemistry. The most notable requirement for synthesis of such systems involves the preparation of TPP derivatives with a uniquely functionalized phenyl ring. Aminoporphyrins are typically obtained by reduction of the corresponding nitroporphyrin. The mononitrophenylporphyrins required can be readily synthesized by reaction of benzaldehyde and nitrobenzaldehyde with pyrrole followed by separation of the mixtures obtained.<sup>75–77</sup> Mono-*ortho*-hydroxy TPP derivatives have also been synthesized by use of empirically optimized aldehyde mixtures.<sup>64</sup>



**Figure 5.** Ferric/cupric oxo- and hydroxo-bridged CcO model systems: Ref A<sup>54</sup>, Ref B<sup>52</sup>, Ref C<sup>58</sup>, Ref D.<sup>60</sup>

Ref A:  $[\text{py}(\text{OEP})\text{Fe}-\text{CN}-\text{Cu}(\text{Me}_6\text{TREN})]^{2+}$   $L_{\text{ax}} = \text{py}$ Ref A:  $[[(\text{Me}_6\text{TREN})\text{Cu}-\text{NC}]_2-(\text{OEP})\text{Fe}]^{3+}$   $L_{\text{ax}} = \text{CNCu}(\text{Me}_6\text{TREN})$ Ref A:  $[\text{py}(\text{OEP})\text{Fe}-\text{CN}-\text{Cu}(\text{Me}_5\text{dien})(\text{OSO}_2\text{CF}_3)]^+$   $L = \text{OTf}^-$ Ref B:  $[\text{py}(\text{OEP})\text{Fe}-\text{CN}-\text{Cu}(\text{Me}_5\text{dien})(\text{Me}_2\text{CO})]^{2+}$   $L = \text{acetone}$ Ref B:  $[(\text{OEP})\text{Fe}-\text{CN}-\text{Cu}(\text{bnpy}_2)(\text{OTf})]^+$ Ref C:  $[\text{py}(\text{OEP})\text{Fe}-\text{CN}-\text{Cu}(\text{TPA})]^{2+}$ Ref D:  $[\text{py}(\text{F}_8\text{-TPP})\text{Fe}-\text{CN}-\text{Cu}(\text{TPA})]^{2+}$   $L_{\text{ax}} = \text{py}$ Ref D:  $[[\text{Cu}(\text{TPA})\text{NC}]_2-(\text{F}_8\text{-TPP})\text{Fe}]^{3+}$   $L_{\text{ax}} = \text{Cu}(\text{TPA})\text{NC}$ Ref B:  $[\text{py}(\text{OEP})\text{Fe}-\text{CN}-\text{Cu}(\text{TIM})]^{2+}$   $Y = (\text{CH}_2)_3$ Ref B:  $[\text{py}(\text{OEP})\text{Fe}-\text{CN}-\text{Cu}(\text{cyclops})]^+$   $Y = \text{OBF}_2\text{O}$ Ref B:  $[(\text{py}(\text{OEP})\text{Fe}-\text{CN})_2-\text{Cu}(\text{cyclam})]^{2+}$   $L = \text{NCFe}(\text{OEP})$ Ref B:  $[(\text{OEP})\text{Fe}^{\text{III}}-\text{NC}-\text{Cu}^{\text{I}}(\text{Me}_5\text{dien})]^+$ Ref C:  $[(\text{OEP})\text{Fe}^{\text{II}}-\text{NC}-\text{Cu}^{\text{I}}(\text{MeNpy}_2)]^+$ Ref C:  $[(\text{OEP}-\text{CH}_2\text{CN})\text{Fe}^{\text{II}}-\text{CN}-\text{Cu}^{\text{I}}(\text{TPA})]^+$ 

**Figure 6.** Cyanide-bridged CcO model systems: Ref. A,<sup>50</sup> Ref. B,<sup>51</sup> Ref. C,<sup>57</sup> Ref. D.<sup>59</sup> Ferric/cupric complexes unless shown otherwise.

Tetraphenylporphyrin-based CcO models with a single *bis-ortho*-substituted phenyl ring have been prepared,<sup>69,78</sup> allowing inclusion of a capping and tail structure. Since the starting porphyrin is  $C_{2v}$  symmetric, there are no stereochemical consequences

to functionalization on either face of the porphyrin, simplifying the preparation.

A number of CcO models based on tetra-*ortho*-aminophenylporphyrin have been synthesized. Tetra-*ortho*-aminophenylporphyrin (TAPP) is obtained as

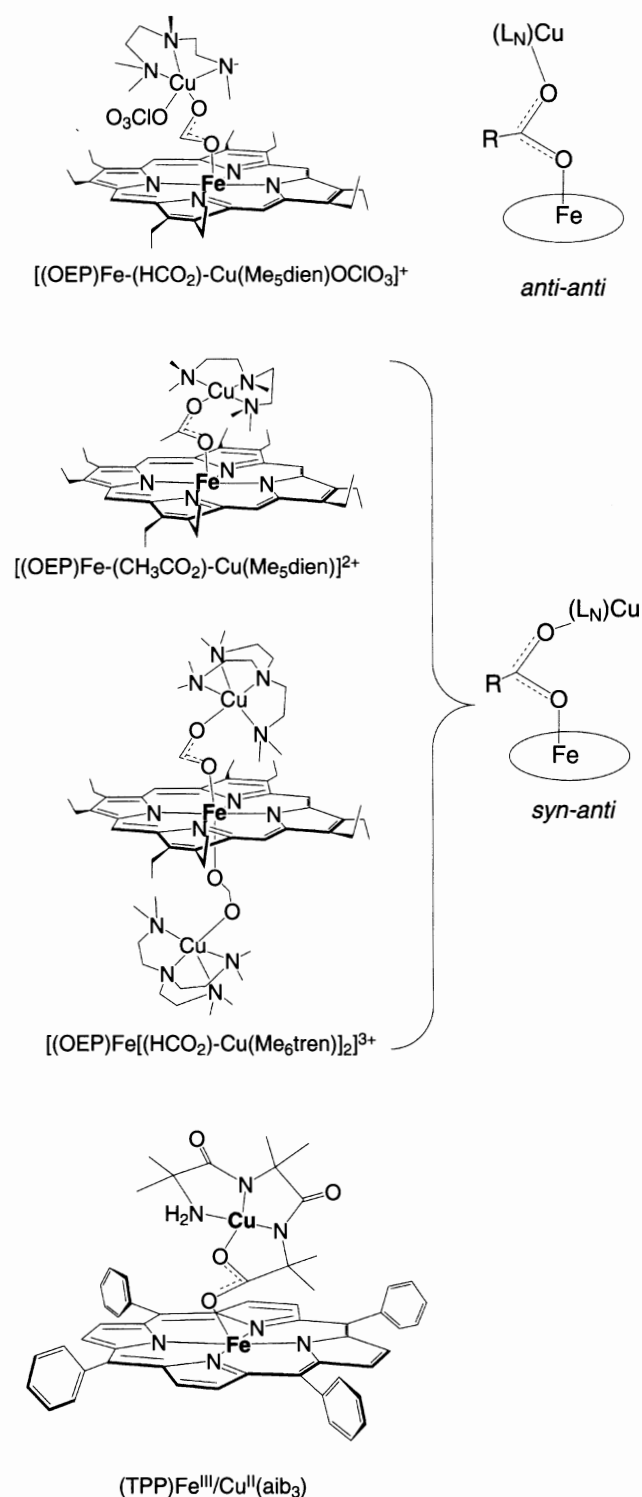
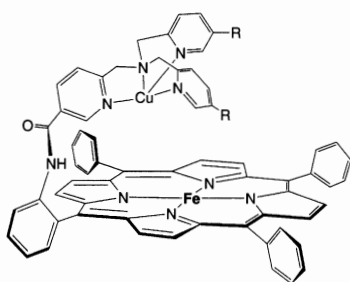


Figure 7. Ferric/cupric carboxylate-bridged CcO model systems.<sup>53</sup>

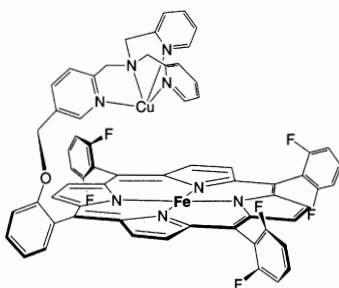
a mixture of four atropisomers,  $\alpha_4$  ( $\alpha,\alpha,\alpha,\alpha$ -TAPP),  $\alpha_3\beta$  ( $\alpha,\alpha,\alpha,\beta$ -TAPP),  $\alpha_2\beta_2$  ( $\alpha,\alpha,\beta,\beta$ -TAPP), and  $\alpha\beta\alpha\beta$ -TAPP, where  $\alpha$  and  $\beta$  designates *ortho*-substituents below or above the porphyrin plane. Examples of  $\alpha_4$ -TAPP,  $\alpha_3\beta$ -TAPP, and  $\alpha\beta\alpha\beta$ -TAPP derived heme/copper terminal oxidase models in Figure 8 are

( $\alpha_4$ -nicotinamide)Fe/Cu, ( $\alpha_3$ TREN<sub>Ph</sub>3 $\beta$ Im<sub>alk</sub>)Fe/Cu, and (Ph-cyclam)Fe/Cu, respectively. These TAPP isomers are chromatographically separable, however, the aminophenyl groups are able to freely rotate about the C<sub>meso</sub>-C<sub>phenyl</sub> bond at elevated temperature, scrambling the amine orientations. Although this mixture of interconvertible isomers presents synthetic challenges, strategies have been developed to manage the atropisomer distribution to realize TAPP as a flexible starting point for a number of superstructured porphyrins. The  $\alpha_3\beta$  pattern, where three amine groups are on one side of the porphyrin plane and a single amine group on the other side of the porphyrin plane, is the most obvious choice to mimic the histidine-ligated *tris*-imidazole Fe/Cu site of CcO (Figure 9).

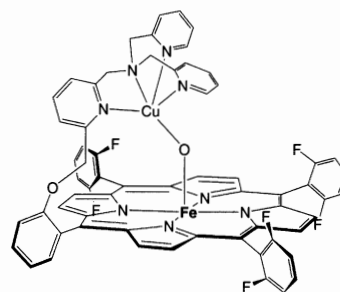
CcO models derived from the  $\alpha_4$ -TAPP<sup>79</sup> have been synthesized for a number of years, and include notable early work with  $\alpha_4$ -nicotinamidophenylporphyrin.<sup>62,80</sup> Differentiation of three of the amine groups from the fourth of  $\alpha_4$ -TAPP has been achieved by control of reaction conditions and stoichiometry, followed by separation of the statistical mixtures obtained.<sup>81-83</sup> In a more sophisticated manner, preparation of an  $\alpha_3\beta$  substitution pattern can be achieved from an  $\alpha_4$ -TAPP, by derivatizing all four of the amino groups with electrophilic (acrylamido or chloroacetamido) pickets (Figure 9).<sup>84a</sup> Addition of a nucleophilic threefold symmetric "cap" structure (e.g., 1,4,7-triazacyclononane, TACN) results in the differentiation of three sites from the fourth. In these derivatives, where three  $\alpha$ -amido pickets are now covalently tethered together, the single unique, untethered arm can be rotated to the opposing face of the porphyrin at elevated temperature to give a 1:1 mixture of  $\alpha_3\{\text{cap}\}\beta\{\text{tail}\}$  and  $\alpha_3\{\text{cap}\}\alpha\{\text{tail}\}$ .<sup>81</sup> Yield of the  $\alpha_3\beta$  isomer is improved if the porphyrin is metalated and the picket to be rotated is derivatized with an axial base. In this case, the driving force of axial base coordination to the metal at the least sterically hindered face of the porphyrin results in enrichment of the desired isomer.<sup>67,68,84</sup> Development of a porphyrin precursor stereochemically preorganized to present an  $\alpha_3\beta$  geometry such that three substituents can be selectively introduced on one face, while a single unique (tail) can be introduced onto the opposing face of the porphyrin was developed by Collman and coworkers.<sup>84b</sup> In this strategy, protection of the atropomeric mixture of TAPP with the bulky trityl group was followed by rotation of the unsubstituted amine groups of this isomeric mixture to the least sterically hindered face, using the driving force of adsorption to a polar alumina surface to realize enrichment (Figure 9).<sup>81,84,85</sup> Trifluoroacetyl protecting



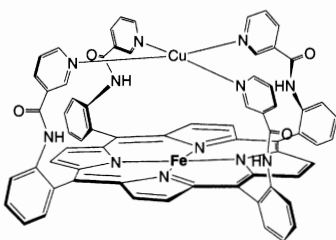
Ref A: (TPP-TMPA)Fe/Cu R=H  
 Ref B: (TPP-5-MeTMPA)Fe/Cu R=Me



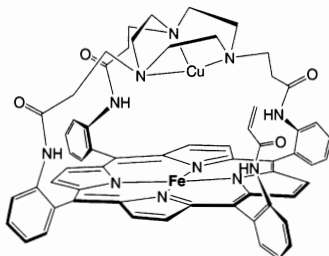
Ref C:  $^5\text{LFe/Cu}$



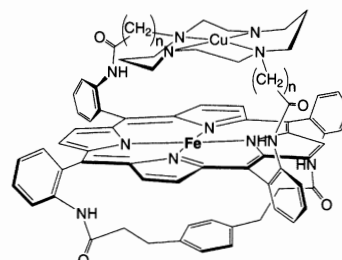
Ref D:  $^6\text{LFe/Cu}$



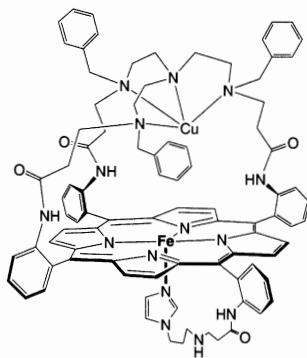
Ref E: ( $\alpha_4$ -nicotinamide)Fe/Cu



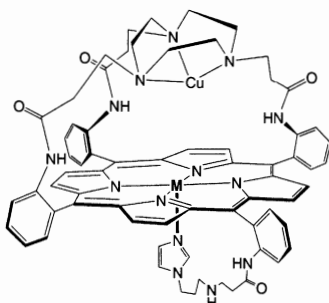
Ref F: ( $\alpha_3\text{TACN}\alpha\text{Acr}$ )Fe/Cu



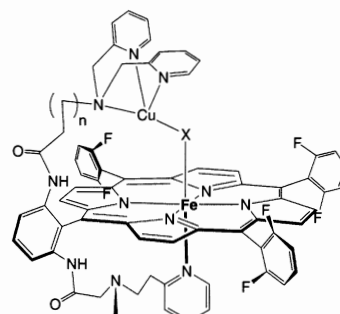
Ref G: (Ph-cyclam)Fe/Cu n=1 or 2



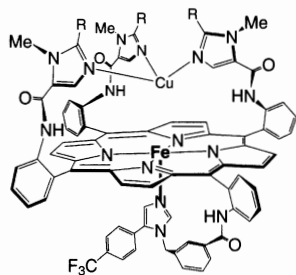
Ref H: ( $\alpha_3\text{TrenPh}\beta\text{Im}_{\text{alk}}$ )Fe/Cu



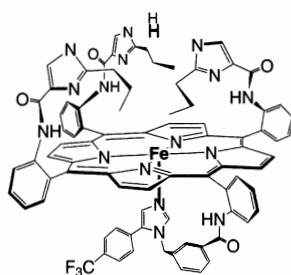
Ref H: M = Fe; ( $\alpha_3\text{TACN}\beta\text{Im}_{\text{alk}}$ )Fe/Cu  
 Ref I: M = Co; ( $\alpha_3\text{TACN}\beta\text{Im}_{\text{alk}}$ )Co/Cu



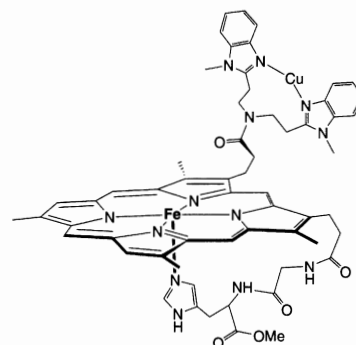
Ref J:  $^3\text{LFe/Cu}$ ; n = 0  
 Ref J:  $^4\text{LFe/Cu}$ ; n = 1



Ref. K: ( $\alpha_3\text{NMeIm}\beta\text{Im}_{\text{PhF}}$ )Fe/Cu R=H  
 Ref. K: ( $\alpha_3\text{NMePrIm}\beta\text{Im}_{\text{PhF}}$ )Fe/Cu R=Pr



Ref. K: ( $\alpha_3\text{NHPrIm}\beta\text{Im}_{\text{PhF}}$ )Fe



Ref L: (DP-GHBB)Fe/Cu

**Figure 8.** Some binuclear CcO oxidase model systems: Ref A<sup>61</sup>, Ref B<sup>71</sup>, Ref C<sup>63</sup>, Ref D<sup>64</sup>, Ref E<sup>62</sup>, Ref F<sup>65</sup>, Ref G<sup>66</sup>, Ref H<sup>67</sup>, Ref I<sup>68</sup>, Ref J<sup>69</sup>, Ref K,<sup>138</sup> Ref L.<sup>86b</sup>

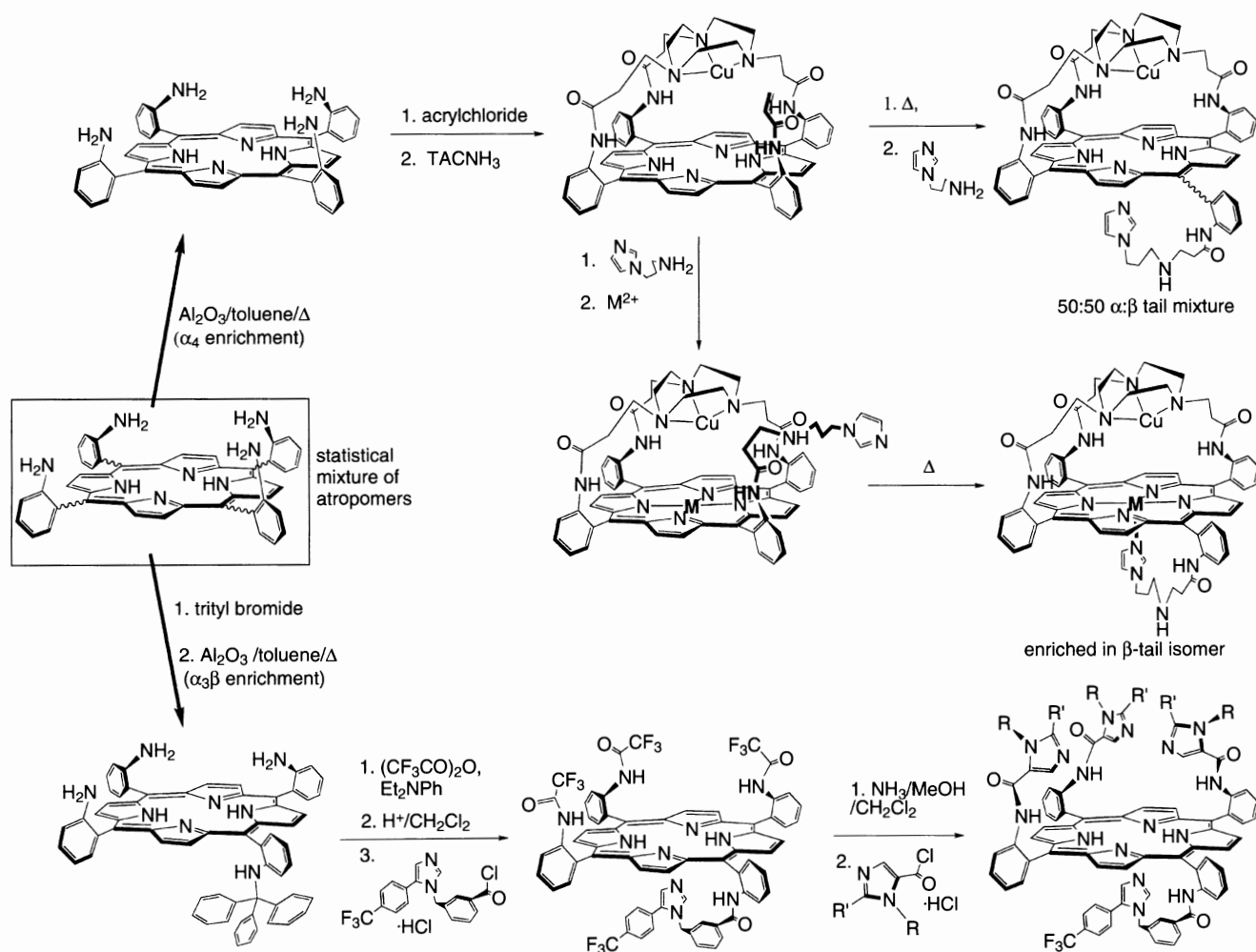


Figure 9. Synthetic routes to CcO models of the  $\alpha_3\beta$  geometry.

groups are subsequently added to improve the ease of purifying the materials by chromatography. By this process, a selectively protected  $\alpha_3\beta$  synthon can be obtained in high yield with multiple opportunities to improve bulk purity of free-base intermediates. Limited use has also been made of the  $\alpha_2\beta_2$ -TAPP isomer as heme/copper terminal oxidase models,<sup>66</sup> in which the distal and proximal components are “strapped” across the porphyrin giving two-point attachment to both structures. As with the mono-functionalized TPP platforms mentioned above, there are no stereochemical consequences to addition of a proximal or distal structure to either side of the  $\alpha_2\beta_2$  aminoporphyrins, simplifying preparation.

The single exception of a binuclear heme/copper terminal oxidase model class that does not utilize a TPP platform is based on deuteroporphyrin. In these systems, one of the two carboxylate side chains of the heme was nonselectively functionalized with a copper-binding group based on benzimidazoles.<sup>86</sup> Unfortunately, the

long and flexible alkyl tether required for attachment of the copper site does not allow for a well-defined Fe–Cu separation, although the porphyrin is certainly the closest analog to the dioxygen binding hemes of heme/copper terminal oxidases.

The earliest attempts to produce structural models of CcO were directed toward understanding the “resting state” of the enzyme and its unusual EPR-silence. This electronic phenomenon was presumed to arise from a ligand bridging the Fe<sup>III</sup> porphyrin and Cu<sup>II</sup> imidazole centers, resulting in a strongly antiferromagnetically coupled (S=2) ground state. Numerous Fe<sup>III</sup>/Cu<sup>II</sup> systems with bridging groups such as O (Figure 5, Section II.B)<sup>70,87–89</sup> S,<sup>90–93</sup> Cl,<sup>62,80,94,95</sup> imidazole,<sup>96–101</sup> and carboxylates (Figure 7, Section II.D)<sup>102</sup> were synthesized. However, these studies uniformly failed to demonstrate properties consistent with the active site of CcO, especially the EPR silence. Later, investigation of new oxygen-derived bridged Fe/Cu models did uncover properties consistent with those observed for



resting-state CcO. These studies, and those pertaining to cyanide, carboxylate, and carbon monoxide inhibited CcO are discussed in the following sections.

## B. OXO AND HYDROXO BRIDGED SYSTEMS

A ligand mediating the EPR silent antiferromagnetically coupled Fe/Cu site of CcO was originally proposed by Van Gelder<sup>103</sup> and later deliberated upon as an oxygen(-II) derived species.<sup>104,105</sup> The first successful demonstration of an antiferromagnetically coupled Fe<sup>III</sup>/Cu<sup>II</sup> system came from Holm and coworkers who structurally characterized a  $\mu$ -oxo complex, (OEP)Fe<sup>III</sup>OCu<sup>II</sup>(Me<sub>6</sub>TREN) (Figure 5). Later, Karlin and coworkers explored several different oxo- and hydroxo-bridged Fe<sup>III</sup>/Cu<sup>II</sup> systems, obtaining structural data in a number of cases.

### 1. Synthesis

The synthesis of Fe<sup>III</sup>-O-Cu<sup>II</sup> assemblies has been approached from three different routes: reaction of (por)Fe<sup>III</sup>OH with a Cu<sup>II</sup>(L<sub>N</sub>) complex containing an exchangeable ligand, reaction of (L<sub>N</sub>)Cu<sup>II</sup>OH with (por)Fe<sup>III</sup>X where X is a poorly coordinating counterion, or by reaction of an Fe<sup>II</sup>/Cu<sup>I</sup> system with dioxygen to eventually yield a  $\mu$ -oxo species. The self-assembled (OEP)Fe<sup>III</sup>-(O/OH)-Cu<sup>II</sup>(L<sub>N</sub>) complexes (L<sub>N</sub> = Me<sub>6</sub>TREN and Me<sub>5</sub>dien) of Holm and coworkers were exclusively synthesized via reaction of (OEP)Fe<sup>III</sup>OCIO<sub>3</sub> with the appropriate (L<sub>N</sub>)Cu<sup>II</sup>OH derivative (Figure 5), in the presence of an equivalent of the sterically hindered phenolate Li(OC<sub>6</sub>H<sub>2</sub>-4-Me-2,6-<sup>t</sup>Bu<sub>2</sub>) as base to provide  $\mu$ -oxo products.<sup>52,54</sup> By contrast, the (F<sub>8</sub>TPP)Fe<sup>III</sup>O-Cu<sup>II</sup>(L<sub>N</sub>) systems (L<sub>N</sub> = TMPA and MeNpy<sub>2</sub>) was synthesized either by reaction of (F<sub>8</sub>TPP)Fe<sup>III</sup>OH with (L<sub>N</sub>)Cu<sup>II</sup>(MeCN) using triethylamine as base, or by reaction of (F<sub>8</sub>TPP)Fe<sup>II</sup> and (L<sub>N</sub>)Cu<sup>I</sup>(MeCN) in oxygenated CH<sub>2</sub>Cl<sub>2</sub> at -80 °C followed by warming to room temperature.<sup>60,106,107</sup> In an analogous manner, a covalently linked model such as (<sup>6</sup>L)Fe<sup>III</sup>OCu<sup>II</sup> can be synthesized by reaction of (<sup>6</sup>L)Fe<sup>II</sup>OH and a Cu<sup>II</sup> salt<sup>64</sup> or by reaction of the reduced Fe<sup>II</sup>/Cu<sup>I</sup> species with dioxygen.<sup>74</sup>

### 2. Solid State Structural Studies

X-ray crystal structures of five (por)Fe<sup>III</sup>-(O/OH)-Cu<sup>II</sup>(L<sub>N</sub>) systems have been determined, and EXAFS data for a further two systems have also been reported. The important structural features revealed by these studies are summarized in Table 1.<sup>52,54,64,74,107,108</sup> With

the exception of <sup>5</sup>LFeOCu (Figure 8), the bimetallic cores of complexes with the same bridging group, (i.e., Fe<sup>III</sup>OCu<sup>II</sup> or Fe<sup>III</sup>-OH-Cu<sup>II</sup>) display similar metric parameters. The Fe-O-Cu linkages are linear with an Fe...Cu separation of 3.57–3.60 Å and the Fe-O bond shorter by 0.08–0.11 Å compared to the Cu-O bond, irrespective of whether the compound is self-assembled or in a binuclear ligand system. In the EXAFS-defined <sup>5</sup>LFeOCu complex, the Fe-O and Cu-O bond lengths are similar to those in the other FeOCu cores, but the FeOCu core is distinctly nonlinear and consequently the Fe...Cu separation is less (3.40 Å). The linear Fe-Cu positioning leads to strong EXAFS multiple atom scattering compared to that of non-linearly positioned Fe-Cu atoms, such as in <sup>5</sup>L and the  $\mu$ -hydroxo systems. The crystallographic evidence of the Fe-N bond lengths and out-of-plane Fe displacement are consistent with high spin Fe<sup>III</sup>. The average Fe-O distances of the CcO models (1.74–1.75 Å) do not appear to be exceptional, and compare to those in [(OEP)Fe<sup>III</sup>]<sub>2</sub>O<sup>109</sup> and [(F<sub>8</sub>TPP)Fe<sup>III</sup>]<sub>2</sub>O<sup>58</sup> of 1.757 Å and 1.760 Å, respectively. Further, the Cu<sup>II</sup>-OFe(por) distances in Table 1 are comparable to the Cu<sup>II</sup>-OH distance in Cu<sup>II</sup>(Me<sub>6</sub>TREN)OH (1.829 Å).

Upon protonation of the  $\mu$ -oxo group, previously linear Fe<sup>III</sup>-O-Cu<sup>II</sup> units cant to ~160° as indicated by the EXAFS<sup>108</sup> and X-ray<sup>52</sup> structure of (OEP)Fe<sup>III</sup>-OH-Cu<sup>II</sup>(Me<sub>5</sub>dien) and EXAFS<sup>107</sup> study of (F<sub>8</sub>TPP)Fe<sup>III</sup>-OH-Cu<sup>II</sup>(TMPA). Despite the number of FeOCu systems structurally characterized, only one – (F<sub>8</sub>TPP)Fe<sup>III</sup>/Cu<sup>II</sup>(TMPA) – has been characterized in its base and protonated form. Since the  $\mu$ -oxo structures show a great deal of structural homology concerning the FeOCu core, this may not be a significant limitation. Compared to the  $\mu$ -oxo complexes, both the Fe-O and Cu-O bonds in the Fe-OH-Cu cores are lengthened and comparable in distance (average Fe-O and Cu-O differences of ~0.02 Å). Metric changes of similar kind have been noted in the protonation of [(OEP)Fe<sup>III</sup>]<sub>2</sub>O.<sup>109</sup> In this case, the near-linear Fe-O-Fe core (172°) tilts to 146° in (OEP)Fe<sup>III</sup>-OH-Fe<sup>III</sup>(OEP), with lengthening of the Fe-O bond from ~1.76 Å to ~1.94 Å. These comparisons indicate that protonation of the oxygen in the heterometallic system disrupts bonding to both metals, but primarily the Fe-O bond, as expected given its greater  $\pi$  bonding component. It would appear to be that stable oxo-bridged systems are generally linear (Fe-O-Cu > 170°), but may be tilted (the EXAFS for (<sup>5</sup>L)Fe<sup>III</sup>OCu<sup>II</sup> indicates an angle of ~140°) while hydroxo-bridged Fe/Cu systems are inherently tilted.

**Table 1.** Structural Parameters (Å or °) of Fe<sup>III</sup>OCu<sup>II</sup> and Fe<sup>III</sup>(OH)Cu<sup>II</sup> Moieties in Structural Heme a<sub>3</sub>/Cu<sub>B</sub> Analogs

Complex	Method <sup>a</sup>	Fe···Cu	Fe–O	Cu–O	Fe–O–Cu	Fe–Ct <sup>b</sup>	Ref.
(OEP)Fe–O–Cu(Me <sub>6</sub> TREN)•MeCN	XR	3.570	1.745	1.829	175.2	0.67	54
(OEP)Fe–O–Cu(Me <sub>6</sub> TREN)•THF	XR	3.575	1.747	1.828	178.2	0.62	54
(OEP)Fe–O–Cu(Me <sub>6</sub> TREN)	XAS	3.57	1.75	–	172		108
(F <sub>8</sub> TPP)Fe–O–Cu(TMPA)	XR	3.596	1.740	1.856	178.2	0.55	58
(F <sub>8</sub> TPP)Fe–O–Cu(TMPA)	XAS	3.55	1.72	1.83	176		107
( <sup>6</sup> L)FeOCu	XR	3.586	1.750	1.848	171.1	0.46	74
( <sup>6</sup> L)FeOCu	XAS	3.59	1.75	1.83	178		64
( <sup>7</sup> L)FeOCu	XAS	3.40	1.77	1.84	141		64
(OEP)Fe–OH–Cu(Me <sub>5</sub> dien)	XR	3.804	1.929	1.954	157.0	0.44	52
(OEP)Fe–OH–Cu(Me <sub>5</sub> dien)	XAS	3.89	1.93	–	161		108
(F <sub>8</sub> TPP)Fe–OH–Cu(TMPA)	XAS	3.66	1.87	1.89	157		107

<sup>a</sup>XR – single-crystal X-ray diffraction; XAS – X-ray absorption spectroscopy.

<sup>b</sup>Displacement of the Fe ion from the 24-atom least-squares plane of the porphyrin core.

Thus, the Fe–(O/OH)–Cu angle does not serve to definitively characterize a bridge as oxo or hydroxo. However, when taken with the shorter M–O bonds of  $\mu$ -oxo systems, oxo and hydroxo bridges can be distinguished in high-resolution structures.

The Fe<sub>a3</sub>/Cu<sub>B</sub> separations in several crystallographically defined oxidized cytochrome oxidases (4.5–5.2 Å) are significantly longer than those found in the  $\mu$ -oxo or  $\mu$ -hydroxo Fe/Cu models. The TOX crystal structure has been interpreted as possessing an oxo/hydroxo bridge at the current resolution level, although the M–O bonds (~2.3 Å) are long compared to the model systems discussed above. Crystalline samples are likely to differ from other “as-isolated” forms of CcO, which can be directly examined by X-ray absorption spectroscopy (XAS) methods. A recent EXAFS structure of bovine CcO has an Fe···Cu separation between 3.89 Å (Cu-edge) and 4.04 Å (Fe-edge), similar to that described by these models for  $\mu$ -hydroxo complexes, give the uncertainties expected due to multiple scattering effects.<sup>110</sup> However, the electron density in the bridge from the bovine CcO study was best fit to a S or Cl atom. An EXAFS structure of a quinol oxidase from *B. subtilis*, revealed a weak iron–copper interaction with an intermetallic separation of ~3.3 Å.<sup>14</sup> This weak interaction was taken to indicate a distinct nonlinear Fe–O–Cu positioning, concluding that a  $\mu$ -hydroxo complex was a possible candidate bridging group at neutral pH.

### 3. Chemical and Electronic Properties

The structural characterization afforded by the examples above supports the formation of Fe<sup>III</sup>–( $\mu$ -oxo/hydroxo)–Cu<sup>II</sup> systems. The coordination geometry at Cu (whether trigonal bipyramidal or square planar) indicates that the partially occupied d-orbital is directed

at the bridging atom, and so may potentially couple to unpaired spins on the Fe<sup>III</sup>, as required for an S=2 ground state. Magnetization, Mossbauer, and nuclear magnetic resonance (NMR) studies provide definitive evidence for an S=2 state.

Variable temperature magnetic susceptibility studies of (OEP)Fe<sup>III</sup>OCu<sup>II</sup>(Me<sub>6</sub>TREN) first demonstrated that a  $\mu$ -oxo bridge in a (por)Fe<sup>III</sup>/Cu<sup>II</sup>(L<sub>N</sub>) binuclear site could propagate sufficiently strong exchange coupling to account for an S=2 ground state in CcO. The magnetic behavior over a temperature range of 4–300 K was well-fit by the Curie–Weiss law  $\chi_m=3.15/(T+2.03)$  with a calculated  $J$  value of 200 cm<sup>-1</sup>. While the corresponding OH-bridged system (OEP)Fe<sup>III</sup>–OH–Cu<sup>II</sup>(Me<sub>6</sub>TREN) has not been reported, magnetic studies on the related (OEP)Fe<sup>III</sup>–OH–Cu<sup>II</sup>(Me<sub>5</sub>dien) system reveal Curie–Weiss behavior over a smaller temperature range (10–100 K), an S=2 ground state and  $J$  value of 170 cm<sup>-1</sup>. The (F<sub>8</sub>TPP)Fe<sup>III</sup>–O–Cu<sup>II</sup>(TMPA) system has a reported coupling constant of  $J=174$  cm<sup>-1</sup>.<sup>58,111</sup> Room temperature magnetic susceptibility determined by NMR (Evan’s method), is available for a range of oxo- and hydroxo-bridged (F<sub>8</sub>TPP)Fe/Cu(L<sub>N</sub>) (L<sub>N</sub> = TMPA, MeNpy<sub>2</sub>) and oxo-bridged (<sup>m</sup>L)Fe/Cu (m=5, 6, Figure 8) systems of Karlin and coworkers. Within this series of complexes based on closely related Fe-porphyrins, the magnetic moments ( $\mu$ -oxo: 4.9–5.1  $\mu_B$ ;  $\mu$ -hydroxo: 5.5–5.6  $\mu_B$ ) present distinct intervals depending on bridge type. Given the limited number of compounds and the data from the (OEP)Fe/Cu(L<sub>N</sub>) complexes, general characterization of bridge type based on magnetization data is not possible. In both  $\mu$ -oxo and  $\mu$ -hydroxo complexes, the magnetic moment is less than the expected sum of uncoupled Fe(5/2) and Cu(1/2) spin systems, suggesting either antiferromagnetic coupling, or a mixed spin Fe<sup>III</sup> state. The latter is considered

unlikely in the presence of a strongly basic oxo donor and can be rejected based on Mossbauer results.

The Mossbauer spectra at 4.2 K of (OEP)Fe<sup>III</sup>OCu<sup>II</sup>-(Me<sub>6</sub>TREN), (OEP)Fe<sup>III</sup>-(O/OH)-Cu<sup>II</sup>(Me<sub>3</sub>dien), and (F<sub>8</sub>TPP)Fe<sup>III</sup>OCu<sup>II</sup>(TMPA) contain a quadrupole doublet in each case, consistent with a high-spin (S=5/2) Fe<sup>III</sup>, indicating the S=2 state is attained by antiferromagnetic coupling to S=1/2 Cu<sup>II</sup>. Within the small set of model compounds to study, it appears that Mossbauer parameters serve to better differentiate oxo from hydroxo bridged ligation, compared to the spin coupling constants (*J*), which do not form distinct ranges for classification. The chemical shifts of oxo bridged Fe<sup>III</sup> systems are larger than the  $\mu$ -hydroxo analogs, consistent with greater electron donation in the former case. In addition, the sign of the  $\Delta E_q$  parameter changes upon protonation, a phenomenon first noted by Karlin and coworkers.<sup>58</sup>

NMR spectroscopy has been used to characterize (por)Fe<sup>III</sup>-(O/OH)-Cu<sup>II</sup>(L<sub>N</sub>) systems. Relaxation broadening and lesser-understood chemical shift trends limit the use of NMR in detecting minor impurities or easily assigning and confidently defining complex ligands in paramagnetic systems. There is extensive literature describing the chemical shift properties of the porphyrin-based *meso*- or pyrrole-H's as a function of Fe oxidation and spin states, which assists in characterization of oxo- and hydroxo-bridged heme a<sub>3</sub>/Cu<sub>B</sub> models.<sup>112,113</sup> Typically, pyrrole shifts of low-spin Fe<sup>III</sup> porphyrins are in the region of -20 ppm, and those of high-spin Fe<sup>III</sup> derivatives, such as (TPP)Fe<sup>III</sup>Cl, are around 80 ppm. Pyrrole resonances of (F<sub>8</sub>TPP)Fe<sup>III</sup>-(O/OH)-Cu<sup>II</sup>(L<sub>N</sub>) occur at 65-75 ppm and this lesser shift compared to the high-spin Fe<sup>III</sup> complexes has been attributed to the antiferromagnetic coupling to the Cu<sup>II</sup> ion and is consistent with a predominately contact-shift origin of the paramagnetically shifted NMR.<sup>58</sup> Pyrrole chemical shifts can become reduced due to intermediate spin mixing in the presence of weak axial ligands, such as in S=3/2 (OEP)Fe<sup>III</sup>ClO<sub>4</sub>. However, in the case of these CcO models, reduction of the pyrrole chemical shift due to intermediate spin mixing was rejected on the basis of the Mossbauer, magnetization, and XR data presented above. The chemical shifts of the  $\beta$ -pyrrolic <sup>1</sup>H NMR resonances for  $\mu$ -hydroxo complexes are 3-5 ppm higher than the  $\mu$ -oxo (deprotonated) analogs, consistent with the larger magnetic moments of  $\mu$ -hydroxo complexes. In a similar manner, the *meso*-H of (OEP)Fe<sup>III</sup>-(O/OH)-Cu<sup>II</sup>(L<sub>N</sub>) systems (17-20 ppm) demonstrate smaller shifts than typical high-spin

(por)Fe<sup>III</sup> complexes (e.g., (OEP)Fe<sup>III</sup>OH, *meso*-H 32 ppm), consistent with antiferromagnetic spin coupling to Cu.<sup>54</sup>

Interconversion of  $\mu$ -oxo and  $\mu$ -hydroxo Fe/Cu systems has been demonstrated by titration with organic acids in acetonitrile and suggests a likely range of  $14 < pK_a < 17$  for (F<sub>8</sub>TPP)Fe<sup>III</sup>-OH-Cu<sup>II</sup>(TMPA).<sup>107</sup> The protonation of two other complexes has been bracketed more carefully:  $16.7 < pK_a$  (F<sub>8</sub>TPP)Fe<sup>III</sup>-OH-Cu<sup>II</sup>(MeNpy<sub>2</sub>)  $< 17.6$ <sup>60</sup> and  $15.6 < pK_a$  (<sup>6</sup>L)Fe<sup>III</sup>-OH-Cu<sup>II</sup>  $< 16.7$ .<sup>60</sup> (<sup>5</sup>L)FeOCu is protonated in a similar range, but it results in Cu<sup>II</sup>-O bond cleavage.<sup>107</sup> Using an argument that aqueous pK<sub>a</sub>'s are  $\sim 7.5$  units lower than those determined in acetonitrile, it has been suggested that these (por)Fe-OH-Cu(L<sub>N</sub>) pK<sub>a</sub>'s correspond to aqueous values of  $\sim 8-9.6 (\pm 2.5)$ .<sup>60,64,107</sup> This aqueous range is intriguing since it is physiologically accessible and supports the possibility that both  $\mu$ -oxo and  $\mu$ -hydroxo species may be present in the biologically active system.

### C. CYANIDE BRIDGED SYSTEMS

The importance of cyanide binding to CcO stems from its use as a biochemical probe of the binuclear site, as well as the fact that its cytotoxicity is mainly due to inhibition of CcO. Since crystallographic studies of cyanide inhibited terminal heme/Cu oxidases have not been successful, crystallography of the model compounds along with infrared studies of the C-N stretching frequencies from both model systems and CcO itself serve to provide insight into possible modes of CN<sup>-</sup> binding in the enzyme. As proposed by Palmer, cyanide binding to the active site of CcO could be either as a tight Fe-CN-Cu bridge (linear or bent); exclusive binding to one metal center only, or strong binding to one metal and a weak interaction to the second metal (or proton in an H-bond).<sup>114</sup> From a combination of magnetic susceptibility, MCD, resonance Raman, and Mossbauer studies, an S=1 ground state was proposed, with a bridging CN<sup>-</sup> presumably mediating the magnetic interaction.<sup>115-122</sup> Thus, it is of interest to use biomimetic models to determine the mode of CN<sup>-</sup> interaction at the binuclear site where either metal is competent to bind the anion.

#### 1. Synthesis

Synthesis of the cyanide bridged Fe<sup>III</sup>/Cu<sup>I/II</sup> systems typically starts with the appropriate (por)Fe<sup>III</sup>CN precursor, prepared by cleavage of the corresponding [(por)Fe<sup>III</sup>]<sub>2</sub>O dimer with Me<sub>3</sub>SiCN.<sup>50</sup> Subsequent

reaction with  $(L_N)Cu^{I/II}$  generates the self-assembled systems depicted in Figure 6. Alternatively, in specific cases where trinuclear  $(L_N)Cu^{II}-NC-Fe^{III}-CN-Cu^{II}(L_N)$  systems have been targeted, the Cu fragment has been used to introduce the  $CN^-$  bridge.<sup>59</sup> Such  $(L_N)Cu^{II}CN$  salts are readily made by metathesis of the appropriate  $(L_N)Cu^{II}Cl$  complex with NaCN or KCN in methanolic solvent mixtures.

## 2. Solid State Structural Studies

Single crystal X-ray diffraction structures have been determined for 14 cyanide bridged (por)Fe/Cu( $L_N$ ) systems (Figure 6). Eleven of these structures concern modeling the fully oxidized ( $Fe^{III}/Cu^{II}$ ) state, two are  $Fe^{III}/Cu^I$  systems and the remaining case is a fully reduced  $Fe^{II}/Cu^I$  derivative. All  $Fe^{III}-CN-Cu^{II}$  systems possess the Fe–C bound linkage isomer where the Fe–C bond varies relatively little (1.86–1.98 Å) and Fe–C–N is essentially linear. A much greater variation in  $Cu^{II}$ –cyanide bonding parameters is observed with ranges of Cu–N bond lengths 1.88–2.45 Å and Cu–N–C angles of 140–177° (Table 2). These  $Fe^{III}/Cu^{II}$  complexes encompass a variety of structural geometries at copper. Figure 10 demonstrates the correlation of Cu–N distance vs. Cu–N–C angle for these compounds although the specific  $Cu^{II}(L_N)$  coordination features leading to this trend are not clear. The coordination at iron is consistent with low spin  $Fe^{III}$  with generally small displacements of Fe from the porphyrin plane toward a second axial base when present. Mononuclear  $NMeIm(OEP)Fe^{III}CN$ <sup>57</sup> and  $py(TPP)Fe^{III}CN$ ,<sup>123</sup> characterized as low-spin hemes, also manifest little displacement of Fe from the porphyrin plane, and

have similar Fe–C–N parameters to the  $Fe^{III}/Cu^{II}$  models. Unlike the copper coordination in the (por)Fe<sup>III</sup>CNCu<sup>II</sup>( $L_N$ ) derivatives, the mononuclear  $Cu^{II}(Me_6TREN)CN$  complex has a linear Cu–C–N moiety. The crystallographically defined partially and fully reduced Fe/Cu models share a number of features in common. Of most significance is the change in the  $CN^-$  binding mode from Fe–CN–Cu<sup>II</sup> to Fe–NC–Cu<sup>I</sup> when Cu<sup>I</sup> is coordinated within the amine cap, whether the iron is in the 2+ or 3+ oxidation state. In these cases, the Fe displacement from the 24-atom plane of the porphyrin core is much greater than the corresponding distances in the  $Fe^{III}-CN-Cu^{II}$  structures consistent with high-spin  $Fe^{III}$  and  $Fe^{II}$ .

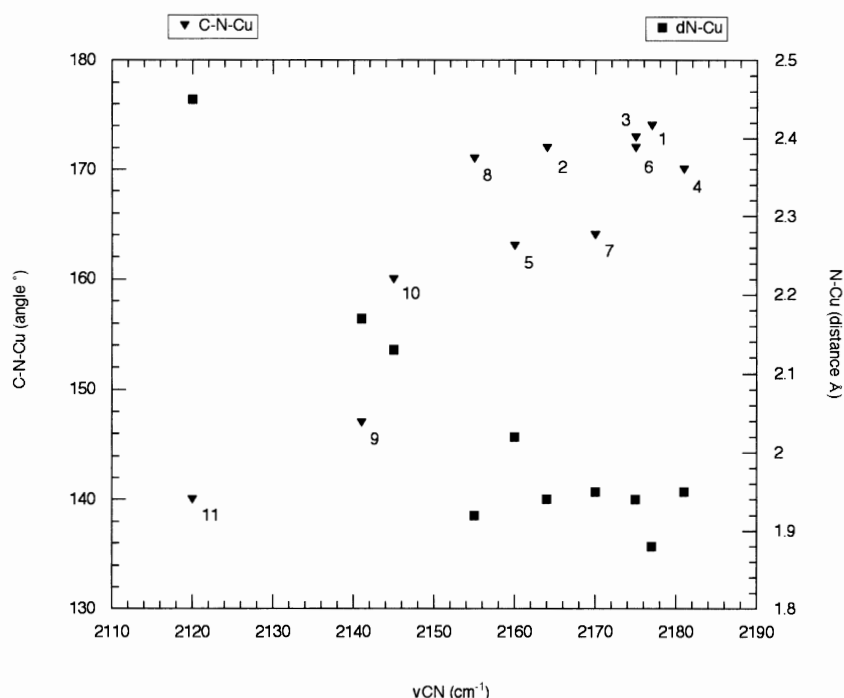
## 3. Chemical and Electronic Properties

The earliest attempt to model cyanide inhibited CcO, based on the ( $\alpha_4$ -nicotinamide)Fe<sup>III</sup>/Cu<sup>II</sup> complex, reproduced some features characteristic of the magnetic and electronic data known for CcO, but lacked crystallographic structural characterization to aid interpretation of the differences observed.<sup>124</sup> Both bovine and bacterial CcO possess an S=1 ferromagnetically coupled ground state with a relatively large zero field splitting (zfs  $\sim 10$  cm<sup>-1</sup>). ( $\alpha_4$ -Nicotinamide)Fe<sup>III</sup>-CN-Cu<sup>II</sup> also possesses an S=1 ground state, but with a small zfs (0.32 cm<sup>-1</sup>), and unlike the fully oxidized  $CN^-$  inhibited CcO, exhibits EPR signals at 4.2 K. Mossbauer spectroscopy of ( $\alpha_4$ -nicotinamide)Fe<sup>III</sup>-CN-Cu<sup>II</sup> ( $\delta = 0.24$  mm/s,  $\Delta E_q = 1.87$  mm/s) indicates larger quadrupole splitting than  $CN^-$  adducts of bovine CcO ( $\delta = 0.28$  mm/s,  $\Delta E_q = 1.25$  mm/s) and *T. thermophilus* CcO ( $\delta = 0.26$  mm/s,  $\Delta E_q = 1.13$  mm/s).

**Table 2.** Bonding Parameters (Å or °) of the Fe–Cyanide–Cu Moieties in Structural Heme  $a_3/Cu_B$  Analogs. Oxidation States are  $Fe^{III}$  and  $Cu^{II}$  Unless Otherwise Noted

Complex	Fe...Cu	Fe–C	C–N	N–Cu	Fe–C–N	C–N–Cu	Fe–Ct <sup>a</sup>	Ref.
Py(OEP)Fe–CN–Cu(Me <sub>6</sub> TREN)	4.94	1.92	1.14	1.88	179	174	–0.053	50
(OEP)Fe–[CN–Cu(Me <sub>6</sub> TREN)] <sub>2</sub>	4.99	1.94	1.14	1.94	173	172	–	50
py(OEP)Fe–CN–Cu(Me <sub>5</sub> dien)•OCMe <sub>2</sub>	4.98	1.91	1.15	1.94	176	173	–0.109	51
py(OEP)Fe–CN–Cu(Me <sub>5</sub> dien)•OTf	4.98	1.90	1.15	1.95	177	170	–0.09	50
py(OEP)Fe–CN–Cu(bnpy) <sub>2</sub>	4.94	1.86	1.13	2.02	176	163	–0.01	51
py(OEP)Fe–CN–Cu(TMPA)	4.99	1.94	1.14	1.94	173	172	–0.02	57
(py)F <sub>8</sub> TPPFe–CN–Cu(TMPA)		1.90	1.14	1.95	175	164	–0.01	59
(F <sub>8</sub> TPP)Fe–[CN–Cu(TMPA)] <sub>2</sub>	4.99	1.98	1.13	1.92	175	171	0.02	59
py(OEP)Fe–CN–Cu(TIM)	5.02	1.91	1.15	2.17	179	147	0.003	51
py(OEP)Fe–CN–Cu(cyclops)	5.11	1.92	1.15	2.13	178	160	–0.031	51
[py(OEP)Fe–CN] <sub>2</sub> –Cu(cyclam)	5.15	1.91	1.14	2.45	177	140	–0.088	51
(OEP)Fe <sup>III</sup> –NC–Cu <sup>I</sup> (Me <sub>5</sub> dien)	4.90	2.00	1.14	1.89	165	169	–0.34	51
(OEP)Fe <sup>II</sup> –NC–Cu <sup>I</sup> (MeNpy <sub>2</sub> )	4.95	2.00	1.15	1.87	162	177	–0.38	57
(OEPCH <sub>2</sub> CN)Fe <sup>II</sup> –NC–Cu <sup>I</sup> (TMPA)	5.05	2.03	1.16	1.87	176	175	–0.62	57

<sup>a</sup>Displacement of the Fe ion from the 24-atom least-squares plane of the porphyrin core.

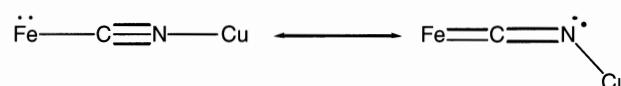


**Figure 10.** Correlation of  $\nu_{\text{CN}}$  with Cu-N distance and Cu-N-C angle in  $(\text{por})\text{Fe}^{\text{III}}\text{CNCu}^{\text{II}}(\text{L}_{\text{N}})$  complexes (the numbers refer to Entries in Table 3).

$(\text{OEP})\text{Fe}^{\text{III}}\text{-CN-Cu}^{\text{II}}(\text{Me}_6\text{TREN})$  appears to be electronically more comparable to cyanide-inhibited  $\text{CcO}$ , based on similarity of its Mossbauer parameters ( $\delta = 0.22$  mm/s,  $\Delta E_{\text{q}} = 1.23$  mm/s) to those of the  $\text{CcO}/\text{CN}^-$  adducts, mentioned above. The complex is also EPR silent at 5 K, consistent with an integer spin system arising from strong ferromagnetic coupling of the low-spin Fe center with the Cu-based electron. In the  $^1\text{H}$  NMR of  $(\text{OEP})\text{Fe}^{\text{III}}\text{-CN-Cu}^{\text{II}}(\text{L}_{\text{N}})$  systems the methylene groups of the OEP appear at 8–12 ppm, consistent with a low-spin heme, while the partly reduced  $(\text{OEP})\text{Fe}^{\text{III}}\text{-CN-Cu}^{\text{I}}(\text{L}_{\text{N}})$  analogs demonstrate resonances in the range of 40–60 ppm, consistent with a high spin  $\text{Fe}^{\text{III}}$ .<sup>57</sup> The pyrrole resonances in  $(\text{F}_8\text{TPP})\text{Fe}^{\text{III}}\text{-CN-Cu}^{\text{II}}(\text{L}_{\text{N}})$  adducts are at –11 to –8 ppm, and its solution magnetic moment of  $2.7 \mu_{\text{B}}$  is consistent with an  $S=1$  ground state.<sup>59</sup> Along with solution UV/vis data for such complexes, this evidences retention of the bridged interaction in solution.

The vibration frequency of  $\text{CN}^-$ ,  $\nu_{\text{CN}}$ , in mononuclear  $(\text{OEP})\text{Fe}^{\text{III}}\text{CN}$  is  $2130 \text{ cm}^{-1}$ . Upon coordination of  $\text{Cu}^{\text{II}}(\text{L}_{\text{N}})$  to the nitrogen of a  $(\text{por})\text{Fe}^{\text{III}}\text{CN}$  group,  $\nu_{\text{CN}}$  increases by  $50\text{--}60 \text{ cm}^{-1}$  as electron density is donated from the cyanide based  $\sigma^*$  to d-orbital of Cu and due to additional kinematic coupling accessible to a bridged CN group.<sup>57</sup> The  $\text{CN}^-$  stretching frequencies for the crystallographically defined  $\text{Fe}^{\text{III}}/\text{Cu}^{\text{II}}$  complexes are displayed in Figure 10 as a function of the Cu-N and

Cu-N-C metric parameters. Despite scatter in the data, a trend of increase in  $\text{CN}^-$  stretching frequency with decreasing Cu-N bond length and increasing Cu-N-C bond angle is apparent. This trend was explained by a simple resonance-bonding picture where a decrease in the C-N bond order occurs as the Cu deviates from linearity.<sup>57</sup>



The  $\text{CN}^-$  stretching frequencies generally change little from solid state to solution, again indicating that the unit remains intact in solution and the angular  $\text{Cu}^{\text{II}}\text{-N-C}$  coordination geometries are largely retained in solution (i.e., are not imposed purely by crystal packing forces). Coincidence with the  $\text{CN}^-$  frequency of bovine and bacterial oxidases ( $2146\text{--}2152 \text{ cm}^{-1}$ )<sup>57</sup> is seen toward the more nonlinear  $\text{Cu}^{\text{II}}\text{-N-C}$  geometries of these models. While the OEP based data of Holm and coworkers appeared to support the notion that a class distinction of linear ( $>173^\circ$ ) and nonlinear ( $140\text{--}163^\circ$ ) C-N-Cu<sup>II</sup> geometry could be made based on the  $\text{CN}^-$  stretching frequency, inclusion of data from Karlin and coworkers (Table 3) makes this distinction of limited practical use since six structures in the angular range of  $170\text{--}174^\circ$  have a frequency spread of  $2155\text{--}2181 \text{ cm}^{-1}$ , within which several structures of  $163\text{--}164^\circ$  also fall. More important

**Table 3.** C–N Stretching Frequencies and Selected Metric Parameters for Structural Heme  $a_3$ /Cu $_B$  Analogs. Entry Number Refers to Values in Figure 10. Oxidation States are Fe<sup>III</sup> and Cu<sup>II</sup> Unless Otherwise Noted

Entry	Complex <sup>a</sup>	N–Cu (Å)	C–N–Cu (°)	$\nu_{CN}$ (cm <sup>-1</sup> )	Ref.
1	py(OEP)Fe–CN–Cu(Me <sub>6</sub> TREN)	1.88	174	2177	50
2	(OEP)Fe–CN–[Cu(Me <sub>6</sub> TREN)] <sub>2</sub>	1.94	172	2164	50
3	py(OEP)Fe–CN–Cu(Me <sub>5</sub> dien)•OCMe <sub>2</sub>	1.94	173	2175	51
4	py(OEP)Fe–CN–Cu(Me <sub>5</sub> dien)•OTf	1.95	170	2181	50
5	py(OEP)Fe–CN–Cu(bnpy) <sub>2</sub>	2.02	163	2160	51
6	py(OEP)Fe–CN–Cu(TMPA)	1.94	172	2175	57
7	py(F <sub>8</sub> TPP)Fe–CN–Cu(TMPA)	1.95	164	2170	59
8	(F <sub>8</sub> TPP)Fe–[CN–Cu(TMPA)] <sub>2</sub>	1.92	171	2155	59
9	py(OEP)Fe–CN–Cu(TIM)	2.17	147	2141	51
10	py(OEP)Fe–CN–Cu(cyclops)	2.13	160	2145	51
11	[py(OEP)Fe–CN] <sub>2</sub> –Cu(cyclam)	2.45	140	2120	51
12	(OEP)Fe <sup>III</sup> –NC–Cu <sup>I</sup> (Me <sub>5</sub> dien)	1.89	169	2100	51
13	(OEP)Fe <sup>II</sup> –NC–Cu <sup>I</sup> (MeNpy <sub>2</sub> )	1.87	177	2072	57
14	(OEPCH <sub>2</sub> CN)Fe <sup>II</sup> –NC–Cu <sup>I</sup> (TMPA)	1.87	175	2099	57

<sup>a</sup>ferric and cupric complexes, unless noted otherwise.

to the characteristic narrow frequency range of CcO-bound CN<sup>-</sup>, model structures within a range of 5 cm<sup>-1</sup> can differ in Cu<sup>II</sup>–N–C angles by more than 10°. Even with this uncertainty range, the low frequency of the enzyme bound CN<sup>-</sup> (2146–2152 cm<sup>-1</sup>) appears to place the fully oxidized Fe<sup>III</sup>–CN–Cu<sup>II</sup> unit in a bent bridging interaction (suggested to be ~160° by Holm and coworkers<sup>57</sup>), in agreement with some studies of heme/copper terminal oxidases.<sup>125,126</sup> However, the result of forming a hydrogen-bonded CN<sup>-</sup> has not been directly examined in such models, a mode of interaction for which arguments have been presented.<sup>127</sup>

The coordination of Cu<sup>I</sup> instead of Cu<sup>II</sup> to (por)Fe<sup>III</sup>CN units results in the isocyano bound heme and causes CN vibrational shift. Fe<sup>III/II</sup>–NC–Cu<sup>I</sup> models display cyanide stretching frequencies some 90 cm<sup>-1</sup> lower than linear Fe<sup>III</sup>–CN–Cu<sup>II</sup> systems (2072–2100 cm<sup>-1</sup>), from which it was deduced that CN( $\pi^*$ ) ← Cu back-donation was the dominant electronic influence. It was not possible to differentiate between Fe<sup>III</sup> and Fe<sup>II</sup> redox states based on the vibrational ranges observed. However, it should be noted that only a single example of an Fe<sup>II</sup>–CN–Cu<sup>I</sup> system was obtained, and this possesses an *N*-alkylated porphyrin core. With the preparation of these reduced Fe/Cu models, an opportunity was afforded to compare the  $\nu_{CN}$  of partly (2093–2132 cm<sup>-1</sup>) and fully (2035–2058 cm<sup>-1</sup>) reduced forms of CN<sup>-</sup> inhibited CcO. Unfortunately, with the range of values determined for the Fe<sup>III/II</sup>–CN–Cu<sup>I</sup> complexes (2072–2100 cm<sup>-1</sup>), and the values expected for (por)Fe<sup>III</sup>CN (~2120–2130 cm<sup>-1</sup>) and (L<sub>N</sub>)Cu<sup>I</sup>CN adducts (2080 cm<sup>-1</sup>), these studies do not allow for unambiguous appraisal of cyanide coordination in the reduced states of the heme  $a_3$ /Cu<sub>B</sub> site.<sup>57</sup>

## D. CARBOXYLATE BRIDGED SYSTEMS

The “as-isolated” preparations of CcO have long been observed to differ in reactivity to substrates and inhibitors depending on the isolation method.<sup>128</sup> One particular observation concerned the isolation of heme/copper oxidases that were either “fast” or “slow” to react with cyanide.<sup>129–132</sup> Enzyme purification methods were developed to minimize the amount of “slow” form, although it was realized that the “fast” form could be generated from “slow” forms by fully reducing, then reoxidizing a sample.<sup>128</sup> The “fast” forms of CcO could be converted to “slow” forms by exposure to low pH,<sup>131</sup> or exogenous formate.<sup>132</sup> Formate-treated CcO showed almost identical kinetic, UV/vis, magnetization, EPR, and resonance Raman properties compared to the isolated “slow” (or “resting oxidized”) form of CcO. “Fast” CcO was found to be high-spin antiferromagnetically coupled Fe<sub>a<sub>3</sub></sub><sup>III</sup>/Cu<sub>B</sub><sup>II</sup> 117,133–135 which was EPR silent,<sup>103</sup> while the “slow” form, also S=2, was EPR active<sup>129,131</sup> due to different zfs and magnetic coupling parameters.<sup>136</sup> These experimental observations fueled speculation into the role of carboxylates at the Fe/Cu active site in CcO preparations and prompted the examination of a carboxylate as a possible bridging element.

### 1. Synthesis

Self-assembled (TPP)Fe<sup>III</sup>/Cu<sup>II</sup>(aib<sub>3</sub>) (aib<sub>3</sub> =  $\alpha$ -aminoisobutyric acid tripeptide, Figure 7), was synthesized by titration of (TPP)Fe<sup>II</sup> with Cu<sup>III</sup>(aib<sub>3</sub>) in THF,<sup>102</sup> a process followed by visible spectroscopy and electrochemistry indicating the formation of a 1:1 complex. The formate and acetate bridged (OEP)Fe<sup>III</sup>/Cu<sup>II</sup>(L<sub>N</sub>)

systems of Holm and coworkers ( $L_N = \text{Me}_5\text{dien}$  and  $\text{Me}_6\text{TREN}$ )<sup>53</sup> were prepared in a similar manner to the  $\mu$ -oxo systems described above, by reaction of  $(\text{OEP})\text{Fe}^{\text{III}}\text{OCIO}_3$  with the appropriate  $(L_N)\text{Cu}^{\text{II}}\text{O}_2\text{CR}$  complex. The latter was readily synthesized by reaction of  $\text{Cu}^{\text{II}}(\text{O}_2\text{CR})_2$  with  $L_N$  in methanol, followed by exchange of one carboxylate for  $\text{ClO}_4^-$ . Alternatively,  $(\text{Me}_5\text{dien})\text{Cu}^{\text{II}}\text{Ac}(\text{ClO}_4)$  was obtained by metathesis of  $\text{Cl}^-$  in  $(\text{Me}_5\text{dien})\text{Cu}^{\text{II}}\text{Cl}-(\text{ClO}_4)$  with  $\text{NaAc}$ .

## 2. Solid State Structural Studies

The three  $(\text{OEP})\text{Fe}^{\text{III}}-\text{RCO}_2-\text{Cu}^{\text{II}}(L_N)$  complexes studied crystallographically all demonstrated a  $\mu-\eta^2$  bridging mode (Figure 7),<sup>53</sup> with one being of the *anti-anti* and the other two being of the *syn-anti* conformation. This has an effect on the Fe/Cu separation with the *anti-anti* conformation of  $(\text{OEP})\text{Fe}^{\text{III}}-(\text{HCO}_2)-\text{Cu}^{\text{II}}(\text{Me}_5\text{dien})$  possessing the longest Fe/Cu distance (5.86 Å), while the two *syn-anti* structures  $(\text{OEP})\text{Fe}^{\text{III}}-(\text{CH}_3\text{CO}_2)-\text{Cu}^{\text{II}}(\text{Me}_5\text{dien})$  and  $(\text{OEP})\text{Fe}^{\text{III}}-[(\text{HCO}_2)-\text{Cu}^{\text{II}}(\text{Me}_6\text{TREN})]_2$  demonstrate Fe/Cu separations of 4.43 Å and 5.42 Å, respectively. The crystallographically determined  $\text{Fe}_{\text{a}_3}/\text{Cu}_{\text{B}}$  separations in CcO are 4.5–5.3 Å. If a bridging carboxylate is present in the heme  $\text{a}_3/\text{Cu}_{\text{B}}$  site of oxidized CcO preparations (whether or not this applies to “slow” CcO), the *anti-anti* conformation is unlikely due to the large intermetallic distance ( $\sim 5.9$  Å) it favors, compared to the *syn-anti* configuration.

## 3. Chemical and Electronic Properties

The  $(\text{TPP})\text{Fe}^{\text{III}}/\text{Cu}^{\text{II}}(\text{aib}_3)$  carboxylate bridged system<sup>102</sup> displayed weak magnetic coupling, but due to thermal, light, and oxygen sensitivity, and corresponding characterization difficulties, the system is of limited use. Magnetization studies have been performed only on  $(\text{OEP})\text{Fe}^{\text{III}}-(\text{HCO}_2)-\text{Cu}^{\text{II}}(\text{Me}_5\text{dien})$ <sup>111</sup>, although  $(\text{OEP})\text{Fe}^{\text{III}}-(\text{CH}_3\text{CO}_2)-\text{Cu}^{\text{II}}(\text{Me}_5\text{dien})$  and  $(\text{OEP})\text{Fe}^{\text{III}}-[(\text{HCO}_2)-\text{Cu}^{\text{II}}(\text{Me}_6\text{TREN})]_2$  are expected to better reflect the *syn-anti* conformation of a carboxylate bridge should it occur at the binuclear site of CcO.<sup>53</sup>  $(\text{OEP})\text{Fe}^{\text{III}}-(\text{HCO}_2)-\text{Cu}^{\text{II}}(\text{Me}_5\text{dien})$  reveals a relatively weak antiferromagnetic coupling ( $J \sim 18 \text{ cm}^{-1}$ ),<sup>111</sup> whereas the formate-inhibited (and as-isolated “slow”) bovine CcO preparations are strongly coupled ( $J > 200 \text{ cm}^{-1}$ ).<sup>135</sup> Thus, it was suggested that if the heme  $\text{a}_3/\text{Cu}_{\text{B}}$  site of the “slow” forms of CcO contains a bridging carboxylate, it would most likely be bound in an  $\mu-\eta^1$  mode (a single O atom bridge), which is expected to provide a stronger coupling pathway. No models have been synthesized to date that explicitly address this

speculation. It is known that “fast” ubiquinol (cytochrome *bo*) oxidase is converted to a “slow” form by addition of formate, but not by lowering pH,<sup>137</sup> whereas “slow” CcO can be generated by both methods. Since the amino acid sequence of CcO and ubiquinol oxidases are very similar, and the structures of these enzymes indicate that endogenous carboxylate residues are not within close proximity to the  $\text{Fe}_{\text{a}_3}/\text{Cu}_{\text{B}}$  site, it appears that formate is not a surrogate for an endogenous carboxylate–residue interaction in the “as-isolated” slow form. It has been proposed that the appearance of the as-isolated “slow” form may be due to interaction with a fatty acid, but it has yet to be demonstrated. It should be noted, however, that cyanide reacts with “fast” CcO many orders of magnitude slower than onset of inhibition by  $\text{CN}^-$  during enzymatic turnover, indicating that *in vivo* cyanide probably reacts via partially reduced Fe/Cu center.<sup>128</sup>

## E. CARBON MONOXIDE ADDUCTS OF (por)Fe<sup>II</sup>/Cu<sup>I</sup> SYSTEMS

Carbon monoxide inhibited CcO is commonly used for flash photolysis experiments and redox control in the study of electron and proton transfers during the reduction of  $\text{O}_2$ . As with cyanide, the stretching frequency of this diatomic molecule has been used as a probe of the  $\text{Fe}_{\text{a}_3}/\text{Cu}_{\text{B}}$  site, thereby aiding the elucidation of structural relationships and dynamics of heme/copper oxidases.<sup>4,20</sup> Although carbon monoxide complexes of a large number of iron porphyrin models have been described previously, little biomimetic emphasis has been placed on carbonyl complexes of bimetallic CcO models. In part, this is due to the requirement for covalently linked models, since CO is not a strong bridging ligand for  $(\text{por})\text{Fe}^{\text{II}}/\text{Cu}^{\text{I}}(L_N)$  complexes.

### 1. Synthesis

Carbonyl adducts of  $\text{Fe}^{\text{II}}$  porphyrins are prepared by exposure to CO gas at room temperature. The CO complexes are usually formed quantitatively, though often require a CO head-gas since binding may be reversible. These characteristics mean that CO adducts are often formed and studied *in situ*.

### 2. Chemical and Spectroscopic Properties

Collman and coworkers have frequently used carbonyl adducts to aid NMR analysis of reduced CcO models. Carbonyl adducts of  $(\text{por})\text{Fe}^{\text{II}}$  complexes coordinated

by a nitrogenous proximal ligand are low-spin,  $d^6$  complexes (i.e., diamagnetic). In this manner, unity of the organic structure can be determined with confidence, and full assignments by simple COSY and NOE experiments are possible. This allows for NMR comparison of free-base and  $\text{Fe}^{\text{II}}\text{CO}$ -metalloporphyrin derivatives (and potentially (por) $\text{FeO}_2$  adducts, Section III below) within the diamagnetic spectral envelope. In addition, porphyrin ring-current induced NMR shifts provides information concerning the spatial disposition of the distal and proximal superstructures.<sup>138</sup> This approach has been used successfully to determine the solution stereochemistry of a series of synthetic heme  $a_3/\text{Cu}_B$  analogs based on the  $\alpha_3\text{NMeIm}\beta\text{Im}_{\text{PhF}}$ ,  $\alpha_3\text{NMePrIm}\beta\text{Im}_{\text{PhF}}$ , and  $\alpha_3\text{NHPrIm}\beta\text{Im}_{\text{PhF}}$  ligands. Thus,  $^1\text{H}$  NMR shifts for the distal imidazole protons of  $\alpha_3\text{NMeIm}\beta\text{Im}_{\text{PhF}}\text{Fe}$  and  $\alpha_3\text{NMePrIm}\beta\text{Im}_{\text{PhF}}\text{Fe}$  indicate that these complexes can be represented by the conformation drawn in Figure 8, where the three imidazole nitrogens are directed toward the center of the binding pocket. In contrast to this, the  $^1\text{H}$  NMR shifts of  $\alpha_3\text{NHPrIm}\beta\text{Im}_{\text{PhF}}\text{Fe}$  suggested a different conformation for this model where the distal imidazole-N's were H-bonded to the amide NH's, thereby contributing to problems with coordination to  $\text{Cu}^{\text{I}}$ .<sup>138</sup>

Comparison of the carbonyl stretching frequency,  $\nu\text{CO}$ , for the mono- and bimetallic models helps understand how a distal metal may affect the Fe-bound CO in a heme  $a_3/\text{Cu}_B$  model. The CO stretching frequency is a convenient probe for detecting structural and electrostatic changes that affect the Fe–CO bonding. For example, a higher  $\nu\text{CO}$  is indicative of a stronger C–O bond due to lesser back-bonding from the metal ion to the carbonyl  $\pi^*$  orbital. Presuming constant porphyrin and axial ligation, an increase in  $\nu\text{CO}$  can be attributed to distortion of the Fe–CO bond or electrostatic destabilization of charge transfer to the CO by polar interactions.<sup>139,140</sup> Collman and coworkers observed<sup>138</sup> that the  $\nu\text{CO}$  of  $(\alpha_3\text{NMeIm}\beta\text{Im}_{\text{PhF}})\text{Fe}^{\text{II}}\text{CO}$  (1979  $\text{cm}^{-1}$ ) and  $(\alpha_3\text{NMePrIm}\beta\text{Im}_{\text{PhF}})\text{Fe}^{\text{II}}\text{CO}$  (1978  $\text{cm}^{-1}$ ) are  $\sim 10\text{cm}^{-1}$  higher than in similar compounds where alkyl groups are present in place of the NMe-imidazoles. This is consistent with the distal imidazole lone-pairs positioned in the vicinity of the FeCO unit, leading to electrostatic destabilization of back-bonding to CO, and is in line with previous biomimetic studies of hemoglobin that sought to examine polarity effects upon  $\text{O}_2/\text{CO}$  discrimination.<sup>139–141</sup> Further, in the Fe/Cu complexes,  $(\alpha_3\text{NMeIm}\beta\text{Im}_{\text{PhF}})\text{Fe}^{\text{II}}\text{CO}/\text{Cu}^{\text{I}}$  and  $(\alpha_3\text{NMeIm}\beta\text{Im}_{\text{PhF}})\text{Fe}^{\text{II}}\text{CO}/\text{Cu}^{\text{I}}$ ,  $\nu\text{CO}$  decreases  $\sim 29\text{cm}^{-1}$  compared

to the Fe-only analogs,<sup>138</sup> consistent with placement of the positive  $\text{Cu}^{\text{I}}$  ion above the (por) $\text{Fe}^{\text{II}}\text{CO}$  unit, leading to electrostatic stabilization of CO back-bonding.

Attempts to identify metal binding residues of CcO were the target of mutagenesis studies for a number of years. Not only did deletion of certain histidines result in loss of  $\text{Cu}_B$ , but a concomitant increase of up to  $20\text{cm}^{-1}$  in the  $\nu\text{CO}$  for  $\text{Fe}_{a_3}\text{CO}$  was noted.<sup>142–144</sup> This was attributed to the absence of the  $\text{Cu}^+$  ion and consequent removal of an electrostatic interaction favorable for back-bonding to CO. Thus, the models  $(\alpha_3\text{NMeIm}\beta\text{Im}_{\text{PhF}})\text{Fe}^{\text{II}}/\text{Cu}^{\text{I}}$  and  $(\alpha_3\text{NMeIm}\beta\text{Im}_{\text{PhF}})\text{Fe}^{\text{II}}/\text{Cu}^{\text{I}}$  are able to reproduce the qualitative trend of  $\nu\text{CO}$  changes due to loss of  $\text{Cu}_B$  in heme/copper oxidases.

In addition, under an atmosphere of CO  $(\alpha_3\text{NMeIm}\beta\text{Im}_{\text{PhF}})\text{Fe}^{\text{II}}\text{CO}/\text{Cu}^{\text{I}}$  demonstrates a second  $\nu\text{CO}$  absorption at  $\sim 2085\text{cm}^{-1}$ .<sup>138</sup> This CO absorption is in a frequency region of CO bound to  $\text{Cu}^{\text{I}}$  with a *tris-N* ligation, indicating that the distal site of this model is able to achieve a  $\text{CuIm}_3$  coordination environment, as required of a structural analog for the active site of CcO. Although  $(\text{L}_N)\text{Cu}^{\text{I}}\text{CO}$  complexes are well documented, this is the only example reported to date for CO binding to the Cu of a binuclear heme  $a_3/\text{Cu}_B$  model. The importance of such an observation lies in the fact that binding of CO to, and release from, heme  $a_3$  proceeds via transient coordination of CO to  $\text{Cu}_B$ .

### III. Reactivity of Heme $a_3/\text{Cu}_B$ Analogs Toward $\text{O}_2$ Under Noncatalytic and Single Turnover Conditions

In contrast to the resting state models designed to elucidate the structural and spectroscopic characteristics of the isolated forms of CcO, a number of model systems, seldom coincident with the aforementioned studies, have been designed to probe the reactivity of a fully reduced Fe/Cu center with  $\text{O}_2$ . Due to the limited stability of the intermediates in such reactions, these systems require *in situ* characterization without the benefit of single crystal X-ray diffraction studies. The metal-dioxygen chemistry of the constituent parts of CcO models, i.e., iron porphyrins and copper–amine systems, is well established. Indeed, metal-dioxygen chemistry has been used to produce some oxo-bridged species as an alternative to the more commonly employed acid/base syntheses. The simplest functionality of CcO to be modeled by a bimetallic system is the



reaction of a (por)Fe<sup>II</sup> and (L<sub>N</sub>)Cu<sup>I</sup> system with oxygen to produce (oxidized) (por)Fe<sup>III</sup> and (L<sub>N</sub>)Cu<sup>II</sup> centers and reduced oxygen products. The questions to be probed by such studies concern the mechanism and stoichiometry of O<sub>2</sub> reaction with reduced Fe/Cu systems, the nature of intermediates, and the eventual identity of the oxidized product(s).

The earliest attempts to probe the metal-dioxygen chemistry of Fe<sup>II</sup>/Cu<sup>I</sup> systems to simply accomplish oxidation of the metal centers and reduction of O<sub>2</sub> were performed with noncovalently linked (por)Fe/Cu(L<sub>N</sub>) systems. Given the high reactivity of both (por)FeO<sub>2</sub> and (L<sub>N</sub>)CuO<sub>2</sub> complexes, this is potentially perilous as it may lead to undesired oxidation of the organic ligands and/or homodinuclear O<sub>2</sub> chemistry as the dominant reaction pathway. The first synthesis of an Fe/Cu oxo-bridged CcO model utilized the known reactivity of dioxygen with (TPP)Fe<sup>II</sup>. At -78° C (TPP)Fe<sup>II</sup> forms, after addition of pyridine, py(TPP)Fe<sup>IV</sup>O (ferryl), a process previously studied in detail.<sup>145</sup> Reaction with a Cu<sup>I</sup> complex (which itself was known to not irreversibly react with O<sub>2</sub>), followed by warming to room temperature, resulted in an oxo-bridged Fe/Cu species.<sup>70</sup> This reaction produces a CcO-related product, (por)Fe<sup>III</sup>O-Cu<sup>II</sup>(L<sub>N</sub>), but not by a mechanism possible at the heme a<sub>3</sub>/Cu<sub>B</sub> site.

While the inclusion of both the Fe and Cu centers on the same ligand scaffold does not exclude the possibility for homodinuclear chemistry to occur, entropic factors should favor intramolecular reactions and thus the desired heterodinuclear chemistry. More advanced ligand designs, although frequently more synthetically onerous, can incorporate features that significantly promote the likelihood of not only achieving the desired heteronuclear chemistry, but also of stabilizing reactive intermediates and providing opportunities to study mechanistic details relevant to CcO. However, a number of reported binuclear porphyrin/amine ligands have not been developed into functional or structural models for CcO.<sup>72,82,146-148</sup> Others have demonstrated dioxygen reactivity of the Fe<sup>II</sup>/Cu<sup>I</sup> system different from that of the Fe<sup>II</sup>-only analog, indirectly implying involvement of the Cu center. For example, Casella and coworkers<sup>86,149</sup> utilized a deuteroporphyrin modified with a pendant benzimidazole arm, which provided Fe and Fe/Cu complexes after metallation (for example, (DP-GHBB)Fe<sup>II</sup>/Cu<sup>I</sup>, Figure 8). Exposure of the Fe system to air resulted in heme degradation, as expected for a *meso*-unsubstituted porphyrin. Exposure of the Fe/Cu analog to air led primarily to oxidation of the

metal centers, in preference to the heme, although the reaction stoichiometry and mechanism were only speculative.

The solution reactivity of a number of systems has been investigated in greater detail in the research groups of Collman, Karlin, and Naruta. These studies are typically comprised of an initial demonstration of the existence of an Fe/O<sub>2</sub>/Cu unit followed by kinetic/mechanistic/electrochemical studies to elaborate on the reaction course leading to O<sub>2</sub> reduction.

### A. CHARACTERIZATION OF PEROXIDE BRIDGED INTERMEDIATES

Although it now appears that the existence of a peroxide intermediate of any appreciable lifetime in CcO is unlikely, such a species can be a relatively stable intermediate in model complexes around which kinetic studies can be made. Fe/Cu peroxide intermediates have been characterized using a combination of techniques including UV/vis, Raman, Mossbauer, and NMR spectroscopies as well as mass spectrometry, manometry, and redox titrations. Eleven different molecular entities have been characterized as possessing “stable” bridging Fe/Cu peroxo groups, in addition to a stable Co/Cu peroxo-bridged CcO model (Table 4).<sup>60,61,65,67-69,71,73,150</sup>

A Soret band blueshift and reduction in extinction coefficients is typically observed upon formation of most dioxygen adducts of ferrous porphyrins.<sup>151</sup> Oxygenation of (por)Fe<sup>II</sup>/Cu<sup>I</sup>(L<sub>N</sub>) complexes is marked by similar changes in the visible spectrum. Since the equilibrium toward dioxygen adduct formation is high, under conditions where the (por)Fe<sup>III</sup>O<sub>2</sub>Cu<sup>II</sup>(L<sub>N</sub>) system is stable, an Fe/Cu system can be titrated with O<sub>2</sub> and monitored by visible spectroscopy to substantiate a 1:1 binding stoichiometry. A 1:1 Fe/Cu:O<sub>2</sub> stoichiometry has been demonstrated for most complexes in Table 4. However, (<sup>5</sup>L)Fe<sup>II</sup>/Cu<sup>I</sup> has a reaction stoichiometry of 2:1, although the nature of this complex is unknown. The binding of O<sub>2</sub> to (F<sub>8</sub>TPP)Fe<sup>II</sup>/Cu<sup>I</sup>(TPMA) is 1:1:1, although upon warming, approximately half the oxygen is liberated from the complex (*vide infra*).

In addition to the demonstration of binding stoichiometry, a technique developed by Collman and coworkers involves a redox titration of peroxo intermediates with the strong single electron reducing agent, cobaltocene. Thus, (α<sub>3</sub>TACNαAcr)FeO<sub>2</sub>Cu (Figure 8) consumes two equivalents of cobaltocene before the fully reduced Fe<sup>II</sup>/Cu<sup>I</sup> system is observed spectrophotometrically with a further two equivalents required

**Table 4.** Chemical and Spectroscopic Parameters of Peroxide Bridged (por)MO<sub>2</sub>Cu(L<sub>N</sub>) (M = Fe, Co) Complexes. See Figure 8 for the Relevant Chemical Structures<sup>a</sup>

Adduct	Raman, <sup>16</sup> O <sub>2</sub> / <sup>18</sup> O <sub>2</sub> , cm <sup>-1</sup>	UV/vis, nm	EPR	NMR, ppm	Mass spec.	(Fe/Cu):O <sub>2</sub> stoichiom. <sup>b</sup>	Redox titration <sup>c</sup>	Stability	Ref.
(TPP-TMPA)FeO <sub>2</sub> Cu	803/759	419, 560	silent	n.r.	<sup>16</sup> O/ <sup>18</sup> O	1:1	n.r.	RT t <sub>1/2</sub> 75 min	61
(TPP-5-MeTMPA)FeO <sub>2</sub> Cu	793/751	n.r.	n.r.	n.r.	n.r.	n.r.	n.r.	n.r.	71
<sup>6</sup> LFeO <sub>2</sub> Cu	787/744	418, 561,632	silent	92 (β-pyr)	<sup>16</sup> O/ <sup>18</sup> O	1:1	> 2eq	RT t <sub>1/2</sub> 60 min	73
<sup>5</sup> LFeO <sub>2</sub> Cu	809/756	n.r.	n.r.	n.r.	n.r.	2:1	n.r.	n.r.	73
<sup>4</sup> LFeO <sub>2</sub> Cu	n.r.	418, 536	silent	D (-80°C)	n.r.	1:1	n.r.	-80°C <sup>d</sup>	69
<sup>3</sup> LFeO <sub>2</sub> Cu	n.r.	418, 536	n.r.	n.r.	n.r.	n.r.	n.r.	-80°C <sup>d</sup>	69
(F <sub>8</sub> TPP)FeO <sub>2</sub> Cu(TMPA)	808/762	412, 558	Silent	68 (β-pyr)	<sup>16</sup> O/ <sup>18</sup> O	1:1:1	n.r.	RT t <sub>1/2</sub> 17 min	150
(F <sub>8</sub> TPP)FeO <sub>2</sub> Cu(MeNpy <sub>2</sub> )	n.r.	422, 542	n.r.	n.r.	n.r.	n.r.	n.r.	-70°C t <sub>1/2</sub> hours	60
NMeIm(α <sub>3</sub> TACNαacr)FeO <sub>2</sub> Cu	758/740	428	n.r.	D	<sup>16</sup> O	1:1	4eq	RT <sup>e</sup>	65
(α <sub>3</sub> TREN <sub>Ph</sub> 3βIm <sub>alk</sub> )FeO <sub>2</sub> Cu	n.r.	n.r.	n.r.	D	n.r.	1:1	4eq	RT <sup>e</sup>	67
(α <sub>3</sub> TACNβIm <sub>alk</sub> )FeO <sub>2</sub> Cu	n.r.	n.r.	n.r.	D	n.r.	1:1	2eq	RT <sup>e</sup>	67
(α <sub>3</sub> TACNβIm <sub>alk</sub> )CoO <sub>2</sub> Cu	804/756	444	n.r.	n.r.	n.r.	1:1	4eq	RT <sup>e</sup> t <sub>1/2</sub> days	68

<sup>a</sup>n.r. – not reported; D – a diamagnetic NMR spectrum.

<sup>b</sup>Complex-O<sub>2</sub> binding stoichiometry defined by UV/vis and/or manometry.

<sup>c</sup>Equivalents of CoCp<sub>2</sub> consumed by the (por)MO<sub>2</sub>Cu(L<sub>N</sub>) adduct, determined by UV/vis or NMR.

<sup>d</sup>Reported as stable at this temperature.

<sup>e</sup>Detectable but decomposes at room temperature.

before an excess of cobaltocene appears (by NMR).<sup>65</sup> This implies that upon 2e reduction, peroxide leaves the Fe<sup>II</sup>/Cu<sup>I</sup> catalyst cavity, but the peroxide released can be further reduced in solution by addition of more CoCp<sub>2</sub>. It is remarkable that the released peroxide does not react with the Fe<sup>II</sup>/Cu<sup>I</sup> complex. Thus, interpretation of this experiment is equivocal on the sole basis of the observed UV/vis spectral changes, and requires supporting chemical or spectroscopic evidence to confirm the nature of all products present after the two-equivalents of CoCp<sub>2</sub> have been added to (α<sub>3</sub>TACNαAcr)FeO<sub>2</sub>Cu. By comparison, (α<sub>3</sub>TACNβIm<sub>alk</sub>)CoO<sub>2</sub>Cu requires four equivalents of CoCp<sub>2</sub> to regenerate the catalyst, and the titration proceeds with isosbestic behavior, which was explained by postulating that the first electron reduction is rate-limiting with partially reduced species being rapidly reduced before leakage. In related work, (α<sub>3</sub>TACNβIm<sub>alk</sub>)FeO<sub>2</sub>Cu and (α<sub>3</sub>TREN<sub>Ph</sub>βIm<sub>alk</sub>)FeO<sub>2</sub>Cu were found to require two and four equivalents of CoCp<sub>2</sub>, respectively, for regeneration of the reduced catalyst.<sup>68</sup> It was suggested that this is consistent with the electrochemical observation of peroxide leakage from the former, but not latter complex under conditions of catalytic turnover on a graphite electrode (see Section IV.D below).<sup>67</sup> The (<sup>6</sup>L)FeO<sub>2</sub>Cu system of Karlin and coworkers also consumes “two or more equivalents of cobaltocene,” however, the product generated is the μ-oxo species rather than the fully reduced catalyst.<sup>73</sup> Presumably, the oxo-bridged analogs in the aforementioned systems of Collman are either never formed, or are much more reactive than (<sup>6</sup>L)FeOCu.

Few cases of the peroxo bridged derivatives are stable enough for mass spectrometry. In conjunction with <sup>16</sup>O/<sup>18</sup>O isotopic substitution, this provides confirmation of a 1:1:1 Fe:Cu:O<sub>2</sub> composition. To date, no peroxo-bridged Fe/Cu complex with a nitrogenous axial base has been characterized by mass spectrometry, perhaps due to lesser stability of the six-coordinate FeO<sub>2</sub><sup>2-</sup> complexes.

The NMR spectrum of a peroxide bridged (por)Fe/Cu(L<sub>N</sub>) system relays information concerning the spin state of the Fe/Cu system, as well as an indication of purity. The O<sub>2</sub><sup>2-</sup> unit provides a strong magnetic exchange pathway between the Fe and Cu centers. In the closest (and most reactive) models of CcO, those containing an axial nitrogenous base, this coupling affords a low-spin Fe<sup>III</sup> center antiferromagnetically coupled to the Cu<sup>II</sup> to provide an S=0 diamagnetic system.<sup>65,67,69</sup> However, diamagnetism alone does not prove the existence of a peroxide bridged Fe/Cu system as an isoelectronic heme-superoxide/copper(I) complex would also be diamagnetic.<sup>65</sup> The correct stereoelectronic environment may allow Cu<sup>I</sup> to charge-stabilize the iron-superoxide adduct while preventing its oxidation to the cupric state necessary to form a peroxo-bridged [Fe<sup>III</sup>O<sub>2</sub>Cu<sup>I</sup>] derivative. The superoxide alternative is of note, since it corresponds to intermediate A in the catalytic cycle of CcO (Figure 4), and as such, is a more biologically relevant target for modeling than the much sought after peroxide bridged complexes. The O–O bond stretching frequency in Fe/Cu dioxygen adducts should readily differentiate a superoxide from a peroxide complex (*vide infra*).

In peroxo bridged systems of five coordinate Fe porphyrins, or those having only a weakly bound sixth ligand,  $S=2$  spin states have been observed with correspondingly paramagnetically shifted and broadened  $^1\text{H}$  NMR spectra. For example, at  $-80^\circ\text{C}$ , the series of compounds  $(^6\text{L})\text{Fe}^{\text{II}}/\text{Cu}^{\text{I}}$ ,  $(^6\text{L})\text{Fe}^{\text{III}}\text{-O}_2\text{-Cu}^{\text{II}}$ , and  $(^6\text{L})\text{Fe}^{\text{III}}\text{OCu}^{\text{II}}$  display broad but dissimilar  $\beta$ -pyrrole resonances in the region of 80–110 ppm. In contrast to the downfield shifts experienced by protons at the  $S=5/2$  heme, protons at the  $S=1/2$   $\text{Cu}^{\text{II}}$  ligand experience upfield shifts to  $-78$  and  $-64$  ppm respectively in the peroxo and oxo bridged species. These proton resonance shifts occurring in opposite directions are consistent with the antiferromagnetically coupled spins of the Fe and Cu centers.<sup>152</sup> Although the NMR spectra in such cases serve to corroborate formation of the peroxo bridged species, no detailed information about structure or composition has been elucidated.

Resonance Raman is an important spectroscopic tool for establishing the existence of a dioxygen adduct in  $\text{CcO}$  models, since the O–O bond order can be directly probed. The experiment requires, however, that resonance enhancement can be achieved and that photolytic decomposition of the Fe/Cu dioxygen adduct not prevail. In principle, the dioxygen adduct of a binuclear model can take on a number of structural forms, as demonstrated in Figure 11. Studies on homonuclear model systems have established the stretching frequencies of  $\text{O}_2$  adducts in Fe and Cu systems. Superoxide bound species such as A and B in Figure 11 are expected to display  $\nu\text{OO}$  in the range of  $1100\text{--}1165\text{ cm}^{-1}$ . The stretching frequencies of the adducts shown in Table 3 are clearly of lower

energy (all but one complex are in the range of  $790\text{--}810\text{ cm}^{-1}$ ), in the region of other complexes characterized with  $\text{O}_2$  in the peroxide oxidation state. The side on  $[(\text{TPP})\text{Fe}^{\text{III}}\text{O}_2]^-$  complex, has  $\nu\text{OO}$  of  $804\text{ cm}^{-1}$ . This is within the range of  $\nu\text{OO}$  values for Fe/Cu systems, but this complex is EPR active, whereas, the reported model systems have been noted as EPR silent. Therefore, a structure such as C in Figure 11 can be excluded as the identity of these Fe/Cu dioxygen complexes. An  $\eta^1$ -peroxo copper(II) complex is expected to have a  $\nu\text{OO}$  of  $\sim 800\text{ cm}^{-1}$ , while the corresponding  $\eta^1$ -hydroperoxo complex should have a frequency of some  $40\text{--}50\text{ cm}^{-1}$  higher.<sup>153,154</sup> However, these are unlikely candidates to describe these Fe/Cu models as the copper complexes are EPR active. A  $\text{Cu}_2(\mu\text{-}1,1\text{-hydroperoxo})$  complex<sup>153</sup> is reported to have a much higher  $\nu\text{OO}$ ,  $\sim 890\text{ cm}^{-1}$ , and as with hydroperoxo D, requires a stoichiometric proton source for formation. Thus, an Fe/Cu dioxygen complex such as E is considered an unlikely structural candidate. Structures F and G are more difficult to distinguish as both are EPR silent. *bis*-Copper dioxygen complexes reveal that  $\mu\text{-}1,2\text{-peroxides}$  have  $\nu\text{OO}$  values ( $830\text{--}880\text{ cm}^{-1}$ ) quite different from  $\mu\text{-}\eta^2\text{:}\eta^2\text{-peroxides}$  ( $730\text{--}765\text{ cm}^{-1}$ ). The observed (por)FeO<sub>2</sub>-Cu(L<sub>N</sub>) peroxide stretches,  $790\text{--}810\text{ cm}^{-1}$ , clearly sit between the *bis*-copper model ranges for  $\mu\text{-}1,2\text{-}$  and  $\mu\text{-}\eta^2\text{:}\eta^2\text{-peroxides}$ . Thus, Raman spectroscopy alone does not necessarily distinguish homo- or heterometallic  $\mu\text{-}1,2$  bridged peroxides, or perhaps even  $\mu\text{-}\eta^2\text{:}\eta^2$  peroxide species in these models. Steric arguments for some complexes<sup>71</sup> disfavor close proximity of L<sub>N</sub> to the porphyrin ring, which is a more demanding requirement for a  $\mu\text{-}\eta^2\text{:}\eta^2\text{-peroxide}$ . However, definitive

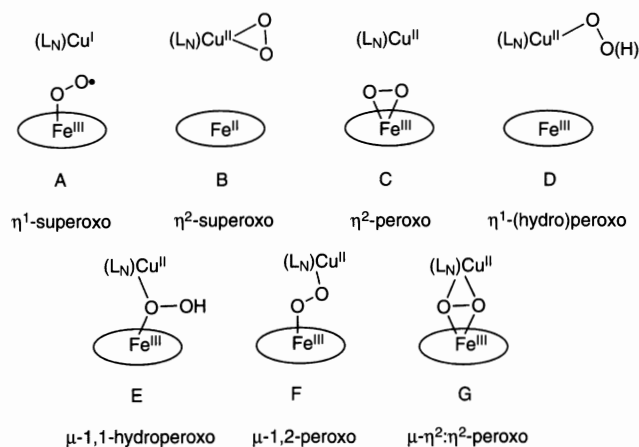


Figure 11. Possible  $\text{O}_2$  binding modes in (por)Fe(OO)Cu(L<sub>N</sub>) complexes.

evidence for a  $\mu$ -1,2-peroxo (por)FeO<sub>2</sub>Cu(L<sub>N</sub>) bridge over a  $\mu$ - $\eta^2$ : $\eta^2$ -peroxide is yet to be obtained.

### B. REACTION OF Fe<sup>II</sup>/Cu<sup>I</sup> CENTERS WITH O<sub>2</sub>

The mechanism of dioxygen reaction with a reduced Fe/Cu system is clearly of importance to biomimetic studies of CcO. However, it has not been until quite recently that a rudimentary picture concerning the elementary steps of oxygen reaction with model systems has emerged. This is due in part to the high reactivity of model systems and susceptibility to photodecomposition.

The simplest reaction mechanism of an Fe/Cu system is demonstrated by the (TPP-TMPA)Fe/Cu system of Naruta and coworkers (Figure 8).<sup>71</sup> Importantly, the study was performed at reduced temperature ( $-90^\circ\text{C}$ ) in a poorly coordinating solvent (toluene). In the absence of axial ligation to Fe, affinity for dioxygen is low, which must be considered in comparing these model systems to each other and to the probable reaction mechanisms of CcO. Indeed, it has been noted that addition of axial base to this system prompts decomposition of the peroxo intermediates.<sup>155</sup> The reaction rate of O<sub>2</sub> with Cu<sup>I</sup>(TMPA) is reported to be  $2 \times 10^4 \text{ M}^{-1} \text{ s}^{-1}$  in EtCN at  $-90^\circ\text{C}$  with activation parameters of  $\Delta H^\ddagger = 32 \pm 4 \text{ kJ/mol}$ ,  $\Delta S^\ddagger = 14 \pm 18 \text{ J/(K mol)}$ ,<sup>71</sup> typical for the reaction of dioxygen with a Cu<sup>I</sup> center. In contrast, the reaction of (TPP-TMPA)Fe<sup>II</sup>/Cu<sup>I</sup> with O<sub>2</sub> is characterized by  $k_{\text{obs}}(-90^\circ\text{C}) = 2.73 \times 10^{-3} \text{ s}^{-1}$  and  $\Delta H^\ddagger = 12.8 \pm 0.3 \text{ kJ/mol}$ ,  $\Delta S^\ddagger = -220 \pm 2 \text{ J/(K mol)}$ , implying a large loss of degrees of freedom in the transition state, not inconsistent with formation of a bridged complex. However, it is not clear if the reaction order with respect to dioxygen and complex was determined. The peroxo product was characterized by resonance Raman, mass spectroscopy, and visible spectroscopy. The peroxide species is one of the most stable known to date ( $t_{1/2} = 75 \text{ min}$  at room temperature<sup>71</sup>) although the product(s) of subsequent decomposition have not been reported.

By contrast, the reactivity of the (F<sub>8</sub>TPP)Fe/Cu(L<sub>N</sub>) systems (L<sub>N</sub> = TMPA,<sup>150</sup> MeNpy<sub>2</sub><sup>60</sup> - Figure 5) and of the complexes (<sup>6</sup>L)Fe/Cu<sup>73</sup> and (<sup>4</sup>L)Fe/Cu (Figure 8)<sup>69</sup> were examined in acetonitrile at reduced temperature ( $-40$  to  $-80^\circ\text{C}$ ). The former two complexes are non-covalently linked Fe/Cu systems (self-assembled in terms of eventual bridged formation), and the latter two contain binucleating ligands. (<sup>4</sup>L)Fe/Cu also has a covalently linked pyridine for axial coordination. The noncovalent systems have been studied by stopped-flow kinetics. Both undergo initial reaction at Fe within the

1 ms mixing time to form the (F<sub>8</sub>TPP)FeO<sub>2</sub> complex ( $\lambda_{\text{max}}$  537 nm, MeCN  $-40^\circ\text{C}$ ), a stable superoxide species at low temperatures. Subsequently, new species evolve, characterized as (F<sub>8</sub>TPP)FeO<sub>2</sub>Cu(L<sub>N</sub>) peroxo bridged complexes. The (F<sub>8</sub>TPP)FeO<sub>2</sub>Cu-(TMPA) complex ( $\lambda_{\text{max}}$  556 nm, MeCN  $-40^\circ\text{C}$ ) has been characterized by resonance Raman ( $\nu_{\text{OO}}$  808/762  $\text{cm}^{-1}$ , <sup>16</sup>O<sub>2</sub>/<sup>18</sup>O<sub>2</sub>), mass spectrometry, visible spectroscopy, and spectrophotometric O<sub>2</sub> titration. The study of this bridged peroxide is complicated by minor side reactions, however, the kinetics are described by the first order parameters,  $k_{\text{obs}}(-90^\circ\text{C}) = 7 \times 10^{-2} \text{ s}^{-1}$  and  $\Delta H^\ddagger = 45 \pm 1 \text{ kJ/mol}$ ,  $\Delta S^\ddagger = -19 \pm 6 \text{ J/(K mol)}$  in acetone. The half-life of the peroxo species is  $\sim 17 \text{ min}$  at  $22^\circ\text{C}$  in acetonitrile. The spectrophotometric titrations indicated that the peroxide complex is indeed a 1:1:1 adduct, but upon warming  $\sim 0.40$ – $0.45 \text{ eq.}$  of dioxygen is released. Thus, two (F<sub>8</sub>TPP)Fe/Cu(TMPA) molecules are used to provide the 4e required for reduction of dioxygen. This is stoichiometrically analogous to the reaction of (TPP)Fe<sup>II</sup> with O<sub>2</sub>, where the dioxygen adduct (TPP)Fe–O<sub>2</sub>–Fe(TPP) decomposes to (TPP)Fe–O–Fe(TPP) while liberating half an equivalent of O<sub>2</sub>.<sup>145</sup> The release of  $\sim 0.5 \text{ eq.}$  of dioxygen certainly opens the possibility for a non-CcO like mechanism of O<sub>2</sub> activation and reduction in (F<sub>8</sub>TPP)-FeO<sub>2</sub>Cu(TMPA).

The reaction of (F<sub>8</sub>TPP)Fe/Cu(MeNpy<sub>2</sub>)<sup>60</sup> has been characterized in a preliminary manner by visible spectroscopy. Reaction of (F<sub>8</sub>TPP)Fe center with dioxygen (THF,  $-70^\circ\text{C}$ ) gives (F<sub>8</sub>TPP)FeO<sub>2</sub> ( $\lambda_{\text{max}}$  416, 536 nm) which upon addition of the Cu complex affords (F<sub>8</sub>TPP)FeO<sub>2</sub>Cu(MeNpy<sub>2</sub>) ( $\lambda_{\text{max}}$  422 nm), the latter decomposes over several hours at  $-70^\circ\text{C}$  to (F<sub>8</sub>TPP)FeOCu(MeNpy<sub>2</sub>) ( $\lambda_{\text{max}}$  446, 558 nm). The spectral changes followed by stopped-flow kinetics (acetone,  $-90^\circ\text{C}$ ), indicate that in a mixture of (F<sub>8</sub>TPP)Fe and Cu(MeNpy<sub>2</sub>), the (F<sub>8</sub>TPP)FeO<sub>2</sub> ( $\lambda_{\text{max}}$  535 nm) complex is formed within the mixing time of the experiment, followed by a species attributed to (F<sub>8</sub>TPP)FeO<sub>2</sub>Cu(MeNpy<sub>2</sub>) ( $\lambda_{\text{max}}$  560 nm), formed with a second order rate constant of  $3.4 \times 10^4 \text{ M}^{-1} \text{ s}^{-1}$ . Subsequent decomposition to the  $\mu$ -oxo product appears to occur in at least two steps. Attempts to follow this reaction in more detail were complicated by photodecomposition, as in the (F<sub>8</sub>TPP)Fe/Cu(TMPA) system.

Room-temperature visible spectroscopy measurements of (<sup>6</sup>L)Fe/Cu ( $\lambda_{\text{max}}$  424, 544 nm, THF) reveal that the (<sup>6</sup>L)FeCu reacts with dioxygen to form an intermediate assigned as (<sup>6</sup>L)FeO<sub>2</sub>Cu ( $\lambda_{\text{max}}$  418, 561, 632 nm, acetone) which decomposes to (<sup>6</sup>L)FeOCu ( $\lambda_{\text{max}}$  438, 556 nm, acetone). This intermediate has an

appreciable stability ( $t_{1/2} = 60$  min, RT in MeCN) and has been characterized as a peroxo adduct by resonance Raman ( $\nu_{OO}$  808/762  $\text{cm}^{-1}$ ,  $^{16}\text{O}_2/^{18}\text{O}_2$ ), mass spectrometry, visible spectroscopy, and spectrophotometric  $\text{O}_2$  titration. Although complicated by a second (unidentified) reaction pathway, in acetone at  $-80^\circ\text{C}$  the peroxo ( $^6\text{L}$ ) $\text{FeO}_2\text{Cu}$  species is observed within the mixing time. While this does not allow for direct claims of observing the first site of  $\text{O}_2$  interaction with the Fe/Cu system, independent observations indicate that initial reaction of  $\text{O}_2$  is at Fe. Studies with the Cu–amine systems that are grafted onto the  $\text{F}_8\text{TPP}$  ligand demonstrate that superoxo ( $(\text{L}_\text{N})\text{CuO}_2$ ) and peroxo ( $(\text{L}_\text{N})\text{CuO}_2\text{Cu}(\text{L}_\text{N})$ ) species are not significantly formed on this time scale. It is presumed that the presence of  $(\text{F}_8\text{TPP})\text{Fe}$  does not alter the reactivity of the  $(\text{L}_\text{N})\text{Cu}$  system, or serve to trap transient species not detectable in the  $(\text{L}_\text{N})\text{Cu}$ -only systems.

Reaction of  $(^4\text{L})\text{Fe}/\text{Cu}$  with dioxygen<sup>69</sup> has been studied at  $-80^\circ\text{C}$ , by bench-top (not stopped-flow) techniques. The first adduct noted is the  $(^4\text{L})\text{FeO}_2\text{Cu}$  species ( $\lambda_{\text{max}}$  418, 536 nm, EtCN  $-80^\circ\text{C}$ ), which decomposes to  $>70\%$   $\mu$ -oxo  $(^4\text{L})\text{FeOCu}$  derivative. Characterization as a peroxo species is based on a diamagnetic NMR spectrum, EPR silence, visible spectroscopy, and spectrophotometric  $\text{O}_2$  titration. The covalently linked axial pyridine is expected to increase the reaction rate of ferrous center with  $\text{O}_2$ , but further studies are needed to determine the details of these reactions for compounds such as  $(^6\text{L})\text{Fe}/\text{Cu}$  and  $(^4\text{L})\text{Fe}/\text{Cu}$ .

#### IV. Functional Analogs of the Dioxygen Reduction Site in Heme/Cu Terminal Oxidases

In addition to spectroscopic models described in the preceding sections, a significant amount of work has been devoted to developing so-called functional heme  $\text{a}_3/\text{Cu}_\text{B}$  analogs, i.e., synthetic porphyrins that effect 4e reduction of  $\text{O}_2$  to  $\text{H}_2\text{O}$  in the presence of reducing equivalents under multiple turnover conditions. Synthesis and studies of functional analogs poses unique challenges. First, in addition to adequately reproducing the immediate coordination environment for both metal ions and the  $\text{Fe}\cdots\text{Cu}$  separation, a functional analog must also have a flexible Fe/Cu core to accommodate reaction intermediates while retaining its structural integrity under catalytic turnover. The latter requirement renders unsuitable synthetic heme  $\text{a}_3/\text{Cu}_\text{B}$  analogs wherein an iron porphyrin and a Cu

complex are held together only by an exogenous bridging ligand (self-assembled systems). Second, the catalytic activity and selectivity of  $\text{O}_2$  reduction must be assessed at least semiquantitatively, preferably under physiologically relevant conditions. In the past few years, a number of Fe porphyrin complexes have been synthesized, which contain a superstructure capable of coordinating the distal cation (Cu) through aliphatic (TREN and TACN) or aromatic (quinoline or imidazole) nitrogens and, in most cases, a covalently attached imidazole or pyridine moiety as a “proximal” ligand to Fe (Figure 12). In contrast, the methodology to assay catalytic activity and selectivity has evolved little between 1980 and 2002. Its limitations remain the major source of confusion regarding what can be called a functional heme  $\text{a}_3/\text{Cu}_\text{B}$  analog and what biologically relevant conclusions can be drawn from such work.

#### A. METHODOLOGIES

No attempts have been reported to carry out catalytic  $\text{O}_2$  reduction homogeneously such that the reductant, the substrate ( $\text{O}_2$ ), and the catalyst are all in solution. A related technique, the spectrophotometric titration of dioxygenated catalyst with a strong reductant, cobaltocene,  $\text{CoCp}_2$  under single-turnover conditions in a non-protic solvent, has been previously discussed (see Section III). The results, however, are not easily interpretable and no mechanistic insights are available from such studies. The method of choice in biomimetic  $\text{O}_2$  reduction has been voltammetry, whereby an electrode serves both as a source of electrons and as a catalyst support. This technique is conceptually similar, and in some respects superior to spectrophotometric and polarographic assays commonly employed to quantify activity of cytochrome oxidase. In electrocatalytic studies a functional heme  $\text{a}_3/\text{Cu}_\text{B}$  analog, which is insoluble in water, is deposited on the surface of a rotating disk electrode (RDE) or on the disk of rotating ring disk electrode (RRDE, Figure 13) and brought in contact with an aqueous buffered (usually to pH 7) electrolyte. Rotating electrode voltammetry<sup>156,157</sup> allows one to quantify the activity and selectivity of the catalyst as a function of the electrochemical potential, by using an appropriate mathematical model to describe the observed catalytic currents. According to a general description of electrochemical kinetics at a chemically modified electrode developed by Andrieux and Saveant,<sup>158</sup> the catalytic  $\text{O}_2$  reduction current generated by a multilayer film of a biomimetic catalyst can be limited not only by the turnover frequency of the



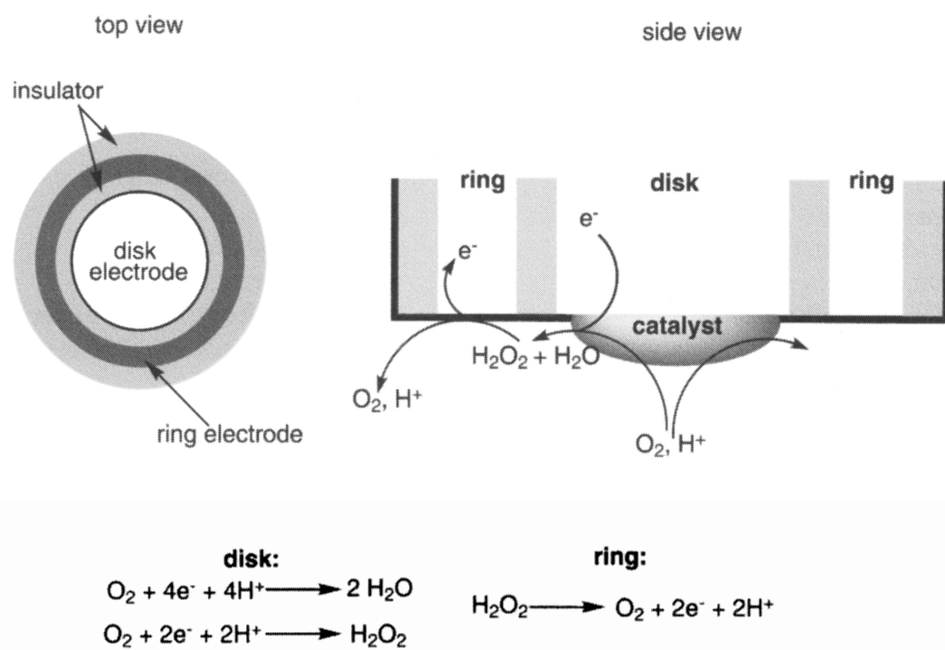


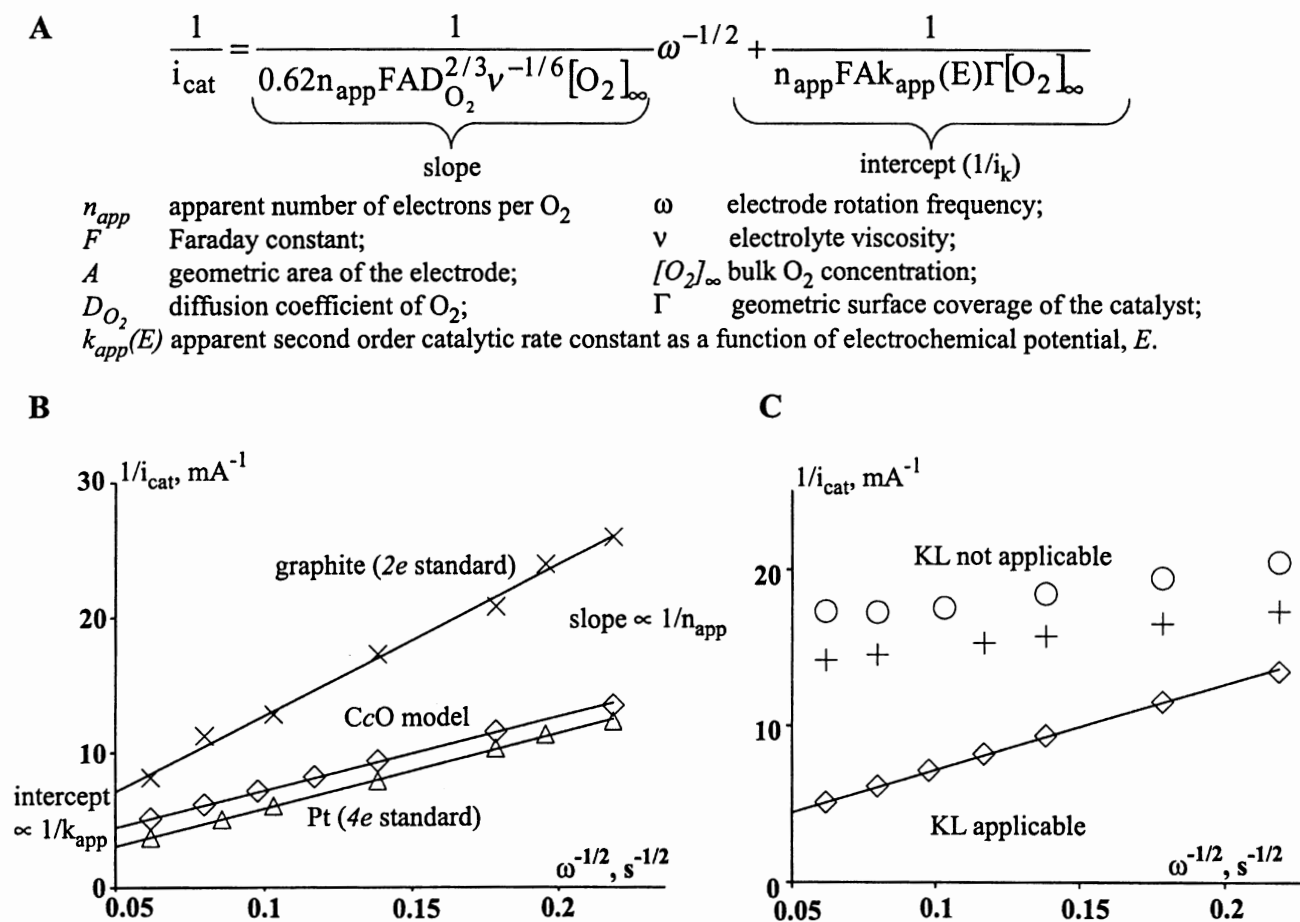
Figure 13. A rotating ring-disk electrode.

exclusively to describe the kinetics of biomimetic  $O_2$  reduction even though in only one case was it shown that the conditions of its applicability were met.<sup>159</sup> In cases when the Koutecky–Levich equation is indeed applicable, the catalytic selectivity (as apparent average number of electrons exchanged per  $O_2$  molecule,  $n_{app}$ ) and catalytic activity (as an apparent second order catalytic rate constant,  $k_{app}$ ) are estimated from the slope and the intercept of the linear  $i_{cat}^{-1}$  vs.  $\omega^{-1/2}$  graph, respectively (Figure 14).<sup>159</sup> The  $0.62FAD_{O_2}^{2/3}\nu^{-1/6}[O_2]_{\infty}$  coefficient, required to derive  $n_{app}$  from the slope, is either calculated based on the literature values of the respective constants or is measured experimentally by carrying out  $O_2$  reduction under identical experimental conditions using a catalyst whose  $n$  value is reliably established, for example graphite ( $n = 2$ ) and thoroughly cleaned Pt ( $n = 4$ , Figure 14B).<sup>159</sup> The latter method may provide more precise estimates of  $n_{app}$  as the values of  $D_{O_2}$ ,  $\nu$  and  $[O_2]_{\infty}$  under given experimental conditions are usually not known with a sufficient precision (e.g., the literature values of  $D_{O_2}$  vary by a factor of 2<sup>157</sup>). More precise estimates of  $k_{app}$  are obtained from a series of  $i_{cat}$  vs.  $\omega$  data collected for  $O_2$  reduction at different surface coverages of the catalyst,  $\Gamma$ . In the regime where the electrocatalytic kinetics<sup>159</sup> follows the Koutecky–Levich behavior, the measured kinetic currents,  $i_k$ , decreases linearly with  $\Gamma$ .

Examples of biomimetic  $O_2$  reduction systems have been reported where the electrode kinetics does not

follow the Koutecky–Levich behavior, either because the overall turnover frequency is partially determined by the rate of charge or substrate transfer within the film or the catalyst is partially saturated with  $O_2$ .<sup>160–162</sup> In some of these cases the  $i_{cat}^{-1}$  vs.  $\omega^{-1/2}$  graphs remain mostly linear but their slopes are lower than they would be if the systems followed the Koutecky–Levich behavior (Figure 14C). Application of the Koutecky–Levich equation in such situations leads to significantly overestimated catalytic selectivities.

The selectivity of the catalyst can also be assayed by a rotating ring disk electrode (RRDE, Figure 13).<sup>156,157</sup> In this setup, the ring electrode serves as an electrochemical sensor of partially reduced oxygen species (PROS:  $H_2O_2$  and  $O_2^-/HO_2$ ) released by the catalytic film at the disk. While the disk potential is scanned, that of the (usually Pt) ring is fixed at an oxidizing potential, so that a fraction of PROS that are hydrodynamically transported from the film–solution interface to the ring is oxidized to  $O_2$ . This oxidation generates a ring current. In order to use the latter to *quantify* catalytic selectivity, one must know what fraction of the PROS generated at the disk is oxidized at the ring (the so-called “ring collection efficiency”). When the Pt ring can be set at a potential at which the rate of the analyte oxidation is much larger than the residence time of the analyte in the ring’s vicinity (i.e., diffusion-limited oxidation), the collection efficiency can be calculated from geometric parameters of the RRDE. However, because Pt is easily passivated toward  $H_2O_2$  oxidation, sufficient



**Figure 14.** (A) The Koutecky–Levich equation. (B) The  $i_{\text{cat}}^{-1}$  vs.  $\omega^{-1/2}$  graphs for  $\text{O}_2$  reduction at an unmodified graphite electrode ( $\times$ ), at a thoroughly cleaned Pt electrode ( $\Delta$ ) and by a heme  $\text{a}_3/\text{Cu}_\text{B}$  analog ( $\diamond$  ( $\alpha_3\text{NRIm}\beta\text{ImPhF}$ ) $\text{Fe}/\text{Cu}$ , Figure 12) deposited on the edge-plane graphite. The solid lines are linear least-squares fits. Adapted from: Boulatov, R.; Collman, J. P.; Shiryayeva, I. M.; Sunderland, C. J. *J. Am. Chem. Soc.* **2002**, *124*, in press. The slope of the line for  $2e$   $\text{O}_2$  reduction at the graphite is twice those for  $4e$   $\text{O}_2$  reduction at Pt and by the biomimetic catalyst. (C)  $i_{\text{cat}}^{-1}$  vs.  $\omega^{-1/2}$  graphs for  $\text{O}_2$  reduction by ( $\alpha_3\text{NRIm}\beta\text{ImPhF}$ ) $\text{Fe}/\text{Cu}$  under conditions of applicability and nonapplicability of the Koutecky–Levich equation. In the latter, the catalyst is partially saturated with  $\text{O}_2$  ( $\circ$ ) or the rate of charge transfer in the catalytic film is comparable to the rate of the  $\text{O}_2$  reduction cycle ( $+$ ).<sup>160a</sup>

overpotential to achieve diffusion-limited ring oxidation of  $\text{H}_2\text{O}_2$  is probably not accessible under most experimental conditions. As a result, the ring collection efficiency of  $\text{H}_2\text{O}_2$  is always lower than the theoretical one (by five-fold and more in some published work). This difference is, however, widely ignored in biomimetic  $\text{O}_2$  reduction studies, so that reported selectivities of most functional heme  $\text{a}_3/\text{Cu}_\text{B}$  analogs (IV.D) are likely overestimated. With adequate precautions,<sup>160</sup> however, the ring current measurements are indispensable for estimation of the catalytic selectivity at potentials where it cannot be obtained from mathematical treatment of the data (e.g., at the most biologically relevant early parts of the catalytic wave). When  $\text{H}_2\text{O}_2$  is the major primary PROS generated by the catalyst, the apparent redox stoichiometry of  $\text{O}_2$  reduction,  $n_{\text{app}}$ , can

be estimated from the collection-efficiency corrected ring-to-disk current ratio,  $i_r/i_d$ , as:  $n_{\text{app}} = 2 \times (2 - i_r/i_d)$ .

There are at least two major limitations in using a film of a synthetic heme  $\text{a}_3/\text{Cu}_\text{B}$  analog deposited on the electrode surface as a model for the catalytic site of cytochrome oxidase under steady-state  $\text{O}_2$  reduction. *In vivo*, electrons are delivered to cytochrome oxidase diffusively one at a time. However, once cytochrome oxidase binds  $\text{O}_2$ , the enzyme does not need external reductants to completely reduce the bound  $\text{O}_2$  to the level of water. This temporal decoupling of  $4e$   $\text{O}_2$  reduction (compounds R through P part of the  $\text{O}_2$  reduction cycle, Figure 4), and oxidation of external reductants (compounds O through R and  $\text{P} \rightarrow \text{F}$  in the case of  $\text{O}_2$  reduction by the mixed-valence enzyme) minimizes the lifetime of catalytic intermediates



containing partially reduced oxygen derivatives, whose release would be cytotoxic. This decoupling is achieved via redox control of the enzyme's  $O_2$  reactivity, so that only the redox states of the enzyme that have a sufficient number of reducing equivalents for complete  $4e^- O_2$  reduction *bind*  $O_2$ . The internal reductants that can be preloaded with electrons before the enzyme binds  $O_2$  are  $Cu_A$ , heme a, the tyrosine residue at the catalytic sites of most heme/Cu oxidases (Figure 3) and  $Cu_B$ . Because of the rapid internal electron transfer,<sup>20,163,164</sup> coupling  $O_2$  reduction to oxidation of these redox sites avoids the danger of a buildup of catalytic intermediates containing partially reduced oxygen.

Normally, a heme  $a_3/Cu_B$  analog in a film at the electrode surface is in a rapid redox equilibrium with the electrode, so that  $O_2$  reduction occurs under the conditions of an excess of electrons of a given potential. At best, this setup reproduces  $O_2$  reduction by fully reduced enzyme with the electrode serving as always reduced  $Cu_A$  and heme a cofactors. Therefore, if a redox cofactor at the heme  $a_3/Cu_B$  site serves mainly as an electron reservoir, its function cannot be probed by an electrode-confined biomimetic analog. The absence of significant differences in the kinetics of  $O_2$  reduction by FeCu and Cu-free forms of functional heme  $a_3/Cu_B$  analogs,<sup>159</sup> wherein the stereoelectronic environment of Fe and Cu is reproduced faithfully, is fully consistent with the commonly accepted role of  $Cu_B$  as an "outer-sphere" reductant to heme  $a_3$ -bound catalytic intermediates. In these Cu-free heme  $a_3/Cu_B$  analogs in physical contact with an electrode, the electrode adequately reproduces the electron donor role of  $Cu_B$  in CcO.

The second limitation of studying functional heme  $a_3/Cu_B$  analogs as films lies in the fact that the observed electrocatalytic behavior is that of the catalytic film as a whole and may not represent the behavior of an isolated molecule (which is more biologically relevant). Firstly, the environment around the catalytic site in a film not only differs notably from that in the protein matrix, but is also potential-dependent.<sup>160b</sup> While immobilization of a model compound at the electrode surface eliminates reaction pathways that are bimolecular in the catalyst (in contrast to solution studies, see Section III.B), stepwise reduction of  $O_2$  to  $H_2O$  at more than one catalytic center (an unlikely biologically relevant mechanism) is possible. Apparent  $4e^- O_2$  reduction by such a film may arise from a two-step mechanism whereby  $H_2O_2$  released by one molecule of the catalyst is reduced by a neighboring molecule (see Section IV.C for further discussion). In the rare cases when this possibility has been explicitly addressed,<sup>68</sup> two

arguments have been invoked to rule it out: (1) the independence of the  $i_r/i_d$  ratios on the electrode rotation rate, and (2) the electrochemical reduction of  $H_2O_2$  being significantly slower than that of  $O_2$  by the same film.

Neither, however, rules out the intermediacy of free  $H_2O_2$ . The  $H_2O_2$  flux reaching the ring during  $O_2$  reduction in a multilayer catalytic film may be determined mainly by the residence time of  $H_2O_2$  in the film (which is rotation-rate-independent) rather than the time an  $H_2O_2$  molecule remains in the vicinity of the disk-electrolyte interface (which is inversely proportional to the electrode rotation rate). Under such conditions,  $i_r/i_d$  would be rotation-rate independent even if free  $H_2O_2$  is generated and reduced further within the film. The dependence of the onset potential at the ring current on the scan rate and the catalyst surface coverage is informative in this respect. If the observed slow catalytic rates of  $H_2O_2$  reduction when it is added to the anaerobic electrolyte are determined mainly by the rate at which  $H_2O_2$  penetrates the film-solution interface, it gives no information of how fast the catalyst reduces/disproportionates  $H_2O_2$  generated *within* the film in incomplete  $O_2$  reduction.

However, the two-step  $O_2$  reduction mechanism is unlikely if several criteria are met.<sup>159</sup> These include overall  $4e^-$  activity of the catalytic film, independence of  $i_r/i_d$  ratios on the catalyst surface coverage, generation of the intermediates which are the most likely sources of  $H_2O_2$  ((por)Fe<sup>II</sup>( $O_2H_x$ )<sup>(x-2)</sup> and (por)Fe<sup>III</sup>( $O_2H_x$ )<sup>(x-1)</sup> ( $x = 1, 2$ ), see Section IV.B) in the turnover-determining step, and the significantly higher stability of the catalyst in reduction of  $O_2$  vs.  $H_2O_2$ .

The dynamics of electron delivery vs.  $O_2$  reduction at the heme  $a_3/Cu_B$  site may be better mimicked either by a water-soluble synthetic analog which receives electrons from the electrode, or by a biomimetic complex incorporated in an inert matrix (e.g., Nafion) on the surface of an electrode. Both methods have been used in  $O_2$  reduction by simple Fe (or Co<sup>81,158</sup>) porphyrins,<sup>165,166</sup> and  $O_2$  reduction by heme/ $Cu_B$  analogs in a lipid film has been studied.<sup>160a</sup> A water-soluble catalyst precludes the use of a rotating ring-disk electrode for detection of partially reduced species, as the oxidation of the catalyst itself on the ring will generate unacceptably high background currents, and the catalyst may also passivate Pt toward  $H_2O_2$  oxidation. It is also difficult to rule out a possibility that the observed electrocatalysis arises mainly from a fraction of the catalyst spontaneously adsorbed on the electrode surface. These issues are avoided for a catalyst

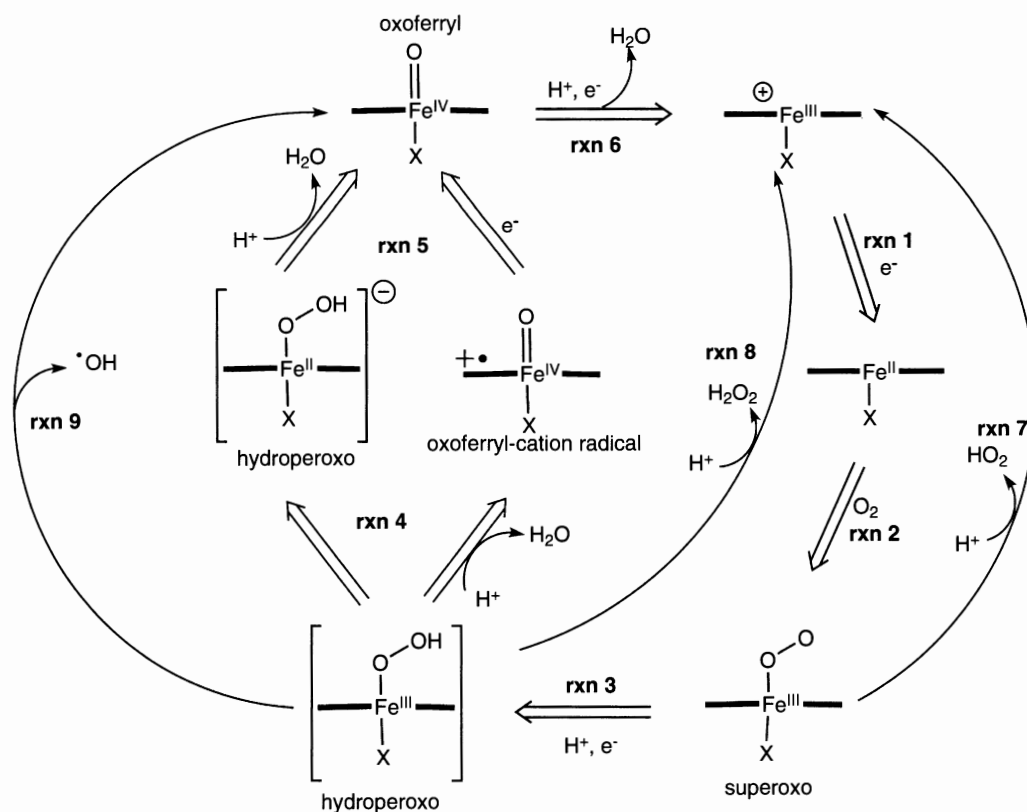
in a matrix because the complex remains confined to the disk, but in this setup either the catalyst must have a reasonable mobility in the matrix,<sup>160,165</sup> or an electron carrier must also be incorporated in the film.<sup>158</sup> The latter however limits the accessible electrochemical potentials to that of the electron carrier.<sup>158</sup>

## B. GENERAL MECHANISM OF ELECTROCATALYTIC O<sub>2</sub> (H<sub>2</sub>O<sub>2</sub>) REDUCTION AT AN IRON PORPHYRIN

Intermediates in O<sub>2</sub> (H<sub>2</sub>O<sub>2</sub>) reduction by a surface-immobilized metalloporphyrin cannot be readily characterized spectroscopically. However, it seems highly likely that the reduction proceeds via intermediates similar to those observed in the heme enzymes of dioxygen metabolism<sup>44</sup> and in reactions of simple Fe porphyrins with O<sub>2</sub> and H<sub>2</sub>O<sub>2</sub> under noncatalytic conditions in homogeneous solutions.<sup>167,168</sup> Behavior of Fe porphyrins in electrocatalytic O<sub>2</sub> (H<sub>2</sub>O<sub>2</sub>) reductions can be understood within such a general mechanism (Figure 15).

It seems likely that the O<sub>2</sub>-binding form of even the simplest catalysts that do not have a built in axial ligand is a five-coordinate ferrous derivative, where axial ligand

X is OH<sup>-</sup>, H<sub>2</sub>O, a buffer molecule or possibly a residue at the graphite surface. The potential at which the ferrous form becomes redox stable contributes to the overpotential of O<sub>2</sub> reduction. Dioxygen binding (reaction 2, Figure 15) yields a formally superoxide, O<sub>2</sub><sup>-</sup>, complex, although this is obviously a limiting description.<sup>169,170</sup> Although there appears to be one example of a side-on ferric-superoxide complex,<sup>222</sup> under catalytic conditions the O<sub>2</sub><sup>-</sup> ligand is most certainly bound end-on. One-electron reduction and protonation of the bound superoxide yields a hydroperoxo intermediate (reaction 3) where both oxygen atoms are formally reduced to the peroxo level (-1). Although ferric-hydroperoxo adducts have not been yet observed spectroscopically, their intermediacy in O<sub>2</sub> and H<sub>2</sub>O<sub>2</sub> reduction is supported by numerous computational studies.<sup>43,171,172</sup> O-O bond heterolysis in the ferric-hydroperoxo adduct (reaction 4) reduces both oxygen atoms to the redox level of H<sub>2</sub>O. One electron for this 2e transformation comes from Fe (Fe<sup>III</sup> → Fe<sup>IV</sup>), whereas the other may come either from the porphyrin (yielding the porphyrin cation-radical) or external reductants (e.g., ferroheme a in the case of fully reduced CcO, see Introduction). Although ferrous-peroxo



**Figure 15.** A general mechanism of O<sub>2</sub> electroreduction by Fe porphyrins. The steps of the main cycle are shown in block arrows, curved arrows depict side reactions that yield partially reduced oxygen byproducts. Release of H<sub>2</sub>O<sub>2</sub> from ferrous-peroxo intermediates is also possible.

intermediates do not form in biological systems, it seems likely that *electrocatalytic* O<sub>2</sub> (H<sub>2</sub>O<sub>2</sub>) reduction at an Fe porphyrin proceeds via such intermediates ( $[(\text{por})\text{Fe}^{\text{II}}(\text{O}_2\text{H}_x)]^{(x-2)}$   $x = 1, 2$ ), particularly at potentials more reducing than biologically relevant. During O–O bond heterolysis in ferrous-peroxo intermediates both electrons most likely come from the Fe, and the reaction bypasses the high-energy oxoferryl-cation radical intermediate. Reduction of the high-potential oxoferryl derivatives regenerates the aerobically stable ferric porphyrin. The ferryl state of many Fe porphyrins is accessible electrochemically at (1 V (vs. NHE, at pH 7)).<sup>160</sup> Both ferrous and ferric porphyrins can react with H<sub>2</sub>O<sub>2</sub>, thereby entering the cycle at the  $[(\text{por})\text{Fe}^{\text{II}}(\text{O}_2\text{H}_x)]^{(x-2)}$  and  $[(\text{por})\text{Fe}^{\text{III}}(\text{O}_2\text{H}_x)]^{(x-1)}$  ( $x = 1, 2$ ) intermediates, respectively.

In contrast to enzymatic heme center, side reactions (curved arrows, Figure 15) that yield partially reduced oxygen species (PROS: superoxide-hydroperoxyl pair, O<sub>2</sub><sup>•−</sup>/HO<sub>2</sub>; H<sub>2</sub>O<sub>2</sub> and free hydroxyl radicals, •OH) are important in determining the reactivity of simple Fe and Co porphyrins. Fe–O bond heterolysis in (por)FeO<sub>2</sub> (especially upon protonation) generates O<sub>2</sub><sup>•−</sup>/HO<sub>2</sub> (autoxidation<sup>170</sup>). Dissociative decomposition of peroxo-level adducts  $((\text{por})\text{M}^{\text{III}}(\text{O}_2\text{H}_x))^{(x-1)}$  and/or  $(\text{por})\text{M}^{\text{II}}(\text{O}_2\text{H}_x)^{(x-2)}$  ( $x = 1, 2$ ) releases free H<sub>2</sub>O<sub>2</sub>. Additionally, O–O bond homolysis in the peroxo intermediate reduces only one oxygen atom to the –2 redox level, whereas the other is liberated as a highly reactive free hydroxyl radical •OH.

Selectivity of electrocatalytic O<sub>2</sub> reduction by most Fe and Co porphyrins is determined mainly by kinetic partitioning among the three decomposition pathways of the peroxo-level intermediates. Within a series of structurally related complexes, this partitioning probably directly correlates with the accessibility of the high-valence states. Since Co<sup>IV</sup> is a very high energy state, simple Co porphyrins do not induce O–O bond cleavage (either homolytic or heterolytic). The less oxidizing ferryl state favors O–O bond cleavage, which in simple Fe porphyrins proceeds via both homolysis<sup>167,173</sup> and heterolysis in competition with release of free peroxide. Indeed, dramatic differences in stability of the O–O bond in peroxo adducts of Co and Fe are well established in many systems.<sup>174</sup> In heme proteins and in more advanced biomimetic catalysts, the proximal and distal environments decrease the activation barrier for O–O bond heterolysis (e.g., via stabilization of the high-valence states<sup>175</sup> and other effects<sup>168</sup>) sufficiently for it to be the dominant decomposition pathway. For these very selective

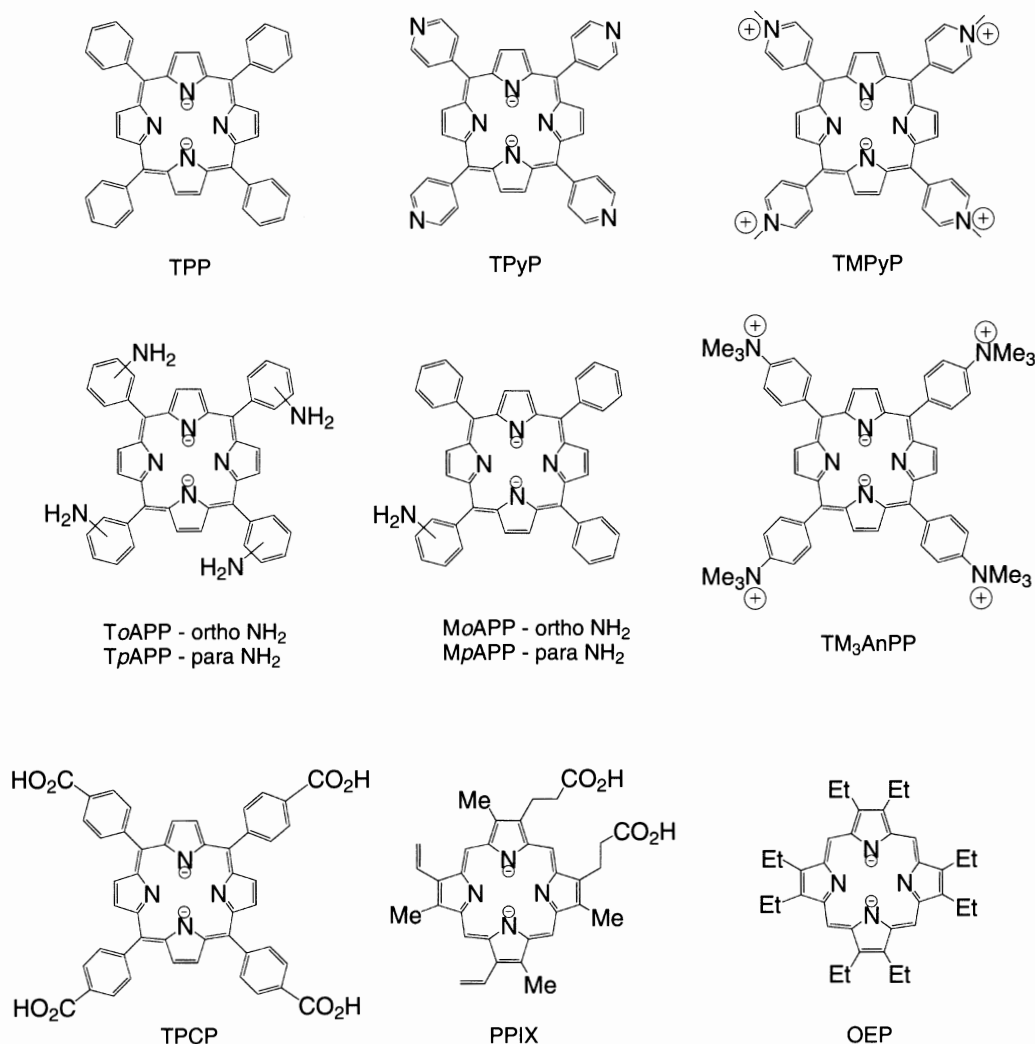
catalysts, autoxidation may become the dominant PROS source.

### C. ELECTROCATALYTIC O<sub>2</sub> REDUCTION BY SIMPLE Fe PORPHYRINS

The electrocatalytic properties of simple Fe porphyrins toward reduction of O<sub>2</sub> and H<sub>2</sub>O<sub>2</sub> provide the necessary background for understanding the structure–function relationship in more biologically relevant analogs. A number of simple Fe porphyrins have been investigated as electrocatalysts of O<sub>2</sub> and H<sub>2</sub>O<sub>2</sub> reduction (Figure 16). There are substantial variations in the quantitative parameters reported by various workers for the same complex (e.g., (TPP)Fe, Entries 1–6 in Table 5),<sup>166,176–183</sup> but the qualitative behavior of all simple Fe porphyrins is similar. Electrocatalytic O<sub>2</sub> reduction usually starts at potentials close to that of the Fe<sup>III/II</sup> couple (measured under anaerobic conditions). An identical pH dependence is observed for the half-wave potentials of the O<sub>2</sub> reduction waves ( $E_{1/2}$ ), and the Fe<sup>III/II</sup> potentials in the absence of O<sub>2</sub> (either 60 or 0 mV/pH depending on the electrolyte acidity, Table 5). This suggests that the turnover rate in the rising part of the catalytic wave depends directly on the surface concentration of the ferrous form with the nonredox turnover determining step (e.g., O<sub>2</sub> binding). The redox stoichiometry of O<sub>2</sub> electroreduction by films of Fe porphyrins is not affected significantly by the pH: they appear to catalyze 4e O<sub>2</sub> reduction over a wide pH range (1–14) in the few cases that have been studied.

Most simple *ferric* porphyrins react only very slowly with H<sub>2</sub>O<sub>2</sub>, whereas the rate of electrocatalytic H<sub>2</sub>O<sub>2</sub> reduction by *ferrous* analogs is comparable to that of O<sub>2</sub> reduction. It was suggested that the reduction of H<sub>2</sub>O<sub>2</sub> proceeds via an outer-sphere mechanism.<sup>178</sup> This is, however, almost certainly incorrect. Outer-sphere reactions of H<sub>2</sub>O<sub>2</sub> have very high kinetic barriers.<sup>169,184</sup> an example is the inertness of a graphite electrode toward H<sub>2</sub>O<sub>2</sub> reduction above ~–800 mV (> 2 V overpotential at pH 7). The reduction most likely proceeds via peroxo adducts  $(\text{por})\text{M}^{\text{III}}(\text{O}_2\text{H}_x)^{(x-1)}$  and/or  $(\text{por})\text{M}^{\text{II}}(\text{O}_2\text{H}_x)^{(x-2)}$  ( $x = 1, 2$ ) (Figure 15). The lower reactivity of Fe<sup>III</sup>-porphyrins toward H<sub>2</sub>O<sub>2</sub> is probably due to both the slower ligand exchange at a ferric vs. a ferrous center and less facile O–O bond cleavage in ferric-peroxo adducts (as it generates more high-energy intermediates, e.g., ferryl-cation radical).

The selectivity of O<sub>2</sub> reduction by multilayer films of many electrode-confined Fe porphyrins is potential-dependent (three major types of the  $i_r - E$  profiles



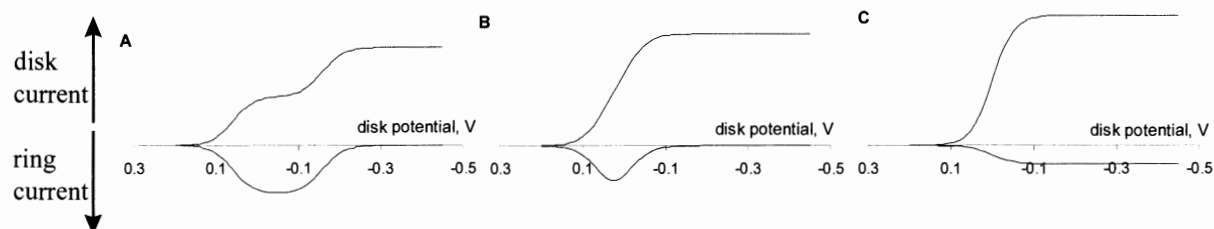
**Figure 16.** Chemical structures and abbreviated names of simple porphyrin ligands whose Fe complexes have been studied as electrocatalysts of O<sub>2</sub> reduction.

observed in O<sub>2</sub> reduction are shown in Figure 17). The apparent redox stoichiometry of O<sub>2</sub> reduction ( $n_{app}$ ) in the rising part of the catalytic wave is often markedly lower than that at the plateau. The 4e O<sub>2</sub> reduction at the plateau is believed to proceed via a two-step mechanism, whereby O<sub>2</sub> reduction by individual Fe porphyrin molecules generate substantial H<sub>2</sub>O<sub>2</sub> flux, but, under the condition of high catalyst-to-substrate ratio, the released H<sub>2</sub>O<sub>2</sub> is further reduced (or disproportionated) by neighboring catalyst molecules before it diffuses out of the film and is detected. The potential-dependent selectivity of a catalytic film indicates a kinetic competition between a potential-independent source of free H<sub>2</sub>O<sub>2</sub> and a potential-dependent sink (or vice versa). Decreasing H<sub>2</sub>O<sub>2</sub> flux at more reducing potentials (Figure 17) is commonly ascribed to an increased fraction of the more reactive-toward-H<sub>2</sub>O<sub>2</sub> ferrous porphyrin.<sup>177</sup> This explanation assumes the presence of

a potential-dependent *sink* (higher fraction of the more reactive Fe<sup>II</sup> species), but the possibility of a potential-dependent *source* as the origin of the selectivity profile cannot at present be ruled out and it may be more consistent with the known chemistry of Fe porphyrins. The catalytic selectivity may increase at potentials where the dominant peroxo-level intermediate changes from ferric-peroxo to ferrous-peroxo (Figure 15). Because O–O bond cleavage in the former is likely less facile than in the latter (*vide supra*), decomposition of [(por)Fe<sup>II</sup>(O<sub>2</sub>H<sub>x</sub>)]<sup>(x-2)</sup> intermediates ( $x = 1, 2$ ) may preferentially proceed via O–O bond cleavage as opposed to peroxide dissociation in the case of [(por)Fe<sup>III</sup>(O<sub>2</sub>H<sub>x</sub>)]<sup>(x-1)</sup> analogs. Within both mechanisms, the 4e activity of simple Fe porphyrins is biologically irrelevant, as O<sub>2</sub> (H<sub>2</sub>O<sub>2</sub>) reduction at enzymatic heme sites does not proceed via ferrous-peroxo intermediates.

**Table 5.** Summary of the Electrocatalytic Properties of Simple Fe Porphyrins Immobilized on an Electrode. See Figure 16 for the Relevant Chemical Structures. All Potentials are vs. the Normal Hydrogen Electrode (NHE)

Catalyst (Figure 16)	E(Fe <sup>III/I</sup> ) <sup>a</sup>	E <sub>1/2</sub> (RDE), V <sup>b</sup>		Selectivity (n <sub>app</sub> ) <sup>c</sup>		pH dependence (pH range)	E <sub>1/2</sub> H <sub>2</sub> O <sub>2</sub>
		pH 0–2	pH 7	at E <sub>1/2</sub>	at plateau		
(TPP)Fe <sup>d</sup>	0	0.35, 0.2 <sup>e</sup>	–	–	3.7 KL		
(TPP)Fe <sup>f</sup>	0.5, 0.1	0.35–0.2	0.1	n.r.	4 KL	60 mV/pH (pH > 3), 0 mV/pH (pH < 3)	
(TPP)Fe <sup>g</sup>	0.1	0.35, 0.2 <sup>e</sup>	–	–	3.7 KL (4 i <sub>r</sub> /i <sub>d</sub> )		0.1
(TPP)Fe <sup>h</sup>	n.r.	0	–	h	3.2 KL		
(TPP)Fe <sup>i</sup>	0.06	0	–	h	3.7 KL		inert
(TPP)Fe <sup>f</sup>	0.5	0.25	–	–	4 KL	0 mV/pH (pH < 7), 60 mV/pH (pH > 7)	0.2
(TpAPP)Fe <sup>d</sup>	0.1	0.2	–	3.5	4 KL		
(ToAPP)Fe <sup>d</sup>	0.1	0.2	–	3.5	4 KL		
(ToAPP)Fe <sup>j</sup>	0.2	0.3	0	j	4 KL, i <sub>r</sub> /i <sub>d</sub>	65 mV/pH (2–7), 0 mV/pH (1, > 7)	
(MpAPP)Fe <sup>d</sup>	0.1	0.2	–	3	3.9 KL		
(MoAPP)Fe <sup>d</sup>	0.1	0.2	–	3	3.9 KL		
(TM <sub>3</sub> AnPP)Fe <sup>k</sup>	0	0.2	0	3.4 (pH 8)	3.8 i <sub>r</sub> /i <sub>d</sub> (pH 8)	55 mV/pH (1–4, 6–8), 0 mV/pH (0–1, 4–6, 8–10)	
(TPCP)Fe <sup>l</sup>	0.3	0.1	–	–	> 2	55 mV/pH (pH 0 – 2)	0.1
(PPIX)Fe <sup>g</sup>	0.1	0.2	0	3	3.8 KL	60 mV/pH (2.5–5.5, > 8.5), 0 mV/pH (1 – 2.5, 5.5–8.5)	0.1
(PPIX)Fe <sup>m</sup>	0	–	–	–	–		0.2
(TPyP)Fe	0.2	0.35	–	3.7	3 KL		0.2
(OEP)Fe <sup>h</sup>	n.r.	0.2	–	h	3.5 KL		
(OEP)Fe <sup>i</sup>	n.r.	0.2	–	h	3.8 KL		

<sup>a</sup>In the absence of a substrate; n.r. – not reported.<sup>b</sup>The half-wave potential of the catalytic wave for O<sub>2</sub> reduction at an RDE. This value depends on the electrode rotation rate, bulk O<sub>2</sub> concentration, pH and in many cases on the scan rate, the amount of the adsorbed catalyst and the nature of the supporting electrolyte.<sup>c</sup>The apparent redox stoichiometry of O<sub>2</sub> reduction. We have calculated the n<sub>app</sub> values at E<sub>1/2</sub> from the presented RRDE LSVs using the collection efficiencies reported by the authors or estimated from an RRDE trace for O<sub>2</sub> reduction on bare electrode. The method by which n<sub>app</sub> was estimated: KL – the Koutecky–Levich plot (Figure 14A); i<sub>r</sub>/i<sub>d</sub> – the ring-to-disk currents ratio when the collection efficiency is reported or could be estimated.<sup>d</sup>The experimental conditions: glassy carbon, O<sub>2</sub> saturated 0.05 M H<sub>2</sub>SO<sub>4</sub>, 100 rpm.<sup>176</sup><sup>e</sup>Two waves (see Figure 17A).<sup>f</sup>The experimental conditions: EPG, O<sub>2</sub> saturated pH 0 electrolyte. The adsorbed catalyst yields 2 surface redox waves, presumably corresponding to two different forms; only the form with the more positive redox potential was reported to be catalytically active. The authors do not mention the presence of two catalytic waves in O<sub>2</sub> reduction; the E<sub>1/2</sub> was reported to be dependent on the surface concentration of the catalysts; the range of the observed E<sub>1/2</sub> values is given.<sup>177</sup> The pH dependence and the E<sub>1/2</sub>(H<sub>2</sub>O<sub>2</sub>) are for the catalyst in solution.<sup>166</sup><sup>g</sup>The experimental conditions: pyrolytic graphite, O<sub>2</sub> saturated 0.1 M HClO<sub>4</sub>, 100 rpm. The pH dependence of the Fe<sup>III/II</sup> potential in the absence of a substrate is shown; the E<sub>1/2</sub> vs. pH dependence appear to be similar.<sup>178</sup><sup>h</sup>Prepared from (por)FeCl.<sup>181</sup> The experimental conditions: glassy-carbon, reported as O<sub>2</sub>-saturated 0.5 M HClO<sub>4</sub> but the shown catalytic currents are about 60–70% of the diffusion limited current at [O<sub>2</sub>] = 1.3 mM. No data are provided to determine the experimental collection efficiency of the RRDE toward H<sub>2</sub>O<sub>2</sub>, the ring current appears to be potential-independent (Figure 17C); a single catalytic wave is observed in linear sweep voltammograms of the (TPP)Fe catalysts.<sup>i</sup>Prepared from [(por)Fe]<sub>2</sub>(μ-O), other parameters are the same as in (h).<sup>j</sup>The experimental conditions: glassy-carbon electrode, air-saturated 0.05 M H<sub>2</sub>SO<sub>4</sub>, 100 rpm; experimental collection efficiency not reported, the i<sub>r</sub> – E profile is similar to that in Figure 17A.<sup>183</sup><sup>k</sup>The experimental conditions: glassy carbon, air-saturated pH 2 electrolyte; 400 rpm.<sup>179</sup><sup>l</sup>The experimental conditions: stationary glassy carbon electrode, air-saturated 0.05 M H<sub>2</sub>SO<sub>4</sub>.<sup>180</sup><sup>m</sup>Covalently attached to a gold electrode; a pH 7 buffered electrolyte.<sup>182</sup>**Figure 17.** Typical linear sweep voltammograms of O<sub>2</sub> reduction by Fe porphyrins immobilized at the disk of a rotating ring-disk electrode: (A) (TPP)Fe, (B) (PPIX)Fe, (C) (TPyP)Fe (see Figure 16 for chemical structures). Shown are simulated traces vs. an arbitrary reference for the disk potential, based on the data in Refs. 177 and 178.

The origin of the low stability of Fe porphyrins during O<sub>2</sub> reduction is not established. Oxidative degradation of Fe porphyrin complexes without *meso* substituents (e.g., OEP and protoporphyrin IX, Figure 16) can proceed via a nucleophilic attack of the Fe-bound superoxo moiety on the *meso* carbon (heme oxygenase mechanism),<sup>44</sup> and a direct attack of H<sub>2</sub>O<sub>2</sub> on the *meso* carbon may also be possible.<sup>185</sup> In contrast, the oxidation mechanism of *meso* substituted porphyrins (which are usually thought to be more resistant to bleaching) is not known. Bimolecular oxygenation of the macrocycle by oxoferryl derivatives appears probable in homogeneous catalytic systems,<sup>186</sup> but such a mechanism is not easily accessible for an adsorbed Fe porphyrin. Although it is generally assumed that H<sub>2</sub>O<sub>2</sub> is primarily responsible for catalyst degradation during O<sub>2</sub> reduction, the most plausible candidate is •OH, which is substantially more reactive, thermodynamically ( $E^0 \sim 2.8$  V) and kinetically, than O<sub>2</sub><sup>-</sup>/HO<sub>2</sub> or H<sub>2</sub>O<sub>2</sub>.<sup>187–189</sup> Indeed, •OH-mediated degradation explains the fact that purely 2e catalysts (simple Co porphyrins) display substantially higher stability (turnover numbers) in electrocatalytic O<sub>2</sub> reduction than many structurally related metalloporphyrins, which catalyze the 4e pathway (Fe porphyrins and *biscobaltdiporphyrins*, see Section V). Thus, the stability of an electrocatalyst during O<sub>2</sub> reduction may provide a qualitative measure of its selectivity toward heterolysis vs. homolysis of the O–O bond. Production of •OH in metalloporphyrin-catalyzed O<sub>2</sub> electroreduction may be assayed using scavengers for partially reduced oxygen species.<sup>159</sup> Regrettably, there has been only a single report on effects of scavengers for O<sub>2</sub><sup>-</sup> (superoxide dismutase, SOD), H<sub>2</sub>O<sub>2</sub> (catalase), and •OH (mannitol) on the stability of an Fe porphyrin, (TMPyP)Fe (Figure 16), in the presence of O<sub>2</sub> and its partially reduced derivatives.<sup>190</sup> Only the presence of catalase led to an increase in the metalloporphyrin stability; the authors concluded that H<sub>2</sub>O<sub>2</sub> is the sole partially reduced oxygen species causing porphyrin bleaching, whereas both O<sub>2</sub><sup>-</sup> and •OH are inert toward the porphyrin. However, the experimental data do not appear sufficient to draw any definitive conclusions. Because •OH is produced from H<sub>2</sub>O<sub>2</sub>, removal of the latter by catalase should decrease production of •OH as well. The lack of the effect of mannitol is more difficult to understand, but it may not be inconsistent with •OH as the bleaching agent. Because •OH is generated in a close proximity of the macrocycle by a homolytic cleavage of the O–O bond in the Fe porphyrin-coordinated hydroperoxide, it may preferentially react with the porphyrin rather than the

added scavenger decreasing the effect of the latter. Effects of other •OH scavengers, such as N<sub>3</sub><sup>-</sup>, carnosine, homocarnosine, and anserine must be investigated before •OH can be ruled out.

The limited stability of Fe catalysts in O<sub>2</sub> reduction may also explain the fact that the apparent selectivity of O<sub>2</sub> reduction at an Fe-porphyrin-modified electrode positively correlates with the amount of deposited metalloporphyrins. As a smaller fraction of “thicker” catalytic films decomposes during a catalytic run, such films manifest higher apparent selectivities, assuming that the intact catalyst is more selective than a partly decomposed analog.

In conclusion, at sufficiently reducing potentials even simple Fe porphyrins, such as (TPP)Fe, (TPyP)Fe, etc., when adsorbed on a graphite electrode, reduce O<sub>2</sub> electrochemically with a remarkably high proportion of the 4e pathway. This 4e O<sub>2</sub> reduction, however, is not biologically relevant, as it proceeds via ferrous-peroxo intermediates, inaccessible in enzymatic heme catalysis. The low stability of most Fe porphyrins in electrocatalytic O<sub>2</sub> reduction even in the regime when apparent 4e O<sub>2</sub> reduction is observed is most likely due to production of hydroxyl radicals, revealing that the catalysis proceeds in part via abiological Fenton chemistry. This illustrates that the capacity to affect 4e O<sub>2</sub> reduction at an arbitrary electrochemical potential and for an arbitrary small number of turnovers is not an indication that a metalloporphyrin adequately reproduces the catalytic mechanism of the heme a<sub>3</sub>/Cu<sub>B</sub> site, and thus can be considered a “functional” analog. Yet, this criterion remains widely abused in biomimetic CcO studies, which leads to unreasonable conclusions regarding the structure–function relationship at the heme a<sub>3</sub>/Cu<sub>B</sub> site.<sup>83,191,192</sup> A minimum requirement for an electrocatalyst to be a functional heme a<sub>3</sub>/Cu<sub>B</sub> analog is its capacity to affect largely 4e O<sub>2</sub> reduction at *physiologically relevant potentials* (e.g., those of cytochrome *c* and ubiquinol, see Introduction) without production of free •OH.

#### D. FUNCTIONAL HEME a<sub>3</sub>/Cu<sub>B</sub> ANALOGS

A number of synthetic heme a<sub>3</sub>/Cu<sub>B</sub> analogs have been screened for their capacity to carry out 4e O<sub>2</sub> reduction at pH ~7 (Figure 12, Table 6).<sup>67,68,160,191–194</sup> However, beyond this, the electrocatalytic properties of these complexes remain virtually unknown. The exception is the (α<sub>3</sub>ImNRβIm<sub>ph</sub>F)Fe/Cu series (R = Me, MePr, HPr Figure 12).<sup>159,160</sup> Among any synthetic porphyrins yet reported, these series most faithfully mimic the

**Table 6.** Electrocatalytic Properties and Reactivity Toward Dioxygen of the Functional Heme  $a_3/Cu_B$  Site Analogs. See Figure 12 for the Relevant Chemical Structures. All Potentials are vs. the Normal Hydrogen Electrode (NHE)

Entry	Catalyst (Figure 12)	$E_{catr}$ , V <sup>a</sup>	$E_{1/2}(O_2)$ , V at pH 7 <sup>b</sup>	Selectivity ( $n_{app}$ ) <sup>c</sup>		Dioxygenation by UV/vis <sup>d</sup>	Ref.
				at $E_{1/2}$	at plateau		
1	$(\alpha_3NRIm\beta Im_{PhF})Fe/Cu^e$	0.1	0.2	~4	4	n.r.	160
2	$(\alpha_3NRIm\beta Im_{PhF})Fe^e$	0.1	0.2	> 3.7–3.8	4	n.r.	160
3	$(\alpha_3Im_N\beta py_{Alk})Fe/Cu$	n.r.	0.2 <sup>f</sup>	n.r.	4 <sup>g</sup>	irreversible	193
4	$(\alpha_3Im_N\beta Im_{Alk})Fe/Cu$	~0.25	0.15	n.r.	4 <sup>g</sup>	irreversible	193
5	$(\alpha_3Im_N\beta Im_{Alk})Fe$	0.25	n.r.	n.r.	n.r.	reversible	193
6	$(\alpha_3quin\alpha Ac)Fe/Cu$	n.r.	0	2.5–3.5	3.4 $i_{lim}$	irreversible	191
7	$(\alpha_3quin\alpha Ac)Fe$	n.r.	0	2.2–3.4	3.5 $i_{lim}$ (3.8 $i_r/i_d$ ) (3.9 $i_r/i_d$ )	reversible	191
8	$(\alpha_3quin\beta Im_{Ph})Fe/Cu$	n.r.	0.1	< 3.1	3.5 $i_{lim}$	irreversible	191
9	$(\alpha_3quin\beta Im_{Ph})Fe$	n.r.	n.m.		3.6 $i_{lim}$	reversible	191
10	$(\alpha_3C_1-TREN_H\alpha Ac)Fe/Cu$	n.r.	0	< 2.6	2.7 $i_r/i_d$	n.r.	192
11	$(\alpha_3C_1-TREN_H\alpha Ac)Fe$	n.r.	0	< 3.8	4 $i_r/i_d$	n.r.	192
12	$(\alpha_3C_2-TREN_H)Fe/Cu$	n.r.	0.05	2.5–3	2.8, $i_{lim}$ (3.2 $i_r/i_d$ )	n.r.	192
13	$(\alpha_3C_2-TREN_H)Fe$	n.r.	0	3.7–3.8	4 $i_r/i_d$	n.r.	192
14	$(\alpha_3TREN_{Ph}3\beta Im_{Alk})Fe/Cu$	~0.15 (Fe); ~-0.2 (Cu) <sup>h</sup>	0.15 <sup>f</sup>	n.r.	4–3.6 <sup>i</sup> KL	j	67
15	$(\alpha_3TACN\beta py_{Alk})Fe/Cu$	n.r.	0.15	n.r.	3.9, KL	irreversible	194
16	$(\alpha_3TACN\beta Im_{Ph})Fe/Cu$	n.r.	0.2	n.r.	3.9 KL	irreversible	194
17	$(\alpha_3TACN\beta Im_{Alk})Fe/Cu$	~0.1 (Fe); ~-0.5 (Cu) <sup>h</sup>	0.15	n.r.	2–3.1 <sup>i</sup>	j	67
18	$(\alpha_3TACN\beta Im_{Alk})Co/Cu$	~0.7 (Co); ~-0.3 (Cu)	0.25	4	3.9 KL	irreversible	68

<sup>a</sup>The redox couple ( $Fe^{III}/Cu^{II}$  or  $Fe^{III}Cu^{II}/Fe^{II}Cu^I$ ) for the graphite-adsorbed catalyst in the absence of a substrate; n.r. – not reported.

<sup>b</sup>The half-wave potential of the catalytic wave for  $O_2$  reduction at an RDE. This value depends on the electrode rotation rate, bulk  $O_2$  concentration, pH and in many cases on the scan rate, the amount of the adsorbed catalyst and the nature of the supporting electrolyte; n.m. – not meaningful (no defined wave).

<sup>c</sup>The apparent redox stoichiometry of  $O_2$  reduction. We have calculated the  $n_{app}$  values at  $E_{1/2}$  from the presented RRDE LSVs using the collection efficiencies reported by the authors or estimated from an RRDE trace for  $O_2$  reduction on bare electrode. The method by which  $n_{app}$  was estimated: KL – the Koutecky–Levich plot;  $i_r/i_d$  – the ring-to-disk currents ratio when the collection efficiency is reported or could be estimated;  $i_{lim}$  – comparison of the limiting current yielded by the catalyst with that given by the standard with a known  $n_{app}$  under the identical experimental conditions. The higher  $n_{app}$  estimated from the  $i_r/i_d$  ratio for several entries illustrated that the reported values by the authors collection efficiencies are significantly overestimated.

<sup>d</sup>Indicates whether formation of the  $O_2$  adduct is reversible; see Section III.B for further details.

<sup>e</sup>The imidazole substitution pattern of the distal superstructure has only a minor effect on electrochemical behavior ( $R = MeIm, HPrIm, MePrIm$ )

<sup>f</sup>The numbers were extracted from the RDE LSVs given in the supplementary information.

<sup>g</sup>“No detectable peroxide leakage”; neither RRDE traces nor  $i_r/i_d$  values are presented and the experimental collection efficiency is not specified.

<sup>h</sup>The peaks labeled as  $Cu^{II}$  are poorly defined and only quasi-reversible, these peaks may not correspond to the  $Cu^{II}$  couple.

<sup>i</sup>The first number refers to the originally reported selectivity; the second  $n$  value was reported later.

<sup>j</sup>“Form < s a > stable 1:1 adduct with  $O_2$  < ... > as demonstrated by UV/vis spectroscopy < ... > has > an apparently diamagnetic NMR spectrum”: no further details were given.

immediate coordination environment of the  $Fe_{a_3}/Cu_B$  core. Under physiologically relevant conditions these biomimetic catalysts reproduce key aspects of the  $O_2$  and  $H_2O_2$  chemistry of the enzyme. First, they affect complete reduction of  $O_2$  to  $H_2O$  at potentials comparable to the midpoint potential of cytochrome  $c$  (Table 6). Second, the pH dependence of the half-wave potentials and other data are consistent with O–O bond activation at these centers proceeding via a slow generation of a formally ferric-hydroperoxo intermediate, followed by its rapid reduction to the level of water. The kinetics is analogous to that proposed for the  $O_2$  reduction step ( $A \rightarrow P$  conversion, Figure 4) at the heme  $a_3/Cu_B$  site.<sup>43</sup> It minimizes the steady-state concentration of the ferric-peroxo

intermediates whose decomposition would release free  $H_2O_2$  (Figure 15). As a result, in contrast to other synthetic Fe porphyrins, the catalysts in the  $(\alpha_3ImNR\beta Im_{PhF})Fe/Cu$  series ( $R = Me, MePr, HPr$ ) effect the 4e  $O_2$  reduction at physiologically relevant potentials without the intermediacy of ferrous-peroxo adducts. Third, the maximum catalytic rate constants of  $O_2$  reduction by the ferrous catalyst and of  $H_2O_2$  reduction by both ferric and ferrous catalysts are comparable to those reported for cytochrome oxidase.<sup>195</sup> Finally, the oxidized catalyst mimics the catalase activity of cytochrome oxidase. This close structural and functional analogy between the heme  $a_3/Cu_B$  site and  $(\alpha_3ImNR\beta Im_{PhF})Fe/Cu$  ( $R = Me, MePr, HPr$ ) biomimetic catalysts allowed the authors

to use these synthetic systems to probe possible physiological effects that Cu<sub>B</sub> may have on the O<sub>2</sub> reduction cycle of this enzyme (apart from the electron donor role, see Section IV.A).<sup>159,160</sup> On the basis of comparative voltammetric studies of the biomimetic complexes in the FeCu as well as Cu-free (monometallic Fe-only and bimetallic FeZn) forms, the authors found that under catalytic conditions, Cu suppresses autoxidation of the ferrous center<sup>159</sup> and decreases the susceptibility to inhibition, particularly by CN<sup>-</sup>.<sup>160c</sup> At physiologically-relevant potentials O<sub>2</sub> reduction by the Cu-free catalysts is accompanied by release of free superoxide as the main source of the partially reduced oxygen byproducts. This was determined from experiments with superoxide scavengers incorporated into catalytic films. In contrast, the FeCu catalyst does not generate detectable amounts of free O<sub>2</sub><sup>-</sup> which accounts for its higher catalytic selectivity. This result suggests that Cu suppresses O<sub>2</sub><sup>-</sup>-releasing heterolytic dissociation of the (por)FeO<sub>2</sub> adduct (autoxidation<sup>170</sup>), an effect that may be biologically beneficial. The Cu has an opposite effect on the affinities of the major heme a<sub>3</sub>/Cu<sub>B</sub> inhibitors, CN<sup>-</sup> and CO, to the Fe-porphyrin center, so that the corresponding adducts of the FeCu catalysts have dissociation constants ~3 times lower than those of the Fe-only analog. A combination of the lower CN<sup>-</sup> affinity to both the oxidized and reduced FeCu catalyst leads to it being up to five times more active than the Fe-only analog in O<sub>2</sub> reduction at physiologically relevant potentials in the presence of CN<sup>-</sup>. The possibility that Cu<sub>B</sub> may have such protective effects on O<sub>2</sub> chemistry of heme a<sub>3</sub> had not been considered prior to this work.

One of the early functional heme a<sub>3</sub>/Cu<sub>B</sub> analogs was a Co porphyrin, (α<sub>3</sub>TACNβIm<sub>Alk</sub>)CoCu (analogous to (α<sub>3</sub>TACNβIm<sub>Alk</sub>)Fe/Cu in Figure 12; Entry 18 in Table 6), which electrocatalytically reduces O<sub>2</sub> to H<sub>2</sub>O at pH 7 and moderate overpotentials.<sup>68</sup> The complex binds O<sub>2</sub> in toluene yielding a bridging peroxo derivative (based on the presence of the IR adsorption at 804 cm<sup>-1</sup>, which shifts to 756 cm<sup>-1</sup> when <sup>18</sup>O<sub>2</sub> is used). The Cu-free analog is a 2e catalyst, as are most monometallic Co porphyrins; so was the bimetallic CoCu complex lacking the covalently attached nitrogenous base. Based on these results, it was concluded that Cu<sub>B</sub> in cytochrome oxidase was essential for the cleavage of the O–O bond, a point yet to be confirmed by biomimetic studies with more relevant FeCu complexes. An increase in n<sub>app</sub> upon introduction of distal Cu into a Co porphyrin bearing imidazole pickets has also been observed.<sup>196</sup> Unfortunately, the

higher redox potentials of Co relative to those of Fe in a comparable coordination environment limits the extent to which Co can be considered a substitute for Fe in redox transformations.

Boitrel, L'Her and coworkers extended this work to a series of Fe-based heme a<sub>3</sub>/Cu<sub>B</sub> analogs and studied O<sub>2</sub> reduction at pH 7 by monometallic Fe-only and bimetallic FeCu porphyrins bearing a TREN-type or trisquinoline superstructures: (α<sub>3</sub>quinβIm<sub>Ph</sub>)Fe(/Cu), (α<sub>3</sub>quinαAc)Fe(/Cu), (α<sub>3</sub>C<sub>1</sub>-TREN<sub>H</sub>αAc)Fe(/Cu), and (α<sub>3</sub>C<sub>2</sub>-TREN<sub>H</sub>αAc)Fe(/Cu) (Figure 12 and Table 6, Entries 6–13).<sup>191,192</sup> They found, in accord with prior work by Anson and coworkers,<sup>177,178</sup> as well as others (see Table 5 in Section IV.C), that the Fe-only catalysts effect 4e O<sub>2</sub> reduction at potentials < ~0 V vs. NHE. Interestingly, in all cases the FeCu complexes displayed dramatically lower selectivities, which the authors ascribed to the fact that “copper center does not interfere with the O<sub>2</sub> molecule bound to Fe” or the “copper ion ... is no longer coordinated.” Neither process, however, should result in the *lower* selectivity relative to the Cu-free catalysts. The Fe···Cu separations in these complexes appear to be comparable to that found in other functional analogs, which is sufficient to accommodate dioxygen ligands in the porphyrin pocket, so that Cu should not sterically interfere with the Fe-centered chemistry. Two alternative explanations seem more likely. First, the synthetic procedure used for Cu insertion may lead to structural degradation of the complex, which may not be obvious from mass-spectral and elemental analyses. Although the bimetallic complexes were prepared in the fully reduced, Fe<sup>II</sup>Cu<sup>I</sup> state amenable to NMR characterization, it was not reported. Alternatively, the poorer selectivity of the FeCu catalysts may be due to their faster degradation during the turnover. These complexes lose catalytic activity very rapidly, which precluded careful electrochemical studies, and this may be related to the fact that many simple Cu salts are excellent Fenton reagents, efficiently converting H<sub>2</sub>O<sub>2</sub> into highly destructive free •OH. The initial small amount of relatively benign H<sub>2</sub>O<sub>2</sub> generated by the intact FeCu catalyst can conceivably be converted into •OH by the Cu ion which leads to more rapid degradation of the bimetallic catalysts and apparently lower selectivities. If this interpretation is correct, Cu coordinated within the TREN<sub>H</sub> and trisquinoline superstructures appears to be in an environment substantially different from that in the heme a<sub>3</sub>/Cu<sub>B</sub> site (where it is not known to manifest Fenton chemistry).



The authors also conclude that “a fifth ligand for the Fe porphyrin is not necessary” for O<sub>2</sub> reduction<sup>191</sup> based on the observation that their catalysts reduce O<sub>2</sub> to H<sub>2</sub>O at the plateau region in the absence of any nitrogenous ligands. However, because the catalysts are exposed to a great excess of both H<sub>2</sub>O and the phosphate buffer, which have substantial ligating power, Fe centers are highly unlikely to remain four coordinate. Moreover, examination of data in Tables 5 and 6 reveals that the biomimetic catalysts that carry a covalently attached nitrogenous axial ligand at pH 7 reduce O<sub>2</sub> at overpotentials ~0.2 V lower than those of the catalysts without such axial ligands (simple Fe porphyrins in Table 5 and Entries 6, 7, 10–13 in Table 6). The lower overpotential is highly biologically relevant since it increases the voltage drop across the respiratory electron transfer chain.

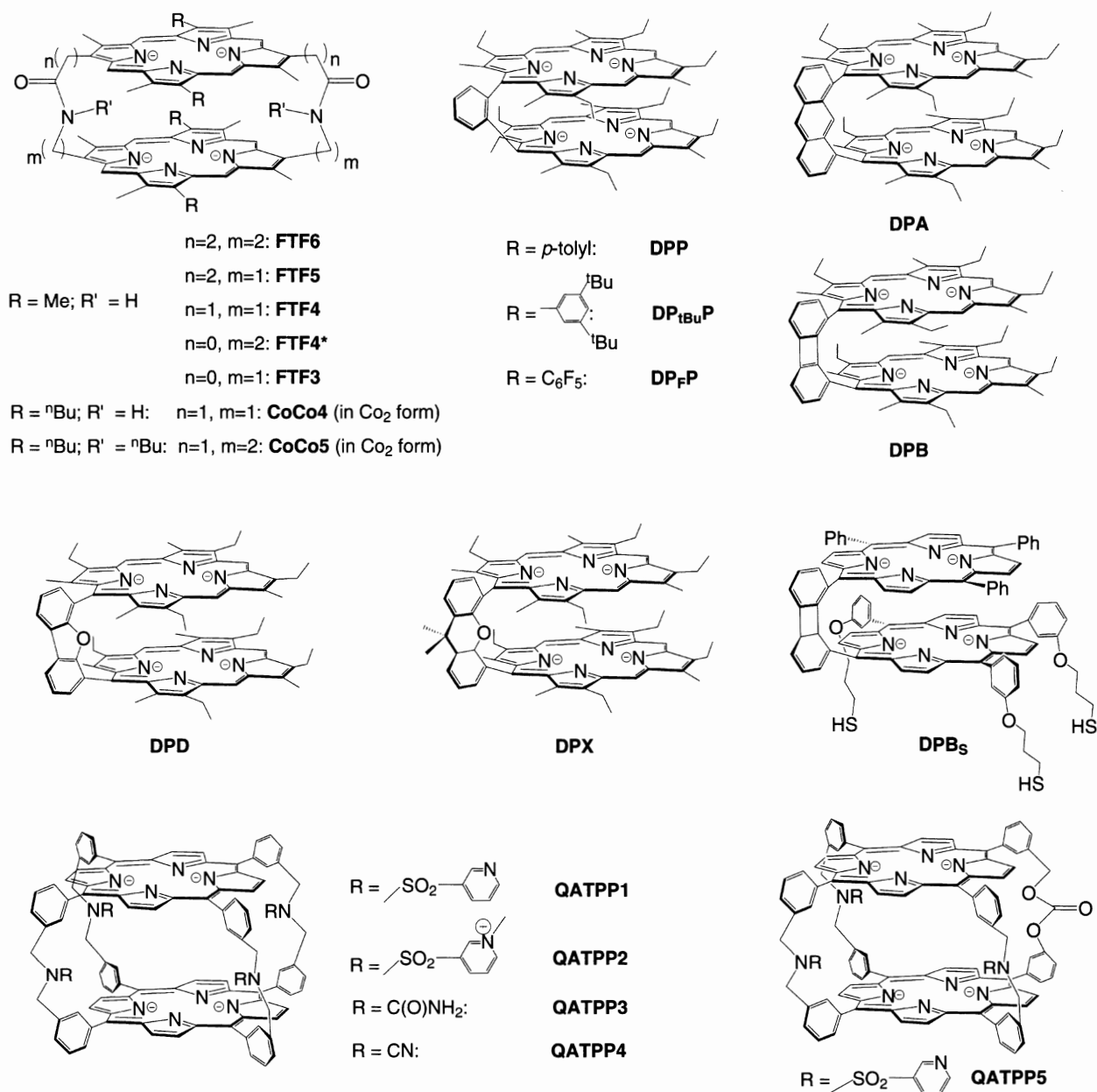
An attempt was made to derive a thermodynamic basis for the different selectivity toward 4e O<sub>2</sub> reduction by two structurally related Cu/Fe porphyrin catalysts ( $\alpha_3$ TREN $\beta$ Im<sub>Alk</sub>)Fe/Cu and ( $\alpha_3$ TACN $\beta$ Im<sub>Alk</sub>)Fe/Cu, (Figure 12 and Table 6, Entries 14 and 17), although it is not entirely clear that Cu is retained in these catalysts during turnover.<sup>67</sup> The authors do not justify the applicability of an equilibrium thermodynamic treatment to an electrochemical transformation occurring at overpotentials in excess of 0.5 V, and it is not apparent why this approach is valid. It appears to be based on an assumption that the sole origin of the overpotential is O<sub>2</sub> binding, which yields a bridging formally peroxo adduct, (por)Fe<sup>III</sup>( $\mu$ -O<sub>2</sub><sup>2-</sup>)Cu<sup>II</sup>(L<sub>N</sub>), whose formation is extremely favorable (pK ~ -33) in the more selective catalyst (( $\alpha_3$ TREN $\beta$ Im<sub>Alk</sub>)Fe/Cu), and substantially less favorable for the less selective analog. Consequently, dissociative decomposition of ( $\alpha_3$ TREN $\beta$ Im<sub>Alk</sub>)Fe–O<sub>2</sub>–Cu with the release of H<sub>2</sub>O<sub>2</sub> is so endergonic that it does not occur to any significant extent even though the catalysis proceeds at potentials close to that of the O<sub>2</sub>/H<sub>2</sub>O<sub>2</sub> couple. While this may be a valid explanation for the difference in the selectivities, it is not supported by experimental data on the nature of the turnover-determining step nor on the relative O<sub>2</sub> affinities of the two complexes (calculated  $\Delta$ pK ~ 28), even under noncatalytic conditions. The conclusions are also weakened by the failure to include the energy of the electrons (which is related to the electrode potential) into the thermodynamic calculations. It thus seems that the relative kinetic and thermodynamic contributions to the selectivity of O<sub>2</sub> reduction catalysis by Fe porphyrins remain an open question.

## V. Cofacial Diporphyrins

Cofacial diporphyrins can be considered as synthetic analogs of the O<sub>2</sub> reduction site in alternative (non heme/Cu) oxidases (see Introduction). In acidic medium, certain cofacial *bis*-Co porphyrins catalytically reduce O<sub>2</sub> with some of the lowest, among molecular electrocatalysts, overpotentials. Cofacial *bismetallodiporphyrins* are one of the very few molecular catalysts definitely displaying bimetallic catalytic cooperativity. As such, these complexes provide important information that may help in a rational design of efficient catalysts for other chemical transformations. Some aspects of cofacial diporphyrin chemistry have been previously reviewed.<sup>197,198</sup>

Cofacial diporphyrins are comprised of two porphyrin macrocycles covalently connected by one to four linkers at *meso* positions, or by two linkers at *trans*  $\beta$ -pyrrolic sites (Figure 18) so as to ensure the face-to-face orientation of the macrocycles. In singly linked cofacial diporphyrins, occasionally referred to as “pillared” diporphyrins, the connecting moiety must be rigid (such as 1,2-phenylene, 1,8-biphenylene, 1,8-anthracene) to restrict rotation of the macrocycles around the axis of the linker. Numerous syntheses of such porphyrins have been reported.<sup>199–204</sup> The molecular structure, and consequently certain chemical properties, depend on the length, the number, and the flexibility of the linkers. Mono- as well as homobi- and heterobimetallic diporphyrins have been studied. When irreversibly adsorbed on an edge-plane graphite electrode in contact with an aqueous electrolyte, several of these complexes are capable of reducing O<sub>2</sub> to H<sub>2</sub>O with a high selectivity at moderate overpotentials (Table 7), although in most cases, O<sub>2</sub> reduction is rather slow. Electrocatalytic reduction of H<sub>2</sub>O<sub>2</sub> is also observed.<sup>205</sup> Although O<sub>2</sub> reduction by cofacial diporphyrins is usually studied only in acidic media (pH 0–2), it appears that the complexes retain their catalytic selectivity at much higher pH (see Section V.C below); this issue, however, has been little studied and literature reports are contradictory.

Cofacial diporphyrins containing at least one Co atom have attracted most attention. The *bis*-Co derivatives are the best catalysts, but as to other metal combinations, there is considerable controversy regarding the nature and the number of metal ions necessary for the 4e activity (see Section V.D below). Electrocatalytic O<sub>2</sub> reduction by homobimetallic diporphyrin complexes of other metals have been studied much less thoroughly; for example, reactivity of



**Figure 18.** Chemical structures and abbreviated names of some cofacial diporphyrins whose metal complexes have been studied as electrocatalysts of  $\text{O}_2$  reduction.

$(\text{DPA})\text{Fe}_2$  appears to be similar to that of simple mononuclear Fe porphyrins (see Section IV.C above).

### A. MOLECULAR STRUCTURE AND PHYSICOCHEMICAL PROPERTIES

The main thrust behind research into cofacial diporphyrins was to develop a catalyst where two metals can simultaneously participate in  $\text{O}_2$  binding and activation. A number of cofacial complexes varying in the intermetallic (M–M) or interplanar (P–P) separations and/or flexibility of the peripheral linkers

connecting the two porphyrin macrocycles (Figure 18) have been studied in this context. In the solid state, the P–P distance depends only slightly on the length of the linker(s), and quite plausibly, is determined by the electronic interactions between the macrocycles ( $\pi$ -stacking). The dominant distortion is the lateral slippage of the two metalloporphyrin moieties, which probably decreases the van der Waals interactions between the two metal ions of the *bimetallic* diporphyrin while maintaining the optimum P–P distance; consequently, the M–M separation varies substantially throughout the series. It is not however known if similar

**Table 7.** Summary of the Relevant Electrocatalytic, Chemical, and Structural Properties of the Selected Cofacial *Biscobaltdiporphyrins*. See Figure 18 for the Relevant Chemical Structures. All Potentials are vs. the Normal Hydrogen Electrode (NHE)

Catalyst (Figure 18)	Group	$E_{\text{cat}}^a$	$E_{1/2}(\text{O}_2), \text{V}$ (pH $\sim 0$ ) <sup>b</sup>	$n_{\text{app}}^c$	M–M/P–P, Å	$[\text{Co}_2(\mu\text{-O}_2)]^{6+ d}$
(FTF4)Co <sub>2</sub>	2	0.86, 0.51	0.7	3.9	3.42/3.54 <sup>236</sup>	yes
(FTF3)Co <sub>2</sub>	2	0.88, 0.58	0.6	$\sim 2$		no?
(FTF4*)Co <sub>2</sub>	2	0.88, 0.59	0.7	$\sim 2$		yes
(FTF5)Co <sub>2</sub>	e	e	0.6	$\sim 3$		yes
(FTF6)Co <sub>2</sub>	1	0.83	0.6	$\sim 2$	6.33/3.87 <sup>f</sup>	no
CoCo4	2	0.93, 0.6	0.7	3.2 – 3.7		yes
CoCo5	2	0.87, 0.54	0.4	2.4	g	yes
(DPB)Co <sub>2</sub>	2	0.88, 0.58	0.7	3.7 – 3.8	3.73/3.81 <sup>204</sup>	yes
(DPA)Co <sub>2</sub>	e	e	0.7	3.7 – 3.8	4.57/3.88 <sup>h</sup>	yes
(DPP)Co <sub>2</sub> <sup>225</sup>	g	0.58 <sup>i</sup>	0.6	3.8	3.85/3.43 <sup>j</sup>	n.r.
(DP <sub>tBu</sub> P)Co <sub>2</sub> <sup>225</sup>			0.4	1.9		n.r.
(DP <sub>F</sub> P)Co <sub>2</sub> <sup>225</sup>			0.4	2.7		n.r.
(DPD)Co <sub>2</sub> <sup>207</sup>	1	0.33 <sup>k</sup>	0.6	3.6	7.78/ <sup>-k</sup>	n.r.
(DPX)Co <sub>2</sub> <sup>207</sup>	2	0.28/0.17 <sup>k</sup>	0.6	3.4	4.58/3.52 <sup>200</sup>	yes
(QATPP1)Co <sub>2</sub> <sup>1</sup>			0.3	3.1	5.0/5.0	n.r.
(QATPP2)Co <sub>2</sub> <sup>1</sup>		0.53	0.3	3.3	5.6/5.5	n.r.
(QATPP3)Co <sub>2</sub> <sup>1</sup>			0.2	2.5	5.2/4.4	n.r.
(QATPP4)Co <sub>2</sub> <sup>1</sup>			0.2	2.6	5.8/5.7	n.r.
(QATPP5)Co <sub>2</sub> <sup>1</sup>			0.1	2.3	5.5/5.3	n.r.

Source: Data are from Ref. 197 unless noted otherwise.

<sup>a</sup>The redox couple ( $[\text{pCo}_2]^{0/+}$  and  $[\text{pCo}_2]^{+/2+}$ ) for the graphite-adsorbed catalyst in the absence of a substrate; n.r. – not reported.

<sup>b</sup>The half-wave potential of the catalytic wave for O<sub>2</sub> reduction at an RDE. This value depends on the electrode rotation rate, bulk O<sub>2</sub> concentration, pH and in many cases on the scan rate, the amount of the adsorbed catalyst and the nature of the supporting electrolyte.

<sup>c</sup>The apparent redox stoichiometry of O<sub>2</sub> reduction at the plateau.

<sup>d</sup>Indicates whether dioxygenated singly reduced diporphyrin forms a bridging superoxo complex; see Section V.B for further details.

<sup>e</sup>For graphite-adsorbed (FTF5)Co<sub>2</sub> a single redox process was reported (at 0.84 V<sup>197</sup>), whereas graphite-adsorbed (DPA)Co<sub>2</sub> manifested two poorly defined waves<sup>224</sup> at 0.87 and 0.57 V. In neither case the number of electrons exchanged is known. In contrast, in benzonitrile solutions reduction of (FTF5)Co<sub>2</sub> proceeds in two single-electron steps (at  $-1.9$  and  $-1.6$  V vs. the ferrocene/ferrocinium (Fc/Fc<sup>+</sup>) couple) and (DPA)Co<sub>2</sub> undergoes a single two-electron redox process at  $\sim -1.6$  V (vs. Fc/Fc<sup>+</sup>)<sup>237</sup>. The measured standard potentials of the Fc/Fc<sup>+</sup> couple (vs. NHE) vary from 0.19 V in acetonitrile to 0.54 V in formamide<sup>238</sup> probably due to variations in the potential of the NHE.<sup>239</sup>

<sup>f</sup>As (FTF6)Cu<sub>2</sub>.<sup>240</sup>

<sup>g</sup>The distances in the structurally analogous *biscopper* dimer having 7-atom linkers are 5.22 and 3.52 Å, respectively.<sup>241</sup>

<sup>h</sup>As (DPA)Ni<sub>2</sub>.<sup>242</sup>

<sup>i</sup>One potential was reported; the number of electrons exchanged was not specified. It seems more plausible that (DPP)Co<sub>2</sub> is a group 2 complex and the 2nd redox wave simply escaped detection.

<sup>j</sup>In the Zn<sub>2</sub> derivative;<sup>201</sup> see also Ref. 243.

<sup>k</sup>Potentials for the graphite-adsorbed catalysts in the absence of O<sub>2</sub> were not reported;  $E_{\text{cat}}$  are for the complexes in C<sub>6</sub>H<sub>5</sub>NO<sub>2</sub> vs. Ag/AgCl. The M–M and P–P values are for (DPD)Zn<sub>2</sub>.<sup>207</sup> the two macrocycles are substantially nonplanar so that the P–P distance is not meaningful.

<sup>l</sup>The M–M and P–P distances are from CHARMM molecular dynamics calculations.<sup>227</sup>

conformations would dominate in a catalyst under steady-state turnover, because formation of intramolecularly bridging O–O intermediates may conceivably compensate for energetically unfavorable steric perturbations and/or less efficient MO interaction of the two porphyrin subunits. The “pillared” diporphyrins appear to be capable of accommodating a wide range of intermetallic separations. In the case of DPD derivatives, these vary from 8.62 Å in (DPD)[Co(OMe)]<sub>2</sub> with the methoxide ligands coordinated inside the cavity, to 7.78 Å in (DPD)Zn<sub>2</sub>, which is free of axial ligands, to 3.50 Å in (DPD)Fe<sub>2</sub>(μ-O).<sup>206,207</sup> Interestingly, the intramolecular bridge in the latter complex appears to be favored thermodynamically over the intermolecular bridge suggesting that only a relatively low-energy distortion of the DPD ligand is necessary to achieve short intermetallic separations. Nonetheless, it is not

apparent to what extent these observations can be used to understand variations in catalytic selectivities of O<sub>2</sub> reduction among *biscobaltdiporphyrins*.

Cofacial diporphyrins are often separated into two groups, based on how much their physicochemical properties (UV/vis, EPR, redox) differ from those expected for monoporphyrins of similar composition. The two macrocycles of group 1 diporphyrin behave independently and similarly to monoporphyrins, whereas those in group 2 analog are electronically coupled and manifest significantly attenuated properties. For example, the Soret bands of group 2 diporphyrins are blueshifted relative to those of monoporphyrins or group 1 analogs. Whereas redox transformations of group 1 diporphyrin derivatives proceed in two-electron steps, those of group 2 analogs are one-electron processes. The electronic structure of group 2

species can be understood in the context of “super-molecular” MOs, which postulates that interactions of the LUMOs and HOMOs of two mutually parallel, closely spaced porphyrins produce new frontier MOs delocalized over both macrocycles.<sup>208,209</sup> Thus, diamagnetism of doubly oxidized group 2 diporphyrins (e.g., [(FTF4)Zn<sub>2</sub>]<sup>2+</sup>)<sup>210</sup> is consistent with removal of an electron pair from a “supermolecular” HOMO. In contrast, the magnetic properties of group 1 metalloporphyrin, [(FTF6)Cu<sub>2</sub>]<sup>2+</sup>, are close to those of non-interacting (por<sup>+</sup>)Cu<sup>II</sup> moieties.

The FTF5 and DPA ligands appear to be borderline and their categorization is controversial; both single two-electron and two one-electron redox couples for oxidation (and/or reduction) have been reported (Table 7). [(FTF5)Zn<sub>2</sub>]<sup>2+</sup> is diamagnetic and by this criterion, FTF5 is a group 2 diporphyrin. The EPR spectrum of [(DPA)Zn<sub>2</sub>]<sup>2+</sup> suggests an equilibrium among S = 1 (ferromagnetically coupled diradical), S = 0 (antiferromagnetically coupled diradical) and S = 1/2 + S = 1/2 (two non interacting radicals) configurations.<sup>210</sup> The situation may arise from both inter- and intramolecular coupling between two singly oxidized macrocycles and is thought to be unique to porphyrin chemistry. This unusual behavior of DPA has not been rationalized, but it was claimed that the anthracene linker is unlikely to be responsible. In this review, FTF5 and DPA derivatives are classified as group 2 porphyrins.

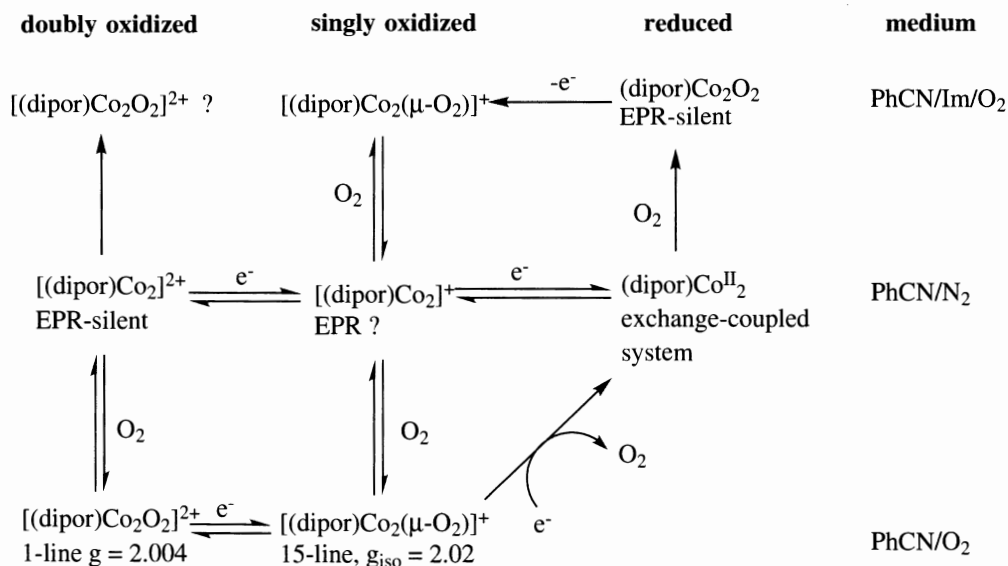
As a result of strong electronic interactions between the two metalloporphyrin units, there is a substantial uncertainty in assigning oxidation states in

mixed-valence group 2 complexes of redox active metals, such as Co. Thus, although reduced neutral Co<sub>2</sub> complexes can be reasonably well described as those of Co<sup>II</sup>, the location (metal vs. porphyrin) of the electron hole(s) in the singly and doubly oxidized derivatives is not known definitively, and may be very sensitive to the medium.<sup>211,212</sup> Possible mixing between frontier porphyrin and metal orbitals, experimentally observed in [(FTF5)Cu<sub>2</sub>]<sup>+</sup>,<sup>212</sup> further complicates the electronic structure of these complexes. Therefore, oxidation state formalism may not always be useful in describing the electronic structure of the mixed-valence group 2 *bismetallodiporphyrins*.

In summary, in the solid state the *bismetallodiporphyrins* without in-cavity bound ligands manifest comparable intramolecular P–P distances, which correlate only weakly with the nature of the linker. In contrast, the latter appears to affect many physicochemical properties of these complexes, so that they can be divided into two categories depending on the degree of the porphyrin-porphyrin interactions: noninteracting (group 1) and strongly interacting (group 2). The physicochemical properties of group 1 *bismetallodiporphyrins* are analogous to those of simple mononuclear metalloporphyrins<sup>212</sup> and will not be discussed further.

## B. NONAQUEOUS DIOXYGEN CHEMISTRY OF GROUP 2 BISCOPALTDIPORPHYRINS

Dioxygen chemistry of group 2 *biscobaltdiporphyrins* (Figure 19) provides a remarkable example of



**Figure 19.** Dioxygen and redox chemistry of group 2 *biscobaltdiporphyrins* in nonaqueous media. The corresponding EPR properties are indicated below the compounds whenever reported. Im–N-methylimidazole, or 1,5-diphenylimidazole; dipor = FTF4, FTF4\*, FTF5, CoCo4, CoCo5, DPX (X = A, B, X).

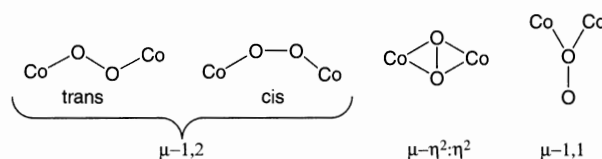
cooperativity and as a result appears to be strikingly different from that of other Group 7–8 metalloporphyrins. The reactivity pattern depends on the interporphyrin and intermetallic separations, as well as on the redox state of the complex. Reduced group 2 *biscobaltdiporphyrins* bind O<sub>2</sub> only in the presence of nitrogenous heterocyclic base, such as imidazole, as do mononuclear Co porphyrins. The diamagnetism of the resulting adducts and the fact that they readily undergo 1e oxidation yielding bridging superoxo derivatives (*vide infra*) are consistent with the formulation of these adduct as intramolecularly bridging peroxo complexes, Co<sup>III</sup>(μ-O<sub>2</sub><sup>2-</sup>)Co<sup>III</sup>.<sup>162,213,214</sup> Despite their diamagnetism, none of these adducts have ever been characterized by NMR.

Although oxidized monomeric Co porphyrins are inert toward O<sub>2</sub>, singly and doubly oxidized group 2 Co<sub>2</sub> derivatives bind O<sub>2</sub> reversibly with unexpectedly high affinities. Even in a noncoordinating solvent (CH<sub>2</sub>Cl<sub>2</sub>), the half-saturation O<sub>2</sub> pressure, p<sub>1/2</sub>(O<sub>2</sub>), for [(DPB)Co<sub>2</sub>]<sup>+</sup> is ~0.2 atm,<sup>204</sup> p<sub>1/2</sub>(O<sub>2</sub>) ~0.01 atm in a weakly coordinating medium (PhCN),<sup>212</sup> whereas in the presence of 1,5-diphenylimidazole (Ph<sub>2</sub>Im) the O<sub>2</sub> adduct could not be deoxygenated.<sup>204</sup> Remarkably, in PhCN p<sub>1/2</sub>(O<sub>2</sub>) for [(FTF4)Co<sub>2</sub>]<sup>+</sup> (0.4 Torr, ~5 × 10<sup>-4</sup> atm), is greater than that of some myoglobins (0.4 – 10 Torr in aqueous buffers).<sup>212</sup> In PhCN, O<sub>2</sub> adducts undergo reversible protonation. It appears reasonably well established that singly oxidized O<sub>2</sub> adducts, [(dipor)Co<sub>2</sub>O<sub>2</sub>]<sup>+</sup> contain bridging superoxide (Figure 19). At room temperature, all these adducts display isotropic or weakly anisotropic EPR signals centered at g ~ 2 with a 15-line superhyperfine splitting indicative of spin coupling to 2 equivalent <sup>57</sup>Co nuclei (nuclear spin 7/2). Collman and coworkers reported that the subtle differences in EPR spectra of [(FTF4)Co<sub>2</sub>(O<sub>2</sub>)]<sup>+</sup> and [(FTF4\*)Co<sub>2</sub>(O<sub>2</sub>)]<sup>+</sup> indicate that the latter complex “has a different, less symmetric configuration” and “the superoxide is preferentially interacting with one of the two cobalt centers,”<sup>214</sup> which presumably explains the puzzlingly different selectivity of O<sub>2</sub> reduction manifested by these two structurally similar complexes. Likewise, under identical conditions the EPR signal of [CoCo5(O<sub>2</sub>)]<sup>+</sup> (n<sub>app</sub> ~ 2.4) is notably more anisotropic than that of [CoCo4(O<sub>2</sub>)]<sup>+</sup> (n<sub>app</sub> > 3.2, Table 7).<sup>213</sup> In contrast, Le Mest and coworkers claimed that the EPR spectra of all dioxygenated group 2 Co<sub>2</sub> porphyrins are very similar: g<sub>iso</sub> = 2.02 (A<sub>iso</sub>, Co = 12 – 14 G), g<sub>||</sub> = 2.09 g<sub>⊥</sub> = 2.00 (A<sub>||</sub> = 15 – 17 G).<sup>212</sup> However, in none of these cases were the experimental EPR spectra simulated computationally nor were donor

atom (O, Co, N) spin densities estimated, so that the interpretation of EPR spectra is somewhat speculative.

In PhCN, doubly oxidized Co<sub>2</sub> group 2 diporphyrins also bind O<sub>2</sub> albeit more weakly than the singly oxidized analogs;<sup>212</sup> the electronic configuration and the O<sub>2</sub> binding mode in the resulting adducts, [(dipor)Co<sub>2</sub>O<sub>2</sub>]<sup>2+</sup> (Figure 19) are least understood. The species was reported<sup>212</sup> to give a single-line EPR spectrum indicative of an S = 1/2 organic radical, but the spin was not quantified. Assuming that the signal does not arise from a minor impurity, it suggests that the O<sub>2</sub> adduct does not contain a doubly oxidized porphyrin, as such species are diamagnetic (e.g., [(FTF4)Zn<sub>2</sub>]<sup>2+</sup>, [(FTF5)Zn<sub>2</sub>]<sup>2+</sup>, [(DPB)Zn<sub>2</sub>]<sup>2+</sup> as are other *bisporphyrin* systems with a “supermolecular” HOMO: [(TPP)<sub>2</sub>Th]<sup>2+</sup>, [(TPP)<sub>2</sub>U]<sup>2+</sup>, and [(OEP)<sub>2</sub>Zr]<sup>2+</sup> (P–P = 3.1 Å)<sup>208,209</sup>. The [(dipor)Co<sub>2</sub>O<sub>2</sub>]<sup>2+</sup> adduct is an even-electron system and must have two unpaired electrons to be EPR active, but the ground state electronic configuration is unknown.

There is a major controversy over which of the three possible bridging modes (Figure 20) is realized in the [(dipor)Co<sub>2</sub>O<sub>2</sub>]<sup>+</sup> adducts. It is generally argued that the Co···Co separation in (FTF4)Co<sub>2</sub> is insufficient to accommodate the μ-1,2 O<sub>2</sub><sup>-</sup> ligand without a substantial distortion of the porphyrin ligand. Although the Co···Co distances in complexes with the μ-superoxo moiety as the only bridging ligand are indeed over 1 Å greater than those in (FTF4)Co<sub>2</sub> (3.42 Å),<sup>215,216</sup> in a very stable μ-superoxo complex, [Co<sub>2</sub>(μ-OH)(μ-O<sub>2</sub>)(μ-NH<sub>2</sub>)(NH<sub>3</sub>)<sub>6</sub>](NO<sub>3</sub>)<sub>3</sub>, the Co<sup>3+</sup> cations are only 2.78 Å apart.<sup>217</sup> The Co···Co distances in between these two extremes are known in doubly bridged analogs.<sup>218</sup> Since FTF4 as a bridging ligand, the Co···Co distance in (FTF4)Co<sub>2</sub> is apparently sufficient to accommodate the *cis*-μ-1,2-O<sub>2</sub><sup>-</sup> moiety, although this binding mode may be precluded by other stereochemical and/or electronic factors. The intermetallic separation arguments are even less persuasive in the DPB and DPP series owing to the apparent capacity of these ligands to accommodate a wide range of Co···Co distances relative to those observed in the solid-state structures of the fully reduced complexes (see Section V.A above). Moreover, if the



**Figure 20.** Possible bridging binding modes of superoxide in *biscobaltdiporphyrins*.

lateral displacement of the macrocycles in DPY (Y = A and to a lesser degree B, P) complexes seen in the solid state (see Section V.A above) is retained in the O<sub>2</sub> adducts the often suggested<sup>212</sup>  $\mu-\eta^2:\eta^2$  binding mode is not possible for geometric reasons.

Unambiguous identification of the O<sub>2</sub><sup>-</sup> binding mode could not be derived from resonance Raman studies of a dioxygenated cofacial diporphyrin similar to (FTF4)Co<sub>2</sub> and of (DPA)Co<sub>2</sub>O<sub>2</sub>.<sup>219</sup> The O–O stretching frequencies,  $\nu(\text{O}_2)$ , of these adducts in CH<sub>2</sub>Cl<sub>2</sub> are very similar: 1081 cm<sup>-1</sup> and 1085 cm<sup>-1</sup>, respectively, despite the different solid-state stereochemistry of the parent (deoxygenated) complexes. These values are comparable to those in dibridged, [(NH<sub>3</sub>)<sub>8</sub>Co<sub>2</sub>( $\mu$ -O<sub>2</sub>)( $\mu$ -NH<sub>2</sub>)]<sup>4+</sup> adducts containing a  $\mu$ -1,2-O<sub>2</sub><sup>-</sup> moiety,<sup>220</sup> but are lower than the  $\nu\text{OO}$  observed in monobridged [L<sub>8</sub>Co<sub>2</sub>( $\mu$ -O<sub>2</sub>)]<sup>5+</sup> complexes (~1100–1125 cm<sup>-1</sup>; L – various neutral ligands).<sup>221</sup> Although no unambiguous examples of CoO<sub>2</sub> units containing a side-on O<sub>2</sub> moiety are known, the  $\nu\text{OO}$  value of side-on O<sub>2</sub> in (TPP)FeO<sub>2</sub> is 89 cm<sup>-1</sup> lower than that in the end-on isomer (1195 vs. 1106 cm<sup>-1</sup>).<sup>222</sup> Finally,  $\nu\text{CoO}$  in (DPA)Co<sub>2</sub>O<sub>2</sub> complex (~628 cm<sup>-1</sup> in CH<sub>2</sub>Cl<sub>2</sub>) is again comparable to those in [(NH<sub>3</sub>)<sub>8</sub>Co<sub>2</sub>( $\mu$ -O<sub>2</sub>)( $\mu$ -NH<sub>2</sub>)]<sup>4+</sup>.<sup>220</sup>

Extended Hückel MO calculations were used to justify the  $\mu-\eta^2:\eta^2$  binding mode (Figure 20) of the dioxygen ligand in [(FTF4)Co<sub>2</sub>O<sub>2</sub>]<sup>2+/+</sup>,<sup>212</sup> although the system is too complex for the result to be reliable. Hoffman and Tatsumi reported<sup>223</sup> that side-on O<sub>2</sub> binding between two d<sup>n</sup>-d<sup>n</sup> metalloporphyrin units (n > 3) is electronically less favorable than the conventional *trans*  $\mu$ -1,2 bridging mode. These calculations, however did not consider possible steric restrictions posed by the bridging diporphyrin.

Dioxygen chemistry of (FTF3)Co<sub>2</sub> complex is different from that of the other group 2 metalloporphyrins, which may be related to the short interporphyrin separation of the FTF3 ligand. Exposure of a (FTF3)Co<sub>2</sub> solution to air in the presence of excess *N*-methylimidazole yields an EPR silent sample, which remains diamagnetic upon addition of I<sub>2</sub>.<sup>214</sup> It was proposed that (FTF3)Co<sub>2</sub> may have no affinity to O<sub>2</sub> under the experimental conditions and cannot be oxidized with I<sub>2</sub>, thereby remaining fully reduced (and presumably anti-ferromagnetically coupled) throughout the manipulations. Alternatively, O<sub>2</sub> binding outside the cavity followed by formation of an intermolecular  $\mu$ -peroxo complex and its decomposition (possibly assisted by the excess imidazole and moisture) can eventually yield a doubly oxidized diamagnetic [(FTF3)Co<sub>2</sub>]<sup>2+</sup>. These possibilities have not been studied and the origin of the

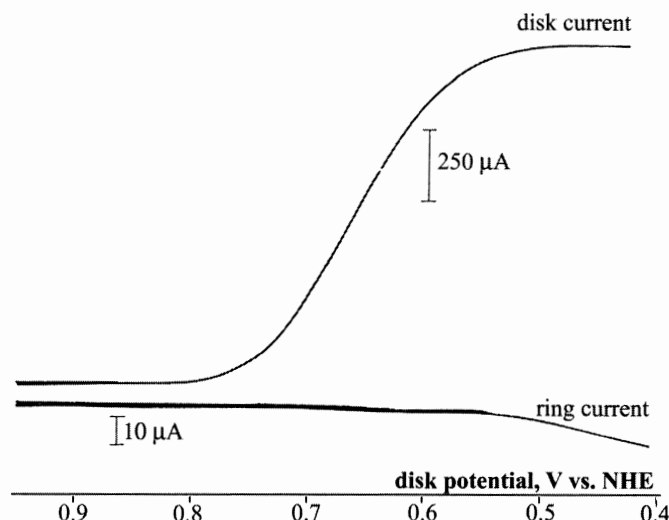
distinct behavior of (FTF3)Co<sub>2</sub> remains somewhat speculative.

In summary, cooperative behavior of the two metal ions determines dioxygen chemistry of group 2 *bis*-Co porphyrins. Unlike monoporphyrin analogs, which bind O<sub>2</sub> only in the reduced (Co<sup>II</sup>) axially ligated form, singly oxidized *bis*cobaltdiporphyrins manifest unusually high O<sub>2</sub> affinities even in the absence of nitrogenous heterocycles. In all studied cases, O<sub>2</sub> binding to singly oxidized group 2 porphyrins (except FTF3) yields bridging  $\mu$ -superoxo adducts, although at present binding mode(s) of the  $\mu$ -O<sub>2</sub><sup>-</sup> moiety is unknown. Whereas O<sub>2</sub> adducts of monometalloporphyrins rapidly autoxidize in the presence of protic sources, [(FTF4)Co<sub>2</sub>(O<sub>2</sub>)]<sup>+</sup> undergoes reversible protonation.

### C. ELECTROCATALYTIC O<sub>2</sub> REDUCTION

Mainly 2e reduction of O<sub>2</sub> to H<sub>2</sub>O<sub>2</sub> catalyzed by group 1 porphyrins likely proceeds via a mechanism similar to that of simple monometallic porphyrins. At sufficiently large M–M separations, there is little or no interaction between the O<sub>2</sub> moiety bound to one Co and the other metal ion, as manifested, for example, by the EPR spectrum of [Co<sub>2</sub>FTF6(O<sub>2</sub>)]<sup>+</sup>.<sup>212</sup> The lack of bimetallic cooperativity is also the most probable reason for exclusive 2e O<sub>2</sub> reduction by a group 2 porphyrin (FTF3)Co<sub>2</sub>, wherein bridging O<sub>2</sub> adducts cannot form due to the too short Co···Co separation. Other group 2 *bis*cobalt porphyrins electrochemically reduce O<sub>2</sub> mostly to H<sub>2</sub>O ( $n_{\text{app}} \approx 4$ : (FTF4)Co<sub>2</sub><sup>197</sup> and (DPY)Co<sub>2</sub> (Y = B, A,<sup>224</sup> P,<sup>225</sup> D<sup>206</sup>), Table 7, Figure 21) or to a mixture of H<sub>2</sub>O and H<sub>2</sub>O<sub>2</sub> ( $n_{\text{app}} \approx 3$ : (FTF5)Co<sub>2</sub>,<sup>197</sup> CoCo4,<sup>213</sup> (DPX)Co<sub>2</sub>,<sup>206</sup> (QATPP1)Co<sub>2</sub> and (QATPP2)-Co<sub>2</sub>,<sup>226,227</sup>).

The high selectivity of (DPY)Co<sub>2</sub> (Y = P, D, A, B) catalysts, despite the different geometry and length of their linkers, may be attributable to the wider range of the M–M distances energetically accessible in these complexes.<sup>200,206</sup> The stereoelectronic effects of the porphyrin peripheral substitution on the selectivity are illustrated in the DPP-DP<sub>tBu</sub>P-DP<sub>F</sub>P series ( $n_{\text{app}} \sim 3.8, 1.9, 2.7$ , respectively).<sup>225</sup> Formation of bridging O<sub>2</sub> adducts of (DP<sub>tBu</sub>P)Co<sub>2</sub>, presumably necessary for the 4e activity, may require sterically unfavorable proximity of the *bis*(*t*-butyl)phenyl groups. The poor selectivity of the (DP<sub>F</sub>P)Co<sub>2</sub> catalyst, whose perfluorophenyl substituents' steric requirements are unlikely to differ notably from those of the *p*-tolyl moieties in DPP, may illustrate the importance of electronic factors, such as the energy of the porphyrin HOMOs. Interestingly, a capacity to carry out



**Figure 21.** A typical linear sweep voltammogram of  $O_2$  reduction at a rotating ring-disk electrode bearing (FTF4)Co<sub>2</sub> in  $O_2$ -saturated 0.5 M trifluoroacetic acid; 100 rpm electrode rotation. Adapted from Collman, J. P.; Anson, F. C.; Barnes, C. E.; Bencosme, C. S.; Geiger, T.; Evitt, E. R.; Kreh, R. P.; Meier, K.; Pettman, R. B. *J. Am. Chem. Soc.* **1983**, *105*, 2694; reprinted by permission; © the American Chemical Society, 1983.

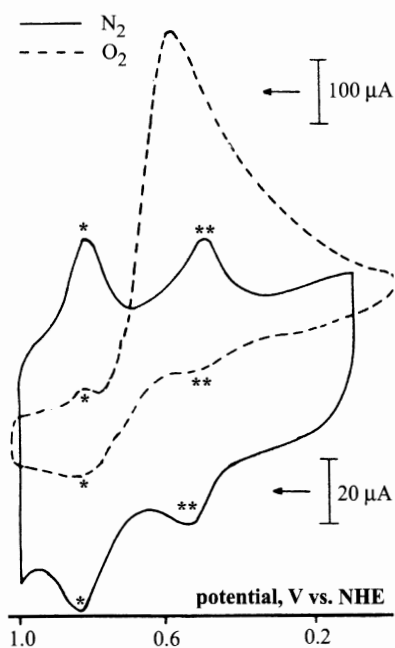
only 2e  $O_2$  reduction by the Co complex of the DPA phthalocyanine analog<sup>228</sup> was suggested to arise from similar electronic perturbations.<sup>210</sup> In contrast, monochlorination of (FTF4)Co<sub>2</sub> at a *meso* position decreases the overpotential of  $O_2$  reduction by ~40 mV and notably increases catalytic selectivity at the plateau.<sup>229</sup> No rationalization has been proposed.

The origin of the poor selectivity of (FTF4\*)Co<sub>2</sub>, (FTF5)Co<sub>2</sub>, CoCo4, CoCo5 ( $n_{app} < 3$ ; Table 7), which are structurally analogous to the most selective biscobaltdiporphyrin-based  $O_2$  reduction catalyst, (FTF4)Co<sub>2</sub> is not obvious. Indeed, all five complexes bind  $O_2$  in nonaqueous medium exclusively in a bridging fashion (forming  $\mu$ -peroxo or  $\mu$ -superoxo derivatives, depending on the oxidation state, see Section V.B above) and their electrochemical properties in the absence of a substrate (Table 7) suggest that the two macrocycles are in a close proximity to display bimetallic cooperativity.

The QATPP-type catalysts<sup>226,227</sup> are inferior to (FTF4)Co<sub>2</sub> and (DPY)Co<sub>2</sub> (Y = A, B, D, P) in terms of both the overpotential and selectivity of  $O_2$  reduction (Table 7). Interestingly, however, there seems to be an inverse correlation between the strength of the porphyrin–porphyrin interactions within the molecule and its catalytic selectivity. Thus, oxidation in DMF of the nonmetalated porphyrin, corresponding to the best catalyst in the series, (QATPP1)Co<sub>2</sub>, proceeds in a single two-electron step (weakly interacting macrocycles), whereas the porphyrin of the less selective catalyst, (QATPP3)Co<sub>2</sub> is oxidized in two one-electron steps (strong macrocycle interaction).

Little is known about the mechanism of  $O_2$  reduction even in the case of best studied catalysts, (FTF4)Co<sub>2</sub> and (DPY)Co<sub>2</sub> (Y = A, B). The catalysis starts at potentials between those of the [(dipor)Co<sub>2</sub>]<sup>2+/+</sup> and [(dipor)Co<sub>2</sub>]<sup>+0</sup> pairs observed under anaerobic conditions. In conjunction with the high  $O_2$  affinity of [(dipor)Co<sub>2</sub>]<sup>+</sup> observed in nonaqueous medium, the onset of  $O_2$  reduction is commonly interpreted to indicate that the [(dipor)Co<sub>2</sub>]<sup>+</sup> is the catalytically active redox state at potentials of the rising part of the  $O_2$  reduction wave. The change of the dominant redox form of the catalyst from [(dipor)Co<sub>2</sub>]<sup>+</sup> to (dipor)Co<sub>2</sub> at ~500 mV was suggested to account for the decrease in the catalytic selectivity (Figure 21), because the reduced catalyst is presumed to be more prone to binding  $O_2$  outside the cavity and thus reducing it in a non-cooperative fashion.

These hypotheses, however, remain largely speculative, mainly because the characteristically high  $O_2$  affinity of [(dipor)Co<sub>2</sub>]<sup>+</sup>, observed in nonaqueous weakly coordinating medium, may not be retained in an aqueous buffer. For example, the position of the [(dipor)Co<sub>2</sub>]<sup>2+/+</sup> redox wave is identical for the catalyst in contact with anaerobic and aerobic buffer (Figure 22) indicating that under these conditions the [(dipor)Co<sub>2</sub>O<sub>2</sub>]<sup>+</sup> adduct does not form, at least on the timescale of the electrochemical scan. This is in contrast to dramatic differences in CVs of (FTF4)Co<sub>2</sub> solutions in anhydrous PhCN under anaerobic and aerobic conditions,<sup>230</sup> indicative of rapid  $O_2$  binding and of [(FTF4)Co<sub>2</sub>]<sup>+</sup> having much higher  $O_2$  affinity than either (FTF4)Co<sub>2</sub> or [(FTF4)Co<sub>2</sub>]<sup>2+</sup>.  $O_2$  binding to

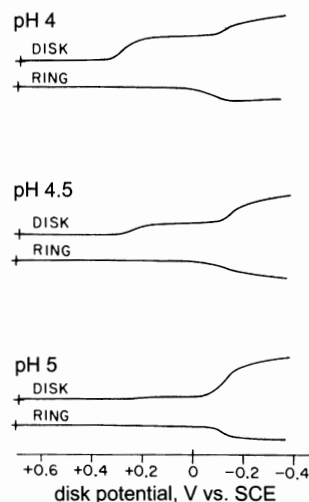


**Figure 22.** The relation between the onset of catalytic  $\text{O}_2$  reduction by  $(\text{FTF4})\text{Co}_2$  (broken line, 10 mV/s scan rate) and the redox potential of the immobilized catalyst in anaerobic electrolyte (solid line, 100 mV/s scan rate; 0.5 M trifluoroacetic acid).  $[(\text{FTF4})\text{Co}_2]^{2+/+}$  and  $[(\text{FTF4})\text{Co}_2]^{+/0}$  redox waves are indicated by \* and \*\*, respectively

$[(\text{dipor})\text{Co}_2]^+$  in contact with an aqueous buffer is likely destabilized by the *bis*aqua coordination of  $\text{Co}^{\text{III}}$ .

The observation that the  $\text{O}_2$  catalysis starts at more oxidative potentials than that of the  $(\text{dipor})\text{Co}_2^{+/0}$  couple under anaerobic conditions does not rule out  $(\text{dipor})\text{Co}_2$  as the catalytically active redox form, as partitioning between  $[(\text{dipor})\text{Co}_2]^+$  and  $(\text{dipor})\text{Co}_2$  in a redox equilibrium is affected by the reactivities of both redox forms with  $\text{O}_2$  (compare, for example,  $\text{Fe}^{\text{III/II}}$  potentials under anaerobic conditions and the half-wave potential of  $\text{O}_2$  reduction waves in Tables 5 and 6). Likewise, alternative explanations are plausible for a decreasing catalytic selectivity at more reducing potentials, but they remain speculative in the absence of experimental data.

The half-wave potentials of  $(\text{FTF4})\text{Co}_2$ -mediated  $\text{O}_2$  reduction at pH 0–3 shifts by  $-60 \text{ mV/pH}$ ,<sup>231</sup> which indicates that the turnover-determining part of the catalytic cycle contains a reversible electron transfer (ET) and a protonation step, or two reversible ETs and two protonation steps. In contrast, if an ET step was irreversible, the pH gradient would be  $60/(n+\alpha) \text{ mV/pH}$ , where  $n$  is the number of electrons transferred in redox equilibria prior to the irreversible ET and  $\alpha$  is the transfer coefficient of the latter. The  $-60 \text{ mV/pH}$  gradient is identical to that manifested by simple Fe porphyrins. A more thorough analysis of the pH dependence requires the knowledge of whether the



**Figure 23.** Linear sweep voltammetry of  $\text{O}_2$  reduction by  $(\text{FTF4})\text{Co}_2$  in contact with unbuffered electrolytes. Reprinted by permission from Durand, R. R., Jr.; Bencosme, C. S.; Collman, J. P.; Anson, F. C. *J. Am. Chem. Soc.* **1983**, *105*, 2710; © the American Chemical Society, 1983.

catalytic rate at the rising part of the wave is substrate-dependent (or the catalyst is saturated with  $\text{O}_2$ ) and is thus not possible at present.

In unbuffered pH 4–5 electrolytes, two catalytic waves are observed (Figure 23);<sup>231</sup> the overall catalytic selectivity at the earlier wave being substantially higher than that of the second one. The currents of the more positive wave are apparently limited by proton mass-transport. Assuming that the second wave does not arise from background  $\text{O}_2$  reduction at graphite electrode, it indicates an increase in the turnover frequency of the catalyst at  $-100 \text{ mV}$  and suggests that  $\text{O}_2$  reduction may proceed via two different mechanisms possibly having different proton stoichiometry. This phenomenon partially explains the controversial literature reports on the pH dependence of catalytic selectivity of *bis*cobaltdiporphyrins. The selectivity of electrocatalytic  $\text{O}_2$  reduction by  $(\text{DPA})\text{Co}_2$  was studied in buffered electrolytes and was reported to be almost pH-independent in the range 0–10.<sup>224</sup> In contrast, the properties of  $(\text{FTF4})\text{Co}_2$  were studied in unbuffered solutions, and the complex was found to be largely a 2e catalyst at pH > 2.<sup>231</sup> This difference is most likely due to the use (or nonuse) of buffers and does not reflect the intrinsic differences in catalytic behavior of the two catalysts. It thus appears likely, that selectivity of  $\text{O}_2$  reduction by *bis*cobaltdiporphyrins like that by Fe porphyrins is nearly pH-independent in buffered electrolytes.

The catalytic activity of *bis*cobaltdiporphyrins appears to be significantly affected by the electrode material. For example, a thiolated analog of  $(\text{DPB})\text{Co}_2$ ,



(DPB<sub>S</sub>)Co<sub>2</sub> (Figure 18), reduces O<sub>2</sub> by an average of ~3.6 electrons when deposited on EPG, but only by ~2.4 electrons when chemisorbed on Au.<sup>232</sup> The result was interpreted as an indication that oxygenated functionalities of the EPG surface provide the necessary ligation to Co. It is not clear if the smaller amount of the active catalyst on a smoother Au surface relative to that of the EPG may contribute to the observed result, for example through faster degradation of the catalytic film.

#### D. CATALYTIC PROPERTIES OF MONOCOBALTDIPORPHYRINS CONTAINING A NONREDOX ACTIVE CATION WITH STRONG LEWIS ACIDITY

Studies of heterobimetallic as well as monocobalt cofacial diporphyrins were motivated in large part by the idea that “the <4e> pathway requires only one redox active <metal center>, but that a Lewis acid center must be present at the oxygen binding site.”<sup>233</sup> This is reminiscent of the effect of hydrogen bonding on the stability and reactivity of O<sub>2</sub> ligands in certain heme proteins.<sup>168</sup> Thus, in myoglobin and hemoglobin, hydrogen bonding from a distal imidazole to both atoms of the coordinated O<sub>2</sub> prevents Fe–O bond heterolysis, thereby *stabilizing* the adduct against autoxidation.<sup>170</sup> In contrast, in catalases and peroxidases, a hydrogen bond only to the distal O atom *facilitates* O–O bond heterolysis in the heme-bound hydroperoxo ligand (so called “pull” effect).<sup>168</sup> It thus seems conceivable that a Lewis acid center may either stabilize a peroxo intermediate against dissociation, or facilitate the O–O bond activation and/or cleavage, depending on the binding mode of the dioxygen ligand ( $\mu\text{-}\eta^2, \eta^2$  or  $\mu\text{-}1,2$ , respectively, Figure 20).

A monometallic complex, (H<sub>2</sub>DPA)Co, manifested remarkably high selectivity at pH = 0 (Table 8) even

though its activity appears to degrade very rapidly during turnover; at higher pH, however, the complex is a substantially 2e catalyst. It was suggested that at low pH, the complex is present largely in the protonated form, [(H<sub>3</sub>DPA)Co]<sup>+</sup>, and protons of the nonmetalated macrocycle “prevent the premature dissociation of, as well as assist in proton transfer to, the partially reduced O<sub>2</sub> coordinated to the cobalt center in the second porphyrin ring.”<sup>224</sup> The selectivity of (H<sub>2</sub>FTF4)Co is somewhat poorer but still well above that of simple (por)Co. The hypothesis that distal protons account for this high selectivity is, however, inconsistent with the observation that Co derivatives of monoporphyrins containing organic moieties with acidic protons at distances approximately similar to that of nonmetalated macrocycle of (H<sub>2</sub>FTF4)Co or (H<sub>2</sub>DPA)Co are largely 2e catalysts.<sup>234</sup>

There seems to be a significant controversy regarding the selectivities of heterobimetallic diporphyrins (Table 8). The literature reports appear to agree that CoCu and CoMn derivatives of both FTF4 and the DPY series (Y = A, B except the unstudied (DPB)CoCu) are 2e catalysts. In contrast, whereas (DPA)CoFe complex was claimed to be as good a catalyst as the monometallic analog, (H<sub>2</sub>DPA)Co, others report that it reduces O<sub>2</sub> only to H<sub>2</sub>O<sub>2</sub> (Entry 3).<sup>235</sup> (DPB)CoFe and (FTF4)CoFe also seem to be poor catalysts. Likewise, catalytic selectivities of (FTF4)CoAl and (DPY)CoAl (Y = A, B), reported by different groups, are strikingly different. Among the heterobimetallic diporphyrins studied to date, (DPA)CoLu and (DPA)CoSc appear to be most selective catalysts, although it is entirely unclear what structural and/or electronic properties of these complexes are responsible for this behavior. It thus remains to be seen whether or under what conditions, a Lewis acid “helper” ion may be sufficient to engender the 4e activity.

**Table 8.** Summary of the Redox Stoichiometry of Electrocatalytic O<sub>2</sub> Reduction by Heterobimetallic Cofacial Diporphyrins

Entry	FTF4 series	$n_{\text{app}}$	DPA series <sup>234</sup>	$n_{\text{app}}$	DPY (Y = A, B) series <sup>235</sup>	$n_{\text{app}}$
1	CoH <sub>2</sub>	3	CoH <sub>2</sub>	3.5		
2	CoCu	2	CoCu	2		
3	CoFe	2.4	CoFe	3.6, 4	CoFe	2
4	CoAl	3			CoAl	2
5	CoMn	2			CoMn	2
6			CoLu <sup>235</sup>	3.7	CoLu(DPB)	2
7	CoAg <sup>231</sup>	3	CoSc <sup>235</sup>	3.7	CoGa	2
8	CoPd	3			CoTi=O	2
9					CoIn	2

Source: Collman, J.P.; Wagenknecht, P.S.; Hutchison, J.E.; *Angew. Chem. Int. Ed. Eng.* **1994**, *33*, 1537, unless noted otherwise.

### E. SUMMARY

Alternative (non-heme/Cu) quinol oxidases are widely distributed among prokaryotes.<sup>6</sup> Little structural information about such enzymes is, however, available. Two most-likely five-coordinate hemes (hemes b and d) are located within the same binding pocket, in close proximity to each other, possibly at the distance that allows formation of a CN<sup>-</sup> bridge. O<sub>2</sub> binding to ferroheme d is established, but the functional role of heme b remains highly controversial. Electrocatalytic O<sub>2</sub> reduction by cofacial diporphyrins clearly demonstrates a possibility of cooperative bimetallic catalysis within a system of two closely spaced metalloporphyrins. While these results pertain mostly to the *biscobalt* derivatives, and the poorly studied Fe<sub>2</sub> analogs appear to manifest no cooperativity, the latter may be caused by the abiological axial ligation of the ferrous centers. Recent progress in synthesis of both cofacial diporphyrins and superstructured monoporphyrins (see Sections II.A and V) may allow the development of a diporphyrin bearing covalently attached axial ligands. Because of their relatively high thermal and chemical stability, cofacial diporphyrins can be metallated with late transition metals, even though such reactions require somewhat more demanding conditions. Bimetallic cooperativity in such complexes may allow catalysis of “difficult” transformations, e.g. nitrogen fixation.

## VI. Summary and Outlook

A great deal of creative effort has been expended in designing, synthesizing, and studying functional and structural models of heme/copper terminal oxidases. Such work has provided a significant body of new information relevant to understanding the chemistry of, and structure/function relationship within, the Fe/Cu catalytic site. This is especially apparent for structural and spectroscopic studies of the fully oxidized heme a<sub>3</sub>/Cu<sub>B</sub> pair.

The design of biomimetic analogs of ever-closer structural similarity to CcO is a continuing area of endeavor. Of note is the absence of studies with bimetallic complexes containing an analog to the histidyl-tyrosine linkage (Figure 3). Inclusion of such a redox active, protic group will certainly add complexity to the chemical behavior of these Fe/Cu models. Before such an advance can be fruitful, a more thorough knowledge of the mechanism of dioxygen binding to, and reduction by, the existing models would be of great benefit. Structural characterization

of binuclear complexes is rare, and no crystallographic data for any of the handful of “stable” peroxide intermediates has been obtained. This may be required to unambiguously assign the binding motif of Fe/O<sub>2</sub>/Cu adducts.

Recent studies have highlighted the importance of  $\mu$ -peroxo Fe/Cu intermediates, and this certainly reflects significant aspects of heme/Cu dioxygen chemistry. However, the focus on uncovering “stable” Fe/Cu bridged peroxides is somewhat dated. The initial inspiration to synthesize “stable” peroxo-bridged complexes lay in the assumption that the P intermediate (Figure 4) was indeed a  $\mu$ -peroxo compound. As this hypothesis has been disproved, it may be better to focus on designing Fe/Cu systems where [Fe<sup>III</sup>O<sub>2</sub><sup>-</sup>...Cu<sup>I</sup>], the analog of intermediate A (Figure 4), is stabilized. With a spatially close, but redox-stable cuprous center, the structural and mechanistic roles of Cu<sub>B</sub> can be probed with more relevant biomimetic complexes.

Although redox cooperativity among the redox cofactors of CcO and the redox control of O<sub>2</sub> binding to the heme a<sub>3</sub>/Cu<sub>B</sub> site have not been targets for biomimetic studies, they are critical for the high selectivity of O<sub>2</sub> reduction manifested by the enzyme.

Development of methodologies to better mimic steady-state O<sub>2</sub> reduction at the heme a<sub>3</sub>/Cu<sub>B</sub> site of CcO under physiologically relevant conditions is probably the most interesting and most challenging area of biomimetic studies of the enzyme. One conceivable direction is multiple-turnover homogeneous catalysis wherein the catalyst, the substrate (O<sub>2</sub> or H<sub>2</sub>O<sub>2</sub>), and the reductant are in one phase. The preferably water-soluble catalysts for such studies must be designed so as to prevent involvement of more than one catalyst molecule in reduction of a single O<sub>2</sub> molecule. Bimolecular processes to be eliminated include not only formation of (por)Fe–O<sub>2</sub>–Fe(por) intermediates but also electron transfer between catalyst molecules and two-step 4e O<sub>2</sub> reduction proceeding via the intermediacy of free H<sub>2</sub>O<sub>2</sub>. Since assaying the selectivity of such homogeneous catalysis voltammetrically is probably impossible, new techniques to detect production of free H<sub>2</sub>O<sub>2</sub> (possibly based on H<sub>2</sub>O<sub>2</sub> scavengers) must be developed.

To date, steady-state O<sub>2</sub> reduction at the heme a<sub>3</sub>/Cu<sub>B</sub> site has been modeled by electrocatalytic O<sub>2</sub> reduction using synthetic analogs deposited on electrode surfaces. As currently practiced, this approach suffers from serious drawbacks (see Section IV.A), which limits the contribution of functional heme a<sub>3</sub>/Cu<sub>B</sub> analogs to

understanding the mechanism of O<sub>2</sub> reduction by the enzyme. To be more biologically relevant, electrocatalytic O<sub>2</sub> reduction needs to be studied at isolated catalytic centers under conditions of limited electron availability during turnover.<sup>160a</sup> This can be achieved, for example, by diluting a biomimetic catalyst in an inert matrix at an electrode surface, wherein it has sufficient mobility to diffuse to and from electrode. Such studies can be based on existing catalysts and electrochemical techniques (rotating disk voltammetry and rotating ring-disk electrode). A more ambitious goal is incorporating biomimetic catalysts into self-assembled monolayers (SAMs) on a gold electrode. This would provide a better-defined chemical environment relative to that in a film at the surface of a graphite electrode. In addition, it would allow control over the rate of electron transfer from the electrode to the catalytic site, thereby mimicking temporal control of electron delivery to the heme a<sub>3</sub>/Cu<sub>B</sub> site as a result of diffusional reaction between cytochrome oxidase and ferrocycytochrome *c* *in vivo*. However, novel cytochrome oxidase model compounds functionalized for incorporation into SAMs are required.

Finally, a true synthetic analog of a heme/Cu oxidase must act as a proton pump. Since the process is based on spatial separation of protons, mimicking it requires well-defined three-dimensional assemblies on nano- or micrometer scale. Due to the challenges in creating such assemblies and a poorly understood molecular basis for directional movement of protons against an electrochemical gradient by CcO, modeling the proton pumping capacity of cytochrome oxidase is probably a far-in-the-future target.

#### ACKNOWLEDGMENTS

J.P.C. thanks his coworkers cited in the appropriate references for their invaluable contributions to biomimetic studies of cytochrome oxidase in his labs. Financial support from the NIH and NSF (J.P.C.) and a Stanford Graduate Fellowship (R.B.) are gratefully acknowledged.

#### REFERENCES

- Garciahorsman, J. A.; Barquera, B.; Rumbley, J.; Ma, J. X.; Gennis, R. B. *J. Bacteriol.* **1994**, *176*, 5587.
- Saraste, M.; Holm, L.; Lemieux, L.; Lubben, M.; Vanderoost, J. *Biochem. Soc. Trans.* **1991**, *19*, 608.
- Ferguson-Miller, S.; Babcock, G. T. *Chem. Rev.* **1996**, *96*, 2889.
- Einarsdottir, O. *Biochim. Biophys. Acta* **1995**, *1229*, 129.
- Pereira, M. M.; Santana, M.; Teixeira, M. *Biochim. Biophys. Acta* **2001**, *1505*, 185.
- Junemann, S. *Biochim. Biophys. Acta* **1997**, *1321*, 107.
- Tsukihara, T.; Aoyama, H.; Yamashita, E.; Tomizaki, T.; Yamaguchi, H.; ShinzawaItoh, K.; Nakashima, R.; Yaono, R.; Yoshikawa, S. *Science* **1995**, *269*, 1069.
- Tsukihara, T.; Aoyama, H.; Yamashita, E.; Tomizaki, T.; Yamaguchi, H.; ShinzawaItoh, K.; Nakashima, R.; Yaono, R.; Yoshikawa, S. *Science* **1996**, *272*, 1136.
- Yoshikawa, S.; ShinzawaItoh, K.; Nakashima, R.; Yaono, R.; Yamashita, E.; Inoue, N.; Yao, M.; Fei, M. J.; Libeu, C. P.; Mizushima, T.; Yamaguchi, H.; Tomizaki, T.; Tsukihara, T. *Science* **1998**, *280*, 1723.
- Iwata, S.; Ostermeier, C.; Ludwig, B.; Michel, H. *Nature* **1995**, *376*, 660.
- Ostermeier, C.; Harrenga, A.; Ermler, U.; Michel, H. *Proc. Natl. Acad. Sci. USA* **1997**, *94*, 10547.
- Abramson, J.; Svensson-Ek, M.; Byrne, B.; Iwata, S. *Biochim. Biophys. Acta* **2001**, *1544*, 1.
- Herrnga, A.; Michel, H. *J. Biol. Chem.* **1999**, *274*, 33296.
- Fann, Y. C.; Ahmed, I.; Blackburn, N. J.; Boswell, J. S.; Verkhovskaya, M. L.; Hoffman, B. M.; Wikstrom, M. *Biochemistry* **1995**, *34*, 10245.
- Mochizuki, M.; Aoyama, H.; ShinzawaItoh, K.; Usui, T.; Tsukihara, T.; Yoshikawa, S. *J. Biol. Chem.* **1999**, *274*, 33403.
- Soulimane, T.; Buse, G.; Bourenkov, G. P.; Bartunik, H. D.; Huber, R.; Than, M. E. *EMBO J.* **2000**, *19*, 1766.
- Abramson, J.; Riistama, S.; Larsson, G.; Jasaitis, A.; Svensson-Ek, M.; Laakkonen, L.; Puustinen, A.; Iwata, S.; Wikstrom, M. *Nature Struct. Biol.* **2000**, *7*, 910.
- Morgan, J. E.; Verkhovskiy, M. I.; Palmer, G.; Wikstrom, M. *Biochemistry* **2001**, *40*, 6882.
- Malmstrom, B. G. *Chem. Rev.* **1990**, *90*, 1247.
- Michel, H.; Behr, J.; Harrenga, A.; Kannt, A. *Annu. Rev. Biophys. Biomol. Str.* **1998**, *27*, 329.
- Michel, H. *Biochemistry* **1999**, *38*, 15129.
- Babcock, G. T. *Proc. Natl. Acad. Sci. USA* **1999**, *96*, 12971.
- Kitagawa, T. *J. Inorg. Biochem.* **2000**, *82*, 9.
- Liebl, U.; Lipowski, G.; Negrerie, M.; Lambry, J. C.; Martin, J. L.; Vos, M. H. *Nature* **1999**, *401*, 181.
- Alben, J. O.; Moh, P. P.; Fiamingo, F. G.; Altschuld, R. A. *Proc. Natl. Acad. Sci. USA* **1981**, *78*, 234.
- Fiamingo, F. G.; Altschuld, R. A.; Moh, P. P.; Alben, J. O. *J. Biol. Chem.* **1982**, *257*, 1639.
- Einarsdottir, O.; Dyer, R. B.; Lemon, D. D.; Killough, P. M.; Hubig, S. M.; Atherton, S. J.; Lopezgarriga, J. J.; Palmer, G.; Woodruff, W. H. *Biochemistry* **1993**, *32*, 12013.
- Iwase, T.; Varotsis, C.; ShinzawaItoh, K.; Yoshikawa, S.; Kitagawa, T. *J. Am. Chem. Soc.* **1999**, *121*, 1415.
- Blackmore, R. S.; Greenwood, C.; Gibson, Q. H. *J. Biol. Chem.* **1991**, *266*, 19245.
- Oliveberg, M.; Malmstrom, B. G. *Biochemistry* **1991**, *30*, 7053.
- Oliveberg, M.; Malmstrom, B. G. *Biochemistry* **1992**, *31*, 3560.
- Bailey, J. A.; James, C. A.; Woodruff, W. H. *Biochem. Biophys. Res. Commun.* **1996**, *220*, 1055.
- Mogi, T.; Hirano, T.; Nakamura, H.; Anraku, Y.; Orii, Y. *FEBS Lett.* **1995**, *370*, 259.
- Fabian, M.; Wong, W. W.; Gennis, R. B.; Palmer, G. *Proc. Natl. Acad. Sci. USA* **1999**, *96*, 13114.
- Proshlyakov, D. A.; Pressler, M. A.; Babcock, G. T. *Proc. Natl. Acad. Sci. USA* **1998**, *95*, 8020.
- Gennis, R. B. *Biochim. Biophys. Acta* **1998**, *1365*, 241.
- Proshlyakov, D. A.; Pressler, M. A.; DeMaso, C.; Leykam, J. F.; DeWitt, D. L.; Babcock, G. T. *Science* **2000**, *290*, 1588.
- Hill, B. C. *J. Biol. Chem.* **1994**, *269*, 2419.

39. Han, S.; Takahashi, S.; Rousseau, D. L. *J. Biol. Chem.* **2000**, *275*, 1910.
40. Morgan, J. E.; Verkhovskiy, M. I.; Wikstrom, M. *Biochemistry* **1996**, *35*, 12235.
41. Sucheta, A.; Szundi, I.; Einarsdottir, O. *Biochemistry* **1998**, *37*, 17905.
42. Ogura, T.; Hirota, S.; Proshlyakov, D. A.; Shinzawa-Ittoh, K.; Yoshikawa, S.; Kitagawa, T. *J. Am. Chem. Soc.* **1996**, *118*, 5443.
43. Blomberg, M. R. A.; Siegbahn, P. E. M.; Babcock, G. T.; Wikstrom, M. *J. Am. Chem. Soc.* **2000**, *122*, 12848.
44. See for example: Sono, M.; Roach, M. P.; Coulter, E. D.; Dawson, J. H. *Chem. Rev.* **1996**, *96*, 2841.
45. Hirota, S.; Mogi, T.; Ogura, T.; Hirano, T.; Anraku, Y.; Kitagawa, T. *FEBS Lett.* **1994**, *352*, 67.
46. Mills, D. A.; Florens, L.; Hiser, C.; Qian, J.; Ferguson-Miller, S. *Biochim. Biophys. Acta* **2000**, *1458*, 180.
47. Behr, J.; Michel, H.; Mantele, W.; Hellwig, P. *Biochemistry* **2000**, *39*, 1356.
48. Verkhovskiy, M. I.; Jasaitis, A.; Verkhovskaya, M. L.; Morgan, J. E.; Wikstrom, M. *Nature* **1999**, *402*, 603.
49. Michel, H. *Nature* **1999**, *402*, 602.
50. Scott, M. J.; Lee, S. C.; Holm, R. H. *Inorg. Chem.* **1994**, *33*, 4651.
51. Scott, M. J.; Holm, R. H. *J. Am. Chem. Soc.* **1994**, *116*, 11357.
52. Scott, M. J.; Zhang, H. H.; Lee, S. C.; Hedman, B.; Hodgson, K. O.; Holm, R. H. *J. Am. Chem. Soc.* **1995**, *117*, 568.
53. Scott, M. J.; Goddard, C. A.; Holm, R. H. *Inorg. Chem.* **1996**, *35*, 2558.
54. Lee, S. C.; Holm, R. H. *J. Am. Chem. Soc.* **1993**, *115*, 11789.
55. Lee, S. C.; Holm, R. H. *J. Am. Chem. Soc.* **1993**, *115*, 5833.
56. Lee, S. C.; Holm, R. H. *Inorg. Chem.* **1993**, *32*, 4745.
57. Lim, B. S.; Holm, R. H. *Inorg. Chem.* **1998**, *37*, 4898.
58. Karlin, K. D.; Nanthakumar, A.; Fox, S.; Murthy, N. N.; Ravi, N.; Huynh, B. H.; Orosz, R. D.; Day, E. P. *J. Am. Chem. Soc.* **1994**, *116*, 4753.
59. Corsi, D. M.; Murthy, N. N.; Young, V. G.; Karlin, K. D. *Inorg. Chem.* **1999**, *38*, 848.
60. Kopf, M. A.; Neuhold, Y. M.; Zuberbuhler, A. D.; Karlin, K. D. *Inorg. Chem.* **1999**, *38*, 3093.
61. Sasaki, T.; Nakamura, N.; Naruta, Y. *Chem. Lett.* **1998**, 351.
62. Buckingham, D. A.; Gunter, M. J.; Mander, L. N. *J. Am. Chem. Soc.* **1978**, *100*, 2899.
63. Martens, C. F.; Murthy, N. N.; Obias, H. V.; Karlin, K. D. *Chem. Commun.* **1996**, 629.
64. Obias, H. V.; vanStrijdonck, G. P. F.; Lee, D. H.; Ralle, M.; Blackburn, N. J.; Karlin, K. D. *J. Am. Chem. Soc.* **1998**, *120*, 9696.
65. Collman, J. P.; Herrmann, P. C.; Boitrel, B.; Zhang, X. M.; Eberspacher, T. A.; Fu, L.; Wang, J. L.; Rousseau, D. L.; Williams, E. R. *J. Am. Chem. Soc.* **1994**, *116*, 9783.
66. Andrioletti, B.; Ricard, D.; Boitrel, B. *New J. Chem.* **1999**, *23*, 1143.
67. Collman, J. P.; Fu, L.; Herrmann, P. C.; Wang, Z.; Rapta, M.; Broring, M.; Schwenninger, R.; Boitrel, B. *Angew. Chem., Int. Ed. Engl.* **1998**, *37*, 3397.
68. Collman, J. P.; Fu, L.; Herrmann, P. C.; Zhang, X. M. *Science* **1997**, *275*, 949.
69. Kopf, M. A.; Karlin, K. D. *Inorg. Chem.* **1999**, *38*, 4922.
70. Saxton, R. J.; Olson, L. W.; Wilson, L. J. *J. Chem. Soc., Chem. Comm.* **1982**, 984.
71. Naruta, Y.; Sasaki, T.; Tani, F.; Tachi, Y.; Kawato, N.; Nakamura, N. *J. Inorg. Biochem.* **2001**, *83*, 239.
72. Tani, F.; Matsumoto, Y.; Tachi, Y.; Sasaki, T.; Naruta, Y. *Chem. Commun.* **1998**, 1731.
73. Ghiladi, R. A.; Ju, T. D.; Lee, D. H.; Moenne-Loccoz, P.; Kaderli, S.; Neuhold, Y. M.; Zuberbuhler, A. D.; Woods, A. S.; Cotter, R. J.; Karlin, K. D. *J. Am. Chem. Soc.* **1999**, *121*, 9885.
74. Ju, T. D.; Ghiladi, R. A.; Lee, D. H.; vanStrijdonck, G. P. F.; Woods, A. S.; Cotter, R. J.; Young, V. G.; Karlin, K. D. *Inorg. Chem.* **1999**, *38*, 2244.
75. Walker, F. A.; Benson, M. J. *Am. Chem. Soc.* **1980**, *102*, 5530.
76. Collman, J. P.; Brauman, J. I.; Doxsee, K. M.; Halbert, T. R.; Bunnenberg, E.; Linder, R. E.; Lamar, G. N.; Delgaudio, J.; Lang, G.; Spartalian, K. *J. Am. Chem. Soc.* **1980**, *102*, 4182.
77. Landrum, J. T.; Grimmett, D.; Haller, K. J.; Scheidt, W. R.; Reed, C. A. *J. Am. Chem. Soc.* **1981**, *103*, 2640.
78. Collman, J. P.; Zhong, M.; Wang, Z.; Rapta, M.; Rose, E. *Org. Lett.* **1999**, *1*, 2121.
79. Collman, J. P.; Gagne, R. R.; Reed, C.; Halbert, T. R.; Lang, G.; Robinson, W. T. *J. Am. Chem. Soc.* **1975**, *97*, 1427.
80. Gunter, M. J.; Mander, L. N.; Murray, K. S.; Clark, P. E. *J. Am. Chem. Soc.* **1981**, *103*, 6784.
81. Collman, J. P.; Brauman, J. I.; Collins, T. J.; Iverson, B. L.; Lang, G.; Pettman, R. B.; Sessler, J. L.; Walters, M. A. *J. Am. Chem. Soc.* **1983**, *105*, 3038.
82. Baeg, J. O.; Holm, R. H. *Chem. Commun.* **1998**, 571.
83. Ricard, D.; L'Her, M.; Richard, P.; Boitrel, B. *Chem. Eur. J.* **2001**, *7*, 3291.
84. (a) Collman, J. P.; Boitrel, B.; Fu, L.; Galanter, J.; Straumanis, A.; Rapta, M. *J. Org. Chem.* **1997**, *62*, 2308. (b) Collman, J. P.; Broring, M.; Fu, L.; Rapta, M.; Schwenninger, R.; Straumanis, A. *J. Org. Chem.* **1998**, *63*, 8082.
85. Lindsey, J. J. *J. Org. Chem.* **1980**, *45*, 5215.
86. (a) Casella, L.; Monzani, E.; Gullotti, M.; Gliubich, F.; Degioia, L. *J. Chem. Soc. Dalton Trans.* **1994**, 3203. (b) Monzani, E.; Casella, L.; Gullotti, M.; Panigada, N.; Franceschi, F.; Papaefthymiou, V. *J. Mol. Catal.* **1997**, *117*, 199.
87. Gunter, M. J.; Mander, L. N.; Murray, K. S. *J. Chem. Soc., Chem. Comm.* **1981**, 799.
88. Chang, C. K.; Koo, M. S.; Ward, B. *J. Chem. Soc., Chem. Comm.* **1982**, 716.
89. Lukas, B.; Miller, J. R.; Silver, J.; Wilson, M. T.; Morrison, I. E. *G. J. Chem. Soc., Dalton Trans.* **1982**, 1035.
90. Elliott, C. M.; Akabori, K. *J. Am. Chem. Soc.* **1982**, *104*, 2671.
91. Serr, B. R.; Headford, C. E. L.; Elliott, C. M.; Anderson, O. P. *J. Chem. Soc., Chem. Comm.* **1988**, 92.
92. Serr, B. R.; Headford, C. E. L.; Anderson, O. P.; Elliot, C. M.; Schauer, C. K.; Akabori, K.; Spartalian, K.; Hatfield, W. E.; Rohrs, B. R. *Inorg. Chem.* **1990**, *29*, 2663.
93. Serr, B. R.; Headford, C. E. L.; Anderson, O. P.; Elliott, C. M.; Spartalian, K.; Fainzilberg, V. E.; Hatfield, W. E.; Rohrs, B. R.; Eaton, S. S.; Eaton, G. R. *Inorg. Chem.* **1992**, *31*, 5450.
94. Gunter, M. J.; Mander, L. N.; McLaughlin, G. M.; Murray, K. S.; Berry, K. J.; Clark, P. E.; Buckingham, D. A. *J. Am. Chem. Soc.* **1980**, *102*, 1470.
95. Berry, K. J.; Clark, P. E.; Gunter, M. J.; Murray, K. S. *New J. Chem.* **1980**, *4*, 581.
96. Dessens, S. E.; Merrill, C. L.; Saxton, R. J.; Ilaria, R. L.; Lindsey, J. W.; Wilson, L. J. *J. Am. Chem. Soc.* **1982**, *104*, 4357.
97. Saxton, R. J.; Wilson, L. J. *J. Chem. Soc., Chem. Comm.* **1984**, 359.
98. Chunplang, V.; Wilson, L. J. *J. Chem. Soc., Chem. Comm.* **1985**, 1761.
99. Brewer, C. T.; Brewer, G. A. *Inorg. Chem.* **1987**, *26*, 3420.
100. Koch, C. A.; Reed, C. A.; Brewer, G. A.; Rath, N. P.; Scheidt, W. R.; Gupta, G.; Lang, G. *J. Am. Chem. Soc.* **1989**, *111*, 7645.
101. Wang, R.; Brewer, G. *Inorg. Chim. Acta* **1993**, *206*, 117.
102. Elliott, C. M.; Jain, N. C.; Cranmer, B. K.; Hamburg, A. W. *Inorg. Chem.* **1987**, *26*, 3655.
103. Van Gelder, B. F. *Biochim. Biophys. Acta* **1969**, *189*, 1.
104. Reed, C. A.; Landrum, J. T. *FEBS Lett.* **1979**, *106*, 265.
105. Caughey, W. S. *Adv. Chem. Ser.* **1971**, *100*, 248.

106. Nanthakumar, A.; Fox, S.; Murthy, N. N.; Karlin, K. D.; Ravi, N.; Huynh, B. H.; Orosz, R. D.; Day, E. P.; Hagen, K. S.; Blackburn, N. J. *J. Am. Chem. Soc.* **1993**, *115*, 8513.
107. Fox, S.; Nanthakumar, A.; Wikstrom, M.; Karlin, K. D.; Blackburn, N. J. *J. Am. Chem. Soc.* **1996**, *118*, 24.
108. Zhang, H. H.; Filipponi, A.; DiCicco, A.; Lee, S. C.; Scott, M. J.; Holm, R. H.; Hedman, B.; Hodgson, K. O. *Inorg. Chem.* **1996**, *35*, 4819.
109. Scheidt, W. R.; Cheng, B.; Safo, M. K.; Cukiernik, F.; Marchon, J. C.; Debrunner, P. G. *J. Am. Chem. Soc.* **1992**, *114*, 4420.
110. Henkel, G.; Muller, A.; Weissgraber, S.; Buse, G.; Soulimane, T.; Steffens, G. C. M.; Nolting, H. F. *Angew. Chem., Int. Ed. Eng.* **1995**, *34*, 1488.
111. Kauffmann, K. E.; Goddard, C. A.; Zang, Y.; Holm, R. H.; Munck, E. *Inorg. Chem.* **1997**, *36*, 985.
112. Walker, F. A.; Simonis, U. In *NMR of Paramagnetic Molecules*. Berliner, L. J., Reuben, J., Eds.; Plenum Press: New York, **1993**; Vol. 12.
113. Goff, H. M. In *NMR of Paramagnetic Molecules*. Gray, H. B., Lever, A. B. P., Eds.; Addison Wesley: Reading, MA, **1983**; Vol. 1.
114. Palmer, G. *J. Bioenerg. Biomembr.* **1993**, *25*, 145.
115. Slebodnick, C.; Fettingner, J. C.; Peterson, H. B.; Ibers, J. A. *J. Am. Chem. Soc.* **1996**, *118*, 3216.
116. Babcock, G. T.; Vickery, L. E.; Palmer, G. *J. Biol. Chem.* **1976**, *251*, 7907.
117. Kent, T. A.; Young, L. J.; Palmer, G.; Fee, J. A.; Munck, E. *J. Biol. Chem.* **1983**, *258*, 8543.
118. Thomson, A. J.; Johnson, M. K.; Greenwood, C.; Gooding, P. E. *Biochem. J.* **1981**, *193*, 687.
119. Thomson, A. J.; Englinton, D. G.; Hill, B. C.; Greenwood, C. *Biochem. J.* **1982**, *207*, 167.
120. Hill, B. C.; Brittain, T.; Englinton, D. G.; Gadsby, P. M. A.; Greenwood, C.; Nicholls, P.; Peterson, J.; Thomson, A. J.; Woon, T. C. *Biochem. J.* **1983**, *215*, 57.
121. Kent, T. A.; Munck, E.; Dunham, W. R.; Filter, W. F.; Findling, K. L.; Yoshida, T.; Fee, J. A. *J. Biol. Chem.* **1982**, *257*, 2489.
122. Babcock, G. T.; Callahan, P. M.; Ondrias, M. R.; Salmeen, I. *Biochemistry* **1981**, *20*, 959.
123. Scheidt, W. R.; Lee, Y. J.; Luangdilok, W.; Haller, K. J.; Anzai, K.; Hatano, K. *Inorg. Chem.* **1983**, *22*, 1516.
124. Gunter, M. J.; Berry, K. J.; Murray, K. S. *J. Am. Chem. Soc.* **1984**, *106*, 4227.
125. Caughey, W. S.; Dong, A.; Sampath, V.; Yoshikawa, S.; Zhao, X. J. *J. Bioenerg. Biomembr.* **1993**, *25*, 81.
126. Tsubaki, M.; Yoshikawa, S. *Biochemistry* **1993**, *32*, 164.
127. Yoshikawa, S.; Mochizuki, M.; Zhao, X. J.; Caughey, W. S. *J. Biol. Chem.* **1995**, *270*, 4270.
128. Moody, A. J. *Biochim. Biophys. Acta* **1996**, *1276*, 6.
129. Brudvig, G. W.; Stevens, T. H.; Morse, R. H.; Chan, S. I. *Biochemistry* **1981**, *20*, 3912.
130. Baker, G. M.; Palmer, G. *Biochemistry* **1987**, *26*, 3038.
131. Baker, G. M.; Noguchi, M.; Palmer, G. *J. Biol. Chem.* **1987**, *262*, 595.
132. Moody, A. J.; Cooper, C. E.; Rich, P. R. *Biochim. Biophys. Acta* **1991**, *1059*, 189.
133. Tweedle, M. F.; Wilson, L. J.; Garciaainiguez, L.; Babcock, G. T.; Palmer, G. *J. Biol. Chem.* **1978**, *253*, 8065.
134. Moss, T. H.; Shapiro, E.; King, T. E.; Beinert, H.; Hartzell, C. *J. Biol. Chem.* **1978**, *253*, 8072.
135. Barnes, Z. K.; Babcock, G. T.; Dye, J. L. *Biochemistry* **1991**, *30*, 7597.
136. Day, E. P.; Peterson, J.; Sendova, M. S.; Schoonover, J.; Palmer, G. *Biochemistry* **1993**, *32*, 7855.
137. Watmough, N. J.; Cheesman, M. R.; Gennis, R. B.; Greenwood, C.; Thomson, A. J. *FEBS Lett.* **1993**, *319*, 151.
138. Collman, J. P.; Sunderland, C. J.; Boulatov, R. *Inorg. Chem.* **2002**, *41*, 2282.
139. Ray, G. B.; Li, X. Y.; Ibers, J. A.; Sessler, J. L.; Spiro, T. G. *J. Am. Chem. Soc.* **1994**, *116*, 162.
140. Spiro, T. G.; Kozlowski, P. M. *Acc. Chem. Res.* **2001**, *34*, 137.
141. Park, K. D.; Guo, K.; Adebodun, F.; Chiu, M. L.; Sligar, S. G.; Oldfield, E. *Biochemistry* **1991**, *30*, 2333.
142. Calhoun, M. W.; Hill, J. J.; Lemieux, L. J.; Ingledew, W. J.; Alben, J. O.; Gennis, R. B. *Biochemistry* **1993**, *32*, 11524.
143. Hosler, J. P.; Kim, Y. K.; Shapleigh, J.; Gennis, R.; Alben, J.; Ferguson-Miller, S.; Babcock, G. *J. Am. Chem. Soc.* **1994**, *116*, 5515.
144. Uno, T.; Mogi, T.; Tsubaki, M.; Nishimura, Y.; Anraku, Y. *J. Biol. Chem.* **1994**, *269*, 11912.
145. Chin, D. H.; Lamar, G. N.; Balch, A. L. *J. Am. Chem. Soc.* **1980**, *102*, 4344.
146. Bag, N.; Chern, S. S.; Peng, S. M.; Chang, C. K. *Inorg. Chem.* **1995**, *34*, 753.
147. Sasaki, T.; Naruta, Y. *Chem. Lett.* **1995**, 663.
148. Thrash, T. P.; Wilson, L. J. *Inorg. Chem.* **2001**, *40*, 4556.
149. Franceschi, F.; Gullotti, M.; Monzani, E.; Casella, L.; Papaefthymiou, V. *Chem. Commun.* **1996**, 1645.
150. Ghiladi, R. A.; Hatwell, K. R.; Karlin, K. D.; Huang, H. W.; Moenne-Loccoz, P.; Krebs, C.; Huynh, B. H.; Marzilli, L. A.; Cotter, R. J.; Kaderli, S.; Zuberbuhler, A. D. *J. Am. Chem. Soc.* **2001**, *123*, 6183.
151. Bertini, I.; Gray, H. B.; Lippard, S. J.; Valentine, J. S. *Bioinorganic Chemistry*. University Science Books: Mill Valley, CA, **1994**.
152. Nanthakumar, A.; Fox, S.; Murthy, N. N.; Karlin, K. D. *J. Am. Chem. Soc.* **1997**, *119*, 3898.
153. Root, D. E.; Mahroof-Tahir, M.; Karlin, K. D.; Solomon, E. I. *Inorg. Chem.* **1998**, *37*, 4838.
154. Schindler, S. *Eur. J. Inorg. Chem.* **2000**, 2311.
155. Naruta, Y.; Sasaki, T.; Nakamura, N.; Kawato, N.; Tani, F.; Tachi, Y. *J. Inorg. Biochem.* **1999**, *74*, 43.
156. Bard, A. J.; Faulkner, L. R. *Electrochemical Methods*. Wiley: New York, **2001**.
157. Opekar, F.; Beran, P. *J. Electroanal. Chem.* **1976**, *69*, 1.
158. Andrieux, C. P.; Saveant, J.-M. In *Molecular Design of Electrode Surfaces*. Murray, R. W., Ed.; Wiley: New York, **1992**; pp. 207-270.
159. Boulatov, R.; Collman, J. P.; Shiryayeva, I. M.; Sunderland, C. J. *J. Am. Chem. Soc.* **2002**, *124*, in press.
160. (a) Collman, J. P.; Boulatov, R. *Angew. Chem., Int. Ed. Eng.* **2002**, *41*, in press. (b) Shiryayeva, I. M.; Collman, J. P.; Boulatov, R.; Sunderland, C. J. *Anal. Chem.* **2002**, submitted. (c) Collman, J. P.; Boulatov, R.; Shiryayeva, I. M.; Sunderland, C. J. *Angew. Chem., Int. Ed. Eng.* **2002**, *41*, in press.
161. Song, E.; Shi, C.; Anson, F. C. *Langmuir* **1998**, *14*, 4315; see Figure 6B.
162. Collman, J. P.; Denisevich, P.; Konai, Y.; Marrocco, M.; Koval, C.; Anson, F. C. *J. Am. Chem. Soc.* **1980**, *102*, 6027.
163. Rich, P. R.; Moody, A. J. In *Bioenergetics*. Graber, P., Milazzo, G., Eds.; Birkhauser: Basel, **1997**; Vol. 4; pp. 418-456.
164. Verkhovsky, M. I.; Morhan, J. E.; Wikstrom, M. *Biochemistry* **1995**, *34*, 7483.
165. Wan, G.-X.; Shigehara, K.; Tsuchida, E.; Anson, F. C. *J. Electroanal. Chem.* **1984**, *179*, 239.
166. Forshey, P. A.; Kuwana, T. *Inorg. Chem.* **1983**, *22*, 699.
167. Nam, W.; Han, H. J.; Oh, S.-Y.; Lee, Y. J.; Choi, M.-H.; Han, S.-Y.; Kim, C.; Woo, S. K.; Shin, W. *J. Am. Chem. Soc.* **2000**, *122*, 8677 and references therein.
168. Watanabe, Y. In *The Porphyrin Handbook*. Kadish, K. M., Smith, K. M., Guillard, R., Eds.; Academic Press: Boston, **2000**; Vol. 4, pp. 97-117.

169. Taube, H. *Prog. Inorg. Chem.* **1986**, *34*, 607.
170. Shikama, K. *Chem. Rev.* **1998**, *98*, 1357.
171. Siegbahn, P. E. M.; Blomberg, M. R. A. *Chem. Rev.* **2000**, *100*, 421.
172. Loew, G. H.; Harris, D. L. *Chem. Rev.* **2000**, *100*, 407.
173. Egawa, T.; Shimada, H.; Ishimura, Y. *J. Biol. Chem.* **2000**, *275*, 34858.
174. See for example Marusak, R. A.; Mears, C. F. In *Active Oxygen in Biochemistry*. Valentine, J. S., Foote, C. S., Greenberg, A., Liebman, J. E., Eds.; Chapman: New York, **1995**, on relative stabilities of Fe<sup>III</sup>-OOH and Co<sup>III</sup>-OOH adducts in bleomycins.
175. See for example Weiss, R.; Mandon, D.; Wolter, T.; Trautwein, A. X.; Muther, M.; Bill, E.; Gold, A.; Jayaraj, K.; Terner, J. *J. Biol. Inorg. Chem.* **1996**, *1*, 377–383 and references therein.
176. Kobayashi, N.; Nishiyama, Y. *J. Electroanal. Chem.* **1984**, *181*, 107.
177. Shi, C.; Anson, F. C. *Inorg. Chem.* **1990**, *29*, 4298.
178. Shigehara, K.; Anson, F. C. *J. Phys. Chem.* **1982**, *86*, 2776.
179. Bettelheim, A.; Parash, R.; Ozer, D. *J. Electrochem. Soc.* **1982**, *129*, 2247.
180. Kobayashi, N.; Osa, T. *J. Electroanal. Chem.* **1983**, *157*, 269.
181. Oyaizu, K.; Haryono, A.; Natori, J.; Shinoda, H.; Tsuchida, E. *Bull. Chem. Soc. Jpn.* **2000**, *73*, 1153.
182. Loetzbecker, T.; Schuhmann, W.; Schmidt, H.-L. *J. Electroanal. Chem.* **1995**, *395*, 339.
183. Su, Y. O.; Kuwana, T.; Chen, S. M. *J. Electroanal. Chem.* **1990**, *288*, 177.
184. Anderson, A. B.; Albu, T. V. *J. Am. Chem. Soc.* **1999**, *121*, 11855.
185. Kalish, H. R.; Latos-Grazynski, L.; Balch, A. L. *J. Am. Chem. Soc.* **2000**, *122*, 12478.
186. Cunningham, I. D.; Danks, T. N.; O'Connell, K. T. A.; Scott, P. W. *J. Chem. Soc., Perkin Trans. 2* **1999**, 2133.
187. Huie, R. E.; Neta, P. In *Reactive Oxygen Species in Biological Systems*. Gilbert, D. L., Colton, C. A., Eds.; Kluwer: New York, **1999**; pp. 33–77.
188. Cabelli, D. E. In *Peroxy Radicals*. Alfassi, Z. B., Ed.; Wiley: New York, **1997**; pp. 407–437.
189. Foote, C. S.; Valentine, J. S.; Greenberg, A.; Liebman, J. E. *Active Oxygen in Chemistry*. Chapman: New York, **1995**; chapters 1, 3.
190. Pasternack, R. F.; Halliwell, B. *J. Am. Chem. Soc.* **1979**, *101*, 1026.
191. Ricard, D.; Didier, A.; L'Her, M.; Boitrel, B. *Chembiochem* **2001**, *2*, 144.
192. Ricard, D.; Andrioletti, B.; M, L. H.; Boitrel, B. *Chem. Commun.* **1999**, 1523.
193. Collman, J. P.; Rapta, M.; Broring, M.; Raptova, L.; Schwenninger, R.; Boitrel, B.; Fu, L.; M, L. H. *J. Am. Chem. Soc.* **1999**, *121*, 1387.
194. Collman, J. P.; Schwenninger, R.; Rapta, M.; Broring, M.; Fu, L. *Chem. Commun.* **1999**, 137.
195. See for example data in Zaslavsky, D.; Gennis, R. B. *Biochim. Biophys. Acta* **2000**, *1458*, 164.
196. Collman, J. P.; Berg, K.; Sunderland, C. J.; Shiryayeva, I. *Inorg. Chem.* **2002**, manuscript in preparation.
197. Collman, J. P.; Wagenknecht, P. S.; Hutchison, J. E. *Angew. Chem., Int. Ed. Engl.* **1994**, *33*, 1537 (small-molecule activation).
198. Barbe, J. M.; Guillard, R. In *The Porphyrin Handbook*. Kadish, K. M., Smith, K. M., Guillard, R., Eds.; Academic Press: Boston, **2000**; Vol. 3, pp. 211–244 (selected physicochemical properties of heterobimetallic biporphyrins).
199. Fletcher, J. T.; Therien, M. J. *J. Am. Chem. Soc.* **2000**, *122*, 12393.
200. Chang, C. J.; Deng, Y.; Heyduk, A. F.; Chang, C. K.; Nocera, D. G. *Inorg. Chem.* **2000**, *39*, 959.
201. Osuka, A.; Nakajima, S.; Nagata, T.; Maruyama, K.; Toriumi, K. *Angew. Chem., Int. Ed. Engl.* **1991**, *30*, 582.
202. Clement, T. E.; Nurco, D. J.; Smith, K. M. *Inorg. Chem.* **1998**, *37*, 1150.
203. Harriman, A.; Sauvage, J. P. *Chem. Soc. Rev.* **1996**, *25*, 41.
204. Collman, J. P.; Hutchison, J. E.; Lopez, M. A.; Tabard, A.; Guillard, R.; Seok, W. K.; Ibers, J. A.; L'Her, M. *J. Am. Chem. Soc.* **1992**, *114*, 9869.
205. Collman, J. P.; Hendricks, N. H.; Leidner, C. R.; Ngameni, E.; L'Her, M. *Inorg. Chem.* **1988**, *27*, 387.
206. Chang, C. J.; Deng, Y.; Nocera, D. G.; Shi, C.; Anson, F. C.; Chang, C. K. *Chem. Commun.* **2000**, 1355.
207. Deng, Y.; Chang, C. J.; Nocera, D. G. *J. Am. Chem. Soc.* **2000**, *122*, 410.
208. Girolami, G. S.; Milam, S. N.; Suslick, K. S. *J. Am. Chem. Soc.* **1988**, *110*, 2011.
209. Girolami, G. S.; Gorlin, P. A.; Milam, S. N.; Suslick, K. S.; Wilson, S. R. *J. Coord. Chem.* **1994**, *32*, 173.
210. Le Mest, Y.; L'Her, M.; Hendricks, N. H.; Kim, K.; Collman, J. P. *Inorg. Chem.* **1992**, *31*, 835.
211. Le Mest, Y.; L'Her, M.; Saillard, J. Y. *Inorg. Chim. Acta* **1996**, *248*, 181.
212. Le Mest, Y.; Inisan, C.; Laouenan, A.; L'Her, M.; Talarmin, J.; El Khalifa, M.; Saillard, J.-Y. *J. Am. Chem. Soc.* **1997**, *119*, 6095.
213. Liu, H. Y.; Weaver, M. J.; Wang, C. B.; Chang, C. K. *J. Electroanal. Chem.* **1983**, *145*, 439.
214. Collman, J. P.; Bencosme, C. S.; Barnes, C. E.; Miller, B. D. *J. Am. Chem. Soc.* **1983**, *105*, 2704.
215. Bernhardt, P. V.; Lawrance, G. A.; Hambley, T. W. *J. Chem. Soc., Dalton Trans.* **1990**, 235 (~ 4.6 Å in (LCO)<sub>2</sub>(μ-O<sub>2</sub>), where L is a tetradentate polyamine ligand).
216. Fronczek, F. R.; Schaefer, W. P.; Marsh, R. E. *Inorg. Chem.* **1975**, *14*, 611 (4.64 Å in Co<sub>2</sub>(CN)<sub>10</sub>(μ-O<sub>2</sub>)K<sub>5</sub>).
217. Spingler, B.; Scanavy-Grigorieff, M.; Werner, A.; Berke, H.; Lippard, S. J. *Inorg. Chem.* **2001**, *40*, 1065.
218. Christoph, G. G.; Marsh, R. E.; Schaefer, W. P. *Inorg. Chem.* **1969**, *8*, 291 (3.24 Å in [Co<sub>2</sub>(NH<sub>3</sub>)<sub>8</sub>(μ-O<sub>2</sub>)(μ-NH<sub>2</sub>)](NO<sub>3</sub>)<sub>4</sub>).
219. Proniewicz, L. M.; Odo, J.; Goral, J.; Chang, C. K.; Nakamoto, K. *J. Am. Chem. Soc.* **1989**, *111*, 2105.
220. Barraclough, C. G.; Lawrance, G. A.; Lay, P. A. *Inorg. Chem.* **1978**, *17*, 3317.
221. Streckas, T. C.; Spiro, T. G. *Inorg. Chem.* **1975**, *14*, 1421.
222. Proniewicz, L. M.; Paeng, I. R.; Nakamoto, K. *J. Am. Chem. Soc.* **1991**, *113*, 3294.
223. Tatsumi, K.; Hoffman, R. *J. Am. Chem. Soc.* **1981**, *103*, 3328.
224. Liu, H. Y.; Abdalmuhdi, I.; Chang, C. K.; Anson, F. C. *J. Phys. Chem.* **1985**, *89*, 665.
225. Park, G. J.; Nakajima, S.; Osuka, A.; Kim, K. *Chem. Lett.* **1995**, 255.
226. Jeon, S.; Almarsson, O.; Karaman, R.; Blasko, A.; Bruce, T. C. *Inorg. Chem.* **1993**, *32*, 2562.
227. Karaman, R.; Jeon, S.; Almarsson, O.; Bruce, T. C. *J. Am. Chem. Soc.* **1992**, *114*, 4899.
228. Kobayashi, N.; Lam, H.; Nevin, W. A.; Janda, P.; Leznoff, C. C.; Lever, A. B. P. *Inorg. Chem.* **1990**, *29*, 3415.
229. Collman, J. P.; Anson, F. C.; Barnes, C. E.; Bencosme, C. S.; Geiger, T.; Evitt, E. R.; Kreh, R. P.; Meier, K.; Pettman, R. B. *J. Am. Chem. Soc.* **1983**, *105*, 2694.
230. Le Mest, Y.; L'Her, M. *J. Chem. Soc., Chem. Comm.* **1995**, 1441.
231. Durand, R. R., Jr.; Bencosme, C. S.; Collman, J. P.; Anson, F. C. *J. Am. Chem. Soc.* **1983**, *105*, 2710.
232. Hutchison, J. E.; Postlethwaite, T. A.; Chen, C.-h.; Hathcock, K. W.; Ingram, R. S.; Ou, W.; Linton, R. W.; Murray, R. W.; Tyvoll, D. A.; Chng, L. L.; Collman, J. P. *Langmuir* **1997**, *13*, 2143.
233. Collman, J. P.; Hendricks, N. H.; Kim, K.; Bencosme, C. S. *J. Chem. Soc., Chem. Comm.* **1987**, 1537.
234. Ni, C. L.; Abdalmuhdi, I.; Chang, C. K.; Anson, F. C. *J. Phys. Chem.* **1987**, *91*, 1158.

235. Guillard, R.; Brandes, S.; Tardieux, C.; Tabard, A.; L'Her, M.; Miry, C.; Gouerec, P.; Knop, Y.; Collman, J. P. *J. Am. Chem. Soc.* **1995**, *117*, 11721.
236. Kim, K.; Collman, J. P.; Ibers, J. A. *J. Am. Chem. Soc.* **1988**, *110*, 4242.
237. Le Mest, Y.; L'Her, M.; Collman, J. P.; Kim, K.; Hendricks, N. H.; Helm, S. *J. Electroanal. Chem.* **1987**, *234*, 277.
238. Heusler, K. E. In *Encyclopedia of Electrochemistry of Elements*. Bard, A. J., Ed.; Dekker: New York, **1973**; Vol. IX A, pp. 230–383.
239. International Committee on Electrochemistry *Pure Appl. Chem.* **1982**, *54*, 1527.
240. Collman, J. P.; Chong, A. O.; Jameson, J. B.; Oakley, R. T.; Rose, E.; Schmittou, E. R.; Ibers, J. A. *J. Am. Chem. Soc.* **1981**, *103*, 516.
241. Hatada, M. H.; Tulinsky, A.; Chang, C. K. *J. Am. Chem. Soc.* **1980**, *102*, 7116.
242. Fillers, J. P.; Ravichandran, K. G.; Abadalmuhdi, I.; Tulinsky, A.; Chang, C. K. *J. Am. Chem. Soc.* **1986**, *108*, 417.
243. Fletcher, J. T.; Therien, M. J. *J. Am. Chem. Soc.* **2000**, *122*, 12393.

# Heme Protein Dynamics: Electron Tunneling and Redox Triggered Folding

63

HARRY B. GRAY and JAY R. WINKLER

Beckman Institute, MC 139-74, California Institute of Technology, Pasadena, California 91125, USA

I. Introduction	51
II. Semiclassical Theory of Electron Transfer	51
III. Reorganization Energies of Ru-Modified Heme Proteins	53
A. Ru-Cytochrome <i>c</i>	53
IV. Electronic Coupling	55
A. Superexchange Coupling	55
B. Tunneling Pathways in Proteins	56
C. Rate/Distance Dependence	56
V. Tunneling Timetables	57
A. Heme Proteins	57
B. Water	58
VI. Tunneling Across Heme Protein-Protein Interfaces	59
VII. Redox-Coupled Folding of Proteins	62
A. Cytochrome <i>c</i>	63
B. Cytochrome <i>b</i> <sub>562</sub>	64
C. Cytochrome <i>c'</i>	65
D. Zn-cytochrome <i>c</i>	67
References	71

## I. Introduction

Proteins containing iron-protoporphyrin IX (heme) play key roles in respiration and photosynthesis. Heme facilitates the transfer of electrons between and through the proteins that are part of the respiratory and photosynthetic machinery. Much work has been done with the goal of understanding the factors that control electron flow through heme proteins (notable electron tunneling experiments are set out in Table 1).<sup>1-81</sup> In this chapter, we will review this work, as well as results from recent studies in which electron transfer has been used both to trigger and to probe heme protein folding.<sup>82-85</sup> Semiclassical theory has been very helpful both in the design and interpretation of experiments, so we start with a brief review of its essential features.

## II. Semiclassical Theory of Electron Transfer

According to semiclassical theory (eq. 1), the rate of electron transfer (ET) from a donor (**D**) to an acceptor (**A**) held at fixed distance and orientation is a function of temperature (*T*), reaction driving force ( $-\Delta G^\circ$ ), a nuclear reorganization parameter ( $\lambda$ ),

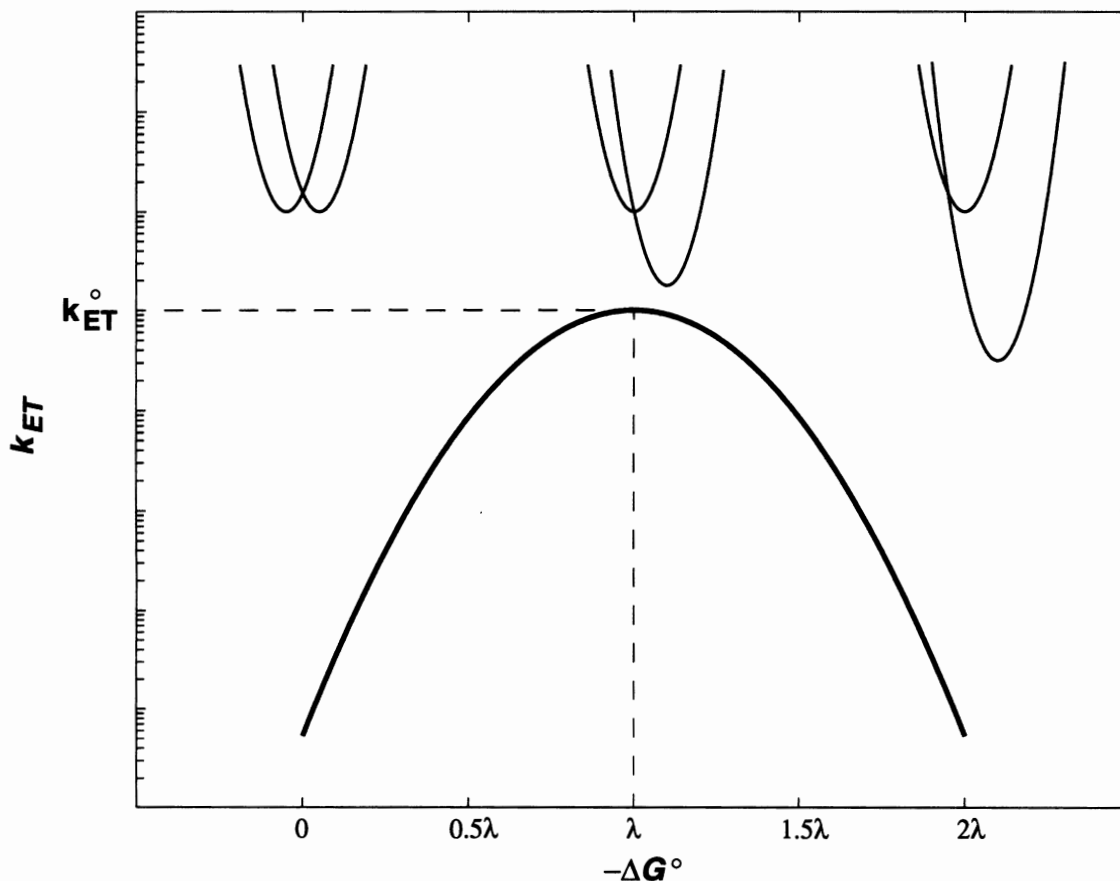
$$k_{\text{ET}} = \sqrt{\frac{4\pi^3}{h^2\lambda k_B T}} H_{\text{AB}}^2 \exp\left\{-\frac{(\Delta G^\circ + \lambda)^2}{4\lambda k_B T}\right\} \quad (1)$$

and an electronic coupling matrix element ( $H_{\text{AB}}$ ).<sup>25,86,87</sup> The reorganization parameter reflects the changes in structure and solvation that result when an electron moves from **D** to **A**. A balance between nuclear reorganization and reaction driving force determines both the transition-state configuration and the height of



**Table 1.** Selected Milestones in Experimental Investigations of Electron Tunneling in Heme Proteins

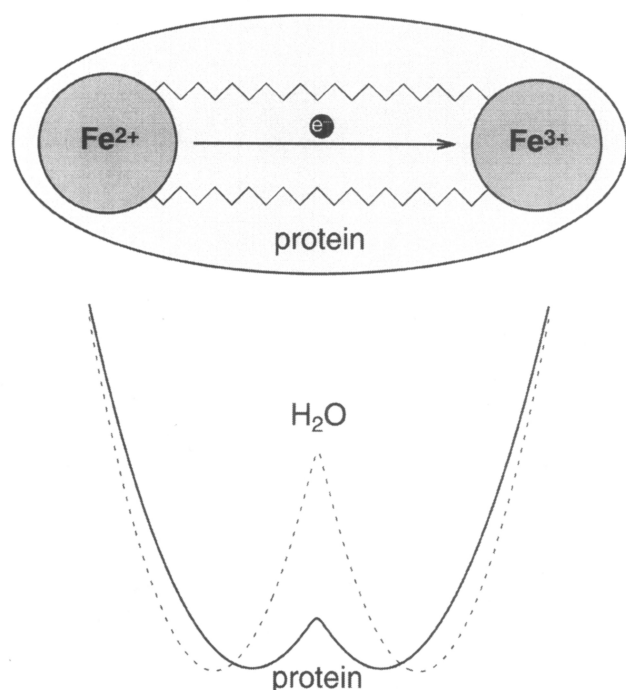
Year	Study	Ref.
1966	Electron tunneling proposed as the mechanism of cytochrome oxidation by the special pair in photosynthetic reaction centers	1
1982	Experimental confirmation of long-distance electron tunneling in proteins (Ru-modified cytochrome <i>c</i> )	49
1983	Electron tunneling in [Zn(II),Fe(II)] hybrid hemoglobin at crystallographically known distance, 25 Å	2
1984	Electron tunneling in a protein-protein physiological pair	11
1991	Flash-quench method for measuring electron tunneling in proteins over many orders of magnitude in time	61
2001	Electron tunneling between proteins in structurally characterized crystals	81

**Figure 1.** ET rate constant vs.  $-\Delta G^\circ$  plot and 3 ET reaction surfaces illustrating eq. 1. Rate constants reach the driving-force optimized value ( $k_{ET}^\circ$ ) when  $-\Delta G^\circ = \lambda$ .

the barrier associated with the ET process. At the optimum driving force ( $-\Delta G^\circ = \lambda$ ), the reaction is activationless, and the rate ( $k_{ET}^\circ$ ) is limited only by the strength of the **D/A** electronic coupling (Figure 1). When **D** and **A** are in van der Waals contact, the coupling strength is usually so large that the ET reaction is adiabatic, that is, it occurs every time the transition-state configuration is formed.<sup>87</sup> In this adiabatic limit, the ET rate is independent of  $H_{AB}$  and the prefactor depends only on the frequency of motion along the reaction coordinate. An ET reaction is nonadiabatic (eq. 1) when the **D/A** interaction is weak and the transition state must be reached many times before an electron is transferred. The electronic coupling element

determines the frequency of crossing from reactants (**D** + **A**) to products (**D**<sup>+</sup> + **A**<sup>-</sup>) in the region of the transition state.

The barriers to electron exchange between hydrated transition metal ions are readily interpreted in terms of semiclassical theory.<sup>25</sup> The 0.66-eV activation energy for electron exchange between aquo ferrous and ferric complexes, for example, implies a 2.7-eV reorganization energy. The major contribution (1.5 eV) is attributed to the 0.14-Å difference in Fe–O bond lengths in the ferric and ferrous ions. The remainder (1.2 eV) arises from repolarization of the aqueous solvent upon electron transfer. When the ferrous and ferric ions are in contact, this large reorganization energy leads to a 100-ms time



**Figure 2.** Schematic representation of the free-energy surfaces for electron exchange between hydrated ferrous and ferric ions in aqueous solution and between the ions complexed in a protein.

constant for electron exchange. Even at short range, then, the barriers to ET between hydrated metal ions are too great for the demands of biological electron flow. To reduce the reorganization energy, proteins must sequester the redox-active metals in hydrophobic cavities, away from the polar aqueous solvent. In this way, a threefold decrease in reorganization energy can be achieved, decreasing the time constant for electron exchange by nine orders of magnitude (Figure 2).

The singular feature of electron transfer is that reactions can proceed at very high rates when **D** and **A** are separated by long distances. The electron tunnels through a potential barrier between **D** and **A**; for a square barrier,  $H_{AB}$  displays an exponential dependence on the distance (**R**) between the reactants.<sup>88</sup> The medium between redox centers is vitally important for long-range ET. Owing to a  $3.5\text{-}\text{\AA}^{-1}$  distance-decay constant ( $\beta$ ), the time required for electron exchange between hydrated ferrous and ferric ions is estimated to be  $10^{17}$  years if the complexes are separated by  $20\text{ \AA}$  in vacuum.<sup>86</sup> Superexchange coupling via hole and electron states of the intervening medium enhances the **D/A** electronic interaction and produces a more gradual decrease in rate with distance. Fill the void between hydrated ferrous and ferric ions with water ( $\beta = 1.65\text{ \AA}^{-1}$ )<sup>89</sup> and the time constant for  $20\text{-}\text{\AA}$  electron exchange decreases dramatically ( $5 \times 10^4$  years), but the reaction

is still far too slow to support biological activity. If the distance decay factor for ET across a polypeptide is comparable to that found for electron tunneling across hydrocarbon bridges ( $\beta = 0.8\text{--}1.0\text{ \AA}^{-1}$ ),<sup>86</sup> then the time for a  $20\text{-}\text{\AA}$  electron exchange between complexed ferrous and ferric ions in the hydrophobic interior of a protein could be in the millisecond to microsecond range. It is clear, then, that in addition to lowering reorganization barriers, the protein plays an important electronic coupling role.

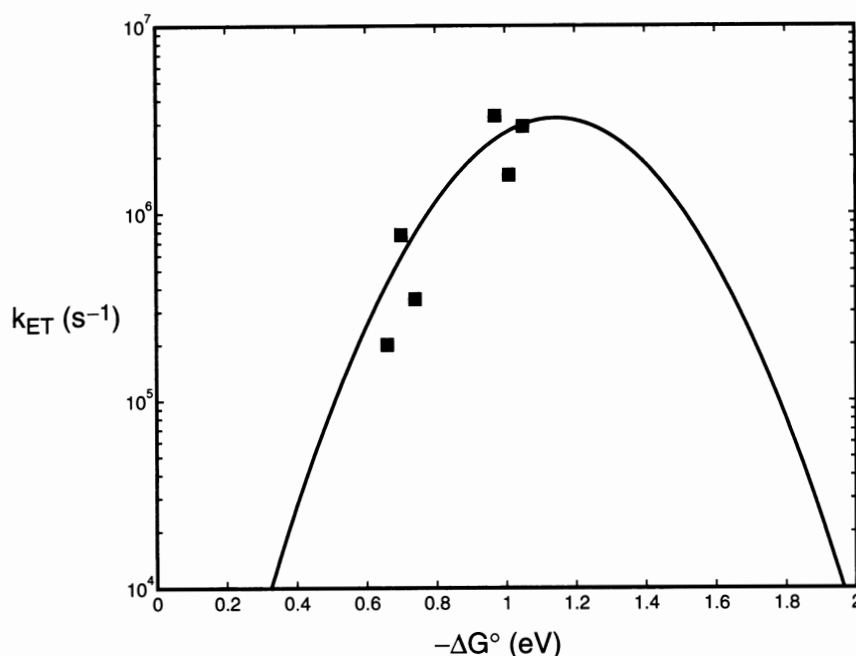
Investigations of the dependences of ET rates on reaction driving force and temperature can be used to evaluate reorganization energies. Although conceptually straightforward, both methods have difficulties. In order to vary the reaction driving force, changes in one or both redox sites are required. These chemical modifications must be chosen with care to ensure that  $\lambda$  does not change along with  $\Delta G^\circ$ . Studies of the temperature dependence of  $k_{ET}$  are easier in principle, but will not provide accurate  $\lambda$  values unless the temperature dependence of  $\Delta G^\circ$  is determined as well.<sup>25</sup>

### III. Reorganization Energies of Ru-Modified Heme Proteins

Investigations of protein–protein ET reactions have led to a better understanding of biological electron flow.<sup>16,90,91</sup> Natural systems, however, often are not amenable to the systematic studies that are required to elucidate the factors that control biological ET reactions. A successful alternative approach involves measurements of ET in heme proteins that have been labeled with redox-active molecules.<sup>74</sup> Ruthenium complexes have been employed as probes in a great many investigations, as Ru(II)-aquo reagents react readily with surface His residues to form stable protein derivatives.

#### A. Ru-CYTOCHROME *c*

ET in a Ru-modified protein was first measured in Ru(NH<sub>3</sub>)<sub>5</sub>(His33)<sup>3+</sup>-ferricytochrome *c*.<sup>49</sup> The rate of Ru<sup>2+</sup> to Fe<sup>3+</sup> electron transfer over a distance of  $18\text{ \AA}$  at a driving force of  $0.2\text{ eV}$  is  $30\text{ s}^{-1}$ . Replacement of the native Fe center in the heme with Zn paved the way for ET measurements at higher driving forces.<sup>64</sup> The driving-force dependence of ET rates in Ru(NH<sub>3</sub>)<sub>4</sub>L(His33)-Zn-cyt *c* (L = NH<sub>3</sub>, pyridine, isonicotinamide) yielded the parameters  $\lambda = 1.15\text{ eV}$  and  $H_{AB} = 0.1\text{ cm}^{-1}$ <sup>64</sup> (Figure 3). According to the Marcus cross relation ( $\lambda_{12} = \frac{1}{2}[\lambda_{11} + \lambda_{22}]$ ), the reorganization energy for the cross reaction between **D**

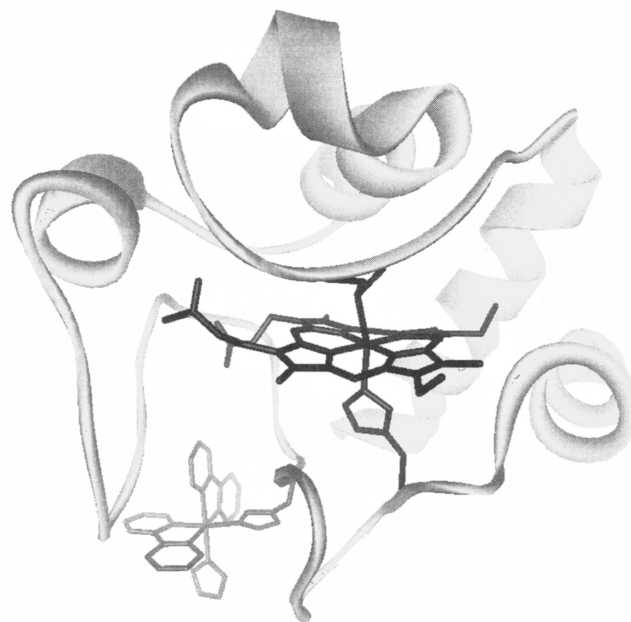


**Figure 3.** Driving-force dependence of intramolecular electron transfer rates in Ru–amine-His33 modified Zn-substituted cytochrome *c* (■). Solid line was generated using eq. 1 and the following parameters:  $\lambda = 1.15$  eV,  $H_{AB} = 0.10$  cm<sup>-1</sup>.

and **A** ( $\lambda_{12}$ ) is the mean of the reorganization energies for electron exchange between **D** and **D**<sup>+</sup> ( $\lambda_{11}$ ) and exchange between **A** and **A**<sup>-</sup> ( $\lambda_{22}$ ).<sup>25</sup> The Fe-cyt *c* self exchange reorganization energy has been estimated to be 0.7 eV.<sup>92</sup> If the Zn-cyt *c* reorganization energy is comparable to that of the Fe protein, then it is apparent that the hydrophilic Ru–amine complex is responsible for about two-thirds of the total reorganization energy in Ru–amine-modified cyt *c* ET reactions ( $\lambda(\text{Ru}^{3+/2+}) = 1.7$  eV). This result is in good agreement with estimates of the self-exchange reorganization energy in  $\text{Ru}(\text{NH}_3)_6^{3+/2+}$ .<sup>25</sup>

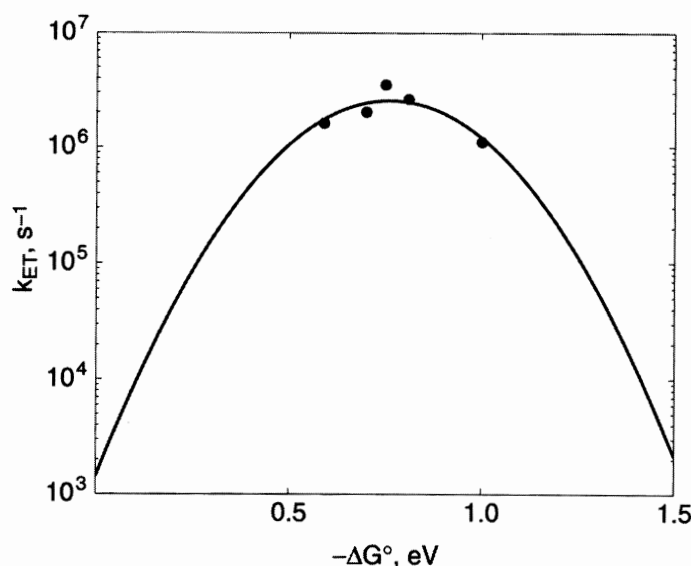
A great deal of work on Ru-modified proteins has employed the  $\text{Ru}(\text{bpy})_2(\text{im})(\text{HisX})^{2+}$  (bpy = 2,2'-bipyridine; im = imidazole) label<sup>74</sup> (Figure 4). In addition to favorable ET properties, these Ru–bpy complexes have long-lived, luminescent metal-to-ligand charge-transfer excited states that can be prepared with short laser pulses. These excited states enable a wider range of ET measurements than is possible with nonluminescent complexes. Furthermore, the bpy ligands raise the  $\text{Ru}^{3+/2+}$  reduction potential (>1 V vs. NHE) so that observed ET rates are close to  $k_{\text{ET}}^\circ$ , improving the reliability of  $H_{AB}$  and  $\lambda$  determinations.

A study of the driving-force dependence of  $\text{Fe}^{2+} \rightarrow \text{Ru}^{3+}$  ET rates in  $\text{Ru}(\text{LL})_2(\text{im})(\text{His33})\text{-Fe-cyt } c$  (LL = bpy, 4,4'-(CH<sub>3</sub>)<sub>2</sub>-bpy, 4,4',5,5'-(CH<sub>3</sub>)<sub>4</sub>-bpy,



**Figure 4.** Ribbon structure representation of a model of the structure of  $\text{Ru}(\text{bpy})_2(\text{im})(\text{His33})^{2+}$ -labeled cytochrome *c*.

4,4'-(CONH(C<sub>2</sub>H<sub>5</sub>))<sub>2</sub>-bpy) gave  $\lambda = 0.74$  eV and  $H_{AB} = 0.095$  cm<sup>-1</sup>.<sup>73,75</sup> (Figure 5). The 0.4-eV decrease in reorganization energy resulting from replacement of the Ru–amine complex with a Ru–bpy label is in excellent agreement with estimates from cross reactions of model complexes.<sup>25</sup>



**Figure 5.** Driving-force dependence of intramolecular electron transfer rates in Ru-bpy-His33 modified Fe-cytochrome *c* (●). Solid line was generated using eq. 1 and the following parameters:  $\lambda = 0.74$  eV,  $H_{AB} = 0.095$  cm<sup>-1</sup>.

The large difference in reorganization energy between Ru–ammine and Ru–bpy modified cytochromes highlights the important role of water in protein electron transfer. The bulky bpy ligands shield the charged metal center from the polar aqueous solution, reducing the solvent reorganization energy. In the same manner, the medium surrounding a metalloprotein active site will affect the reorganization energy associated with its ET reactions. A hydrophilic active site will lead to larger reorganization energies than a hydrophobic site. Consequently, the kinetics of protein ET reactions will be very sensitive to the active-site environment.

The rates of heme reduction by  $*Ru^{2+}$  and  $Ru^+$  in Ru(His33)cytochrome *c* have been examined at very high driving forces ( $1.3 \text{ eV} \leq -\Delta G^\circ \leq 1.9 \text{ eV}$ ).<sup>75</sup> The semiclassical theory predicts significant inverted effects in this driving-force regime, but at driving forces above 1.3 eV rates leveled at a value eightfold below the maximum ET rate. Rate/energy leveling is a common phenomenon, particularly in excited-state ET reactions; formation of electronically excited products is a likely explanation for the absence of inverted effects.<sup>75</sup> In the case of cytochrome *c* heme reduction by  $Ru^+$ , reactions that form low-lying metal-to-ligand charge transfer excited states of the ferroheme ( $Fe(d\pi) \rightarrow$  Porphyrin ( $\pi^*$ ); 1.05–1.3 eV) should be faster than reactions forming ground-state products. The low-lying excited states of ferro- and ferrihememes are likely to mask inverted driving-force effects in the ET reactions of heme proteins.

## IV. Electronic Coupling

Nonadiabatic ET reactions are characterized by weak electronic interaction between the reactants and products at the transition-state nuclear configuration ( $H_{AB} \ll k_B T$ ). This coupling is directly related to the strength of the electronic interaction between the donor and acceptor.<sup>93</sup> When donors and acceptors are separated by long distances ( $> 10 \text{ \AA}$ ), direct overlap of their wavefunctions is vanishingly small; the material between the two redox sites must mediate the coupling.

For electron tunneling through a square potential barrier, the electronic coupling matrix element ( $H_{AB}$ ) drops off exponentially with increasing **D/A** separation.<sup>88,94</sup> The height of the tunneling barrier relative to the energies of the **D/A** states determines the distance-decay constant ( $\beta$ ). Hopfield estimated  $\beta \sim 1.4 \text{ \AA}^{-1}$  on the basis of measurements of the temperature dependence of ET from a cytochrome to the oxidized special pair of chlorophylls in the photosynthetic reaction center of *Chromatium vinosum*.<sup>88</sup> His analysis predicted that the heme edge of the cytochrome would be  $8 \text{ \AA}$  from the nearest edge of the special pair; later structural studies revealed that the actual distance was somewhat greater ( $12.3 \text{ \AA}$ ).<sup>45</sup>

### A. SUPEREXCHANGE COUPLING

Coupling **D** to **A** through electronic interactions with the intervening bridge is called superexchange. If

oxidized states of the bridge mediate the coupling, the process is referred to as “hole transfer”; mediation by reduced bridge states is known as “electron transfer.” In 1961, McConnell developed a nearest-neighbor superexchange coupling model to describe charge-transfer interactions between donors and acceptors separated by spacers comprised of identical repeat units.<sup>95</sup> The total coupling ( $H_{AB}$ ) is given as the product of the coupling-decays for each bridge site ( $\epsilon$ ). For a bridge built from identical repeat units separated by  $m$  bonds,  $H_{AB}$  will be proportional to  $\epsilon^m$ . In this model, the ET rate constant will exhibit an exponential dependence on the number of bonds separating **D** and **A**; experimental studies on synthetic **D-br-A** complexes support this prediction.<sup>86</sup>

### B. TUNNELING PATHWAYS IN PROTEINS

The McConnell superexchange model is too simplistic for a protein intervening medium because of the complex array of bonded and nonbonded contacts between **D** and **A**. An important advance was made by Onuchic *et al.*, who developed a generalized tunneling pathway (TP) superexchange coupling model that reduces the diverse interactions between the atoms in a folded polypeptide to a set of three types of contacts: covalent bonds, hydrogen bonds, and through space contacts.<sup>66</sup> Each type of contact is assigned a coupling decay value ( $\epsilon_C$ ,  $\epsilon_H$ , and  $\epsilon_S$ ), which permits implementation of a search algorithm for finding optimal coupling pathways through proteins. The total coupling of a single pathway is given as a product of the couplings for the individual links (eq. 2).<sup>66</sup>

$$H_{AB} \propto \prod \epsilon_C \prod \epsilon_H \prod \epsilon_S \quad (2)$$

A tunneling pathway can be described in terms of an effective covalent tunneling path comprised of  $n$  (non-integral) covalent bonds, with a total length equal to  $\sigma_l$  (eq. 3). The relationship between  $\sigma_l$  and the direct **D–A** distance (**R**) reflects the coupling efficiency of a pathway.

$$H_{AB} \propto (\epsilon_C)^n \quad (3a)$$

$$\sigma_l = n \times 1.4 \text{ \AA} / \text{bond} \quad (3b)$$

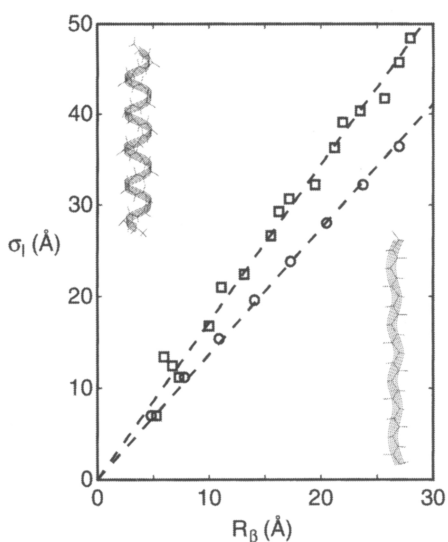
The variation of ET rates with **R** is expected to depend upon the coupling decay for a single covalent bond ( $\epsilon_C$ ); the magnitude of  $\epsilon_C$  depends critically upon the energy of the tunneling electron relative to the energies of the bridge hole and electron states.

### C. RATE/DISTANCE DEPENDENCE

The **D–A** distance decay of protein ET rate constants depends on the capacity of the polypeptide matrix to mediate distant electronic couplings. If dominant coupling pathways mediate long-range electron transfer in proteins, then single-site mutations could have profound effects on enzyme function. In addition, if single pathways operate in biological ET reactions, then they have presumably been optimized through natural selection. These consequences of tunneling pathways impart a certain lack of robustness into the protein structure/function relationship. Concerns about this issue led Dutton and coworkers to propose that a folded polypeptide matrix behaves like a glassy solvent, imposing a uniform barrier (UB) to electron tunneling.<sup>45</sup> Analysis of a variety of ET rates, especially those from the photosynthetic reaction center, produced a universal distance-decay constant for protein electron transfer that was in remarkable agreement with Hopfield’s estimate ( $1.4 \text{ \AA}^{-1}$ ).<sup>45</sup> Disagreements over the appropriate **D/A** distance measure (edge-to-edge, center-to-center) fueled disputes about whether the large body of protein ET data supports a homogeneous barrier model, or whether a structure-dependent model is necessary. Recently, the UB model has been amended to include the packing density of the protein matrix.<sup>48</sup> Although this model ignores bond connectivity, it does embody many of the same elements as the TP model by accounting for, in a rudimentary fashion, the protein structure dependence of long-range couplings.

The great strength of the TP model is that a straightforward analysis of a protein structure identifies residues that are important for mediating long-range coupling. Employing this model, Beratan, Betts, and Onuchic predicted in 1991 that proteins comprised largely of  $\beta$ -sheet structures would be more effective at mediating long-range couplings than those built from  $\alpha$  helices.<sup>31</sup> This analysis can be taken a step further by comparing the coupling efficiencies of individual protein secondary structural elements ( $\beta$  sheets,  $\alpha$  helices). The coupling efficiency can be determined from the variation of  $\sigma_l$  as a function of **R**. A linear  $\sigma_l/\mathbf{R}$  relationship implies that  $k_{ET}^0$  will be an exponential function of **R**; the distance-decay constant is determined by the slope of the  $\sigma_l/\mathbf{R}$  plot and the value of  $\epsilon_C$ .<sup>74</sup>

A  $\beta$  sheet is comprised of extended polypeptide chains interconnected by hydrogen bonds; the individual strands of  $\beta$  sheets define nearly linear coupling pathways along the peptide backbone spanning  $3.4 \text{ \AA}$  per residue. The tunneling length for a  $\beta$  strand exhibits an



**Figure 6.** Plot of calculated tunneling path length ( $\sigma_l$ ) vs.  $\beta$ -carbon separation ( $R_\beta$ ) for ET along an idealized  $\alpha$  helix (■, using the standard H-bond coupling parameters in the TP model) and a  $\beta$  strand (●).

excellent linear correlation with  $\beta$ -carbon separation ( $R_\beta$ ); the best linear fit with zero intercept yields a slope of  $1.37 \sigma_l/R_\beta$  (distance-decay constant =  $1.0 \text{ \AA}^{-1}$ ) (Figure 6). Couplings across a  $\beta$  sheet depend upon the ability of hydrogen bonds to mediate the **D/A** interaction. The standard parameterization of the TP model defines the coupling decay across a hydrogen bond in terms of the heteroatom separation. If the two heteroatoms are separated by twice the  $1.4\text{-\AA}$  covalent-bond distance, then the hydrogen-bond decay is assigned a value equal to that of a covalent bond. Longer heteroatom separations lead to weaker predicted couplings but, as yet, there is no experimental confirmation of this relationship.

In the coiled  $\alpha$ -helix structure, a linear distance of just  $1.5 \text{ \AA}$  is spanned per residue. In the absence of mediation by hydrogen bonds,  $\sigma_l$  is a very steep function of  $R_\beta$ , implying that an  $\alpha$  helix is a poor conductor of electronic coupling ( $2.7 \sigma_l/R_\beta$ , distance-decay constant =  $1.97 \text{ \AA}^{-1}$ ). If the hydrogen-bond networks in  $\alpha$  helices mediate coupling, then the Beratan–Onuchic parameterization of hydrogen-bond couplings suggests a  $\sigma_l/R_\beta$  ratio of  $1.72$  (distance-decay constant =  $1.26 \text{ \AA}^{-1}$ ) (Figure 6). Treating hydrogen bonds as covalent bonds further reduces this ratio ( $1.29 \sigma_l/R_\beta$ , distance-decay constant =  $0.94 \text{ \AA}^{-1}$ ). Hydrogen-bond interactions, then, will determine whether  $\alpha$  helices are vastly inferior to or are slightly better than  $\beta$  sheets in mediating long-range electronic couplings. It is important to note that the coiled helical structure leads to poorer  $\sigma_l/R_\beta$  correlations, especially for values of  $R_\beta$  under  $10 \text{ \AA}$ . In this distance region, the TP model predicts little

variation in coupling efficiencies for the different secondary structures.

## V. Tunneling Timetables

Plots of coupling-limited tunneling times ( $1/k_{\text{ET}}^\ominus$ ) vs. distance (**R**) are called tunneling timetables.<sup>74</sup> When comparing tunneling times from systems with different donors and/or acceptors, it can be difficult to identify a proper distance measure. So-called edge-to-edge distances are often employed but there are many ambiguities, not the least of which is defining the set of atoms that constitute the edges of **D** and **A**. For planar aromatic molecules (e.g., chlorophylls, pheophytins, quinones), edge–edge separations are usually defined on the basis of the shortest distance between aromatic carbon atoms of **D** and **A**. In transition-metal complexes (e.g., Fe–heme, Ru–ammine, Ru–bpy), however, atoms on the periphery are not always well coupled to the central metal, and empirical evidence suggests that metal–metal distances are more appropriate.

### A. HEME PROTEINS

ET rates have been measured in eight different Ru(bpy)<sub>2</sub>(im)(HisX)<sup>2+</sup> derivatives of wild-type and mutant cytochromes *c* (Table 2).<sup>61,65,70,72</sup> Maximum ET rates do not correlate well with a simple exponential distance dependence (Figure 7). Two modified proteins, for example, have comparable ET rates (Ru(His72),  $9.0 \times 10^5 \text{ s}^{-1}$ ; Ru(His39),  $3.2 \times 10^6 \text{ s}^{-1}$ ), yet the Ru–Fe distances differ by  $6.5 \text{ \AA}$  (His72,  $13.8 \text{ \AA}$ ; His39,  $20.3 \text{ \AA}$ ). Moreover, the **D/A** distances in the Ru(His39) and Ru(His62) derivatives are nearly identical ( $20.3$  and  $20.2 \text{ \AA}$ , respectively), yet their maximum ET rates differ by a factor of 300 ( $3.2 \times 10^6$  and  $1.0 \times 10^4 \text{ s}^{-1}$ , respectively). The scatter in the data illustrates conclusively that the UB model does not adequately describe long-range couplings in proteins; a model that takes into account the structure of the bridging medium is required to explain the data.

Donor–acceptor pairs separated by  $\alpha$  helices include the heme–Ru redox sites in two Ru-modified myoglobins, Ru(bpy)<sub>2</sub>(im)(HisX)-Mb (X = 83, 95) (Table 3).<sup>96</sup> The tunneling pathway from His95 to the Mb–heme is comprised of a short section of  $\alpha$  helix terminating at His93, the heme axial ligand. The coupling for the [Fe<sup>2+</sup> → Ru<sup>3+</sup>(His95)]-Mb ET reaction<sup>96</sup> is of the same magnitude as that found in Ru-modified azurins with comparable **D–A** spacings. This result is consistent with the TP model, which predicts very little difference in the coupling efficiencies of  $\alpha$  helices and  $\beta$  sheets at small

**Table 2.** Driving-Force Optimized Intramolecular ET Rates and Ru–Fe Distances in Ru(bpy)<sub>2</sub>(im)(His)<sup>2+</sup>-Modified cyt c

Modified His <sup>a</sup>	$k_{ET}^o, s^{-1}$	R, Å	Ref.
33 <sup>b</sup>	$2.7 \times 10^6$	17.9	61
39 <sup>c</sup>	$3.3 \times 10^6$	20.3	65
54 <sup>d,e</sup>	$3.4 \times 10^4$	22.5	72
54(Ile52) <sup>d,f</sup>	$5.8 \times 10^4$	21.5	72
58 <sup>d,g</sup>	$6.0 \times 10^4$	20.2	70
62 <sup>d,h</sup>	$1.0 \times 10^4$	20.2	65
66 <sup>d,i</sup>	$1.1 \times 10^6$	18.9	70
72 <sup>b,j</sup>	$9.4 \times 10^5$	13.8	65

<sup>a</sup>The horse heart numbering system is used for all of the cytochromes c.

<sup>b</sup>Horse-heart cytochrome c.

<sup>c</sup>*Candida krusei* cytochrome c.

<sup>d</sup>*Saccharomyces cerevisiae* cytochrome c.

<sup>e</sup>Lys54His, Cys102Ala double mutant.

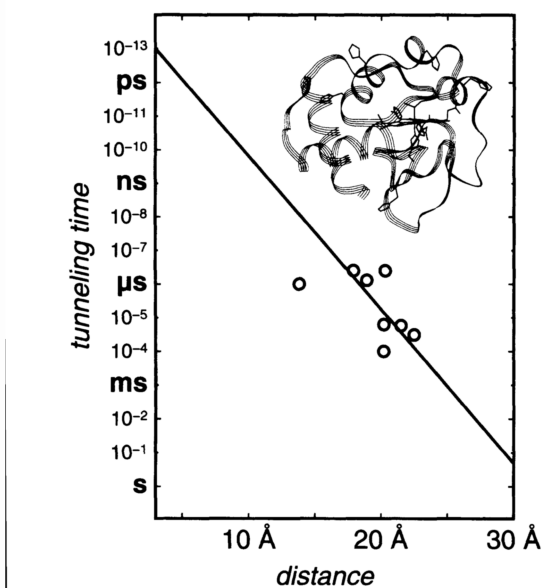
<sup>f</sup>Lys54His, Asn52Ile, Cys102Ala triple mutant.

<sup>g</sup>Leu58His, His39Gln, Cys102Ser triple mutant.

<sup>h</sup>Asn62His mutant.

<sup>i</sup>Glu66His, His39Gln, Cys102Ser triple mutant.

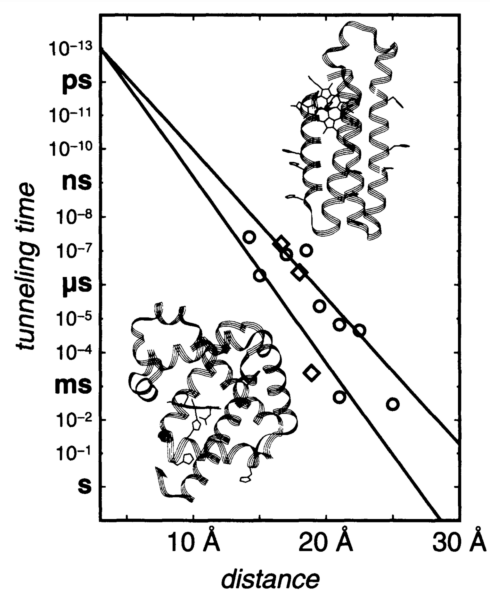
<sup>j</sup>Lys72His semisynthetic variant.

**Figure 7.** Tunneling timetable for ET in Ru-modified cytochrome c. The solid line illustrates a  $1.05 \text{ \AA}^{-1}$  distance decay.**Table 3.** Driving-Force Optimized Intramolecular ET Rates and Ru–Fe Distances in Ru(bpy)<sub>2</sub>(im)(His)<sup>2+</sup>-Modified Mb<sup>a</sup>

Modified His	$k_{ET}^o, s^{-1}$	R, Å
70	$1.6 \times 10^7$	16.6
83	$2.5 \times 10^3$	18.9
95	$2.3 \times 10^6$	18.0

<sup>a</sup>Reference 96.

D–A separations. The [Fe<sup>2+</sup> → Ru<sup>3+</sup>(His83)]-Mb [83] tunneling time, however, is substantially longer than those found in  $\beta$ -sheet structures at similar separations, in accord with the predicted distance-decay constant for an  $\alpha$  helix (Figure 8).

**Figure 8.** Tunneling timetable for ET in Ru-modified myoglobin ( $\diamond$ ) and cytochrome  $b_{562}$  ( $\circ$ ). The solid lines illustrate the TP predictions for coupling along  $\beta$ -strands ( $\beta = 1.0 \text{ \AA}^{-1}$ ) and  $\alpha$ -helices ( $\beta = 1.3 \text{ \AA}^{-1}$ ).**Table 4.** Driving-Force Optimized Intramolecular ET Rates and Ru–Fe Distances in Ru(bpy)<sub>2</sub>(im)(His)<sup>2+</sup>-Modified cyt  $b_{562}$ <sup>a</sup>

Modified His	$k_{ET}^o, s^{-1}$	R, Å
12	$2.6 \times 10^7$	14.2
15	$1.9 \times 10^6$	15.0
19	$6.7 \times 10^4$	21.0
63	$7.9 \times 10^6$	17.0
70	$2.3 \times 10^5$	19.5
73	$4.9 \times 10^2$	21.0
86	$2.9 \times 10^2$	25.0
89	$4.4 \times 10^4$	22.5
92	$1.0 \times 10^7$	18.5

ET rate data are available for nine Ru-modified derivatives of cytochrome  $b_{562}$ , a four-helix-bundle protein (Table 4).<sup>79</sup> The tunneling times for Ru-modified  $b_{562}$  exhibit far more scatter than was found for Ru-modified azurin. Two derivatives exhibit ET rates close to those predicted for coupling along a simple  $\alpha$  helix, and several others lie close to the  $\beta$ -strand decay (Figure 8). In these proteins, as in Ru(His70)Mb, the intervening medium is not a simple section of  $\alpha$  helix. Coupling across helices, perhaps on multiple interfering pathways, is likely to produce a complex distance dependence.

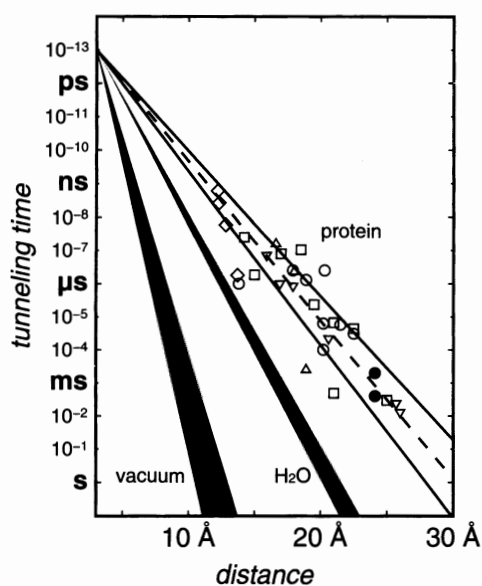
## B. WATER

The relevant solvent for protein electron transfer is water. Indeed, aqueous solution redox processes pervade chemistry and biology, and ET reactions in

water have been among the most intensively studied.<sup>25,86,87</sup> In 1984, Larsson suggested that long-range ET in water would be inefficient ( $\beta = 2.4 \text{ \AA}^{-1}$ ) because of the large energy gap between the hole states of water and those of **D** and **A**.<sup>97</sup> More recent theoretical treatments, however, have produced  $\beta$  values in the 1.0 to  $1.8 \text{ \AA}^{-1}$  range.<sup>98,99</sup>

An experimental investigation of  $\text{Ru}(\text{tpy})_2^{2+}$  (tpy = 2,2':6,2''-terpyridine) luminescence quenching by  $\text{Fe}(\text{OH})_6^{3+}$  in aqueous acidic glasses has produced a distance-decay constant of  $1.65 \pm 0.05 \text{ \AA}^{-1}$ , a value substantially larger than that for ET across saturated alkane spacers ( $0.9 \text{ \AA}^{-1}$ ).<sup>100</sup> The average distance-decay constant found for tunneling through proteins is  $1.1 \text{ \AA}^{-1}$ , although there is significant deviation from a simple exponential distance dependence because proteins do not provide a homogeneous tunneling barrier. The region representing the distance decay for coupling through water ( $\beta=1.6\text{--}1.7 \text{ \AA}^{-1}$ ) demonstrates that, although better than a vacuum ( $\beta=3\text{--}4 \text{ \AA}^{-1}$ ), tunneling  $20 \text{ \AA}$  through water is at least 100 times slower than tunneling through protein or hydrocarbon bridges.

The tunneling timetable for water and proteins is shown in Figure 9. Virtually all of the observed protein ET rates fall in a zone bound by the predicted distance decays for  $\alpha$  helices ( $1.3 \text{ \AA}^{-1}$ ) and  $\beta$  strands ( $1.0 \text{ \AA}^{-1}$ ).



**Figure 9.** Tunneling timetable for ET in Ru-modified proteins: azurin ( $\nabla$ ); cytochrome *c* ( $\circ$ ); myoglobin ( $\Delta$ ); cytochrome *b*<sub>562</sub> ( $\square$ ); and HiPIP ( $\diamond$ ). Rates for ET reactions in crystals of tuna cytochrome *c* doped with Zn-cytochrome *c* are indicated by solid circles. The solid lines illustrate the TP predictions for coupling along  $\beta$ -strands ( $\beta = 1.0 \text{ \AA}^{-1}$ ) and  $\alpha$ -helices ( $\beta = 1.3 \text{ \AA}^{-1}$ ); the dashed line illustrates a  $1.1 \text{ \AA}^{-1}$  distance decay. Distance decay for electron tunneling through water is shown as a grey wedge. Estimated distance dependence for tunneling through vacuum is shown as the black wedge.

The data provide compelling support for coupling mediated by the sigma-bonded framework of the protein. The relatively large  $\beta$  value for water indicates that, in addition to large reorganization barriers, this ubiquitous biological solvent also imposes a large tunneling barrier to long-range ET. The poor coupling efficiency of water suggests that pathways involving interstitial water molecules in proteins may not be as effective as all-peptide pathways.

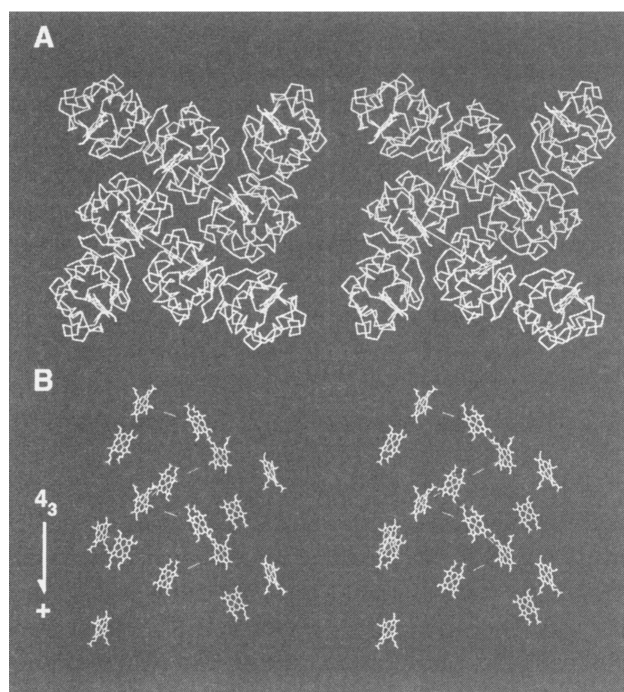
## VI. Tunneling Across Heme Protein–Protein Interfaces

Simple theoretical models (e.g., uniform barrier, tunneling pathway) do not capture all of the critical factors that control the rates of intraprotein ET reactions. Refined pathway models are being developed that, in most cases, aim to identify the atoms most responsible for mediating donor–acceptor electronic couplings.<sup>43</sup> Most of the definitive work has centered on molecules with fixed donor–acceptor distances and orientations, such as proteins covalently modified with redox-active units<sup>74,79,101–103</sup> or proteins that contain both donors and acceptors.<sup>17,104</sup> This work has established that redox centers within proteins are coupled electronically through the chemical-bond framework of the intervening medium.<sup>29,74,79,101–105</sup> How protein dynamics affect long-range couplings is currently an issue of great interest. Very-long-range reactions proceed too slowly to sustain many biological transformations. Multistep tunneling processes, even with endergonic intermediate steps, can compete effectively with single-step long-range reactions.<sup>48,79</sup> Long-range ET reactions via a series of real intermediates, rather than the virtual intermediates implicated in pathway models, may play important roles in many biochemical transformations.<sup>106</sup>

Electron transfer between proteins is understood less well, as it involves at least three steps: (i) association of the donor and acceptor, (ii) electron tunneling within the donor–acceptor complex, and (iii) dissociation of the oxidized and reduced products.<sup>16,20,91</sup> Because the dynamics of the first and the third steps obscure the electron tunneling reaction, many studies have focused on the ET properties of stable protein–protein complexes in solution.<sup>16,103,107</sup> It has been difficult to interpret the results, however, as neither the donor–acceptor docking geometries nor the conformations of these complexes are known.

Recent work has shown that a protein crystal containing photoactivatable donors and acceptors at





**Figure 10.** Stereo views of tuna cytochrome *c* crystal packing (space group  $P4_3$ ). The asymmetric unit contains two molecules. This packing produces a 24.1-Å separation between the metal centers of adjacent molecules. (a) View down the  $P4_3$  axis, straight lines connect the iron centers. (b) View of the heme orientation along the  $P4_3$  axis. Broken lines connect hemes that are involved in ET reactions.

specific lattice sites is an ideal medium for investigating the dependence of tunneling rates on structure. In the crystal lattice of tuna cytochrome *c* (cyt *c*),<sup>108</sup> chains of cyt *c* molecules form helices with a 24.1-Å separation between neighboring metal centers (Figure 10). All other metal–metal distances in the lattice are greater than 30 Å, with estimated electron tunneling times that are at least three orders of magnitude slower.<sup>74</sup> Thus, the heme groups can be treated as ordered in a one-dimensional chain, separated by identical protein and solvent media. By doping Zn-cyt *c* into this lattice, interprotein ET reactions can be triggered by laser excitation.<sup>81</sup> The triplet state of Zn-cyt *c* (\*Zn-cyt *c*) is generated in high yield with 550- or 580-nm excitation. This highly reducing excited state ( $E^\circ \approx -0.8$  V) reacts with Fe(III)-cyt *c* ( $E^\circ \approx 0.25$  V) to generate Fe(II)-cyt *c* and the Zn-cyt *c* cation radical, Zn-cyt *c*<sup>•+</sup> ( $E^\circ \approx 0.9$  V).<sup>51</sup> In a dark reaction, Zn-cyt *c*<sup>•+</sup> and Fe(II)-cyt *c* recombine to yield the ground-state species. Of special interest is the finding that the rates of tunneling reactions across a protein–protein interface closely match those for intraprotein ET over similar donor–acceptor separations.

We initially looked for ET by measuring the decay kinetics of \*Zn-cyt *c* using transient absorption

spectroscopy. \*Zn-cyt *c* has intense absorption in the 450- to 500-nm range, whereas the ground-state molecule does not. In pure Zn-cyt *c* crystals, the excited-state decay could be fit satisfactorily to a monoexponential function with a rate constant of  $\sim 80$  s<sup>-1</sup> ( $k_{\text{int}}$ , intrinsic decay rate constant), similar to that measured in solution.<sup>51</sup> In Fe(III):Zn-cyt *c* cocrystals, the decay is considerably faster and better described by a biexponential function. We assign the fast phase ( $k_{\text{fast}} = 400 \pm 100$  s<sup>-1</sup>) to ET from \*Zn-cyt *c* to Fe(III)-cyt *c*, where the electron tunneling rate ( $k_{\text{ET}} = k_{\text{fast}} - k_{\text{int}}$ ) is 320 s<sup>-1</sup>. The slower phase ( $k_{\text{slow}} = 70 \pm 20$  s<sup>-1</sup>) closely matches the intrinsic decay of \*Zn-cyt *c*, which is consistent with a distribution of cyt *c* molecules in the crystals; a fraction of Zn-cyt *c* molecules is adjacent to only two other Zn molecules and hence decays without undergoing an ET process. Accordingly, the amplitude of the slow phase grows relative to the fast phase as the Zn fraction in the cocrystals increases.

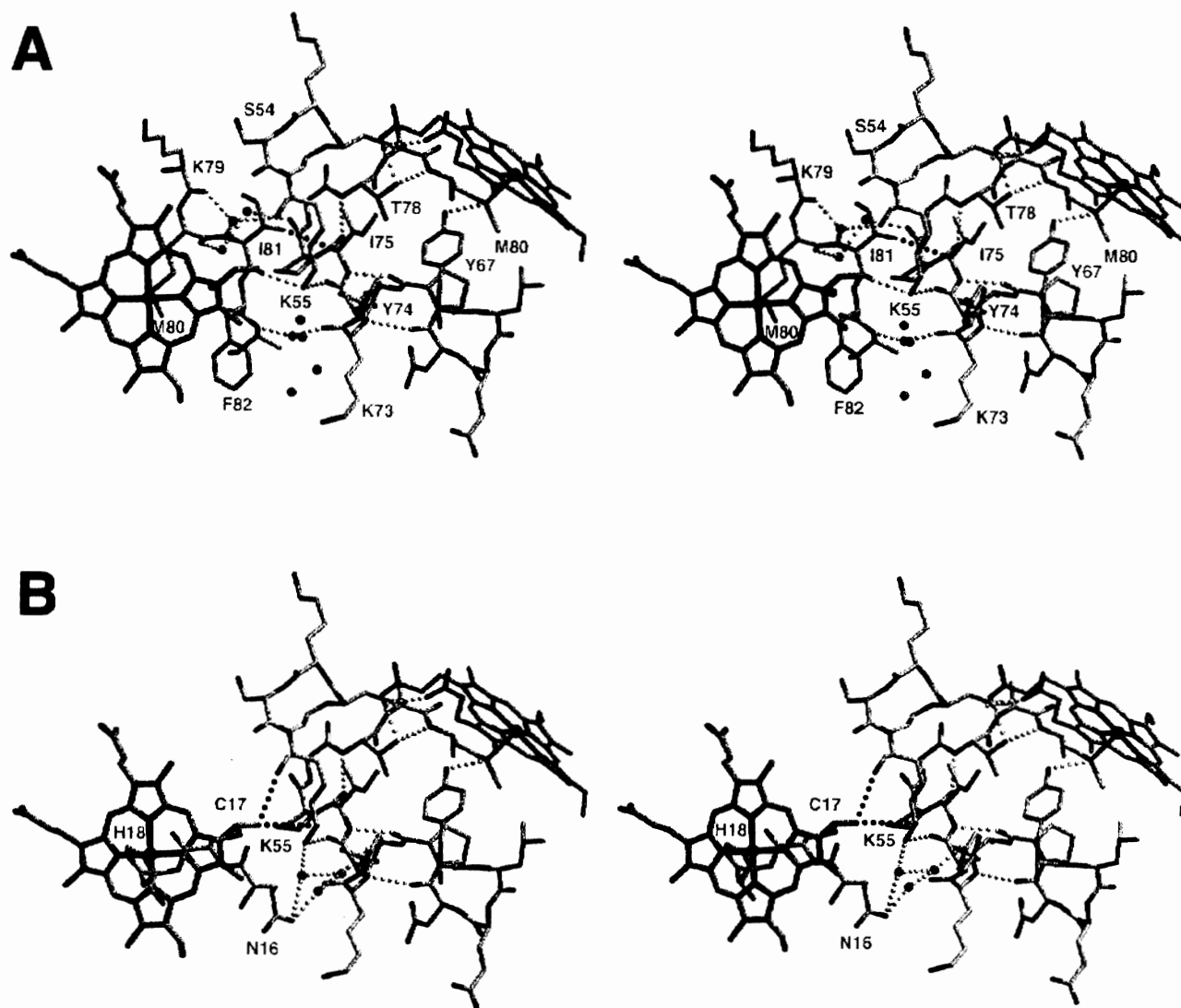
As controls, we examined Fe(II):Zn-cyt *c* and Co(III):Zn-cyt *c* cocrystals – ET in the former case is disfavored thermodynamically, whereas in the latter case there is a large barrier owing to a high Co(III/II) reorganization energy ( $> 2.4$  eV).<sup>109</sup> \*Zn-cyt *c* decay in both cases was slow and monoexponential, with rate constants [68 s<sup>-1</sup> for Fe(II) and 78 s<sup>-1</sup> for Co(III)] that were essentially the same as those observed in pure Zn-cyt *c* crystals. Zemel and Hoffman<sup>110</sup> reported fast \*Zn-porphyrin (\*Zn-P) decay at high pulse energies attributable to triplet–triplet energy transfer in Zn hemoglobin (24.1-Å metal–metal separation). Although a similarly fast decay channel was apparent in pure Zn-cyt *c* crystals ( $> 4$  mJ per pulse), it was less than 20% of the total amplitude at the pulse energies ( $< 800$  μJ) used in our experiments. Moreover, no such power dependence of the excited-state decay was observed in Fe(III):Zn-cyt *c* cocrystals, indicating that the contribution of triplet–triplet energy transfer to the fast decay kinetics was negligible.

The search for ET products proved to be challenging. First, absorbance measurements in the Soret region are precluded in crystals, owing to high extinction coefficients ( $\text{abs}_{424} \approx 65$  for a 50-μm thick crystal) and, second, Fe(II)-cyt *c* formation in the Q-band region is difficult to monitor, as the isosbestic point for Zn-cyt *c* and \*Zn-cyt *c* (540 nm) coincides with that for Fe(II)- and Fe(III)-cyt *c*. Our efforts to detect Zn-cyt *c*<sup>•+</sup> were successful, because in the deep red region of the spectrum the molar absorbance of this cation radical greatly exceeds that of \*Zn-cyt *c*.<sup>51</sup> The transient kinetics probed at 675 nm reveal a prompt absorbance

increase caused by \*Zn-cyt *c* formation, followed by a slower rise corresponding to production of Zn-cyt  $c^{\bullet+}$ .<sup>81</sup> The time constant for the subsequent decay of the 675-nm absorbance matches that measured at 470 nm, indicating that charge recombination is faster than charge separation. A biexponential fit to the 675-nm data yields the following rate constants:  $320 \pm 100 \text{ s}^{-1}$  for \*Zn-cyt *c*  $\rightarrow$  Fe(III)-cyt *c* ET, and  $2000 \pm 500 \text{ s}^{-1}$  for the Fe(II)-cyt *c*  $\rightarrow$  Zn-cyt  $c^{\bullet+}$  reaction.

Rapid relay of electrons by redox enzymes necessarily involves short-lived, weakly bound protein-protein complexes. The recognition sites between proteins in

such complexes tend to be smaller ( $< 1200 \text{ \AA}^2$ ) and include more water molecules than the interfaces between subunits in oligomeric proteins.<sup>111</sup> In fact, the protein-protein interface between cyt *c* and CcP ( $770 \text{ \AA}^2$ )<sup>112</sup> is very small compared with other interfaces; there are 17 van der Waals contacts and 13 water molecules (two of which form bridging hydrogen bonds across the interface) but only one direct hydrogen bond bridging the two proteins. The interprotein interactions in crystals of tuna cyt *c* are similar (Figure 11):  $760 \text{ \AA}^2$  of surface area is buried in an interface with 31 van der Waals contacts, 16 water molecules (3 bridging), and one direct hydrogen



**Figure 11.** Stereoview of heme groups and the intervening solvent medium. Residues below (a) and above (b) the heme plane on the left-hand side are shown separately. The side- and main-chain atoms of 14 residues on each molecule participate in the interface, burying  $400 \text{ \AA}^2$  of solvent-accessible surface area on Mol<sub>*i*</sub> and  $360 \text{ \AA}^2$  on Mol<sub>*i+1*</sub>. Close contacts in the interface include those between Ile81<sub>*i*</sub> and Ile75<sub>*i+1*</sub>, and the heme vinyl, and Lys55<sub>*i+1*</sub>. The side chain of Lys55<sub>*i+1*</sub> and the peptide carbonyl of Ile81<sub>*i*</sub> form the only direct protein-protein hydrogen bond. Water-bridged hydrogen bonds link the main chain of Phe82<sub>*i*</sub> to that of Lys73<sub>*i+1*</sub>, the side chain of Asp16<sub>*i*</sub> to that of Lys55<sub>*i+1*</sub>, and the main chain of Ile81<sub>*i*</sub> to both the main and side chains of Lys55<sub>*i+1*</sub>. A series of two or more water molecules (dark spheres) mediates additional hydrogen bonds between interfacial residues.

bond. In addition, a heme vinyl group makes direct contacts across the interface in both the cyt *c*–cyt *c* and the CcP–cyt *c* complexes. Electron tunneling across hydrogen-bonded interfaces is well established,<sup>113–115</sup> and the coupling across one or two water molecules (<5 Å) should not be much weaker than that over a comparable distance of peptide.<sup>89</sup> Our finding that the rates of ET between cytochromes *c* in a crystal fall well within the range that has been established for Ru proteins with similar donor–acceptor separations (Figure 9)<sup>89</sup> indicates that small interaction zones, such as that between Zn-cyt *c* and Fe-cyt *c*, are quite effective in mediating interprotein redox reactions.

## VII. Redox-Coupled Folding of Proteins

Proteins do not fold by randomly searching a large number of nearly degenerate configurations; instead, an ensemble of unfolded molecules must traverse a complicated energy landscape to reach a thermodynamically stable structure.<sup>116–120</sup> The fastest nuclear motions in proteins, rotations about single bonds, occur on the picosecond time scale and accompany both secondary- and tertiary-structure forming processes.<sup>121</sup> Short segments of secondary structure (e.g.,  $\alpha$  helices) can be formed in nanoseconds,<sup>122</sup> whereas the large scale, collective motions associated with the development of tertiary structure fall in the microsecond to millisecond range. Misfolded structures or traps are frequently encountered in folding processes; escape from these traps (e.g., proline isomerization) can take seconds or even minutes.<sup>123</sup> Understanding the key events in folding and identifying any partially folded intermediates are major goals of theoretical<sup>116–120,124,125</sup> and experimental<sup>126–133</sup> work.

The formal potentials for heme cofactors in the interiors of proteins often are shifted substantially from their aqueous solution values (Figure 12).<sup>134–136</sup> A thermodynamic cycle can be drawn connecting oxidized and reduced proteins in both folded and unfolded configurations (Figure 13).<sup>82,137</sup> If the active-site reduction potentials are different for the folded and unfolded states ( $\Delta E_f^\circ \equiv E_f^\circ - E_u^\circ$ ), then the free energies of folding the oxidized and reduced proteins will differ by a comparable amount ( $\Delta\Delta G_f^\circ \equiv \Delta G_{f,OX}^\circ - \Delta G_{f,RED}^\circ$ ).

Under normal conditions in aqueous solution, both the oxidized and reduced forms of redox proteins are usually folded;  $\Delta E_f^\circ$  reflects the relative stabilities of the two forms. Addition of denaturants

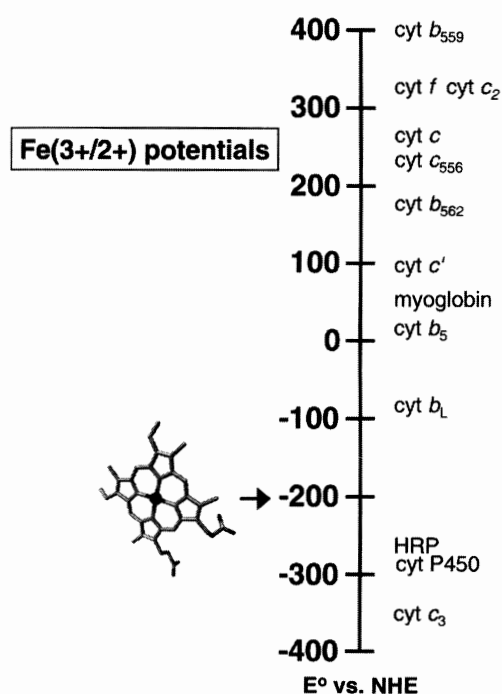


Figure 12. Redox potentials of heme proteins and for a heme in aqueous solution.

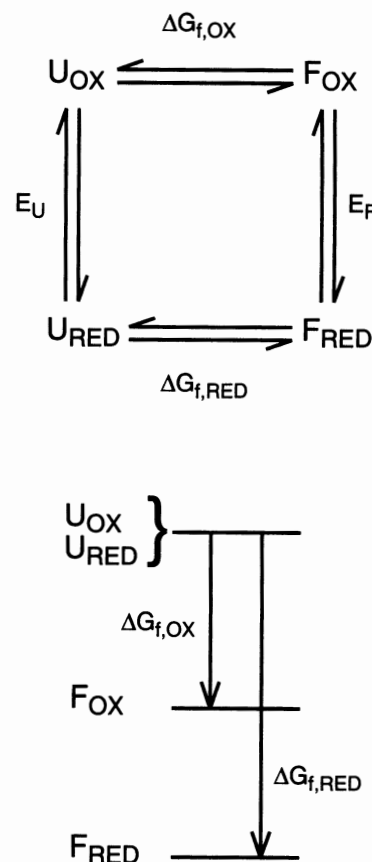


Figure 13. Thermodynamic cycle and free-energy diagram for the oxidized (OX) and reduced (RED) states of unfolded (U) and folded (F) forms of a redox-active protein.

(e.g., urea, guanidine hydrochloride (GuHCl)) to protein solutions induces unfolding; the folding free energies under these conditions ( $\Delta G_f$ ) often are found to be linear functions of the denaturant concentration ([D], eq. 4).<sup>138,139</sup>

$$\Delta G_f = \Delta G_f^\circ + m_D[D] \quad (4)$$

Indeed, linear extrapolation to infinite dilution of a  $\Delta G_f$  vs. [D] plot is commonly employed to estimate  $\Delta G_f^\circ$ .<sup>140</sup> In redox proteins with large values of  $\Delta E_f^\circ$ , and comparable values of  $m_{D,OX}$  and  $m_{D,RED}$ , it is possible to find denaturing conditions where one oxidation state of the protein is fully unfolded while the other is fully folded.<sup>141</sup>

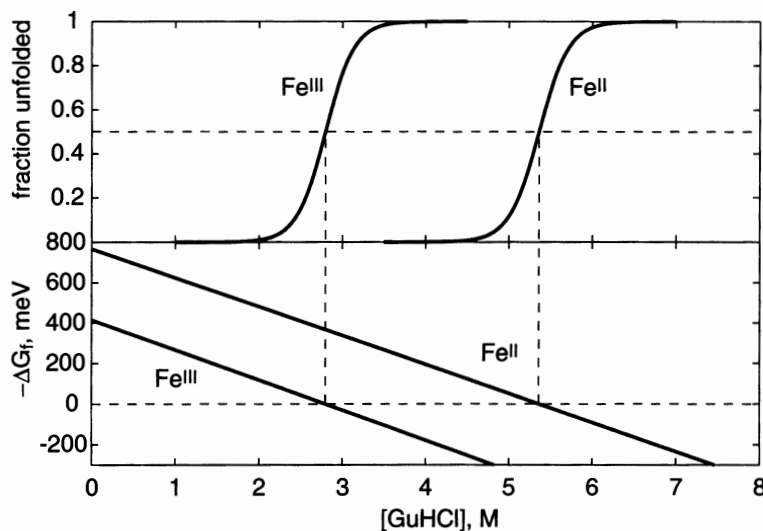
The coupling of folding free energies and redox potentials is clearly illustrated by the unfolding behavior of horse heart cytochrome *c* (Figure 14).<sup>82,83,142</sup> In the folded protein, the formal potential of the heme cofactor is 0.38-V greater than its value in aqueous solution. Consequently, the reduced protein has a more favorable folding free energy than the oxidized protein ( $\Delta\Delta G_f^\circ = 42 \text{ kJ mol}^{-1}$ ). The unfolding midpoints occur at denaturant concentrations of 2.8 M ( $\Delta G_{f,OX}/m_{D,OX}$ ) and 5.3 M ( $\Delta G_{f,RED}/m_{D,RED}$ ) for oxidized and reduced proteins, respectively. Notably, the values of  $m_{D,OX}$  and  $m_{D,RED}$  are quite similar (14.3 and 13.8  $\text{kJ mol}^{-1} \text{ M}^{-1}$ , respectively).<sup>142</sup> There is a range of denaturant concentrations in which  $\geq 99\%$  of the oxidized protein is unfolded and  $\geq 99\%$  of the reduced protein is folded. In this range, electron injection into the ferriheme of the unfolded protein will initiate a folding reaction.<sup>82,83,143,144</sup> Similarly, electron removal from the reduced folded protein will induce unfolding.

An attractive feature of ET-triggered folding is the availability of many well-established techniques for rapidly injecting and removing electrons from proteins on time scales as short as a few nanoseconds. Electronically excited  $\text{Ru}(\text{bpy})_3^{2+}$  ( $^*\text{Ru}(\text{bpy})_3^{2+}$ ) is a powerful reductant ( $E^\circ(\text{Ru}^{3+}/^*\text{Ru}^{2+}) = -0.85 \text{ V vs. NHE}$ ) and its 600-ns decay time makes it an excellent reagent for triggering folding reactions on the microsecond time scale.<sup>82</sup> Furthermore, the millisecond-time-scale reoxidation of the reduced protein by  $\text{Ru}(\text{bpy})_3^{3+}$  regenerates the initial species and permits extensive signal averaging.

Complete folding of a protein can require tens to hundreds of milliseconds. Consequently, irreversible photochemical ET reagents are required to study the entire range of folding dynamics. We have found that NADH is an effective irreversible photochemical sensitizer for injecting electrons into unfolded proteins.<sup>143,145</sup> Two-photon, 355-nm excitation of this reagent generates two powerful reductants, a solvated electron and  $\text{NAD}^\bullet$ ;<sup>146</sup> both reductants reduce unfolded heme proteins ( $\sim 100 \mu\text{M}$ ) in about 100  $\mu\text{s}$ . The combination of  $^*\text{Ru}(\text{bpy})_3^{2+}$  and NADH permits investigations of 1  $\mu\text{s}$  to  $> 1 \text{ s}$  folding events of heme proteins.

### A. CYTOCHROME *c*

The early events in  $\text{Fe}^{\text{II}}\text{-cyt}_U c$  folding have been examined using  $^*\text{Ru}(\text{bpy})_3^{2+}$  as the photochemical sensitizer.<sup>82,145</sup> In 3.5 M GuHCl, the first-order decay rate for  $^*\text{Ru}(\text{bpy})_3^{2+}$  is a linear function of the concentration of  $\text{Fe}^{\text{III}}\text{-cyt}_U c$ . This observation is consistent with a bimolecular ET reaction between

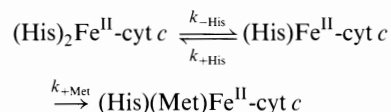


**Figure 14.** GuHCl denaturation curves and unfolding isotherms for oxidized ( $\text{Fe}^{\text{III}}$ ) and reduced ( $\text{Fe}^{\text{II}}$ ) cytochrome *c*.

\*Ru(bpy)<sub>3</sub><sup>2+</sup> and Fe<sup>III</sup>-cyt<sub>U</sub> *c*. After the rapid change in absorbance following electron injection into unfolded cytochrome *c*, there is no substantial variation in the spectrum of the reduced protein for a time period of up to 200 μs. NADH was used as the sensitizer to study ferrocycytochrome *c* folding between 100 μs and 1 s. Following reduction of horse heart Fe<sup>II</sup>-cyt<sub>U</sub> *c* at pH 7 ([GuHCl] = 3.2 M), the transient difference spectrum is characteristic of a low-spin, six-coordinate ferroheme, suggesting that the ferrous ion in the unfolded protein remains axially coordinated to two His ligands. Only minor changes in Soret absorbance are observed in the time range from a few microseconds to several milliseconds after electron injection; significant changes in the heme spectrum occur 50–100 ms after injection. The difference spectrum measured 400 ms after reduction of Fe<sup>II</sup>-cyt<sub>U</sub> *c* closely matches that of folded Fe<sup>II</sup>-cyt *c*. Importantly, there is no spectroscopic evidence for a high-spin intermediate in the folding of Fe<sup>II</sup>-cyt *c* at neutral pH.

The heme axial-ligand set in unfolded cytochrome *c* is a sensitive function of the solution pH. At lower pH, nonnative histidine binding is disfavored (p*K*<sub>a</sub> ~ 5.3); the oxidized heme is high-spin and the axial ligands are His18 and water ((H<sub>2</sub>O)(His)Fe<sup>III</sup>-cyt<sub>U</sub> *c*).<sup>145,147–149</sup> Under such conditions, Fe<sup>III</sup>-cyt<sub>U</sub> *c* folding is markedly faster than at neutral pH and a single kinetic phase is observed when folding is probed by Trp fluorescence and S(Met80)→Fe<sup>III</sup> charge-transfer absorption.<sup>127,128</sup>

Transient absorption measurements of ET-triggered ferrocycytochrome *c* folding reveal a central role for ligand binding and dissociation kinetics. This is due, in large part, to the fact that the heme spectrum is far more sensitive to the Fe coordination sphere than it is to the polypeptide conformation. A three-component kinetics model describes our observations:



The general solution to the rate law for this model predicts biphasic kinetics. Above pH 6, ferrocycytochrome *c* folding is slow and monophasic (*k*<sub>obs</sub> = 1–20 s<sup>-1</sup>; [GuHCl] = 3.1 M). Since we observe only (His)<sub>2</sub>Fe<sup>II</sup>-cyt *c* and (His)(Met)Fe<sup>II</sup>-cyt *c*, we can invoke the steady-state approximation for (His)Fe<sup>II</sup>-cyt *c*. In this limit, the kinetics will be exponential with an observed rate constant given by:

$$k_{\text{obsd}} = \frac{k_{-\text{His}}k_{+\text{Met}}}{k_{+\text{His}} + k_{+\text{Met}}}$$

At high pH, then, folding could be limited by Met80 binding (*k*<sub>+His</sub> ≫ *k*<sub>+Met</sub>; *k*<sub>obsd</sub> ~ *k*<sub>+Met</sub>*k*<sub>-His</sub>/*k*<sub>+His</sub>), or by nonnative His dissociation (*k*<sub>+Met</sub> ≫ *k*<sub>+His</sub>; *k*<sub>obsd</sub> ~ *k*<sub>-His</sub>).

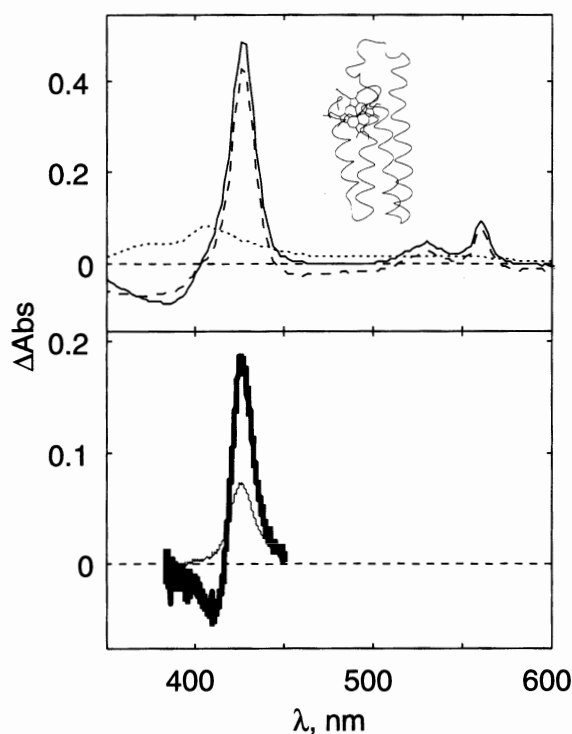
Below pH 6, the folding kinetics are biphasic, and all three of the ligation states of the reduced heme can be detected in the transient absorption spectra. Under these conditions, the steady-state approximation is not valid. The faster kinetics phase reflects the equilibration between (His)<sub>2</sub>Fe<sup>II</sup>-cyt *c* and (His)Fe<sup>II</sup>-cyt *c*, with a pH-dependent rate constant given by *k*<sub>+His</sub> + *k*<sub>-His</sub>. The rate constant for the slower step corresponds to *k*<sub>+Met</sub> = 16(5) s<sup>-1</sup>. If *k*<sub>+Met</sub> does not vary substantially with pH, then it is likely that *k*<sub>-His</sub> limits ferrocycytochrome *c* folding above pH 6.

## B. CYTOCHROME *b*<sub>562</sub>

A requirement for kinetics studies of folding is that the heme cofactor remain bound to the unfolded protein. When the heme is dissociated from the unfolded protein, its bimolecular capture would likely be the rate-limiting process. Surprisingly, ET triggering can be employed to study the folding of a four-helix-bundle protein, cytochrome *b*<sub>562</sub>.<sup>143</sup> Although the porphyrin is not covalently attached to the protein, the heme iron is ligated axially by the side chains of Met7 and His102.

As expected for a heme protein with a 0.18-V reduction potential, titrations with GuHCl confirm that reduced cytochrome *b*<sub>562</sub> is more stable toward unfolding than the oxidized protein.<sup>143,150,151</sup> Unfolding experiments probed using circular dichroism and Soret-band absorbance gave identical results, consistent with a two-state process. In contrast to the *bis*-His ligation of unfolded cytochrome *c*, absorption spectra of the unfolded cytochrome *b*<sub>562</sub> indicate that the heme iron is high-spin in both oxidation states. Oxidized cytochrome *b*<sub>562</sub> is fully denatured at 2 M GuHCl, whereas reduced cytochrome *b*<sub>562</sub> does not unfold below 6 M GuHCl. The oxidized protein refolds upon dilution of GuHCl, and the refolding kinetics show no protein-concentration dependence, indicating that the heme is still associated with the protein in the unfolded state. It is possible that the Fe<sup>III</sup>-N(His102) bond is still intact in the unfolded protein.

Electron injection into unfolded, oxidized cytochrome *b*<sub>562</sub> (Fe<sup>III</sup>-cyt<sub>U</sub> *b*<sub>562</sub>) produces a significant amount of folded, reduced protein (Fe<sup>II</sup>-cyt<sub>F</sub> *b*<sub>562</sub>) at GuHCl concentrations between 2 and 3 M. The transient difference spectrum measured 200 μs after laser excitation of NADH in the presence of Fe<sup>III</sup>-cyt<sub>U</sub>



**Figure 15.** (upper) Difference absorption spectra between reduced, unfolded protein and oxidized unfolded protein (dotted line) and between reduced, folded protein and oxidized, unfolded protein (solid line). Difference absorption spectrum of cytochrome  $b_{562}$  measured before and after photochemical electron injection (dashed line). (inset) Backbone structure of cytochrome  $b_{562}$ . (lower) Transient absorption spectra recorded 200  $\mu\text{s}$  (thin line) and 2 ms (thick line) after electron injection into a sample of unfolded, oxidized cytochrome  $b_{562}$ . Spectra taken after 2 ms (up to 400 ms) show no further change in absorption.

$b_{562}$  (Figure 15) is consistent with that of a high-spin  $\text{Fe}^{\text{II}}$  heme. The spectrum measured 2 ms after excitation (Figure 15) indicates the formation of a low-spin  $\text{Fe}^{\text{II}}$  heme, and closely matches that expected for  $\text{Fe}^{\text{II}}$ -cyt $_F b_{562}$ . The ferrocyanochrome  $b_{562}$  folding kinetics can be described by a dominant kinetics phase with a first-order rate constant of  $800 \pm 200 \text{ s}^{-1}$  at a driving force of  $\sim 25 \text{ kJ/mol}$  (2.5 M GuHCl). At a similar driving force,  $\text{Fe}^{\text{II}}$ -cyt $_U c$  folds much more slowly ( $10 \text{ s}^{-1}$ ). The absence of nonnative His ligands is certainly one explanation for the faster folding of cytochrome  $b_{562}$ ; but even at reduced pH, the rate of Met80 binding to the ferroheme in cytochrome  $c$  ( $16(5) \text{ s}^{-1}$ ) is far slower than in cytochrome  $b_{562}$ .

### C. CYTOCHROME $c'$

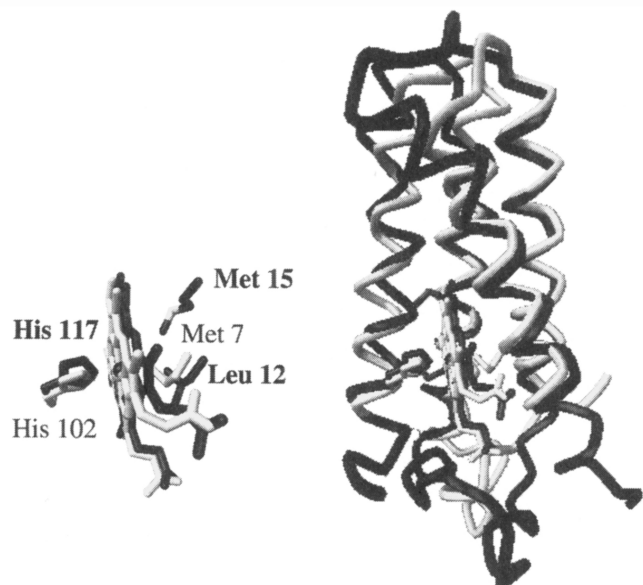
Although folded  $\text{Fe}^{\text{II}}$ -cyt  $b_{562}$  was observed within milliseconds after reduction of the unfolded oxidized protein, no more than half of the reduced protein successfully developed native structure.<sup>152</sup> Rapid heme dissociation from the polypeptide ( $k_{\text{diss}} \sim 2\text{--}7 \times 10^3 \text{ s}^{-1}$ ) limited the yield of the folding reaction. The heme-loss step selects fast-folding conformations from the

unfolded ensemble; if there are slow-folding components, they cannot be detected. Under these circumstances, the observed kinetics reflect heme-dissociation dynamics rather than folding.

Cytochrome  $c'$  (cyt  $c'$ ) from the photosynthetic bacterium *Rhodospseudomonas palustris* is a monomeric, soluble, 125-residue, four-helix-bundle heme protein. Importantly, the porphyrin is bound to the polypeptide with two thioether links near the C terminus (Cys113 and Cys116).<sup>153–155</sup> Although sharing just 19% sequence identity and 40% similarity,<sup>156</sup> cyt  $c'$  and cyt  $b_{562}$  have quite similar folds (1.6-Å RMSD in  $\alpha$ -carbon position) (Figure 16).<sup>157,158</sup> Cyt  $b_{562}$  has a six-coordinate, low-spin heme with Met7 and His102 axial ligands ( $(^{\text{H}102\text{N}})\{\text{PorN}_4\text{Fe}^{\text{III}}\}(\text{M}7\text{S})^+$ ) and a reduction potential of 180 mV vs. NHE.<sup>157,159</sup> Cyt  $c'$  has a high-spin, five-coordinate heme, axially ligated by His117 ( $(^{\text{H}117\text{N}})\{\text{PorN}_4\text{Fe}^{\text{III}}\}^+$ ) and a reduction potential of 100 mV.<sup>160–165</sup> In cyt  $c'$ , the side chain of Leu12 fills the space occupied by a sixth ligand in cyt  $b_{562}$  (Figure 16, inset);<sup>158</sup> movement of this bulky group is necessary for ligand binding.

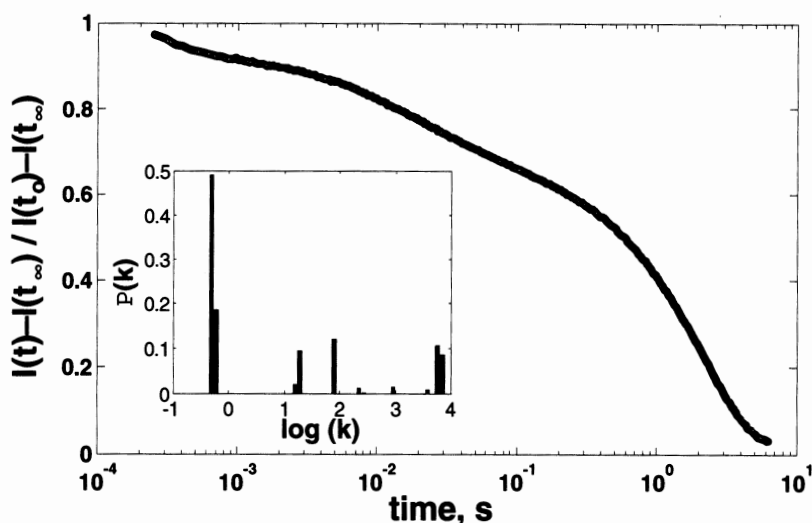
The  $\text{Fe}^{\text{III/II}}$  reduction potential is high enough to permit ET triggering of  $\text{Fe}^{\text{II}}$ -cyt  $c'$  folding in

the 2.0–2.9-M guanidine hydrochloride (GuHCl) concentration range. Fe<sup>II</sup>-cyt *c'* folding has been initiated by rapid electron injection ( $\sim 100 \mu\text{s}$ ) into unfolded oxidized protein ( $[\text{GuHCl}] = 2.02\text{--}2.54 \text{ M}$ ) following two-photon laser excitation of NADH.<sup>145,146</sup> Under these conditions, heme reduction is slower than binding of the nonnative sixth ligand. Highly heterogeneous kinetics were



**Figure 16.** Comparison of the structures of cytochrome  $b_{562}$  and cytochrome  $c'$ . In cytochrome  $b_{562}$  (gray), the heme iron is axially ligated to His-102 and Met-7, whereas in cytochrome  $c'$  (black), the heme has only one axial ligand (His-117) with the side chain of Leu-12 at the other axial site. The nearest methionine residue in cytochrome  $c'$  (Met-15) also is shown. Backbone atoms of four  $\alpha$ -helices of cytochrome  $c'$  are superimposed on the corresponding atoms in cytochrome  $b_{562}$ , with a calculated rms deviation of 1.6 Å.

observed in studies where the progress of the folding reaction was monitored by heme absorption in the Soret and Q-band regions from  $10^{-4}$  to 1 s after excitation. A small fraction ( $\sim 20\%$ ) of the population forms a high-spin heme species in about a millisecond. Complete formation of the fully folded ensemble requires several seconds (Figure 17). Rate constants for Fe<sup>II</sup>-cyt *c'* span a range from  $10^3$  to  $10^{-1} \text{ s}^{-1}$  revealing fast- ( $7.0 \times 10^3 \text{ s}^{-1}$ , 8%;  $5.7 \times 10^3 \text{ s}^{-1}$ , 9%), intermediate- ( $9.0 \times 10^2$  to  $1.5 \times 10^1 \text{ s}^{-1}$ , 24%), and slow-folding ( $5.9 \times 10^{-1} \text{ s}^{-1}$ , 16%;  $4.8 \times 10^{-1} \text{ s}^{-1}$ , 43%) components in the protein ensemble (Figure 17 inset). Although the relative populations and the number of different rate constants vary slightly for kinetics measured at different wavelengths, heterogeneous behavior is always observed. On very long time scales, oxidation of the reduced protein leads to some uncertainty in the extracted rate constants (although the samples were carefully deoxygenated, trace amounts of oxygen were always present). The transient difference spectrum recorded 100  $\mu\text{s}$  after electron injection is characteristic of a mixture of five-coordinate, high-spin and six-coordinate, low-spin ferrohemes, suggesting that the slower folding populations are misligated. The difference spectra measured at 1 and 500 ms have been fit to a combination of the [(Fe<sup>II</sup>-folded)–(Fe<sup>III</sup>-unfolded)] and [(Fe<sup>II</sup>-unfolded)–(Fe<sup>III</sup>-unfolded)] molar difference spectra. The resulting folded and unfolded populations (1 ms, 25% folded, 75% unfolded; 500 ms, 52% folded, 48% unfolded) are consistent with the measured amplitude changes in the single wavelength kinetics.



**Figure 17.** Normalized folding kinetics (observed at 440 nm, black line) fit to 80 rate constants spanning logarithmically  $10^5$  to  $10^{-2} \text{ s}^{-1}$  (gray line) using a nonnegative least-squares algorithm. (Inset) The projected population of rate constants: ( $7.0 \times 10^3 \text{ s}^{-1}$  (8%);  $5.7 \times 10^3 \text{ s}^{-1}$  (9%);  $9.2 \times 10^2$  (1%);  $2.2 \times 10^2$  (1%);  $7.9 \times 10^1$  (11%);  $1.9 \times 10^1$  (9%);  $1.5 \times 10^1$  (2%);  $5.9 \times 10^{-1}$  (16%);  $4.8 \times 10^{-1}$  (43%)).

It is reasonable to expect that topologically homologous proteins would fold at similar rates, yet cytochromes  $b_{562}$  and  $c'$  display quite disparate folding kinetics. Apparently, there are factors beyond structural topology that must be considered in order to explain the folding kinetics of these four-helix bundles. Three key features of cytochromes  $b_{562}$  and  $c'$  are likely to contribute to the differences in folding kinetics: covalent attachment of the porphyrin to the polypeptide; nonnative heme-ligand traps; and folding driving force.

The rapid dissociation of the heme from unfolded  $\text{Fe}^{\text{II}}$ -cyt  $b_{562}$  limits the time scale for observation of folding kinetics. Since the porphyrin is covalently attached in  $\text{Fe}$ -cyt  $c'$ , the folding kinetics cover a far wider time range and are considerably more complex. A fraction of the unfolded  $\text{Fe}^{\text{II}}$ -cyt  $c'$  ensemble refolds rapidly, but several seconds are required for the entire sample to fold. Proline isomerization is known to inhibit protein folding<sup>166</sup> but is unlikely to be responsible for the slow  $\text{Fe}$ -cyt  $c'$  kinetics. Although there are four proline residues in the cyt  $c'$  sequence, the observed folding rates depend on denaturant concentration, and are substantially faster than typical proline isomerizations.<sup>166</sup> It is interesting to note that the fast-folding fraction of  $\text{Fe}^{\text{II}}$ -cyt  $c'$  is roughly comparable to the yield of folded  $\text{Fe}^{\text{II}}$ -cyt  $b_{562}$ . It is possible, then, that if heme dissociation could be inhibited,  $\text{Fe}^{\text{II}}$ -cyt  $b_{562}$  would display slower and more complex folding kinetics.

The refolding of  $\text{Fe}^{\text{II}}$ -cyt  $c'$  can be described qualitatively by a kinetic partitioning mechanism.<sup>167,168</sup> At the instant that folding is initiated, a fraction of the denatured proteins will have adopted conformations that can smoothly and rapidly fold to the native structure. The fast-folding population of  $\text{Fe}^{\text{II}}$ -cyt  $c'$  would correspond to this group. Folding of the remaining fraction is frustrated by transient trapping in local minima on the folding energy landscape. Escape from these misfolded structures is an activated process that slows formation of the native structure. The partition factor that determines the balance between fast- and slow-folding populations depends on the primary sequence as well as the refolding conditions.<sup>167-172</sup> Simulated folding kinetics of model three-helix-bundle proteins<sup>169,170</sup> point to a central role for the folding free-energy gap in determining the partitioning between fast- and slow-track folding. The heterogeneous folding kinetics of  $\text{Fe}^{\text{II}}$ -cyt  $c'$  are strikingly similar to the simulated folding kinetics of a small-gap three-helix-bundle.<sup>170</sup>

Nonnative methionine ligands in unfolded  $\text{Fe}^{\text{II}}$ -cyt  $c'$  contribute to the heterogeneity of the folding kinetics. In

addition to the fast-folding population, there are intermediate ( $\sim 10^2 \text{ s}^{-1}$ ) and slow-folding ( $< 1 \text{ s}^{-1}$ ) components. Iron-sulfur bond dissociation is not rate-limiting because ferroheme-methionine ligand exchange is faster than either folding phase.<sup>173</sup> In the presence of CO, the nonnative Met ligands are displaced from the ferroheme and folding is dominated by a slow phase with a time constant of  $\sim 350 \text{ ms}$ . Similarly,  $\text{Fe}^{\text{III}}$ -cyt  $c'$  folding is not complicated by heme-ligand binding and a single 1-s phase predominates. These observations suggest that, in the absence of misligation, cyt  $c'$  requires 500–1000 ms to adopt a folded structure. The presence of an intermediate ( $\sim 10^2 \text{ s}^{-1}$ ) folding phase in  $\text{Fe}^{\text{II}}$ -cyt  $c'$  implies that nonnative methionine ligation can, in some instances, facilitate refolding. On a free-energy basis, the  $\text{Fe}$ -cyt  $c'$  folding kinetics more closely resemble those of cytochrome  $c$  than those of the non-heme helical-bundle proteins. Nonnative ligand binding clearly can perturb heme protein folding; it is likely that noncovalent, nonnative heme-polypeptide contacts represent additional sources of frustration.

#### D. Zn-CYTOCHROME $c$

The reactivity of a polypeptide can be an extremely sensitive indicator of structural heterogeneity. With a carefully selected probe reaction, a bimodal distribution of protein conformations would exhibit biphasic kinetics, whereas a single-mode distribution would react in a single phase. The key requirement is that the probe reaction be fast compared to the time scale of folding ( $< 10^{-4}$  to  $> 10^1 \text{ s}$ ). Electron-transfer reactions are excellent folding probes because rates at high driving forces are determined by the distance and medium separating the two redox partners.<sup>74</sup> Buried redox centers in proteins often exchange electrons rather slowly with reagents in solution. Unfolding will greatly increase the accessibility of a redox cofactor and can lead to much faster ET. Compact intermediates might be expected to exhibit ET rates somewhere between those of the folded and unfolded molecules.

The folding landscape of Zn(II)-substituted cytochrome  $c$  (Zn-cyt  $c$ )<sup>174</sup> has been investigated using ET reactivity probes.<sup>85</sup> Zn-cyt  $c$  is structurally homologous to the native protein ( $\text{Fe}$ -cyt  $c$ ), which has been studied in great detail.<sup>173,175-177</sup> A nonnative axial ligand (His 26 or His 33) replaces Met 80 at neutral pH in denatured horse heart  $\text{Fe}$ -cyt  $c$ ;<sup>149</sup> the rate-limiting folding step in this case is correction of heme misligation. Owing to weaker binding and faster substitution at the sixth coordination site, replacement of Fe with Zn will

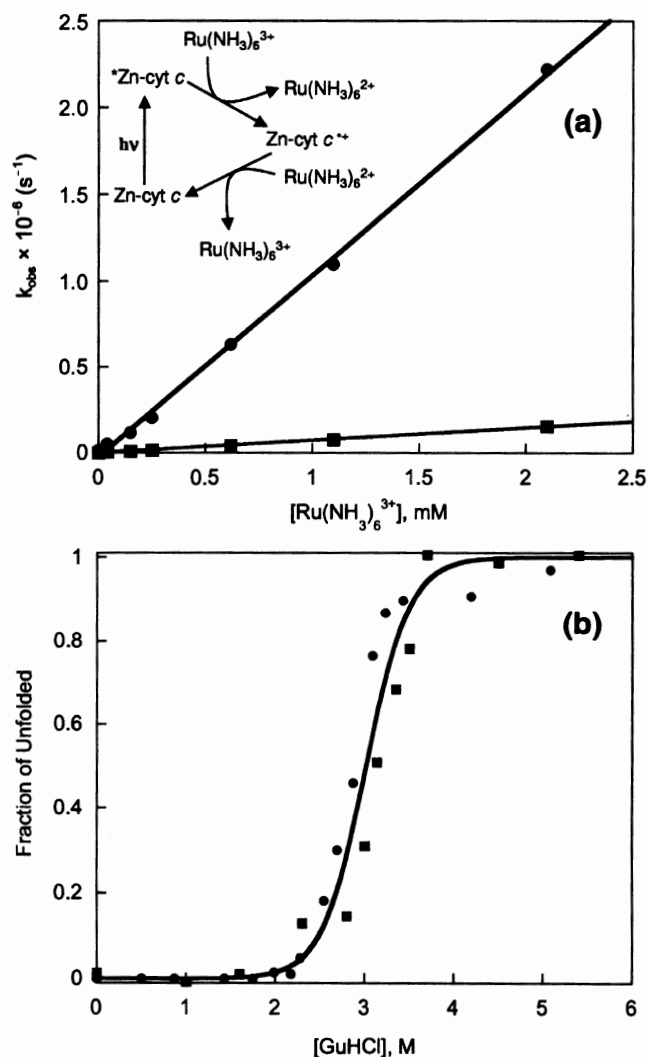


eliminate axial ligand traps during refolding.<sup>178</sup> The key advantage of the Zn-substituted protein is the availability of a long-lived ( $\tau \sim 15$  ms), powerfully reducing ( $E^\circ = -0.8$  V vs. NHE) triplet excited state ( $^*Zn\text{-cyt } c$ ), which can be prepared in 90% yield<sup>179</sup> with 580-nm laser excitation.<sup>51</sup>

Addition of guanidine hydrochloride (GuHCl) to solutions of Zn-cyt *c* produces a blueshift in the Soret absorption band (folded,  $\lambda_{\text{max}} = 426$  nm; unfolded,  $\lambda_{\text{max}} = 418$  nm), giving a species with a spectrum similar to that of Zn(II)-substituted myoglobin ( $\lambda_{\text{max}} = 414$  nm).<sup>59</sup> GuHCl unfolding curves generated from Soret absorp-

tion and far-UV CD spectra show that the stability of folded Zn-cyt *c* is comparable to that of the Fe(III) form (Fe(III):  $\Delta G_f^\circ = -40(1)$  kJ mol<sup>-1</sup>, [GuHCl]<sub>1/2</sub> = 2.8(1) M; Zn(II):  $\Delta G_f^\circ = -35(2)$  kJ mol<sup>-1</sup>, [GuHCl]<sub>1/2</sub> = 2.9(1) M).<sup>83,136</sup> In contrast to Fe-cyt *c*, the Zn center in the unfolded protein should not be ligated by any peptide side chain other than the native His 18.<sup>178</sup>

Triplet-excited Zn-cyt *c* is quenched by  $Ru(NH_3)_6^{3+}$ , producing Zn-cyt *c*<sup>•+</sup> and  $Ru(NH_3)_6^{2+}$  (Figure 18, inset). The reported quenching rate constant measured under native conditions is  $1.4 \times 10^7$  M<sup>-1</sup> s<sup>-1</sup>.<sup>51</sup> Moderate concentrations of GuHCl (< 1.0 M) do not unfold the



**Figure 18.** (a) ET quenching of  $^*Zn\text{-cyt } c$  by  $Ru(NH_3)_6^{3+}$  (inset: reaction scheme) in deoxygenated GuHCl solution (2.85 M, 100 mM sodium phosphate, pH 7). The  $^*Zn\text{-cyt } c$  decay under these conditions is biexponential and both observed rate constants vary linearly with  $[Ru(NH_3)_6^{3+}]$ . The second-order rate constants extracted from these measurements are attributed to bimolecular ET reactions of folded ( $7.2 \times 10^7$  M<sup>-1</sup>s<sup>-1</sup>, red squares) and unfolded ( $1.0 \times 10^9$  M<sup>-1</sup>s<sup>-1</sup>, blue circles) protein. (b) Denaturation curve for Zn-cyt *c* generated from Soret absorption (red squares) and ET rate (blue circles) data. Zn-cyt *c* was prepared from commercial horse heart protein according to standard procedures.<sup>174</sup> Guanidine hydrochloride and  $[Ru(NH_3)_6]Cl_3$  were from commercial sources and used without additional purification.

protein, but accelerate  $\text{Ru}(\text{NH}_3)_6^{3+}$  quenching, presumably because of the increased ionic strength.<sup>180</sup> Under denaturing conditions ( $[\text{GuHCl}] > 3 \text{ M}$ ), the quenching reaction is 100 times faster ( $1.4 \times 10^9 \text{ M}^{-1} \text{ s}^{-1}$ ,  $[\text{GuHCl}] = 3.5 \text{ M}$ ) than that measured in the absence of GuHCl. At a GuHCl concentration corresponding to the midpoint of Zn-cyt *c* unfolding (2.85 M), the  $\text{Ru}(\text{NH}_3)_6^{3+}$  quenching kinetics are biexponential. Both rate constants exhibit a linear dependence on  $[\text{Ru}(\text{NH}_3)_6^{3+}]$  giving respective values of  $7.2 \times 10^7$  and  $1.0 \times 10^9 \text{ M}^{-1} \text{ s}^{-1}$  for folded and unfolded ensembles (Figure 18). The latter quenching rate is very high, owing to the greater accessibility of the Zn-porphyrin in the unfolded protein. The \*Zn-cyt *c* ET kinetics are generally consistent with a two-state unfolding process. The unfolding isotherm generated from ET kinetics exhibits a transition midpoint at 2.8(1) M GuHCl, in good agreement with those obtained from far-UV CD and heme absorption measurements (Figure 18).<sup>174</sup>

Changes in Zn-cyt *c* Soret absorption (418 and 426 nm) after stopped-flow dilution of denaturant (initial  $[\text{GuHCl}] = 3.4 \text{ M}$ ; final  $[\text{GuHCl}] = 1.20\text{--}2.60 \text{ M}$ ) were examined: the transient absorption kinetics are exponential functions and the observed rate constants depend linearly on denaturant concentration, decreasing from  $1.3 \pm 0.2 \times 10^2 \text{ s}^{-1}$  at 1.20 M GuHCl to  $1.1 \pm 0.1 \times 10^1 \text{ s}^{-1}$  at 2.60 M GuHCl. The extrapolated time constant for refolding in the absence of denaturant is about a millisecond. The Zn-cyt *c* folding rate is about 10 times higher than that of the Fe(III) protein at comparable driving forces,<sup>175,176</sup> consistent with the absence of heme misligation.

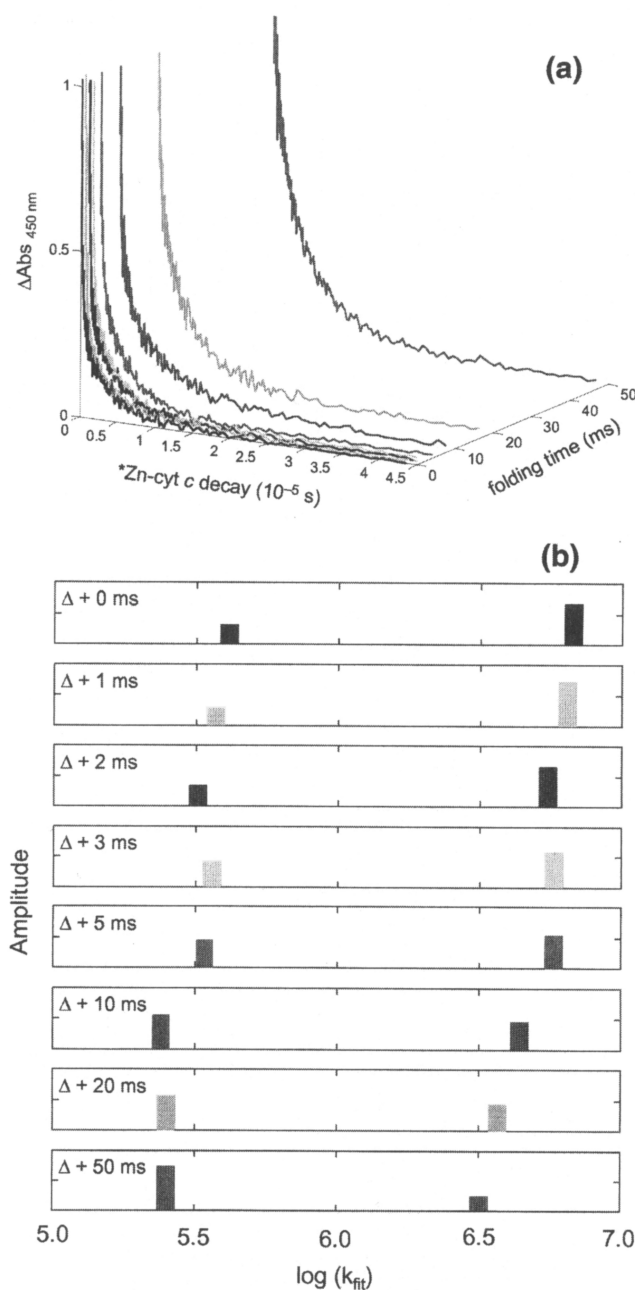
More complex Zn-cyt *c* folding becomes apparent when the process is probed with transient absorption measurements (450 nm) of \*Zn-cyt *c*/Ru(NH<sub>3</sub>)<sub>6</sub><sup>3+</sup> ET kinetics. As the polypeptide chain folds around the porphyrin, the \*Zn-cyt *c* ET rate decreases from its value in the unfolded protein ( $\sim 7 \times 10^6 \text{ s}^{-1}$ ,  $[\text{Ru}(\text{NH}_3)_6^{3+}] = 3\text{--}5 \text{ mM}$ ) to that characteristic of folded molecules ( $\sim 2.5 \times 10^5 \text{ s}^{-1}$ ). Biphasic \*Zn-cyt *c* decay kinetics are observed during protein refolding; biexponential functions provide adequate fits to the \*Zn-cyt *c* kinetics, although the residuals suggest that more than just two decay components are present. Fits to the kinetics recorded 1 ms after GuHCl dilution to 1.46 M reveal that two-thirds of the excited Zn-porphyrins decay in a fast phase ( $7 \pm 2 \times 10^6 \text{ s}^{-1}$ ) attributable to largely unfolded protein; the remaining third exhibits a rate constant ( $3.5 \pm 1.5 \times 10^5 \text{ s}^{-1}$ ) closer to that expected for folded molecules. ET kinetics

measured at longer folding times remain biphasic with the amplitude of the faster component decreasing in favor of an increase in the amplitude of the slow component (Figure 19).

Both rate constants extracted from biexponential fits to the \*Zn-cyt *c* decay kinetics decrease by about a factor of two as the folding reaction proceeds (1 ms,  $7 \pm 2 \times 10^6$ ,  $3.5 \pm 1.5 \times 10^5 \text{ s}^{-1}$ ; 50 ms,  $3 \pm 2 \times 10^6$ ,  $2.2 \pm 0.4 \times 10^5 \text{ s}^{-1}$ ) (Figure 19). This variation in quenching efficiency, although close to the uncertainties in our measured rate constants, may reflect a gradual collapse of polypeptide structures during folding. It is important to note, however, that biexponential functions only approximate the \*Zn-cyt *c* decay kinetics. It is likely that the two rate constants extracted from these fits represent the average ET rates of two heterogeneous populations of polypeptides, one largely unfolded, the other compact. In this case, the shifts in \*Zn-cyt *c* decay constants could reflect subtle changes in the composition of these two groups during protein folding.

The amplitudes of the two \*Zn-cyt *c* decay phases vary exponentially with folding time and the rate constant ( $33 \text{ s}^{-1}$ ,  $[\text{GuHCl}] = 1.46 \text{ M}$ ) is in reasonable agreement with that measured by Soret absorption spectroscopy. It is noteworthy that, at the earliest measured folding times (1 ms), there are significant amplitudes in *both* the fast and slow \*Zn-cyt *c* ET phases ( $\sim 67\%$  fast;  $\sim 33\%$  slow). This is substantially more than would be expected on the basis of the stopped-flow dead-time ( $\sim 1 \text{ ms}$ ) and the observed rate constants. Measurements of \*Zn-cyt *c* kinetics at different GuHCl concentrations consistently extrapolate back to a “burst-phase” ensemble<sup>175,176,181,182</sup> with a 2:1 ratio of fast and slow ET components: these results demonstrate that the burst ensemble is heterogeneous; molecules in one-third of the protein population have compact structures, and ones in the remaining fraction have exposed Zn-porphyrins.

It is apparent that there is underlying complexity in Zn-cyt *c* folding. The fraction of the burst ensemble ( $\sim 1/3$ ) with slow \*Zn-cyt *c* decay kinetics could be fully folded protein or an ensemble of compact nonnative structures. The former possibility would be an example of “fast-track” folding,<sup>167,170,183</sup> where about a third of the unfolded Zn-cyt *c* molecules adopt conformations that can refold very quickly. The remaining protein molecules have relatively exposed porphyrin groups, and fold on a substantially longer time scale. Alternatively, the 2:1 ratio of fast:slow \*Zn-cyt *c* decay components formed immediately after dilution of



**Figure 19.** Zn-cyt *c* folding probed by ET kinetics. (a) Folding initiated by stopped-flow denaturant dilution (final concentrations: [GuHCl] = 1.46 M; [Zn-cyt *c*] = 10  $\mu\text{M}$ ; [Ru(NH<sub>3</sub>)<sub>6</sub><sup>3+</sup>] = 4 mM; pH 7) and monitored by laser transient absorption measurements of \*Zn-cyt *c* decay (450 nm, signals normalized to an initial value of 1.0) at different delay times after mix was complete (0, 1, 2, 3, 5, 10, 20, and 50 ms). (b) Rate constants and relative amplitudes from biexponential fits of \*Zn-cyt *c* decay data measured during protein folding. The observed rate constants decrease by about a factor of two as folding proceeds.

[GuHCl] may reflect a shift in the equilibrium between unfolded and compact nonnative structures. Although it is often assumed that native solvent conditions will strongly favor compact structures, the \*Zn-cyt *c* ET kinetics clearly indicate that two-thirds of the molecules in the burst intermediates have highly exposed porphyrins. Ultimately, the entire protein ensemble folds

because, at low [GuHCl], the native structure is much more stable than unfolded conformations.

#### ACKNOWLEDGMENT

Our research on heme proteins has been supported by the National Institutes of Health, the National Science

Foundation, and the Arnold and Mabel Beckman Foundation.

## REFERENCES

- De Vault, D.; Chance, B. *Biophys. J.* **1966**, *6*, 825–846.
- McGourty, J. L.; Blough, N. V.; Hoffman, B. M. *J. Am. Chem. Soc.* **1983**, *105*, 4470–4472.
- Peterson-Kennedy, S. E.; McGourty, J. L.; Kalweit, J. A.; Hoffman, B. M. *J. Am. Chem. Soc.* **1986**, *108*, 1739–1746.
- Hoffman, B. M.; Ratner, M. A. *J. Am. Chem. Soc.* **1987**, *109*, 6237–6243.
- Hoffman, B. M.; Ratner, M. A.; Wallin, S. A. *Energetics and Dynamics of Gated Reactions*. Johnson, M., Ed.; American Chemical Society: Washington, DC, **1990**; Vol. 226, pp. 125–146.
- Nocek, J. M.; Stemp, E. D. A.; Finnegan, M. G.; Koshy, T. I.; Johnson, M. K.; Margoliash, E.; Mauk, A. G.; Smith, M.; Hoffman, B. M. *J. Am. Chem. Soc.* **1991**, *113*, 6822–6831.
- Wallin, S. A.; Stemp, E. D. A.; Everest, A. M.; Nocek, J. M.; Netzel, T. L.; Hoffman, B. M. *J. Am. Chem. Soc.* **1991**, *113*, 1842–1844.
- Everest, A. M.; Wallin, S. A.; Stemp, E. D. A.; Nocek, J. M.; Mauk, A. G.; Hoffman, B. M. *J. Am. Chem. Soc.* **1991**, *113*, 4337–4338.
- Kuila, D.; Baxter, W. W.; Natan, M. J.; Hoffman, B. M. *J. Phys. Chem.* **1991**, *95*, 1–3.
- King, B. C.; Hawkrigide, F. M.; Hoffman, B. M. *J. Am. Chem. Soc.* **1992**, *114*, 10603–10608.
- Simolo, K. P.; McLendon, G. L.; Mauk, M. R.; Mauk, A. G. *J. Am. Chem. Soc.* **1984**, *106*, 5012–5013.
- McLendon, G.; Zhang, Q.; Wallin, S. A.; Miller, R. M.; Billstone, V.; Spears, K. G.; Hoffman, B. M. *J. Am. Chem. Soc.* **1993**, *115*, 3665–3669.
- Stemp, E. D. A.; Hoffman, B. M. *Biochemistry* **1993**, *32*, 10848–10865.
- Zhou, J. S.; Hoffman, B. M. *J. Am. Chem. Soc.* **1993**, *115*, 11008–11009.
- Zhou, J. S.; Nocek, J. M.; DeVan, M. L.; Hoffman, B. M. *Science* **1995**, *269*, 204–207.
- Nocek, J. M.; Zhou, J. S.; DeForest, S.; Priyadarshy, S.; Beratan, D. N.; Onuchic, J. N.; Hoffman, B. M. *Chem. Rev.* **1996**, *96*, 2459–2489.
- Dick, L. A.; Malfant, I.; Kuila, D.; Nebolsky, S.; Nocek, J. M.; Hoffman, B. M.; Ratner, M. A. *J. Am. Chem. Soc.* **1998**, *120*, 11401–11407.
- McLendon, G.; Miller, J. R. *J. Am. Chem. Soc.* **1985**, *107*, 7811–7816.
- McLendon, G.; Pardue, K.; Bak, P. *J. Am. Chem. Soc.* **1987**, *109*, 7540–7541.
- McLendon, G.; Hake, R. *Chem. Rev.* **1992**, *92*, 481–490.
- Simmons, J.; McLendon, G.; Qiao, T. *J. Am. Chem. Soc.* **1993**, *115*, 4889–4890.
- Isied, S. S.; Kuehn, C.; Worosila, G. *J. Am. Chem. Soc.* **1984**, *106*, 1722–1726.
- Sun, J.; Wishart, J. F.; Isied, S. S. *Inorg. Chem.* **1995**, *34*, 3998–4000.
- Twitchett, M. B.; Ferrer, J. C.; Siddarth, P.; Mauk, A. G. *J. Am. Chem. Soc.* **1997**, *119*, 435–436.
- Marcus, R. A.; Sutin, N. *Biochim. Biophys. Acta* **1985**, *811*, 265–322.
- Beratan, D. N.; Onuchic, J. N.; Hopfield, J. J. *J. Chem. Phys.* **1987**, *86*, 4488–4498.
- Beratan, D. N.; Onuchic, J. N. *Photosynth. Res.* **1989**, *22*, 173–186.
- Onuchic, J. N.; Beratan, D. N. *J. Chem. Phys.* **1990**, *92*, 722–733.
- Beratan, D. N.; Betts, J. N.; Onuchic, J. N. *Science* **1991**, *252*, 1285–1288.
- Onuchic, J. N.; Andrade, P. C. P.; Beratan, D. N. *J. Chem. Phys.* **1991**, *95*, 1131–1138.
- Beratan, D. N.; Betts, J. N.; Onuchic, J. N. *Science* **1991**, *252*, 1285–1288.
- Betts, J. N.; Beratan, D. N.; Onuchic, J. N. *J. Am. Chem. Soc.* **1992**, *114*, 4043–4046.
- Beratan, D. N.; Betts, J. N.; Onuchic, J. N. *J. Phys. Chem.* **1992**, *96*, 2852–2855.
- Skourtis, S. S.; Beratan, D. N. *JBIC* **1997**, *2*, 378–386.
- Skourtis, S. S.; Beratan, D. N. *J. Phys. Chem. B* **1997**, *101*, 1215–1234.
- Kumar, K.; Kurnikov, I. V.; Beratan, D. N.; Waldeck, D. H.; Zimmt, M. B. *J. Phys. Chem. A* **1998**, *102*, 5529–5541.
- Roitberg, A. E.; Holden, M. J.; Mayhew, M. P.; Kurnikov, I. V.; Beratan, D. N.; Vilker, V. L. *J. Am. Chem. Soc.* **1998**, *120*, 8927–8932.
- Beratan, D. N.; Skourtis, S. S. *Curr. Opin. Chem. Biol.* **1998**, *2*, 235–243.
- de Andrade, P. C. P.; Onuchic, J. N. *J. Chem. Phys.* **1998**, *108*, 4292–4298.
- Regan, J. J.; Onuchic, J. N. *Adv. Chem. Phys.* **1999**, *107*, 497–553.
- Stuchebrukhov, A. A.; Marcus, R. A. *J. Phys. Chem.* **1995**, *99*, 7581–7590.
- Daizadeh, I.; Medvedev, E. S.; Stuchebrukhov, A. A. *Proc. Natl. Acad. Sci. USA* **1997**, *94*, 3703–3708.
- Daizadeh, I.; Guo, J.-X.; Stuchebrukhov, A. A. *J. Chem. Phys.* **1999**, *110*, 8865–8868.
- Medvedev, D. M.; Daizadeh, I.; Stuchebrukhov, A. A. *J. Am. Chem. Soc.* **2000**, *122*, 6571–6582.
- Moser, C. C.; Keske, J. M.; Warncke, K.; Farid, R. S.; Dutton, P. L. *Nature* **1992**, *355*, 796–802.
- Farid, R. S.; Moser, C. C.; Dutton, P. L. *Curr. Opin. Struct. Biol.* **1993**, *3*, 225–233.
- Moser, C. C.; Page, C. C.; Chen, X.; Dutton, P. L. *JBIC* **1997**, *2*, 393–398.
- Page, C. C.; Moser, C. C.; Chen, X.; Dutton, P. L. *Nature* **1999**, *402*, 47–52.
- Winkler, J. R.; Nocera, D. G.; Yocom, K. M.; Bordignon, E.; Gray, H. B. *J. Am. Chem. Soc.* **1982**, *104*, 5798–5800.
- Nocera, D. G.; Winkler, J. R.; Yocom, K. M.; Bordignon, E.; Gray, H. B. *J. Am. Chem. Soc.* **1984**, *106*, 5145–5150.
- Elias, H.; Chou, M. H.; Winkler, J. R. *J. Am. Chem. Soc.* **1988**, *110*, 429–434.
- Crutchley, R. J.; Ellis, W. R., Jr.; Gray, H. B. *J. Am. Chem. Soc.* **1985**, *107*, 5002–5004.
- Mayo, S. L.; Ellis, W. R.; Crutchley, R. J.; Gray, H. B. *Science* **1986**, *233*, 948–952.
- Axup, A. W.; Albin, M.; Mayo, S. L.; Crutchley, R. J.; Gray, H. B. *J. Am. Chem. Soc.* **1988**, *110*, 435–439.
- Karas, J. L.; Lieber, C. M.; Gray, H. B. *J. Am. Chem. Soc.* **1988**, *110*, 599–600.
- Meade, T. J.; Gray, H. B.; Winkler, J. R. *J. Am. Chem. Soc.* **1989**, *111*, 4353–4356.
- Bowler, B. E.; Meade, T. J.; Mayo, S. L.; Richards, J. H.; Gray, H. B. *J. Am. Chem. Soc.* **1989**, *111*, 8757–8759.
- Gray, H. B.; Malmström, B. G. *Biochemistry* **1989**, *28*, 7499–7505.
- Cowan, J. A.; Gray, H. B. *Inorg. Chem.* **1989**, *28*, 2074–2078.
- Therien, M. J.; Selman, M. A.; Gray, H. B.; Chang, I.-J.; Winkler, J. R. *J. Am. Chem. Soc.* **1990**, *112*, 2420–2422.
- Chang, I.-J.; Gray, H. B.; Winkler, J. R. *J. Am. Chem. Soc.* **1991**, *113*, 7056–7057.
- Therien, M. J.; Bowler, B. E.; Selman, M. A.; Gray, H. B.; Chang, I.-J.; Winkler, J. R. *Long-Range Electron Transfer in Heme Proteins: Porphyrin-Ruthenium Electronic Couplings in Three*

- Ru(His)Zn-Cytochromes c*. Bolton, J. R., Mataga, N., McLendon, G., Eds.; American Chemical Society: Washington, DC, **1991**; Vol. 228, pp. 191–199.
63. Jacobs, B. A.; Mauk, M. R.; Funk, W. D.; MacGillivray, R. T. A.; Mauk, A. G.; Gray, H. B. *J. Am. Chem. Soc.* **1991**, *113*, 4390–4394.
  64. Winkler, J. R.; Gray, H. B. *Chem. Rev.* **1992**, *92*, 369–379.
  65. Wuttke, D. S.; Bjerrum, M. J.; Winkler, J. R.; Gray, H. B. *Science* **1992**, *256*, 1007–1009.
  66. Onuchic, J. N.; Beratan, D. N.; Winkler, J. R.; Gray, H. B. *Annu. Rev. Biophys. Biomol. Struct.* **1992**, *21*, 349–377.
  67. Wuttke, D. S.; Bjerrum, M. J.; Chang, I.-J.; Winkler, J. R.; Gray, H. B. *Biochim. Biophys. Acta* **1992**, *1101*, 168–170.
  68. Winkler, J. R.; Gray, H. B. *Pure Appl. Chem.* **1992**, *64*, 1257–1262.
  69. Casimiro, D. R.; Wong, L.-L.; Colón, J. L.; Zewert, T. E.; Richards, J. H.; Chang, I.-J.; Winkler, J. R.; Gray, H. B. *J. Am. Chem. Soc.* **1993**, *115*, 1485–1489.
  70. Casimiro, D. R.; Richards, J. H.; Winkler, J. R.; Gray, H. B. *J. Phys. Chem.* **1993**, *97*, 13073–13077.
  71. Casimiro, D. R.; Muheim, A.; Richards, J. R.; Arnold, F. H.; Winkler, J. R.; Gray, H. B. *J. Inorg. Biochem.* **1993**, *51*, 232.
  72. Karpishin, T. B.; Grinstaff, M. W.; Komar-Panicucci, S.; McLendon, G.; Gray, H. B. *Structure* **1994**, *2*, 415–422.
  73. Bjerrum, M. J.; Casimiro, D. R.; Chang, I.-J.; Di Bilio, A. J.; Gray, H. B.; Hill, M. G.; Langen, R.; Mines, G. A.; Skov, L. K.; Winkler, J. R.; Wuttke, D. S. *J. Bioenerg. Biomemb.* **1995**, *27*, 295–302.
  74. Gray, H. B.; Winkler, J. R. *Annu. Rev. Biochem.* **1996**, *65*, 537–561.
  75. Mines, G. A.; Bjerrum, M. J.; Hill, M. G.; Casimiro, D. R.; Chang, I.-J.; Winkler, J. R.; Gray, H. B. *J. Am. Chem. Soc.* **1996**, *118*, 1961–1965.
  76. Low, D. W.; Winkler, J. R.; Gray, H. B. *J. Am. Chem. Soc.* **1996**, *118*, 117–120.
  77. Berglund, J.; Pascher, T.; Winkler, J. R.; Gray, H. B. *J. Am. Chem. Soc.* **1997**, *119*, 2464–2469.
  78. Winkler, J. R.; Gray, H. B. *JBIC* **1997**, *2*, 399–404.
  79. Winkler, J. R.; Di Bilio, A.; Farrow, N. A.; Richards, J. H.; Gray, H. B. *Pure Appl. Chem.* **1999**, *71*, 1753–1764.
  80. Wilker, J. J.; Dmochowski, I. J.; Dawson, J. H.; Winkler, J. R.; Gray, H. B. *Angew. Chem., Int. Ed. Engl.* **1999**, *38*, 89–92.
  81. Tezcan, F. A.; Crane, B. R.; Winkler, J. R.; Gray, H. B. *Proc. Natl. Acad. Sci. USA* **2001**, *98*, 5002–5006.
  82. Pascher, T.; Chesick, J. P.; Winkler, J. R.; Gray, H. B. *Science* **1996**, *271*, 1558–1560.
  83. Mines, G. A.; Pascher, T.; Lee, S. C.; Winkler, J. R.; Gray, H. B. *Chem. Biol.* **1996**, *3*, 491–497.
  84. Telford, J. R.; Wittung-Stafshede, P.; Gray, H. B.; Winkler, J. R. *Acc. Chem. Res.* **1998**, *31*, 755–763.
  85. Lee, J. C.; Chang, I.-J.; Gray, H. B.; Winkler, J. R. *J. Mol. Biol.* **2002**, *320*, 159–164.
  86. Balzani, V. *Electron Transfer in Chemistry*. Wiley-VCH: Weinheim, **2001**.
  87. Gray, H. B.; Ellis, W. R., Jr. *Electron Transfer*. Bertini, I., Gray, H. B., Lippard, S. J., Valentine, J. S., Eds.; University Science Books: Mill Valley, CA, **1994**, pp. 315–363.
  88. Hopfield, J. J. *Proc. Natl. Acad. Sci. USA* **1974**, *71*, 3640–3644.
  89. Ponce, A.; Gray, H. B.; Winkler, J. R. *J. Am. Chem. Soc.* **2000**, *122*, 8187–8191.
  90. Millett, F.; Miller, M. A.; Geren, L.; Durham, B. *J. Bioenerg. Biomemb.* **1995**, *27*, 341–351.
  91. Davidson, V. L. *Acc. Chem. Res.* **2000**, *33*, 87–93.
  92. Andrew, S. M.; Thomasson, K. A.; Northrup, S. H. *J. Am. Chem. Soc.* **1993**, *115*, 5516–5521.
  93. Newton, M. D. *J. Phys. Chem.* **1988**, *92*, 3049–3056.
  94. Wasielewski, M. R. *Distance Dependencies of Electron-Transfer Reactions*. Fox, M. A., Chanon, M., Eds.; Elsevier: Amsterdam, **1988**.
  95. McConnell, H. M. *J. Chem. Phys.* **1961**, *35*, 508–515.
  96. Langen, R.; Colón, J. L.; Casimiro, D. R.; Karpishin, T. B.; Winkler, J. R.; Gray, H. B. *JBIC* **1996**, *1*, 221–225.
  97. Larsson, S. *J. Phys. Chem.* **1984**, *88*, 1321–1323.
  98. Miller, N. E.; Wander, M. C.; Cave, R. J. *J. Phys. Chem. A* **1999**, *103*, 1084–1093.
  99. Benjamin, I.; Evans, D.; Nitzan, A. *J. Chem. Phys.* **1997**, *106*, 6647–6654.
  100. Smalley, J. F.; Feldberg, S. W.; Chidsey, C. E. D.; Linford, M. R.; Newton, M. D.; Liu, Y.-P. *J. Phys. Chem.* **1995**, *99*, 13141–13149.
  101. Langen, R.; Chang, I.-J.; Germanas, J. P.; Richards, J. H.; Winkler, J. R.; Gray, H. B. *Science* **1995**, *268*, 1733–1735.
  102. Winkler, J. R. *Curr. Opin. Chem. Biol.* **2000**, *4*, 192–198.
  103. Mei, H.; Wang, K.; Peffer, N.; Weatherly, G.; Cohen, D. S.; Miller, M.; Pielak, G.; Durham, B.; Millett, F. *Biochemistry* **1999**, *38*, 6846–6854.
  104. Farver, O.; Pecht, I. *JBIC* **1997**, *2*, 387–392.
  105. Daizadeh, I.; Gehlen, J. N.; Stuchebrukhov, A. A. *J. Chem. Phys.* **1997**, *106*, 5658–5666.
  106. Jortner, J.; Bixon, M.; Langenbacher, T. L.; Michel-Beyerle, M. E. *Proc. Natl. Acad. Sci. USA* **1998**, *95*, 12759–12765.
  107. Pletneva, E. V.; Fulton, D. B.; Kohzuma, T.; Kostic, N. M. *J. Am. Chem. Soc.* **2000**, *122*, 1034–1046.
  108. Takano, T.; Dickerson, R. E. *Proc. Natl. Acad. Sci. USA* **1980**, *77*, 6371.
  109. Sun, J.; Su, C.; Wishart, J. F. *Inorg. Chem.* **1996**, *35*, 5893–5901.
  110. Zemel, H.; Hoffman, B. M. *J. Am. Chem. Soc.* **1981**, *103*, 1192–1201.
  111. Lo Conte, L.; Chothia, C.; Janin, J. *J. Mol. Biol.* **1999**, *285*, 2177–2198.
  112. Pelletier, H.; Kraut, J. *Science* **1992**, *258*, 1748–1755.
  113. de Rege, P. J. F.; Williams, S. A.; Therien, M. J. *Science* **1995**, *269*, 1409–1413.
  114. Kirby, J. P.; Roberts, J. A.; Nocera, D. G. *J. Am. Chem. Soc.* **1997**, *119*, 9230–9236.
  115. Yang, J.; Seneviratne, D.; Arbatin, G.; Andersson, A. M.; Curtis, J. C. *J. Am. Chem. Soc.* **1997**, *119*, 5329–5336.
  116. Bryngelson, J. D.; Onuchic, J. N.; Wolynes, P. G. *Proteins: Struct. Func. Gen.* **1995**, *21*, 167–195.
  117. Dill, K. A.; Chan, H. S. *Nature Struct. Biol.* **1997**, *4*, 10–19.
  118. Shakhnovich, E. I. *Curr. Opin. Struct. Biol.* **1997**, *7*, 29–40.
  119. Lazaridis, T.; Karplus, M. *Science* **1997**, *278*, 1928–1931.
  120. Onuchic, J. N.; Lutheyschulten, Z.; Wolynes, P. G. *Annu. Rev. Phys. Chem.* **1997**, *48*, 545–600.
  121. Chen, L. X.-Q.; Petrich, J. W.; Fleming, G. R.; Perico, A. *Chem. Phys. Lett.* **1987**, *139*, 55–61.
  122. Williams, S.; Causgrove, T. P.; Gilman, R.; Fang, K. S.; Callender, R. H.; Woodruff, W. H.; Dyer, R. B. *Biochemistry* **1996**, *35*, 691–697.
  123. Koide, S.; Dyson, H. J.; Wright, P. E. *Biochemistry* **1993**, *32*, 12299–12310.
  124. Karplus, M.; Weaver, D. L. *Prot. Sci.* **1994**, *3*, 650–668.
  125. Zwanzig, R. *Proc. Natl. Acad. Sci. USA* **1995**, *92*, 9801–9804.
  126. Jones, C. M.; Henry, E. R.; Hu, Y.; Chan, C.-K.; Luck, S. D.; Bhuyan, A.; Roder, H.; Hofrichter, J.; Eaton, W. A. *Proc. Natl. Acad. Sci. USA* **1993**, *90*, 11860–11864.
  127. Elöve, G.; Bhuyan, A. K.; Roder, H. *Biochemistry* **1994**, *33*, 6925–6935.
  128. Sosnick, T. R.; Mayne, L.; Hiller, R.; Englander, S. W. *Nature Struct. Biol.* **1994**, *1*, 149–156.
  129. Baldwin, R. L. *BioEssays* **1994**, *16*, 207–210.
  130. Fersht, A. R. *Curr. Opin. Struct. Biol.* **1995**, *5*, 79–84.
  131. Ptitsyn, O. B. *Adv. Protein Chem.* **1995**, *47*, 83–229.
  132. Englander, S. W.; Mayne, L. *Annu. Rev. Biophys. Biomol. Struct.* **1992**, *21*, 243–265.

133. Plaxco, K.; Dobson, C. M. *Curr. Opin. Struct. Biol.* **1996**, *6*, 630–636.
134. Churg, A. K.; Warshel, A. *Biochemistry* **1986**, *25*, 1675–1681.
135. Tezcan, F. A.; Winkler, J. R.; Gray, H. B. *J. Am. Chem. Soc.* **1998**, *120*, 13383–13388.
136. Tezcan, F. A. Ph.D. Thesis, California Institute of Technology, **2001**.
137. Bixler, J.; Bakker, G.; McLendon, G. *J. Am. Chem. Soc.* **1992**, *114*, 6938–6939.
138. Chen, B.-L.; Baase, W. A.; Nicholson, H.; Schellman, J. A. *Biochemistry* **1992**, *31*, 1464–1476.
139. Matouschek, A.; Otzen, D. E.; Itzhaki, L. S.; Jackson, S. E.; Fersht, A. R. *Biochemistry* **1995**, *34*, 13656–13662.
140. Yao, M.; Bolen, D. W. *Biochemistry* **1995**, *34*, 3771–3781.
141. Winkler, J. R.; Wittung-Stafshede, P.; Leckner, J.; Malmström, B. G.; Gray, H. B. *Proc. Natl. Acad. Sci. USA* **1997**, *94*, 4246–4249.
142. Mines, G. A.; Winkler, J. R.; Gray, H. B. *Spectroscopic Studies of Ferrocytochrome c Folding*. Solomon, E. I., Hodgson, K. O., Eds.; American Chemical Society: Washington DC, **1998**.
143. Wittung-Stafshede, P.; Gray, H. B.; Winkler, J. R. *J. Am. Chem. Soc.* **1997**, *119*, 9562–9563.
144. Wittung-Stafshede, P.; Malmström, B. G.; Winkler, J. R.; Gray, H. B. *J. Phys. Chem. A* **1998**, *102*, 5599–5601.
145. Telford, J. R.; Tezcan, F. A.; Gray, H. B.; Winkler, J. R. *Biochemistry* **1999**, *38*, 1944–1949.
146. Orii, Y. *Biochemistry* **1993**, *32*, 11910–11914.
147. Babul, J.; Stellwagen, E. *Biochemistry* **1972**, *11*, 1195–1200.
148. Muthukrishnan, K.; Nall, B. T. *Biochemistry* **1991**, *30*, 4706–4710.
149. Colón, W.; Wakem, L. P.; Sherman, F.; Roder, H. *Biochemistry* **1997**, *36*, 12535–12541.
150. Kita, K.; Konishi, K.; Anraku, Y. *J. Biol. Chem.* **1984**, *259*, 3368–3374.
151. Fisher, M. T. *Biochemistry* **1991**, *30*, 10012–10018.
152. Wittung-Stafshede, P.; Lee, J. C.; Winkler, J. R.; Gray, H. B. *Proc. Natl. Acad. Sci. USA* **1999**, *96*, 6587–6590.
153. Meyer, T. E.; Kamen, M. D. *Adv. Protein Chem.* **1982**, *35*, 105–212.
154. Moore, G. R.; McClune, G. J.; Clayden, N. J.; Williams, R. J. P.; Alsaadi, B. M.; Angstrom, J.; Ambler, R. P.; van Beeumen, J.; Tempst, P.; Bartsch, R. G.; Meyer, T. E.; Kamen, M. D. *Eur. J. Biochem.* **1982**, *123*, 73–80.
155. Moore, G. R.; Pettigrew, G. W. *Cytochromes c: Evolutionary, Structural, and Physicochemical Aspects*. Springer-Verlag: New York, **1990**.
156. Ambler, R. P.; Bartsch, R. G.; Daniel, M.; Kamen, M. D.; McLellan, L.; Meyer, T. E.; Beeumen, J. V. *Proc. Natl. Acad. Sci. USA* **1981**, *78*, 6854–6857.
157. Hamada, K.; Bethge, P. H.; Mathews, F. S. *J. Mol. Biol.* **1995**, *247*, 947–962.
158. Shibata, N.; Iba, S.; Misaki, S.; Meyer, T. E.; Bartsch, R. G.; Cusanovich, M. A.; Morimoto, Y.; Higuchi, Y.; Yasuoka, N. *J. Mol. Biol.* **1998**, *284*, 751–760.
159. Moore, G. R.; Williams, R. J. P.; Peterson, J.; Thomson, A. J.; Mathews, F. S. *Biochim. Biophys. Acta* **1985**, *829*, 83–96.
160. Klerk, H. D.; Bartsch, R. G.; Kamen, M. D. *Biochim. Biophys. Acta* **1965**, *97*, 275–280.
161. Streckas, T. C.; Spiro, T. G. *Biochim. Biophys. Acta* **1974**, *351*, 237–245.
162. Fujii, S.; Yoshimura, T.; Kamada, H.; Yamaguchi, K.; Suzuki, S.; Shidara, S.; Takakuwa, S. *BBA Prot. Struct. Molec. Enzym.* **1995**, *1251*, 161–169.
163. Clark, K.; Dugad, L. B.; Bartsch, R. G.; Cusanovich, M. A.; Mar, G. N. L. *J. Am. Chem. Soc.* **1996**, *118*, 4654–4664.
164. Jackson, J. T.; Mar, G. N. L.; Bartsch, R. G. *J. Biol. Chem.* **1983**, *258*, 1799–1805.
165. Barakat, R.; Streckas, T. C. *Biochim. Biophys. Acta* **1982**, *679*, 393–399.
166. Schmid, F. X.; Mayr, L. M.; Mücke, M.; Schönbrunner, E. R. *Adv. Protein Chem.* **1993**, *44*, 25–66.
167. Thirumalai, D.; Klimov, D. K.; Woodson, S. A. *Theor. Chem. Acc.* **1997**, *96*, 14–22.
168. Thirumalai, D.; Klimov, D. K. *Curr. Opin. Struct. Biol.* **1999**, *9*, 197–207.
169. Zhou, Y.; Karplus, M. *Nature* **1999**, *401*, 400–403.
170. Zhou, Y.; Karplus, M. *J. Mol. Biol.* **1999**, *293*, 917–951.
171. Shea, J.-E.; Onuchic, J. N.; Brooks III, C. L. *J. Chem. Phys.* **2000**, *113*, 7663–7671.
172. Shea, J.-E.; Onuchic, J. N.; Brooks III, C. L. *Proc. Natl. Acad. Sci. USA* **1999**, *96*, 12512–12517.
173. Hagen, S. J.; Hofrichter, J.; Eaton, W. A. *J. Phys. Chem. B* **1997**, *101*, 2352–2365.
174. Vanderkooi, J. M.; Landesberg, R.; Hayden, G.; Owen, C. S. *Eur. J. Biochem.* **1977**, *81*, 339–347.
175. Shastry, M. C. R.; Sauder, J. M.; Roder, H. *Acc. Chem. Res.* **1998**, *31*, 717–725.
176. Englander, S. W.; Sosnick, T. R.; Mayne, L. C.; Shtilerman, M.; Qi, P. X.; Bai, Y. *Acc. Chem. Res.* **1998**, *31*, 737–744.
177. Pierce, M. M.; Nall, B. T. *Prot. Sci.* **1997**, *6*, 618–627.
178. Scheidt, W. R.; Kastner, M. E.; Hatano, K. *Inorg. Chem.* **1978**, *17*, 706–710.
179. Sudha, B. P.; Dixit, N.; Moy, V. T.; Vanderkooi, J. M. *Biochemistry* **1984**, *23*, 2103–2107.
180. Wherland, S.; Gray, H. B. *Proc. Natl. Acad. Sci. USA* **1976**, *73*, 2950–2954.
181. Akiyama, S.; Takahashi, S.; Ishimori, K.; Morishima, I. *Nature Struct. Biol.* **2000**, *7*, 514–520.
182. Sauder, J. M.; Roder, H. *Folding & Design* **1998**, *3*, 293–301.
183. Mirny, L. A.; Abkevich, V.; Shakhnovich, E. I. *Folding & Design* **1996**, *1*, 103–116.

# Chiral Metalloporphyrins and Their Use in Enantiocontrol

# 64

JEAN-CLAUDE MARCHON and RENÉ RAMASSEUL

Laboratoire de Chimie Inorganique et Biologique, Département de Recherche Fondamentale sur la Matière Condensée, CEA-Grenoble, 38054 Grenoble, France

I. Introduction . . . . .	75
II. Syntheses of Chiral Porphyrins and Metalloporphyrins . . . . .	76
A. Chiral <i>meso</i> -Substituted Porphyrins . . . . .	76
B. Other Chiral Porphyrins . . . . .	76
C. Chiral di- and tri-Porphyrin Arrays . . . . .	76
III. Enantiocontrol with Chiral Metalloporphyrins . . . . .	76
A. Asymmetric Catalytic Oxidation. . . . .	76
1. Epoxidation . . . . .	76
2. Other Oxidations. . . . .	84
B. Asymmetric Catalytic Aziridination . . . . .	90
C. Asymmetric Catalytic Cyclopropanation . . . . .	90
D. Chiral Recognition . . . . .	94
E. Memory Systems . . . . .	102
F. Miscellaneous Applications . . . . .	102
IV. Transition Metal Chiroporphyrins . . . . .	111
A. Synthesis of Chiroporphyrins . . . . .	111
B. Chiroporphyrin Stereochemistry . . . . .	113
1. Free Bases. . . . .	113
2. Conformational Switches . . . . .	114
C. Spin States of Fe(III) Chiroporphyrins . . . . .	114
D. Asymmetric Additions to Olefins Catalyzed by Mn(III) Chiroporphyrins . . . . .	117
1. Epoxidation . . . . .	117
2. Aziridination . . . . .	118
E. Enantioselective Binding of Chiral Ligands by Metallochiroporphyrins . . . . .	118
F. Irreversible Binding of Amines to Co(III) Chiroporphyrins . . . . .	121
G. Chiroporphyrin Derivatizing Agents for Chiral Analysis by NMR Spectroscopy . . . . .	123
V. Perspectives . . . . .	124
References . . . . .	126

## I. Introduction

The aim of this chapter is to provide an overview of the syntheses of chiral porphyrin derivatives, and to summarize the uses of such compounds in enantioselective control. Complete coverage of the literature is provided up to mid-2001. As chiral porphyrins constitute a subset of the porphyrin field, some of the topics which are covered in this chapter have been reviewed in previous volumes of *The Porphyrin*

*Handbook*, for example in Chapters 2,<sup>1</sup> 27,<sup>2</sup> 28,<sup>3</sup> 31,<sup>4</sup> or 46.<sup>5</sup> Rather than duplicating this earlier coverage, an attempt has been made to provide an exhaustive but concise overview of the field. Thus, this chapter has been organized as a database in which chiral porphyrins are classified according to their structures (Section II) and their uses in enantiocontrol (Section III). Selected applications of chiroporphyrins, a subclass of chiral porphyrins developed in the authors' laboratory since 1994, are illustrated as examples in Section IV.

## II. Syntheses of Chiral Porphyrins and Metalloporphyrins

Selected aspects of this field have been reviewed.<sup>6,7</sup> The simplest way to confer chirality to a porphyrin is to link at least one chiral substituent to it. Numerous easily accessible porphyrins possess at least a carboxylic, phenolic, amino, or hydroxyl group, which are good candidates for attaching chiral substituents.<sup>8–35</sup> Thus, most of the known chiral porphyrins are *meso*-substituted by an enantiopure chiral group. Selected examples are illustrated in Figure 1. Such substituted systems can be obtained either by tailing, as mentioned above, or by condensation of pyrrole with a chiral aldehyde. In both cases, the chiral moiety often is obtained via a multistep synthesis. The overall yield of the chiral porphyrin is consequently often poor. An alternative access to an enantiopure chiral porphyrin is by resolution of the mixture of the two enantiomers (see paragraph II.B).

### A. CHIRAL *meso*-SUBSTITUTED PORPHYRINS

Numerous chiral porphyrins have been obtained from appropriately *ortho*-substituted tetraphenylporphyrins (Figure 2). A popular strategy uses elaboration on the *ortho* amino substituents of selected atropisomers of *meso*-tetra(*o*-aminophenyl)porphyrin<sup>29,36–73</sup> (Figure 3). A reliable synthetic route to tetra(*o,o'*-diaminophenyl)porphyrin derivatives<sup>65</sup> now allows elaboration on both faces of the porphyrin (Figure 4).

Some chiral porphyrins were also obtained by modification of the *o*-, *m*-, and *p*-carboxy appendages of *meso*-tetracarboxyphenylporphyrin<sup>29,48,54,55,74–77</sup> (Figure 5), or of the *bis*-face-substituted analog<sup>91</sup> (Figure 6). Collman's threitol-strapped porphyrins were prepared from *meso*-tetra (*o*-hydroxyphenyl)porphyrins<sup>78,79</sup> (Figure 7). The so-called "twin-coronet" porphyrins<sup>80,81</sup> were derived from *meso*-(*o,o'*-octahydroxy)tetraphenyl porphyrin, which was also used to prepare other chiral porphyrins<sup>82–85</sup> (Figure 8). Other types of tailed chiral porphyrins have been described.<sup>86,87</sup>

The synthesis of *meso*-substituted porphyrins by the Lindsey method has been reviewed in Chapter 2 of *The Porphyrin Handbook*.<sup>1</sup> Aromatic aldehydes are reacted with pyrrole in dichloromethane solution in the presence of an acid catalyst to give a porphyrinogen which is subsequently oxidized by DDQ leading to a *meso*-tetraarylporphyrin. This method can be used to obtain chiral porphyrins directly if the starting aldehyde is chiral, as will be seen below (Figure 9). If not, tailing

of the porphyrin with chiral substituents can be done as mentioned above.<sup>88–91</sup>

Preformed chiral aryl aldehydes were subjected to Lindsey conditions leading to the so-called "chiral wall"<sup>92</sup> and "chiral fortress"<sup>93</sup> porphyrins (Figure 10). A series of *D*<sub>4</sub>-symmetric,<sup>94–98</sup> glycosylated,<sup>99–106</sup> and various other chiral tetra-substituted porphyrin systems<sup>107–121</sup> have been described (Figure 10). Chiral *meso*-tetraalkylporphyrins<sup>122–134</sup> are also obtained from chiral alkyl aldehydes by the Lindsey method (Figure 11).

### B. OTHER CHIRAL PORPHYRINS

Numerous planar chiral *N*-alkylporphyrins have been obtained.<sup>135–143</sup> Single-armed porphyrins,<sup>144</sup> chiral "strapped" porphyrins with diastereotopic faces,<sup>145,146</sup> 5,10-diaryl-porphyrins,<sup>147–150,345</sup> Tröger's base derivatives,<sup>151–154</sup> and various other chiral porphyrins<sup>155–162</sup> have been prepared (Figure 12).

### C. CHIRAL DI- AND TRI-PORPHYRIN ARRAYS

A number of chiral porphyrin dimers<sup>163–183</sup> and trimers<sup>184–188,344,345</sup> have been described, and some are illustrated in Figure 13.

## III. Enantiocontrol with Chiral Metalloporphyrins

A number of reviews on various aspects of enantiocontrol with chiral metalloporphyrins have been published. These include chiral porphyrins as model receptors for chiral recognition,<sup>189–192</sup> models of synthetic enzymes based on porphyrins and steroids,<sup>193</sup> biomimetic oxidation catalysts.<sup>194</sup>

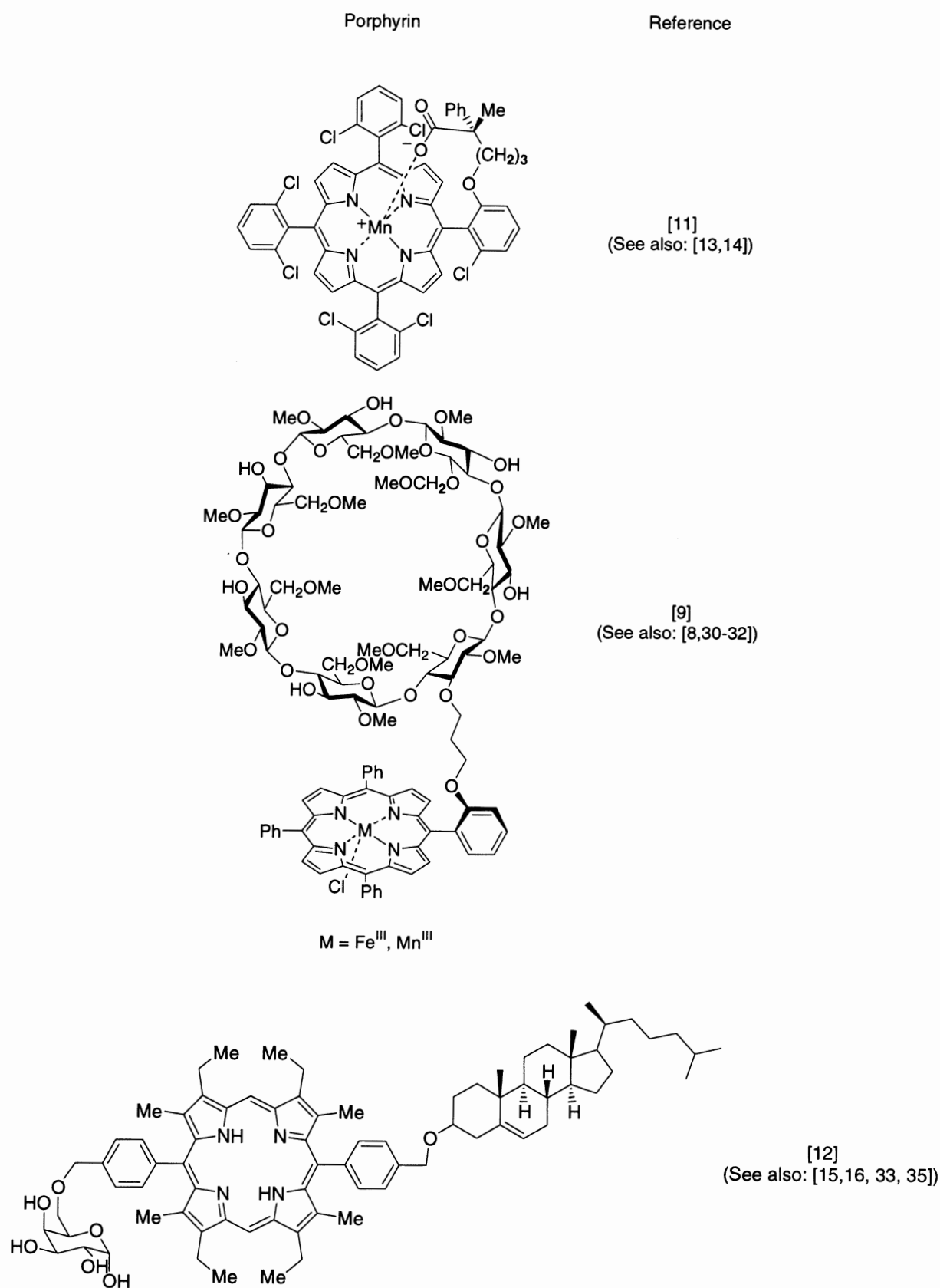
### A. ASYMMETRIC CATALYTIC OXIDATION

The design of porphyrin catalysts for the asymmetric epoxidation of substituted alkenes (Figure 14) has been reviewed.<sup>195–207</sup>

#### 1. Epoxidation

Groves's seminal work on asymmetric hydroxylation, epoxidation, and sulfoxidation catalyzed by vaulted binaphthyl metalloporphyrins<sup>44</sup> (Figure 3) is a reference paper for all further studies. For catalytic asymmetric epoxidation, enantiomeric excesses (ee's) were in the range 20–72%. This work is of academic interest as the experiments are nonstoichiometric; the substrate is in tenfold excess relative to the oxygen donor, thus





**Figure 1.** Examples of chiral porphyrins which are *meso*-substituted by enantiopure group(s) from the chiral pool.

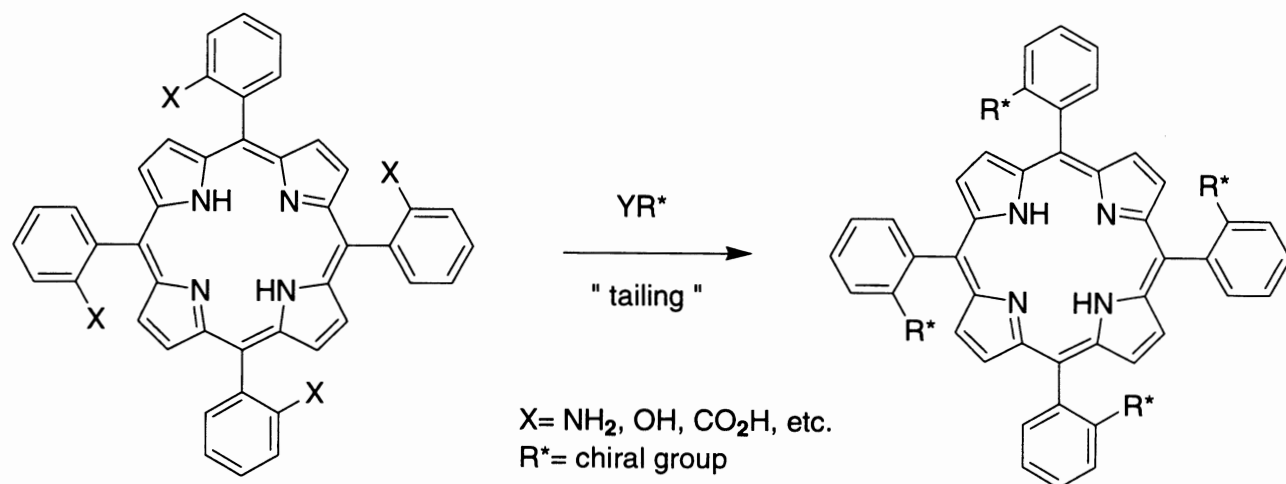


Figure 2. Access to chiral porphyrins from *ortho*-substituted *meso*-tetraphenylporphyrins.

preventing large scale application. A later investigation by Groves and coworkers, using FT-NMR  $T_1$  relaxation techniques,<sup>37</sup> addressed the question of the origins of chiral induction by this and related systems. (*R*)-styrene oxide was obtained in >90% ee in the initial stages of styrene epoxidation with  $\text{F}_5\text{PhIO}$  catalyzed by a new chiral vaulted porphyrin that carries (*S*)-binaphthyl-L-alanine straps across both faces of the porphyrin macrocycle. The transition state for olefin epoxidation with high-valent metal-oxo species was modeled by coordinating epoxides to paramagnetic copper complexes of the corresponding ligands. The epoxide enantiomer that better fits the chiral cavity of the catalyst, as revealed by  $T_1$  relaxation measurements, was also the major product of catalytic olefin epoxidation. These results are consistent with the "lock-and-key" mechanism of asymmetric catalysis by metalloporphyrins.<sup>37</sup>

In another pioneering study by Mansuy and coworkers, a chiral "basket-handle" iron porphyrin<sup>45</sup> (Figure 3) catalyzed the epoxidation of 4- $\text{ClC}_6\text{H}_4\text{CH}:\text{CH}_2$  by PhIO to give 50% excess of the (*R*) epoxide, whereas chiral "picket" iron porphyrins catalyzed the same reaction to give 12–21% excess of the (*S*)-epoxide.<sup>46,208</sup>

During the following period, chiral metalloporphyrins have been used with moderate success in catalytic asymmetric epoxidation of phenyl-substituted alkenes.<sup>11,42,86,102–104,108,109,111,131,209,210</sup>

#### a. Terpene-Derived $D_4$ -Symmetric Metalloporphyrins

The chloromanganese complexes of  $D_4$ -symmetric porphyrins obtained by Kodadek and coworkers from

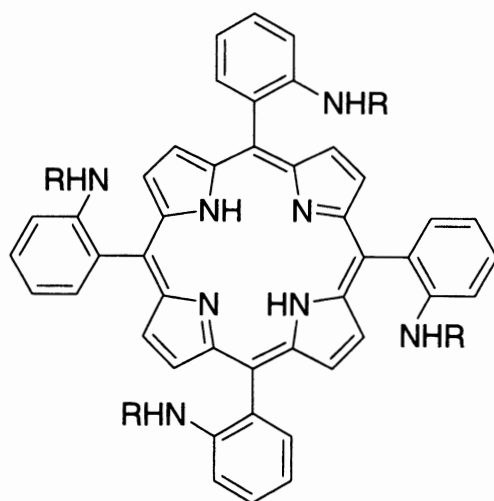
the cyclic ketone 1-(*R*)-(+)-nopinone<sup>95</sup> (Figure 10) are good catalysts for the epoxidation of terminal alkenes, providing epoxides with ee's of 70% with high turnover numbers.

A manganese complex of the  $D_4$ -symmetrical porphyrin prepared by Halterman<sup>96,97</sup> (Figure 10) was used as a catalyst for the asymmetric epoxidation of aromatic substituted alkenes in the presence of excess NaOCl. The epoxidations of terminal or *cis*-disubstituted alkenes were complete within 4 h with yields above 90% and enantioselectivities ranging from 41 to 76% ee. Reactivity changes were observed with Mn complexes of sterically and electronically modified  $D_4$ -symmetric tetraarylporphyrin ligands<sup>98</sup> (Figure 10) in catalytic epoxidations, the methoxy derivative giving slightly improved selectivity (83% ee with *cis*- $\beta$ -methylstyrene).

A ruthenium complex of an enantiomerically pure, Halterman-type porphyrin<sup>96</sup> (Figure 10) was used in the catalytic asymmetric epoxidation of olefins with 2,6-dichloropyridine *N*-oxide as terminal oxidant to afford epoxides in good yields and with enantioselectivities up to 77%.<sup>211</sup> A dioxoruthenium(VI) complex of a similar  $D_4$ -chiral porphyrin<sup>212,213</sup> exhibited catalytic activity toward aerobic enantioselective epoxidation of prochiral alkenes with enantioselectivity up to 77% ee at an oxygen pressure of 8 atm.

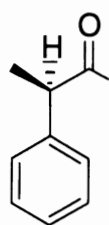
#### b. Strapped Metalloporphyrins

Chiral  $C_2$ -symmetric "twin-coronet" porphyrins containing chiral binaphthyl<sup>80</sup> or bitetralin<sup>81</sup> moieties (Figure 8) were found to catalyze asymmetric epoxidation of olefins with high enantioselectivity. Chiral

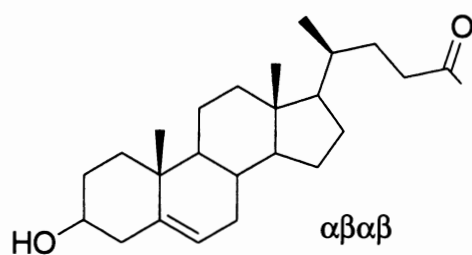


R=

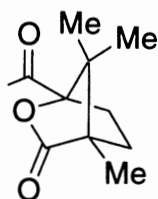
Reference

 $\alpha\beta\alpha\beta$ 

[36]

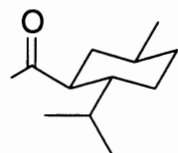
 $\alpha\beta\alpha\beta$ 

[40]



[42]

(See also : [29], [54], [55])



[52]

**Figure 3.** Selected chiral porphyrins obtained from *meso*-tetra(*o*-aminophenyl)porphyrin (literature citations are given in brackets).


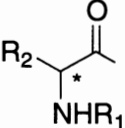
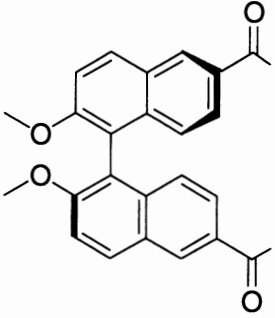
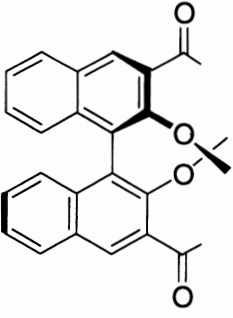
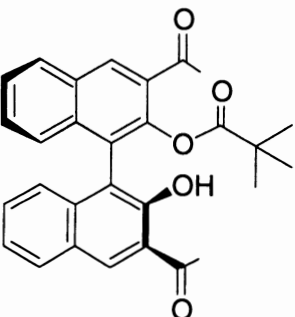
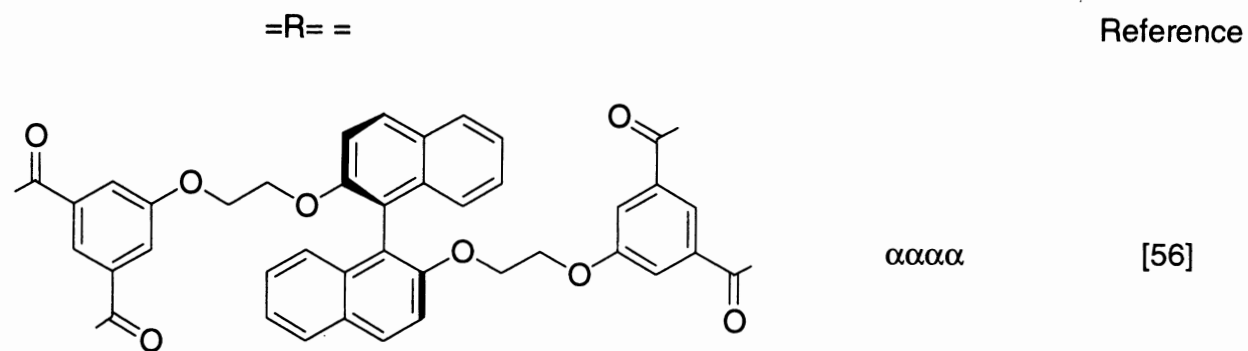
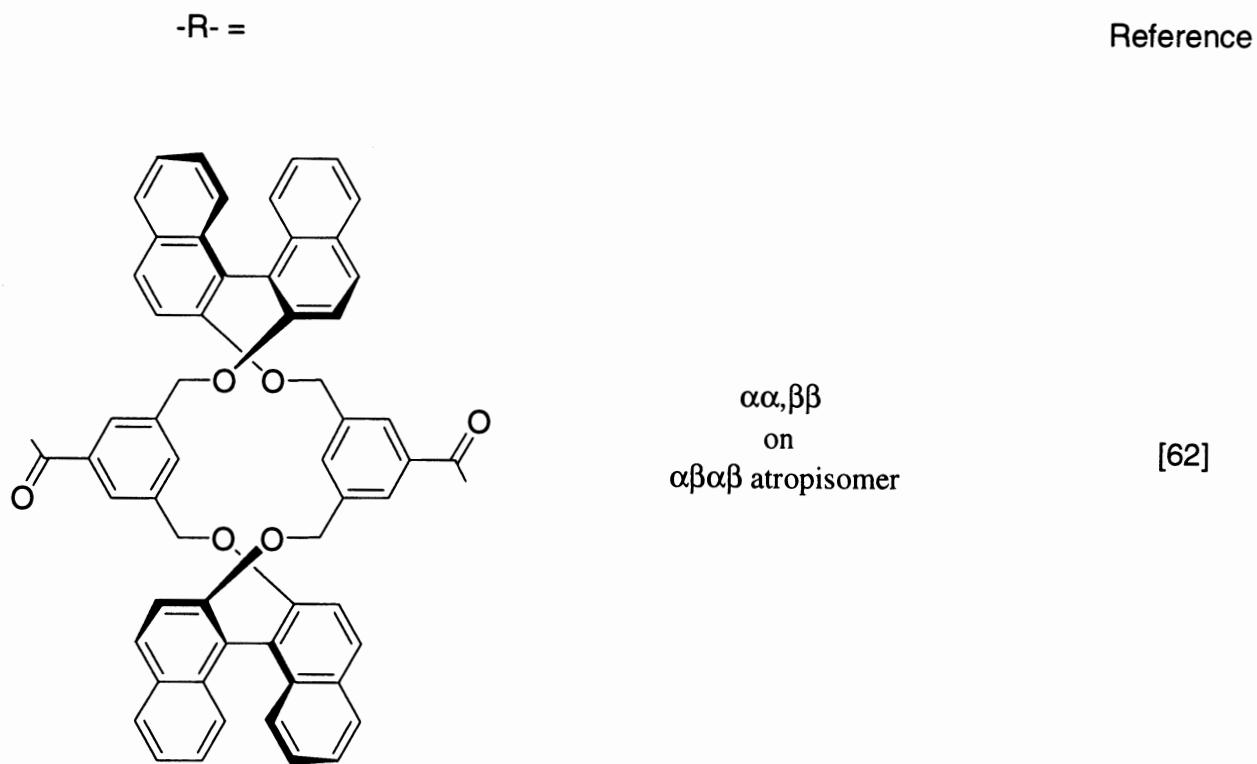
R=	Reference		
	[60]		
	$R_1 = \text{Boc}$ $\text{Boc}$ $\text{benzoyl}$	$R_2 = \text{CH}_3$ $\text{Pro residue}$ $\text{Gln residue}$	[71]
-R- =	Reference		
	$\alpha\alpha, \beta\beta$ on $\alpha\beta\alpha\beta$ atropisomer	[44]	
	$\alpha\alpha, \beta\beta$ on $\alpha\alpha\beta\beta$ atropisomer	[58]	
	$\alpha\alpha, \alpha\alpha$ on $\alpha\alpha\alpha\alpha$ atropisomer	[73]	

Figure 3. Continued.



(+), (-) and meso

Figure 3. Continued.

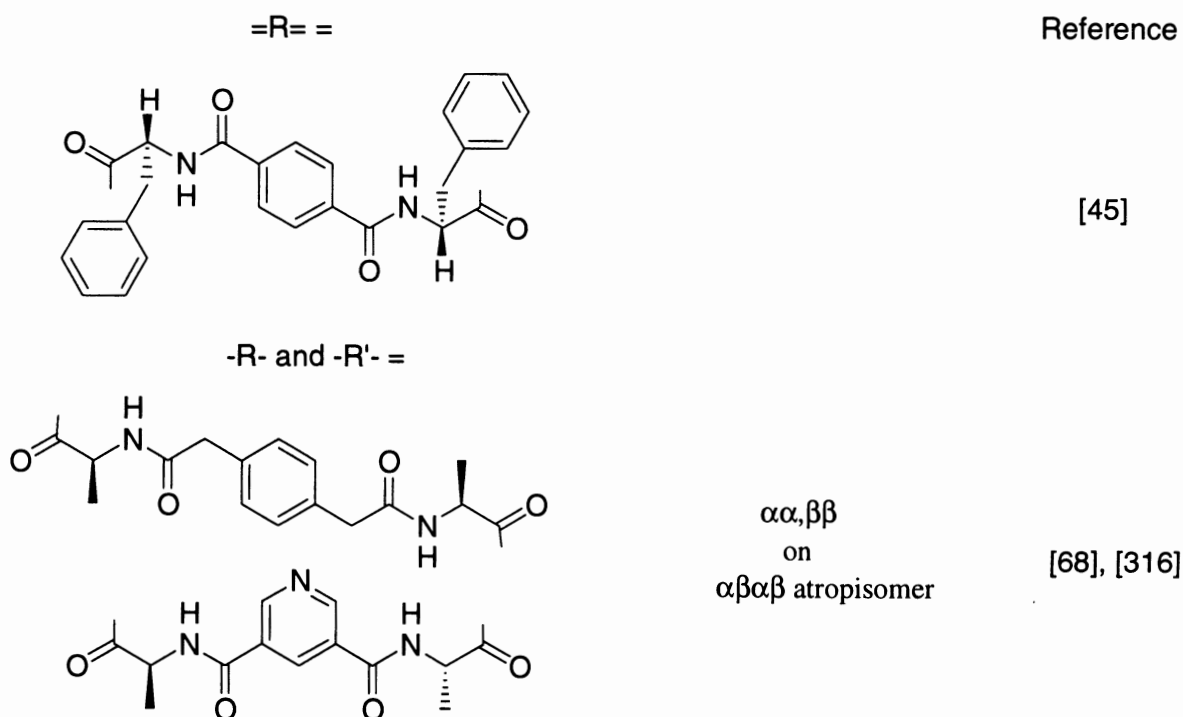


Figure 3. Continued.

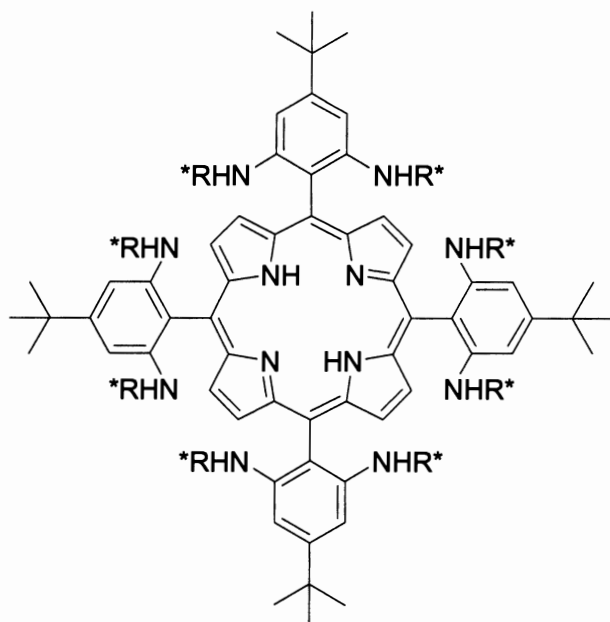
bitetralin-strapped “twin-coronet” porphyrins catalyzed epoxidation of styrenes substituted with electron-withdrawing groups in high ee (61–89%) and high product selectivity.<sup>81,214–216</sup> Each face of these porphyrins forms a chiral substrate-binding site and is sterically protected from oxidative catalyst deterioration. In the catalytic oxidation of styrene derivatives with the iron porphyrins and iodosobenzene, the highest ee (89%) was observed for 2-nitrostyrene.

Collman’s chiral iron “binap-capped” porphyrin<sup>62</sup> (Figure 3) was used to catalyze the asymmetric epoxidation of various unsubstituted aromatic olefins with ee’s in the range 21–63%. Unfunctionalized olefins were stereoselectively epoxidized with PhIO in the presence of threitol-strapped<sup>79</sup> manganese porphyrin complexes (Figure 7). Up to 88% ee was obtained in the epoxidation of 1,2-dihydronaphthalene with one of these derivatives, when a bulky imidazole ligand was used to block the unhindered face of the porphyrin catalyst.<sup>78,79</sup>

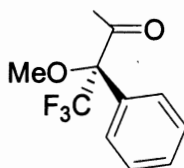
A series of  $D_2$ -symmetric chiral *trans*-dioxo-ruthenium(VI) porphyrins<sup>217</sup> (Figure 8) can effect enantioselective epoxidation of *trans*- $\beta$ -methylstyrene in up to 70% ee; a 76% ee was attained for the oxidation of cinnamyl chloride. The facial selection for *trans*-alkene epoxidation was explained by a “head-on approach” model.

The diamide prepared from *tetrakis*(2-aminophenyl)-porphyrin and 2,2’-dimethoxy-1,1’-binaphthalene-3,3’-dicarbonyl chloride<sup>58</sup> (Figure 3) is an efficient catalyst for the asymmetric epoxidation of terminal olefins. Exceptionally high ee’s and turnover numbers were obtained with some simple olefins.<sup>58</sup> UV–vis spectroscopy was used to study the selective binding of enantiomeric pairs of chiral epoxides to the corresponding  $\alpha\alpha\beta\beta$  binaphthyl-strapped Al porphyrin; the binding selectivity correlates to the enantioselectivity in the epoxidation of alkenes catalyzed by its Fe analog.<sup>218</sup>

The enantioselective epoxidation of terminal aromatic olefins by pyridine *N*-oxides catalyzed by a chiral ruthenium porphyrin catalyst<sup>219</sup> (Figure 8) proceeds with up to 80% ee. Similar ruthenium porphyrins were shown to be most selective catalysts for asymmetric epoxidation of terminal and *trans*-disubstituted olefins. The same catalysts display some selectivity in kinetic resolution of secondary alcohols and in what appears to be the first example of catalytic enantioselective hydroxylation of tertiary alkanes.<sup>220</sup> The enantioselectivity in the first catalytic conversion of styrene to its epoxide by a homochiral ruthenium porphyrin displayed a remarkable sensitivity to the solvent and the identity of the oxidant. The latter phenomenon clearly indicates that several high valent intermediates with different selectivities participate in



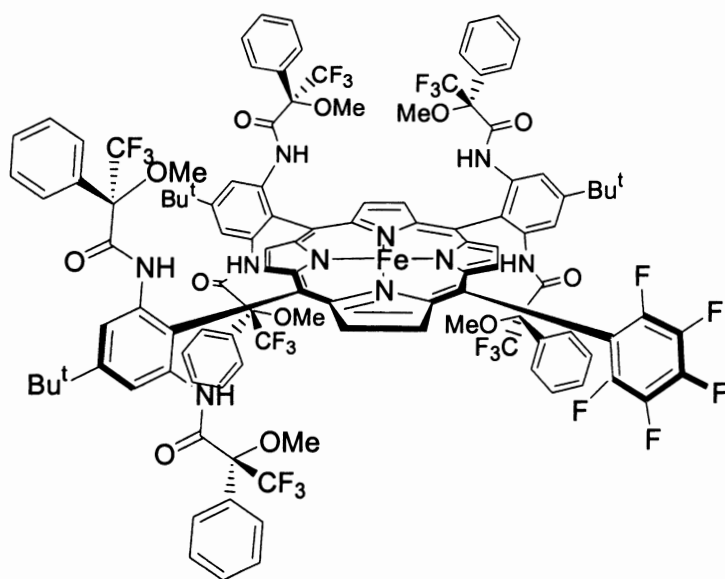
R=



Reference

[65]

Example of a mixed-substituent porphyrin:



[65]

( See also : [347] )

Figure 4. Selected chiral porphyrins obtained from *meso*-tetra(*o,o'*-diaminophenyl)-porphyrin.

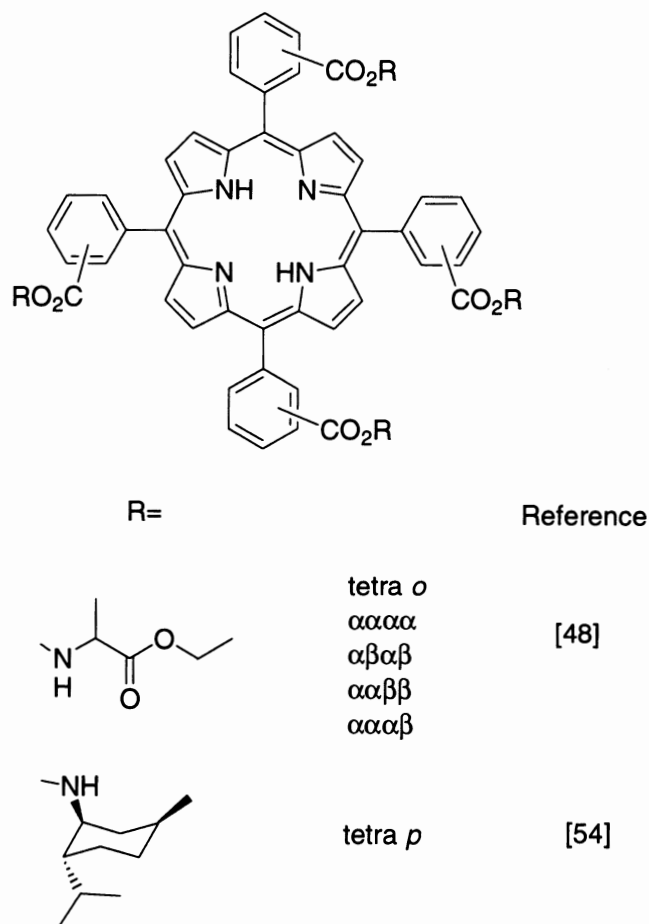


Figure 5. Selected chiral porphyrins obtained from *meso*-tetra(carboxyphenyl)porphyrin isomers.

oxygen atom transfer from catalyst to substrate.<sup>221</sup> Three metal complexes of one particular homochiral porphyrin were investigated as catalysts for enantioselective epoxidation of unfunctionalized olefins under various reaction conditions. Much better results were obtained with the iron and ruthenium complexes than with the manganese derivative.<sup>222</sup>

### c. Miscellaneous Metalloporphyrins

Manganese complexes of a series of  $\alpha\beta\alpha\beta$ -*meso*-tetraalkylporphyrins derived from a chiral cyclopropylaldehyde<sup>132</sup> (Figure 11), called chiorporphyrins (see Section IV), gave good ee's (60–86%) in 1,2-dihydro-naphthalene epoxidation. The observed excess of the 1*S*,2*R* epoxide was consistent with the *Re* face selectivity expected on steric grounds for the “side-on approach” of the substrate.<sup>133,223</sup>

Asymmetric epoxidation of olefins catalyzed by manganese complexes of chiral “strapped” porphyrins with diastereotopic faces<sup>145</sup> (Figure 12) was achieved

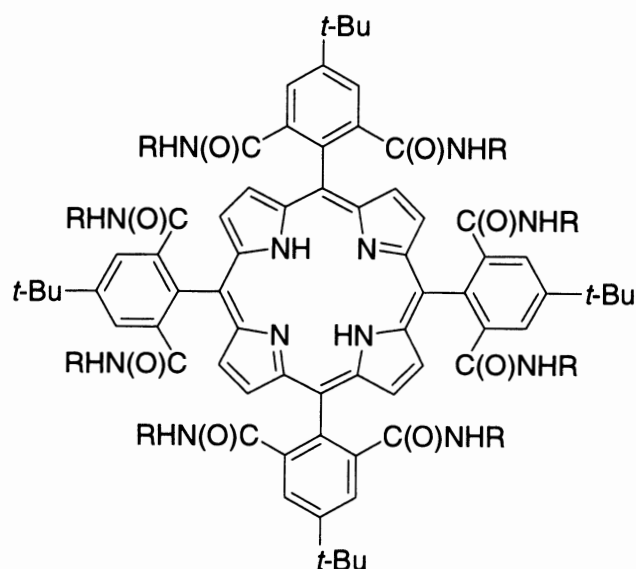
in the presence of imidazole, and the optically active epoxides were obtained in 42–58% ee. When imidazole was absent, the epoxides with the opposite configuration were formed in lower ee. In the presence of imidazole, the enantioselectivity of the reaction depended on the structure of the strap in the catalyst, while no such dependence was observed in the absence of imidazole.

## 2. Other Oxidations

### a. Hydroxylation

The first catalytic asymmetric hydroxylations reported by Groves *et al.* were obtained with a chiral iron “vaulted” porphyrin<sup>44</sup> (Figure 3); the ee's were in the range 40–72%.<sup>224</sup> A metal derivative of Halterman's chiral  $D_4$ -symmetric dinorbornabenzene tetraarylporphyrin<sup>96</sup> (Figure 10) was used as catalyst for hydroxylation of benzylic methylene groups by iodosylbenzene with 9–53% ee.<sup>97</sup> The corresponding  $D_4$ -symmetric dioxoruthenium(VI) porphyrin can effect stoichiometric and catalytic enantioselective hydroxylation of





R=	Reference
	[91]
	[91]
	[91]

Figure 6. Selected chiral porphyrins obtained from *meso*-tetra(*o,o'*-dicarboxyphenyl)-porphyrin.

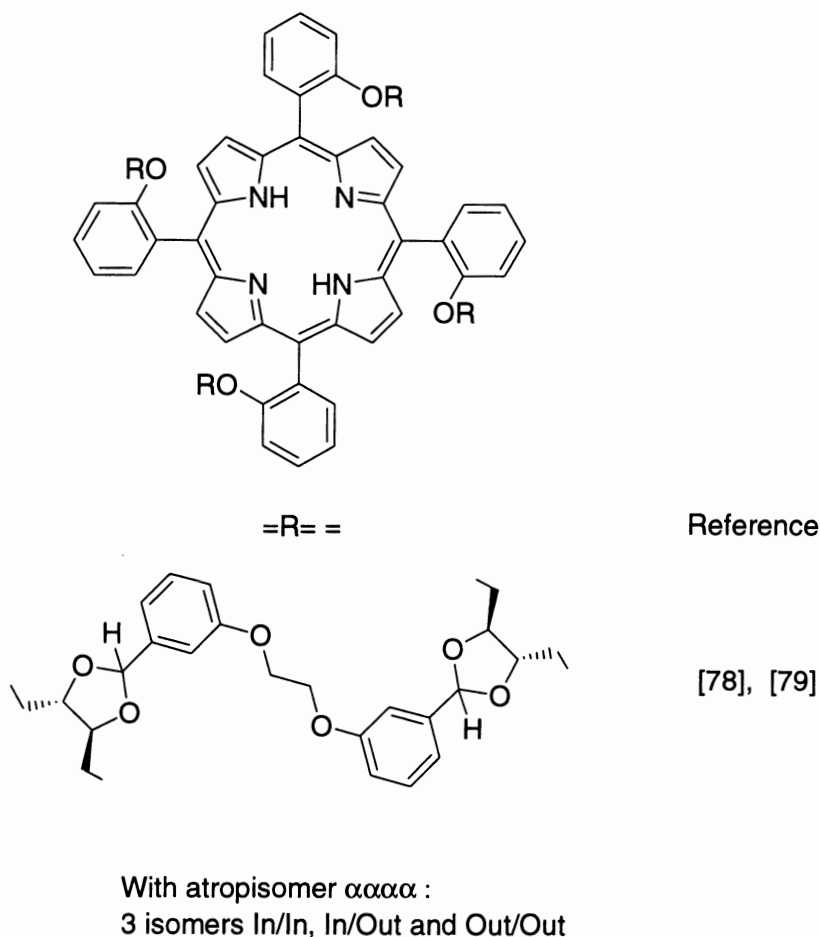
benzylic C–H bonds to give enantio-enriched aryl alcohols, the highest ee of 76% being attained in the catalytic oxidation of 1-ethyl-4-methylbenzene with 2,6-dichloropyridine *N*-oxide as terminal oxidant.<sup>225</sup>

### b. Various Oxidations

2,6-Permethylated- $\beta$ -cyclodextrin-linked iron and manganese porphyrins<sup>9</sup> (Figure 1) catalyze the enantioselective oxygenation of a racemic mixture of (*S*) and (*R*)- $\alpha$ -pinene with molecular oxygen under irradiation with visible light<sup>10</sup> (Figure 15). A 67% ee was obtained for (*S*)- $\alpha$ -pinene oxide. Low ee values (*ca.* 5%) were obtained with iodobenzene as oxidant.

Stereoselective oxidations by deuterohemin-L-phenylalanyl-poly-L-alanine complexes were interpreted in terms of the interaction between the chiral substrates and the peptide chains of the deuterohemin complexes.<sup>13</sup> Stereoselective catalytic oxidations of chelated deuterohemin-glycyl-L-histidine complexes suggest that phenolic substrates are capable of interacting with the catalyst from the proximal side, which contains the chiral histidine center. This disposition is reminiscent of the aromatic substrate mode of interaction in peroxidases.<sup>14</sup>

Stereoselective tryptophan-2,3-dioxygenase model reactions of the racemic tryptophan derivatives, *N*-acetyl-L-(+)- and *N*-acetyl-D-(–)-tryptophan methyl



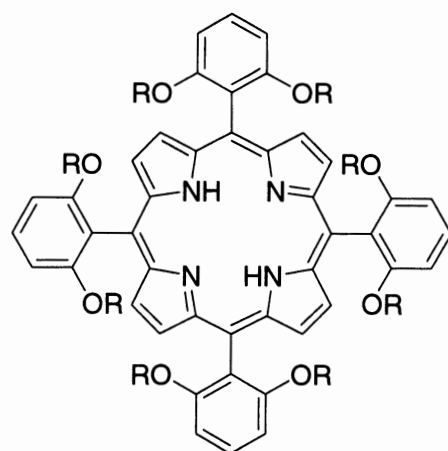
**Figure 7.** Selected chiral porphyrins obtained from *meso*-tetra(*o*-hydroxyphenyl)porphyrin (adapted from reference 79).

esters (abbreviated Ac-L-Trp-OMe and Ac-D-Trp-OMe), were performed with Mn complexes of a chiral porphyrin.<sup>29,54,55</sup> The predominant generation of methyl 2-D-(–)-acetamido-3-(2-formamidobenzoyl) propionate was achieved to 23.3% ee<sup>55</sup> (Figure 16) in the catalytic system using the Mn complex of  $\alpha,\alpha,\alpha,\alpha$ -*tetrakis*[*o*-(L-(–)-camphanoyl-amido)phenyl]-porphyrin (Figure 3). Stereoselective oxidation of enantiomeric amines (*R*(+)- or *S*(–)- $\alpha$ -phenylethylamine) has also been performed with the chiral iron(III) porphyrin complexes.<sup>74,75</sup> Tryptophan-2,3-dioxygenase-like activity of a manganese porphyrin bound to bovine serum albumin modified with poly(ethylene glycol) has been observed in the stereoselective dioxygenolyses of Ac-L- and Ac-D-Trp-OMe.<sup>226</sup> Stereoselective dioxygenolyses of the pyrrole ring in Ac-L- and Ac-D-Trp-OMe were performed with a manganese porphyrin covalently bound to bovine serum albumin. An enantioselective ratio of up to 1.63 ( $k_L/k_D$ ) in 18 vol% THF/H<sub>2</sub>O (pH 9.3) under an O<sub>2</sub> atmosphere at 298 K was achieved.<sup>227</sup>

A dioxoruthenium(VI) picket-fence porphyrin complex ( $\alpha\beta,\alpha\beta$  isomer) bearing optically active  $\alpha$ -methoxy- $\alpha$ -(trifluoromethyl)phenylacetyl residues on both sides of the porphyrin plane<sup>60</sup> (Figure 3) oxidizes racemic benzyl(methyl)(phenyl)phosphine to give optically active phosphine oxide (41% ee) and proceeds with retention of configuration at the phosphorus atom (Figure 17). A mechanism for phosphine oxidation involving kinetic resolution to give an oxoruthenium(IV) intermediate has been proposed.<sup>228,229</sup>

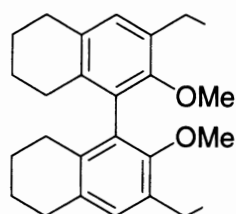
Prochiral alkyl sulfides gave sulfoxides with 14–48% ee with iron “vaulted” porphyrins (Figure 3).<sup>44</sup> “Basket-handle” iron porphyrins bearing (*S*)-naphthylpropionamide at the *meso* positions of tetra(*o*-aminophenyl)porphyrin are active as catalysts for oxygen atom transfer from iodosylbenzene and *tert*-butyl hydroperoxide to sulfides.<sup>41,61</sup> Oxidation of PhSMe gave (*S*)-PhS(O)Me in 79% yield and 15% ee.

Aryl alkyl sulfides were also oxidized enantioselectively to chiral sulfoxides in the presence of



-R- =

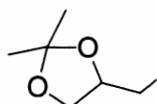
Reference



[81]

2 isomers, "eclipsed" and "staggered"

R=



[82]

(See also : [85], [217], [219], [220])

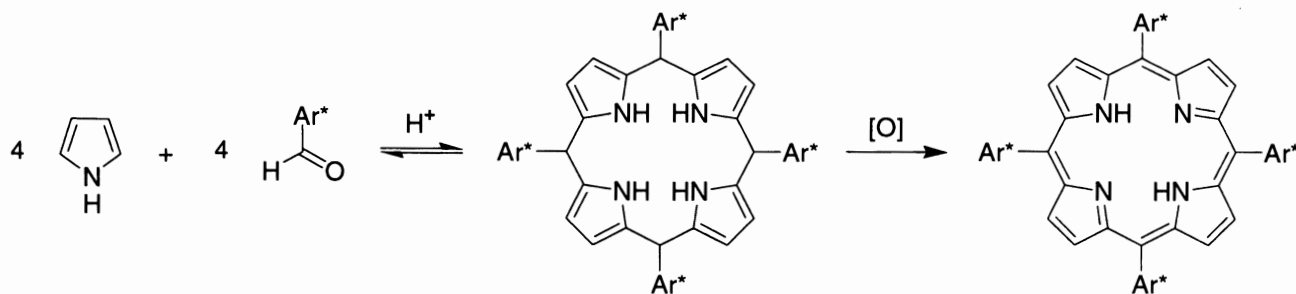
Figure 8. Selected chiral porphyrins obtained from *meso*-tetra(*o,o'*-dihydroxyphenyl)-porphyrin.

Figure 9. Synthesis of chiral porphyrins from chiral aromatic aldehydes.

stoichiometric amounts of iodosylbenzene and catalytic amounts of Halterman's  $D_4$ -symmetric manganese-tetraarylporphyrin<sup>96</sup> (Figure 10); enantioselectivities ranging from 40 to 68% ee were obtained.<sup>97,230</sup> "Twin-coronet" Fe porphyrins<sup>81</sup> (Figure 8) were used to catalyze the stereoselective oxidation of  $\text{MeSC}_6\text{H}_4\text{R}$ .<sup>231,232</sup>

Asymmetric oxidation of aryl sulfides by iodosylbenzene has also been achieved using iron porphyrin catalysts derived from the antipodes of a  $C_2$ -chiral, 1,4-xylylene-strapped porphyrin<sup>145</sup> (Figure 12), and gave the corresponding sulfoxides in 18–71% ee.<sup>233</sup>

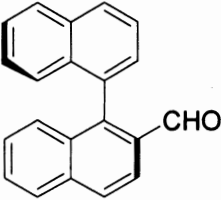
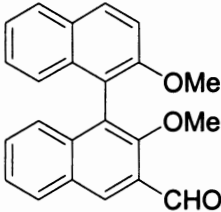
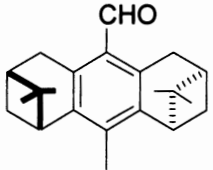
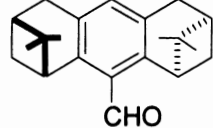
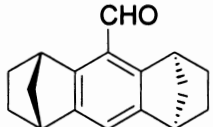
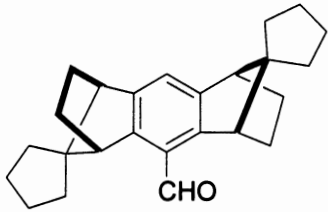
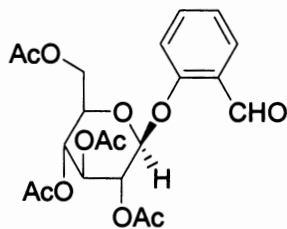
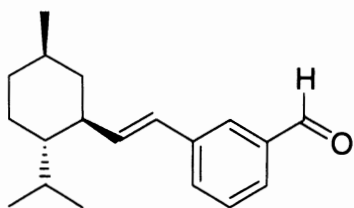
Ar-CHO	Reference
	[92] (See also: [93,110,111])
	[110]
	[95]
	[96]
	[96]
	[98]
	[99] (See also: [121])

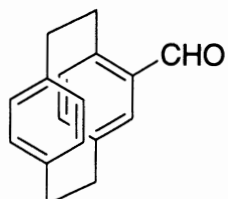
Figure 10. Selected chiral aromatic aldehydes used in the synthesis of chiral porphyrins.

Ar-CHO

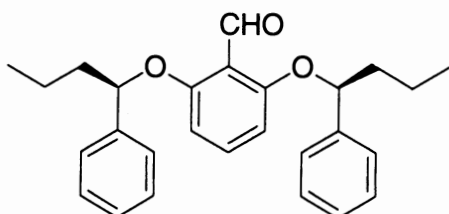
Reference



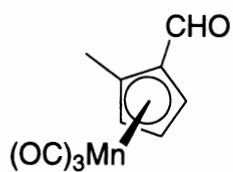
[107]



4 stereoisomers

[109]  
(See also: [108])

[120]



[118]

OHC-Ar-R-Ar-CHO

Reference

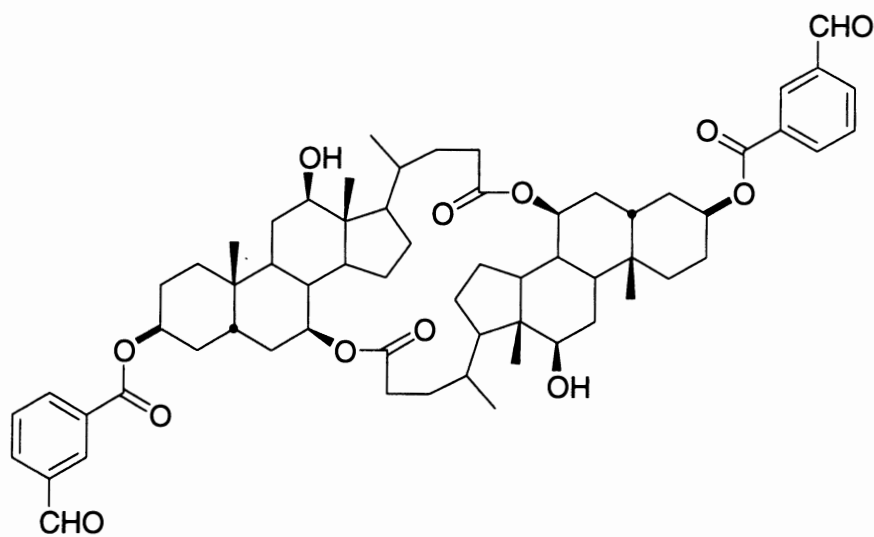
[113]  
(See also: [114], [115], [262])

Figure 10. Continued.

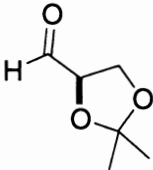
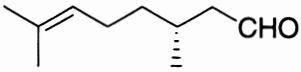
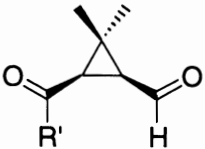
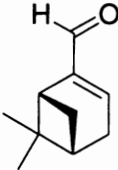
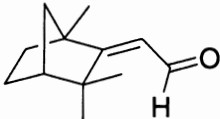
R-CHO	Reference
	[123] (See also: [122,124,125,127,128])
	[129]
	[132]
	[133]
	[131]

Figure 11. Selected chiral aliphatic aldehydes used in the synthesis of chiral porphyrins.

### c. Amidation

Ruthenium(II) and manganese(III) complexes of Halterman's porphyrin<sup>96</sup> (Figure 10) catalyze the asymmetric amidation of saturated C–H bonds of ethylbenzene and ethylnaphthalene to form the corresponding amides in up to 85% yield with 45–58% ee.<sup>234</sup>

## B. ASYMMETRIC CATALYTIC AZIRIDINATION

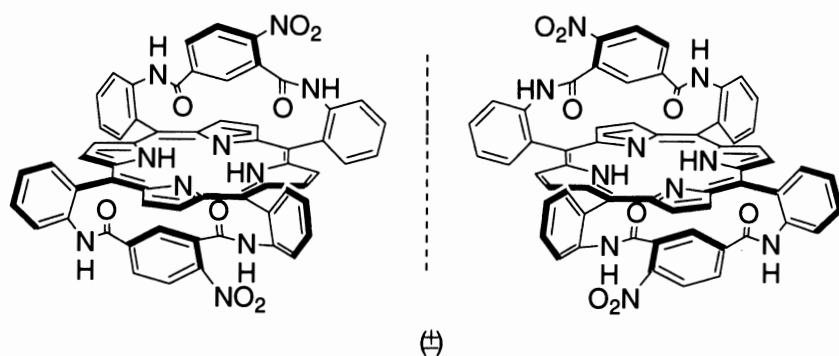
The use of ruthenium-tosylimido porphyrin complexes for aziridination of alkenes has been reviewed.<sup>196</sup> A *D*<sub>4</sub>-manganese(III) porphyrin<sup>96</sup> (Figure 10) was utilized to catalyze the aziridination of styrene-type substrates with ee ranging from 43 to 68%. Evidence for a Mn(IV) reactive intermediate in the catalytic cycle was obtained from spectroscopic studies and organic product analysis (Figure 18).<sup>235</sup>

Catalytic asymmetric aziridination of styrene by [*N*-(*p*-toluenesulfonyl)imino]phenyliodinane was achieved by manganese and iron complexes of tetramethylchiro-porphyrin<sup>132</sup> (abbreviated TMCP, see Figure 19); opposite enantioselectivities were obtained with the two metal centers<sup>236</sup> (see Section IV).

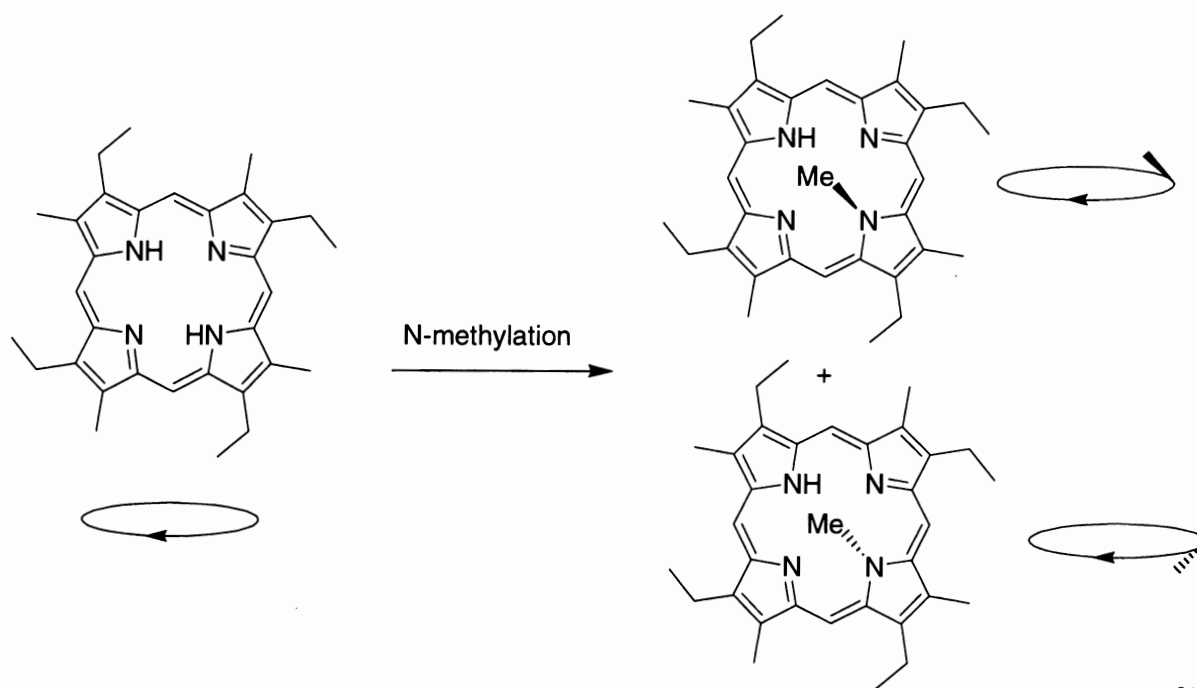
## C. ASYMMETRIC CATALYTIC CYCLOPROPANATION

The iodorrhodium derivatives of the so-called “chiral wall” porphyrin<sup>92</sup> (Figure 10) is an extremely active catalyst for the asymmetric cyclopropanation of alkenes by ethyl diazoacetate. Moderate enantioselectivities are observed.<sup>93,237</sup> The reaction is unusual in that it provides *syn*-cyclopropanes as the major product except in one case. Mono-, di-, and tri-substituted aliphatic olefins react at nearly equivalent rates, but tetrasubstituted alkenes are cyclopropanated poorly, especially when

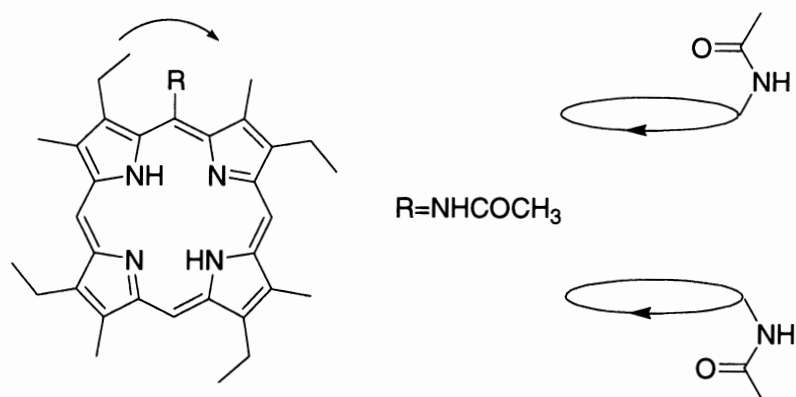
Reference



[51]  
(See also : [259])



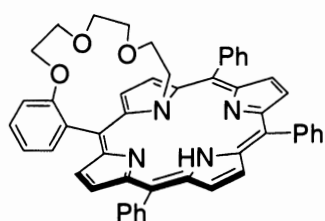
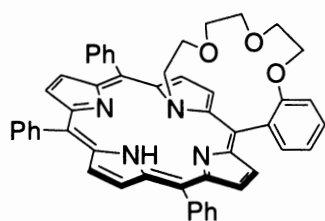
[138]  
(See also : [317])



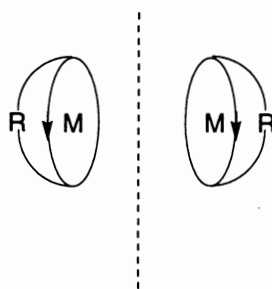
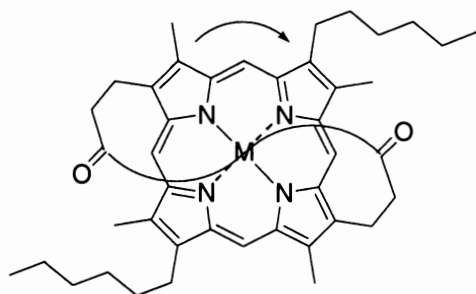
[140]  
(See also:  
[139,144, 146])

Figure 12. Selected examples of nonclassical chiral porphyrins.

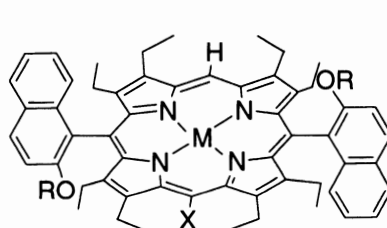
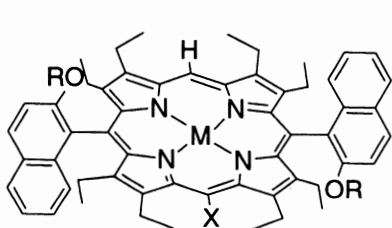
Reference



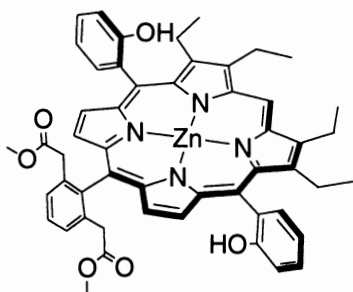
[143]



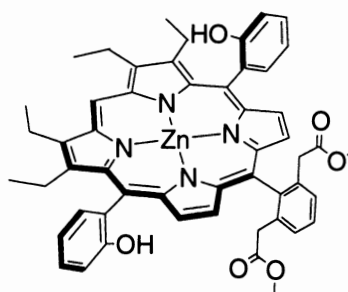
[145]

$$R = \text{NHCH}_2\text{-(p-C}_6\text{H}_4\text{)-CH}_2\text{NH}$$


[147]  
(See also: [148])



(R,R)



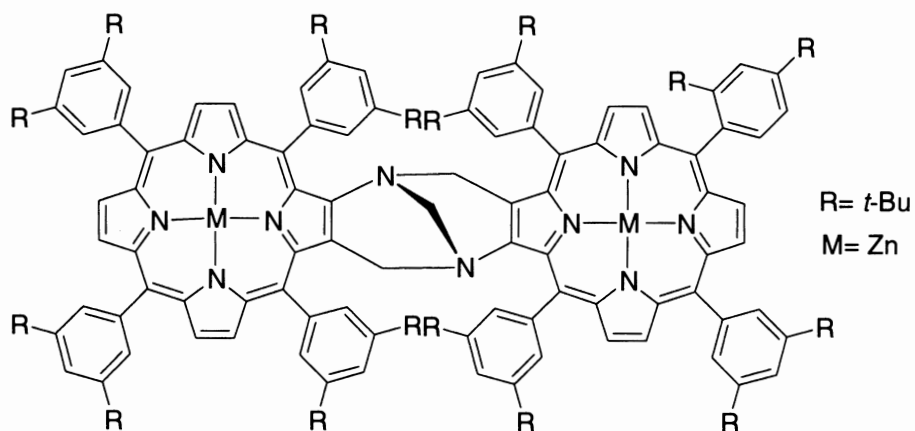
(S,S)

[149]  
(See also : [263])

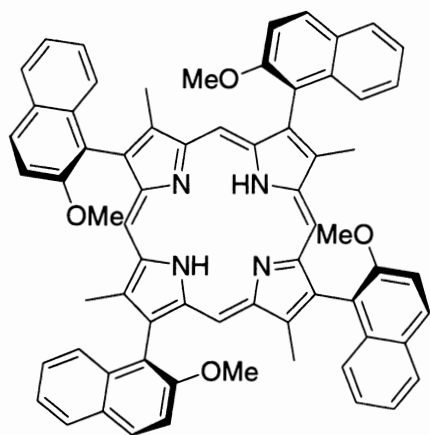
Figure 12. Continued.



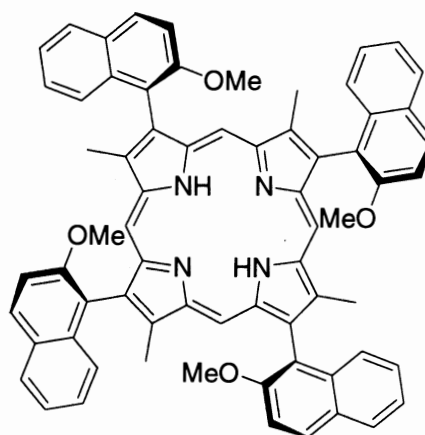
## Reference



[151]  
(See also: [152-154])

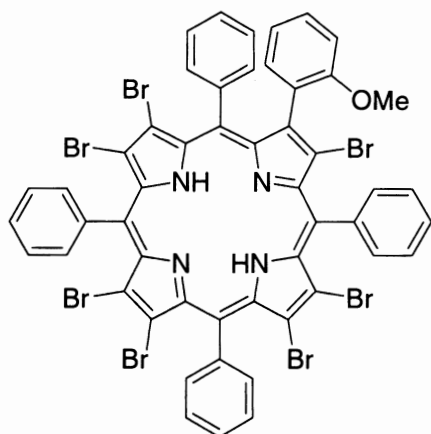


(*S,S,S,S*)



(*R,R,R,R*)

[155]



4 isomers

[158]

Figure 12. Continued.

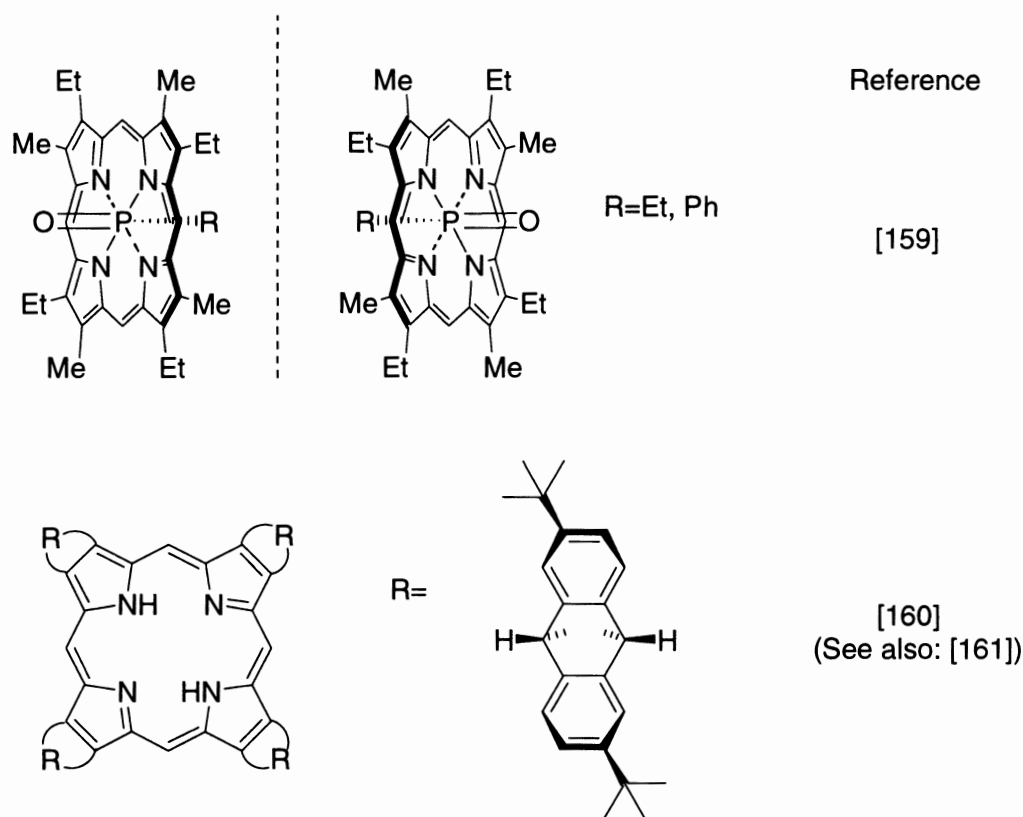


Figure 12. Continued.

a crowded catalyst is used. In the case of bulkier aromatic alkenes, extremely high *cis/trans* substrate selectivity is observed.<sup>238</sup>

Cyclopropanation of alkenes with ethyl diazoacetate was catalyzed by ruthenium complexes of a chiral tetraphenylporphyrin derivative<sup>60</sup> (Figure 3).<sup>239,240</sup> An enantiomerically pure ruthenium catalyst derived from Halterman's porphyrin<sup>96</sup> (Figure 10) was an active and selective catalyst for the asymmetric cyclopropanation of olefins with diazo compounds.<sup>241</sup> At a catalyst loading of only 0.15 mol%, quantitative yields, excellent diastereoselectivities (*trans* : *cis* 96 : 4) and high ee's (up to 91%) of the product cyclopropanes were achieved in the reaction of styrene with ethyl diazoacetate. Intermolecular cyclopropanation of styrene and its derivatives with ethyl diazoacetate catalyzed by a chiral ruthenium porphyrin afforded the corresponding cyclopropyl esters in up to 98% ee with high *trans/cis* ratios of up to 36 and extremely high catalyst turnovers.<sup>242,244</sup>

Asymmetric cyclopropanation of styrene by an enantiopure carbenoid catalyzed by simple metalloporphyrins was found to be much more efficient and selective than the alternative approach, the combination of metal complexes of enantiopure porphyrins and a nonchiral diazo ester.<sup>243</sup>

#### D. CHIRAL RECOGNITION

This topic has been reviewed in a previous volume of *The Porphyrin Handbook*<sup>5</sup> and in the open literature.<sup>245</sup> Chiral porphyrins and metalloporphyrins provide a potentially useful framework for the design of artificial receptors combining several unique features:

1. An approximately planar structure owing to the  $\pi$ -electron conjugation. This allows a facile design of receptors having a geometrically well-defined binding pocket consisting of a porphyrin framework and chiral recognition groups.
2. A number of possible central metals with varying recognition potentialities.
3. Several distinct functionalization sites: *meso* and  $\beta$ -positions, central metal, and inner nitrogens.
4. Chromophores for detecting subtle changes in interactions between porphyrin and surrounding molecules. UV-vis, circular dichroism, fluorescence, and resonance Raman spectroscopy can be used to probe the intermolecular interactions. <sup>1</sup>H NMR spectroscopy is also useful owing to the large ring current effects on the chemical shifts of the protons close to the porphyrin plane.<sup>189</sup>

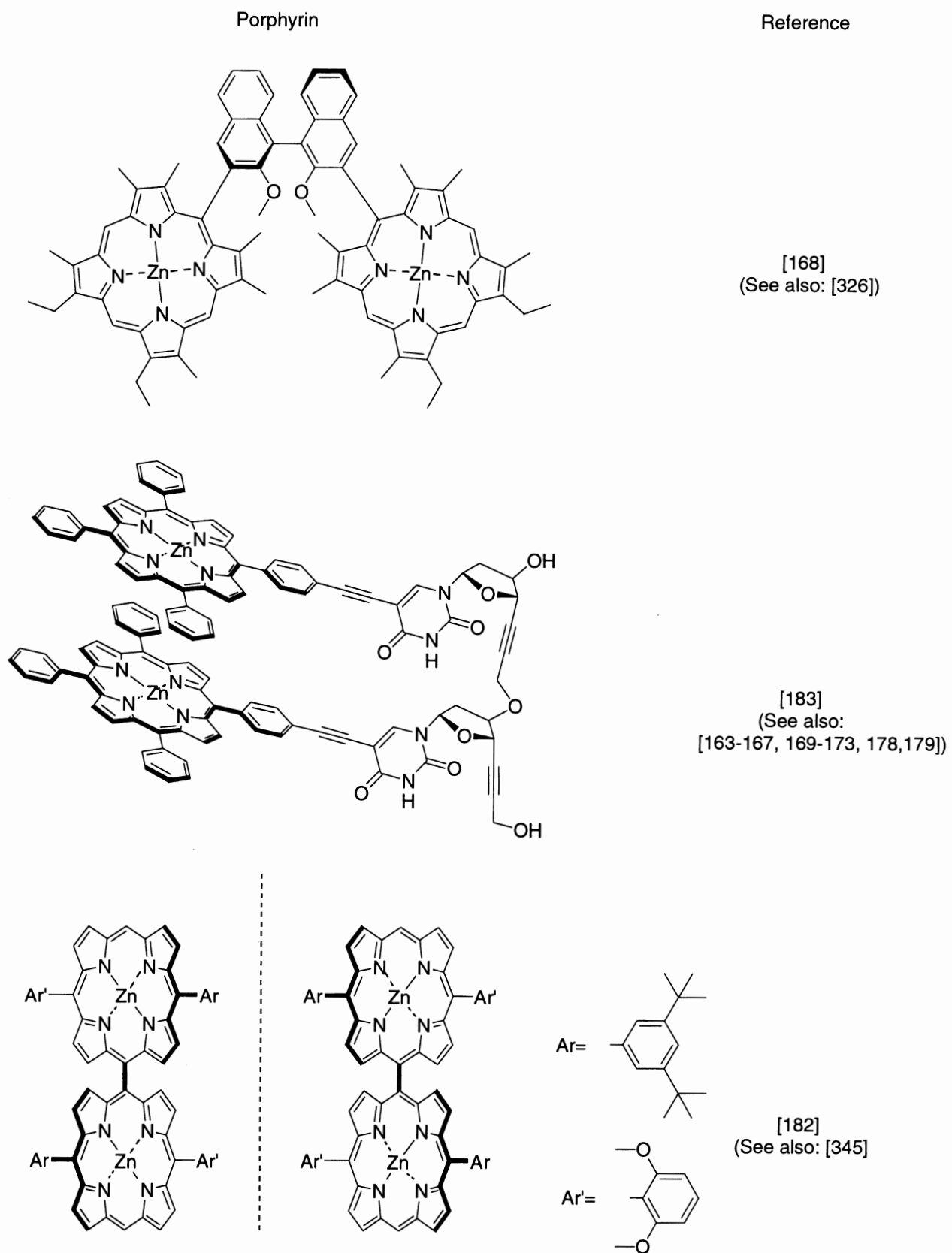


Figure 13. Selected examples of chiral di- and tri-porphyrin arrays.

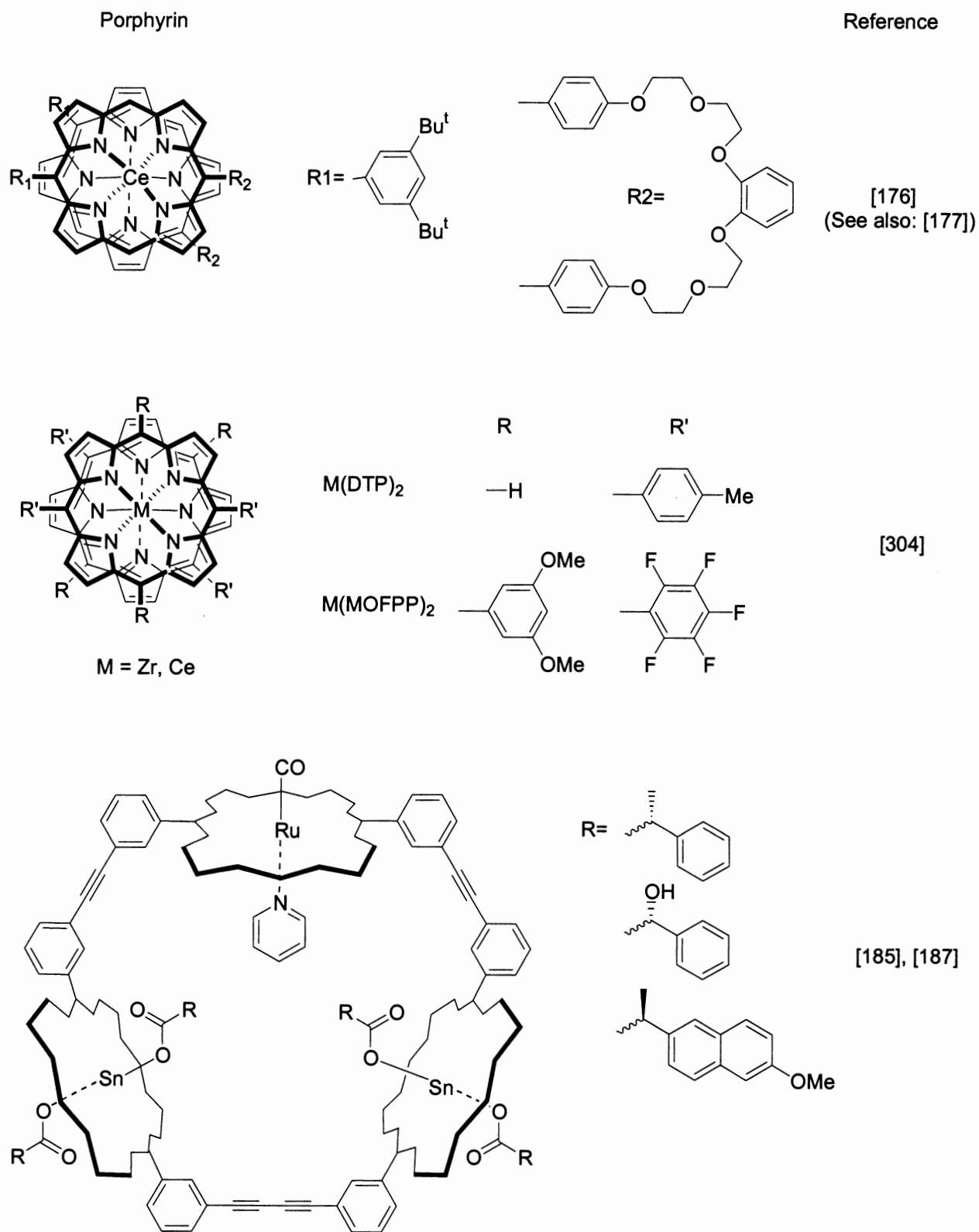


Figure 13. Continued.

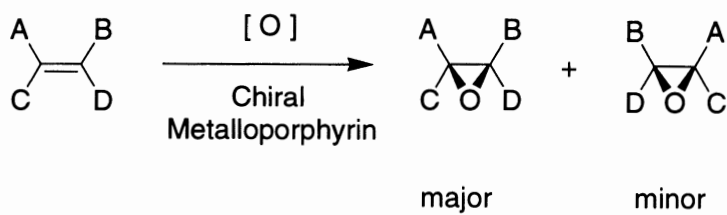


Figure 14. Asymmetric olefin epoxidation catalyzed by a chiral metalloporphyrin.

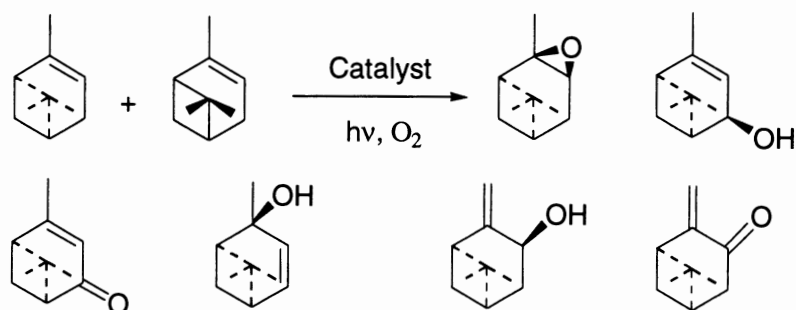


Figure 15. Enantioselective oxygenation of racemic  $\alpha$ -pinene (adapted from reference 10).

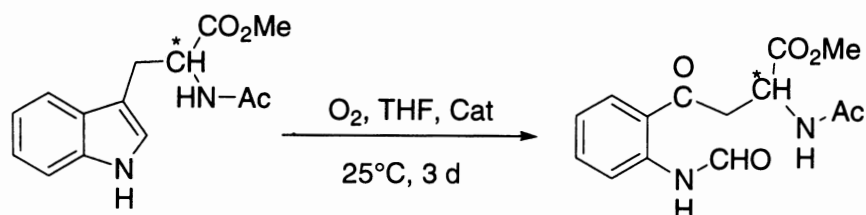


Figure 16. Stereoselective tryptophan-2,3-dioxygenase model reaction.

Reference

[29], [54], [55]

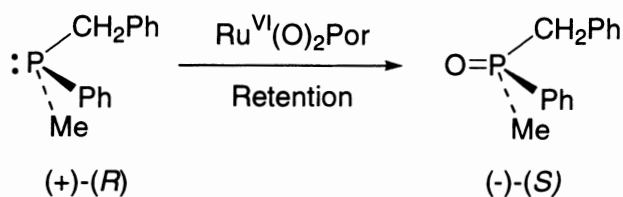


Figure 17. Phosphine oxidation with retention of configuration at the phosphorus atom.

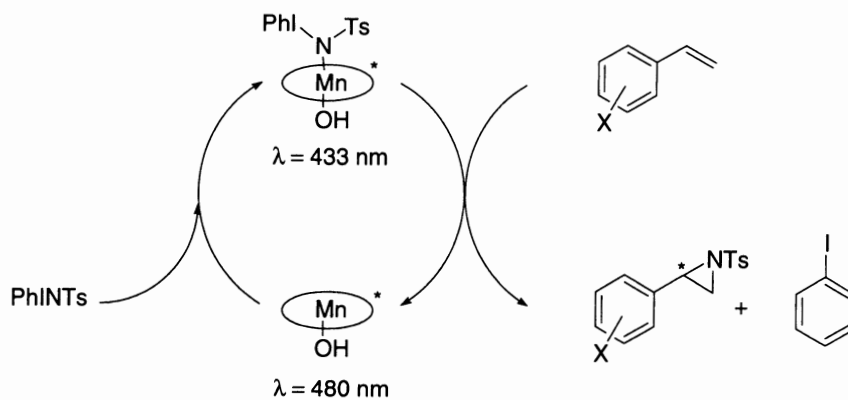
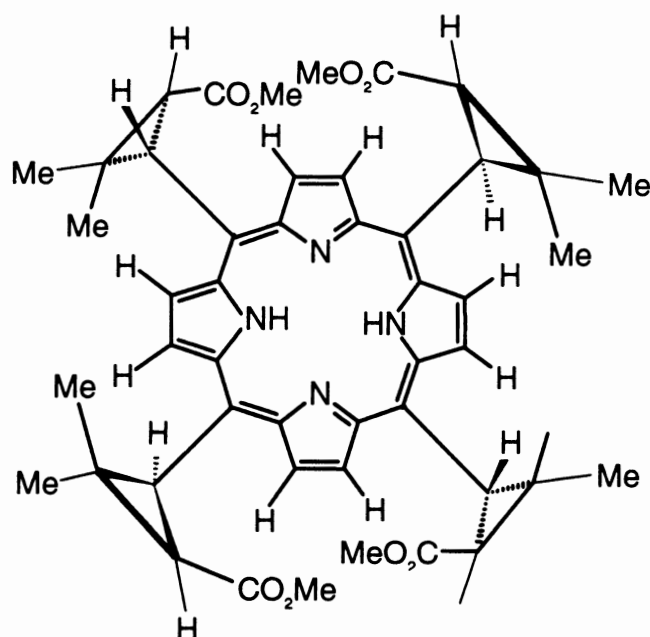


Figure 18. Intermediates in the catalytic aziridination of styrene derivatives.



**Figure 19.** Tetramethylchiroporphyrin: chiral porphyrin obtained from the methyl ester of (1*R*)-*cis*-cinaldehyde.

**Table 1.** Summary of Chiral Ligand Recognition by Porphyrins and Metalloporphyrins

Metal center	Axial ligand	Reference
Zn(II)	Amine	249, 267
None, Zn(II), Ru(II)	Alcohol	110, 246, 247
Co(III), Zn(II), Rh(III)	Amino alcohol	250, 252, 267
None, Zn(II), Rh(III)	Amino acid	25, 51, 71, 72, 146, 149, 253–260, 263, 264, 267
Ru(II), Ru(VI)	Amino ester	261, 262, 265, 266
Ru(II)	Phosphine	59, 60
Ru(II)	Isocyanide	82

Recognition of ligand absolute configuration has been achieved using chiral metalloporphyrins for various types of chiral ligands and several types of metal centers. An overview is given in Table 1.

#### a. Amines

Equilibria of the reactions with chiral amines of a Zn(II) “picket-fence” porphyrin complex bearing optically active substituents were studied by Inamo and Yoneda.<sup>249</sup> Stability constants were determined by spectrophotometric titration in dichloromethane solution. Chiral recognition in the complexation of amine to the  $\alpha,\beta,\alpha,\beta$ -isomer of the complex was observed for 1-(1-naphthyl)ethylamine with the ratio of the binding constant of  $K_S/K_R = 2.4$ .<sup>249</sup>

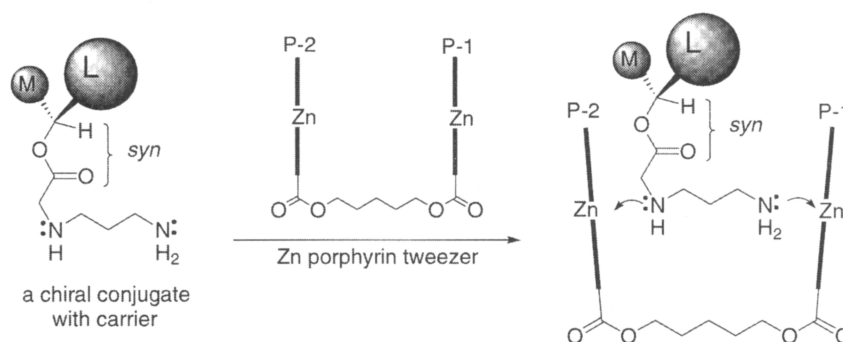
Induced circular dichroism in a porphyrin tweezer has been used for enantiomeric differentiation of guest diamines.<sup>267</sup> The tweezer was composed of two zinc

tetraphenylporphyrin units connected by a pentanediol spacer (Figure 20). Binding of the diamine to porphyrin tweezer led to a unique arrangement of the effective electric transition moments which gave rise to a coupled CD. Enantiomeric diamines showed mirror image CD spectra, from which absolute configurations could be assigned.<sup>267</sup>

#### b. Alcohols

Porphyrins with four *meso*-1,1'-binaphthyl substituents bearing 2-methoxy groups<sup>110</sup> (Figure 10) or hydrogen bond donating 2-hydroxy groups were obtained as the (*R,S*)- $\alpha,\beta,\alpha,\beta$ -atropisomer. The latter was found to bind mono-, di-, and tri-saccharides. Sugar binding was easily monitored in the visible wavelength region. IR, Raman, and <sup>1</sup>H NMR spectra indicated strong complexation of  $\beta$ -D-methylglucopyranose in water and DMSO. Association constants indicated a significant preference for di- and tri-saccharides (D- $\alpha$ -lactose, D- $\beta$ -lactose, D-trehalose, maltotriose) over monosaccharides (D-glucose, D-fructose, D-galactose).<sup>110</sup>

A semisynthetic receptor composed of a zinc porphyrin bridged by a steroidal diol<sup>113</sup> (Figure 10) was shown to complex alcohols and saccharides in nonpolar solvents by a combination of Lewis acid coordination and hydrogen bonding.<sup>247</sup> Comparison of binding constants to those obtained with the components of the receptor (zinc porphyrin alone, or steroidal diol alone) allowed an understanding of the physical basis of polyol recognition in terms of the binding



**Figure 20.** A zinc porphyrin tweezer for the determination of absolute configuration of primary amino groups or secondary hydroxyl groups linked to a single stereogenic center.

properties of the floor (zinc porphyrin) and roof (steroidal diol). Addition of pyranosides to the receptor in dichloromethane solution produced a striking color change from pink to green, implying sugar coordination to the Zn center, and allowing convenient analysis by UV titration. Binding isotherms indicated a 1:1 stoichiometry. Pyranosides were bound in the order: mannose > glucose > galactose, reflecting their “stickiness order” to the roof. This binding selectivity was rationalized on the basis of both the inherent receptor selectivity and the degree of intramolecular hydrogen bonding in the ligand. Moderate enantioselectivity was observed between the L and D enantiomers of a *n*-octyl-substituted  $\alpha$ -glucoside.<sup>247</sup>

The carbonylruthenium(II) complex Ru(CO)(TMCP) of tetramethylchiorporphyrin<sup>132</sup> (Figure 19) is able to discriminate the two enantiomers of a chiral alcohol ligand which binds on the axial coordination site *trans* to the carbonyl. Preferential binding of the (*R*) enantiomer was observed by <sup>1</sup>H NMR spectroscopy of the mixture of diastereomeric complexes obtained by addition of the racemic alcohol (see Section IV).<sup>246</sup>

### c. Amino Alcohols

A similar behavior was observed for the binding of amino alcohols to the chlorocobalt(III) complex CoCl(TMCP) of tetramethylchiorporphyrin<sup>132</sup> (Figure 19), but the kinetics of the dissociation and binding steps leading to an equilibrium state were considerably slower than with the carbonylruthenium(II) complex.<sup>252</sup> The enantioselection of amino alcohol ligands on the Co(III) center involves statistical complex formation in a first step, followed by slow ligand dissociation and fast ligand binding resulting in the selection of the (*R*) enantiomer over a period of 20–80 h. The final equilibrium ratios [R]/[S] measured by <sup>1</sup>H NMR were 1.2, 2.0, and 2.7 ( $\pm 0.1$ ) for

(*R,S*)-prolinol, (*R,S*)-2-aminobutanol, and (*R,S*)-2-aminopropanol, respectively.<sup>252</sup> The X-ray structures of the (*R*) and (*S*)-prolinol *bis*-adducts (see Section IV) revealed a multipoint bonding between host and guest that integrates two hydrogen bonds in addition to the coordination bond.<sup>252</sup> A slightly weaker hydrogen bonding of the (*S*) enantiomer has been proposed as the origin of the thermodynamic preference for the (*R*)-enantiomer.<sup>252</sup>

The iodorrhodium(III) complex RhI(TMCP) of tetramethylchiorporphyrin was prepared and its X-ray structure was determined.<sup>250</sup> In contrast to the corresponding chlorocobalt(III) complex CoCl(TMCP), this chiral metallohost has a single site available for ligand coordination *trans* to the iodine atom, and it affords a 1:1 adduct with (*R*)- or (*S*)-2-aminopropanol. RhI(TMCP) binds *rac*-2-aminopropanol with an enantioselective ratio [R]/[S] of 5.5 in favor of the (*R*)-enantiomer at the thermodynamic equilibrium after several days.<sup>250</sup> When compared to the analogous experiment performed with the corresponding cobalt(III) complex ([R]/[S] = 2.7), this result shows that enantiodiscrimination can be metal-dependent.<sup>250</sup>

### d. Amino Acids

*Trans*-5,15-(2-hydroxy-1-naphthyl)octaethylporphyrin<sup>147</sup> (Figure 12) was prepared by the coupling of two different dipyrromethanes with 2-hydroxynaphthaldehyde. Its racemic chlororrhodium(III) complex forms diastereomeric 1:1 adducts with L-amino acid methyl esters. The HPLC behavior of these adducts suggested that chiral recognition takes place in the presence of the HPLC adsorbent.<sup>255</sup> The Rh(III) complex acts as a bifunctional receptor for phenylalanine and leucine methyl esters via simultaneous coordination of the amine group to Rh(III) and H-bonding interaction between the hydroxy group of the host and the ester

group of the ligand. The adduct formation is practically irreversible when the *trans* axial ligand is Cl, but is reversible when the ligand is CH<sub>2</sub>COCH<sub>3</sub>. The weaker H-bonding interaction brings about selectivity for amino ester binding over amine in CHCl<sub>3</sub>, corresponding to a stabilization energy of 2.1 kcal/mol, and also plays a crucial role in reversible amino acid extraction from neutral aqueous solutions.<sup>256</sup>

An intrinsic chiral recognition host, [*trans*-5,15-*bis*(2-hydroxyphenyl)-10-[2,6-*bis*(methoxy-carbonylmethyl)phenyl]-2,3,17,18-tetraethylporphyrinato] zinc(II)<sup>149</sup> (Figure 12) was synthesized and found to show an enantioselectivity of *ca.* 2:1 for L- and D-amino acid esters having nonpolar residues. A reversed enantioselectivity of *ca.* 1:2 was observed for L- and D-serine benzyl ethers.<sup>149</sup>

The reaction of  $\alpha,\alpha,\beta,\beta$ -*tetrakis*(2-aminophenyl)porphyrin (Figure 2, X = NH<sub>2</sub>) having an achiral framework with dissymmetric bridging reagents (bridge = 1-nitro-2,5-phenylene, or 1-nitro-2,4-phenylene,<sup>51</sup> see Figure 3) yielded *meso* and racemic porphyrins. Enantioselective hosts were obtained from the enantiopure free bases<sup>51</sup> (Figure 12) by Zn insertion. The Zn complexes formed 1:1 adducts with amino acid esters, and their enantioselectivity toward amino acid esters was quite high, presumably because the two NH groups have very different acidities owing to the electron-withdrawing effects of the nitro group.<sup>51,259</sup> The ee's for phenylalanine methyl ester, alanine methyl ester, valine methyl ester, and leucine ethyl ester at 20°C in CH<sub>2</sub>Cl<sub>2</sub> were 75–80%. In the ligand–receptor complex, three interactions, the Zn···NH<sub>2</sub> coordination, NH···O=C hydrogen bonding, and the phenyl group···side chain steric interaction, are simultaneously operating, leading to the high observed enantioselectivity.<sup>51</sup>

A chiral triphenylporphyrin derivative which had two recognition groups in addition to the Lewis acid center: a hydrogen-bonding donor (OH), and a steric interaction/hydrogen-bonding acceptor (CH<sub>2</sub>COOCH<sub>3</sub>)<sup>149,263</sup> (Figure 12) was prepared. This compound behaved as an enantioselective receptor for amino acid derivatives. <sup>1</sup>H NMR studies and determinations of binding constants among a series of amino acid ligands suggested that the Zn···NH<sub>2</sub> coordination and OH···O=C hydrogen bonding determine the ligand orientation. Subsequent interactions between the CH<sub>2</sub>COOCH<sub>3</sub> group of the host and the side chain of amino acid ester guest become different for L- and D-amino acid esters. This receptor showed binding for amino acid esters with moderate ee's in the range 33–47% at 15°C in CHCl<sub>3</sub>. The ee increased with

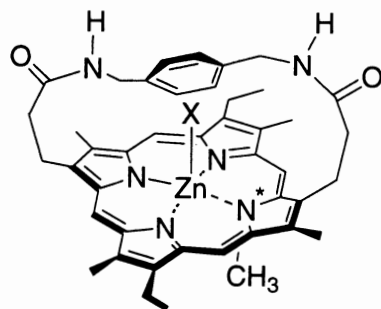
increasing the hydrogen-bonding energy between the OH group of the host and the C=O group of the guest, demonstrating that chiral discrimination originates from restriction of the rotational freedom of the guest via ditopic binding. Interestingly, the D/L-enantioselectivity was predictable from the nature of the ligand–receptor interactions. One enantiomer of the host systematically preferred the L-enantiomer of most of the amino acid esters except for serine. This enantioselectivity was rationalized by assuming that steric repulsion exists between the CH<sub>2</sub>COOCH<sub>3</sub> group in that enantiomer of the host and the side chain groups of most amino acid esters, while attractive hydrogen bonding exists between the CH<sub>2</sub>COOCH<sub>3</sub> group and the serine OH group. On the basis of these results, a general formalism for multipoint recognition was elaborated, and it was proposed that chiral recognition is achieved by combination of three recognition interactions between host and guest.<sup>254</sup> A helical Ru(II) *bis*(terpyridine) complex bearing two Zn(II) porphyrin units, designed as a potential enantioselective host for amino acids, has been mentioned.<sup>253</sup>

A chiral zinc strapped *N*-methylated porphyrin with molecular asymmetry, featuring a metal atom to bind a carboxylate anion and a rigid *p*-xylylene strap anchored via two amide linkages<sup>145</sup> (Figure 12), was synthesized from *meso*porphyrin II with enantiotopic faces, and its enantiomers were resolved by HPLC.<sup>146</sup> With this chiral receptor, highly enantioselective binding was achieved for the carboxylate anions of *N*-benzyloxycarbonyl-, *tert*-butoxycarbonyl-, 3,5-dinitrobenzoyl-, and acetyl-amino acids. IR and NMR studies demonstrated the crucial role of the hydrogen-bonding interaction between the receptor and substrates in the chiral recognition.<sup>146</sup>

Resolution of a *bis*porphyrin derived from Tröger's base<sup>151</sup> (Figure 12) afforded homochiral clefts that tightly bind histidine esters in 80–86% ee and lysine benzyl ester in 48% ee. The histidine esters are bound in fixed conformations that can be readily detected by <sup>1</sup>H NMR spectroscopy as a result of the large dispersion of proton resonances by the ring currents of the two porphyrins.<sup>257</sup>

A hydrophobic steroid-porphyrin-based receptor<sup>262</sup> (Figure 10) capable of multipoint recognition in organic solvents was solubilized directly in water by incorporation inside micelles. Micellar recognition was most effective when both hydrogen bonding and solvophobic forces acted together, leading to increased chiral discrimination of hydrophobic amino acid derivatives.<sup>262</sup>





**Figure 21.** A chiral zinc porphyrin with an  $\alpha,\alpha'$ -xylylenediamide strap. The (*S*) enantiomer is enantioselectively incorporated into poly(L-glutamic acid).

In competitive complexation of *Z*-amino acids (*N*-benzyloxycarbonyl-amino acids) in  $\text{CDCl}_3$ , a synthetic receptor such as zinc *N*-methylmesoporphyrin II having a xylylenediamido strap<sup>258</sup> (Figure 21) preferred *Z*-glycine over other *Z*-amino acids, where an excellent selectivity (> 90%) was achieved when *Z*-beta-alanine, *Z*-sarcosine, *Z*-leucine, or *Z*-proline was the competitor. In contrast, in competitive binding of *Z*-amino acid anions in a  $\text{CHCl}_3$ /water biphasic system, the host preferred substrates with hydrophobic side chains.<sup>258</sup>

Several chiral threonine-tailed porphyrins were synthesized and reported in the Chinese literature.<sup>25</sup> Their Zn complexes exhibited significant chiral recognition toward phenylalanine ethyl esters, and a possible recognition mode was suggested.<sup>25</sup>

Three chiral zinc tetraphenylporphyrin derivatives with protected amino acids as stereogenic groups<sup>71,72</sup> were synthesized (Figure 3), and their chiral recognition of amino acid methyl esters was investigated using UV-vis spectrophotometric titration. High enantioselectivities up to 21.5 were obtained.<sup>71,72</sup> The minimal energy conformation of these chiral zinc (II) porphyrins was studied by using molecular mechanics method. A molecular dynamics simulation of the chiral recognition process showed that the host prefers the D-amino acid esters, which is consistent with the experimental results.<sup>264</sup>

#### e. Amino Esters

Oxidation and chiral recognition of racemic amino esters by a dioxoruthenium (VI) picket-fence porphyrin complex  $\alpha,\beta,\alpha,\beta$  isomer bearing two optically active  $\alpha$ -methoxy- $\alpha$ -(trifluoromethyl) phenylacetyl residues<sup>60</sup> (Figure 3) on each side of the porphyrin plane led to

#### Reference

[258], [318]

the formation of mixed-ligated imino ester/amino ester Ru(II) complexes.<sup>265</sup> The same complexes were also obtained by anodic oxidation at a constant potential of the corresponding *bis*(amino ester) ruthenium(II) porphyrins. The electrochemical data were found consistent with a mechanism involving a Ru(IV) intermediate formed by disproportionation of a Ru(III) species.<sup>266</sup>

The synthesis of a (carbonyl)(valine methyl ester)-ruthenium(II) complex of the same chiral picket-fence porphyrin complex<sup>60</sup> (Figure 3) was described. For various amino esters, chiral recognition was observed for the complexation of the ligand with up to 52% ee for *tert*-leucine methyl ester. The dissociation rate constants of the two enantiomers of valine methyl ester were determined by <sup>1</sup>H NMR using magnetization transfer experiments, showing that the origin of the enantioselectivity in favor of the (L)-valine (*ca.* 2.6 : 1) resides in the difference between the kinetics of the axial ligand dissociation of the two enantiomers.<sup>261</sup>

The corresponding *bis*(amino ester)ruthenium(II) complexes of the chiral picket-fence porphyrin isomers<sup>60</sup> (Figure 3) were synthesized. With the valine methyl ester complex, a chiral recognition was observed for the oxidation of the ligand yielding a mixed-ligated imino ester/amino ester ruthenium(II) complex with 66% ee.<sup>260</sup>

#### f. Phosphines

The ruthenium(II) complex of this same picket-fence porphyrin<sup>60</sup> (Figure 3) exhibited chiral recognition in the complexation of racemic benzylmethylphenylphosphine. The reaction led to the formation of one of three possible diastereoisomeric products with high stereoselectivity (>95%).<sup>60</sup> The regiochemistry of axial

ligation by methyldiphenylphosphine was also described.<sup>59</sup>

### g. Isocyanides

The preparation of a chiral porphyrin bearing eight optically active pickets,<sup>82</sup> four on each side of the porphyrin plane (Figure 8), was described. Chiral recognition in the complexation of racemic isocyanide to the ruthenium(II) complex led to the formation of three stereoisomers with low stereoselectivity (15%).<sup>82</sup>

## E. MEMORY SYSTEMS

A saddle-shaped, fully-substituted porphyrin with  $D_2$ -symmetry such as 2,3,7,8,12,13,17,18-octamethyl-5,15-*bis*(2',6'-dimethoxyphenyl)-10,20-diphenylporphine<sup>268</sup> (Figure 22), upon mixing with (*R*)- or (*S*)-mandelic acid, formed a diastereoisomeric dimandelate complex which showed optical activity as a consequence of the strong inclination to a thermodynamically favorable isomer. Upon dissolution in acetic acid, the dimandelate complex was converted into an enantiomeric diacetate complex, which again exhibited optical activity with a half-life of 200 h at 23°C. The CD profiles of the dimandelate and diacetate complexes reflected the absolute configuration of mandelic acid. The optical activity of the dimandelate was erased upon exposure to visible light, but it was automatically retrieved when the light was switched off.<sup>268</sup> Extension of this work to a series of fully substituted chiral porphyrins having different numbers of *o*-dimethoxyphenyl groups at the *meso*-positions showed that different chiral transfer efficiencies and ring inversion activities could be obtained. Thermal racemization profiles of the protonated porphyrins in a variety of achiral carboxylic acids indicated that the ring inversion rate is dependent on the

steric factor as well as the acidity of the carboxylic acid solvent.<sup>269</sup>

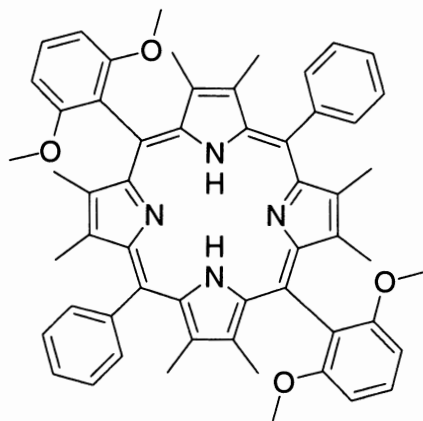
Numerous studies of supramolecular chirogenesis by coordination of a chiral ligand to an achiral metalloporphyrin system have been published.<sup>270–277</sup> The achiral *syn* folded (face-to-face conformation) host molecule of the ethane-bridged *bis*(zinc porphyrin) transforms into the corresponding chiral extended *anti bis*-ligated species in the presence of enantiopure amine guests (Figure 23). The mechanism of the supramolecular chirogenesis is based upon the screw formation in *bis*(zinc porphyrin), arising from steric interactions between the largest substituent at the ligand's asymmetric carbon and peripheral alkyl groups of the neighboring porphyrin ring pointing toward the covalent bridge. The screw direction is determined by the guest's (amines) absolute configuration resulting in a positive chirality induced by (*S*)-enantiomers due to the formation of the right-handed screw, and a negative chirality produced by the left-handed screw of (*R*)-enantiomers. The screw magnitude is strongly dependent upon the structure of the chiral guests.<sup>276</sup>

## F. MISCELLANEOUS APPLICATIONS

Miscellaneous properties and applications of chiral porphyrins, and various phenomena involving chiral porphyrins are listed in Table 2 and summarized below.

### a. Catalysts of Various Asymmetric Reactions

The aluminium complex of the  $D_4$ -symmetric dinorbornabenzene-derived Halterman's porphyrin<sup>96</sup> (Figure 10) catalyzes Diels–Alder reactions of isoprene or cyclopentadiene as the diene, and acrolein, methylvinylketone, or methyl acrylate as the dienophile

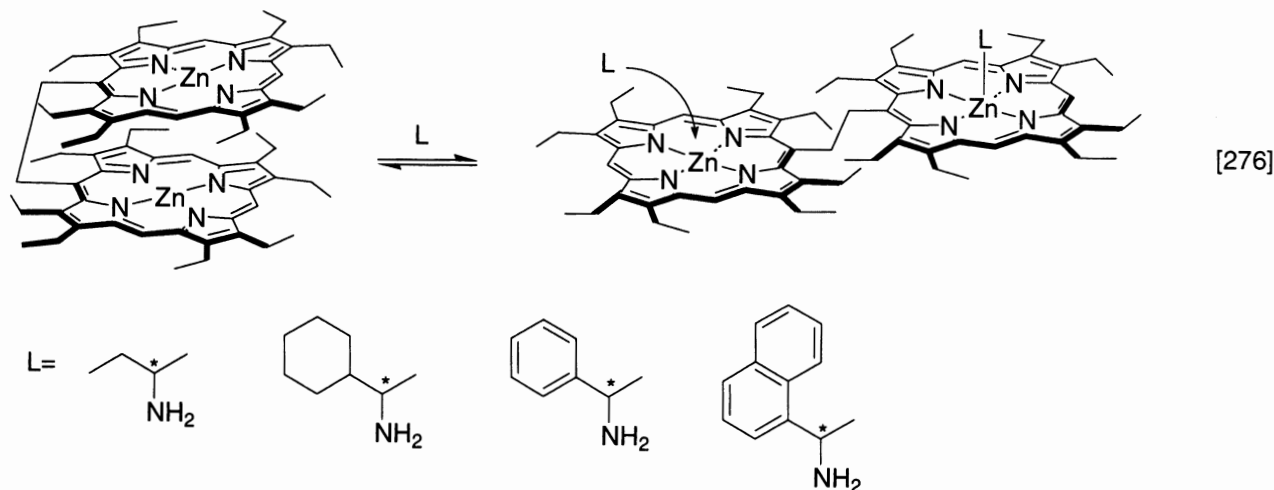


**Figure 22.** A saddle-shaped porphyrin which exhibits "chirality memory" of its adduct with (*R*)- or (*S*)-mandelic acid (adapted from reference 276).

## Reference

[268]

Reference



**Figure 23.** Supramolecular chirality induction by coordination of an optically active amine to a zinc octaethylporphyrin dimer.

**Table 2.** Miscellaneous Properties and Uses of Chiral Porphyrins

Topic	Reference
Catalysts of various asymmetric reactions	97, 278–280
Porphyrin tweezers	300, 301
Chirality probes	302, 303
Chiral metal <i>bis</i> -porphyrinate double-deckers	304, 305
Chiral assemblies and aggregates of porphyrins	19, 24, 27, 187, 295, 323–327, 330
Optical properties of chiral porphyrin conjugates	8, 17, 18, 24, 26, 48, 281–294, 296–299
Biochemical applications	76, 77, 88, 89, 127, 291, 306–322
Stirring effects on supramolecular chirogenesis	328, 329

with 5–20% ee.<sup>97</sup> Chiral *N*-substituted porphyrin free bases having a conformationally locked asymmetric nitrogen atom catalyzed Michael addition of thiophenols to cycloalkenones (Figure 24), where the reaction proceeded enantioselectively when the catalyst having a xylylene strap anchored via two secondary amido linkages was employed (Figure 21).<sup>278</sup>

A protein-hybrid photocatalyst prepared by covalently binding Ru<sup>II</sup>(CO)(py)(TCPP) (TCPP = *meso-tetrakis*(4-carboxyphenyl)porphyrin, see Figure 5 (R = H); py = pyridine) to bovine serum albumin (BSA), reduced  $\Lambda$ -Co(acac)<sub>3</sub> (acac = acetylacetonate) enantioselectively under photoirradiation.<sup>279</sup>

The iron complexes of *meso*tetraarylporphyrins bearing a peptide chain induce Soret-band splitting characteristic of the cytochrome P450 model

compounds. The hydrophobic environment and site separation of the protein have been mimicked by grafting the porphyrin on a highly cross-linked polystyrene. Control of axial ligation of the mercaptide has been activated through covalent linkage of a peptide chain including the cysteine.<sup>280</sup>

### b. Tweezers

The nonchiral 5,10,15,20-*tetrakis*(4-boronophenyl)porphyrin and 5,10,15,20-*tetrakis*[*N*-(2- or 4-boronophenyl)methylpyridinium]porphyrin formed a 1 : 1 complex, which gave specific exciton-coupling bands in CD spectroscopy only in the presence of glucose and xylose among monosaccharides. The structural examination established that only these monosaccharides can bridge two porphyrins by covalent-bond formation with boronic acids and twist them asymmetrically.<sup>300</sup> Similarly, [(dihydroxyboryl)phenyl]porphinatoiron(III) complexes were synthesized and the saccharide-binding ability of their  $\mu$ -oxo dimers was investigated.<sup>301</sup> The saccharide-binding process with boronic acids can be conveniently monitored by CD spectroscopy. The  $\mu$ -oxo dimer with 4-(hydroxyboryl) groups can bind glucose and galactose among monosaccharides with extremely high selectivity and sensitivity (association constants 10<sup>4</sup>–10<sup>5</sup> dm<sup>3</sup>mol<sup>-1</sup>), whereas the  $\mu$ -oxo dimer with 3-(hydroxyboryl) groups shows only a weak affinity with these monosaccharides. A similar trend was also observed for disaccharides. The former  $\mu$ -oxo dimer, which is formed in a self-assembled manner in aqueous alkaline solution, acts as an excellent pair of artificial “sugar tweezers.”<sup>301</sup>

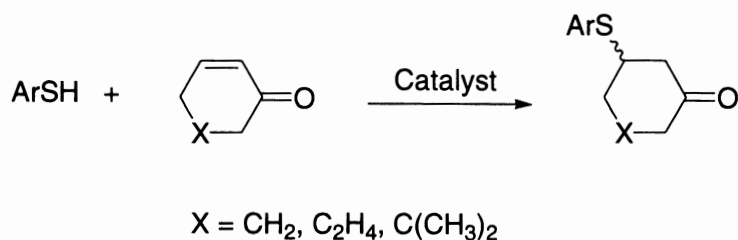


Figure 24. Asymmetric Michael addition of thiophenols to cycloalkenones.

### c. Chirality Probes

A general microscale protocol for the determination of absolute configurations of primary amino groups or secondary hydroxyl groups linked to a single stereogenic center has been described. The chiral substrates are linked to the achiral trifunctional bidentate carrier molecule (3-aminopropylamino)acetic acid and the resultant conjugates are then complexed with a dimeric zinc porphyrin host giving rise to 1:1 host/guest sandwiched complexes<sup>302</sup> (Figure 20). These complexes exhibit exciton-coupled bisignate CD spectra due to stereodifferentiation leading to preferred porphyrin helicity. Since the chiral sense of twist between the two porphyrins in the complex is dictated by the stereogenic center of the substrate, the sign of the couplet determines the absolute configuration at this center. The twist of the porphyrin tweezer in the complex can be predicted from the relative steric sizes of the groups flanking the stereogenic center, such that the bulkier group protrudes from the complex sandwich. In certain  $\alpha$ -hydroxy esters and  $\alpha$ -amino esters, electronic factors and hydrogen bonding govern the preferred conformation of the complex, and hence the CD spectra.<sup>302,303</sup>

### d. Metal bisPorphyrinate Double-Deckers

Reduction of a chiral cerium bisporphyrinate double-decker complex Ce(MOFPP)<sub>2</sub> (MOFPP = 5,15-*bis*(3,5-dimethoxyphenyl)-10,20-*bis*(pentafluorophenyl)porphyrin dianion)<sup>304</sup> (Figure 13) with sodium anthracenide in dioxane at 20° resulted in acceleration of the porphyrin ligand rotation (= racemization) by a factor of >300. Photoreduction of Ce(MOFPP)<sub>2</sub> in dioxane also resulted in enhancing the ligand rotation activity of the complex. However, oxidation of a chiral zirconium complex Zr(DTP)<sub>2</sub> (DTP = 5,15-ditolylporphyrin dianion)<sup>304</sup> (Figure 13) with phenoxathiinium hexachloroantimonate or FeCl<sub>3</sub> resulted in deceleration of the acid-induced racemization in THF, where monocationic and dicationic forms of the complex racemized 21 and 99 times more slowly than the neutral

complex, respectively.<sup>304</sup> A nonchiral Ce(IV) *bis*-(porphyrinate) double-decker scaffold bearing two pairs of boronic acid groups is a scaffold for the effective binding of oligosaccharides (maltooligosaccharides and laminarioligosaccharides) in aqueous media to form 1:2 saccharide complexes, and shows positive, homotropic allosterism with Hill coefficients of 1.6–2.0.<sup>305</sup>

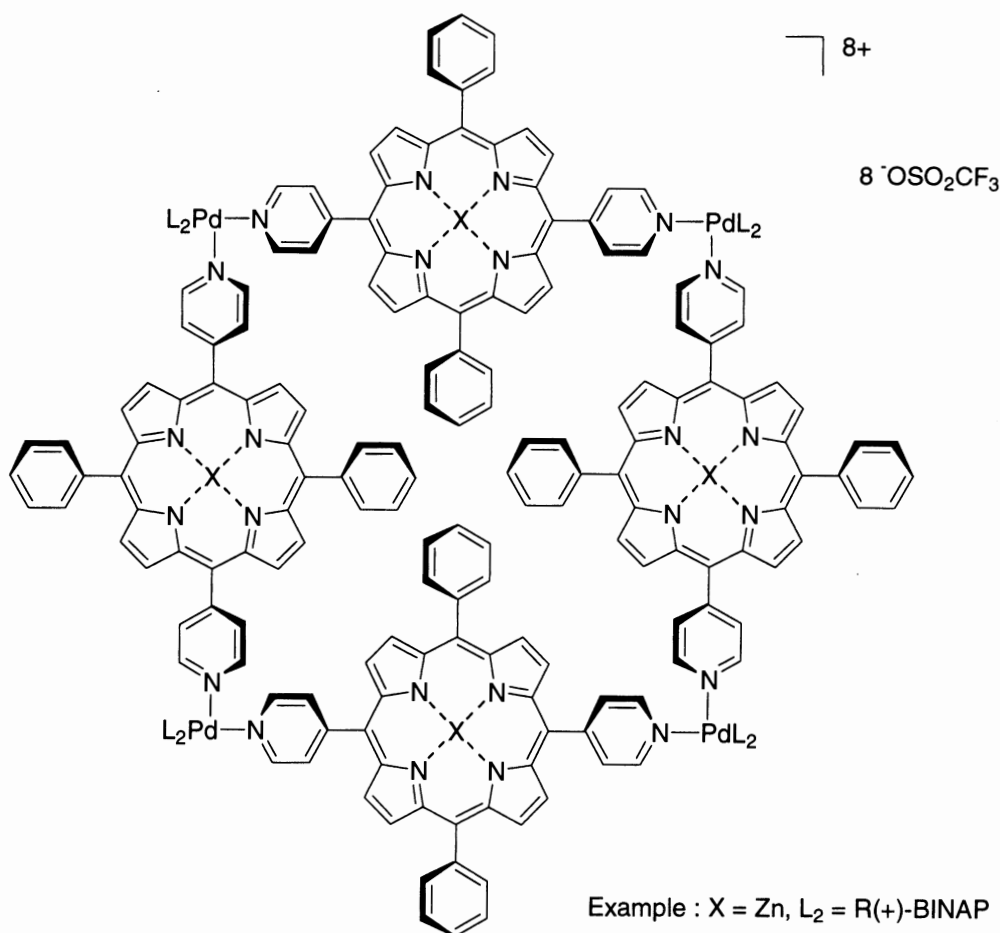
### e. Chiral Assemblies and Aggregates of Porphyrins

The NMR spectra of hematoporphyrin-IX derivatives were studied. The two chiral centers caused a splitting of the signals of the *meso* protons. The dimeric association of dihemim was shown to have a displaced sandwich structure.<sup>330</sup>

A cyclic trimeric porphyrin host<sup>187</sup> has been synthesized (Figure 13). Binding of the octahedral aluminum *tris*[3-(4-pyridyl)acetylacetonate] guest ligand into the complementary cavity of the host induced an asymmetry, which was readily detected by NMR spectroscopy.<sup>187</sup>

Self-assembly of predesigned angular and linear dipyriddyldiphenylporphyrin modules (DPyDPP) with bisphosphine-coordinated Pd(II) and Pt(II) angular and linear modules leads to cyclic porphyrin arrays containing two or four units and ranging in size from 15 to 39 Å (Figure 25).<sup>325</sup> Restriction in rotation of *trans*-DPyDPP groups around the axis defined by the terminal metal-N bonds distorts the symmetry of the tetramers, but the rotation is unrestricted at elevated temperatures. Chiral metal triflates containing *R*(+)- or *S*(-)-BINAP phosphines promote formation of enantiomeric macrocycles with a puckered geometry. CD spectra of the chiral macrocycles reveal a strong exciton coupling between the porphyrin chromophores in the tetramers. Emission spectra reveal moderate fluorescence quenching of the dipyriddyldiphenylporphyrin fluorophores upon treatment with metal triflates and concomitant incorporation into the macrocycles.<sup>325</sup>

Easily accessible protoporphyrin IX 13,17-*bis*(glycosamides) form colloidal aqueous solutions which are



**Figure 25.** A cyclic tetrameric porphyrin array obtained by self-assembly of a dipyrrolyldiphenylporphyrin module.

stable for several months or longer. Electron micrographs show ribbons of an approximate width of 4 nm and lengths of between 20 nm (D-glucosamide) and 5  $\mu\text{m}$  (D,L-mannosamide). CD spectra reveal complex exciton splittings. Fluorescence was not present in the aggregate and the aggregates did not quench the fluorescence of the added porphyrins. Two stacked face-to-face dimers with lateral shifts of half a molecule in each direction and no dipole–dipole interactions are proposed to connect to twisted ribbons by strong edge-to-edge interactions.<sup>327</sup>

Chiral-twisted iron(III) porphyrin dimers connected by (*R*)- and (*S*)-2,2'-dimethoxy-1,1'-binaphthyl spacers<sup>326</sup> (Figure 13) were self-assembled, characterized by CD spectra and formed high molecular weight polynuclear species through  $\mu$ -oxo dimers. The  $\mu$ -oxo stacks of Sn(IV) porphyrins rearrange to staircase-type and lateral aggregates upon replacement of the O ligands by chloride ions.<sup>326</sup> The lateral aggregation of Sn(IV) 2,18-dipropionate porphyrins in HCl at pH 0–0.5 is favored by 8,13-Et groups instead of the natural 8,13-vinyl groups of protoporphyrin IX and is impeded by H

atoms at these positions. Replacement of axial chloride counterions to the Sn(IV) central ions by cyanate counterions at pH 4.5 leads to similar aggregates if the cyanate ions are connected by H bonding to acetic or lactic acid. In this case, aggregation is not necessarily impeded by H atoms at positions 8 and 13. D- and L-lactic acid enforce chiral assemblies of the Sn(IV) deuteroporphyrin di-Me ester complex with mirror image CD spectra ( $\theta \approx 8 \times 10^5 \text{ deg cm}^2 \text{ dmol}^{-1}$ ), whereas the gluconoyl hydrazide-substituted Sn(IV) deuteroporphyrin does not form aggregates at all.<sup>324</sup>

The self-aggregation of chiral threonine-linked porphyrins and their zinc(II) complexes in water–alcohol system and water–alcohol–NaCl system has been studied by CD, UV–vis absorption spectra, and fluorescence spectra methods. The experimental results indicate that chiral threonine-linked porphyrins and their zinc(II) complexes have two different kinds of aggregates in water–alcohol system and water–alcohol–NaCl system. The aggregates in water–alcohol–NaCl system may have helical structures.<sup>24</sup> Absorption spectra of Langmuir–Blodgett (LB) films formed by a

chiral amino acid porphyrin and its mixture with stearic acid have been investigated.<sup>27</sup>

Amphiphilic  $\alpha$ -helix peptides carrying porphyrin moieties were designed and synthesized. The tetraphenylporphyrins were able to be fixed and arranged with a chiral twist in a three-dimensional structure constructed by the amphiphilic assembly of the  $\alpha$ -helices.<sup>19</sup>  $\alpha$ -Helical polyglutamic acid was used as a matrix to form chiral H- and J-type aggregates of the anionic *meso-tetrakis*(4-sulfonatophenyl)porphine in the presence of cationic porphyrins.<sup>323</sup>

#### f. Optical Properties of Chiral Porphyrin Conjugates

(1) *Fluorescence.* Linked porphyrin-cyclodextrin compounds<sup>8</sup> (Figure 1) exhibit perturbed electronic absorption and emission spectra which are consistent with their adopting two conformations, one extended with little interaction between the porphyrin and cyclodextrin, and the other folded with the cyclodextrin weakly complexed to the porphyrin. Quenching of the porphyrin excited state by benzoquinone was examined by measurement of the fluorescence lifetime as a function of quinone concentration; the results suggest that the porphyrin excited state can be quenched intermolecularly by benzoquinone and also intramolecularly by quinone complexed within the cyclodextrin cavity.<sup>8</sup>

Several dendritic poly(L-lysine)s containing porphyrinic sites have been prepared.<sup>286-289</sup> Dendritic poly(L-lysine)s combining thirty-two free base- and Zn(II)-porphyrins in scramble fashion were synthesized

and they exhibit highly efficient (85%) fluorescence energy transfer from Zn(II)-porphyrins to free base-porphyrins.<sup>286</sup>

A series of glycosylated porphyrins have been synthesized with the aim of studying the structural dependence of porphyrin cellular localization and efficiency in photodynamic therapy. The association of nonaggregated forms of porphyrins to unilamellar liposomes, modeling the lipid bilayer of a biological membrane, was studied by fluorescence spectroscopy at neutral pH. On mixing with liposomes, amphiphilic porphyrin derivatives exhibit an increase in their fluorescence intensity and lifetime. The localization of liposome-bound dyes was studied by fluorescence labeling of (a) the lipid region in interaction with both lipid chains and headgroups or (b) the carbohydrate chain region of lipids.<sup>290,291</sup>

A Pd(II) porphyrin was covalently linked to a chiral lanthanide complex and effectively sensitizes near-IR emission from Nd and Yb (Figure 26). Sensitization is enhanced in the absence of oxygen and in the presence of a nucleic acid.<sup>299</sup>

(2) *Photoinduced electron-transfer.* Synthetic peptide-bridged porphyrin-quinone molecules<sup>285</sup> (Figure 27) give photoinduced electron transfer from porphyrin to quinone in 2-methyltetrahydrofuran.

(3) *Induced circular dichroism.* L-Amino acids attached to the atropisomers of *meso-tetrakis*(*o*-aminophenyl)porphyrin (Figure 3, R = H) and *meso-tetrakis*(*o*-carboxyphenyl)porphyrin (Figure 5, R = H), induced

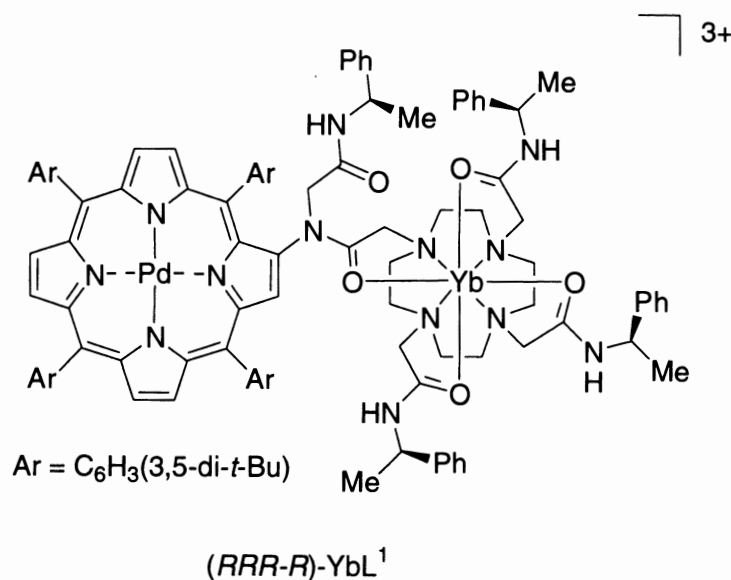
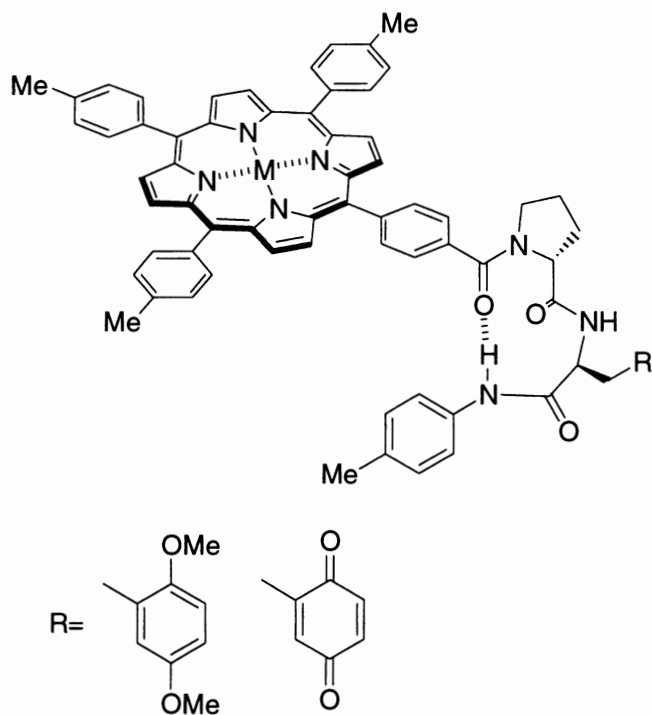


Figure 26. A chiral lanthanide complex-palladium porphyrin conjugate.

## Reference



[285]

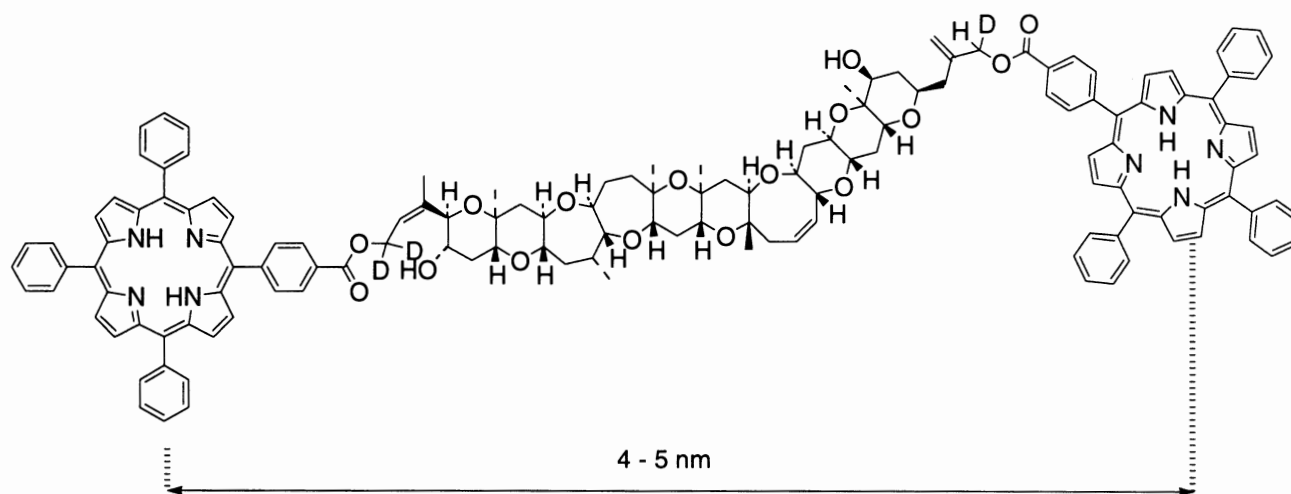
Figure 27. A peptide-bridged porphyrin-quinone dyad (adapted from reference 285).

CD at the Soret band of the porphyrins to an extent which depended on the conformation of the atropisomer.<sup>48</sup>

A chiral amino acid was covalently linked to (5-(2-carboxylphenyl)-10,15,20-triphenylporphinato) zinc(II) ZnCOTPP via amide formation.<sup>26</sup> As a heme protein model, the resulting chiral amino acid-linked porphinatozinc(II) complex, AA-ZnCOTPP (AA = amino acid residue), was designed to study the relation of the induced CD (ICD) of heme protein and the intramolecular interaction. The complexes exhibited split ICD in the Soret region. The ICD of AA-ZnCOTPP in the Soret region also indicates that an amino acid residue interacts with a porphyrin plane and the intramolecular interaction makes the conformation of an amino acid residue relatively fixed. Electronic absorption spectra demonstrate that a hydroxyl group of the amino acid residue coordinates to a Zn atom of the porphinatozinc(II) complex in Thr-ZnCOTPP (Thr = threonine) and Ser-ZnCOTPP (Ser = serine) and the coordination interaction between the amino acid residue and a porphyrin moiety is weak in Leu-COZnTPP (Leu = leucine). AA-ZnCOTPP represents a unique system which allowed a study of the CD features which arise from

the heme moiety directly rather than from heme protein model compound, as was done previously.<sup>26</sup> Another study was made with L- and D-phenylalanine bridged Zn bis-porphyrins.<sup>298</sup>

(4) *Exciton-coupled circular dichroism*. Exciton-coupled circular dichroism studies with chiral porphyrin derivatives of philanthotoxin<sup>17</sup> and steroid diol diesters<sup>18</sup> have been published. The scope and limitations of porphyrin chromophores for structural studies by the exciton coupled circular dichroic (CD) method has been delineated.<sup>292</sup> A distance dependence of the porphyrin coupling was investigated in the range between 10 and 50 Å. Over short interchromophoric distances, significant changes in the conformational distribution introduced by the bulky porphyrin chromophores were observed. Over longer distances, the porphyrins showed *ca.* 10-fold sensitivity increase over commonly used chromophores, and an effective direction for the interacting porphyrin transition moments was assigned by comparison. Porphyrins at the termini of dimeric steroids and brevetoxin B (Figure 28) exhibited exciton coupling over interchromophoric distances up to 50 Å.<sup>292,294</sup> These results represent the porphyrins as



**Figure 28.** A chiral porphyrin derivative of philanthotoxin for structural studies by the exciton-coupled circular dichroic method.

promising reporter chromophores for extending the exciton coupled CD method to structural studies of biopolymers.

A new concept based on exciton coupled circular dichroism (CD) for assigning absolute configurations to a single chiral center \*CXYSL, where X is  $-\text{OH}$  or  $-\text{NH}_2$ , Y is an acyclic chain with terminal OH or  $-\text{NH}_2$ , and S (small) and L (large) represent sterically distinct groups, has been proposed.<sup>293</sup> It consists of a one step attachment of porphyrins to X and Y followed by CD measurement. The key event is intramolecular porphyrin  $\pi,\pi$ -stacking, which converts the flexible, acyclic substrate into a rigid stacked conformation characterized by bisignate exciton split CD curves. Since the stacked conformer is sterically controlled by the two groups, S and L, the sign of the exciton split CD is directly governed by the spatial arrangement of these groups.

(5) *Vibrational circular dichroism.* Intense vibrational CD (VCD) bands for the azide antisymmetric stretching vibration in the azide complex of a  $C_2$ -chiral strapped iron porphyrin have been observed.<sup>297</sup> This is the first case in which the extremely strong VCD band has been measured for a ligand vibration of iron porphyrin without an apo-protein. The VCD spectrum of myoglobin azide shortly after reconstitution with its own heme exhibited a weak band but over time the intensity with negative sign gradually recovered. The combination of these two results suggests that the chiral environment produced by the peripheral substituents on the porphyrin ring, which give rise to a diastereotopic plane, is responsible for the generation of the intense VCD in hemoproteins whereas specific interactions of distal residues with the porphyrin ring

and the ligands in halo-proteins are not always necessary.<sup>297</sup>

Room-temperature Q-band electronic MCD, CD, and optical spectra were reported for the first time for two free and nucleic acid-bound cationic metallo-porphyrins, such as the Cu(II) or Pt(II) complexes of *meso-tetrakis(N-methylpyridyl)porphyrin*.<sup>296</sup> The results suggested that the Pt complex is symmetrically intercalated between adjacent GC base pairs, specifically at 5'GC3' sites, with each of two adjacent 4-*N*-methylpyridyl groups extending into each of the major and minor grooves.<sup>296</sup>

### g. Biochemical Applications

(1) *Helical porphyrin-containing peptides.* Molecular modeling of  $\alpha$ -helical peptide H-(Leu-Ser-Leu-Aib-Leu-Ser-Leu)<sub>3</sub>-NH<sub>2</sub> (Aib =  $\alpha$ -aminoisobutyric acid), which exhibits channel-forming properties, suggested that the channel consists of a parallel four-helix bundle, although other aggregation states are also possible.<sup>77</sup> To control the aggregation state of the peptide, tetraphilin, a conjugate consisting of four copies of the helical peptide attached to *meso-tetrakis(3-carboxyphenyl)porphyrin* was prepared. The resulting conjugate formed proton-selective channels in planar bilayers composed of diphtanoyl phosphatidylcholine.<sup>77</sup>

Four amphiphilic  $\alpha$ -helical peptides were hybridized with the  $\alpha,\alpha,\alpha,\alpha$ -isomer of *meso-tetra(o-carboxyphenyl)porphyrin* to synthesize a picket-fence-type four- $\alpha$ -helix bundle polypeptide.<sup>76</sup> The peptide sequence was designed so that the hybrid polypeptide could penetrate into phospholipid bilayers. CD spectra showed that the hybrid folds in a complete four  $\alpha$ -helix bundle structure both in methanol and dipalmitoylphosphatidylcholine



vesicles. Further studies on membrane protein models have been published.<sup>88,89</sup>

$\alpha,\alpha,\alpha,\alpha$ -Tetrakis(2-amino-5-dodecyloxyphenyl)porphyrin synthesized under mild conditions possesses two amino groups and two dodecyloxy groups on each face of the porphyrin plane.<sup>89</sup> It was combined with a fragment of alamethicin, a typical membrane peptide, to give a porphyrin-polypeptide hybrid, in which two hydrophobic polypeptides existed on each face of the porphyrin. This conjugate was successfully embedded into the lipid bilayer membrane. The resulting mixed vesicle showed the CD profile of a helical peptide. A membrane-penetrating columnar structure of  $\alpha,\alpha,\alpha,\alpha$ -tetrakis(2-peptidyl-5-dodecyloxyphenyl)porphyrin in the lipid bilayer membrane was suggested.<sup>89</sup>

Amphiphilic  $\alpha$ -helix peptides carrying porphyrin or flavin moieties were synthesized.<sup>308</sup> The tetraphenylporphyrin and 7-acetyl-10-methylisoalloxazine were able to be fixed and arranged with a chiral twist in a 3D structure constructed by the amphiphilic folding of  $\alpha$ -helices. Assembly of the peptides on a gold electrode was examined.<sup>308</sup>

5-[4-( $\alpha$ -Bromoacetamido)phenyl]-10,15,20-tritolyloporphyrin was incorporated into a single-chain two- $\alpha$ -helix peptide containing 29 amino acids via the thiol side chain of a Cys residue.<sup>307</sup> Two molecules of two- $\alpha$ -helix peptide connecting free base porphyrin were strongly associated to form a four- $\alpha$ -helix bundle structure by hydrophobic interaction among  $\alpha$ -helix segments and porphyrin rings in aqueous solution. The dimer formation was demonstrated by gel filtration chromatography and various spectroscopic measurements. The Soret band in the UV-vis spectrum was broadened and redshifted in aqueous solution. In the fluorescence spectrum with excitation at the Soret band, the emission at 650 nm was quenched to 40% of the intensity measured in methanol. At the Soret band was observed a strongly split CD signal, which demonstrated the chiral assembly of a pair of porphyrins in a left-handed sense. The dimerized Fe(III)-porphyrin-linked two- $\alpha$ -helix peptide was examined for biomimetic peroxidase-like activity with  $\text{H}_2\text{O}_2$  or 3-chloroperbenzoic acid (MCPBA) as the oxidant. The  $k_{\text{cat}}/K_M$  value for the oxidation of 3,7-bis(dimethylamino)-10-methyl carbamoyl phenothiazine by the polypeptide with MCPBA was increased by 5000 times compared to that with  $\text{H}_2\text{O}_2$ . This fact suggested that Fe(III) porphyrin was located in the hydrophobic core and more easily accommodated an organic oxidant than did  $\text{H}_2\text{O}_2$  alone.<sup>307</sup> A single-chain 49-mer-peptide tethering iron(III)-porphyrin via *bis*-histidine coordination

exhibited peroxidase activity toward linoleic acid hydroperoxide.<sup>306</sup>

Treatment of poly(L-glutamic acid) with the racemic zinc complex of a chiral porphyrin having an  $\alpha,\alpha'$ -xylylenediamide strap<sup>318</sup> (Figure 21) gave an assembly in which the (*S*) enantiomer was enantioselectively incorporated. It is the first chiral receptor capable of recognizing the helical sense of poly(glutamic acid) in solution.<sup>318</sup>

Apocytochrome *b562*, a naturally occurring host molecule with an exceptionally high conformational stability, recognized the structures of synthetic metalloporphyrins in reconstitution.<sup>319</sup> Among manganese porphyrins containing peripheral propionate residues, the protoporphyrin IX complex, which has two proximal propionate functionalities, was preferred over the other manganese complexes by a factor of more than 100 in terms of the association constants *K*. In reconstitution with a chiral zinc II *meso*porphyrin with a 1,4-xylylenediamide strap ZnP, the (*R*) enantiomer was highly preferred over the (*S*); the ratio  $K_R/K_S$  was as large as 30. The apoprotein also recognized the absolute configuration of an *N,N'*-dimethylated analog ( $K_R/K_S = 23$ ). The high enantioselectivity of the apoprotein allowed the perfect separation of racemic ZnP in a competitive one-pot reconstitution.<sup>319</sup>

Peptide dendrimers in which amphiphilic  $\alpha$ -helix peptides were introduced at the end groups of poly-amidoamine dendrimers were synthesized.<sup>322</sup> Some of these novel synthetic biopolymers have an enormous molecular weight, about 160 kDa, and a regulated amino acid sequence and three-dimensional conformation. The peptide dendrimers bound  $\text{Fe}^{\text{III}}$ - or  $\text{Zn}^{\text{II}}$ -*meso*porphyrin IX per two  $\alpha$ -helices; this afforded a multimetalloporphyrin assembly similar to the natural light-harvesting antennae in photosynthetic bacteria.<sup>322</sup>

(2) *Glycosylated porphyrins*. Water soluble porphyrin-sugar hybrid species bearing two or four glycosidic units appended at the *meso* positions of the central macrocycle through robust C-C bonds were prepared.<sup>127</sup> Two Pd derivatives proved to be efficient reagents for the selective cleavage of double strand DNA into form II nicked circular DNA upon exposure to visible light at room temperature in aqueous media.<sup>127</sup>

Amphiphilic glycoconjugated porphyrins, benzochlorin, and azaporphyrins were reported. The effect and interaction of these porphyrin derivatives with different cell organelles and macromolecules in photodynamic therapy is dependent on their chemical

structure.<sup>310</sup> Several derivatives were found to be efficient photosensitizers in an *in vitro* assay using the human tumoral cell line HT29. Glycosylated benzochlorin and azaporphyrins, whose absorption bands in the red region of the visible spectrum are substantially increased as compared to porphyrins, display a good photocytotoxicity on tumor cells after irradiation with wavelength above 590 nm.<sup>312</sup>

(3) *Miscellaneous.* Water and carbon monoxide binding to *bis*-ansa porphyrins have been investigated and the possibility of linear free energy relationships connecting this series with amino acid basket-handle porphyrins<sup>68</sup> (Figure 3) was discussed.<sup>316</sup> The synthesis and NMR characterization of chiral *meso*porphyrins bearing  $\alpha$ -methoxy- $\alpha$ -(trifluoromethyl)phenylacetyl residues (Figure 29) have been reported.<sup>321</sup> The phototoxicity with circular polarized light and intracellular localization in L1210 cells were described as preliminary results.<sup>321</sup>

Resolution of the antipodes of chiral  $\sigma$ -alkyl- and  $\sigma$ -arylcobalt(III) complexes of etioporphyrin I was first achieved,<sup>317</sup> where the latter was much more stable than the former toward thermal racemization (Figure 12). Use of these antipodes for stereochemical studies on the mechanism of reversible Co–N transfer of alkyl and aryl groups in cobalt porphyrins revealed that the transfers from Co to N and from N to Co both take place in intramolecular fashion.<sup>317</sup>

An antibody–metalloporphyrin assembly that catalyzes the enantioselective oxidation of aromatic sulfides to sulfoxides has been described.<sup>309</sup> Antibody SN37.4 was elicited against a water-soluble tin(IV) porphyrin containing an axial  $\alpha$ -naphthoxy ligand. The catalytic assembly comprising antibody SN37.4 and a

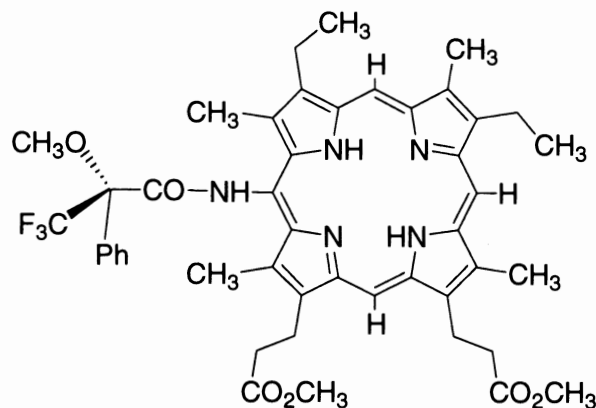
ruthenium(II) porphyrin cofactor exhibited typical enzyme characteristics, such as predetermined oxidant and substrate selectivity, enantioselective delivery of oxygen to the substrate and Michaelis–Menten saturation kinetics. This assembly, which promotes a complex, multistep catalytic event, represents a close model of natural heme-dependent oxidation enzymes.<sup>309</sup>

The substrate stereochemistry of porphyrinogen carboxy-lyase which catalyzes the decarboxylation of the four acetate side chains of uroporphyrinogen III has been determined.<sup>320</sup> The chiral analysis showed that in the porphyrinogen carboxy-lyase reaction, both protons at each methylene of uroporphyrinogen III remain intact in coproporphyrinogen III and that the reaction proceeds with retention of configuration at the methylene C atoms of all four acetate side chains.<sup>320</sup>

Novel porphyrin-binding peptides were designed on the basis of an antigen-binding site of an antiheme monoclonal antibody.<sup>315</sup> The synthetic peptides were modified with a pyrene moiety. The spectroscopic measurements revealed that the synthetic peptides bound a porphyrin effectively.<sup>315</sup>

#### *h. Stirring Effects on Supramolecular Chirogenesis*

Homoassociation of achiral diprotonated *meso*-*tetra*-*kis*(sulfonatophenyl)porphyrins in acid solutions show spontaneous symmetry breaking, which can be detected by CD.<sup>328,329</sup> The CD spectra are due to differential scattering and differential absorption contributions, the relative significance of which is related to the shape and size of the homoassociation. When an earlier model, designed for the association of these diprotonated porphyrins (J aggregates with the geometry of stepped sheets of intramolecular-stabilized zwitterions), was applied to an exciton-coupling point-dipole



**Figure 29.** A *meso*porphyrin derivative with a chiral  $\alpha$ -methoxy- $\alpha$ -(trifluoromethyl)-phenylacetyl residue.

approximation, the folding of the one-dimensional homoassociation explained the CD signals detected. An effect of the vortex direction, caused by stirring or rotary evaporation, upon the exciton chirality sign was detected. This vortex effect can be attributed to enhancement of the chirality fluctuations that originate in the diffusion-limited aggregation to high molecular-weight homoassociates. The phenomenon could be general for supramolecular systems that are obtained under kinetic control, and its detection would be possible when inherent chiral chromophores were being generated in the association process.<sup>328,329</sup>

#### IV. Transition Metal Chiroporphyrins

The development of chiral metalloporphyrins by Marchon and coworkers has been focused on the elaboration of a synthon called "biocartol," which is available from agrochemical sources. This cyclopropane derivative has two vicinal stereogenic centers with aldehydic and carboxylic substituents in a *cis* configuration, leading to the formation of a five-membered hemiacetal ring which is the stable form observed in the solid state (Figure 30). Biocartol is an intermediate in the industrial synthesis of deltamethrin, an enantiopure pyrethroid insecticide,<sup>346</sup> and it is available in crystalline form of high enantiomeric purity (Table 3).

The availability of biocartol from an industrial source, and the presence in this molecule of a carboxylic acid group in *cis* position next to an aldehyde group, allowed access to a new series of chiral porphyrins. While the aldehyde group is suited to the construction of the porphyrin ring by condensation with pyrrole, the *cis* carboxylic group is ideally located for synthetic elaboration near the center of the porphyrin, where reactive metal species are formed in a catalytic process. Thus, biocartol esters and amides (Figure 31) were used as starting materials of a new family of chiral porphyrins called "chiroporphyrins." In addition to mild catalysts for asymmetric epoxidation and aziridination,

investigation of their coordination chemistry has led to the discovery of enantioselective receptors of chiral ligands (such as alcohols, amines, aziridines), and of chiral derivatizing agents for the determination of enantiomer composition of amines and amino acids by <sup>1</sup>H NMR spectroscopy. A summary of the synthesis and stereochemistry of chiroporphyrins and metallochiroporphyrins, and of their uses in enantioselective control, is given below.

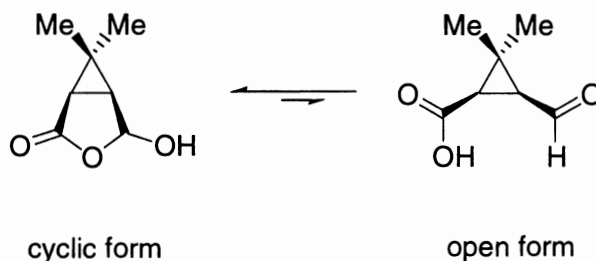
#### A. SYNTHESIS OF CHIROPORPHYRINS

Biocartol esters (Figure 31) are good synthons for the preparation of porphyrins bearing chiral cyclopropyl groups on the four *meso* positions. A novel synthesis of these esters has been worked out, which involves dithiolane protection of the aldehyde function, and is satisfactory in terms of both the yield and the stereochemical purity of the product. An alternative, much simpler access has been found recently; it involves deprotonation of biocartol followed by nucleophilic attack of the resulting carboxylate on a suitable bromo- or iodoalkyl derivative.<sup>132</sup> The synthesis of biocartol amides has also been explored, and a convenient synthesis of the very bulky *N,N*-disubstituted amides has been worked out (Figure 31).

The prototypic tetramethylchiroporphyrin H<sub>2</sub>TMCP (Figure 19), is accessible in one step from the methyl ester.<sup>133</sup> The related chiroporphyrins derived from the ethyl, benzyl, *tert*-butyl, neopentyl, bornyl, *m*(and *p*)-nitrophenyl esters, and from various *N,N*-disubstituted amides, have been prepared (Figure 32).<sup>132,134</sup> Whereas most chiroporphyrin syntheses generally exhibit low

**Table 3.** Biocartol Nomenclatures

Molecular formula	C <sub>7</sub> H <sub>10</sub> O <sub>3</sub>
Registry number	73611-02-6
CA index name	(1 <i>R</i> ,4 <i>R</i> ,5 <i>S</i> )-4-hydroxy-6,6-dimethyl-3-oxabicyclo[3.1.0]hexan-2-one
Other names	(-)-1 <i>R</i> - <i>cis</i> -caronaldehyde (-)-biocartol (-)-caronaldehyde



**Figure 30.** Cyclic and open forms of (1*R*)-*cis*-caronaldehyde.

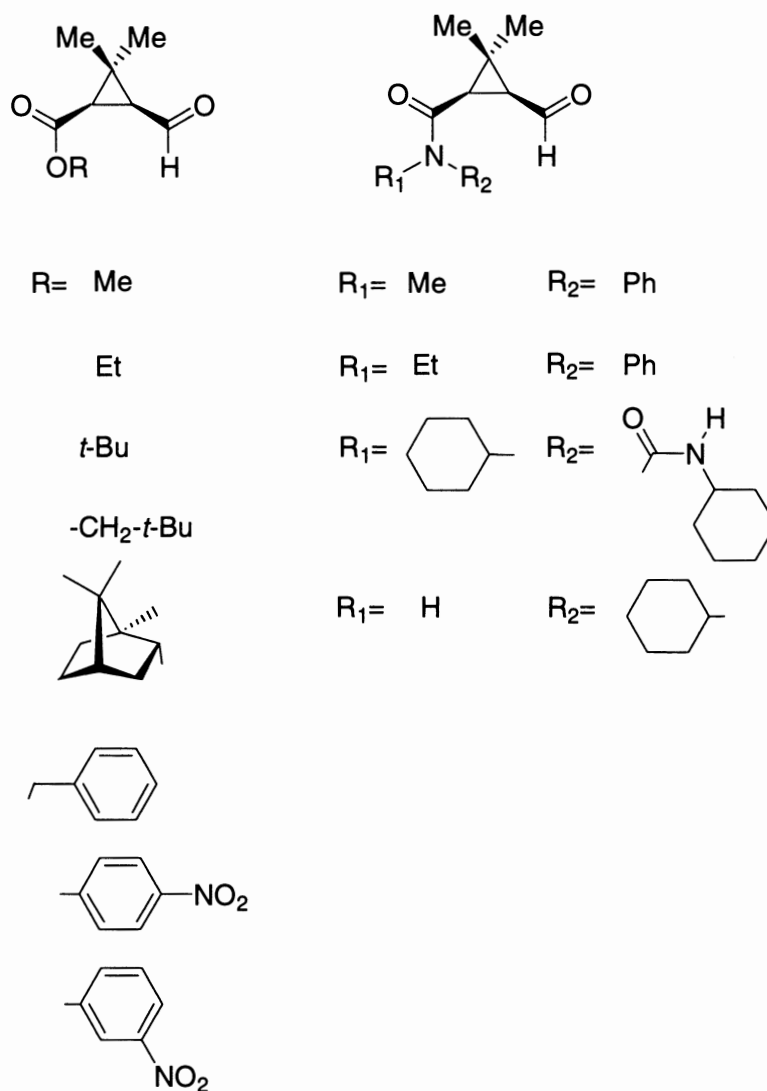


Figure 31. Ester and amide derivatives of (1*R*)-cis-caronaldehyde.

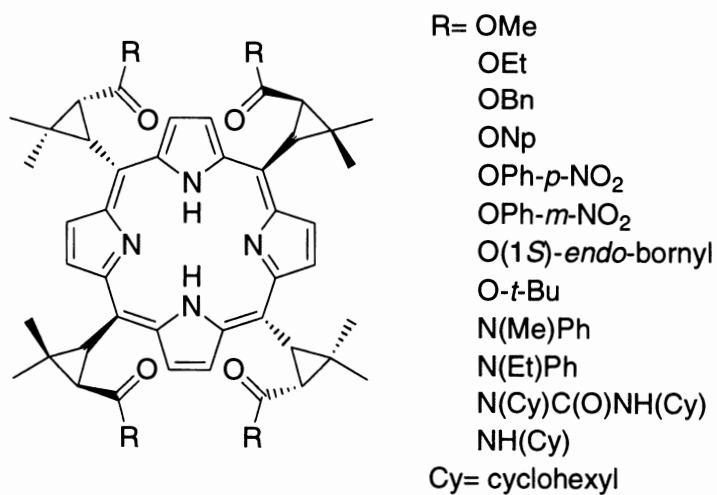
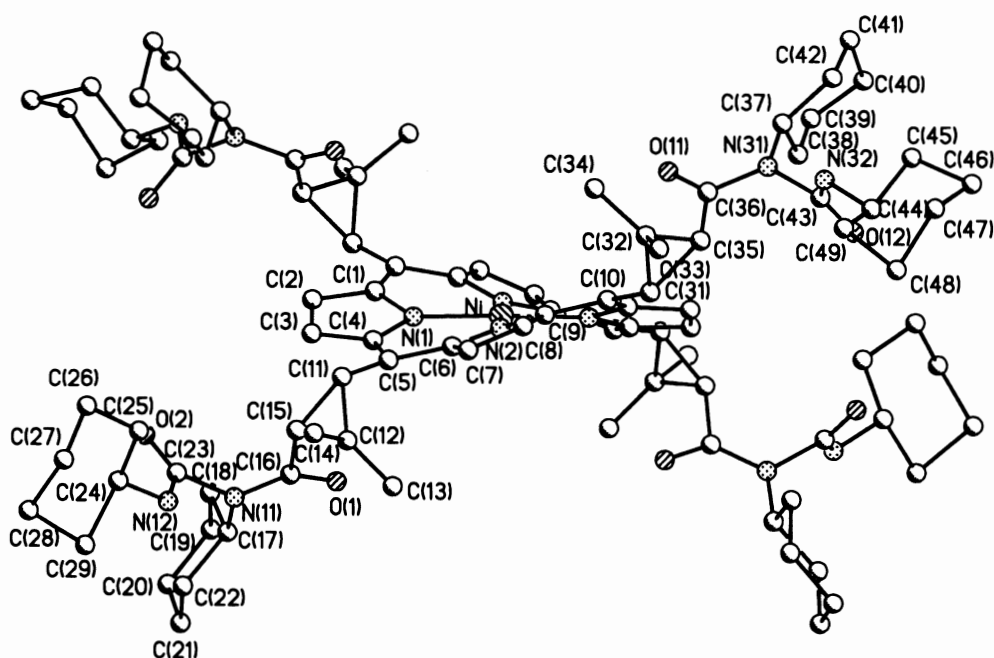


Figure 32. A series of chiorporphyrins obtained from esters and amides of (1*R*)-cis-caronaldehyde.



**Figure 33.** X-ray structure of the nickel complex of a chiorporphyrin with *N*-acylurea substituents (R = N(Cy)C(O)NH(Cy) in Figure 32). (Pérollier, C.; Pécaut, J.; Ramasseul, R.; Marchon, J.-C.; Bau, R. *Chem. Commun.* (Cambridge) **1999**, 1597) - Reproduced by permission of The Royal Society of Chemistry.

yields (5–25%), the chiorporphyrin with *N*-acylurea substituents (Figure 33) was obtained in 60% yield. This surprising result has been explained by complementary intramolecular hydrogen-bonding interactions between *N*-acylurea substituents which direct the cyclization of the tetrapyrrolic intermediate.<sup>134</sup> Complexation with various metals have provided an extended family of chiral metallomacrocycles in which stereodirecting groups of variable steric bulk and polarity are located near the plane of the porphyrin ring and close to the metal center, and thus are able to interact with potential substrates.

## B. CHIROPORPHYRIN STEREOCHEMISTRY

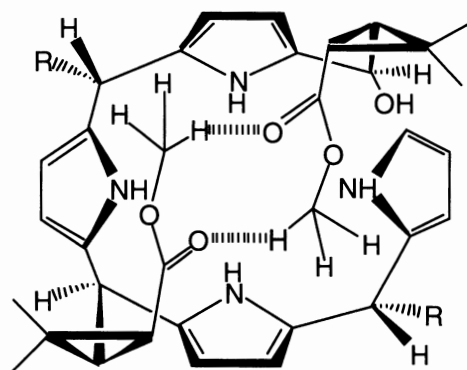
### 1. Free Bases

The synthesis of chiorporphyrins from biocartol derivatives by the Lindsey method is remarkably selective; it always affords the thermally stable  $\alpha\beta\alpha\beta$  conformer, and none of the other possible conformers ( $\alpha\alpha\alpha\alpha$ ,  $\alpha\alpha\alpha\beta$ ,  $\alpha\alpha\beta\beta$ ) has been detected so far. This unusual product selectivity saves the need of a tedious separation of atropisomers by chromatography, which is usual in classical syntheses of chiral porphyrins by elaboration on tetra(*o*-aminophenyl)porphyrin for example. This selectivity has been attributed to the formation of C–H···O hydrogen bonds between

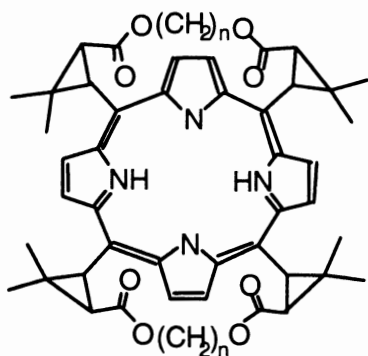
opposite *meso* ester substituents in a  $\alpha,\beta,\alpha,\beta$ -substituted tetrapyrrole intermediate, which leads to facile cyclization to the corresponding  $\alpha,\beta,\alpha,\beta$ -porphyrinogen (Figure 34).<sup>132</sup>

The alternating up-down-up-down orientations of the bulky *meso* substituents in the  $\alpha\beta\alpha\beta$  chiorporphyrin free bases and metal complexes have an important effect on the porphyrin core, which adopts a nonplanar conformation of the so-called “ruffle” type (Figure 33). In a ruffled porphyrin, opposite pyrrole rings are counterrotated so that the *meso* carbon atoms are alternatively displaced above and below the mean porphyrin plane. This distortion mode is seen in the crystal structures of square-planar Ni(II)<sup>134,223,335,339</sup> or octahedral Co(III)<sup>248,332</sup> and Ru(II)<sup>246</sup> chiorporphyrin complexes for example; it is also observed in resonance Raman spectra by a decrease in the frequencies of structure-sensitive lines in the region 1300–1700 cm<sup>-1</sup>.<sup>331,340</sup> Five-coordinate complexes such as MnCl(TMCP),<sup>236</sup> FeCl(TMCP),<sup>337</sup> and CoCl-(TMCP)<sup>248</sup> exhibit a mixture of the “ruffle” and “dome” distortions.

One exception to the  $\alpha\beta\alpha\beta$  rule has been found recently in the synthesis of “bridled chiorporphyrins” (Figure 35), in which the ester functions on adjacent *meso* substituents are linked by a strap of adjustable length ( $n = 8$  to 16 methylene groups). While long straps ( $n = 9$  to 16) lead to the  $\alpha\beta\alpha\beta$  conformer as usual, the compound with short bridles ( $n = 8$ )



**Figure 34.** Conformation of an  $\alpha,\beta,\alpha,\beta$ -substituted tetrapyrrole intermediate, preorganized by weak C–H...O hydrogen bonds between methyl ester substituents, which leads to facile cyclization to the porphyrinogen. For the sake of clarity, only the H-bonding pattern on the top face is shown, and each of the two *meso* substituents on the bottom face is abbreviated as R. Reprinted with permission from Pérollier, C.; Mazzanti, M.; Simonato, J.-P.; Launay, F.; Ramasseul, R.; Marchon, J.-C. *Eur. J. Org. Chem.* **2000**, 583. Copyright 2000 Wiley-VCH.



**Figure 35.** Bridled chiroporphyrins. The ruffling of the porphyrin induced by the  $\alpha\beta\alpha\beta$  conformation is restricted by the bridles.

surprisingly is formed as the  $\alpha^4$  conformer exclusively, presumably because 8-methylene straps are too short to allow the formation of an  $\alpha,\beta,\alpha,\beta$ -substituted tetrapyrrole. This unusual stereochemistry has been confirmed by the crystal structure of the zinc(II) complex (Figure 36).<sup>334</sup> The  $\alpha\alpha\alpha\alpha$  (or  $\alpha^4$ ) conformation is correlated to an almost planar porphyrin core. This observation corroborates the notion that the ubiquitous ruffled distortion is correlated to the  $\alpha\beta\alpha\beta$  conformation.

## 2. Conformational Switches

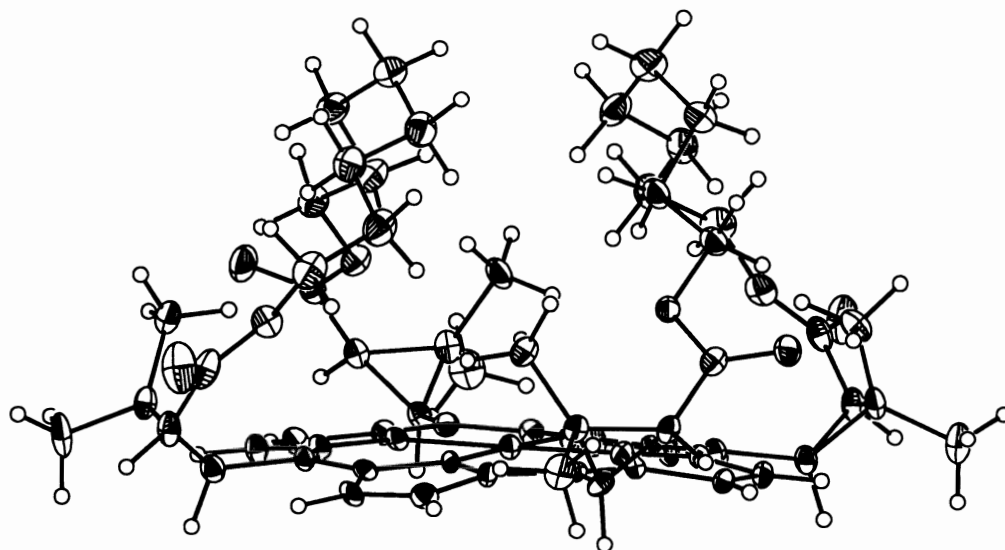
Nickel(II) insertion into the  $\alpha^4$ -chiroporphyrin with short bridles ( $n = 8$ ) surprisingly induced a complete switch to the  $\alpha\beta\alpha\beta$  conformer (Figure 37).<sup>334</sup> Marchon and coworkers have suggested that the  $\alpha^4 \rightarrow \alpha\beta\alpha\beta$  conformation change which is observed upon Zn(II)  $\rightarrow$  Ni(II) substitution in the strapped chiroporphyrin may be related to the coordination requirements of the two metals and to the constraints induced by the short straps. While Zn(II) with its full  $d^{10}$  complement

shows long Zn–N bonds compatible with the flat porphyrin core of the  $\alpha^4$ -free base, square-planar  $d^8$  Ni(II) with its vacant antibonding  $d_{x^2-y^2}$  orbital requires short Ni–N bonds which are obtained by ruffling of the core. In this distorted core conformation, the 8-methylene straps apparently are too short to stride over their adjacent cyclopropyl substituent, which are forced to rotate toward the opposite face of the porphyrin. The low rotation barrier usually observed in ruffled nickel(II) porphyrins may facilitate this motion, which results in the  $\alpha\beta\alpha\beta$  complex.<sup>334</sup>

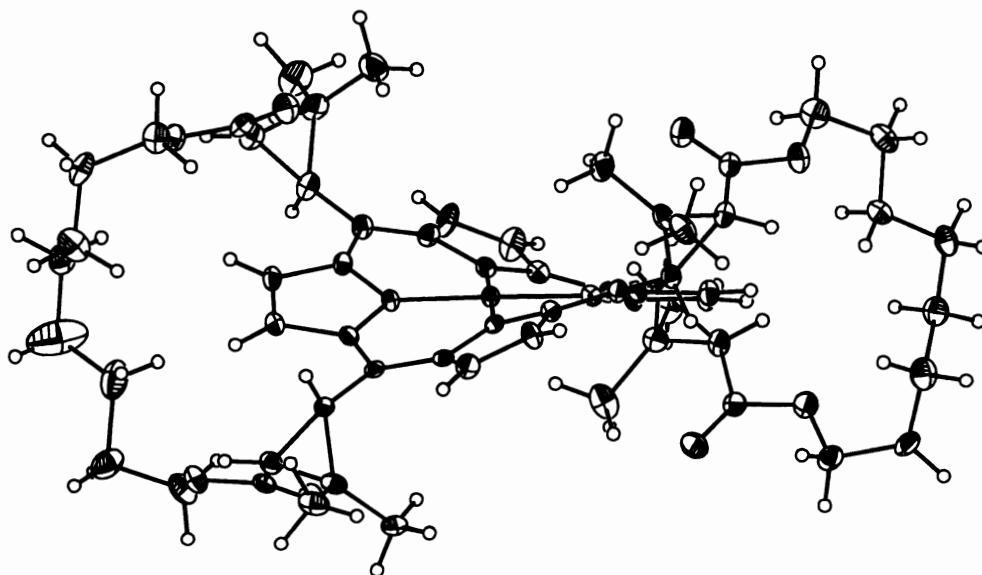
A “Venus flytrap” zinc porphyrin which reversibly swings between an open  $\alpha\beta\alpha\beta$  (Figure 38) and a closed  $\alpha^4$  form (Figure 39) upon binding and dissociation of pyridine has also been reported.<sup>333</sup> In that case, the conformation change has been attributed to a low rotation barrier in the domed pyridine complex and to the stabilization of the  $\alpha^4$  conformer by attractive  $\pi$ – $\pi$  and C–H  $\cdots$   $\pi$  interactions between the pyridine ligand and the surrounding phenyl rings of the *meso* substituents.

## C. SPIN STATES OF Fe(III) CHIROPORPHYRINS

A ruffled conformation of a metalloporphyrin results in short metal–nitrogen bonds, which usually destabilize the metal  $d_{x^2-y^2}$  orbital. The presence of two bulky substituents on opposite *meso* positions on either face of an  $\alpha\beta\alpha\beta$  metallochiroporphyrin restricts the orientation of a planar axial ligand within a vacant groove along the other *meso*–*meso* diagonal on each face. This orientation effect will destabilize the metal  $d_{xy}$  orbital in a five- or six-coordinate complex. Both these effects may have important consequences on the ground spin states of iron(III) complexes of chiroporphyrins.



**Figure 36.** ORTEP view of a zinc chiorporphyrin complex with short bridles (8 methylene groups), showing the  $\alpha^4$  conformation.



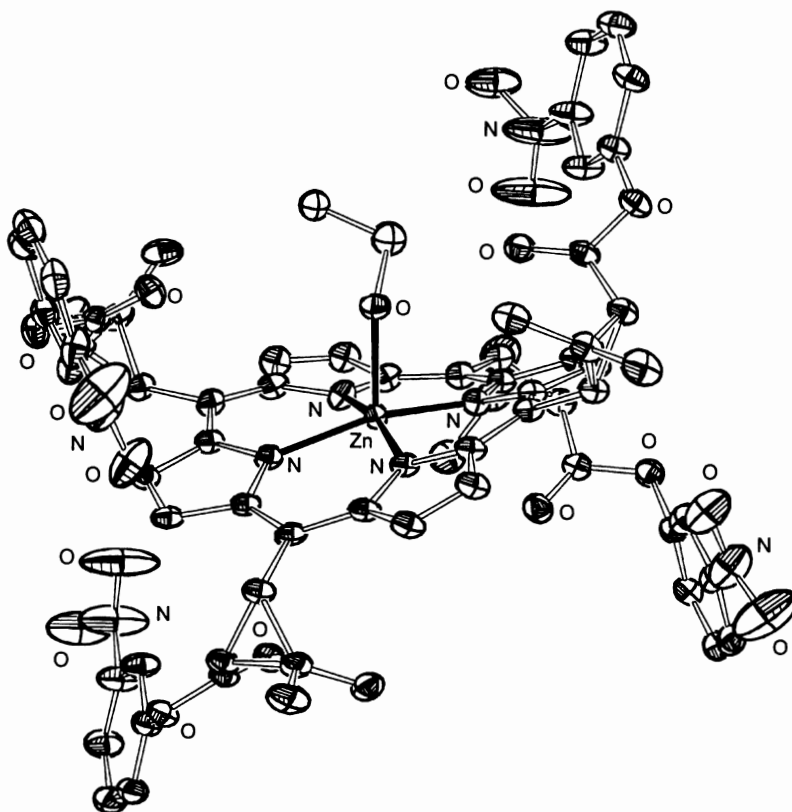
**Figure 37.** ORTEP view of a nickel chiorporphyrin complex with short bridles (8 methylene groups), showing the  $\alpha\beta\alpha\beta$  conformation.

The X-ray structure of FeCl(TMCP) shows a five-coordinate high-spin iron(III) center in a strongly ruffled and domed porphyrin. A consequence of the  $\alpha\beta\alpha\beta$  conformation is seen in the short equatorial bond distances ( $\text{Fe-N}(\text{av}) = 2.034(9) \text{ \AA}$ ), but despite these unusually short bonds this complex has a high-spin ( $S = 5/2$ ) ground state.<sup>337</sup>

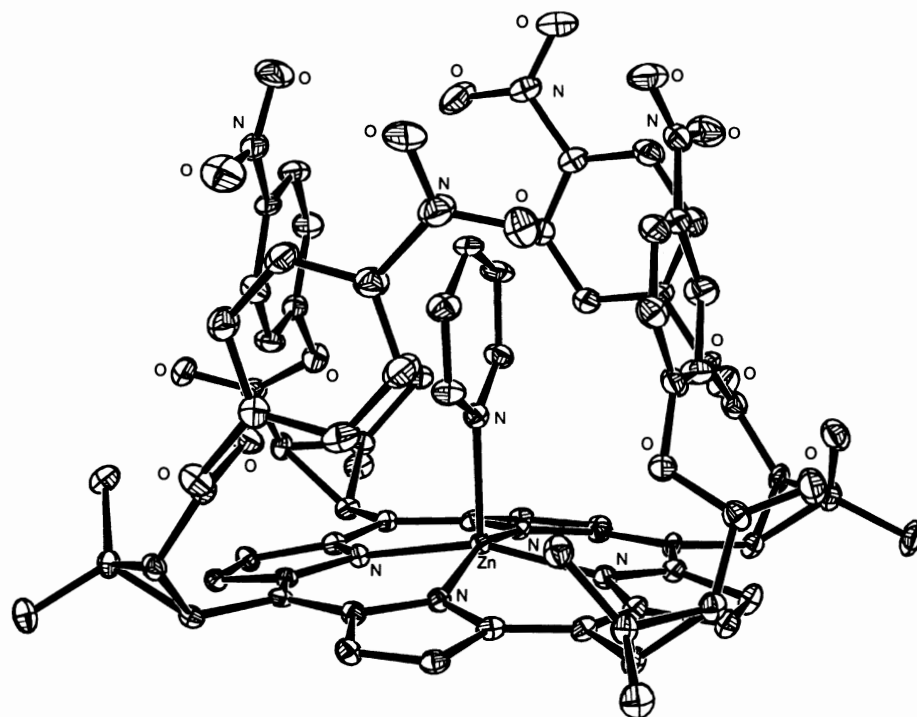
Low-spin ( $S = 1/2$ ) complexes are formed by reaction of FeCl(TMCP) with imidazoles, and they have been studied by means of 1D and 2D  $^1\text{H}$  NMR spectroscopy. The chemical shift of ( $\beta$ -H pyrrole

resonances has been used as a sensitive probe of the electronic state of the iron(III) center. Coordination of sterically hindered imidazoles results in a stable conformation in which the two imidazole planes are perpendicular, due to the orientation effect of the  $\alpha\beta\alpha\beta$  substitution pattern, and in the stabilization of the rare  $(d_{xz}, d_{yz})^4(d_{xy})^1$  electronic state.<sup>336</sup>

Crystal field theory indicates that increasing tetragonal distortion in ferric porphyrins (e.g., decreasing axial field strength) leads from low-spin to high-spin states, and that it will eventually stabilize the mid-spin



**Figure 38.** ORTEP view of the open form of a “Venus flytrap” porphyrin, showing the  $\alpha\beta\alpha\beta$  conformation. Reprinted with permission from Mazzanti, M.; Marchon, J.-C.; Shang, M.; Scheidt, W. R.; Jia, S.; Shelnut, J. A. *J. Am. Chem. Soc.* **1997**, 119, 12400. Copyright 1997 American Chemical Society.



**Figure 39.** ORTEP view of the closed form of a “Venus flytrap” porphyrin, showing the  $\alpha^4$  conformation. Reprinted with permission from Mazzanti, M.; Marchon, J.-C.; Shang, M.; Scheidt, W. R.; Jia, S.; Shelnut, J. A. *J. Am. Chem. Soc.* **1997**, 119, 12400. Copyright 1997 American Chemical Society.



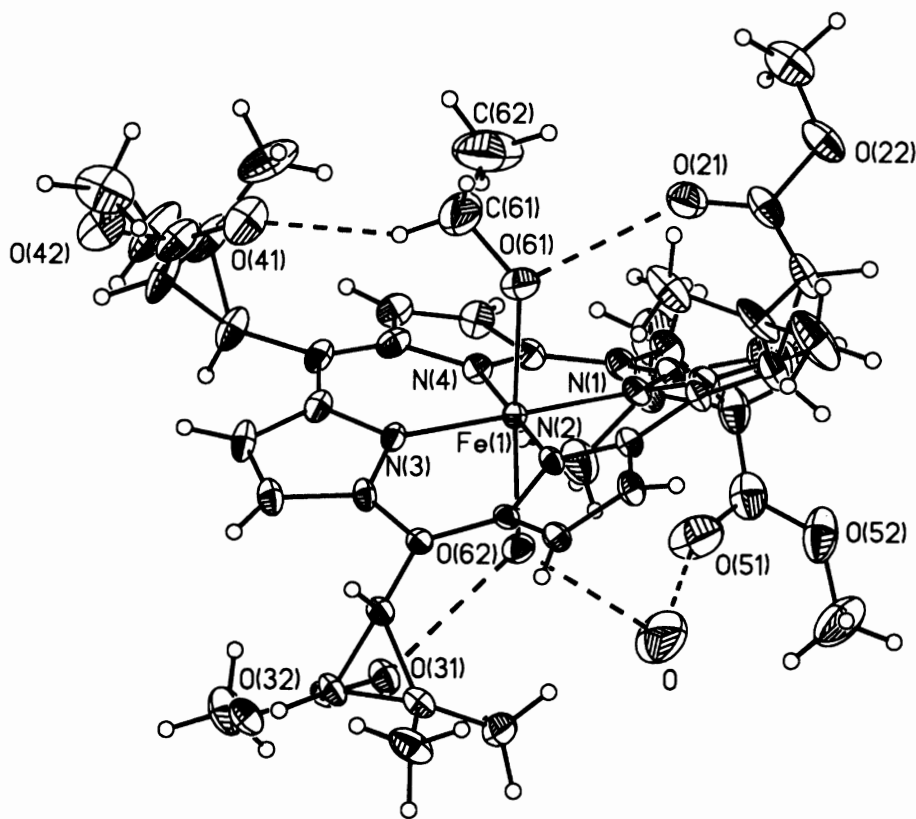
state ( $S = 3/2$ ) when the  $d_{z^2}$  orbital is close in energy to the  $d_{xy}$ ,  $d_{xz}$ , and  $d_{yz}$  and singly occupied, and the  $d_{x^2-y^2}$  is considerably higher in energy and vacant. Many attempts to stabilize the mid-spin state ( $S = 3/2$ ) of ferric porphyrins in six-coordinate complexes with very weak axial ligands have resulted rather in mixed-spin states ( $S = 3/2, 5/2$ ) in which the  $d_{x^2-y^2}$  orbital is not completely depopulated. These results suggested that the elusive pure mid-spin state might be stabilized by combining the favorable effects of a weak axial field strength and of a small macrocycle hole in a ruffled ferric chiroporphyrin. Axial ligand exchange by reaction of  $\text{FeCl}(\text{TMCP})$  with silver perchlorate in ethanol–chloroform led to ethanol-ligated ferric chiroporphyrins. Two distinct crystalline products containing a *bis*-ethanol complex  $[\text{Fe}^{\text{III}}(\text{EtOH})_2(\text{TMCP})]\text{ClO}_4$  and three variants of a mixed ethanol–water complex  $[\text{Fe}^{\text{III}}(\text{EtOH})(\text{H}_2\text{O})(\text{TMCP})]\text{ClO}_4$  have been structurally characterized in the solid state (Figure 40). The small hole of the ruffled chiroporphyrin and the weak axial oxygen ligation result in strongly tetragonally distorted complexes. All the spectroscopic data, and especially the

EPR spectra, are consistent with a ground state which is mid-spin ( $S = 3/2$ ) as expected.<sup>338</sup>

#### D. ASYMMETRIC ADDITIONS TO OLEFINS CATALYZED BY Mn(III) CHIROPORPHYRINS

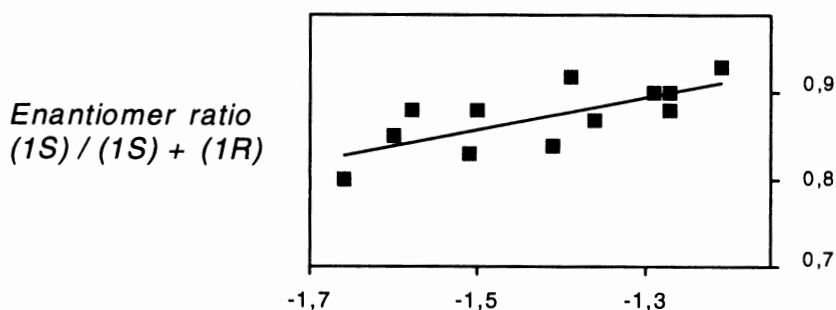
##### 1. Epoxidation

The chloromanganese(III) complexes of an extensive series of  $D_2$ -symmetric chiroporphyrins derived from enantiopure biocartol esters and amides, in which potentially stereogenic groups sit on the porphyrin ring in the vicinity of the metal binding site (Figure 32), have been prepared and their performance as asymmetric epoxidation catalysts have been investigated.<sup>133, 223</sup> The observed excess of the (1*S*, 2*R*) epoxide of dihydronaphthalene was consistent with the *Re* face selectivity expected on steric grounds for the side-on approach of the substrate. Among the eight ester derivatives, those with the bulkier substituents induced the larger enantioselectivities, and the disubstituted amides which are even bulkier brought the stereoinduction to the highest levels (86% ee). The



**Figure 40.** ORTEP view of the cation of  $[\{\text{Fe}^{\text{III}}(\text{EtOH})(\text{H}_2\text{O})(\text{TMCP})\}(\text{H}_2\text{O})]^+\text{ClO}_4^-$ , showing the hydrogen bond array between coordinated ethanol and water, interstitial water, and carbonyl groups of the chiroporphyrin *meso* substituents. Reprinted with permission from Simonato, J.-P.; Pécaut, J.; Le Pape, L.; Oddou, J.-L.; Jeandey, C.; Shang, M.; Scheidt, W. R.; Wojaczynski, J.; Wolowiec, S.; Latos-Grazynski, L.; Marchon, J.-C. *Inorg. Chem.* **2000**, *39*, 3978. Copyright 2000 American Chemical Society.

### Chemical shift of NH protons



**Figure 41.** Plot of the enantiomer composition of the 1*S*,2*R* epoxide obtained in the asymmetric epoxidation of 1,2-dihydronaphthalene by a series of manganese chiroporphyrins as a function of the NMR chemical shift (ppm) of the central NH protons of the corresponding chiroporphyrin free bases (see Figure 32). Reprinted with permission from Pérollier, C.; Pécaut, J.; Ramasseul, R.; Marchon, J.-C. *Inorg. Chem.* **1999**, *38*, 3758. Copyright 1999 American Chemical Society.

enantioselectivity of 1,2-dihydronaphthalene epoxidation was found to reflect the degree of nonplanar distortion of the porphyrin observed in solution.<sup>223</sup> A structure–enantioselectivity correlation is presented in Figure 41, in which the enantiomeric composition *ec* of the major (1*S*, 2*R*) epoxide is plotted as a function of the NMR chemical shift of the central NH protons of the corresponding metal-free chiroporphyrins in CDCl<sub>3</sub> solution. This correlation indicates that the enantioselectivity induced by the manganese complex increases as the aromatic character of the corresponding porphyrin free base decreases, i.e., as its degree of ruffling increases. Interestingly, this correlation is valid only for solution conformations; the crystal structures of nine nickel derivatives have been solved (see one representative example in Figure 42), but the correlation does not hold for solid-state conformations.<sup>339</sup>

Since the origin of the ruffled distortion is the congestion induced by the bulky *meso* substituents near the porphyrin ring in an  $\alpha\beta\alpha\beta$  conformation, it has not been possible to conclude whether the determinant of asymmetric induction is a conformational or a steric effect, or both. In an attempt to resolve these two influences, a series of chiroporphyrins in which the ester functions on adjacent *meso* substituents are linked by a strap of adjustable length ( $n = 8$  to 16 methylene groups) have been designed (Figure 35). It was expected that the ruffling induced by the  $\alpha\beta\alpha\beta$  conformation could be restricted by these bridles, and that the resulting distortion could be tuned by the strap length while the substituent volume and electronic effects would remain unchanged. Investigations by resonance Raman and <sup>1</sup>H NMR spectroscopies have shown that the ruffling in solution could indeed be controlled by the bridle length, and that the enantioselectivity induced by the bridled

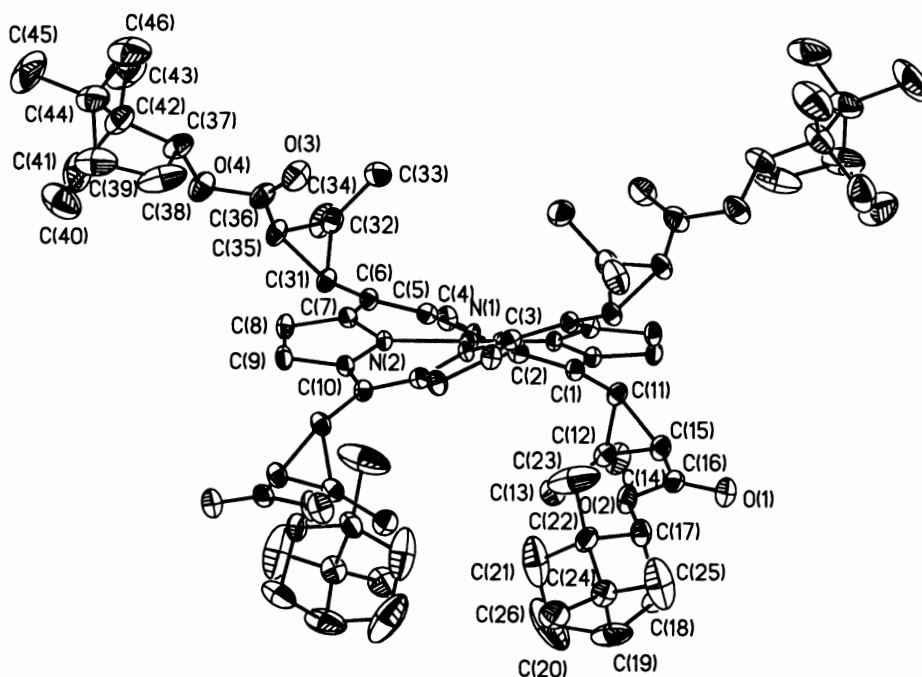
manganese catalysts (Figure 43) increases as the ruffling of the porphyrin increases, i.e., twisting the porphyrin ring is beneficial to the asymmetric induction.<sup>340</sup>

## 2. Aziridination

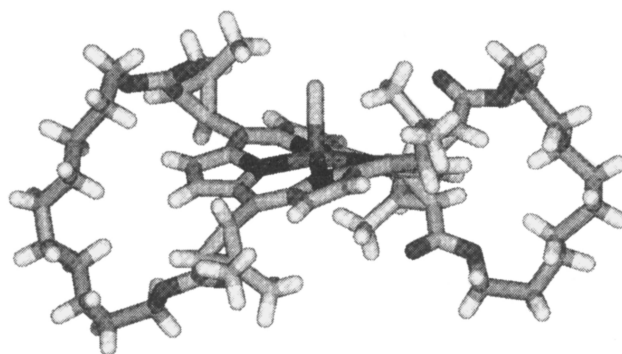
Catalytic asymmetric aziridination of styrene by [*N*-(*p*-toluenesulfonyl)imino]-phenyliodinane has been achieved by manganese and iron tetramethylchiroporphyrins. Opposite enantioselectivities have been obtained with the two metal centers (Figure 44). Possible mechanisms have been proposed to explain this unexpected result.<sup>236</sup>

## E. ENANTIOSELECTIVE BINDING OF CHIRAL LIGANDS BY METALLOCHIROPORPHYRINS

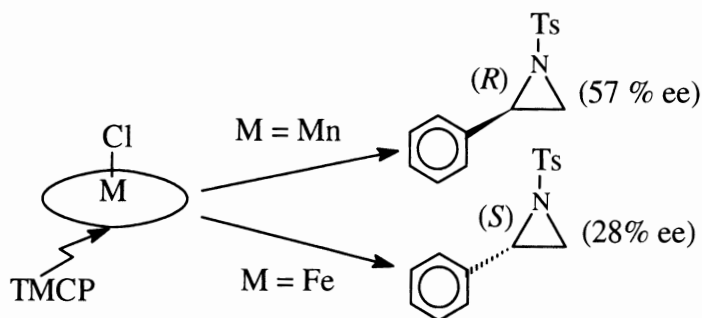
A (carbonyl)ruthenium(II) complex of tetramethylchiroporphyrin H<sub>2</sub>TMCP was found to be an enantioselective receptor of chiral aliphatic alcohols.<sup>246</sup> The X-ray structure of the six-coordinate complex Ru(CO)(EtOH)(TMCP) (Figure 45) showed that the *cis* configuration of the ester and porphyrin groups on each cyclopropane constrains the methyl ester groups to lie on the porphyrin ring, with the carbonyl oxygen atoms nearly eclipsing four  $\alpha$  pyrrole carbon atoms. One methyl of the *gem*-dimethyl group in each cyclopropane also lies on the porphyrin ring, thus defining a C<sub>2</sub>-symmetric groove of *ca.* 3–4 Å width along a C<sub>meso</sub> – C<sub>meso</sub> axis on each face of the porphyrin. The carbonyl and ethanol axial ligands of ruthenium(II) are accommodated within each of the two grooves; the latter is disordered with both the hydroxyl and methylene groups equally distributed over two C<sub>2</sub>-related sites. This unusual off-axis location of the hydroxyl oxygen



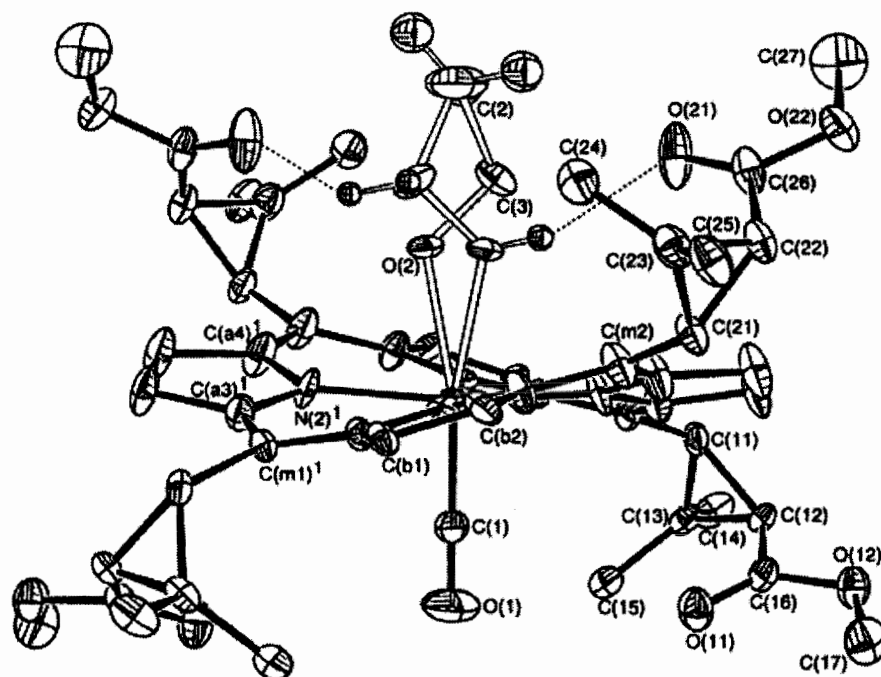
**Figure 42.** ORTEP view of the nickel chiorporphyrin with bornyl ester substituents ( $R = O\text{-}(1S)\text{-endo-bornyl}$  in Figure 32), showing the bornyl groups pointing outward on the upper face and inward on the lower face. Reprinted with permission from Pérollier, C.; Pécaut, J.; Ramasseul, R.; Marchon, J.-C. *Inorg. Chem.* **1999**, *38*, 3758. Copyright 1999 American Chemical Society.



**Figure 43.** Stick representation of the X-ray structure of a chloromanganese(III) chiorporphyrin with 10-methylene bridges.



**Figure 44.** Antagonistic metal-directed inductions in catalytic asymmetric aziridination by manganese and iron tetramethylchiorporphyrins. (Simonato, J.-P.; Pécaut, J.; Marchon, J.-C.; Scheidt, W. R. *Chem. Commun. (Cambridge)* **1999**, 989) - Reproduced by permission of The Royal Society of Chemistry.



**Figure 45.** ORTEP view of the structure of Ru(CO)(EtOH)(TMCP), showing the  $C_2$  symmetry and ruffled conformation of the chiorporphyrin complex. The two symmetry-related sites of the disordered ethanol ligand are shown, but the hydrogen atoms are drawn for one site only. Hydrogen bonds are indicated by dotted lines. Reprinted with permission from Mazzanti, M.; Veyrat, M.; Ramasseul, R.; Marchon, J.-C.; Turowska-Tyrk, I.; Shang, M.; Scheidt, W. R. *Inorg. Chem.* **1996**, *35*, 3733. Copyright 1996 American Chemical Society.

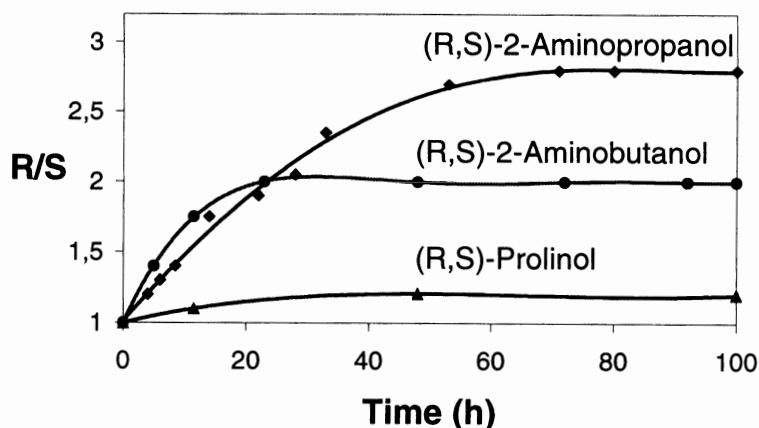
atom is the result of a hydrogen bond to the neighboring carbonyl oxygen atom. The latter was apparent in the IR spectrum as a broad absorption near  $3440\text{ cm}^{-1}$  in the O–H stretch region and by a splitting of the C=O stretching frequency. Similarly, the conformation of the methylene group reflects a weak C–H $\cdots$ O hydrogen bond to the other carbonyl group.

The room-temperature  $^1\text{H}$  NMR spectrum showed the signature of the ethanol axial ligand as two broad resonances which were assigned to the methyl and methylene groups of the coordinated ethanol molecule in fast exchange with free ethanol. At  $-50^\circ\text{C}$ , four sharp, well-resolved resonances appeared at high field, which were assigned to either methylene proton, and to the methyl and hydroxyl protons of coordinated ethanol, respectively.

Axial ligand exchange was readily obtained by addition of excess ( $\pm$ )-2-octanol (*ca.* 6 equiv.) to a  $\text{CD}_2\text{Cl}_2$  solution of the Ru(II) complex at room temperature. At  $-50^\circ\text{C}$  the  $^1\text{H}$  NMR spectrum showed the expected resonances of coordinated 2-octanol in the region between  $-5$  and  $0$  ppm. Particularly striking was the appearance of the hydroxylic protons as two well-resolved doublets ( $\delta = -4.70$  and  $-4.60$ ) of unequal intensities, immediately revealing enantioselective coordination to the chiral ruthenium(II) center with

a selection ratio of *ca.* 2.2. Detailed low-temperature  $^1\text{H}$ - $^1\text{H}$  DQF-COSY experiments on the individual complexes of (*R*)- and (*S*)-2-octanol led to the identification of the (*R*)-enantiomer as the preferentially bound axial ligand. Selective binding of the (*R*)-enantiomer was similarly observed for 2-butanol with a binding ratio  $K_R/K_S = \text{ca. } 2$ . Molecular modeling revealed complementary geometries of the *n*-alkyl substituent and linear groove, suggesting that increased van der Waals contacts for the (*R*)-2-butanol and (*R*)-2-octanol complexes can contribute to the observed (*R*)-enantioselection.<sup>246</sup>

Upon addition of 2-aminopropanol, 2-aminobutanol, or prolinol to the chlorocobalt(III) complex of tetramethylchiorporphyrin CoCl(TMCP) in  $\text{CDCl}_3$  solution, a cationic 2:1 adduct was obtained quantitatively, in which two amino alcohol ligand are N-bound to the Co(III) center. When the added amino alcohol was racemic, the resonances of the two cobalt-bound enantiomers initially appeared in a 1:1 intensity ratio. However, monitoring the  $^1\text{H}$  NMR spectrum over a period of several days revealed slow axial ligand exchange, as the resonances of the bound (*R*) enantiomer gradually increase in intensity at the expense of those of the (*S*) enantiomer.<sup>252</sup> A plot of the enantioselection ratio  $[R]/[S]$  as a function of time shows that



**Figure 46.** Plot of the enantioselection ratio  $[R]/[S]$  as a function of time for the adducts of  $\text{CoCl}(\text{TMCP})$  with  $(R,S)$ -2-aminopropanol,  $(R,S)$ -2-aminobutanol, and  $(R,S)$ -prolinol. The host-guest system reaches thermodynamic equilibrium in 20–80 h, depending on the amino alcohol guest. Reprinted with permission from Simonato, J.-P.; Pécaut, J.; Marchon, J.-C. *J. Am. Chem. Soc.* **1998**, *120*, 7363. Copyright 1998 American Chemical Society.

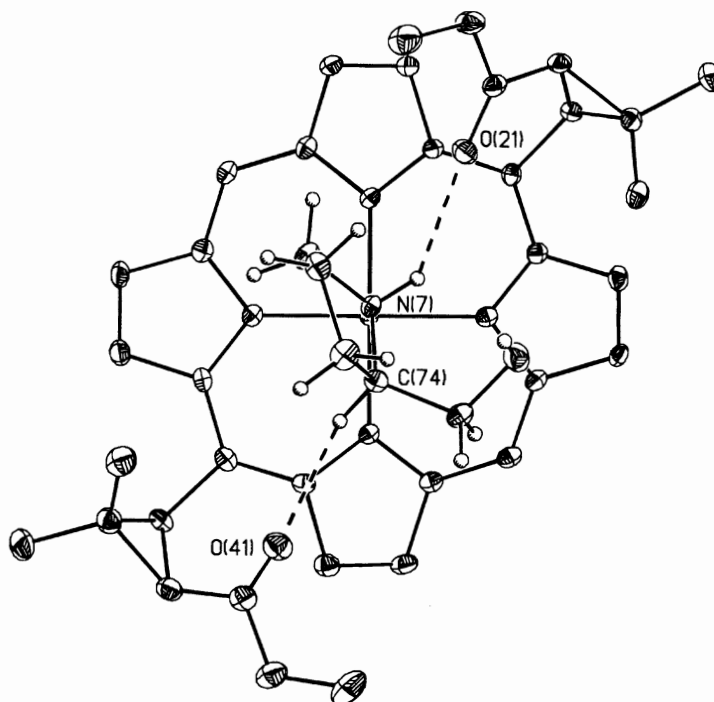
the host-guest system reaches thermodynamic equilibrium in 1–3 days depending on the aminoalcohol guest (Figure 46). The final equilibrium ratios  $[R]/[S]$  measured by  $^1\text{H}$  NMR were 2.7, 2.0, and 1.2 ( $\pm 0.1$ ) for  $(R,S)$ -2-aminopropanol,  $(R,S)$ -2-aminobutanol, and  $(R,S)$ -prolinol, respectively. In each case, the  $(R)$  enantiomer is the preferentially bound ligand at equilibrium. Since the axial  $\text{Co-N}$  bonds presumably have similar energies in the  $(R)$  and  $(S)$  complexes, the preference for  $(R)$  aminoalcohol is the result of stronger noncoordinate binding to the chiroporphyrin host. The time dependence of the enantioselection ratio suggests that equilibration takes place by a dissociative pathway, and that the rate-determining step is the dissociation of the aminoalcohol axial ligand.<sup>252</sup>

The X-ray structures of the  $(R)$  and  $(S)$ -prolinol *bis*-adducts of  $\text{CoCl}(\text{TMCP})$  show that steric exclusion constrains the prolinol ligands to lie along the chiral grooves which span the porphyrin ring, with similar conformations of the five-membered rings and  $\text{N-H}\cdots\text{O}=\text{C}$  hydrogen bonds to a carbonyl group of the host (Figures 47 and 48). The opposite absolute configurations of  $C_2$  in the  $(R)$  and  $(S)$ -prolinol ligands result in different patterns of interaction with the *meso* substituents. In the  $(S)$ -prolinol complex, the methylene of the hydroxymethyl group  $C_{1'}$  of each  $(S)$ -prolinol ligand is involved in a weak  $\text{C-H}\cdots\text{O}=\text{C}$  hydrogen bond to a *meso* carbonyl group. In contrast, it is the asymmetric carbon atom  $C_2$  of each  $(R)$ -prolinol ligand which is involved in a  $\text{C-H}\cdots\text{O}=\text{C}$  hydrogen bond, and the bond is a little shorter. The preferential binding of  $(R)$ -prolinol in solution at equilibrium has been attributed to this stronger hydrogen bond.<sup>252</sup>

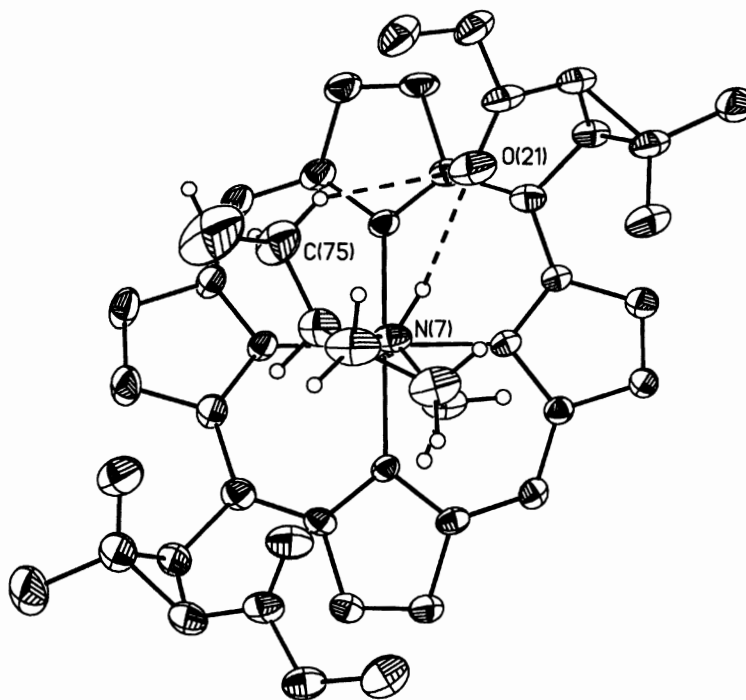
#### F. IRREVERSIBLE BINDING OF AMINES TO $\text{Co}(\text{III})$ CHIROPORPHYRINS

Primary amines bind to the diamagnetic cobalt(III) center of  $\text{CoCl}(\text{TMCP})$  to form cationic *bis*-adducts in which the  $^1\text{H}$  NMR resonances of the axial ligands are shifted upfield of tetramethylsilane by the porphyrin ring current. Coordinated enantiopure 2-alkylamines exhibit NMR signals for the protons of the amine group which are characteristic of their  $(R)$  or  $(S)$  absolute configuration. The *bis*-complexes of the same amines in racemic form exist as three different species,  $(R,R)$ ,  $(R,S)$ , and  $(S,S)$ , and the observed 1:2:1 relative abundance of the three species indicates that there is no enantioselection by the chiral host in that case. This result suggests that the system is not at thermodynamic equilibrium and that distribution of the *bis*-amine adducts is under kinetic control (Figure 49). With its ability to induce good resolution of axial ligand  $^1\text{H}$  NMR resonances and slow dissociation kinetics of its *bis*-adducts,  $\text{CoCl}(\text{TMCP})$  is a useful chiral NMR shift reagent for conformational studies of chiral amines,<sup>248</sup> and for the determination of the absolute configuration of amino acids.<sup>341</sup>

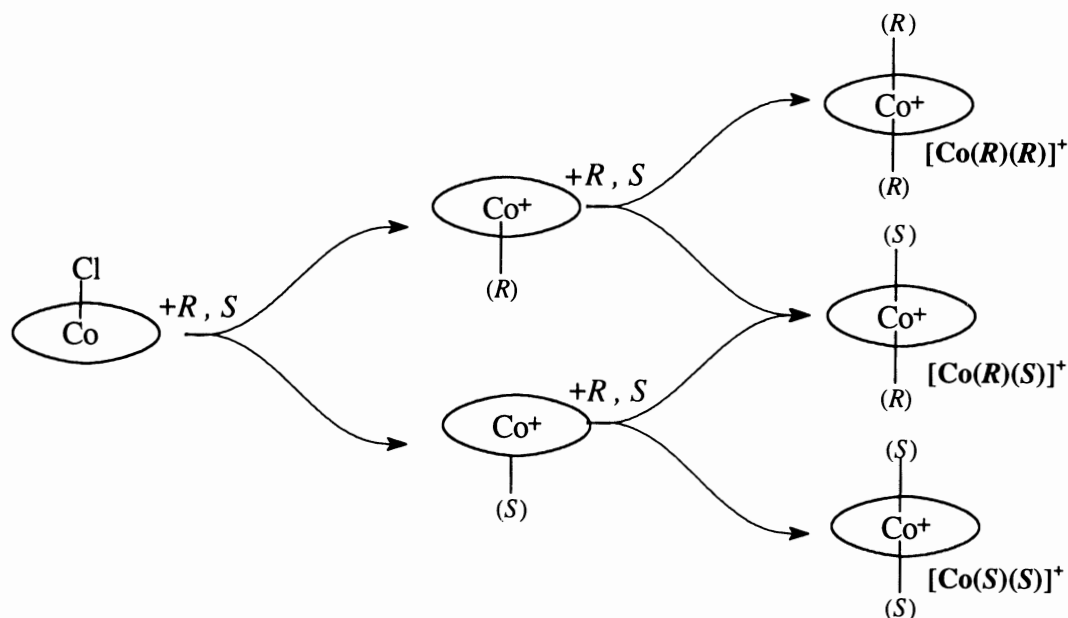
Likewise, the binding of chiral aziridines to  $\text{CoCl}(\text{TMCP})$  is strong and irreversible, and therefore it is not enantioselective. Using standard solutions containing various ratios of two amine enantiomers, we have shown that the observed distribution of diastereomeric products accurately reflects the enantiomer composition of the chiral ligand.<sup>251</sup> Like the  $\text{Co}(\text{III})$  reagent, chiroporphyrin complexes with other inert metal centers like  $\text{Rh}(\text{III})$  have potential applications in chiral analysis by NMR spectroscopy.<sup>250</sup>



**Figure 47.** ORTEP view of the X-ray structure of the cobalt(III) chiroporphyrin-*bis*[(*R*)-prolinol] cationic complex showing the hydrogen bonding pattern between a (*R*)-prolinol guest and two carbonyl groups of the host on the top face. The other (*R*)-prolinol axial ligand and the two *meso* substituents on the bottom face have been omitted for clarity. The enantiodifferentiating hydrogen bond distances are C(74)···O(41) 3.230(2) Å (top), and C(64)···O(51) 3.186(1) Å (bottom, not shown). Reprinted with permission from Simonato, J.-P.; Pécaut, J.; Marchon, J.-C. *J. Am. Chem. Soc.* **1998**, *120*, 7363. Copyright 1998 American Chemical Society.



**Figure 48.** ORTEP view of the X-ray structure of the cobalt(III) chiroporphyrin-*bis*[(*S*)-prolinol] cationic complex showing the hydrogen bonding pattern between a (*S*)-prolinol guest and two carbonyl groups of the host on the top face. The other (*S*)-prolinol axial ligand and the two *meso* substituents on the bottom face have been omitted for clarity. The enantiodifferentiating hydrogen bond distances are C(75)···O(21) 3.400(2) Å (top), and C(65)···O(31) 3.381(2) Å (bottom, not shown). Reprinted with permission from Simonato, J.-P.; Pécaut, J.; Marchon, J.-C. *J. Am. Chem. Soc.* **1998**, *120*, 7363. Copyright 1998 American Chemical Society.



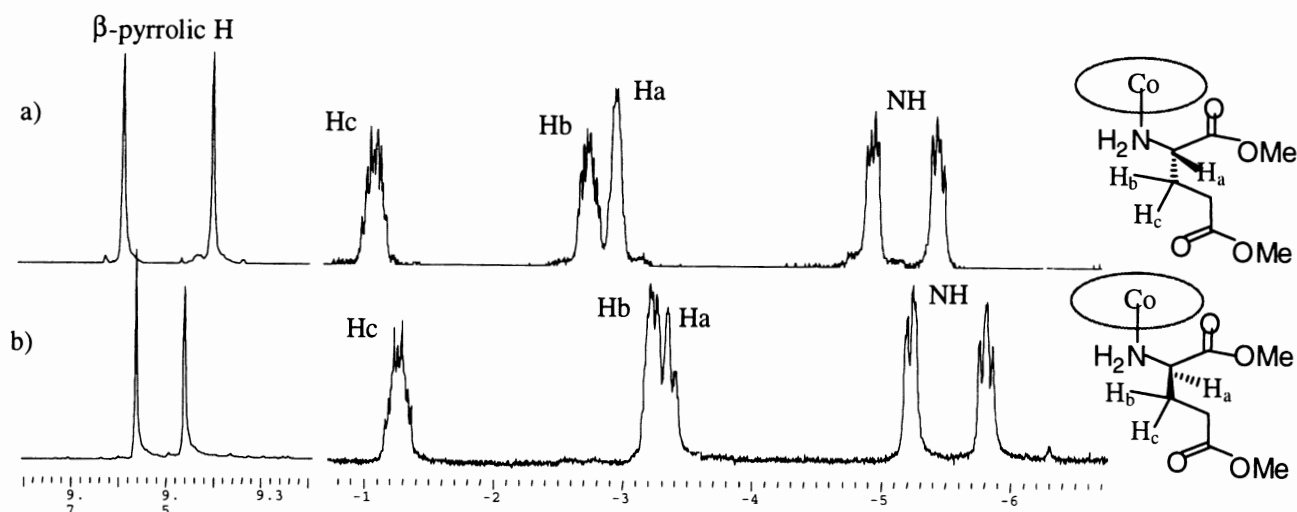
**Figure 49.** Irreversible binding of chiral aliphatic amines to  $\text{CoCl(TMCP)}$ , resulting in statistical ratios of the three diastereomeric *bis*-adducts.

### G. CHIROPORPHYRIN DERIVATIZING AGENTS FOR CHIRAL ANALYSIS BY NMR SPECTROSCOPY

In a typical experiment, 2 equiv of amino acid methyl ester  $L^*$  were added to a 3 mg sample of  $\text{CoCl(TMCP)}$  in  $\text{CDCl}_3$  solution in a NMR tube at room temperature, and the *bis*-adduct was formed quantitatively and without any detectable kinetic resolution.<sup>343</sup> The influences of the chiral cavity and of the porphyrin ring current of **1** on the protons of  $L^*$  were seen in the high field region of the NMR spectrum of the *bis*-adduct  $[\text{Co}(L^*)_2(\text{TMCP})]^+ \text{Cl}^-$ . The  $(R)$  and  $(S)$  ligands gave well resolved spectral signatures at 200 MHz, and their relative concentrations could be readily determined by peak integration. Good agreement was found with values obtained by chiral chromatography for standard solutions of  $(R)$ - and  $(S)$ -phenylalanine methyl esters with ee's in the range 5–95%. Relevant spectra for the methyl esters of  $(R)$  and  $(S)$  glutamic acids as representative examples are shown in Figure 50. A remarkable feature of the spectra is the large value of the diastereomeric dispersion  $\Delta\delta = |\delta_R - \delta_S|$  observed for equivalent protons of  $(R)$  and  $(S)$  ligands, which can be as high as 0.5 ppm, as shown for  $H_b$  in Figure 50. The spectral simplicity observed in most cases indicates that the amino ester ligand adopts a single, well-defined conformation within the cavity of  $[\text{Co(TMCP)}]^+$ .<sup>343</sup>

The stereochemistries of several adducts of  $(R)$ - and  $(S)$ -amino acid methyl esters with  $\text{CoCl(TMCP)}$  have

been elucidated by X-ray crystallography. They explain the large diastereomeric dispersions observed in the  $^1\text{H}$  NMR spectra of the adducts.<sup>343</sup> The crystal structures of the four  $(R)$  *bis*-adducts [ $(R)$ -Ile,  $(R)$ -Ala,  $(R)$ -Thr, and  $(R)$ -Tyr] shown in Figure 51 exhibit a number of conserved features. Two hydrogen bonds connect the amino ester to the carbonyl groups of opposite *meso* substituents of the porphyrin:  $\text{N-H}\cdots\text{O}$ , always with the same hydrogen of the amine, and  $\text{C-H}\cdots\text{O}$  with the hydrogen on the asymmetric carbon. The methyl ester group of the axial ligand lies on the porphyrin macrocycle, nearly parallel to its mean plane, at a distance of 3.5–3.7 Å, suggesting a weakly bonding  $\pi$ - $\pi$  interaction. Thus, the weak bonds which involve three substituents of the  $(R)$  asymmetric carbon of the axial ligand impose a unique conformation of this guest within the cavity of the host, and project the fourth substituent outward. It was anticipated that in a  $(S)$  adduct at least one of the three weak interactions is necessarily lost; if the two hydrogen bonds are maintained, the ester and alkyl substituents must exchange places as a consequence of the  $(S)$  absolute configuration of the asymmetric carbon. The crystal structure of the adduct of  $(S)$ -Glu dimethyl ester (Figure 52) confirms this expectation. Interestingly, a different conformation of the coordinated amino ester is found on each of the two faces of the chiroporphyrin complex. One face shows a stereochemistry (A) similar



**Figure 50.** Selected signals of the  $^1\text{H}$  NMR spectra of the *bis*-adducts of (*R*)- and (*S*)-glutamic acid methyl esters with  $\text{CoCl}(\text{TMCP})$ , showing the exceptionally large diastereomeric dispersion. Top: (*S*)(*S*) adduct; bottom: (*R*)(*R*) adduct.

to that of the (*R*) adducts, with exactly the same pattern of opposite  $\text{N-H}\cdots\text{O}$  and  $\text{C-H}\cdots\text{O}$  hydrogen bonds; the expected permutation of the alkyl and ester substituents of the asymmetric carbon is indeed observed, and the  $\pi$ -stacking interaction is therefore lost. The conformation (B) found on the other face is totally different; while the three intermolecular bonds which were present in the (*R*) adducts are observed, the  $\text{N-H}\cdots\text{O}$  interaction surprisingly involves the other amine hydrogen. This has required a *ca.*  $120^\circ$  turn around the  $\text{Co-N}$  bond; this rotation allows the ester group to  $\pi$ -stack on the ring, and it projects the fourth (alkyl) substituent outward. The  $\text{C-H}\cdots\text{O}$  hydrogen bond is as usual. We relate the (B) conformation to the changes in NMR spectrum which are seen in aged samples after several weeks, and we conclude that both (*S*) ligands in a fresh sample of the *bis*-adduct exhibit the (A) conformation. The permutation of ester and alkyl substituents of the asymmetric carbon seen in (A) puts the alkyl protons at very different elevations above the porphyrin, where they are subject to significantly different ring current effects. This explains the exceptionally large diastereomeric dispersion which is seen for protons such as  $\text{H}_d$ .

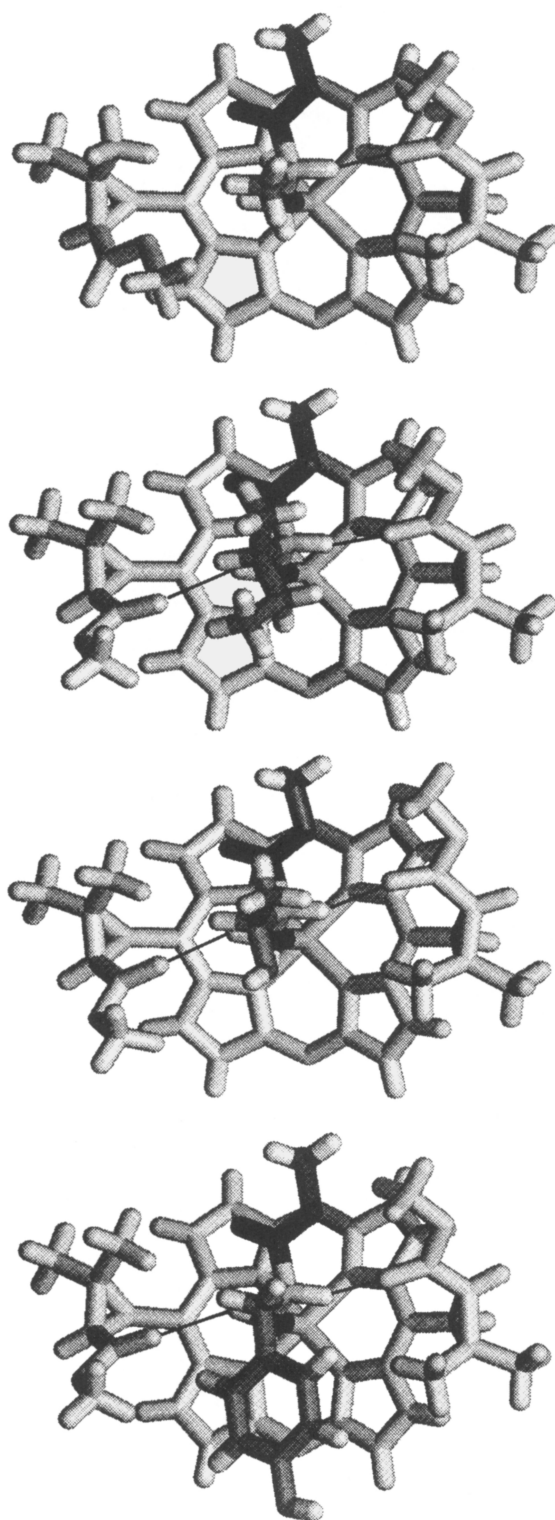
In summary, the hydrogen bonding capabilities of  $\text{CoCl}(\text{TMCP})$  allow the conformation of coordinated amino esters to be uniquely defined within the chiral cavity on the time scale of NMR analysis, and the porphyrin ring current amplifies the chemical shift differences between the diastereomeric adducts. Taken together, these structural features make this chiral

cobalt complex a very powerful derivatizing agent for the chiral analysis of amino acid derivatives.<sup>342,343,348</sup>

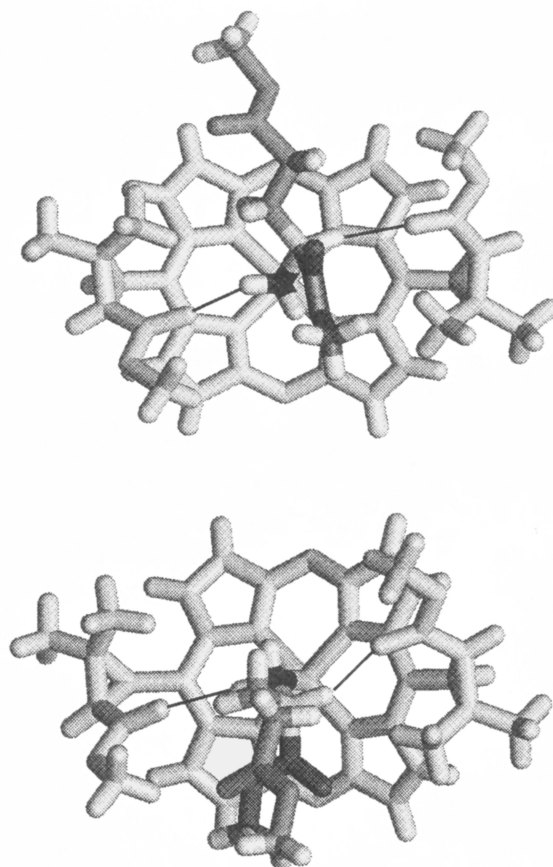
## V. Perspectives

Among the myriads of chiral metalloporphyrin structures which have been designed, thanks to the ingenuity of chemists during the last two decades, so far only a dozen or two have met some success in asymmetric catalysis, and perhaps a handful will stand out as practical catalysts for synthetic purposes. As far as asymmetric industrial processes are concerned, there is still a long way to go in order to achieve with chiral metalloporphyrins the high standards of enantioselectivity and cost effectiveness shown by the chiral metallosalens for example. However, asymmetric catalysis is only one facet of enantioselective control, and chiral metalloporphyrins may find a bright future in related fields, such as the development of selectors for enantiomer resolution, or of derivatizing agents for the spectroscopic analysis of enantiomer mixtures. Seemingly infinite possibilities are available for appending chiral structures to porphyrins, for combining porphyrins in chiral arrays, or for assembling porphyrins in chiral supramolecular aggregates. The potential of these arrays and aggregates seems to be considerable, and initial results may provide an impetus for further developments. Efforts in these fields will probably continue unabated, providing new clues on the determinants of enantioselectivity and new ways to adjust it at will, and bringing out new chemistry of practical interest.





**Figure 51.** Conserved conformation and hydrogen bond pattern of a (*R*)-amino acid methyl ester ligand as seen in the crystal structures of four (*R*) *bis*-adducts of CoCl(TMCP). The second ligand and *meso*-substituents on the bottom faces have been omitted for clarity. Downward from top: (*R*)-Ala, (*R*)-Ile, (*R*)-Thr, (*R*)-Tyr. Hydrogen bonds are indicated by black lines. The N–H···O interaction is not seen in the representation shown for (*R*)-Ala, since the methyl ester of the *meso* substituent on the left side has its carbonyl group oriented outward. However, it is seen on the other face (not shown for clarity), which has a twofold disorder of the amino ester ligand. Reprinted with permission from Claeys-Bruno, M.; Toronto, D.; Pécaut, J.; Bardet, M.; Marchon, J. C. *J. Am. Chem. Soc.*, **2001**, *123*, 11067. Copyright 2001 American Chemical Society.



**Figure 52.** Conformations and hydrogen bond patterns of a (*S*)-amino acid methyl ester ligand as seen in the crystal structure of a *bis*-adduct of CoCl(TMCP) with (*S*)-Glu. Top: (*S*)-Glu (conformation A); bottom: (*S*)-Glu (conformation B). Only the top faces are shown; the second ligand and *meso*-substituents on the bottom faces have been omitted for clarity. Hydrogen bonds are indicated by black lines. Reprinted with permission from Claeys-Bruno, M.; Toronto, D.; Pécaut, J.; Bardet, M.; Marchon, J. C. *J. Am. Chem. Soc.*, **2001**, *123*, 11067. Copyright 2001 American Chemical Society.

### ACKNOWLEDGMENTS

The authors are grateful to the many coworkers who contributed to the discovery and development of chiroporphyrins in their laboratory.

### REFERENCES

- Lindsey, J. S. In *The Porphyrin Handbook*. Kadish, K. M., Smith, K. M., Guilard, R., Eds.; Academic Press: Boston, **2000**; Vol. 1, pp. 45–118.
- Groves, J. T.; Shalyaev, K.; Lee, J. In *The Porphyrin Handbook*. Kadish, K. M., Smith, K. M., Guilard, R., Eds.; Academic Press: Boston, **2000**; Vol. 4, pp. 17–40.
- Suslick, K. S. In *The Porphyrin Handbook*. Kadish, K. M., Smith, K. M., Guilard, R., Eds.; Academic Press: Boston, **2000**; Vol. 4, pp. 41–64.
- Meunier, B.; Robert, A.; Pratiel, G. Bernadou, J. In *The Porphyrin Handbook*. Kadish, K. M., Smith, K. M., Guilard, R., Eds.; Academic Press: Boston, **2000**; Vol. 4, pp. 119–188.
- Ogoshi, H.; Mizutani, T.; Hayashi, T.; Kuroda, Y. In *The Porphyrin Handbook*. Kadish, K. M., Smith, K. M., Guilard, R., Eds.; Academic Press: Boston, **2000**; Vol. 6, pp. 279–340.
- Collman, J. P.; Wang, Z. *Chemtracts* **1999**, *12*, 229–263.
- Rose, E.; Quelquejeu, M.; Kossanyi, A.; Boitrel, B. *Coord. Chem. Rev.* **1998**, *178–180 (Pt. 2)*, 1407–1431.
- Gonzalez, M. C.; Weedon, A. C. *Can. J. Chem.* **1985**, *63*, 602.
- Weber, L.; Imiolczyk, I.; Haufe, G.; Rehored, D.; Hennig, H. *J. Chem. Soc., Chem. Commun.* **1992**, 301–303.
- Weber, L.; Hommel, R.; Behling, J.; Haufe, G.; Hennig, H. *J. Am. Chem. Soc.* **1994**, *116*, 2400–2408.
- Banfi, S.; Montanari, F.; Pozzi, G.; Quici, S. *Gazz. Chim. Ital.* **1993**, *123*, 617–621.
- Hombrecher, H. K.; Schell, C.; Thiem, J. *Bioorg. Med. Chem. Lett.* **1996**, *6*, 1199–1202.
- Casella, L.; Gullotti, M.; De Gioia, L.; Bartesaghi, R.; Chillemi, F. *J. Chem. Soc., Dalton Trans.* **1993**, 2233–2239.
- Monzani, E.; Linati, L.; Casella, L.; De Gioia, L.; Favretto, M.; Gullotti, M.; Chillemi, F. *Inorg. Chim. Acta* **1998**, *273*, 339–345.
- Hombrecher, H. K.; Ohm, S.; Koll, D. *Tetrahedron* **1996**, *52*, 5441–5448.
- Wandreakar, V.; Trumble, W. R.; Czuchajowski, L. *J. Heterocycl. Chem.* **1996**, *33*, 1775–1783.
- Huang, D.; Matile, S.; Berova, N.; Nakanishi, K. *Heterocycles* **1996**, *42*, 723–736.
- Matile, S.; Berova, N.; Nakanishi, K.; Novkova, S.; Philipova, I.; Blagoev, B. *J. Am. Chem. Soc.* **1995**, *117*, 7021–7022.

19. Mihara, H.; Haruta, Y.; Sakamoto, S.; Nishino, N.; Aoyagi, H. *Chem. Lett.* **1996**, 1–2.
20. Wang, Y.; Liu, Y.; Han, S. *Huaxue Shiji* **2000**, 22, 205–206. (CAN 133:350370).
21. Liu, Y.-Q.; Han, S.-T. *Guangpu Shiyanshi* **2000**, 17, 91–94. (CAN 133:43363).
22. Liu, Y.-Q.; Zhang, Y.-M.; Han, S.-T. *Guangpu Shiyanshi* **2000**, 17, 286–289. (CAN 134:4799).
23. Li, J.; Zhao, Y.; Zhang, H.; Cheng, J. *Guijinshu* **1997**, 18, 33–36. (CAN 128:29769).
24. Peng, X.; Huang, J.; Ji, L. *Chin. Sci. Bull.* **2000**, 45, 418–421. (CAN 133:150391).
25. Luo, G.; Liu, H.; Huang, J.; Peng, X.; Ji, L. *Zhongshan Daxue Xuebao, Ziran Kexueban* **1997**, 36, 125–126. (CAN 128:308723).
26. Peng, X.-B.; Huang, J.-W.; Mei, W.-J.; Ji, L.-N. *Synth. React. Inorg. Met.-Org. Chem.* **2000**, 30, 791–802.
27. Ouyang, J.-M.; Zhang, Z.-M.; Huang, C.-X.; Yao, X.-Q.; Liu, H.-Y.; Hu, X.-M. *Colloids Surf., A* **2000**, 175, 99–104.
28. Yoshinaga, K.; Itoh, N.; Kito, T. *Polym. J. (Tokyo)* **1991**, 23, 65–68.
29. Sagawa, T.; Ohkubo, K. *J. Mol. Catal. A: Chem.* **1996**, 113(1–2), 269–281.
30. Kuroda, Y.; Hiroshige, T.; Ogoshi, H. *J. Chem. Soc., Chem. Commun.* **1990**, 22, 1594–1595.
31. Kuroda, Y.; Ito, M.; Sera, T.; Ogoshi, H. *J. Am. Chem. Soc.* **1993**, 115, 7003–7004.
32. Carofiglio, T.; Fornasier, R.; Lucchini, V.; Simonato, L.; Tonellato, U. *J. Org. Chem.* **2000**, 65, 9013–9021.
33. Snip, E.; Shinkai, S.; Reinhoudt, D. N. *Tetrahedron Lett.* **2001**, 42, 2153–2156.
34. Cazelles, J.; Robert, A.; Meunier, B. *C. R. Acad. Sci., Ser. IIC: Chim.* **2001**, 4, 85–89.
35. Feng, X.; Senge, M. O. *J. Chem. Soc., Perkin Trans. 1* **2001**, 1030–1038.
36. Groves, J. T.; Myers, R. S. *J. Am. Chem. Soc.* **1983**, 105, 5791–5796.
37. Groves, J. T.; Crowley, S. J.; Shalyaev, K. V. *Chirality* **1998**, 10, 106–119.
38. Groves, J. T.; Neumann, R. *J. Am. Chem. Soc.* **1987**, 109, 5045–5047.
39. Groves, J. T.; Neumann, R. *J. Org. Chem.* **1988**, 53, 3891–3893.
40. Groves, J. T.; Neumann, R. *J. Am. Chem. Soc.* **1989**, 111, 2900–2909.
41. Zhou, Q.; Chen, K.; Zhu, Z. *J. Mol. Catal.* **1992**, 72, 59–65.
42. Licoccia, S.; Paci, M.; Tagliatesta, P.; Paolesse, R.; Antonaroli, S.; Boschi, T. *Magn. Reson. Chem.* **1991**, 29, 1084–1091.
43. Kuroda, Y.; Egawa, Y.; Seshimo, H.; Ogoshi, H. *Chem. Lett.* **1994**, 2361–2364.
44. Groves, J. T.; Viski, P. *J. Org. Chem.* **1990**, 55, 3628–3634.
45. Renaud, J. P.; Battioni, P.; Mansuy, D. *New J. Chem.* **1987**, 11, 279–290.
46. Mansuy, D.; Battioni, P.; Renaud, J. P.; Guerin, P. *J. Chem. Soc., Chem. Commun.* **1985**, 155–156.
47. Maillard, P.; Schaeffer, C.; Huel, C.; Lhoste, J. M.; Mometeau, M. *J. Chem. Soc., Perkin Trans. 1* **1988**, 3285–3296.
48. Nishino, N.; Mihara, H.; Hasegawa, R.; Yanai, T.; Fujimoto, T. *J. Chem. Soc., Chem. Commun.* **1992**, 692–694.
49. Boitrel, B.; Lecas, Nawrocka, A.; Rose, E. *Tetrahedron Lett.* **1992**, 33, 227–230.
50. Boitrel, B.; Lecas, A.; Renko, Z.; Rose, E. *New J. Chem.* **1989**, 13, 73–99.
51. Kuroda, Y.; Kato, Y.; Higashioji, T.; Hasegawa, J.-Y.; Kawanami, S.; Takahashi, M.; Shiraishi, N.; Tanabe, K.; Ogoshi, H. *J. Am. Chem. Soc.* **1995**, 117, 10950–10958.
52. Pfeiffer, H. P.; Sander, H.; Breitmaier, E. *Liebigs Ann. Chem.* **1987**, 725–726.
53. Takagi, S.; Miyamoto, T. K.; Sasaki, Y. *Bull. Chem. Soc. Jpn.* **1985**, 58, 447–454.
54. Ohkubo, K.; Sagawa, T.; Kuwata, M.; Hata, T.; Ishida, H. *J. Chem. Soc., Chem. Commun.* **1989**, 352–354.
55. Ohkubo, K.; Sagawa, T.; Ishida, H. *Inorg. Chem.* **1992**, 31, 2682–2688.
56. Collman, J. P.; Zhang, X.; Hembre, R. T.; Brauman, J. I. *J. Am. Chem. Soc.* **1990**, 112, 5356–5357.
57. Nagasaki, T.; Fujishima, H.; Shinkai, S. *Chem. Lett.* **1994**, 989–992.
58. Collman, J. P.; Wang, Z.; Straumanis, A.; Quelquejeu, M.; Rose, E. *J. Am. Chem. Soc.* **1999**, 121, 460–461.
59. Le Maux, P.; Bahri, H.; Simonneaux, G. *Tetrahedron* **1993**, 49, 1401–1408.
60. Le Maux, P.; Bahri, H.; Simonneaux, G. *J. Chem. Soc., Chem. Commun.* **1991**, 1350–1352.
61. Zhou, Q.; Chen, K.; Zhu, Z. *J. Mol. Catal.* **1991**, 64, L19–L21.
62. Collman, J. P.; Zhang, X.; Lee, V. J.; Brauman, J. I. *J. Chem. Soc., Chem. Commun.* **1992**, 1647–1649.
63. Lecas, A.; Renko, Z.; Rose, E. *Tetrahedron Lett.* **1985**, 26, 1019–1022.
64. Nishino, N.; Mihara, H.; Kiyota, H.; Kobata, K.; Fujimoto, T. *J. Chem. Soc., Chem. Commun.* **1993**, 162–163.
65. Rose, E.; Soleilhavoup, M.; Christ-Tomasino, L.; Moreau, G.; Collman, J. P.; Quelquejeu, M.; Straumanis, A. *J. Org. Chem.* **1998**, 63, 2042–2044.
66. Boitrel, B.; Lecas, A.; Rose, E. *J. Chem. Soc., Chem. Commun.* **1989**, 349–350.
67. Boitrel, B.; Camilleri, E.; Fleche, Y.; Lecas, A.; Rose, E. *Tetrahedron Lett.* **1989**, 30, 2923–2926.
68. Richard, P.; Rose, E.; Boitrel, B. *Inorg. Chem.* **1998**, 37, 6532–6534.
69. Boitrel, B.; Lecas, A.; Rose, E. *Tetrahedron Lett.* **1988**, 29, 5653–5656.
70. Collman, J. P.; Wang, Z.; Straumanis, A. *J. Org. Chem.* **1998**, 63, 2424–2425.
71. Wang, C. Z.; Zhu, Z. A.; Li, Y.; Yun, T. C.; Wen, X.; Fang, M. M.; Chan, W. L.; Chan, A. S. C. *New J. Chem.* **2001**, 25, 801–806.
72. Wang, C.-Z.; Zhu, Z.-A.; Li, Y.; Chen, R.-T. *Wuji Huaxue Xuebao* **2001**, 17, 244–248. (AN 2001:215709).
73. Kossanyi, A.; Tani, F.; Nakamura, N.; Naruta, Y. *Chem.-Eur. J.* **2001**, 7, 2862–2872.
74. Ohkubo, K.; Sagawa, T.; Minamoto, Y. *J. Mol. Catal.* **1994**, 91, 7–17.
75. Ohkubo, K.; Sagawa, T.; Minamoto, Y. *J. Mol. Catal.* **1993**, 85, L7–L11.
76. Mihara, H.; Nishino, K.; Hasegawa, R.; Fujimoto, T. *Chem. Lett.* **1992**, 1805–1808.
77. Akerfeldt, K. S.; Kim, R. M.; Camac, D.; Groves, J. T.; Lear, J. D.; DeGrado, W. F. *J. Am. Chem. Soc.* **1992**, 114, 9656–9657.
78. Collman, J. P.; Lee, V. J.; Zhang, X.; Ibers, J. A.; Brauman, J. I. *J. Am. Chem. Soc.* **1993**, 115, 3834–3835.
79. Collman, J. P.; Lee, V. J.; Kellen-Yuen, C. J.; Zhang, X.; Ibers, J. A.; Brauman, J. I. *J. Am. Chem. Soc.* **1995**, 117, 692–703.
80. Naruta, Y.; Tani, F.; Maruyama, K. *Chem. Lett.* **1989**, 1269–1272.
81. Naruta, Y.; Ishihara, N.; Tani, F.; Maruyama, K. *Chem. Lett.* **1991**, 1933–1936.
82. Galardon, E.; Lukas, M.; Le Maux, P.; Simonneaux, G. *Tetrahedron Lett.* **1999**, 40, 2753–2756.
83. Galardon, E.; Lukas, M.; Le Maux, P.; Toupet, L.; Roisnel, T.; Simonneaux, G. *Acta Crystallogr., Sect. C: Cryst. Struct. Commun.* **2000**, C56, 955–956.

84. Matsu-Ura, M.; Tani, F.; Nakayama, S.; Nakamura, N.; Naruta, Y. *Angew. Chem., Int. Ed. Engl.* **2000**, *39*, 1989–1991.
85. Ini, S.; Kapon, M.; Cohen, S.; Gross, Z. *Tetrahedron: Asymmetry* **1996**, *7*, 659–662.
86. Ohkatsu, Y.; Watanabe, T.; Goto, T.; Wakita, M. *Bull. Chem. Soc. Jpn.* **1994**, *67*, 742–747.
87. Li, Y.; Han, S.; Qie, W.; Xie, H. *Gaodeng Xuexiao Huaxue Xuebao* **1996**, *17*, 586–588. (CAN 125:142404).
88. Arai, T.; Kobata, K.; Mihara, H.; Fujimoto, T.; Nishino, N. *Bull. Chem. Soc. Jpn.* **1995**, *68*, 1989–1998.
89. Arai, T.; Tsukuni, A.; Kawazu, K.; Aoi, H.; Hamada, T.; Nishino, N. *J. Chem. Soc., Perkin Trans. 2* **2000**, 1381–1390.
90. Kuroda, Y.; Hiroshige, T.; Sera, T.; Shirowa, Y.; Tanaka, H.; Ogoshi, H. *J. Am. Chem. Soc.* **1989**, *111*, 1912–1913.
91. Nakagawa, H.; Nagano, T.; Higuchi, T. *Org. Lett.* **2001**, *3*, 1805–1807.
92. O'Malley, S.; Kodadek, T. *J. Am. Chem. Soc.* **1989**, *111*, 9116–9117.
93. O'Malley, S.; Kodadek, T. *Organometallics* **1992**, *11*, 2299–2302.
94. Barry, J.; Kodadek, T. *Tetrahedron Lett.* **1994**, *35*, 2465–2468.
95. Barry, J. F.; Campbell, L.; Smith, D. W.; Kodadek, T. *Tetrahedron* **1997**, *53*, 7753–7776.
96. Halterman, R. L.; Jan, S. T. *J. Org. Chem.* **1991**, *56*, 5253–5254.
97. Halterman, R. L.; Jan, S.-T.; Nimmons, H. L.; Standlee, D. J.; Khan, M. A. *Tetrahedron* **1997**, *53*, 11257–11276.
98. Halterman, R. L.; Jan, S.-T.; Abdulwali, A. H.; Standlee, D. J. *Tetrahedron* **1997**, *53*, 11277–11296.
99. Maillard, P.; Gaspard, S.; Guerquin-Kern, J. L.; Momenteau, M. *J. Am. Chem. Soc.* **1989**, *111*, 9125–9127.
100. Maillard, P.; Guerquin-Kern, J. L.; Huel, C.; Momenteau, M. *J. Org. Chem.* **1993**, *58*, 2774–2780.
101. Maillard, P.; Vilain, S.; Huel, C.; Momenteau, M. *J. Org. Chem.* **1994**, *59*, 2887–2890.
102. Vilain-Deshayes, S.; Maillard, P.; Momenteau, M. *J. Mol. Catal. A: Chem.* **1996**, *113*, 201–208.
103. Vilain, S.; Maillard, P.; Momenteau, M. *J. Chem. Soc., Chem. Commun.* **1994**, 1697–1698.
104. Vilain-Deshayes, S.; Robert, A.; Maillard, P.; Meunier, B.; Momenteau, M. *J. Mol. Catal. A: Chem.* **1996**, *113*, 23–34.
105. Oulmi, D.; Maillard, P.; Guerquin-Kern, J.-L.; Huel, C.; Momenteau, M. *J. Org. Chem.* **1995**, *60*, 1554–1564.
106. Zhang, X.-B.; Guo, C.-C.; Chen, S.-H.; Shen, G.-L.; Yu, R.-Q. *Fresenius' J. Anal. Chem.* **2001**, *369*, 422–427.
107. Marx, T.; Breitmair, E. *Liebigs Ann. Chem.* **1992**, 183–185.
108. Rispens, M. T.; Manfredi, A.; Pozzi, G.; Banfi, S.; Quici, S. *J. Mol. Catal. A: Chem.* **1998**, *136*, 13–22.
109. Banfi, S.; Manfredi, A.; Montanari, F.; Pozzi, G.; Quici, S. *J. Mol. Catal. A: Chem.* **1996**, *113*, 77–86.
110. Rusin, O.; Kral, V. *Chem. Commun. (Cambridge)* **1999**, 2367–2368.
111. Reginato, G.; Di Bari, L.; Salvadori, P.; Guillard, R. *Eur. J. Org. Chem.* **2000**, *7*, 1165–1171.
112. Halterman, R. L.; Mei, X. *Tetrahedron Lett.* **1996**, *37*, 6291–6294.
113. Bonar-Law, R. P.; Sanders, J. K. M. *J. Chem. Soc., Chem. Commun.* **1991**, 574–577.
114. Bonar-Law, R. P.; Mackay, L. G.; Sanders, J. K. M. *J. Chem. Soc., Chem. Commun.* **1993**, 456–458.
115. Mackay, L.; Bonar-Law, R. P.; Sanders, J. K. M. *J. Chem. Soc., Perkin Trans. 1* **1993**, 1377–1378.
116. Bonar-Law, R. P.; Sanders, J. K. M. *J. Chem. Soc., Perkin Trans. 1* **1995**, 3085–3096.
117. Tamiaki, H.; Onishi, M. *Tetrahedron: Asymmetry* **1999**, *10*, 1029–1032.
118. Loim, N. M.; Kondratenko, M. A.; Grishko, E. V.; Sokolov, V. I. *Izv. Akad. Nauk, Ser. Khim.* **1994**, 959–961. (CAN 122:187734).
119. Ema, T.; Jittani, M.; Sazkai, T.; Utaka, M. *Tetrahedron Lett.* **1998**, *39*, 6311–6314.
120. Foxon, S. P.; Lindsay Smith, J. R.; O'Brien, P.; Reginato, G. *J. Chem. Soc., Perkin Trans. 2* **2001**, 1145–1153.
121. Pasetto, P.; Chen, X.; Drain, C. M.; Franck, R. W. *Chem. Commun. (Cambridge)* **2001**, 81–82. Erratum: *ibid.* **2001**, 507.
122. Maillard, P.; Huel, C.; Momenteau, M. *Tetrahedron Lett.* **1992**, *33*, 8081–8084.
123. Cornia, M.; Casiraghi, G.; Binacchi, S.; Zanardi, F.; Rassu, G. *J. Org. Chem.* **1994**, *59*, 1226–1230.
124. Cornia, M.; Valenti, C.; Capacchi, S.; Cozzini, P. *Tetrahedron* **1998**, *54*, 8091–8106.
125. Casiraghi, G.; Cornia, M.; Zanardi, F.; Rassu, G.; Ragg, E.; Bortolini, R. *J. Org. Chem.* **1994**, *59*, 1801–1808.
126. Casiraghi, G.; Cornia, M.; Rassu, G.; Del Sante, C.; Spanu, P. *Nat. Prod. Lett.* **1992**, *1*, 45–50.
127. Cornia, M.; Menozzi, M.; Ragg, E.; Mazzini, S.; Scarafoni, A.; Zanardi, F.; Casiraghi, G. *Tetrahedron* **2000**, *56*, 3977–3983.
128. Cornia, M.; Binacchi, S.; Del Soldato, T.; Zanardi, F.; Casiraghi, G. *J. Org. Chem.* **1995**, *60*, 4964–4965.
129. Cornia, M.; Capacchi, S.; Porcari, S.; Tarasconi, P. *Tetrahedron: Asymmetry* **1997**, *8*, 2885–2887.
130. Cornia, M.; Capacchi, S.; Ferrari, M. B.; Tarasconi, P.; Albertini, R.; Pinelli, S. *Tetrahedron: Asymmetry* **1999**, *10*, 1599–1616.
131. Proess, G.; Hevesi, L. *J. Mol. Catal.* **1993**, *80*, 395–401.
132. Pérollier, C.; Mazzanti, M.; Simonato, J.-P.; Launay, F.; Ramasseul, R.; Marchon, J.-C. *Eur. J. Org. Chem.* **2000**, 583–589.
133. Veyrat, M.; Maury, O.; Faverjon, F.; Over, D. E.; Ramasseul, R.; Marchon, J. C.; Turowska-Tyrk, I.; Scheidt, W. R. *Angew. Chem., Int. Ed. Engl.* **1994**, *33*, 220–223.
134. Pérollier, C.; Pécaut, J.; Ramasseul, R.; Marchon, J.-C.; Bau, R. *Chem. Commun. (Cambridge)* **1999**, 1597–1598.
135. De Matteis, F.; Jackson, A. H.; Gibbs, A. H.; Rao, K. R. N.; Atton, J.; Weerasinghe, S.; Hollands, C. *FEBS Lett.* **1982**, *142*, 44–48.
136. Abraham, R. J.; Smith, K. M.; Bobe, F. W.; Minnetian, O. M. *Org. Magn. Reson.* **1984**, *22*, 771–774.
137. De Matteis, F.; Harvey, C.; Martin, S. R. *Biochem. J.* **1986**, *238*, 263–268.
138. Kubo, H.; Aida, T.; Inoue, S.; Okamoto, Y. *J. Chem. Soc., Chem. Commun.* **1988**, 1015–1017.
139. Konishi, K.; Takahata, Y.; Aida, T.; Inoue, S.; Kuroda, R. *J. Am. Chem. Soc.* **1993**, *115*, 1169–1170.
140. Konishi, K.; Mori, Y.; Aida, T.; Inoue, S. *Inorg. Chem.* **1995**, *34*, 1292–1294.
141. Gaudemer, A.; Gaudemer, F.; Merienne, C. *Org. Magn. Reson.* **1983**, *21*, 83–85.
142. De Matteis, F.; Gibbs, A. H.; Martin, S. R.; Milek, R. L. B. *Biochem. J.* **1991**, *280*, 813–816.
143. Ishimaru, Y.; Sumida, S.; Iida, T. *Chem. Commun. (Cambridge)* **1997**, 2187–2188.
144. Konishi, K.; Miyazaki, K.; Aida, T.; Inoue, S. *J. Am. Chem. Soc.* **1990**, *112*, 5639–5640.
145. Konishi, K.; Oda, K.; Nishida, K.; Aida, T.; Inoue, S. *J. Am. Chem. Soc.* **1992**, *114*, 1313–1317.
146. Konishi, K.; Yahara, K.; Toshishige, H.; Aida, T.; Inoue, S. *J. Am. Chem. Soc.* **1994**, *116*, 1337–1344.

147. Ogoshi, H.; Saita, K.; Sakurai, K.; Watanabe, T.; Toi, H.; Aoyama, Y.; Okamoto, Y. *Tetrahedron Lett.* **1986**, *27*, 6365–6368.
148. Aoyama, Y.; Saita, K.; Toi, H.; Ogoshi, H.; Okamoto, Y. *Tetrahedron Lett.* **1987**, *28*, 4853–4856.
149. Mizutani, T.; Ema, T.; Tomita, T.; Kuroda, Y.; Ogoshi, H. *J. Chem. Soc., Chem. Commun.* **1993**, 520–522.
150. Hatano, K. *Chem. Pharm. Bull.* **1985**, *33*, 4116–4119.
151. Crossley, M. J.; Hambley, T. W.; Mackay, L. G.; Try, A. C.; Walton, R. *J. Chem. Soc., Chem. Commun.* **1995**, 1077–1079.
152. Reek, J. N. H.; Schenning, A. P. H. J.; Bosman, A. W.; Meijer, E. W.; Crossley, M. J. *Chem. Commun. (Cambridge)* **1998**, 11–12.
153. Yeow, E. K. L.; Sintic, P. J.; Cabral, N. M.; Reek, J. N. H.; Crossley, M. J.; Ghiggino, K. P. *Phys. Chem. Chem. Phys.* **2000**, *2*, 4281–4291.
154. Allen, P. R.; Reek, J. N. H.; Try, A. C.; Crossley, M. J. *Tetrahedron: Asymmetry* **1997**, *8*, 1161–1164.
155. Furusho, Y.; Aida, T.; Inoue, S. *J. Chem. Soc., Chem. Commun.* **1994**, 653–655.
156. Omote, M.; Ando, A.; Takagi, T.; Koyama, M.; Kumadaki, I.; Shiro, M. *Heterocycles* **1998**, *47*, 65–68.
157. Brunner, H.; Agrifoglio, G. *Inorg. Chim. Acta* **1984**, *90*, 209–213.
158. Muzzi, C. M.; Medforth, C. J.; Smith, K. M.; Jia, S.-L.; Shelnut, J. A. *Chem. Commun. (Cambridge)* **2000**, 131–132.
159. Konishi, K.; Suezaki, M.; Aida, T. *Tetrahedron Lett.* **1999**, *40*, 6951–6955.
160. Schwenninger, R.; Ramondenc, Y.; Wurst, K.; Schlogl, J.; Krautler, B. *Chem.-Eur. J.* **2000**, *6*, 1214–1223.
161. Schwenninger, R.; Schlogl, J.; Maynollo, J.; Gruber, K.; Ochsenbein, P.; Burgi, H.-B.; Konrat, R.; Krautler, B. *Chem.-Eur. J.* **2001**, *7*, 2676–2686.
162. Kusch, D.; Montforts, F.-P. *Tetrahedron: Asymmetry* **1995**, *6*, 867–870.
163. Ema, T.; Nemugaki, S.; Tsuboi, S.; Utaka, M. *Tetrahedron Lett.* **1995**, *36*, 5905–5908.
164. Flores, V.; Nguyen, C. K.; Sindelar, C. A.; Vasquez, L. D.; Shachter, A. M. *Tetrahedron Lett.* **1996**, *37*, 8633–8636.
165. Takeuchi, M.; Chin, Y.; Imada, T.; Shinkai, S. *Chem. Commun. (Cambridge)* **1996**, 1867–1868.
166. Ema, T.; Misawa, S.; Negmugaki, S.; Sakai, T.; Utaka, M. *Chem. Lett.* **1997**, 487–488.
167. Liu, H.-Y.; Huang, J.-W.; Tian, X.; Jiao, X.-D.; Luo, G.-T.; Ji, L.-N. *Chem. Commun. (Cambridge)* **1997**, 1575–1576.
168. Hayashi, T.; Nonoguchi, M.; Arya, T.; Ogoshi, H. *Tetrahedron Lett.* **1997**, *38*, 1603–1606.
169. Li, Z.-Y.; Liang, J.-L.; Li, C. *Chin. J. Chem.* **2000**, *18*, 565–570.
170. Arai, T.; Maruo, N.; Sumida, Y.; Korosue, C.; Nishino, N. *Chem. Commun. (Cambridge)* **1999**, 1503–1504.
171. Liu, H.-Y.; Huang, J.-W.; Tian, X.; Jiao, X.-D.; Luo, Guo-T.; Ji, L.-N. *Inorg. Chim. Acta* **1998**, *272*, 295–299.
172. Liu, H.-Y.; Hu, X.-M.; Ying, X.; Liu, Y.; Huang, J.; Huang, J.-W.; Ji, L.-N.; Tian, X.; Yang, L.; Zhu, Q.-X. *Gaodeng Xuexiao Huaxue Xuebao* **1999**, *20*, 849–851. (CAN 131:210702).
173. Liu, H.-Y.; Hu, X.-M.; Ying, X.; Liu, Y.; Huang, J.; Huang, J.-W.; Tian, X.; Ji, L.-N. *Mater. Sci. Eng., C* **1999**, *C10*, 33–38. (CAN 132:160387).
174. Jiang, H.; Huang, X.; Nakanishi, K.; Berova, N. *Tetrahedron Lett.* **1999**, *40*, 7645–7649.
175. Ema, T.; Misawa, S.; Nemugaki, S.; Sakai, T.; Utaka, M. *J. Inorg. Biochem.* **1997**, *67*, 416.
176. Tashiro, K.; Fujiwara, T.; Konishi, K.; Aida, T. *Chem. Commun. (Cambridge)* **1998**, 1121–1122.
177. Tashiro, K.; Konishi, K.; Aida, T. *Angew. Chem., Int. Ed. Engl.* **1997**, *36*, 856–858.
178. Liu, H. Y.; Ying, X.; Hu, X. M.; Gu, Y. L.; Liu, Y.; Huang, J. W.; Ji, L. N. *Chin. Chem. Lett.* **1999**, *10*, 209–212. (CAN 131:164580).
179. Liu, H.-Y.; Huang, J.-W.; Tian, X.; Hu, X.-M.; Ji, L.-N. *Gaodeng Xuexiao Huaxue Xuebao* **1998**, *19*, 511–513. (CAN 129:22523).
180. Zaoying, L.; Jianglin, L.; Cong, L.; Wei, X. *Synth. Commun.* **2000**, *30*, 917–922.
181. Li, Z.-Y.; Liang, J.-L.; Li, C.; Xu, W. *Wuhan Univ. J. Nat. Sci.* **1999**, *4*, 249–250. (CAN 132:151583).
182. Yoshida, N.; Osuka, A. *Tetrahedron Lett.* **2000**, *41*, 9287–9291.
183. Solladié, N.; Gross, M. *Tetrahedron Lett.* **1999**, *40*, 3359–3362.
184. Vidal-Ferran, A.; Muller, C. M.; Sanders, J. K. M. *J. Chem. Soc., Chem. Commun.* **1994**, 2657–2658.
185. Webb, S. J.; Sanders, J. K. M. *Inorg. Chem.* **2000**, *39*, 5920–5929.
186. Arai, T.; Takei, K.; Nishino, N.; Fujimoto, T. *Chem. Commun. (Cambridge)* **1996**, 2133–2134.
187. Mackay, L. G.; Anderson, H. L.; Sanders, J. K. M. *J. Chem. Soc., Chem. Commun.* **1992**, 43–44.
188. Solladié, N.; Hamel, A.; Gross, M. *Tetrahedron Lett.* **2000**, *41*, 6075–6078.
189. Ogoshi, H.; Mizutani, T. *Acc. Chem. Res.* **1998**, *31*, 81–89.
190. Ogoshi, H.; Mizutani, T. *Yuki Gosei Kagaku Kyokaiishi* **1996**, *54*, 906–917.
191. Ogoshi, H.; Kuroda, Y.; Mizutani, T.; Hayashi, T. *Pure Appl. Chem.* **1996**, *68*, 1411–1415.
192. Kuroda, Y.; Ogoshi, H. *Synlett* **1994**, *5*, 319–324.
193. Bonar-Law, R. P.; Mackay, L. G.; Walter, C. J.; Marvaud, V.; Sanders, J. K. M. *Pure Appl. Chem.* **1994**, *66*, 803–810.
194. Suslick, K. S.; Van Deusen-Jeffries, S. In *Comprehensive Supramolecular Chemistry*. Atwood, J. L., Davies, J. E. D., MacNicol, D. D., Vögtle, F., Lehn, J. M. Eds.; Elsevier: Oxford, **1996**; Vol. 5, pp. 141–170.
195. Rose, E.; Quelquejeu, M.; Pandian, R. P.; Lecas-Nawrocka, A.; Vilar, A.; Ricart, G.; Collman, J. P.; Wang, Z.; Straumanis, A. *Polyhedron* **2000**, *19*, 581–586.
196. Che, C.-M.; Yu, W.-Y. *Pure Appl. Chem.* **1999**, *71*, 281–288.
197. Campbell, L. A.; Kodadek, T. *J. Mol. Catal. A: Chem.* **1996**, *113*, 293–310.
198. Gonsalves, A. M. D. R.; Pereira, M. M. *J. Mol. Catal. A: Chem.* **1996**, *113*, 209–221.
199. Collman, J. P.; Zhang, X.; Lee, V. J.; Uffelman, E. S.; Brauman, J. I. *Science (Washington, D. C., 1883-)* **1993**, *261*, 1404–1411.
200. Inoue, S.; Aida, T.; Konishi, K. *J. Mol. Catal.* **1992**, *74*, 121–129.
201. Meunier, B. *Chemtracts: Inorg. Chem.* **1991**, *3*, 120–123.
202. Gupta, A. D.; Bhuniya, D.; Singh, V. K. *J. Indian Inst. Sci.* **1994**, *74*, 71–89. (CAN 122:105537).
203. Naruta, Y. *Metalloporphyrins Catal. Oxid.* **1994**, 241–259.
204. Halterman, R. L. *Transition Met. Org. Synth.* **1998**, *2*, 300–306.
205. Katsuki, T. *Curr. Org. Chem.* **2001**, *5*, 663–678.
206. Robert, A.; Meunier, B. *Biomimetic Oxid. Catal. Transition Met. Complexes* **2000**, 543–562.
207. Boschi, T.; Licoccia, S.; Paolesse, R.; Tagliatesta, P. *Catal. Met. Complexes* **1994**, *17 (Metalloporphyrins Catalyzed Oxidations)*, 239–267.
208. Battioni, P.; Renaud, J. P.; Bartoli, J. F.; Reina-Artiles, M.; Fort, M.; Mansuy, Daniel. *J. Am. Chem. Soc.* **1988**, *110*, 8462–8470.
209. Maillard, P.; Guerquin-Kern, J. L.; Momenteau, M. *Tetrahedron Lett.* **1991**, *32*, 4901–4904.
210. Ohkatsu, Y.; Watanabe, T.; Hayakawa, M. *Nihon Yukagakkaiishi* **1998**, *47*, 577–584. (CAN 129:172337).

211. Berkessel, A.; Frauenkron, M. *J. Chem. Soc., Perkin Trans. 1* **1997**, 2265–2266. Erratum: *ibid.*, **1998**, 629.
212. Lai, T.-S.; Zhang, R.; Cheung, K.-K.; Che, C.-M.; Lai, T.-S.; Kwong, H.-L. *Chem. Commun. (Cambridge)* **1998**, 1583–1584.
213. Lai, T.-S.; Kwong, H.-L.; Zhang, R.; Che, C.-M. *J. Chem. Soc., Dalton Trans.* **1998**, 3559–3564.
214. Naruta, Y.; Tani, F.; Ishihara, N.; Maruyama, K. *J. Am. Chem. Soc.* **1991**, *113*, 6865–6872.
215. Naruta, Y.; Tani, F.; Maruyama, K. *Tetrahedron Lett.* **1992**, *33*, 6323–6326.
216. Naruta, Y.; Ishihara, N.; Tani, F.; Maruyama, K. *Bull. Chem. Soc. Jpn.* **1993**, *66*, 158–166.
217. Zhang, R.; Yu, W.-Y.; Lai, T.-S.; Che, C.-M. *Chem. Commun. (Cambridge)* **1999**, 409–410. Erratum: *ibid.* **1999**, 757.
218. Collman, J. P.; Wang, Z.; Linde, C.; Fu, L.; Dang, L.; Brauman, J. I. *Chem. Commun. (Cambridge)* **1999**, 1783–1784.
219. Gross, Z.; Ini, S. *Inorg. Chem.* **1999**, *38*, 1446–1449.
220. Gross, Z.; Ini, S. *Org. Lett.* **1999**, *1*, 2077–2080.
221. Gross, Z.; Ini, S.; Kapon, M.; Cohen, S. *Tetrahedron Lett.* **1996**, *37*, 7325–7328.
222. Gross, Z.; Ini, S. *J. Org. Chem.* **1997**, *62*, 5514–5521.
223. Pérollier, C.; Pécaut, J.; Ramasseul, R.; Marchon, J.-C. *Inorg. Chem.* **1999**, *38*, 3758–3759.
224. Groves, J. T.; Viski, P. *J. Am. Chem. Soc.* **1989**, *111*, 8537–8538.
225. Zhang, R.; Yu, W.-Y.; Lai, T.-S.; Che, C.-M. *Chem. Commun. (Cambridge)* **1999**, 1791–1792. Erratum: *ibid.* **1999**, 2441.
226. Sagawa, T.; Ishida, H.; Urabe, K.; Yoshinaga, K.; Ohkubo, K. *J. Chem. Soc., Perkin Trans. 2* **1993**, 1–5.
227. Sagawa, T.; Ishida, H.; Urabe, K.; Ohkubo, K. *Chem. Lett.* **1991**, 2083–2086.
228. Le Maux, P.; Bahri, H.; Simonneaux, G. *J. Chem. Soc., Chem. Commun.* **1994**, 1287–1288.
229. Le Maux, P.; Bahri, H.; Simonneaux, G.; Toupet, L. *Inorg. Chem.* **1995**, *34*, 4691–4697.
230. Halterman, R. L.; Jan, S. T.; Nimmons, H. L. *Synlett* **1991**, 791–792.
231. Naruta, Y.; Tani, F.; Maruyama, K. *J. Chem. Soc., Chem. Commun.* **1990**, 1378–1380.
232. Naruta, Y.; Tani, F.; Maruyama, K. *Tetrahedron: Asymmetry* **1991**, *2*, 533–542.
233. Chiang, L. C.; Konishi, K.; Aida, T.; Inoue, S. *J. Chem. Soc., Chem. Commun.* **1992**, 254–256.
234. Zhou, X.-G.; Yu, X.-Q.; Huang, J.-S.; Che, C.-M. *Chem. Commun. (Cambridge)* **1999**, 2377–2378.
235. Lai, T.-S.; Che, C.-M.; Kwong, H.-L.; Peng, S.-M. *Chem. Commun. (Cambridge)* **1997**, 2373–2374.
236. Simonato, J.-P.; Pécaut, J.; Marchon, J.-C.; Scheidt, W. R. *Chem. Commun. (Cambridge)* **1999**, 989–990.
237. O'Malley, S.; Kodadek, T. *Tetrahedron Lett.* **1991**, *32*, 2445–2448.
238. Maxwell, J. L.; O'Malley, S.; Brown, K. C.; Kodadek, T. *Organometallics* **1992**, *11*, 645–652.
239. Galardon, E.; Le Maux, P.; Simonneaux, G. *Chem. Commun. (Cambridge)* **1997**, 927–928.
240. Galardon, E.; Roue, S.; Le Maux, P.; Simonneaux, G. *Tetrahedron Lett.* **1998**, *39*, 2333–2334.
241. Frauenkron, M.; Berkessel, A. *Tetrahedron Lett.* **1997**, *38*, 7175–7176. Erratum: *ibid.* **1998**, *39*, 727.
242. Lo, W.-C.; Che, C.-M.; Cheng, K.-F.; Mak, T. C. W. *Chem. Commun. (Cambridge)* **1997**, 1205–1206. Erratum: *ibid.* **1997**, 2249.
243. Gross, Z.; Galili, N.; Simkhovich, L. *Tetrahedron Lett.* **1999**, *40*, 1571–1574.
244. Che, C.-M.; Huang, J.-S.; Lee, F.-W.; Li, Y.; Lai, T.-S.; Kwong, H.-L.; Teng, P.-F.; Lee, W.-S.; Lo, W.-C.; Peng, S.-M.; Zhou, Z.-Y. *J. Am. Chem. Soc.* **2001**, *123*, 4119–4129.
245. Ogoshi, H.; Mizutani, T. *Curr. Opin. Chem. Biol.* **1999**, *3*, 736–739.
246. Mazzanti, M.; Veyrat, M.; Ramasseul, R.; Marchon, J.-C.; Turowska-Tyrk, I.; Shang, M.; Scheidt, W. R. *Inorg. Chem.* **1996**, *35*, 3733–3734.
247. Bonar-Law, R. P.; Sanders, J. K. M. *J. Am. Chem. Soc.* **1995**, *117*, 259–271.
248. Toronto, D.; Sarrazin, F.; Pécaut, J.; Marchon, J.-C.; Shang, M.; Scheidt, W. R. *Inorg. Chem.* **1998**, *37*, 526–532.
249. Inamo, M.; Yoneda, I. *Inorg. Chem. Commun.* **1999**, *2*, 331–333.
250. Simonato, J.-P.; Pécaut, J.; Marchon, J.-C. *Inorg. Chim. Acta* **2001**, *315*, 240–244.
251. Simonato, J.-P.; Chappellet, S.; Pécaut, J.; Baret, P.; Marchon, J.-C. *New J. Chem.* **2001**, *25*, 714–720.
252. Simonato, J.-P.; Pécaut, J.; Marchon, J.-C. *J. Am. Chem. Soc.* **1998**, *120*, 7363–7364.
253. Livoreil, A.; Hayashi, T.; Sauvage, J. P.; Ogoshi, H. *J. Inorg. Biochem.* **1997**, *67*, 117.
254. Ogoshi, H.; Ema, T.; Kato, Y.; Mizutani, T.; Kuroda, Y. *Supramol. Chem.* **1995**, *6*, 115–124.
255. Aoyama, Y.; Uzawa, T.; Saita, K.; Tanaka, Y.; Toi, H.; Ogoshi, H.; Okamoto, Y. *Tetrahedron Lett.* **1988**, *29*, 5271–5274.
256. Aoyama, Y.; Yamagishi, A.; Asagawa, M.; Toi, H.; Ogoshi, H. *J. Am. Chem. Soc.* **1988**, *110*, 4076–4077.
257. Crossley, M. J.; Mackay, L. G.; Try, A. C. *J. Chem. Soc., Chem. Commun.* **1995**, 1925–1927.
258. Zheng, J.-Y.; Konishi, K.; Aida, T. *Tetrahedron* **1997**, *53*, 9115–9122.
259. Kuroda, Y.; Kato, Y.; Higashioji, T.; Ogoshi, H. *Angew. Chem., Int. Ed. Engl.* **1993**, *32*, 723–724.
260. Morice, C.; Le Maux, P.; Simonneaux, G.; Toupet, L. *J. Chem. Soc., Dalton Trans.* **1998**, 4165–4172.
261. Galardon, E.; Le Maux, P.; Bondon, A.; Simonneaux, G. *Tetrahedron: Asymmetry* **1999**, *10*, 4203–4210.
262. Bonar-Law, R. P. *J. Am. Chem. Soc.* **1995**, *117*, 12397–12407.
263. Mizutani, T.; Ema, T.; Tomita, T.; Kuroda, Y.; Ogoshi, H. *J. Am. Chem. Soc.* **1994**, *116*, 4240–4250.
264. Wang, C.-Z.; Zhu, Z.-A.; Li, Y.; Chen, R.-T.; Wen, X.; Miao, F.-M.; Chan, A. S. C. *Gaodeng Xuexiao Huaxue Xuebao* **2001**, *22*, 262–264. (AN 2001:315720).
265. Morice, C.; Le Maux, P.; Simonneaux, G. *Tetrahedron Lett.* **1996**, *37*, 6701–6704.
266. Morice, C.; Le Maux, P.; Moinet, C.; Simonneaux, G. *Inorg. Chim. Acta* **1998**, *273*, 142–150.
267. Huang, X.; Rickman, B. H.; Borhan, B.; Berova, N.; Nakanishi, K. *J. Am. Chem. Soc.* **1998**, *120*, 6185–6186.
268. Furusho, Y.; Kimura, T.; Mizuno, Y.; Aida, T. *J. Am. Chem. Soc.* **1997**, *119*, 5267–5268.
269. Mizuno, Y.; Aida, T.; Yamaguchi, K. *J. Am. Chem. Soc.* **2000**, *122*, 5278–5285.
270. Sugasaki, A.; Ikeda, M.; Takeuchi, M.; Robertson, A.; Shinkai, S. *J. Chem. Soc., Perkin Trans. 1* **1999**, 3259–3264.
271. Bellacchio, E.; Lauceri, R.; Gurrieri, S.; Scolaro, L. M.; Romeo, A.; Purrello, R. *J. Am. Chem. Soc.* **1998**, *120*, 12353–12354.
272. Borovkov, V. V.; Lintuluoto, J. M.; Inoue, Y. *Org. Lett.* **2000**, *2*, 1565–1568.
273. Borovkov, V. V.; Lintuluoto, J. M.; Fujiki, M.; Inoue, Y. *J. Am. Chem. Soc.* **2000**, *122*, 4403–4407.
274. Borovkov, V. V.; Lintuluoto, J. M.; Inoue, Y. *J. Phys. Chem. A* **2000**, *104*, 9213–9219.
275. Purrello, R.; Raudino, A.; Scolaro, L. M.; Loisi, A.; Bellacchio, E.; Lauceri, R. *J. Phys. Chem. B* **2000**, *104*, 10900–10908. Erratum: *ibid.* **2001**, *105*, 2474.

276. Borovkov, V. V.; Lintuluoto, J. M.; Inoue, Y. *J. Am. Chem. Soc.* **2001**, *123*, 2979–2989.
277. Borovkov, V. V.; Yamamoto, N.; Lintuluoto, J. M.; Tanaka, T.; Inoue, Y. *Chirality* **2001**, *13*, 329–335.
278. Ito, A.; Konishi, K.; Aida, T. *Tetrahedron Lett.* **1996**, *37*, 2585–2588.
279. Hamada, T.; Ishida, H.; Kuwada, M.; Ohkubo, K. *Chem. Lett.* **1992**, 1283–1286.
280. Niedercorn, F.; Ledon, H.; Tkatchenko, I. *New J. Chem.* **1988**, *12*, 897–906.
281. Huang, X.; Nakanishi, K.; Berova, N. *Chirality* **2000**, *12*, 237–255.
282. Tsukube, H.; Shinoda, S. *Enantiomer* **2000**, *5*, 13–22.
283. Peng, X.; Le, Z.; Cai, J. *Huaxue Jinzhan* **1999**, *11*, 327–332. (CAN 131:348602; AN 1999:623395).
284. Shinoda, S. *Kagaku (Kyoto)* **1997**, *52*, 66–67. (CAN 126:196464; AN 1997:104488).
285. Tamiaki, H.; Maruyama, K. *Chem. Lett.* **1993**, 1499–1502.
286. Kato, T.; Uchiyama, M.; Maruo, N.; Arai, T.; Nishino, N. *Chem. Lett.* **2000**, 144–145.
287. Kato, T.; Maruo, N.; Akisada, H.; Arai, T.; Nishino, N. *Chem. Lett.* **2000**, 890–891.
288. Maruo, N.; Uchiyama, M.; Kato, T.; Arai, T.; Nishino, N.; Akisada, H. *Chem. Commun. (Cambridge)* **1999**, 2057–2058.
289. Maruo, N.; Nishino, N. *Kobunshi Ronbunshu* **1997**, *54*, 731–737. (CAN 128:22745).
290. Csik, G.; Balog, E.; Voszka, I.; Tolgyesi, F.; Oulmi, D.; Maillard, P.; Momenteau, M. *J. Photochem. Photobiol., B* **1998**, *44*, 216–224.
291. Oulmi, D.; Maillard, P.; Vever-Bizet, C.; Momenteau, M.; Brault, D. *Photochem. Photobiol.* **1998**, *67*, 511–518.
292. Matile, S.; Berova, N.; Nakanishi, K.; Fleischhauer, J.; Woody, R. W. *J. Am. Chem. Soc.* **1996**, *118*, 5198–5206.
293. Matile, S.; Berova, N.; Nakanishi, K. *Enantiomer* **1996**, *1*, 1–12.
294. Matile, S.; Berova, N.; Nakanishi, K. *Chem. Biol.* **1996**, *3*, 379–392.
295. Ouyang, J.-M.; Zhang, Z.-M.; Gu, Z.-J. *Spectrosc. Lett.* **2000**, *33*, 633–642.
296. Barnes, N. R.; Schreiner, A. F.; Dolan, M. A. *J. Inorg. Biochem.* **1998**, *72*, 1–12.
297. Teraoka, J.; Yamamoto, N.; Matsumoto, Y.; Kyogoku, Y.; Sugeta, H. *J. Am. Chem. Soc.* **1996**, *118*, 8875–8878.
298. Liu, H.; Ying, X.; Hu, X.; Liu, Y.; Huang, J.; Huang, J.; Ji, L.; Yao, Z.; Zhang, J. *Guangpuxue Yu Guangpu Fenxi* **2000**, *20*, 495–497. (CAN 133:341872).
299. Beeby, A.; Dickins, R. S.; Fitzgerald, S.; Govenlock, L. J.; Parker, D.; Williams, J. A. G.; Maupin, C. L.; Riehl, J. P.; Siligardi, G. *Chem. Commun. (Cambridge)* **2000**, 1183–1184.
300. Arimori, S.; Takeuchi, M.; Shinkai, S. *Chem. Lett.* **1996**, 77–78.
301. Takeuchi, M.; Imada, T.; Shinkai, S. *Bull. Chem. Soc. Jpn.* **1998**, *71*, 1117–1123.
302. Kurtan, T.; Nesnas, N.; Li, Y.-Q.; Huang, X.; Nakanishi, K.; Berova, N. *J. Am. Chem. Soc.* **2001**, *123*, 5962–5973.
303. Kurtan, T.; Nesnas, N.; Koehn, F. E.; Li, Y.-Q.; Nakanishi, K.; Berova, N. *J. Am. Chem. Soc.* **2001**, *123*, 5974–5982.
304. Tashiro, K.; Konishi, K.; Aida, T. *J. Am. Chem. Soc.* **2000**, *122*, 7921–7926.
305. Sugasaki, A.; Ikeda, M.; Takeuchi, M.; Shinkai, S. *Angew. Chem., Int. Ed. Engl.* **2000**, *39*, 3839–3842.
306. Tomizaki, K.-Y.; Nishino, H.; Kato, T.; Miike, A.; Nishino, N. *Chem. Lett.* **2000**, 648–649.
307. Tomizaki, K.-Y.; Murata, T.; Kaneko, K.; Miike, A.; Nishino, N. *J. Chem. Soc., Perkin Trans. 2* **2000**, 1067–1074.
308. Mihara, H.; Sakamoto, S.; Haruta, Y.; Aoyagi, H. *Pept. Chem.* **1995**, *33*, 517–520.
309. Nimri, S.; Keinan, E. *J. Am. Chem. Soc.* **1999**, *121*, 8978–8982.
310. Csik, G.; Balog, E.; Voszka, I.; Tolgyesi, F.; Oulmi, D.; Maillard, P.; Momenteau, M. *J. Photochem. Photobiol., B* **1998**, *44*, 216–224.
311. Voszka, I.; Galantai, R.; Maillard, P.; Csik, G. *J. Photochem. Photobiol., B* **1999**, *52*, 92–98.
312. Momenteau, M.; Maillard, P.; De Belinay, M.-A.; Carrez, D.; Croisy, A. *J. Biomed. Opt.* **1999**, *4*, 298–318.
313. Carre, V.; Jayat, C.; Granet, R.; Krausz, P.; Guilloton, M. *Photochem. Photobiol.* **1999**, *69*, 55–60.
314. Takahashi, M.; Ueno, A.; Mihara, H. *Pept. Sci.* **1999**, *36*, 395–396.
315. Takahashi, M.; Ueno, A.; Uda, T.; Mihara, H. *Bioorg. Med. Chem. Lett.* **1998**, *8*, 2023–2026.
316. Tetreau, C.; Boitrel, B.; Rose, E.; Lavalette, D. *J. Chem. Soc., Chem. Commun.* **1989**, 1805–1806.
317. Konishi, K.; Sugino, T.; Aida, T.; Inoue, S. *J. Am. Chem. Soc.* **1991**, *113*, 6487–6491.
318. Konishi, K.; Kimata, S.-I.; Yoshida, K.; Tanaka, M.; Aida, T. *Angew. Chem., Int. Ed. Engl.* **1996**, *35*, 2823–2825.
319. Ishida, Y.; Konishi, K.; Aida, T.; Nagammune, T. *Chem.-Eur. J.* **1998**, *4*, 1148–1153.
320. Barnard, G. F.; Akhtar, M. *J. Chem. Soc., Perkin Trans. 1* **1979**, 2354–2360.
321. Poignant, G.; Bourseul, A.; Geze, C.; Le Plouzenec, M.; Le Maux, P.; Bondon, A.; Simonneaux, G.; Moinet, C.; Vonarx, V.; Patrice, T. *Tetrahedron Lett.* **1996**, *37*, 7511–7514.
322. Sakamoto, M.; Ueno, A.; Mihara, H. *Chem.-Eur. J.* **2001**, *7*, 2449–2458.
323. Purrello, R.; Scolaro, L. M.; Bellacchio, E.; Gurrieri, S.; Romeo, A. *Inorg. Chem.* **1998**, *37*, 3647–3648.
324. Rosengarten, B.; Botcher, C.; Schulz, A.; Fuhrhop, J.-H.; Siggel, U. *J. Porphyrins Phthalocyanines* **1998**, *2*, 273–284.
325. Fan, J.; Whiteford, J. A.; Olenyuk, B.; Levin, M. D.; Stang, P. J.; Fleischer, E. B. *J. Am. Chem. Soc.* **1999**, *121*, 2741–2752.
326. Kimura, M.; Kitamura, T.; Sano, M.; Muto, T.; Hanabusa, K.; Shirai, H.; Kobayashi, N. *New J. Chem.* **2000**, *24*, 113–114.
327. Fuhrhop, J. H.; Demoulin, C.; Boettcher, C.; Koening, J.; Siggel, U. *J. Am. Chem. Soc.* **1992**, *114*, 4159–4165.
328. Rubires, R.; Farrera, J.-A.; Ribo, J. M. *Chem.-Eur. J.* **2001**, *7*, 436–446.
329. Ribo, J. M.; Crusats, J.; Sagues, F.; Claret, J.; Rubires, R. *Science (Washington, DC, U. S.)* **2001**, *292*, 2063–2066.
330. Babushkina, T. A.; Kirillova, G. V.; Ponomarev, G. V. *Khim. Geterotsikl. Soedin.* **1996**, 198–204. (CAN 125:142409).
331. Jentzen, W.; Simpson, M. C.; Hobbs, J. D.; Song, X.; Ema, T.; Nelson, N. Y.; Medforth, C. J.; Smith, K. M.; Veyrat, M.; Mazzanti, M.; Ramasseul, R.; Marchon, J. C.; Takeuchi, T.; Goddard, W. A. III; Shelnutt, J. A. *J. Am. Chem. Soc.* **1995**, *117*, 11085–11097.
332. Simonato, J.-P.; Pécaut, J.; Marchon, J.-C. *Inorg. Chim. Acta* **2000**, *304*, 288–292.
333. Mazzanti, M.; Marchon, J.-C.; Shang, M.; Scheidt, W. R.; Jia, S.; Shelnutt, J. A. *J. Am. Chem. Soc.* **1997**, *119*, 12400–12401.
334. Gazeau, S.; Pécaut, J.; Marchon, J. C. *Chem. Comm.* **2001**, 1644–1645.
335. Gazeau, S.; Pécaut, J.; Marchon, J. C. *Compt. Rend. Acad. Sci., Sér. IIC, Chimie* **2002**, *5*, 27–31.
336. Wolowiec, S.; Latos-Grazynski, L.; Mazzanti, M.; Marchon, J.-C. *Inorg. Chem.* **1997**, *36*, 5761–5771.
337. Mazzanti, M.; Marchon, J.-C.; Wojaczynski, J.; Wolowiec, S.; Latos-Grazynski, L.; Shang, M.; Scheidt, W. R. *Inorg. Chem.* **1998**, *37*, 2476–2481.
338. Simonato, J.-P.; Pécaut, J.; Le Pape, L.; Oddou, J.-L.; Jeandey, C.; Shang, M.; Scheidt, W. R.; Wojaczynski, J.; Wolowiec, S.; Latos-Grazynski, L.; Marchon, J.-C. *Inorg. Chem.* **2000**, *39*, 3978–3987.
339. Pécaut, J.; Pérollier, C.; Ramasseul, R.; Marchon, J.-C. *Compt. Rend. Acad. Sci., Sér. IIC, Chimie* **2000**, *3*, 743–746.

340. Gazeau, S.; Pécaut, J.; Haddad, R.; Shelnut, J. A.; Marchon, J. C. *Eur. J. Inorg. Chem.* **2002**, 2956–2960.
341. Toronto, D.; Marchon, J. C. *PCT Int. Appl.* **1998**, 30 pp. CODEN: PIXXD2 WO 9840758 A1 19980917. Application: WO 98-FR492 19980311. Priority: FR 97-2940 19970312. (CAN 129:260858; AN 1998:624035)
342. Claeys-Bruno, M.; Bardet, M.; Marchon, J. C. *Compt. Rend. Acad. Sci., Sér. IIC, Chimie* **2002**, 5, 21–25.
343. Claeys-Bruno, M.; Toronto, D.; Pécaut, J.; Bardet, M.; Marchon, J. C. *J. Am. Chem. Soc.* **2001**, 123, 11067–11068.
344. Wojaczynski, J.; Latos-Grazynski, L.; Olmstead, M. M.; Balch, A. L. *Inorg. Chem.* **1997**, 36, 4548–4554.
345. Wojaczynski, J.; Latos-Grazynski, L.; Chmielewski, P. J.; Van Calcar P.; Balch, A. L. *Inorg. Chem.* **1999**, 38, 3040–3050.
346. Tessier, J. *Chem. Ind. (London)* **1984**, 199–204.
347. Liu, S. Q.; Pécaut, J.; Marchon, J. C. *Eur. J. Inorg. Chem.* **2002**, 1823–1826.
348. Claeys-Bruno, M.; Bardet, M.; Marchon, J. C. *Magn. Reson. Chem.* **2002**, 40, 647–652.



# Carbene Complexes of Metalloporphyrins and Heme Proteins

65

GÉRARD SIMONNEAUX<sup>a</sup> and PAUL LE MAUX<sup>b</sup>

<sup>a</sup>Organométallique et Catalyse, Chimie et Moléculaires, Université de Rennes 1, 35042 Rennes, France

<sup>b</sup>Laboratoire de Chimie Organométallique et Biologique, UMR CNRS 6509, Institut de Chimie, Université de Rennes 1, 35042 Rennes cedex, France

I. Introduction . . . . .	134
A. Carbenes . . . . .	134
B. Metal–Carbene Binding . . . . .	134
II. Structure and Bonding . . . . .	134
A. X-ray Methods . . . . .	134
B. Spectroscopic Characterization . . . . .	135
C. Metal–Carbene Formalism . . . . .	135
III. Methods of Synthesis of Metal–Carbene Bond in Porphyrins . . . . .	136
A. Preparation from Polyhalogenated Precursors Under Reducing Conditions . . . . .	136
B. Preparation from Diazo Compounds . . . . .	137
C. Preparation from Zero-Valent Metalloporphyrin Dianions . . . . .	137
D. Preparation from Isonitrile Complexes . . . . .	137
E. Preparation from Iodonium Ylide . . . . .	138
F. Insertion of Zero-Valent Metals into the C–N Bond of <i>N,N'</i> -Bridged Porphyrins . . . . .	138
IV. Synthetic Metal–Carbene Porphyrin Derivatives and Their Reactivity . . . . .	139
A. Group 6 . . . . .	139
B. Group 7 . . . . .	139
1. Manganese . . . . .	139
C. Group 8 . . . . .	139
1. Iron . . . . .	139
2. Ruthenium . . . . .	143
3. Osmium . . . . .	145
D. Group 9 . . . . .	146
1. Cobalt . . . . .	146
2. Rhodium . . . . .	147
E. Group 10 . . . . .	148
1. Nickel . . . . .	148
F. Group 11 . . . . .	148
1. Copper . . . . .	148
G. Group 12 . . . . .	148
1. Zinc . . . . .	148
V. Metalloporphyrins as Catalysts for Carbene Transfer . . . . .	148
A. Cyclopropanation . . . . .	148
B. Insertion . . . . .	150
C. Sigmatropic Rearrangements . . . . .	151
D. Olefination of Aldehydes . . . . .	152
VI. Carbenes as Ligands to Heme Proteins . . . . .	152
A. Cytochromes P450 . . . . .	152
B. Myoglobin and Hemoglobin . . . . .	155
Conclusion . . . . .	156
References . . . . .	156

## I. Introduction

### A. CARBENES

Carbenes are divalent species possessing two non-bonding electrons, either paired or unpaired.<sup>1,2</sup> The multiplicity of their ground state is thus either singlet  $S_0$  or triplet  $T_1$ .<sup>3,4</sup> Triplet carbenes can be considered as diradicals and singlet carbenes are electron deficient species which possess a nonbonding pair of electrons. The nature of the ground state ( $S_0$  or  $T_1$ ) depends on the ability of the adjacent groups to withdraw electrons from, or to supply electrons to, the carbene atoms. Thus, electronegative substituents will favor a singlet ground state.<sup>1,4</sup> Heteroatom donor groups on a carbene center render the originally degenerate orbitals on carbon unequal in energy, thus enhancing the nucleophilicity. Stable compounds in the carbene category have been made recently and definite structural and electronic information is now available.<sup>2,5,6</sup> The basic principles of "free" carbene reactivity in organic synthesis are outside of the purpose of this chapter and there is an extensive literature on carbenes which is too vast to be cited in its entirety here.<sup>1-4,7-9</sup>

### B. METAL-CARBENE BINDING

It has been well known for several decades that divalent carbon species of the type:  $CR^1R^2$ , where one of the two substituents at the carbene carbon atom is bonded via a heteroatom ( $R^1 = \text{alkyl}$ ,  $R^2 = \text{OR}$ ,  $\text{NR}_2$ ) exhibit  $\sigma$ -donor and  $\pi$ -acceptor properties upon binding to transition metals.<sup>10</sup> In general, a "double bond," between the metal and the carbon results, depending somewhat on the nature of  $R^1$  and  $R^2$  groups. More generally, the literature discriminates between electrophilic (Fisher) carbenes<sup>10</sup> and nucleophilic (Schrock) carbenes.<sup>11,12</sup>

Comprehensive reviews on metal-carbene compounds in organometallic chemistry are available<sup>1,12-18</sup> and this general topic will not be discussed here. We shall rather focus on the metalloporphyrin and heme protein area.

This chapter is subdivided into five parts which correspond to the major aspects of carbene complexation involving metal porphyrin models and heme proteins. The chapter is organized as follows: Part 1 deals with structure and bonding properties of metal-carbene porphyrins; Part 2 is devoted to methods of synthesis of metal-carbene bonded complexes in porphyrins; Part 3 summarizes the synthesis and reactivity of synthetic carbene metalloporphyrins; Part 4 reviews various reactions involving carbene transfers catalyzed by metal porphyrins and Part 5 covers the coordination chemistry of carbene-heme proteins. Abbreviations are summarized in Table 1.

## II. Structure and Bonding

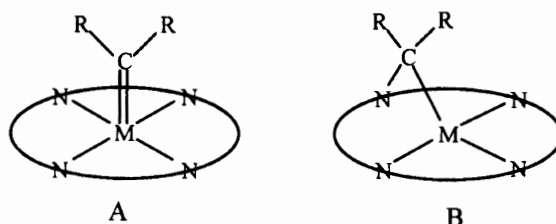
### A. X-RAY METHODS

From the reactions of various carbene precursors, it appears that the nature of the adduct depends on the nature of the coordinating metal and even on the nature of the porphyrin. Two main binding modes are possible as shown in Scheme 1. The carbene is an axial metalloporphyrin ligand or is inserted into a nitrogen-metal bond. These two structural types have been established by single-crystal X-ray crystallography. Structural data for carbene-metal porphyrin complexes are summarized in Table 2. Although a large series of carbene complexes of metalloporphyrins have been synthesized, only a few of the compounds have been characterized by single-crystal X-ray diffraction analysis. For the compounds of the group 6 (Fe, Ru, and Os), there is a complete series. Two papers dealing with the theoretical interaction of metalloporphyrins with carbenes to give axial-metal or nitrogen-metal inserted complexes have been published.<sup>19,20</sup>

Turning to the metal-carbene complexes where the carbene is inserted into one of the metal-nitrogen bonds, structural data are also available.<sup>21-23</sup> In these complexes (Ni and Fe), the porphyrin macrocycle is largely distorted and the metal is bound to three of the four pyrrole nitrogens and the carbene carbon (and chloride in

**Table 1.** List of Abbreviations

Abbreviation	Name
(TPP)H <sub>2</sub>	Tetraphenylporphyrin
(TTP)H <sub>2</sub>	Tetratolylporphyrin
(TPFPP)H <sub>2</sub>	Tetrapentafluorophenylporphyrin
(T- <i>p</i> -ClPP)H <sub>2</sub>	Tetra- <i>p</i> -chlorophenylporphyrin
(TMP)H <sub>2</sub>	Tetramesitylporphyrin
(OEP)H <sub>2</sub>	Octaethylporphyrin



**Scheme 1**

**Table 2.** X-ray Structural Data for Axial Carbene and Carbide Complexes of Metalloporphyrins

Complex	Molecular parameters <sup>a</sup>	Reference
(TPP)Fe(CCl <sub>2</sub> )(H <sub>2</sub> O)	Fe–C 1.83(3) Fe–N <sup>b</sup> 1.984(4) Fe–O 2.13(3)	60
(TPP)Ru[C(CO <sub>2</sub> Et) <sub>2</sub> ](THF)	Ru–C 1.829(9) Ru–N <sup>b</sup> 2.046(6) Ru–O 2.293(6)	51
(P*)Ru(CPh <sub>2</sub> ) <sup>c</sup>	Ru–C 1.860(6) Ru–N <sup>b</sup> 2.044(5)	52
(P*)Ru[C(Ph)(CO <sub>2</sub> CH <sub>2</sub> CH=CH <sub>2</sub> ) <sup>c</sup>	Ru–C 1.847(3) Ru–N <sup>b</sup> 2.037(2)	52
(TTP)(Os(CHSiMe <sub>3</sub> )(THF)	Os–C 1.79(2) Os–N <sup>c</sup> 2.034(4) Os–O 2.328(3)	105
(TTP)Os[C(C <sub>6</sub> H <sub>4</sub> - <i>p</i> -Me <sub>3</sub> ) <sub>2</sub> ](THF)	Os–C 1.865(5) Os–N <sup>b</sup> 2.050(7) Os–O 2.328(3)	105
(TPFPP)Os(CPh <sub>2</sub> )	Os–C 1.870(2) Os–N <sup>b</sup> 2.041(2)	27
(TPFPP)Os(CPh <sub>2</sub> ) <sub>2</sub>	Os–C 2.035(2) Os–C 2.027(3) Os–N <sup>b</sup> 2.044(2)	27
(TPP)Rh[C(NHCH <sub>2</sub> Ph) <sub>2</sub> ] (CNCH <sub>2</sub> Ph)PF <sub>6</sub>	Rh–C 2.030(11) Rh–N 2.039(10) Rh–C 2.064(13)	55
[(TPP)Fe] <sub>2</sub> C	Fe–C 1.675(4) Fe–N 1.980(4)	69
(TPP)FeCRe(CO) <sub>4</sub> Re(CO) <sub>5</sub>	Fe–C 1.605(13) Fe–N 1.982(10) Re–C 1.957(12)	71

<sup>a</sup>Bond lengths are reported in Å.<sup>b</sup>Average value.<sup>c</sup>P\* is the dianion of 5,10,15,20-tetrakis-[(1*S*,4*R*,5*R*,8*S*)-1,2,3,4,5,6,7,8-octa-hydro-1,4:5,8-dimethano anthracene-9-yl] porphyrin.

the iron complex) (Table 3). In the cobalt complex, two ethoxycarbonylmethylene groups are inserted between the metal and the nitrogen atoms of two different pyrrole rings.<sup>24</sup>

## B. SPECTROSCOPIC CHARACTERIZATION

The <sup>13</sup>C chemical shifts of the carbene complex vary from 210 to 315 ppm in the iron series (Table 4). These large differences have been interpreted by taking into account the more electrophilic nature of the carbene atom due to a possible stabilization of a positive charge by an alkyl group in some cases (Scheme 2).<sup>25</sup> An increase of the chemical shift is also noted in going from the mono-carbene to the *bis*-carbene adduct.<sup>26,27</sup> For example in Table 4, the <sup>13</sup>C chemical shift of the diphenyl carbene increases from 273.6 to 313.8 ppm with osmium

**Table 3.** X-ray Structural Data for M–N Inserted Carbene Complexes of Metalloporphyrins

Complex	Molecular parameters <sup>a</sup>	Reference
(TPP)Ni[CH(CO <sub>2</sub> Et)]	Ni–C 1.905(4) Ni–N 1.911(3) Ni–N 1.910(3) Ni–N 1.905(4)	21
(TPP)Fe[C=C( <i>p</i> -ClC <sub>6</sub> H <sub>4</sub> ) <sub>2</sub> ]Cl	Fe–C 1.914(7) Fe–N 1.990(5) Fe–Cl 2.290(2)	22
(TPP)Fe[C=C( <i>p</i> -ClC <sub>6</sub> H <sub>4</sub> ) <sub>2</sub> ]Cl	Fe–C 1.921(5) Fe–N 2.002(4) Fe–N 1.991(4) Fe–N 1.985(4) Fe–Cl 2.299(1)	23
(OEP)Co(CHCO <sub>2</sub> Et) <sub>2</sub> (NO <sub>3</sub> <sup>−</sup> )	Co–C 1.98(1) Co–C 2.00(1) Co–N 1.90(1) Co–N 1.93(1)	24

<sup>a</sup>Bond lengths are reported in Å.

porphyrins.<sup>27</sup> This may be related to a concomitant increase of the reactivity toward nucleophilic olefins.<sup>27</sup>

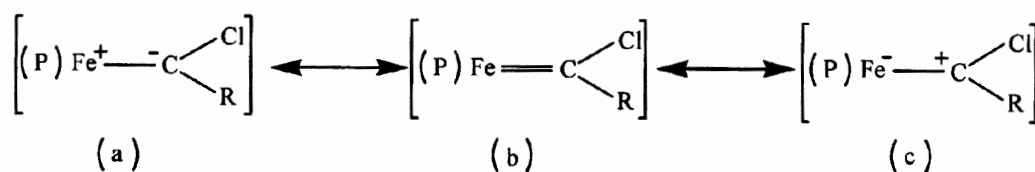
Hyperporphyrin spectra, showing a “split Soret” band for carbene complexes of metalloporphyrins have been predicted.<sup>28</sup> Actually, addition of alkylthiolates to (TPP)Fe(II)[C=C(*p*-Cl-C<sub>6</sub>H<sub>4</sub>)<sub>2</sub>] resulted in the formation of an hyperporphyrin spectrum with Soret peaks at  $\lambda = 385$  and 461 nm.<sup>29</sup> A hyperporphyrin spectrum has also been reported for (TPP)Mn(CCl<sub>2</sub>) in the presence of added thiol.<sup>30</sup> The position of the redshifted Soret peak in the iron complex is very close to that reported for carbene complexes of cytochrome P450<sup>31,32</sup> and confirms the ligation of a cysteinyl axial ligand *trans* to the carbene in the cytochrome P450 complex. Such a result is characteristic of sulfur binding to metalloporphyrins containing a strong iron–carbon bond. This was first reported for carbon monoxide complexation to cytochrome P450Fe(II).<sup>33</sup>

## C. METAL–CARBENE FORMALISM

The formalism generally adopted for late-transition-metal complexes is a formally neutral carbene fragment bonded to M(II) in the group 6 compound,<sup>20</sup> but carbene complexes have been also described as M(IV) complexes on the basis of Mössbauer results.<sup>34,35</sup> In a theoretical study on the structure of iron carbene derivatives, (TPP)FeCCl<sub>2</sub> was considered as a d<sup>6</sup> electron system.<sup>19</sup> Carbene adducts of metalloporphyrins have been also considered as carbon analogs of the porphyrin-iron-oxo species on the basis of similarity in the electronic spectra.<sup>19,22,36</sup>

**Table 4.**  $^{13}\text{C}$  NMR Chemical Shifts of Carbene Complexes of Metalloporphyrins

Complex	$^{13}\text{C}$ NMR (ppm)	Solvent	Reference
(TPP)Fe(CCl) <sub>2</sub>	224.7	CDCl <sub>3</sub>	30
(TPP)Fe[C(Cl)(CH <sub>2</sub> C <sub>6</sub> H <sub>5</sub> )]	266.4	CDCl <sub>3</sub>	67
(TPP)Fe[C(Cl)(C <sub>6</sub> H <sub>5</sub> )]	288.5	CDCl <sub>3</sub>	67
(TPP)Fe[C(Cl)(CN)]	210.0	CDCl <sub>3</sub>	25
(TPP)Fe[C(Cl)(CO <sub>2</sub> C <sub>2</sub> H <sub>5</sub> )]	234.0	CDCl <sub>3</sub>	25
(TPP)Fe[C(Cl)(CH <sub>2</sub> OH)]	302.7	CDCl <sub>3</sub>	25
(TPP)Fe[C(Cl)(C <sub>6</sub> H <sub>5</sub> CHOH)]	303.0	CDCl <sub>3</sub>	25
(TPP)Fe[C(Cl)(CH <sub>3</sub> CHOH)]	312.0	CDCl <sub>3</sub>	25
(TPP)Fe[C(Cl)(SeCH <sub>2</sub> C <sub>6</sub> H <sub>5</sub> )]	265.1	CDCl <sub>3</sub>	48
[(TMP)Ru] <sub>2</sub> (μ-C <sub>2</sub> H <sub>2</sub> )	263.8	C <sub>6</sub> D <sub>6</sub>	100
(TPP)Ru[C(CO <sub>2</sub> Et) <sub>2</sub> ]	271.4	CDCl <sub>3</sub>	51
(TPFPP)Ru[C(CO <sub>2</sub> Et) <sub>2</sub> ]	285.8	CDCl <sub>3</sub>	51
(TPP)Ru[C(H)(PO(O <i>i</i> -Pr) <sub>2</sub> )]	290	CDCl <sub>3</sub>	152
(P*)Ru[C(Ph) <sub>2</sub> ]	315	CDCl <sub>3</sub>	52
(P*)Ru[C(Ph)(CO <sub>2</sub> CH <sub>2</sub> CHCH <sub>2</sub> )]	285	CDCl <sub>3</sub>	52
(TTP)Os[C(H)(Si(CH <sub>3</sub> ) <sub>3</sub> )]	295.5	C <sub>6</sub> D <sub>6</sub>	26
(TTP)Os[C( <i>p</i> -CH <sub>3</sub> -C <sub>6</sub> H <sub>4</sub> ) <sub>2</sub> ]	264.6	C <sub>6</sub> D <sub>6</sub>	26
Os(TTP)[C( <i>p</i> -CH <sub>3</sub> -C <sub>6</sub> H <sub>4</sub> ) <sub>2</sub> ] <sub>2</sub>	305.5	C <sub>6</sub> D <sub>6</sub>	26
(TPFPP)Os[C(Ph) <sub>2</sub> ]	273.6	CDCl <sub>3</sub>	27
(TPFPP)Os[C(Ph) <sub>2</sub> ] <sub>2</sub>	313.8	CDCl <sub>3</sub>	27
(TPP)Mn(CCl) <sub>2</sub>	264.5	CDCl <sub>3</sub>	30



Scheme 2

### III. Methods of Synthesis of Metal–Carbene Bond in Porphyrins

The first synthesis of a transition metal–carbene complex by Fischer and Maasböl opened up a large research field in organometallic chemistry.<sup>37</sup> Many new preparative routes were developed and a wide variety of carbene complexes were prepared. A number of reviews have appeared covering this area as a whole<sup>13,38</sup> or in part.<sup>1</sup> This chapter will concentrate only on synthetic routes having a range of applicability in metalloporphyrin chemistry. Different approaches for the synthesis of metal–carbene porphyrins are possible. First, the transformation of a non-carbene ligand into a carbene ligand is feasible. In this case, the carbon atom is already attached to the metal in the metalloporphyrin complex. The addition of a carbene ligand precursor to the metalloporphyrin offers a second possibility.<sup>14</sup> Modification of a metal–carbene porphyrin to yield a different metal–carbene porphyrin may also be possible.

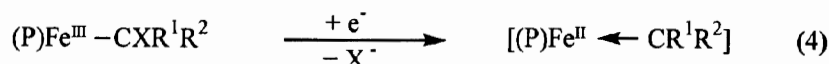
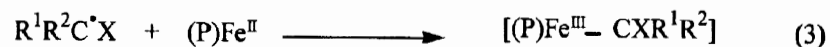
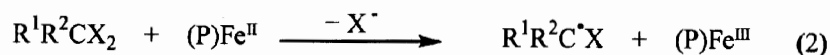
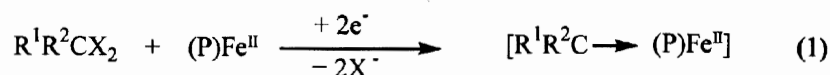
Finally, metalloporphyrins with an intramolecular-bridged carbene fragment inserted into the metal–

nitrogen bond have been prepared.<sup>39,40</sup> Their preparation will also be described in this chapter.

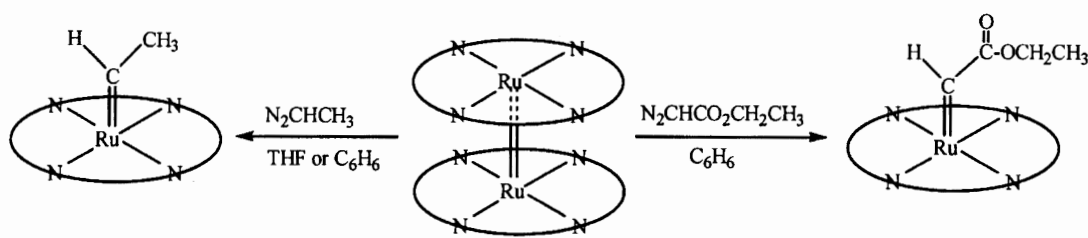
#### A. PREPARATION FROM POLYHALOGENATED PRECURSORS UNDER REDUCING CONDITIONS

The report of the first isolated metalloporphyrin–carbene complex in 1977 by Mansuy and coworkers<sup>41</sup> generated widespread interest in this class of organometallic compounds. The synthetic strategy was to use a suitable carbene ligand precursor (e.g., polyhalogenated compounds) which is first attached to the metal complex and then modified during the synthesis (Scheme 3).<sup>42</sup> In this case, the procedure is associated with a change of the formal oxidation state of the iron center and possible formation of  $\sigma$ -alkyl-iron complexes as intermediates.<sup>43–47</sup> This method can be extended to polyhalogenated substrates bearing a heteroatom on the carbon atom such as in the case of C<sub>6</sub>H<sub>5</sub>CH<sub>2</sub>SeCCl<sub>3</sub>.<sup>48</sup>

The reaction of (TPP)MnCl with CCl<sub>4</sub> and excess iron powder (or NaBH<sub>4</sub>) also resulted in the formation



Scheme 3



Scheme 4

of a Mn carbene complex using the strategy reported by Mansuy.<sup>21</sup>

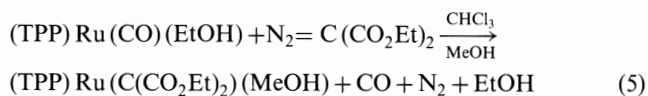
## B. PREPARATION FROM DIAZO COMPOUNDS

The decomposition of diazo compounds by transition metal complexes is one of the best methods in chemistry for new synthetic methodologies.<sup>17</sup> This method can be used for catalytic reactions or for synthesis of carbene complexes with metalloporphyrins.

Ruthenium and osmium porphyrin carbene complexes can be prepared by a reaction of double-bonded porphyrin dimers with diazoalkanes.<sup>20,26,49</sup> As an example, the treatment of  $[(\text{TTP})\text{Ru}]_2$  with diazoethane or ethyl diazomethyl acetate produces  $(\text{TTP})\text{Ru}(\text{CHCH}_3)$  and  $(\text{TTP})\text{Ru}(\text{CHCO}_2\text{CH}_2\text{CH}_3)$ , respectively (Scheme 4). The fourteen-electron complex, ruthenium 5,10,15,20-tetramesitylporphyrin, also reacts with ethyl diazoacetate to give quantitatively a metalloporphyrin carbene complex.<sup>50</sup> A biscarbene osmium porphyrin complex has been prepared from diphenyldiazomethane as a reactive precursor.<sup>27</sup>

Using diazoethyl malonate as a precursor, a carbene complex as shown in eq 5 was obtained which was stable enough to determine its X-ray structure.<sup>51</sup> Optically active ruthenium carbene complexes were also prepared using diazo derivatives as precursors.<sup>52</sup>  $\alpha$ -keto carbene

complexes of iron porphyrins were prepared by addition of diazoketone to Fe(II) porphyrins.<sup>39,53</sup>

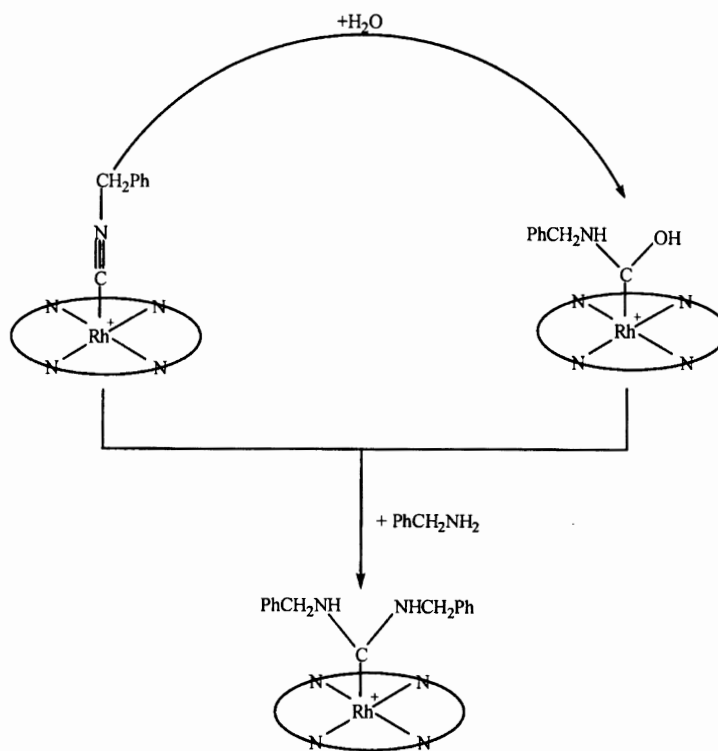
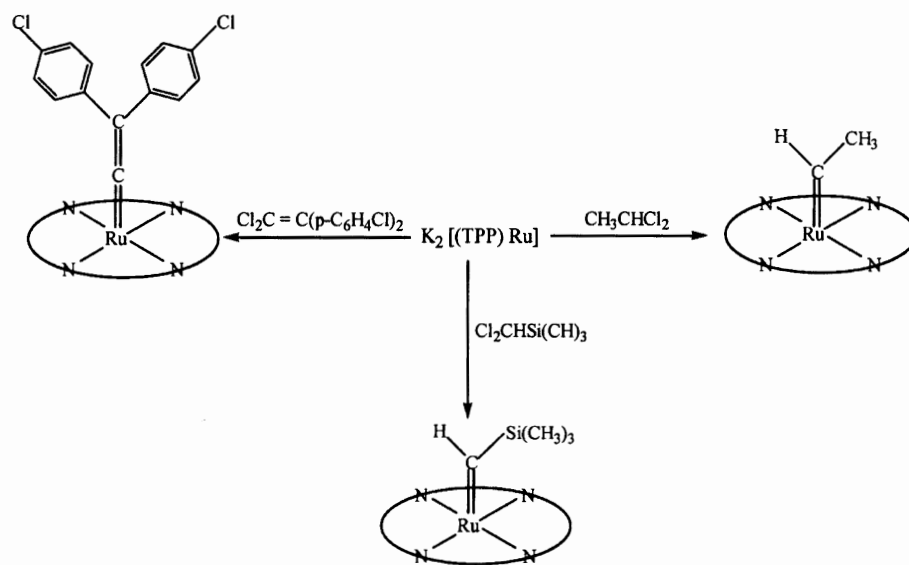


## C. PREPARATION FROM ZERO-VALENT METALLOPORPHYRIN DIANIONS

The reaction of ruthenium porphyrin dianion such as  $\text{K}_2[(\text{TTP})\text{Ru}]$  with a geminal dihalide leads to the corresponding carbene complexes. Thus, it was possible to prepare the vinylidene species  $(\text{TTP})\text{Ru}[(\text{C}=\text{C}-(p\text{-C}_6\text{H}_4\text{Cl})_2)]$ ,  $(\text{TTP})\text{Ru}[\text{CHSi}(\text{CH}_3)_3]$  and  $(\text{TTP})\text{Ru}[\text{CHCH}_3]$  using  $\text{Cl}_2\text{C}=\text{C}(p\text{-C}_6\text{H}_4\text{Cl})_2$ ,  $\text{Cl}_2\text{CHSi}(\text{CH}_3)_3$  and  $\text{CH}_3\text{CHCl}_2$  as organic electrophiles, respectively (Scheme 5).<sup>20,54</sup>

## D. PREPARATION FROM ISONITRILE COMPLEXES

It is well known that isocyanides coordinated to transition metals react with alcohols or amines leading to the formation of carbene complexes.<sup>13,15</sup> Although this method is generally used with palladium and platinum complexes, it can also be successfully used with rhodium derivatives. Thus, Boschi *et al.* reported



that *bis*(isocyanide) Rh(III) porphyrins undergo nucleophilic attack of alcohols leading to the formation of cationic carbene derivatives (Scheme 6).<sup>55</sup>

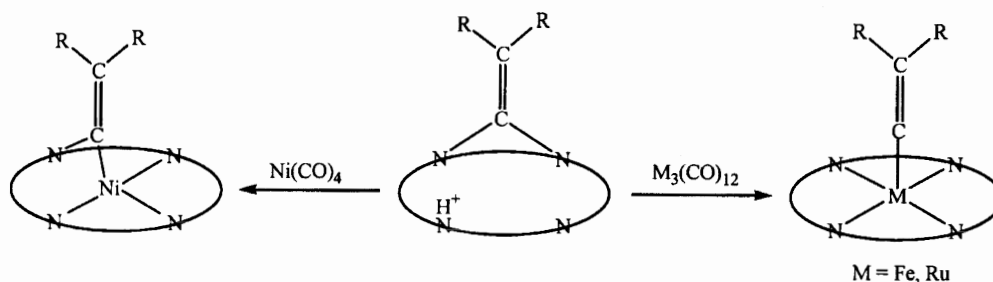
#### E. PREPARATION FROM IODONIUM YLIDE

$\alpha$ -Ketocarbene iron porphyrin complexes were prepared by reaction of Fe(II) porphyrins with iodonium ylids at  $-40^\circ\text{C}$ .<sup>53</sup> However, the carbene complex

was stable only below  $-30^\circ\text{C}$  and this reaction is not a general route leading to iron porphyrin carbenes.

#### F. INSERTION OF ZERO-VALENT METALS INTO THE C-N BOND OF *N,N'*-BRIDGED PORPHYRINS

Treatment of an *N,N'*-bridged porphyrin with an excess of  $\text{Fe}_3(\text{CO})_{12}$  or  $\text{Ru}_3(\text{CO})_{12}$  yields the metal-carbene complexes of (TPP)Fe and (TPP)Ru, respectively with



Scheme 7

good (Fe: 90%) to moderate (Ru: 40%) yields.<sup>56</sup> In contrast, the reaction of  $\text{Ni}(\text{CO})_4$  with the  $N,N'$ -bridged porphyrin takes a different course where only one C–N bond is broken. This reaction yields a different complex in which a carbene moiety is inserted into the Ni–N bond of a nickel porphyrin (Scheme 7). Similar complexes were previously reported by a different route using diazo derivatives.<sup>21,39,57,58</sup>

#### IV. Synthetic Metal–Carbene Porphyrin Derivatives and Their Reactivity

Two different metalloporphyrin carbene complexes have been reported. These are the axially symmetric complex with multiple metal–carbon order and the metal–nitrogen inserted complex (Scheme 1). The relative stability of the two types, A and B, has been previously discussed.<sup>19</sup> A carbene fragment in a metalloporphyrin should insert in an M–N bond when the molecule has a  $d^8$  electronic configuration and/or the d orbitals of the central metal are lowered in energy.<sup>19</sup> Occupancy of two electrons in the M–C(carbene)  $\pi^*$  level seems to be the reason that the  $d^8$  molecule tends toward geometry B rather than A (Scheme 1). Considering the strong  $\sigma$ -donor and  $\pi$ -acceptor character of a carbene ligand, it is also expected that the addition of  $\sigma$ -donor or a  $\pi$ -acceptor would weaken the M=C bond, thus destabilizing structure A.

##### A. GROUP 6

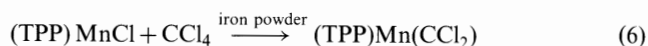
To our knowledge, there is no evidence of the existence of metallocarbene complexes in group 6 of the periodic table.

##### B. GROUP 7

###### 1. Manganese

The reaction of  $(\text{TPP})\text{MnCl}$  with excess iron powder or sodium borohydride resulted in the formation of  $(\text{TPP})\text{Mn}(\text{CCl}_2)$  (eq 6).<sup>30</sup> Purification of the manganese–carbene complex was similar to the purification of

the iron–carbene porphyrin analog.<sup>41</sup> The carbene complex was characterized by  $^{13}\text{C}$  NMR, the spectrum showing the carbene resonance at 264.5 ppm. Complexation of *n*-butanethiol to the carbene complex resulted in the formation of a split-Soret band, as expected for sulfur ligand binding to a metalloporphyrin.<sup>28</sup>



##### C. GROUP 8

###### 1. Iron

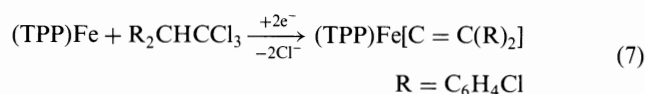
###### a. Syntheses

The first isolated metalloporphyrin–carbene complex was reported in 1977 by Mansuy and coworkers<sup>41</sup> and was an iron porphyrin carbene complex. It was suggested by the authors that iron carbene complexes could be involved in the metabolism of xenobiotics. Thus, the five-coordinated  $(\text{TPP})\text{Fe}(\text{CCl}_2)$  was prepared as a purple red solid by treatment of  $(\text{TPP})\text{FeCl}$  with  $\text{CCl}_4$  in the presence of excess of iron powder (90% yield).<sup>41</sup> It must be emphasized that the possible formation of carbene complexes after reduction of iron deuteroporphyrin in  $\text{CCl}_4$  was initially proposed by Braut and coworkers.<sup>59</sup> An original method of reduction by aqueous sodium dithionite solution was described but, under these conditions, it was not possible to isolate any complex although the reaction leads to a compound of unusually good stability toward air.

A later crystal structure of a related six-coordinate complex,  $(\text{TPP})\text{Fe}(\text{CCl}_2)(\text{H}_2\text{O})$ , confirmed the formation of such a  $\text{CCl}_2$  complex which was also the first example of a dihalogenated carbene complex of a transition metal.<sup>60</sup> In this complex, the overall deviations from the planarity of the porphyrin core are very small (0.03 Å) and the iron atom is not significantly displaced from this plane. The average length of the equivalent Fe–N bonds (1.984(4) Å) and the distances within the porphyrin core are in good agreement with values reported for other low-spin iron porphyrins.<sup>61,62</sup> Resonance Raman spectra of

the same carbene complexes have also been reported.<sup>63</sup> This synthesis was an opening route to other carbene complexes since various polyhalogenated compounds,  $\text{RCX}_3$ , react similarly with iron porphyrins leading to the corresponding porphyrin iron carbene complexes. A large series of iron carbene porphyrins were synthesized, starting from  $(\text{TPP})\text{FeCl}$  and polyhalogenated compounds in the presence of an excess of reducing agent. Thus, the carbenes  $\text{CCl}_2$ ,<sup>41</sup>  $\text{CBr}_2$ ,<sup>42</sup>  $\text{CF}_2$ ,<sup>42</sup>  $\text{CFCl}$ ,<sup>42</sup>  $\text{CFBr}$ ,<sup>42</sup>  $\text{CClCN}$ <sup>64</sup> have been attached to the iron atom by reaction with  $\text{CCl}_4$ ,  $\text{CBr}_4$ ,  $\text{CF}_2\text{Br}_2$ ,  $\text{CFCl}_3$ ,  $\text{CFBr}_3$ , and  $\text{CCl}_3\text{CN}$ , respectively.

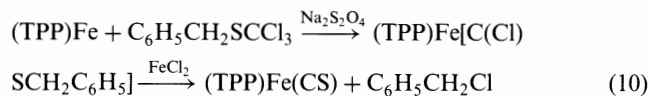
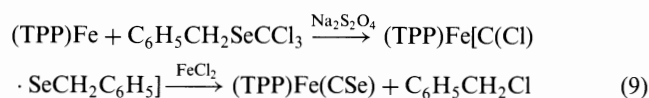
The stable complex formed during the reaction between DDT (2,2-bis(*p*-chlorophenyl)-1,1,1-trichloroethane), a widely used insecticide, and iron porphyrins under reducing condition is a nice example of such carbene formation (eq 7). Actually, these carbene complexes were the first reported vinylidene carbene complexes of an iron porphyrin.<sup>65</sup> The syntheses were then extended to other chlorocarbenes having an electron withdrawing group on the carbene carbon atom such as  $\text{CCIX}$  yielding  $(\text{TPP})\text{Fe}(\text{CCIX})$  ( $\text{X} = \text{CO}_2\text{Et}$ ).<sup>64</sup> However, these complexes were less stable than  $(\text{TPP})\text{Fe}(\text{CCl}_2)$ , due to an increase in reactivity toward nucleophiles.



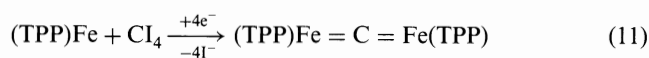
Characterization of the  $(\text{TPP})\text{Fe}(1,3\text{-benzodioxol-2-carbene})$  complex (eq 8a) was also reported, giving indirect evidence for the presence of this carbene as a ligand in the benzodioxole-derived cytochrome P450 complex (eq 8b).<sup>36,66</sup>

$\text{Fe}(\text{TPP})(\text{C}(\text{Cl})\text{SeCH}_2\text{C}_6\text{H}_5)$ <sup>48</sup> and  $\text{Fe}(\text{TPP})(\text{C}(\text{Cl})\text{SR})$  ( $\text{R} = \text{C}_6\text{H}_5, \text{CH}_2\text{C}_6\text{H}_5$ )<sup>67</sup> were also prepared as

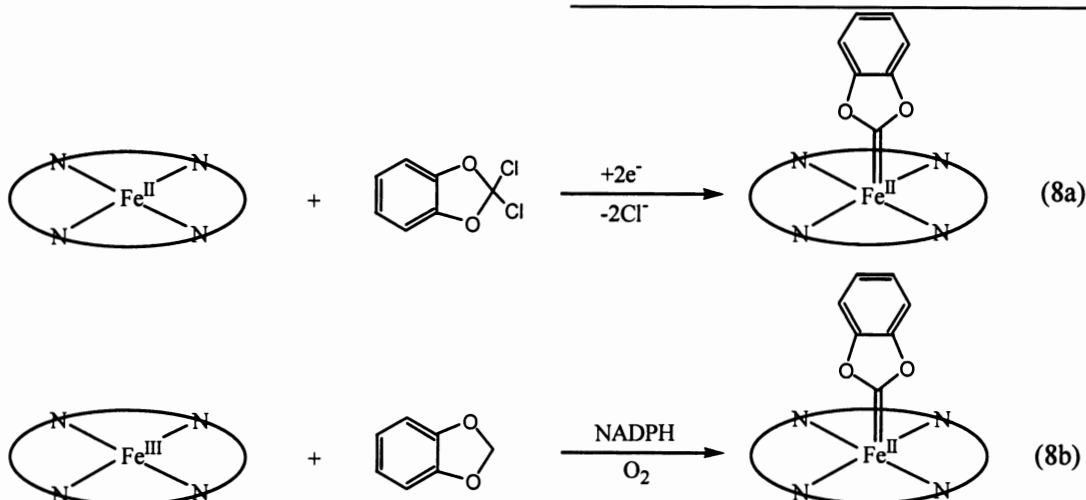
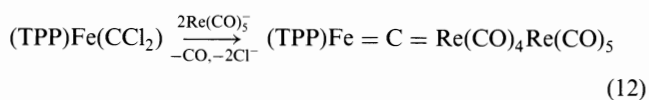
precursors of the selenocarbonyl and thiocarbonyl complexes, respectively (eqs 9 and 10).



A  $\mu$ -carbido dimeric complex,  $[(\text{TPP})\text{Fe}]_2\text{C}$  is formed upon reaction with carbon tetraiodide (eq 11).<sup>68</sup> This was the first example of a transition-metal complex of the type  $\text{M}=\text{C}=\text{M}$  involving a formally dicarbenic carbon atom ligand bridging two transition metals.



The X-ray structure of this complex was reported by Bottomley and coworkers.<sup>69</sup> Remarkably, the electronic structure of such a complex was predicted before its preparation.<sup>19</sup> Reduction of trichloromethyltrimethylsilane by iron(II) tetraarylporphyrins in the presence of a reducing agent also leads to the carbide complex.<sup>70</sup> This surprising result can be explained by the involvement of an unstable  $\alpha$ -silylcarbene ferroporphyrin complex. More recently, a heterometallic  $\mu_2$ -carbido complex was isolated from the reaction of a dichloro carbene iron porphyrin and pentacarbonylrhenate (eq 12).<sup>71</sup> The X-ray structure of this trinuclear complex,  $[(\text{TPP})\text{Fe}=\text{C}=\text{Re}(\text{CO})_4\text{Re}(\text{CO})_5]$ , shows a 1,3-dimetalla-allene system.





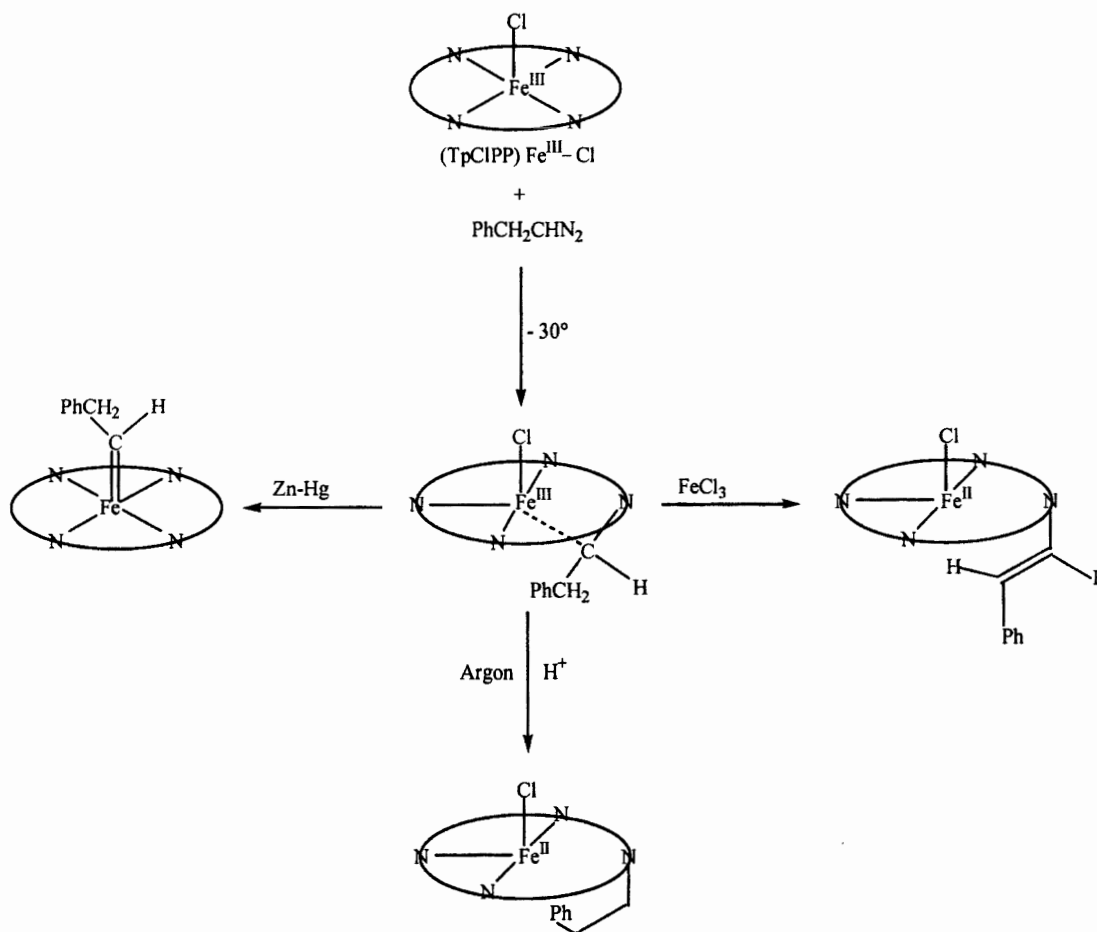
Bridged carbene complexes were also reported in the iron series. Thus, a bridged carbene complex with a vinylidene group inserted into an Fe–N bond of (TPP)FeCl was independently reported by Mansuy and coworkers<sup>22,72</sup> and Balch and coworkers.<sup>23,73</sup> An X-ray analysis of the complex (TPP)Fe[C=C(*p*-ClC<sub>6</sub>H<sub>4</sub>)<sub>2</sub>]Cl was reported by two different groups.<sup>22,74</sup> In this compound, the metal is five-coordinated by three of the four pyrrole nitrogens, a chlorine atom and the carbon of the vinylidene group. A 1.914(7) Å (Fe–C) distance and 1.387(6) Å (Fe–N) distance was found, respectively, for the carbene inserted group. The four pyrrole nitrogens are approximately coplanar and the iron atom is displaced out of this plane by 0.3 Å. Magnetic susceptibility, electron spin resonance, and Mössbauer spectroscopic studies indicate that this complex is described as an iron(III) complex with an *S*=3/2 ground state.<sup>75</sup> Later, reaction of the diazocompound PhCH<sub>2</sub>CHN<sub>2</sub> with (T-*p*-ClIPP)Fe also led to a bridged carbene complex with a PhCH<sub>2</sub>CH moiety inserted between the iron

and a pyrrole nitrogen atom (Scheme 8).<sup>39</sup> Reduction of this intermediate spin complex gives the corresponding diamagnetic axial carbene complex. This reaction also confirms the intermediate formation of a bridged carbene species upon reaction of PhCH<sub>2</sub>CHN<sub>2</sub> with cytochrome P450 which was previously reported by Ortiz de Montellano and coworkers.<sup>76,77</sup> Similar intermediates were also suggested during the inactivation of sydnones by P450.<sup>76</sup>

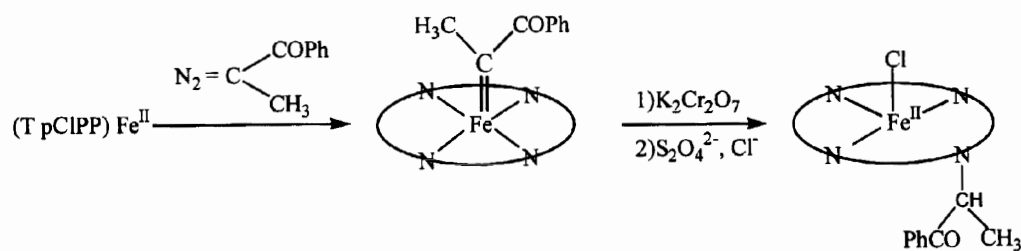
### b. Reactivity

The reversible one-electron oxidation of the vinylidene complex (TPP)Fe(C=CAR<sub>2</sub>) induces the carbene ligand to adopt a bridging structure<sup>22,75,78</sup> giving a complex with an intermediate spin iron(III).<sup>75</sup> Further oxidation results in the formation of a *N,N'*-4-vinylidene-bridged porphyrin.<sup>79</sup>

Addition of alkylthiolates to porphyrin–iron–carbene complexes immediately gave new complexes characterized by their hyperporphyrin spectra.<sup>29</sup>



Scheme 8

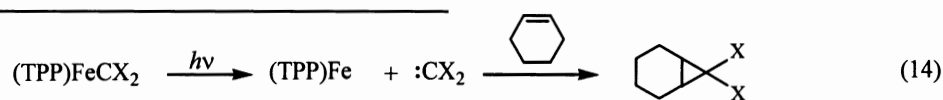
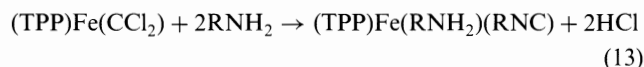


Scheme 9

Similar spectra were obtained with the analogous iron thiocarbonyl complexes,<sup>80</sup> suggesting that these complexes have similar electronic structures.

Iron-porphyrin model reactions have been reported for several steps of metabolic oxidation of sydnone by cytochrome P450.<sup>76,77</sup> Thus, diazoketones react with iron(II) porphyrins to give iron-carbene complexes and then *N*-alkylporphyrins after a one  $\pi$  electron oxidation. In this case, a migration of the carbene moiety to the pyrrole nitrogen is observed (Scheme 9).<sup>53</sup> Similar results were obtained with PhCH<sub>2</sub>CH<sub>2</sub>N<sub>2</sub>.<sup>39</sup>

The dichlorocarbene complex (TPP)Fe(CCl<sub>2</sub>) is a useful synthetic intermediate forming isocyanide complexes upon reaction with primary amines (eq 13).<sup>81</sup>



A possible application to the synthesis of labeled <sup>13</sup>C (or <sup>14</sup>C) isocyanides using <sup>13</sup>CCl<sub>4</sub> (or <sup>14</sup>CCl<sub>4</sub>) was suggested. Later, a kinetic investigation established two alternate mechanisms for the reaction of primary amines with (TPP)Fe(CCl<sub>2</sub>).<sup>82</sup> Both the formation of the mixed-ligated complex (TPP)Fe(CNR)(RNH<sub>2</sub>) and the *bis*(amino) complex (TPP)Fe(RNH<sub>2</sub>)<sub>2</sub> was detected depending on the basicity or the steric hindrance of the primary amine (RNH<sub>2</sub>).

An unusual intramolecular rearrangement of an iron carbene complex yielding an *N,N'*-*cis* bridged tetraarylporphyrin was reported.<sup>79</sup> This rearrangement results from oxidation with FeCl<sub>3</sub> of the corresponding vinylidene iron complex obtained from reaction of DDT with tetraanisylporphyrin iron chloride under reducing conditions. An intermediate in which the carbene has been inserted into an iron-nitrogen bond was also suggested by analogy with cobalt porphyrin carbene chemistry.<sup>24,83</sup>

Iron porphyrin carbenes and vinylidenes are photoactive and possess a unique photochemistry since the mechanism of the photochemical reaction suggests the liberation of "free" carbene species in solution.<sup>84,85</sup> These "free" carbenes can react with olefins to form cyclopropanes (eq 14). The photochemical generation of the free carbene fragment from a transition metal-carbene complex has not been previously observed.<sup>86,87</sup> Although the photochemistry of both Fischer and Schrock-type carbene has been investigated, no examples of homolytic carbene dissociation have yet been found. In the case of the metalloporphyrin carbene complexes, the lack of other coordinatively labile species and the stability of the resulting fragment both contribute to the reactivity of the iron-carbon double bond. Thus, this photochemical behavior is quite different to that previously observed with other classes of carbene complexes.<sup>87,88</sup>

The reductive electrochemistry of iron-carbene porphyrins has been investigated in aprotic solvents.<sup>89</sup> With the vinylidene complex, there is a 2e+H<sup>+</sup> reduction of the ligand leading to the formation of the corresponding iron(II) vinyl complex. The energies required to reduce by two electrons the other carbene complexes are quite similar.<sup>89</sup> The dichlorocarbene complex is an exception because the reduction is facilitated by the extreme instability of the one-electron intermediate. Formation of  $\sigma$ -alkyl iron(II) porphyrins has been confirmed by independent synthesis.<sup>45</sup> The  $\sigma$ -alkyl iron(III) porphyrins can then be obtained by a one-electron reoxidation reaction. These results are based on an electrochemical investigation of the reduction of carbene complexes in aprotic media.<sup>45</sup> The electrochemistry of organometallic iron porphyrin complexes has been reported by Guilard *et al.*<sup>90</sup>

Reaction of trimethylsilyldiazomethane with [(OEP)-Fe<sup>III</sup>](ClO<sub>4</sub>) gave an *N,N'*-ethanobridged porphyrin via a possible bridged carbene complex.<sup>91</sup> The chemistry of

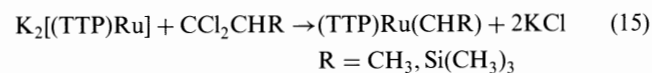
the naturally occurring iron porphyrins and other iron, cobalt, and ruthenium porphyrins has been reviewed by Setsune and Dolphin.<sup>92</sup> The chemical properties of carbene iron porphyrins and their relationships with *N*-alkyliron(III) porphyrins and  $\sigma$ -alkyl iron(III) porphyrins have been discussed in this review. Thus, the organometallic chemistry of iron porphyrins may serve as an excellent basis for elucidating the mechanism of the catalytic reactions in which the cytochromes P450 play an important role, in particular toward the formation of carbene iron species.

Carbene intermediates have also been identified as products of the reduction of polyhalogenated methanes by iron porphyrins in the presence of cysteine.<sup>93</sup> Such a process seems to be of particular interest because of its potential applicability in the treatment of wastes as well as in remediation approaches to removing polyhalogenated methanes from contaminated soils.

## 2. Ruthenium

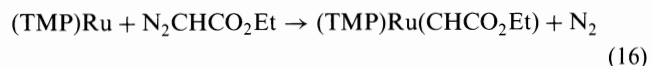
The first ruthenium porphyrin carbene complex was reported by Balch and coworkers<sup>56</sup> by metalation of an *N,N'*-vinyl-bridged porphyrin<sup>79,94</sup> with  $\text{Ru}_3(\text{CO})_{12}$  (Scheme 7). In this reaction, both of the C–N bonds (vinyl) were broken. Surprisingly, this reaction also yields two ruthenium(II) dicarbonyl complexes in which the *N,N'*-vinyl-bridged remains intact, but the ruthenium has been inserted into a pyrrole C–N bond.<sup>95,96</sup> Upon heating, these two complexes are converted to the axial ruthenium carbene complex.

Cleavage of a ruthenium dimer such as  $[(\text{TTP})\text{Ru}]_2$ <sup>97</sup> upon treatment with diazoalkanes and diazoesters affords the corresponding carbene complexes,  $(\text{TTP})\text{Ru}(\text{CHCO}_2\text{CH}_2\text{CH}_3)$  and  $(\text{TTP})\text{Ru}(\text{CHCH}_3)$ , respectively (Scheme 4).<sup>49,54</sup> These carbene complexes were the first such metalloporphyrin species to contain a proton on the carbene carbon atom. Unfortunately, the methylene carbene complex was not detected when diazomethane was used as the reagent. Instead, the ethylene complex was formed. The carbene complexes were also prepared by interaction of geminal dihalides with zero-valent ruthenium porphyrins such as  $\text{K}_2[(\text{TTP})\text{Ru}]$  by the same authors (eq 15).<sup>54</sup>

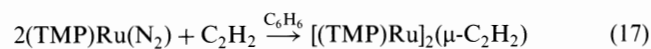


It was later demonstrated that decomposition of a dialkyl ruthenium(IV) porphyrin also yields the carbene species  $(\text{TPP})\text{Ru}(\text{CHCH}_3)$  due to  $\alpha$ -abstraction.<sup>98</sup> More recently,<sup>50</sup> it was reported that addition of ethyl

diazomethyl acetate to the fourteen electron species,  $(\text{TMP})\text{Ru}$ <sup>99</sup> also affords  $(\text{TMP})\text{Ru}(\text{CHCO}_2\text{CH}_2\text{CH}_3)$  in a more classical route (eq 16).

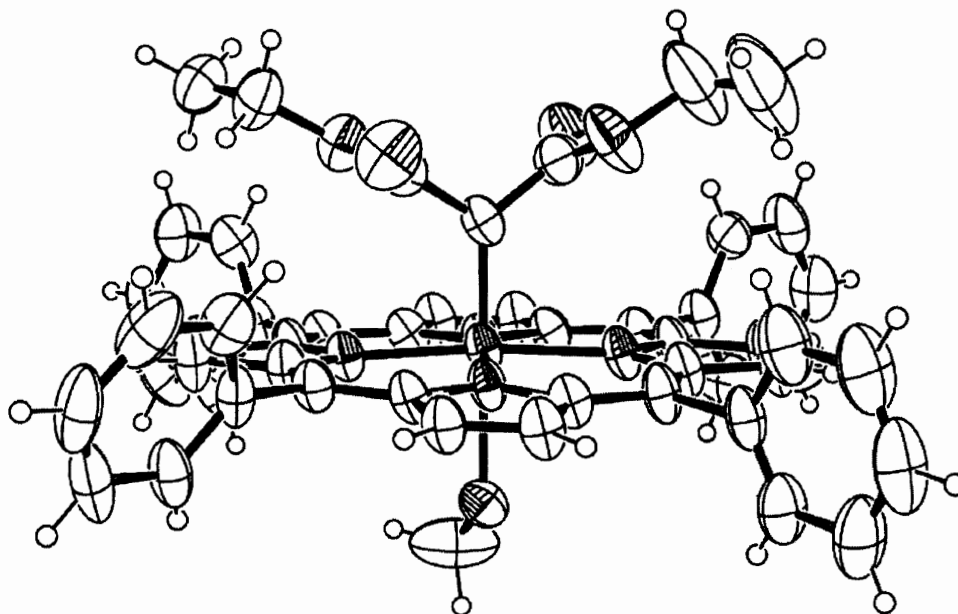


The reaction of  $(\text{TMP})\text{Ru}$  with ethyne to produce a  $\mu$ -biscarbene complex  $[(\text{TMP})\text{Ru}]_2(\mu\text{-C}_2\text{H}_2)$  was reported by Rajapakse *et al.* (eq 17).<sup>100</sup> It is worth noting that formation of the carbene complex appears to require at least laboratory light to proceed, the  $\text{C}_2\text{H}_2$  reaction being stopped in the dark. This complex was characterized by  $^1\text{H}$  and  $^{13}\text{C}$  NMR ( $\delta = 263.8$  ppm). A possible formation of a  $\pi$ -acetylene ruthenium complex was ruled out on the basis of the spectroscopic data and a comparison with a rhodium complex  $[(\text{OEP})\text{Rh}]_2(\mu\text{-C}_2\text{H}_2)$  which was formulated as a  $\text{Rh}\text{-CH}=\text{CH}\text{-Rh}$  unit.<sup>101</sup> In contrast to  $\text{C}_2\text{H}_2$  itself,  $\text{PhCCPh}$  and  $\text{PhCCH}$  form 1:1 complexes with  $(\text{TMP})\text{Ru}$ .<sup>100</sup> Similar acetylene rearrangements in the reaction with ruthenium porphyrinogen have been recently reported by Floriani and coworkers.<sup>102</sup>



The first X-ray structure of a ruthenium porphyrin carbene complex was reported by Simonneaux and coworkers (Figure 1).<sup>51</sup> To stabilize the ruthenium carbene complex, ethyl diazomalonate was used instead of ethyl diazomethyl acetate, as it was previously reported in the *bis*(oxazolinyl)pyridine (pybox) series.<sup>103</sup> The presence of this complex as an intermediate in cyclopropanation was also discussed in relation with stoichiometric transfer to alkenes (*vide infra*).<sup>104</sup>

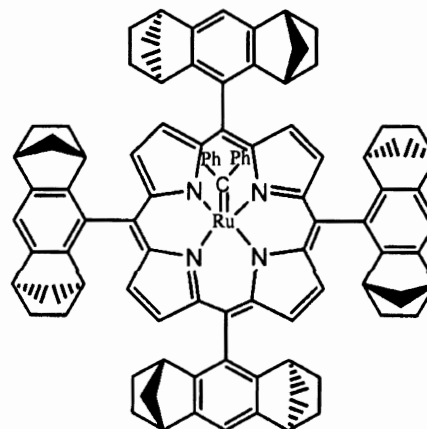
Figure 1 illustrates the molecular structure of  $(\text{TPP})\text{Ru}(\text{C}(\text{CO}_2\text{Et})_2)(\text{MeOH})$ .<sup>51</sup> The coordination sphere of the ruthenium atom consists of four pyrrole nitrogen atoms, one carbon atom from the carbene ligand and one oxygen atom from the methanol group. As expected for a six-coordinate complex, the porphyrin ligand is nearly planar. However, the ruthenium atom is slightly out of the mean porphyrin plane 0.12 Å toward the carbene ligand. A similar situation was previously observed for an osmium(II) porphyrin carbene complex,  $(\text{TTP})\text{Os}(\text{CHSiMe}_3)(\text{THF})$ ,<sup>105</sup> and a rhodium(III) porphyrin carbene complex,  $(\text{TPP})\text{Rh}[\text{C}(\text{NHCH}_2\text{Ph})_2](\text{CNCH}_2\text{Ph})\text{PF}_6$ .<sup>55</sup> The geometry of the coordination sphere is octahedral. The carbene fragment is slightly distorted since the angle is  $112.2(7)^\circ$  which is significantly smaller than the  $120^\circ$  angle for ideal  $\text{sp}^2$  hybridization as it has



**Figure 1.** Molecular structure of  $(\text{TPP})\text{Ru}[\text{C}(\text{CO}_2\text{Et})_2(\text{MeOH})]$  (adapted from Galardon, E.; Le Maux, P.; Toupet, L.; Simonneaux, G. *Organometallics* **1998**, *17*, 565–569).

been previously reported for an osmium porphyrin carbene complex.<sup>105</sup> Steric interactions between the two ethoxy groups of the carbene fragment and the phenyl groups of the porphyrin may explain this result. The Ru–C distance of 1.829(9) Å is slightly shorter than ruthenium–carbon double bonds reported for other molecular structures of ruthenium carbene complexes. For example, the ruthenium–carbon distances in  $\text{RuCl}_2(\text{pybox})[\text{C}(\text{CO}_2\text{Me})_2]$  (pybox: *bis*(oxazolinyl)-pyridine),<sup>103</sup>  $\text{Ru}(\text{Cl}_2)(\text{PPh}_3)(\text{CH}=\text{CH}=\text{CPh}_2)$ <sup>106</sup> and  $\text{CpRuI}(\text{CO})[\text{C}(\text{OEt})\text{Ph}]$ <sup>107</sup> are 1.880(7), 1.887(7), and 1.997(52) Å, respectively. For comparison, the M=C distances of the other carbene complexes which have been characterized by single-crystal X-ray diffraction analysis are reported in Table 2.

Recently, two X-ray structures of chiral ruthenium carbene complexes were reported.  $(P^*)\text{Ru}(\text{CPh}_2)$  and  $(P^*)\text{Ru}[\text{C}(\text{Ph})(\text{CO}_2\text{CH}_2\text{CH}=\text{CH}_2)]$  were obtained by reaction of the chiral carbonyl ruthenium complex  $(P^*)\text{Ru}(\text{CO})(\text{EtOH})$  ( $P^* = 5,10,15,20$ -*tetrakis*-(1*S*,4*R*,5*R*,8*S*)-1,2,3,4,5,6,7,8-octahydro-1,4:5,8-dimethanoanthracene-9-yl]porphyrin dianion) with the corresponding diazomethyl derivatives (Figure 2).<sup>52</sup> Both complexes contain a five-coordinate ruthenium atom that is situated in a slightly distorted square-pyramidal coordination sphere with the carbene C atom at the vertex site. For the diphenyl carbene complex, the Ru–C distance is 1.860(6) Å and the ruthenium atom is displaced from the mean plane of the four pyrrole nitrogen atoms toward the carbene C atom by 0.19 Å.



**Figure 2.** Schematic structure of the chiral complex showing the Ru–carbene bond (adapted from Che, C. M.; Huang, J. S.; Lee, F. W.; Li, Y.; Lai, T. S.; Kwong, H. L.; Tang, P. F.; Lee, W. S.; Lo, W. C.; Peng, S. M.; Zhou, Z. Y. *J. Am. Chem. Soc.* **2001**, *123*, 4119–4129).

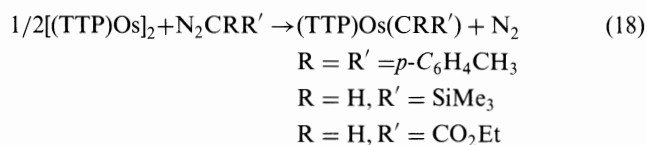
For  $(P^*)\text{Ru}[\text{C}(\text{Ph})(\text{CO}_2\text{CH}_2\text{CH}=\text{CH}_2)]$ , the Ru–C distance is 1.847(3) Å and the ruthenium atom is displaced from the mean plane of the four pyrrole nitrogen atoms toward the carbene C atom by 0.22 Å. Five-coordinate carbenes and their solvent adducts or even *bis*-carbene species were suggested as intermediates in the cyclopropanation reactions (*vide infra*).<sup>52</sup>

The isolation of a diamagnetic bridging methylene complex  $[(\text{OEP}-N-\mu\text{-CH}_2)\text{Ru}(\text{CH}_3)](\text{BF}_4)$  from decomposition of  $[(\text{OEP}-N-\text{CH}_3)\text{Ru}(\text{CH}_3)](\text{BF}_4)$  was also possible. This complex has been characterized by

$^1\text{H}$  NMR and partially by an X-ray structure.<sup>40</sup> Unfortunately, reduction of this complex did not result in formation of an axial methylene carbene complex as was postulated by James and Dolphin.<sup>108</sup> Although  $\text{M}=\text{CH}_2$  species have been prepared,<sup>109,110</sup> similar metalloporphyrin complexes are not yet known. Ruthenium carbene complexes which are involved in catalytic reactions will be discussed below.

### 3. Osmium

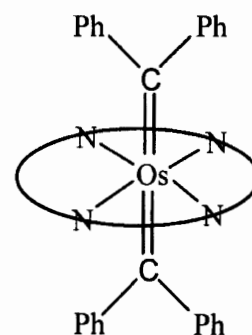
A series of osmium *meso*-tetra-*p*-tolyl-porphyrin carbene complexes,  $(\text{TTP})\text{Os}(\text{CRR}')(\text{R}, \text{R}' = p\text{-tolyl}; \text{R} = \text{H}, \text{R}' = \text{SiMe}_3 \text{ or } \text{CO}_2\text{Et})$  were first prepared by Woo and Smith<sup>26</sup> by treating  $[(\text{TTP})_2\text{Os}]$  with the appropriate diazoalkanes (eq 18). As an indirect method, one of these carbene complexes can also be prepared by reaction of the silylene complex  $(\text{TTP})\text{Os}(\text{SiEt}_2)(\text{THF})$ <sup>111</sup> with di-*p*-tolyl diazomethane.



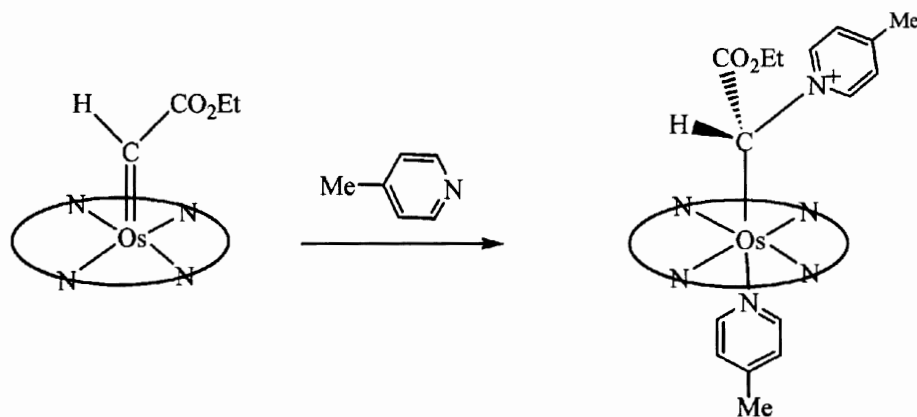
Addition of 4-substituted pyridine derivatives to  $(\text{TTP})\text{Os}(\text{CHCO}_2\text{Et})$  affords stable osmium ylide complexes (Scheme 10).<sup>112</sup> The same group also reported the molecular structure of the two carbene complexes  $(\text{TTP})\text{Os}(\text{CHSiMe}_3)(\text{THF})$  and  $(\text{TTP})\text{Os}[\text{C}(\text{C}_6\text{H}_4\text{-}p\text{-Me})_2](\text{THF})$ .<sup>105</sup> As expected for a six coordinate complex, the porphyrin in  $(\text{TTP})\text{Os}[\text{C}(\text{C}_6\text{H}_4\text{-}p\text{-Me})_2](\text{THF})$  is nearly planar but the osmium atom is slightly out of the mean porphyrin plane 0.14 Å toward the carbene atom. The Os–C (carbene) distance is 1.865(5) Å and the carbene ligand is slightly distorted since the angle formed by the carbene

carbon atom and the two adjacent carbon atoms is  $113.0(4)^\circ$ , a value which is significantly smaller than the  $120^\circ$  angle for ideal  $\text{sp}^2$  hybridization. Similar data were obtained with  $(\text{TTP})\text{Os}(\text{CHSiMe}_3)(\text{THF})$ .<sup>105</sup> The presence of a *trans bis*-carbene species was also mentioned but the complex was contaminated with the mono-carbene species.

Very recently Che and coworkers<sup>27</sup> were able to isolate and characterize a pure *bis*-carbene  $(\text{TPFPP})\text{Os}(\text{CPh}_2)_2$  (Figure 3). The *bis*-carbene species represents the first structurally characterized *trans-bis*-carbene metal complex whose carbene groups are not stabilized by heteroatoms. The related pentacoordinated mono-carbene complex was also prepared and characterized by an X-ray structure. A comparison of the reactivity of these complexes with olefins suggests that the *bis*-carbene species acts as an intermediate in cyclopropanation. Thus, the inertness of the mono-carbene complex toward stoichiometric styrene cyclopropanation and the observation of an efficient cyclopropanation of styrene in the presence of the *bis*-carbene complex as a catalyst support this suggestion.<sup>27</sup>



**Figure 3.** Schematic structure of  $(\text{TPFPP})\text{Os}(\text{CPh}_2)_2$  showing the two Os-carbene bonds (adapted from Li, Y.; Huang, J. S.; Zhou, Z. Y.; Che, C. M. *J. Am. Chem. Soc.* **2001**, *123*, 4843–4844).



**Scheme 10**

## D. GROUP 9

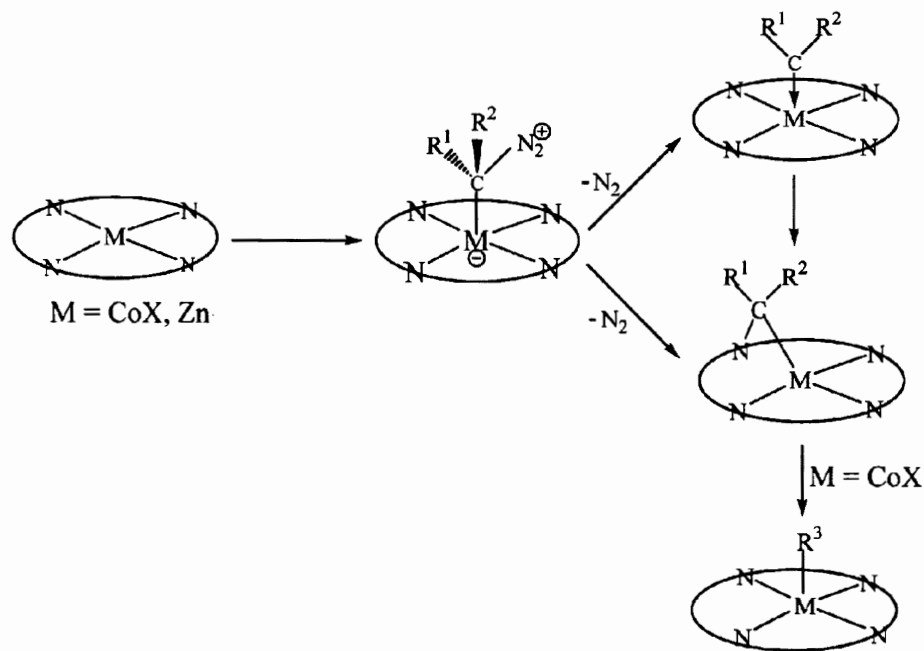
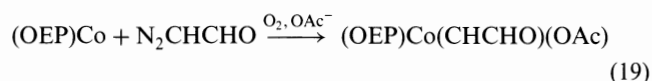
## 1. Cobalt

Reaction of cobalt(III) porphyrins with ethyl diazoacetate leads to the formal insertion of ethoxy carbonyl carbene into the cobalt–nitrogen bond to give the corresponding cobalt(III) adduct.<sup>83,113</sup> (TPP)Co<sup>II</sup> was shown to proceed similarly to (OEP)Co<sup>II</sup>, although the products are less stable.<sup>114</sup> A 1:2 adduct of cobalt(III) porphyrin and ethoxycarbonyl carbene, (OEP)Co(CHCO<sub>2</sub>Et)<sub>2</sub>(NO<sub>3</sub><sup>-</sup>), has been also prepared.<sup>24</sup> The possible formation of an axial carbene cobalt complex as an intermediate has been proposed but without any experimental evidence. It should be mentioned, however, that the studies of interaction of diazoalkanes and metalloporphyrins reported by Callot and Schaeffer were the first to suggest that the exchange of an organic fragment between the metal and nitrogen proceeded via a bridged intermediate.<sup>115</sup> The electronic factors determining the geometries of carbene complexes of metalloporphyrins have been discussed by Tatsumi and Hoffmann.<sup>19</sup> It was suggested that the carbene fragment in the metalloporphyrin should insert into a M–N bond when the d levels have low energies, which is the case for cobalt(III) porphyrins. This possibility was also discussed by Brothers and Collman in 1986.<sup>20</sup>

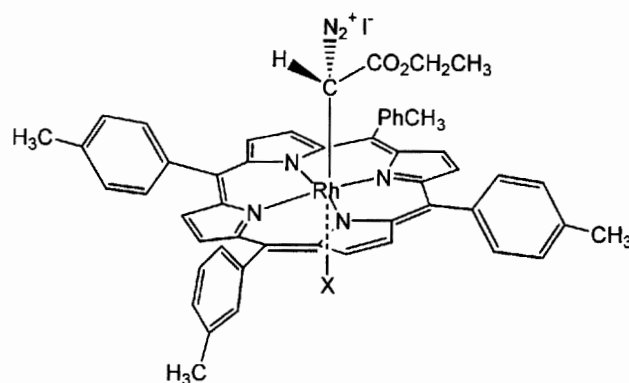
The treatment of cobalt(III) porphyrins with various diazo alkanes was also reported by Callot and Schaeffer<sup>116,117</sup> giving vinyl or halomethyl-cobalt(III)

porphyrins with high yields instead of the Co–N carbene-inserted compounds. However, a reaction pathway involving insertion of a carbene moiety into the Co–N bond was proposed as an initial step, by analogy with previous results reported by Johnson and co-workers.<sup>83</sup> The reactions of tosylhydrazones of aryl ketones with cobalt(III) porphyrins in the presence of triethylamine also gave  $\alpha$ -styrylcobalt(III) porphyrins. It is a reaction without preparation of the diazo compound as an intermediate.<sup>118</sup> A general scheme (Scheme 11) for the reaction of diazoalkanes with metalloporphyrins, including cobalt derivatives, was discussed by the same authors, also suggesting the possible formation of an axial carbene species.<sup>119</sup>

The insertion of formylcarbene into a Co–N bond of cobalt porphyrin with the cobalt being air oxidized to the +3 state was reported by addition of diazoacetaldehyde to (OEP)Co<sup>II</sup> (eq 19).<sup>58</sup> Although the complex is thermally unstable, it was found pure enough to be characterized spectroscopically (<sup>1</sup>H NMR and visible spectroscopy). Similar reactions were obtained with trivalent cobalt porphyrins such as (OEP)CoBr and [(OEP)Co(H<sub>2</sub>O)]ClO<sub>4</sub>. Controlled-potential electrolysis of these complexes gave *N*-alkylporphyrins, in the presence of acetic acid for the removal of cobalt.<sup>58</sup>



Scheme 11



**Figure 4.** Schematic structure showing the complexation of ethyl diazoacetate on the rhodium atom (adapted from Brown, K. C.; Kodadek, T. *J. Am. Chem. Soc.* **1992**, *114*, 8336–8338)

## 2. Rhodium

Several major differences exist between the cobalt(III) and rhodium(III) porphyrin reactivity in presence of diazoalkanes.<sup>119</sup> First, the insertion of a carbene fragment between Rh and N is not observed. In contrast, ethyl diazoacetate gave an adduct possessing a metal–carbon bond (Figure 4). Second, the rhodium porphyrins catalyze the cyclopropanation of olefins in the presence of diazo derivatives. Thus, Callot and coworkers first reported that Rh(III) porphyrins catalyze the decomposition of ethyl diazoacetate and the carbene transfer to cyclohexene to give a mixture of norcaradiene esters.<sup>119–121</sup> More recently, asymmetric cyclopropanations of alkenes catalyzed by chiral rhodium porphyrin were also reported.<sup>122,123</sup> In these reactions, an axial carbene–rhodium complex was proposed<sup>124</sup> as an intermediate but without any experimental characterization. Brown and Kodadek succeeded in characterizing a rhodium porphyrin–ethyl diazoacetate adduct possessing a metal–carbon bond.<sup>124</sup> However, the <sup>13</sup>C and <sup>1</sup>H NMR spectra suggest that it is a novel iodoalkyl complex resulting from the formal insertion of a carbene fragment into the Rh–I bond. These authors also succeeded to characterize a rhodium porphyrin diazoalkyl adduct that results from the stoichiometric condensation of rhodium catalyst and ethyl diazoacetate (Figure 4). Their interpretation argues that metalcarbene formation is a necessary prerequisite for cyclopropanation and that the reaction does not occur by an S<sub>N</sub>2-like displacement of N<sub>2</sub> by the alkene.<sup>125</sup> However, the formation of a metal–carbene complex still needs to be confirmed in the rhodium case.

The first carbene synthesis of a rhodium porphyrin was reported by Boschi and coworkers using a different method.<sup>55</sup> It is well known that isocyanides coordinated

to transition metals react with alcohols or amines leading to the formation of carbene compounds.<sup>13</sup> Thus, [(TPP)Rh(CNBz)<sub>2</sub>]PF<sub>6</sub> undergoes nucleophilic attack of methanol leading to the formation of cationic carbene derivatives. To confirm the structure of the carbene complex, the crystal and molecular structure of (TPP)Rh(CNBz)[C(NHCHPh)<sub>2</sub>]PF<sub>6</sub> was also determined.<sup>55</sup> The coordination sphere of the rhodium atom consists of four pyrrole nitrogen atoms, one carbon atom from the carbene ligand and one carbon atom from the isocyanide group. The rhodium–N bond distances are all nearly equivalent, lying in the narrow range of 2.015(10)–2.057(10) Å.<sup>55</sup> The average value 2.037 Å is normal for the trivalent rhodium ion and in fairly good agreement with values reported for other rhodium(III) porphyrin complexes by X-ray diffraction. For examples, the rhodium–N bond distance is 2.031 (5) Å in the (OEP)Rh(CH<sub>3</sub>) complex<sup>126</sup> and 2.020 (6) Å in the (TPP)Rh(CH<sub>2</sub>Cl) complex.<sup>127</sup> The carbon atom of the carbene ligand is bonded to the rhodium atom at a distance of 2.030(11) Å. The hybridization of the carbene carbon atom is clearly sp<sup>2</sup>, as indicated by the planarity of the RhCNN system and the bond angles at carbon, all close to 120°. These complexes react with ligands (L=P(OMe)<sub>3</sub>, PPh<sub>3</sub>, PhCH<sub>2</sub>NC) leading to the formation of the cationic mixed-ligated species (porphyrin)-Rh[C(NHCHPh)<sub>2</sub>](L)PF<sub>6</sub>. When stronger nucleophiles were used such as methoxide, the formation of neutral amido or alkyl complexes was observed.<sup>55</sup>

The reaction of rhodium(III) porphyrins with acetylenes to give β-chlorovinyl rhodium(III) porphyrins has been reported by Ogoshi and coworkers (eq 20).<sup>128</sup> The formation of acyl rhodium(III) porphyrin complexes is also observed. It was suggested that this reaction proceeds through a cationic intermediate which is subject to resonance stabilization due to a carbene

structure. However, no alkoxy-carbene ligand could be isolated, even in the reaction of (OEP)RhCl with 3-butyne-1-ol under anhydrous conditions.



Although the first representatives of four-coordinate cationic carbene rhodium(I) complexes containing non-Fischer-type carbene ligands have been recently reported,<sup>129</sup> a characterization of similar rhodium porphyrin complexes is still missing, to the best of our knowledge.

## E. GROUP 10

### 1. Nickel

The reaction of *N*-alkyl porphyrins with nickel(II) salts<sup>130,131</sup> causes large rearrangements yielding nickel homoporphyrins<sup>131–133</sup> and a carbene inserted into Ni–N bond of (TPP)Ni.<sup>21,57</sup> The crystal and molecular structure of the carbene complex showed a largely distorted macrocycle with large distances between the opposite pyrrole nitrogen atoms (*vide infra*).<sup>21</sup> Thus, the nickel atom is tetracoordinated with the nitrogen atoms of only three pyrrole rings and with the carbon atom of the carbene fragment. The Ni–C bond length of 1.905(4) Å is close to that expected for a pure  $\sigma$  bond. The four nitrogen atoms of the pyrroles are approximately coplanar but the nickel and carbon atoms are displaced from the porphyrin plane by 0.19 and 1.04 Å, respectively. This carbene complex is analogous to the cobalt(III) congener but is air stable.<sup>83,113</sup> The X-ray structure of the endo epimer of the homoporphyrin Ni(II) complex has also been determined, showing a highly distorted macrocyclic ring and a nickel atom in a square-planar coordination. In this case, the carbene insertion is located between two pyrrole rings.<sup>133</sup>

A new carbene nickel porphyrin has also been prepared by Balch and coworkers<sup>56</sup> but by an entirely different route. Treatment of *N,N'*-bridged tetraphenylporphyrin (TPPC=C(*p*-ClC<sub>6</sub>H<sub>4</sub>)<sub>2</sub>) with Ni(CO)<sub>4</sub> yields the (TPP)Ni(C=C(*p*-ClC<sub>6</sub>H<sub>4</sub>)<sub>2</sub>) complex in which one N–C bond is broken (Scheme 7). In this complex, the vinyl carbene moiety is also inserted into the Ni–N bond of a nickel porphyrin.

## F. GROUP 11

### 1. Copper

The reaction of (OEP)Cu<sup>II</sup> with ethyl diazoacetate yields mainly two isomeric chlorins formed formally by

carbene addition to the cross-conjugated double bond of the porphyrin ring. A small amount of the *meso*-ethoxycarbonylmethyloctaethylporphyrin is also observed.<sup>134,135</sup> A possible formation of a metal–carbene complex as an intermediate was suggested (but not observed) in these reactions because the elimination of nitrogen from aliphatic diazo-compounds catalyzed by copper derivatives is a well-known reaction.<sup>13</sup>

## G. GROUP 12

### 1. Zinc

A general scheme for the reaction of Zn(II) porphyrins with diazoalkanes has been discussed by Callot and Schaeffer.<sup>115</sup> (TPP)Zn or (OEP)Zn reacts with diazoacetates in the presence of copper salts to yield *N*-alkylporphyrins, chlorin, and bacteriochlorin zinc derivatives.<sup>136,137</sup> More substituted diazo derivatives such as N<sub>2</sub>C(CO<sub>2</sub>Me)<sub>2</sub> also give homoporphyrins with Zn tetraphenylporphyrin. The possible formation of a carbene inserted in the Zn–N bond of (TPP)Zn was postulated by analogy with the behavior of cobalt porphyrins but without any experimental evidence.<sup>115</sup> The mechanism of the reaction, in the absence of copper salts, has also been studied. In this case, *N*-alkyl metalloporphyrins were mainly formed.<sup>138</sup>

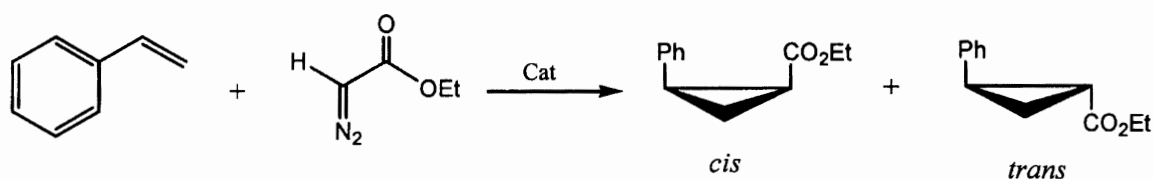
## V. Metalloporphyrins as Catalysts for Carbene Transfer

### A. CYCLOPROPANATION

Enantioselective carbene transfer to olefins is an important area of asymmetric synthesis.<sup>103,139–141</sup> Recent growth in the area of transition metal porphyrin chemistry has, in part, been driven by the increased interest associated with metal-catalyzed cyclopropanation.

The use of metalloporphyrins as cyclopropanation catalysts originated with Callot who reported that (TPP)RhI provided a *cis* preference for the cyclopropanation of styrene with ethyl diazoacetate (Scheme 12).<sup>120,121</sup> This was quite unexpected because cyclopropanation of *cis*-olefin using diazoesters and metal derivatives as catalysts usually gives the *trans* cyclopropyl ester as the major product.<sup>142</sup> The *cis*-selectivity increased with the size of the substituents at the *meso* position and suggested a preferential direction of approach of the alkene toward a rhodium carbene complex.<sup>121</sup> In order to rationally design more selective catalysts, the secondary kinetic isotope effect for the





Scheme 12

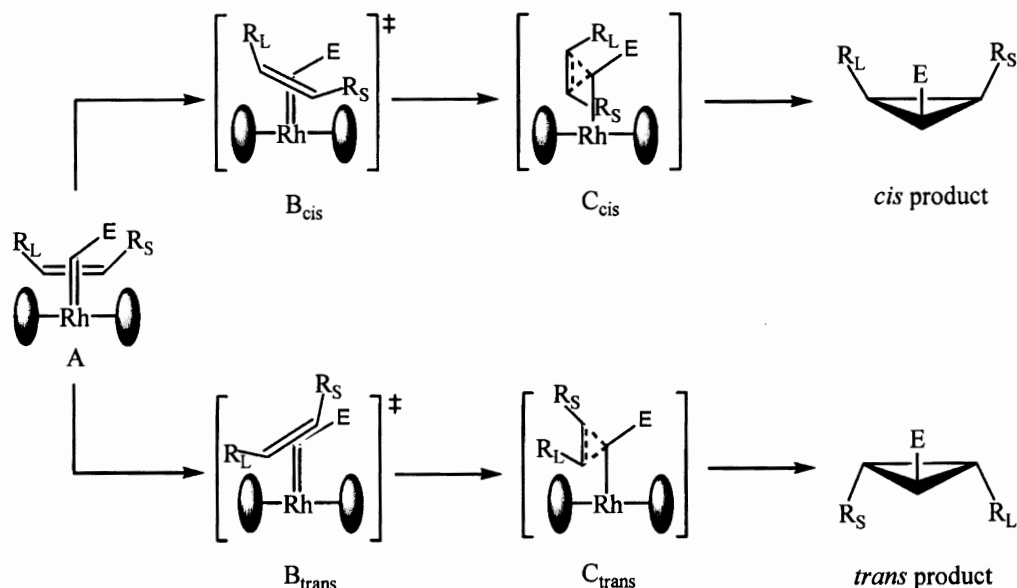
cyclopropanation of styrene- $d_8$  was determined in a competition reaction by Brown and Kodadek.<sup>124</sup> The authors concluded that there is little rehybridization of the alkene in the transition state of the carbene transfer step because no detectable secondary isotope effect was detected (Scheme 12). An active intermediate, a rhodium porphyrin diazoalkyl adduct, has been also isolated during the course of this reaction.<sup>125,143</sup> More thorough mechanistic work in this area is, however, complicated by the lack of synthetic routes to rhodium porphyrin carbene complexes.<sup>127</sup> Indeed, only a single example of such species has so far been prepared.<sup>55</sup> Such a situation is also observed with dirhodium carboxylate catalysts since the first stable dirhodium(II) carbenoid has been recently isolated and its structure determined by X-ray crystallography.<sup>144</sup> It was also found that ethyl diazoacetate in 2-methylnaphthalene solution formed two cyclopropane isomers with (TPFPP)RhI as a catalyst.<sup>145</sup> Recently, the possibility of generating cyclopropane carboxylate esters from olefins and amino esters by diazotization using sodium nitrite and acid in the presence of (TPP)RhI as catalyst was explored by Barrett *et al.*<sup>146</sup> The one-pot synthesis of cyclopropanes from glycine ethyl ester hydrochloride avoids the need to isolate ethyl diazoacetate and the cyclopropane derivatives were generally obtained in a good yield. Unfortunately, all attempts to extend the methodology by replacement of glycine ethyl ester hydrochloride with the corresponding ester salts of alanine, cysteine, serine, phenylalanine, or phenylglycine failed. Asymmetric cyclopropanation of alkenes catalyzed by a chiral rhodium porphyrin was also reported but a moderate enantioselectivity was observed.<sup>123,147</sup>

Examples involving osmium<sup>148,149</sup> and iron<sup>150</sup> porphyrins as catalysts have also been reported but the catalysts mainly provide a *trans* product. A mechanism for iron porphyrin-catalyzed cyclopropanation was proposed by Kodadek and coworkers.<sup>150</sup> A transition state for carbene transfer which is reached later than in the rhodium porphyrin catalyzed reaction is suggested. In this case, the olefin is parallel to the metalcarbene and significant bonding has occurred. This geometry explains why 1,2 disubstituted alkenes are poor

substrates since there is a steric interaction between the porphyrin ring and the alkene (Scheme 13).<sup>150</sup>

The catalytic production of olefins, diethyl maleate, and fumarate, from ethyl diazoacetate has been reported with osmium<sup>26</sup> and ruthenium<sup>50</sup> porphyrins. Despite the periodic relationship of ruthenium to iron and osmium and the syntheses of different carbene complexes of ruthenium porphyrins, developed by Collman *et al.*,<sup>49,54,98</sup> it is only very recently that cyclopropanation<sup>104,151,152</sup> and ethyl diazoacetate insertion into heteroatom bond reactions<sup>153</sup> were observed using ruthenium porphyrins as catalysts. The details of the catalytic reaction of diazoesters with simple olefins catalyzed with ruthenium porphyrins have been reported.<sup>154</sup> Product yields, stereoselectivities and regioselectivities for ruthenium porphyrin-catalyzed cyclopropanation reactions of ethyl diazoacetate with styrene derivatives are compared with observed stereoselectivities for cyclopropanation reactions catalyzed with other metalloporphyrin catalysts. Linear correlations are observed when the rates for competitive cyclopropanation or product stereoisomer ratio are plotted against Hammett constants of various ring-substituted groups on the styrenes.<sup>154</sup> Isomeric distributions for the cyclopropanation of isoprene and 1,3-pentadiene with ethyl diazoacetate and competition studies of the cyclopropanation have also been reported. All of these results agree with a major electronic and steric influence on both the regiochemical and stereochemical control in the catalytic cyclopropanation reactions.<sup>154</sup> Recently, it was discovered that ruthenium porphyrins catalyze effective cyclization of  $\gamma$ -alkoxy- $\alpha$ -diazo- $\beta$ -ketoesters to form 1,3-dioxolanes selectively.<sup>155</sup> Reaction of (TTP)Ru(CO) with a diazo ketoester affords a ruthenium-carbene complex which has been isolated.<sup>155</sup>

There has also been a renewal of interest in reactions catalyzed by ruthenium(II) porphyrin complexes, simultaneously with the development of new chiral ruthenium porphyrins.<sup>156-159</sup> Although these reactions focus mainly on asymmetric epoxidation of olefins,<sup>160,161</sup> in some cases asymmetric cyclopropanations were very successful. As a recent example, the intermolecular cyclopropanation of styrene and its derivatives with



Scheme 13

ethyl diazoacetate afforded the corresponding cyclopropyl esters in up to 98% ee with high *trans/cis* ratios of up to 36 and extremely high catalyst turnovers of up to  $1.1 \times 10^4$ .<sup>52</sup> The structure of the metalloporphyrin is given in Figure 2. Asymmetric intramolecular cyclopropanations were also reported with the same catalyst.<sup>52</sup> In this case, the decomposition of a series of allylic diazoacetates afforded the cyclopropyl lactones in up to 85% ee. Both the inter- and intramolecular cyclopropanation were proposed to proceed via a reactive chiral ruthenium carbene intermediate. The enantioselectivities in these processes were rationalized on the basis of the X-ray crystal structures of closely related stable chiral carbene complexes obtained from the reaction of the chiral complex with  $N_2CPh_2$  and  $N_2C(Ph)CO_2CH_2CH=CH_2$ .

Frauenkron and Berkessel,<sup>162</sup> and Che *et al.*,<sup>151</sup> independently reported that the ruthenium complex of the same chiral porphyrin, can be used to catalyze the cyclopropanation of styrene. The synthesis of this chiral porphyrin was previously reported by Halterman and Jan.<sup>157</sup> This reaction is particularly interesting since the enantiomeric excesses are quite high (90%). Surprisingly, changing the solvent from 1,2-dichloroethane to benzene resulted in an inversion of the absolute configuration of the major enantiomer for the *cis*-cyclopropane and no change for the *trans*-cyclopropane.<sup>162</sup>

Gross *et al.*<sup>163</sup> described asymmetric cyclopropanation of styrene by an enantiopure carbenoid by ruthenium porphyrins as a catalyst. A comparison with the classical approach, chiral porphyrin and non chiral carbenoid, provides significant insight into the

mechanistic aspects of these reactions. Using different metal porphyrin complexes (Ru, Fe, Os, and Rh), the authors clearly demonstrate that the absolute configuration of the major diastereomer is related not to the metal but rather to the structure of the porphyrin.

Further insight into the mechanism of osmium(II) porphyrin catalyzed cyclopropanation of alkenes by diazoalkanes was reported by Woo and coworkers.<sup>149</sup> A mono-carbene complex,  $(TTP)Os(CHCO_2Et)$ , has been isolated but is not the catalytically active species. An electron withdrawing ligand *trans* to the carbene activates the carbon fragment toward transfer to an olefin. Substrate reactivity profiles and labeling studies are consistent with a *trans*-osmium(II) *bis*-carbene species as the active catalyst.<sup>149</sup>

## B. INSERTION

Rhodium(III) porphyrins are known to catalyze the insertion of carbethoxycarbenes from ethyl diazoacetate into the C–H bonds of saturated compounds with yields up to 20–25% corresponding to a large increase of the primary/secondary selectivity.<sup>164</sup> In this case the substrates ( $C_6$  to  $C_{12}$  *n*-alkanes) were used as solvents. The rhodium porphyrins,  $(TPP)RhI$ ,  $(TMP)RhI$ , and  $(OEP)RhI$  efficiently catalyze carbene insertion in O–H bonds, leading to ethers by using ethyl diazoacetate under mild conditions.<sup>165</sup> Using  $(TMP)RhI$  as catalyst, a stereoselective insertion reaction was observed with the order of primary > secondary > tertiary for various alcohols.

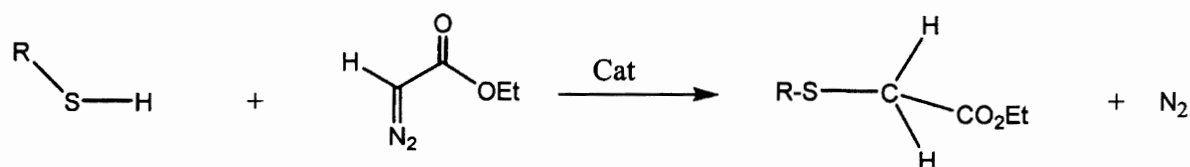
The ruthenium porphyrins, (TPP)RuCO and (TMP)RuCO catalyze carbene insertion into S–H bonds, leading to dialkyl and alkyl aryl sulfides using ethyl diazoacetate under mild conditions. The insertion process is regiospecific since dithiothreitol reacts to give the S–H insertion product without any trace of the ether compound (Scheme 14).<sup>153</sup> With a homochiral porphyrin ruthenium complex, asymmetric insertions were obtained but with low enantioselectivities.<sup>166</sup>

The ruthenium porphyrins, (TPP)Ru(CO) and (TMP)Ru(CO) also catalyze carbene insertion into N–H bonds.<sup>153</sup> Thus, the complex (TMP)Ru(CO) reacts with ethyl diazoacetate in the presence of alkyl and aromatic amines to give the corresponding *N*-substituted glycine ethyl esters (Scheme 15). Both primary and secondary amines react with EDA but it is necessary to add simultaneously the diazo ester and the substrate into the solution to avoid too large excess of

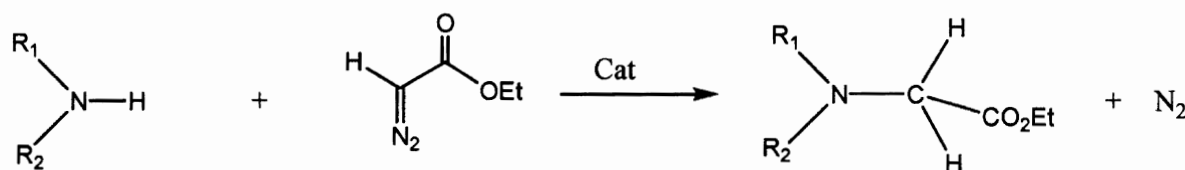
amine in the presence of the catalyst. The nucleophilic amines clearly coordinate to the ruthenium and, to a certain extent, poison the catalyst.

### C. SIGMATROPIC REARRANGEMENTS

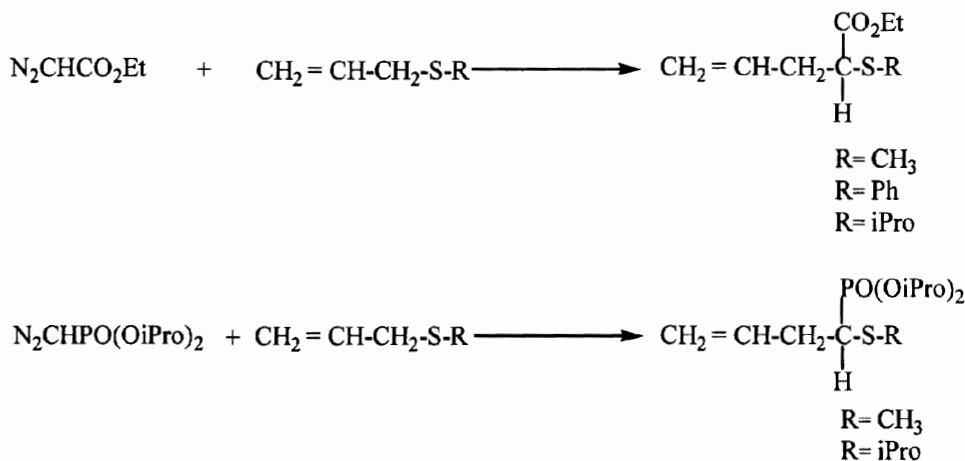
The catalytic effectiveness of ruthenium porphyrins for ylide generation in reactions of ethyl diazoacetate and diisopropyl diazomethylphosphonate with some allylic substrates was described for the first time by Simonneaux and coworkers (Scheme 16).<sup>167</sup> These reactions result in products of the [2,3]-sigmatropic rearrangement of intermediate allylic ylides. It was demonstrated that simple ruthenium porphyrins are highly effective catalysts for carbenoid reactions with alkyl allyl sulfides and alkyl allyl amines providing the *formal C–S or C–N* insertion rather than the more classical cyclopropanation. To fully characterize the catalytic properties of the porphyrin compound, it was



Scheme 14



Scheme 15

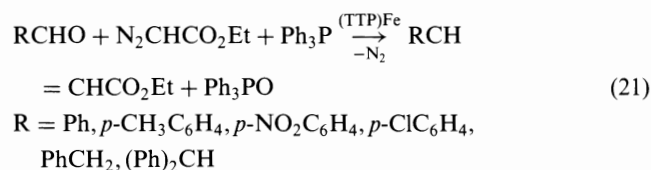


Scheme 16

also shown that, in the competition process between ylide generation and the insertion of the diazo compound into heteroatom-hydrogen bond, only the Z-H (Z = N or S) insertion compound is observed.<sup>167</sup>

#### D. OLEFINATION OF ALDEHYDES

A novel extension of the catalytic activity of metalloporphyrins with the first use of (TPP)Fe<sup>II</sup> as a catalyst for the efficient and selective olefination of aldehydes has been recently reported by Woo and coworkers.<sup>168</sup> Olefination of aromatic and aliphatic aldehydes (eq 21) was achieved in excellent yield (> 85%) at ambient temperature using ethyl diazoacetate and triphenylphosphine in presence of catalytic amount of (TTP)Fe. Ethyl maleate and fumarate were also observed as side products.



In the proposed mechanism, the iron porphyrin serves to catalytically convert the diazo reagent and phosphine to the corresponding phosphorane. Then the phosphorane produces a new olefin and phosphine oxide on reaction with aldehyde.<sup>168</sup> Although other metal complexes can catalyze this reaction,<sup>169,170</sup> the iron system seems to be especially efficient.

## VI. Carbenes as Ligands to Heme Proteins

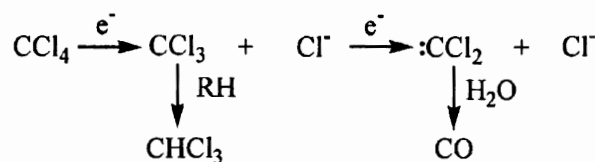
### A. CYTOCHROMES P450

Although carbenes are not natural substrates in biological systems, their formation (interactions) with heme proteins has been extensively studied. Initial experiments were carried out in the 1970–1980s, and several short reviews on carbene formations during interactions of heme proteins with xenobiotics are available.<sup>36,42,92,171,172</sup> Thus, the literature before 1980 will be summarized first and more recent results then will be highlighted.

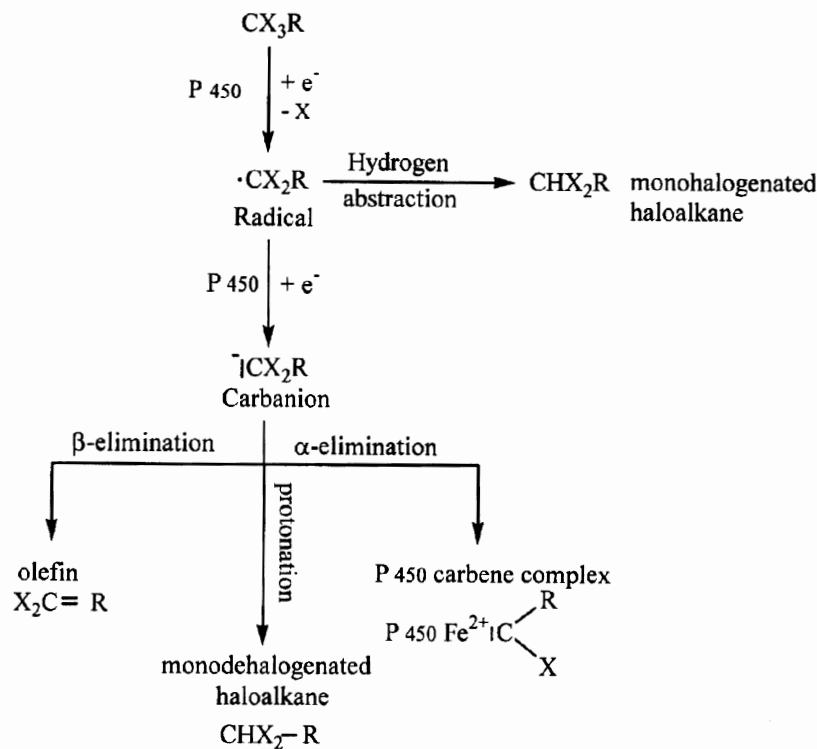
Evidence was first presented in 1974 and then in 1977 for microsomal cytochrome P450 carbene complexes by Ullrich, Mansuy and coworkers.<sup>31,32</sup> Carbon tetrachloride is a hepatotoxic molecule, resulting in the formation of trichloromethyl radicals which are responsible for lethal cellular damages.<sup>173</sup> Initially, the concept for the toxicity of carbon tetrachloride was discussed in a paper of Ullrich and Schnabel in 1973 on carbanion species as ligands of cytochrome P450.<sup>174</sup> Later it was proposed that a two-step reduction of CCl<sub>4</sub> to the CCl<sub>3</sub><sup>-</sup> anion would liberate a chloride ion to yield the highly reactive dichlorocarbene (Scheme 3).<sup>32</sup> Carbon monoxide and chloroform, two other metabolites that result from the reduction of CCl<sub>4</sub>, were detected in incubations that contained P450 and dithionite or in complete systems (P450 and reductase) (Scheme 17).<sup>32,175</sup> The metabolism of carbon tetrachloride and its relationship to lipid peroxidation has been investigated in hepatic microsomes and in reconstituted monooxygenase systems.<sup>175</sup> The results, obtained using purified enzymes, demonstrate that cytochrome P450 can catalyze both the one- and the two-electron reductions of CCl<sub>4</sub> (Scheme 17). It seems also from these studies that the cytochrome P450-mediated reduction of CCl<sub>4</sub> and CCl<sub>4</sub>-induced lipid peroxidation are independent reactions.

The mechanism of the reductive dehalogenation of polyhalogenated compounds by microsomal cytochrome P450 has been studied in detail.<sup>176</sup> The main products of the *in vitro* metabolism of hexa and pentachloroethane were tetra and trichloroethene, respectively. In this case, the reductive dehalogenation probably proceeds by two sequential one-electron reductions forming first a radical and then a carbanion. The carbanion may undergo protonation, alpha or beta elimination forming a mono-halogenated alkane, a carbene or an olefin, respectively (Scheme 18).<sup>176</sup>

Since halothane (CF<sub>3</sub>CHClBr) is one of the most widely used polyhalogenated anaesthetics, a possible formation of carbene species during the interaction of halothane and cytochrome P450 was also proposed by analogy with the results obtained with CCl<sub>4</sub> (eq 22). This hypothesis was tested by producing



Scheme 17



trifluoromethyl carbene chemically from a diazo derivative and by then studying its interaction with rat liver cytochrome P450.<sup>31</sup> The similarity of the halothane induced difference spectrum with that obtained from trifluoro diazoethane suggests the formation of the corresponding carbenoid complex with halothane ( $\lambda_{\max}=470$  nm).



Other cytochrome P450-carbene complexes were found under anaerobic reducing conditions with various polyhalogenated methanes such as  $\text{CBr}_4$ ,  $\text{CCl}_4$ ,  $\text{CCl}_3\text{F}$ ,  $\text{CCl}_3\text{Br}$ ,  $\text{CClCN}$ ,  $\text{CHI}_3$ ,  $\text{CHBr}_3$ , and  $\text{CHCl}_3$ , showing absorption bands between 450 and 480 nm.<sup>32,177</sup> Carbon monoxide is detected as a metabolic product. Carbon monoxide is a known hydrolysis product of dihalogeno carbenes.<sup>178,179</sup> Comparison of cytochrome P450 complex formation using liver microsomal preparations from phenobarbital and 3,4-benzopyrene treated rats showed differences which could be accounted for by a decreasing stability of the halogenomethane complex when the 3,4-benzopyrene induced form is used.<sup>32</sup>

Complexes in which the halocarbon is  $\sigma$ -bonded to the ferric prosthetic heme groups are formed in preference to carbene complexes was also suggested.<sup>47,180</sup> The oxidation of heme proteins by alkyl

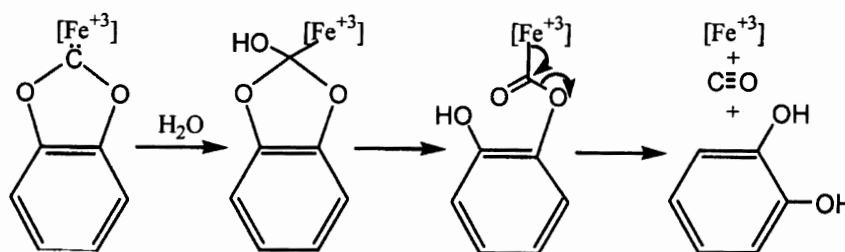
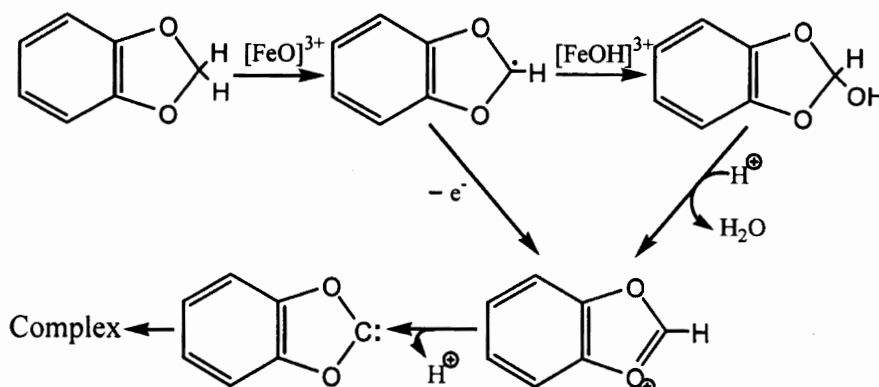
halides was studied by Castro and coworkers.<sup>181,182</sup> It has been argued that halocarbons only give unstable  $\sigma$ -bonded complexes and, for some time, the reality of cytochrome P450-carbene complexes was discussed.<sup>181,182</sup> Actually, these studies discounted the possibility of carbene intermediates arising during cytochrome P450<sub>CAM</sub>-dependent reduction of halogenated methane. However, the data invoked in supporting this view are not convincing because they were obtained in an experimental system in which the complexes with Soret maxima at long wavelengths were not observed.<sup>183</sup> More recent studies,<sup>184</sup> under anaerobic reducing conditions with bacterial cytochrome P450<sub>CAM</sub>, confirm previous results obtained by the groups of Ullrich and Mansuy.<sup>31,32</sup> It was also shown that a purified reconstituted cytochrome P450 containing system is capable of reductive dehalogenation of  $\text{CCl}_4$ . It is now well known that halogenated hydrocarbons interact with models of cytochrome P450 to form iron carbene derivatives.<sup>41,60</sup>

Cytochrome P450 inactivation was observed during reductive metabolism of hydrochlorofluorocarbons, which have been developed as candidate substitutes for the ozone-depleting chlorofluorocarbons.<sup>185</sup> Rat liver microsomes were used providing indirect evidence for the involvement of both P4502E1 and P4502B1/2. The reaction with 1,1-dichloro-2,2,2-trifluoroethane is

prevented by both carbene and free-radical scavengers, providing indirect evidence of a possible role of reactive carbene species in the mechanism. Indeed, various other hydrochlorofluorocarbons are biotransformed by cytochrome P450 to oxygenated products such as 1,1-dichloro-1-fluoroethane.<sup>186</sup>

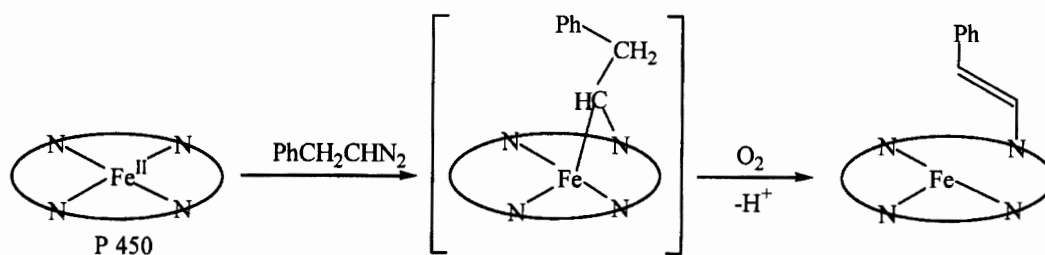
Two theoretical investigations of the anaerobic reduction of halogenated alkanes by cytochrome P450 were also reported in order to predict the reactivity of the substrates.<sup>187,188</sup> An anaerobic reduction cycle for polyhalogenated substrates has been proposed.<sup>187</sup> The strengths of C–H bonds in halogenated methanes were theoretically calculated to correlate to the activity of the radical produced in anaerobic reduction.

The 1,3-benzodioxole derivatives are oxidatively metabolized by cytochrome P450 monooxygenases with formation of very stable complexes of this cytochrome in the ferrous state, characterized by a Soret peak at 455 nm.<sup>189,190</sup> Direct evidence for the presence of 1,3-benzodioxol-2-carbene complexes of cytochrome P450 (eq 8b) came from model studies (eq 8a).<sup>66,191,192</sup> Structure–activity relationships in the interaction of alkoxymethylenedioxybenzene derivatives with microsomal mixed-function oxidase *in vivo* have been reported<sup>193</sup> and the mechanism of this reaction has also been discussed in a review by Ortiz de Montellano (Scheme 19).<sup>194</sup>

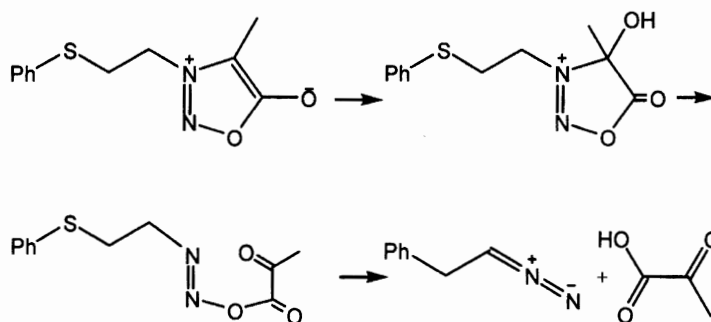


The metabolism of aryldioxymethylene compounds to catechol, carbon monoxide, and formic acid is consistent with hydroxylation of the carbene complex (Scheme 20).<sup>194</sup>

The interactions of related derivatives, methylenedioxyphenyl HIV protease inhibitors with ferrous P450 have been recently examined.<sup>195</sup> It has also been proposed that a carbene is the reactive intermediate generated from these derivatives, which coordinates to the prosthetic heme of P450. Complex formation is reduced when the substituent on the methylenedioxyphenyl moiety is an electron-withdrawing group which destabilizes the carbene–iron complex, whereas, if the substituent is electron-donating, complex formation is increased and stabilized.<sup>195</sup> The electron-donating stabilization of the metabolite-P450 complex was previously observed with other similar derivatives.<sup>196,197</sup> Catechol formation of the aryldioxymethylene derivatives is now well documented. P450 enzymes mediate the hydroxylation of the methylene carbon of many drugs, and resulting hydroxylated intermediates can undergo hydrolysis to yield the catechol intermediate. The metabolism of dimethyl-4,4'-dimethoxy-5,6,5',6'-dimethylene dioxybiphenyl-2,2'-dicarboxylate, an hepatic drug, by cytochrome P450 is a recent example of such behavior.<sup>198</sup> Regiochemical differences in cytochrome P450 isozymes responsible for the oxidation of



Scheme 21



Scheme 22

methylenedioxyphenyl groups by rabbit liver have been observed.<sup>199</sup> In particular, it was suggested that complex formation with methylenedioxyamphetamine was not due to the carbene pathway involving the methylene dioxy group but was due to oxidation of the amino group.

The metabolism of sydnone, which are a pharmacology interesting class of drugs,<sup>200</sup> has been shown to be a mechanism-based inactivator of microsomal P450 (Scheme 21).<sup>194</sup> Enzymatic destruction is accompanied by the formation of *N*-vinylprotoporphyrin IX. It was first suggested that intermediate formation of diazo compounds<sup>201</sup> (Scheme 22) from sydnone metabolism gives bridged Fe–C–N iron carbene complexes.<sup>194</sup> To better define the mechanism of these reactions, other sydnone substrates that do not have a leaving group were also examined in order to explain the formation of *N*-alkyl heme adduct.<sup>77</sup> Reaction of the same diazoalkane with iron-porphyrin models confirms the formation of the carbene complexes as precursors of the *N*-alkyl porphyrins.<sup>39</sup>

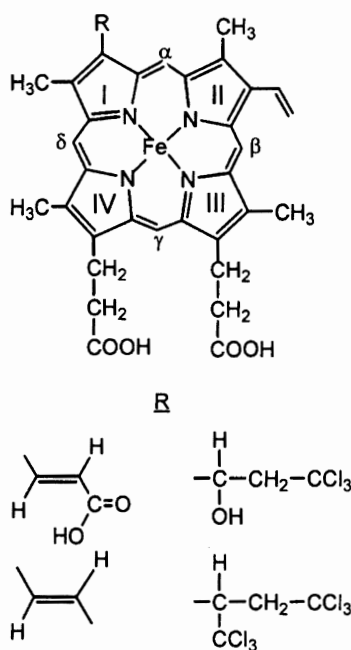
Bacterial cytochrome P450 has been used as an excellent model to better understand bacterial reductive dehalogenation biochemistry.<sup>183,184</sup> Thus, the binding of halogenated pollutants to cytochrome P450<sub>CAM</sub> has been investigated. Hexachloroethane was found to bind more tightly to Fe(III)-P450<sub>CAM</sub> than the physiological substrate camphor.<sup>184</sup> In this study, it was found that the enzyme catalyzed a single turnover stoichiometric

reduction of CFC<sub>3</sub> to carbon monoxide, indicating a carbene intermediate in the reaction pathway.<sup>184</sup> A similar carbene pathway to CO has been proposed during reduction of CFC<sub>3</sub> by cobalamins or a methanogenic bacterium.<sup>202</sup> It is also known that fluorine substituents stabilize carbenes.<sup>203</sup> However, the reported data do not discriminate between potential free or iron-bound heme carbene intermediates.

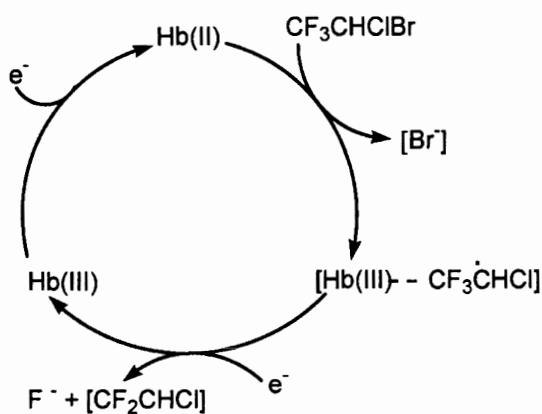
Finally, photocarbenes have been used to probe the active site of cytochrome P450 2B4. Spiro[adamantane-2,2'-diazirine] which produces adamantyl carbene under photolysis, binds tightly to P450 2B4 (*K*<sub>s</sub>=3.2 μM) giving a normal substrate binding difference spectrum.<sup>204</sup> The results after irradiation were interpreted as the presence of an active site carbene reacting by three competing pathways: capture of the heme sixth ligand to yield 2-adamantol or 2-adamantanecarbonitrile, capture of an unbound active site water molecule to yield adamantol, and covalent attachment to a protein residue.<sup>204</sup>

## B. MYOGLOBIN AND HEMOGLOBIN

The oxidation of heme proteins by alkyl halides was studied by Castro and coworkers.<sup>205</sup> The oxidation of deoxymyoglobin and deoxyhemoglobin by bromomalonitrile has been reported as yielding metmyoglobin, methemoglobin and malonitrile.<sup>205,206</sup> The reductive metabolism of BrCCl<sub>3</sub> by ferrous deoxymyoglobin leads



Scheme 23



Scheme 24

to the formation of three major modified heme products (Scheme 23) and a protein-bound heme adduct which were identified.<sup>207</sup> All of these metabolites appear to result from an initial regiospecific attack of the trichloromethyl radical on the vinyl group of the heme.

More recently, the reductive activation of halothane ( $\text{CF}_3\text{CHBrCl}$ ), which is a hepatotoxic anaesthetic molecule, by human hemoglobin results in the modification of the prosthetic heme.<sup>208</sup> The inhibition of the reaction by adding exogenous CO or the spin trapping agent *N*-*t*-butyl- $\alpha$ -phenyl nitron to the incubation mixture indicated that (i) a reduced and free heme iron is required by Hb to activate the halogenated substrate, and (ii) the formation of free radical species is responsible for Hb inactivation. However no carbene

species were detected in these reactions. The mechanism is shown in Scheme 24.

## Conclusion

A large amount of work has been accomplished over the years on the synthesis and characterization of the metal-carbene group in synthetic carbene metalloporphyrins and carbene heme proteins. Evidence of carbene formation during the metabolism of various drugs is still increasing. For example, it is probable that the availability of new drugs<sup>209</sup> such as recent HIV protease inhibitors<sup>195</sup> or other drugs,<sup>198</sup> will generate more discoveries involving new aspects of the carbene chemistry relevant to biological systems.

This survey also illustrates that metalloporphyrins are versatile catalysts that can be used in many different reactions involving carbene transfer. Their development will be considerably widened in the future, with possible application in asymmetric catalysis.

## REFERENCES

1. Demonceau, A.; Hubert, A. J.; Noels, A. F. *Metal Promoted Selectivity in Organic Synthesis*. Noels, A. F., Graziani, M., Hubert, A. J. Eds.; Kluwer Academic Publishers: Dordrecht, **1991**; 237–259.
2. Bourissou, D.; Guerret, O.; Gabbai, F. P.; Bertrand, G. *Chem. Rev.* **2000**, *100*, 39–91.
3. Tomioka, H. *Acc. Chem. Res.* **1997**, *30*, 315–321.
4. Herrmann, W. A.; Köcher, C. *Angew. Chem. Int. Ed. Engl.* **1997**, *36*, 2162–2187.



5. Igau, A.; Grutzmacher, H.; Baceiredo, A.; Bertrand, G. *J. Am. Chem. Soc.* **1988**, *110*, 6463–6466.
6. Arduengo, A. J., III; Dias, H. V. R.; Harlow, R. L.; Kline, M. *J. Am. Chem. Soc.* **1992**, *114*, 5530–5534.
7. Kirmse, W. In *Carbene Chemistry*. Academic Press: New York, **1964**; 1st edn.
8. Moss, R. A.; Jones, M. J. *Carbenes*. Wiley: New York, **1973**; Vol. 1.
9. Moss, R. A.; Jones, M. J. *Carbenes*. Wiley: New York, **1975**; Vol. 2.
10. Fischer, E. O. *Adv. Organometal. Chem.* **1976**, *14*, 1–32.
11. Schrock, R. R. *J. Am. Chem. Soc.* **1976**, *98*, 5399–5400.
12. Schrock, R. R. *Acc. Chem. Res.* **1979**, *12*, 98–104.
13. Cardin, D. J.; Cetinkaya, B.; Lappert, M. F. *Chem. Rev.* **1972**, *72*, 545–574.
14. Herrmann, W. A. *Angew. Chem. Int. Ed. Engl.* **1978**, *17*, 800–812.
15. Dotz, K. H.; Fischer, H.; Hofmann, P.; Kreissl, F. R.; Schubert, U.; Weiss, K. *Transition Metal Carbene Complexes*. Verlag Chemie: Weinheim, **1983**.
16. Brookhart, M.; Studabaker, W. B. *Chem. Rev.* **1987**, *87*, 411–432.
17. Doyle, M. P. *Comprehensive Organometallic Chemistry II* **1994**, Vol. 12, 421–468.
18. Trnka, T. M.; Grubbs, R. H. *Acc. Chem. Res.* **2001**, *34*, 18–29.
19. (a) Tatsumi, K.; Hoffmann, R. *Inorg. Chem.* **1981**, *20*, 3771–3784.  
(b) Tatsumi, K.; Hoffmann, R.; Whangbo, M.H. *J. Chem. Soc., Chem. Commun.* **1980**, 509–511.
20. Brothers, P. J.; Collman, J. P. *Acc. Chem. Res.* **1986**, *19*, 209–215.
21. Chevrier, B.; Weiss, R. *J. Am. Chem. Soc.* **1976**, *98*, 2985–2990.
22. Chevrier, B.; Weiss, R.; Lange, M.; Chottard, J. C.; Mansuy, D. *J. Am. Chem. Soc.* **1981**, *103*, 2899–2901.
23. Latos-Grazynski, L.; Cheng, R. J.; La Mar, G. N.; Balch, A. L. *J. Am. Chem. Soc.* **1981**, *103*, 4270–4272.
24. Batten, P.; Hamilton, A. L.; Johnson, A. W.; Mahendran, M.; Ward, D.; King, T. J. *Chem. Soc. Perkin 1* **1977**, 1623–1628.
25. Guerin, P.; Battioni, J. P.; Chottard, J. C.; Mansuy, D. *J. Organometal. Chem.* **1981**, *218*, 201–209.
26. Woo, L. K.; Smith, D. A. *Organometallics* **1992**, *11*, 2344–2346.
27. Li, Y.; Huang, J. S.; Zhou, Z. Y.; Che, C. M. *J. Am. Chem. Soc.* **2001**, *123*, 4843–4844.
28. Loew, G. H.; Herman, Z. S.; Rhomer, M.; Goldblum, A.; Pudzianowski, A. *Ann. N.Y. Acad. Sci.* **1981**, *367*, 192–218.
29. Lange, M.; Battioni, J. P.; Mansuy, D.; Lexa, D.; Saveant, J. M. *J. Chem. Soc., Chem. Commun.* **1981**, 888–890.
30. Jones, T. K.; McPherson, C.; Chen, H. L.; Kendrick, M. J. *Inorg. Chim. Acta* **1993**, *206*, 5–7.
31. Mansuy, D.; Nastainczyk, W.; Ullrich, V. *Naunyn-Schmiedeberg's Arch. Pharmacol.* **1974**, *285*, 315–324.
32. Wolf, C. R.; Mansuy, D.; Nastainczyk, W.; Deutschmann, G.; Ullrich, V. *Mol. Pharmacol.* **1977**, *13*, 698–705.
33. Hanson, L. K.; Eaton, W. A.; Sligar, S. G.; Gunsalus, I. C.; Gouterman, M.; Connell, C. R. *J. Am. Chem. Soc.* **1976**, *98*, 2672–2674.
34. English, D. R.; Hendrickson, D. N.; Suslick, K. S. *Inorg. Chem.* **1983**, *22*, 367–368.
35. Lu, D.; Paeng, I. R.; Nakamoto, K. *J. Coord. Rev.* **1991**, *83*, 3–12.
36. Mansuy, D.; Chottard, J. C.; Lange, M.; Battioni, J. P. *J. Mol. Catal.* **1980**, *7*, 215–226.
37. Fischer, E. O.; Maasböl, A. *Angew. Chem., Int. Ed. Engl.* **1964**, *3*, 580–581.
38. Fischer, H. *Transition Metal Carbene Complexes*. Verlag Chemie: Weinheim, **1983**; 1–72.
39. Artaud, I.; Gregoire, N.; Leduc, P.; Mansuy, D. *J. Am. Chem. Soc.* **1990**, *112*, 6899–6905.
40. Seyler, J. W.; Safford, L. K.; Fanwick, P. E.; Leidner, C. R. *Inorg. Chem.* **1992**, *31*, 1545–1547.
41. Mansuy, D.; Lange, M.; Chottard, J. C.; Guerin, P.; Morliere, P.; Brault, D.; Rougee, M. *J. Chem. Soc., Chem. Commun.* **1977**, 648–649.
42. Mansuy, D. *Pure Appl. Chem.* **1980**, *52*, 681–690.
43. Brault, D.; Bizet, C.; Morliere, M.; Rougee, M.; Land, E. J.; Santus, R.; Swallow, A. J. *J. Am. Chem. Soc.* **1980**, *102*, 1015–1020.
44. Brault, D.; Neta, P. *J. Am. Chem. Soc.* **1981**, *103*, 2705–2710.
45. Lexa, D.; Saveant, J. M.; Battioni, J. P.; Lange, M.; Mansuy, D. *Angew. Chem., Int. Ed. Engl.* **1981**, *20*, 578–579.
46. Mansuy, D.; Fontecave, M.; Battioni, J. P. *J. Chem. Soc., Chem. Commun.* **1982**, 317–319.
47. Mansuy, D.; Battioni, J. P. *J. Chem. Soc., Chem. Commun.* **1982**, 638–639.
48. Battioni, J. P.; Mansuy, D.; Chottard, J. C. *Inorg. Chem.* **1980**, *19*, 791–792.
49. Collman, J. P.; Brothers, P. J.; McElwee-White, L.; Rose, E.; Wright, L. J. *J. Am. Chem. Soc.* **1985**, *107*, 4570–4571.
50. Collman, J. P.; Rose, E.; Venburg, G. D. *J. Chem. Soc., Chem. Commun.* **1993**, 934–935.
51. Galardon, E.; Le Maux, P.; Toupet, L.; Simonneaux, G. *Organometallics* **1998**, *17*, 565–569.
52. Che, C. M.; Huang, J. S.; Lee, F. W.; Li, Y.; Lai, T. S.; Kwong, H. L.; Teng, P. F.; Lee, W. S.; Lo, W. C.; Peng, S. M.; Zhou, Z. Y. *J. Am. Chem. Soc.* **2001**, *123*, 4119–4129.
53. Artaud, I.; Gregoire, N.; Battioni, J. P.; Dupré, D.; Mansuy, D. *J. Am. Chem. Soc.* **1988**, *110*, 8714–8716.
54. Collman, J. P.; Brothers, P. J.; McElwee-White, L.; Rose, E. *J. Am. Chem. Soc.* **1985**, *107*, 6110–6111.
55. Boschi, T.; Licocchia, S.; Paolesse, R.; Tagliatesta, P.; Pelizzi, G.; Vitali, F. *Organometallics* **1989**, *8*, 330–336.
56. Chan, Y. W.; Renner, M. W.; Balch, A. L. *Organometallics* **1983**, *2*, 1888–1889.
57. Callot, H. J.; Tschamber, T.; Chevrier, B.; Weiss, R. *Angew. Chem., Int. Ed. Engl.* **1975**, *14*, 567–568.
58. Setsune, J. I.; Dolphin, D. *Organometallics* **1984**, *3*, 440–443.
59. Brault, D.; Rougee, M.; Momenteau, M. *J. Chim. Phys.* **1971**, *98*, 1621–1629.
60. Mansuy, D.; Lange, M.; Chottard, J. C.; Bartoli, J. F.; Chevrier, B.; Weiss, R. *Angew. Chem., Int. Ed. Engl.* **1978**, *17*, 781–782.
61. Scheidt, W. R.; Reed, C. A. *Chem. Rev.* **1981**, *81*, 543–555.
62. Scheidt, W. R. *Systematics of the Stereochemistry of Porphyrins and Metalloporphyrins*, In *The Porphyrin Handbook*. Kadish, K. M., Smith, K. M., Guillard, R., Eds.; Academic Press: Boston, **2000**; Vol. 3, pp. 49–112.
63. Chottard, G.; Battioni, P.; Battioni, J. P.; Lange, M.; Mansuy, D. *Inorg. Chem.* **1981**, *20*, 1718–1722.
64. Mansuy, D.; Guerin, P.; Chottard, J. C. *J. Organometal. Chem.* **1979**, *171*, 195–201.
65. Mansuy, D.; Lange, M.; Chottard, J. C. *J. Am. Chem. Soc.* **1978**, *100*, 3213–3214.
66. Mansuy, D.; Battioni, J. P.; Chottard, J. C.; Ullrich, V. *J. Am. Chem. Soc.* **1979**, *101*, 3971–3973.
67. Battioni, J. P.; Chottard, J. C.; Mansuy, D. *Inorg. Chem.* **1982**, *21*, 2056–2062.
68. Mansuy, D.; Lecomte, J. P.; Chottard, J. C.; Bartoli, J. F. *Inorg. Chem.* **1981**, *20*, 3119–3121.
69. Goedken, V. L.; Deakin, M. R.; Bottomley, L. A. *J. Chem. Soc.* **1982**, 607–608.
70. Battioni, J. P.; Dupre, D.; Mansuy, D. *J. Organometal. Chem.* **1981**, *214*, 303–309.
71. Beck, W.; Knauer, W.; Robl, C. *Angew. Chem., Int. Ed. Engl.* **1990**, *29*, 318–320.
72. Mansuy, D.; Lange, M.; Chottard, J. C. *J. Am. Chem. Soc.* **1979**, *101*, 6437–6439.
73. Balch, A. L.; Cheng, R. J.; La Mar, G. N.; Latos-Grazynski, L. *Inorg. Chem.* **1985**, *24*, 2651–2656.

74. Olmstead, M. M.; Cheng, R. J.; Balch, A. L. *Inorg. Chem.* **1982**, *21*, 4143–4148.
75. Mansuy, D.; Morgenstern-Badarau, I.; Lange, M.; Gans, P. *Inorg. Chem.* **1982**, *21*, 1427–1430.
76. Ortiz de Montellano, P. R.; Grab, L. A. *J. Am. Chem. Soc.* **1986**, *108*, 5584–5589.
77. Grab, L. A.; Swanson, B. A.; Ortiz de Montellano, P. R. *Biochemistry* **1988**, *27*, 4805–4814.
78. Balch, A. L.; Chan, Y. W.; La Mar, G. N.; Latos-Grazynski, L.; Renner, M. W. *Inorg. Chem.* **1985**, *24*, 1437–1443.
79. Wisnieff, T. J.; Gold, A.; Evans, Jr, S. A. *J. Am. Chem. Soc.* **1981**, *103*, 5616–5618.
80. Mansuy, D.; Battioni, J. P.; Chottard, J. C. *J. Am. Chem. Soc.* **1978**, *100*, 4311–4312.
81. Mansuy, D.; Lange, M.; Chottard, J. C.; Bartoli, J. F. *Tetrahedron Lett.* **1978**, 3027–3030.
82. Bruice, T. C.; Furter, P. G.; Ball, S. S. *J. Am. Chem. Soc.* **1981**, *103*, 4578–4580.
83. Johnson, A.; Ward, D.; Batten, P.; Hamilton, A. L.; Shelton, G.; Elson, C. M. *J. Chem. Soc., Perkin Trans I* **1975**, 2076–2085.
84. Ziegler, C. J.; Suslick, K. S. *J. Am. Chem. Soc.* **1996**, *118*, 5306–5307.
85. Ziegler, C. J.; Suslick, K. S. *J. Organometal. Chem.* **1997**, *528*, 83–90.
86. Crabtree, R. H. *Organometallic Chemistry of the Transition Metals*. Wiley: New York, 2nd edn. **1994**.
87. Rooney, A. D.; McGarvey, J. J.; Gordon, K. C. *Organometallics* **1995**, *14*, 107–113.
88. Pourreau, D. B.; Geoffroy, G. L. *Adv. Organometal. Chem.* **1985**, *24*, 249–352.
89. Battioni, J. P.; Lexa, D.; Mansuy, D.; Saveant, J. M. *J. Am. Chem. Soc.* **1983**, *105*, 207–215.
90. Guilard, R.; Tabard, A.; Van Caemelbecke, E.; Kadish, K. M. *The Porphyrin Handbook*. Academic Press: Boston, **2000**; Vol. 3, pp. 295–345.
91. Setsune, J. I.; Iida, T.; Kitao, T. *Tetrahedron Lett.* **1988**, *29*, 5677–5680.
92. Setsune, J. I.; Dolphin, D. *Can. J. Chem.* **1987**, *65*, 459–467.
93. Buschman, J.; Angst, W.; Schwarzenbach, R. P. *Environ. Sci. Technol.* **1999**, *33*, 1015–1020.
94. Lange, M.; Mansuy, D. *Tetrahedron Lett.* **1981**, *22*, 2561–2564.
95. Chan, Y. W.; Wood, F. E.; Renner, M. W.; Hope, H.; Balch, A. *J. Am. Chem. Soc.* **1984**, *106*, 3380–3381.
96. Balch, A. L.; Chan, Y. W.; Olmstead, M. M.; Renner, M. W.; Wood, F. E. *J. Am. Chem. Soc.* **1988**, *110*, 3897–3902.
97. Collman, J. P.; Barnes, C. E.; Swepston, P. N.; Ibers, J. A. *J. Am. Chem. Soc.* **1984**, *106*, 3500–3510.
98. Collman, J. P.; McElwee-White, L.; Brothers, P. J.; Rose, E. *J. Am. Chem. Soc.* **1986**, *108*, 1332–1333.
99. Camenzind, M. J.; James, B. R.; Dolphin, D. *J. Chem. Soc., Chem. Commun.* **1986**, 1137–1139.
100. Rajapakse, N.; James, B. R.; Dolphin, D. *Can. J. Chem.* **1990**, *68*, 2274–2277.
101. Setsune, J. I.; Yoshida, Z. I.; Ogoshi, H. *J. Chem. Soc., Perkin Trans. I* **1982**, 983–987.
102. Bonomo, L.; Stern, C.; Solari, E.; Scopelliti, R.; Floriani, C. *Angew. Chem., Int. Ed. Engl.* **2001**, *40*, 1449–1452.
103. Nishiyama, H.; Aoki, K.; Itoh, H.; Iwamura, T.; Sakata, N.; Kurihara, O.; Motoyama, Y. *Chem. Lett.* **1996**, 1071–1072.
104. Galardon, E.; Le Maux, P.; Simonneaux, G. *J. Chem. Soc., Chem. Commun.* **1997**, 927–928.
105. Djukic, J. P.; Smith, D. A.; Young, V. G.; Woo, L. K. *Organometallics* **1994**, *13*, 3020–3026.
106. Nguyen, S. T.; Johnson, L. K.; Grubbs, R. H. *J. Am. Chem. Soc.* **1992**, *114*, 3974–3975.
107. Adams, H.; Bailey, N. A.; Ridgway, C.; Taylor, B. F.; Walter, S. J.; Winter, M. J. *J. Organometal. Chem.* **1990**, *394*, 349–364.
108. Ke, M.; Rettig, S. J.; James, B. R.; Dolphin, D. *J. Chem. Soc., Chem. Commun.* **1987**, 1110–1112.
109. Schrock, R. R. *J. Am. Chem. Soc.* **1975**, *97*, 6577–6578.
110. Tilset, M.; Bodner, G. S.; Senn, D. R.; Gladysz, J. A.; Parker, V. D. *J. Am. Chem. Soc.* **1987**, *109*, 7551–7553.
111. Woo, L. K.; Smith, D. A.; Young, V. G. *Organometallics* **1991**, *10*, 3977–3982.
112. Djukic, J. P.; Young, V. G.; Woo, L. K. *Organometallics* **1994**, *13*, 3995–4003.
113. Batten, P.; Hamilton, A.; Johnson, A.; Shelton, G.; Ward, D. *J. Chem. Soc., Chem. Commun.* **1974**, 550–551.
114. Johnson, A. W.; Ward, D. *J. Chem. Soc., Perkin Trans I* **1977**, 720–723.
115. Callot, H.; Schaeffer, E. *New. J. Chem.* **1980**, *4*, 307–309.
116. Callot, H. J.; Schaeffer, E. *Tetrahedron Lett.* **1977**, 239–242.
117. Callot, H. J.; Schaeffer, E. *J. Organometal. Chem.* **1978**, *145*, 91–99.
118. Callot, H. J.; Schaeffer, E. *J. Organometal. Chem.* **1980**, *193*, 111–115.
119. Callot, H.; Schaeffer, E. *New. J. Chem.* **1980**, *4*, 311–314.
120. Callot, H. J.; Piechocki, C. *Tetrahedron Lett.* **1980**, *21*, 3489–3492.
121. Callot, H. J.; Metz, F.; Piechocki, C. *Tetrahedron* **1982**, *38*, 2365–2369.
122. O'Malley, S.; Kodadek, T. *Organometallics* **1992**, *11*, 2299–2302.
123. Maxwell, J. L.; O'Malley, S.; Brown, K. C.; Kodadek, T. *Organometallics* **1992**, *11*, 645–652.
124. Brown, K. C.; Kodadek, T. *J. Am. Chem. Soc.* **1992**, *114*, 8336–8338.
125. Maxwell, J. L.; Brown, K. C.; Bartley, D. W.; Kodadek, T. *Science* **1992**, *256*, 1544–1547.
126. Tanaka, A.; Syal, S. K.; Sasada, Y.; Omura, T.; Ogoshi, H.; Yoshida, Z. *Acta Cryst.* **1976**, *B32*, 62–65.
127. Collman, J. P.; Boulatov, R. *Inorg. Chem.* **2001**, *40*, 560–563.
128. Ogoshi, I.; Setsune, J. I.; Nando, Y.; Yoshida, Z. I. *J. Organometal. Chem.* **1978**, *159*, 329–339.
129. Bleuel, E.; Weberndörfer, B.; Werner, H. *J. Organometal. Chem.* **2001**, *617–618*, 502–510.
130. Callot, H. J.; Tschamber, T. *Tetrahedron Lett.* **1974**, 3155–3158.
131. Callot, H. J.; Tschamber, T. *Tetrahedron Lett.* **1974**, 3159–3162.
132. Callot, H. J.; Tschamber, T. *J. Am. Chem. Soc.*, **1975**, *97*, 6175–6180.
133. Chevrier, B.; Weiss, R. *J. Am. Chem. Soc.* **1975**, *97*, 1416–1421.
134. Callot, H. J.; Johnson, A. W. *J. Chem. Soc., Chem. Commun.* **1969**, 749–750.
135. Callot, H. J.; Johnson, A. W.; Sweeney, A. J. *J. Chem. Soc. Perkin I* **1973**, 1424–1427.
136. Callot, H. *Bull. Soc. Chim. Fr.* **1972**, 4387–4391.
137. Callot, H. J. *Tetrahedron Lett.* **1972**, 1011–1014.
138. Callot, H.; Tschamber, T. *Bull. Chem. Soc. Fr.* **1973**, 3192–3198.
139. Nishiyama, H.; Itoh, Y.; Matsumoto, H.; Park, S. B.; Itoh, K. *J. Am. Chem. Soc.* **1994**, *116*, 2223–2224.
140. Nishiyama, H.; Itoh, Y.; Suwagata, Y.; Matsumoto, H.; Aoki, K.; Itoh, K. *Bull. Chem. Soc. Jpn.* **1995**, *68*, 1247–1262.
141. Doyle, M. P.; Forbes, D. C. *Chem. Rev.* **1998**, *98*, 911–935.
142. Doyle, M. P. *Chem. Rev.* **1986**, *86*, 919–939.
143. Bartley, D. W.; Kodadek, T. *J. Am. Chem. Soc.* **1993**, *115*, 1656–1660.
144. Snyder, J. P.; Pawda, A.; Stengel, T.; Arduengo, I.; A. J.; Jockisch, A.; Kim, H. J. *J. Am. Chem. Soc.* **2001**, *123*, 11318–11319.
145. Yang, J.; Breslow, R. *Tetrahedron Lett.* **2000**, *41*, 8063–8067.
146. Barrett, A. G. M.; Braddock, D. G.; Lenoir, I.; Tone, I. *J. Org. Chem.* **2001**, *66*, 8260–8263.
147. O'Malley, S.; Kodadek, T. *Organometallics* **1992**, *11*, 2299–2302.

148. Smith, D. A.; Reynolds, D. N.; Woo, L. K. *J. Am. Chem. Soc.* **1993**, *115*, 2511–2513.
149. Hamaker, C. G.; Djukic, J. P.; Smith, D. A.; Woo, L. K. *Organometallics* **2001**, *20*, 5189–5199.
150. Wolf, J. R.; Hamaker, C. G.; Djukic, J. P.; Kodadek, T.; Woo, L. K. *J. Am. Chem. Soc.* **1995**, *117*, 9194–9199.
151. Lo, W. C.; Che, C. M.; Cheng, K. F.; Mak, T. C. W. *J. Chem. Soc., Chem. Commun.* **1997**, 1205–1206.
152. Simonneaux, G.; De Montigny, F.; Paul-Roth, C.; Gulea, M.; Masson, S. *Tetrahedron Lett.* **2002**, *43*, 3685–3687.
153. Galardon, E.; Le Maux, P.; Simonneaux, G. *J. Chem. Soc., Perkin Trans. 1* **1997**, 2455–2456.
154. Galardon, E.; Le Maux, P.; Simonneaux, G. *Tetrahedron* **2000**, *56*, 615–621.
155. Zheng, S. L.; Yu, W. Y.; Che, C. M. *Org. Lett.* **2002**, *4*, 889–892.
156. Le Maux, P.; Bahri, H.; Simonneaux, G. *J. Chem. Soc., Chem. Commun.* **1991**, 1350–1352.
157. Halterman, R. L.; Jan, S. T. *J. Org. Chem.* **1991**, *56*, 5253–5254.
158. Ini, S.; Kapon, M.; Cohen, S.; Gross, Z. *Tetrahedron: Asymmetry* **1996**, *7*, 659–662.
159. Lai, T. S.; Kwong, H. L.; Zhang, R.; Che, C. M. *J. Chem. Soc., Dalton Trans.* **1998**, 3559–3564.
160. Gross, Z.; Ini, S.; Kapon, M.; Cohen, S. *Tetrahedron Lett.* **1996**, *37*, 7325–7328.
161. Berkessel, A.; Frauenkron, M. *J. Chem. Soc. Perkin Trans.* **1997**, 2265–2266.
162. Frauenkron, M.; Berkessel, A. *Tetrahedron Lett.* **1997**, *38*, 7175–7176.
163. Gross, Z.; Galili, N.; Simkhovich, L. *Tetrahedron Lett.* **1999**, *40*, 1571–1574.
164. Callot, H.; Metz, F. *Tetrahedron Lett.* **1982**, *23*, 4321–4324.
165. Hayashi, T.; Kato, T.; Kaneko, T.; Asai, T.; Ogoshi, H. *J. Organometal. Chem.* **1994**, *473*, 323–327.
166. Galardon, E.; Roué, S.; Le Maux, P.; Simonneaux, G. *Tetrahedron Lett.* **1998**, *39*, 2333–2334.
167. Simonneaux, G.; Galardon, E.; Paul-Roth, C.; Gulea, M.; Masson, S. *J. Organometal. Chem.* **2001**, *617–618*, 360–363.
168. Mirafzal, G. A.; Cheng, G.; Woo, L. K. *J. Am. Chem. Soc.* **2002**, *124*, 176–177.
169. Fujimura, O.; Honma, T. *Tetrahedron Lett.* **1998**, *39*, 625–626.
170. Shen, Y.; Zhang, Y.; Zhou, Y. *J. Chem. Soc., Chem. Commun.* **1998**, 2195–2196.
171. Mansuy, D. *Inorg. Chim. Acta* **1983**, *79*, 9–10.
172. Ortiz de Montellano, P. R. E. *Cytochrome P-450: Structure, Mechanism and Biochemistry*. Plenum Press: New York, **1986**.
173. Recknagel, R. O.; Glence, E. A. *J. CRC Crit. Rev. Toxicol.* **1973**, *2*, 263–296.
174. Ullrich, V.; Schnabel, K. H. *Drug Metab. Disposition* **1973**, *1*, 176–182.
175. Wolf, C. R.; Harrelson, W. G.; Nastainczyk, W. M.; Philpot, R. M.; Kalyanaraman, B.; Mason, R. P. *Mol. Pharmacol.* **1980**, *18*, 553–558.
176. Nastainczyk, W.; Ahr, H.; Ulrich, W. *Adv. Exper. Med. Biol.* **1981**, *136*, 799–808.
177. Wolf, C. R.; Mansuy, D.; Nastainczyk, W.; Ullrich, V. *Microsomes Drug Oxid. Proc. Int. Symp., 3rd* **1976**, 240–246.
178. Hine, J.; Dowell, A. M. *J. Am. Chem. Soc.* **1954**, *76*, 2688–2692.
179. Castro, C. E.; Kray, J., W. C. *J. Am. Chem. Soc.* **1966**, *88*, 4447–4455.
180. Ruf, H. H.; Ahr, H.; Nastainczyk, W.; Ullrich, V.; Mansuy, D.; Battioni, J. P.; Montiel-Montoya, R.; Trautwein, A. *Biochemistry* **1984**, *23*, 5300–5306.
181. Bartnicki, E. W.; Belser, N. O.; Castro, C. E. *Biochemistry* **1978**, *17*, 5582–5586.
182. Castro, C. E.; Wade, R. S. *J. Org. Chem.* **1985**, *50*, 5342–5351.
183. Castro, C. E.; Wade, R. S.; Belser, N. O. *Biochemistry* **1985**, *24*, 204–210.
184. Li, S.; Wackett, L. P. *Biochemistry* **1993**, *32*, 9355–9361.
185. Ferrara, R.; Tolando, R.; King, L. J.; Manno, M. *Toxicol. Appl. Pharmacol.* **1997**, *143*, 420–428.
186. Tolando, R.; Ferrara, R.; Eldirdiri, N. I.; King, L. J.; Manno, M. *Xenobiotica* **1996**, *26*, 425–435.
187. Luke, B. T.; Loew, G. H.; McLean, A. D. *J. Am. Chem. Soc.* **1987**, *109*, 1307–1317.
188. Luke, B. T.; Loew, G. H.; McLean, A. D. *J. Am. Chem. Soc.* **1988**, *110*, 3396–3400.
189. Philpot, R. M.; Hogson, E. *Chem. Biol. Interact.* **1971**, *4*, 185–190.
190. Franklin, M. R. *Xenobiotica* **1971**, *1*, 581–591.
191. Mansuy, D. *Review in Biochemical Toxicology* **1981**, Vol. 3, pp. 283–320.
192. Mansuy, D.; Battioni, P. In *The Porphyrin Handbook*. Kadish, K. M., Smith, K. M., Guillard, R. Eds.; Academic Press: San Diego, **2000**; Vol. 4, pp. 1–15.
193. Murray, M.; Wilkinson, C. F.; Marcus, C.; Dube, C. E. *Mol. Pharmacol.* **1983**, *24*, 129–136.
194. Ortiz de Montellano, P. R.; Reich, N. O. In *Cytochrome P-450, Structure, Mechanism and Biochemistry*, Ed.; Plenum Press: New York, **1986**; pp. 281–283.
195. Chiba, M.; Nishime, J. A.; Wu-Chen, I.; Vastag, K. J.; Sahly, Y. S.; Kim, B. M.; Dorsey, B. D.; Vacca, J. P.; Lin, J. H. *Biochem. Pharmacol.* **1998**, *56*, 223–230.
196. Yu, L. S.; Wilkinson, C. F.; Anders, M. W. *Biochem. Pharmacol.* **1980**, *29*, 1113–1122.
197. Murray, M.; Hetnarski, K.; Wilkinson, C. F. *Xenobiotica* **1985**, *15*, 369–379.
198. Baek, M. S.; Kim, J. Y.; Myung, S. W.; Yim, Y. H.; Jeong, J. H.; Kim, D. H. *Drug. Metab. Dispos.* **2001**, *29*, 381–388.
199. Kumagai, Y.; Lin, L. Y.; Philpot, R. M.; Yamada, Y.; Oguri, K.; Yoshimura, H.; Cho, A. K. *Mol. Pharmacol.* **1992**, *42*, 695–702.
200. Stewart, F. H. C. *Chem. Rev.* **1964**, *64*, 129–147.
201. White, E. H.; Egger, N. *J. Am. Chem. Soc.* **1984**, *106*, 3701–3703.
202. Krone, V. E.; Thauer, R. K.; Hogenkamp, H. P. C.; Steinbach, K. *Biochemistry* **1991**, *30*, 2713–2719.
203. Dolbier, W. R. J.; Burkholder, C. R. *J. Org. Chem.* **1990**, *55*, 589–594.
204. Miller, J. P.; White, R. E. *Biochemistry* **1994**, *33*, 807–817.
205. Bartnicki, E. W.; Belser, N. O.; Castro, C. E. *Biochemistry* **1978**, *17*, 5582–5586.
206. Wade, R. S.; Castro, C. E. *J. Am. Chem. Soc.* **1973**, *95*, 231–234.
207. Osawa, Y.; Highet, R. J.; Murphy, C. M.; Cotter, R. J.; Pohl, L. R. *J. Am. Chem. Soc.* **1989**, *111*, 4462–4467.
208. Tolando, R.; Cazzaro, S.; Ferrara, R.; Rezzadore, M.; Manno, M. *Biochem. Pharmacol.* **1995**, *49*, 233–241.
209. Chiba, M.; Jin, L.; Neway, W.; Vacca, J. P.; Tata, J. R.; Chapman, K.; Lin, J. H. *Drug. Metab. Dispos.* **2001**, *29*, 1–3.

# Metalloporphyrins in the Biomimetic Oxidation of Lignin and Lignin Model Compounds: Development of Alternative Delignification Strategies

CLAUDIA CRESTINI and PIETRO TAGLIATESTA

Dipartimento di Scienze e Tecnologie Chimiche, Tor Vergata University, Via Della Ricerca scientifica, 00133, Rome, Italy

I. Introduction . . . . .	161
II. Lignin . . . . .	162
A. Occurrence and Biological Role . . . . .	162
B. Lignin Structure . . . . .	163
C. Lignin Degradation: Importance of Pulping and Bleaching Processes in the Industrial Production of Paper . . . . .	163
III. Lignin Degradation Enzymes Containing Porphyrins Prosthetic Group . . . . .	167
A. Lignin Peroxidase (LiP) . . . . .	168
B. Manganese Peroxidase (MnP) . . . . .	169
IV. Models of Lignin Degradation Enzymes. . . . .	171
A. LiP Models . . . . .	171
B. MnP Models . . . . .	172
V. Metalloporphyrins as Biomimetic Systems for Lignin and Lignin Model Compounds Degradation . . . . .	174
A. Oxidation of Lignin Model Compounds . . . . .	175
1. Oxidation of Monomeric Lignin Model Compounds. . . . .	175
2. Oxidation of Dimeric Lignin Model Compounds . . . . .	183
B. Aerobic Oxidations. . . . .	193
C. Oxidation of Lignin . . . . .	195
D. Oxidation of Pulps . . . . .	197
E. Development of Porphyrin-Mediator Systems . . . . .	198
VI. Conclusions . . . . .	200
References . . . . .	201

## I. Introduction

Abbreviations used for porphyrin rings. TPP: *meso-tetrakis* phenylporphyrin; TMP: *meso-tetrakis*(mesityl)porphyrin; TDCPP: *meso-tetrakis*(2,6-dichlorophenyl)porphyrin; TF<sub>5</sub>PP: *meso-tetrakis*(pentafluorophenyl)porphyrin; TPPS: *meso-tetrakis*(*p*-sulfonatophenyl)porphyrin; TSP(Cl<sub>8</sub>)P: *meso-tetrakis*(sulfonatophenyl) $\beta$ -octachloroporphyrin; TDCPPS: *meso-tetra*(2,6-dichloro-3-sulfonatophenyl)porphyrin; TDCS<sub>4</sub>P(Cl<sub>8</sub>)P: *meso-tetrakis*(2,6-dichloro-3-sulfonatophenyl) $\beta$ -octachloroporphyrin; TMP(Br)<sub>8</sub>S: *meso-tetrakis*(3-sulfonato-mesityl) $\beta$ -octachloroporphyrin; TMPS: *meso-tetrakis*(3-sulfonato-mesityl)porphyrin; TF<sub>5</sub>PS<sub>4</sub>P: *meso-tetrakis*(pentafluoro-phenyl) $\beta$ -tetrasulfonatoporphyrin; TF<sub>4</sub>PS<sub>4</sub>P: *meso-tetrakis*(2,3,5,6-tetrafluoro-3-tetra-sulfonatophenyl)porphyrin; TpyMeP: *meso-tetrakis*(tetramethylpyridinio)porphyrin; TF<sub>5</sub>PP: *meso-tetrakis*(pentafluorophenyl)-porphyrin.

A main goal in the development of catalytic processes in chemistry is the mimicking of biological transformations. The objective of this research is to perform reactions in a context isolated from the biological one, and to use a catalyst less expensive as compared to the enzyme itself. A modern approach to the development of new catalytic systems goes beyond these intentions. In this review are described some pivotal strategies for the design of new and efficient catalytic systems which can mimic the course of biological processes in the oxidative

degradation of lignin and lignin model compounds, a key step for industrial paper production processes. Such systems should also provide a wider margin of catalyst stability, conversion yields, selectivity in the reaction, and lower substrate selectivity than the enzyme itself. The goal is the development of a system that is both environmentally friendly and economically suitable for the scale up to plant dimensions.

In the paper production processes, environmental concerns have prompted the study of pulping and bleaching sequences to avoid the use of chlorinated compounds. Several totally chlorine free (TCF) processes have been developed, which include, for example, the use of oxygen, hydrogen peroxide, and ozone as stoichiometric oxidants.<sup>1</sup> However, their major drawback consists in a lack of selectivity in the degradation of lignin, which leads to the partial degradation of the cellulose contained in pulps and ultimately in a lower final pulp yield. The reason for this lack of selectivity in the oxidation reactions is mainly due to the formation of common radical intermediates such as hydroxyl radicals that are able to attack both cellulose and lignin.<sup>2</sup> The selective removal of lignin in wood is accomplished in nature by the white-rot basidiomycetes fungi. Such fungi are able to produce three classes of ligninolytic enzymes: laccases, lignin peroxidases (LiP), and manganese dependent peroxidases (MnP).<sup>3-5</sup> The former are oxygenases with an active site containing four copper atoms. The oxidation of phenolic lignin subunits is performed, in the presence of oxygen, by the generation of phenoxy radicals. LiP and MnP are enzymes that can perform the heterolytic oxygen transfer from hydrogen peroxide to the active center. MnP is able to oxidize only phenolic lignin substructures, while LiP, due to its higher redox potential, can oxidize also nonphenolic substrates. The active site of these enzymes is constituted by a heme center, the protoporphyrin IX (iron-PPIX) (Figure 1).<sup>6</sup>

Synthetic metalloporphyrins are biomimetic catalysts that can yield highly oxidized oxo-metalloporphyrin species. They have been used as lignin peroxidase models, and their potentiality for lignin degradation has been a subject of several studies.<sup>7-9</sup>

In this review, we describe the structure and properties of lignin and lignin degrading enzymes. We will also focus attention on delignification systems. In this context, the use of several synthetic porphyrins in the oxidative degradation of pulps, lignin, and lignin model compounds are described in detail. Recent solid supported porphyrin heterogeneous catalysts and the use of the "mediator" concept in the oxidation of lignin

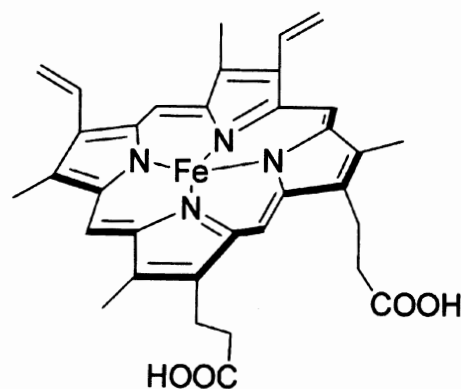


Figure 1. Protoporphyrin IX (iron-PPIX).

will be also described. The best catalytic systems will be analyzed to suggest their possible industrial applications.

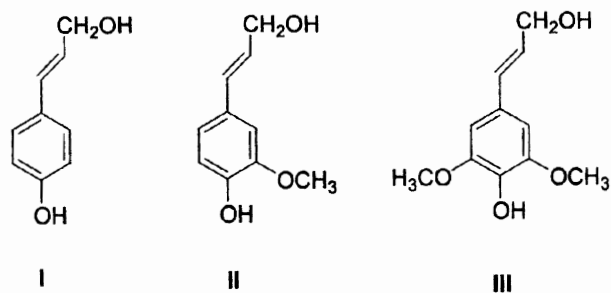
## II. Lignin

### A. OCCURRENCE AND BIOLOGICAL ROLE

Lignin is the second most abundant biopolymer on earth<sup>10</sup> and is a characteristic chemical and morphological component of the tissues of higher plants such as pteridophytes and spermatophytes. The amount of lignin in plants is quite variable and ranges from approximately 30% of the dry weight of softwoods and 20% of hardwoods, while herbaceous angiosperms as well as many monocotyledons are less lignified.<sup>11-13</sup> Lignin increases the mechanical strength properties of plants and provides resistance to biodegradation and environmental stresses. From the industrial point of view, the process of paper making requires the chemical or mechanical separation of the cellulosic fibers from lignin or other lignified plant material. This process, that proceeds through chemical transformations, is known as delignification process and is at the basis of the pulp and paper industry.<sup>14,15</sup>

The understanding of lignin structure is based on the elucidation of its biosynthesis. The primary precursors and building units of all the lignins are the *p*-hydroxycinnamyl alcohols, *p*-coumaryl alcohol I, coniferyl alcohol II, and sinapyl alcohol III (Figure 2).

The biosynthesis of lignin precursors proceeds through the shikimic acid pathway with the initial formation of  $\alpha$ -amino acids (L)-phenylalanine and (L)-tyrosine that are the starting substances for the phenylpropanoid metabolism (cinnamic acid pathway). The cinnamic acid pathway leads, among other derivatives, to the formation of the three cinnamyl alcohols. Lignification in the plant cell wall is initiated by the



**Figure 2.** Structures of *p*-hydroxycinnamyl alcohols; *p*-coumaryl alcohol **I**, coniferyl alcohol **II**, and sinapyl alcohol **III**.

enzymatic formation of phenoxy radicals of the cinnamyl alcohol precursors (Figure 3). The bond formation between the different possible mesomeric forms (I–V) generate several types of subunits all present in the lignin polymer.<sup>16,17</sup>

It is now accepted that the enzymatically generated phenoxy radicals react without the intervention of other enzymes.<sup>18</sup> The principal coupling modes of the radicals are shown in Figure 3. The relative electron densities determine the frequency of different sites involved in coupling reactions. Quantum mechanical calculations suggest that the phenoxy radicals have the highest  $\Pi$ -electron densities at the oxygen atom, thus favoring the formation of aryl ether bonds as the  $\beta$ -O-4 bond. Among the products, highly reactive quinone methides are formed which further react by addition to various nucleophiles (Figure 3).

## B. LIGNIN STRUCTURE

The lignin macromolecule cannot be described by a simple combination of one or few monomeric units by one or few types of linkages; it is rather the result of a random coupling of different units with different regiochemistry. This implies that repetitive units are not present, even at an oligomeric level. Lignin structure can be described in terms of relative abundance of the various monomeric constituents and on their interunit linkages. The composition of lignin shows a high heterogeneity based on its origin. Gymnosperm lignins are composed by guaiacyl units with minor amounts of syringyl- and *p*-hydroxyphenylpropane units. Monocotyledon lignins are guaiacyl-syringyl-*p*-hydroxyphenyl lignins, while dicotyledon lignins are composed by guaiacyl and syringyl units.<sup>19–21</sup> Lignin average molecular weights range from 7000 to 20,000, but the value is strongly dependent on the isolation method and molecular weight determination techniques. Several models of the lignin polymer have been developed in order to represent the overall structure,

on the basis of the frequency of building units and interunit linkages. Figure 4 shows a schematic representation of the lignin structure proposed by Brunow *et al.* in which are described all the main types of linkages present in the polymer.<sup>22</sup>

Lignin carbohydrate bonds are possible due to the reaction of quinone methides with various lignols and carbohydrates during lignin biosynthesis (Figure 5). The lignin carbohydrate bonds are mainly benzyl ether or esters from ferulic or *p*-coumaric acids, which are found to be esterified with carbohydrates and etherified with lignin.<sup>23,24</sup> These bonds are degraded in the pulp and paper process. In Table 1 are reported the frequencies of the major linkages in hardwood and softwood lignins.<sup>25,26</sup>

On the basis of such frequencies, phenolic and non-phenolic dimeric lignin model compounds have been synthesized with the aim to study the reactivity of the single lignin subunits during pulping, bleaching, or more generally during oxidation processes. In Figure 5 are reported lignin model compounds representing the major interunit linkages<sup>27–30</sup> used in oxidation reactions with metalloporphyrins. Free phenolic biphenyl 5-5' units are present in lignin only in low amount,<sup>22</sup> while most of them are etherified in the dibenzodioxocine unit 5-5-O-4. Such units are easily cleaved during pulping (see below) to regenerate biphenyl 5-5' substructures. Diarylpropane units are not present in native lignin, but are formed during pulping processes by the condensation of two adjacent aromatic rings.<sup>31,32</sup> In Figure 6, dimeric lignin model compounds oxidized in the presence of metalloporphyrins are reported.

## C. LIGNIN DEGRADATION: IMPORTANCE OF PULPING AND BLEACHING PROCESSES IN THE INDUSTRIAL PRODUCTION OF PAPER

Pulp and paper industry interest is mainly focused on the selective elimination of lignin from wood in order to get cellulose pulps for paper production. This process requires selective reagents and mild reaction conditions in order to obtain the highest cellulose yield at a lower cost.<sup>33</sup> Traditionally, a coarse pulping process is followed by a bleaching treatment aimed at eliminating the residual lignin present on pulps that is responsible for paper yellowing. Chemical pulping reactions are divided into two types: alkaline pulping and sulfite pulping. The simple treatment of wood chips with sodium hydroxide causes degradation of lignin and polysaccharides. Improved alkaline pulping processes use sulfide in the presence of small amounts of anthraquinone to

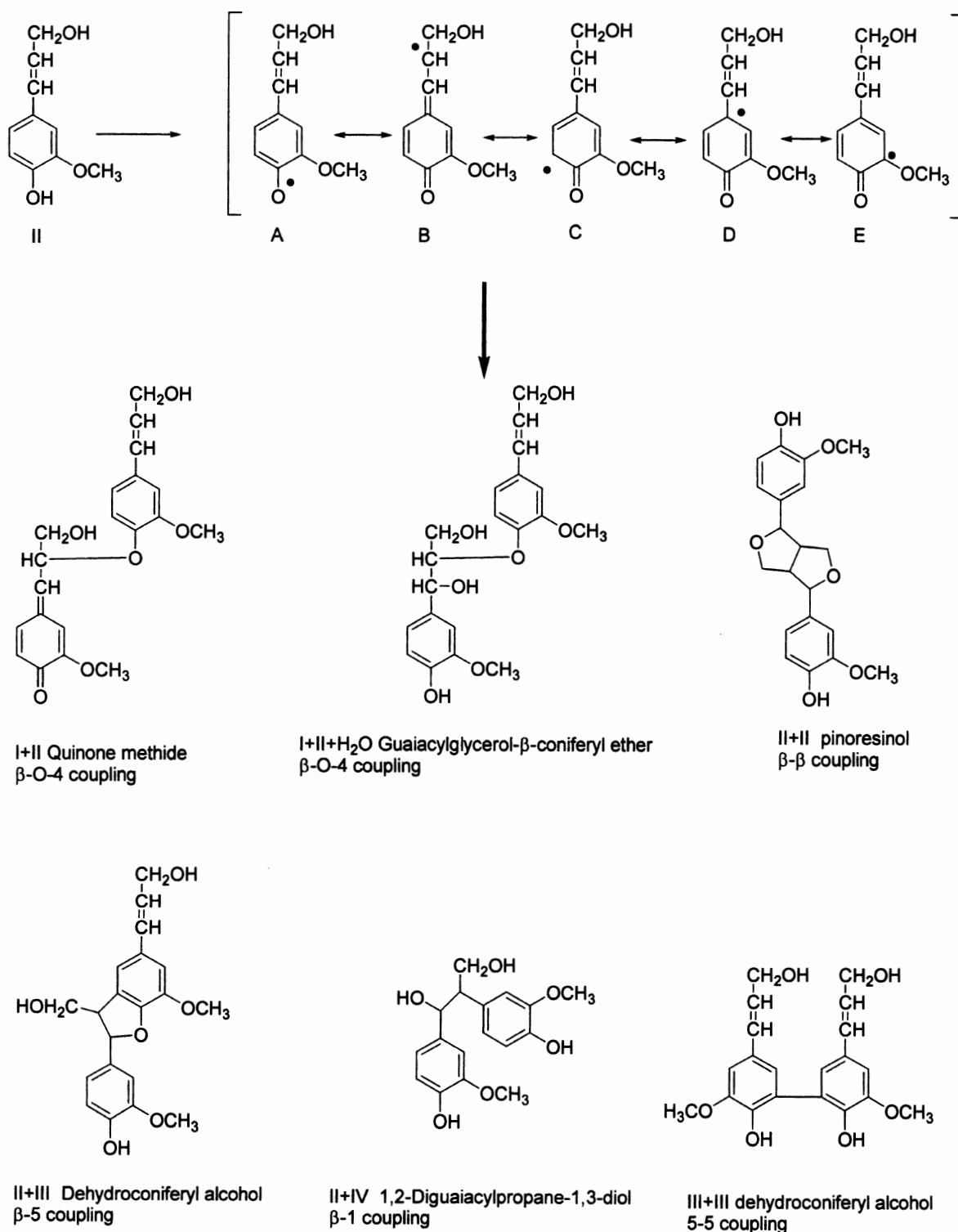
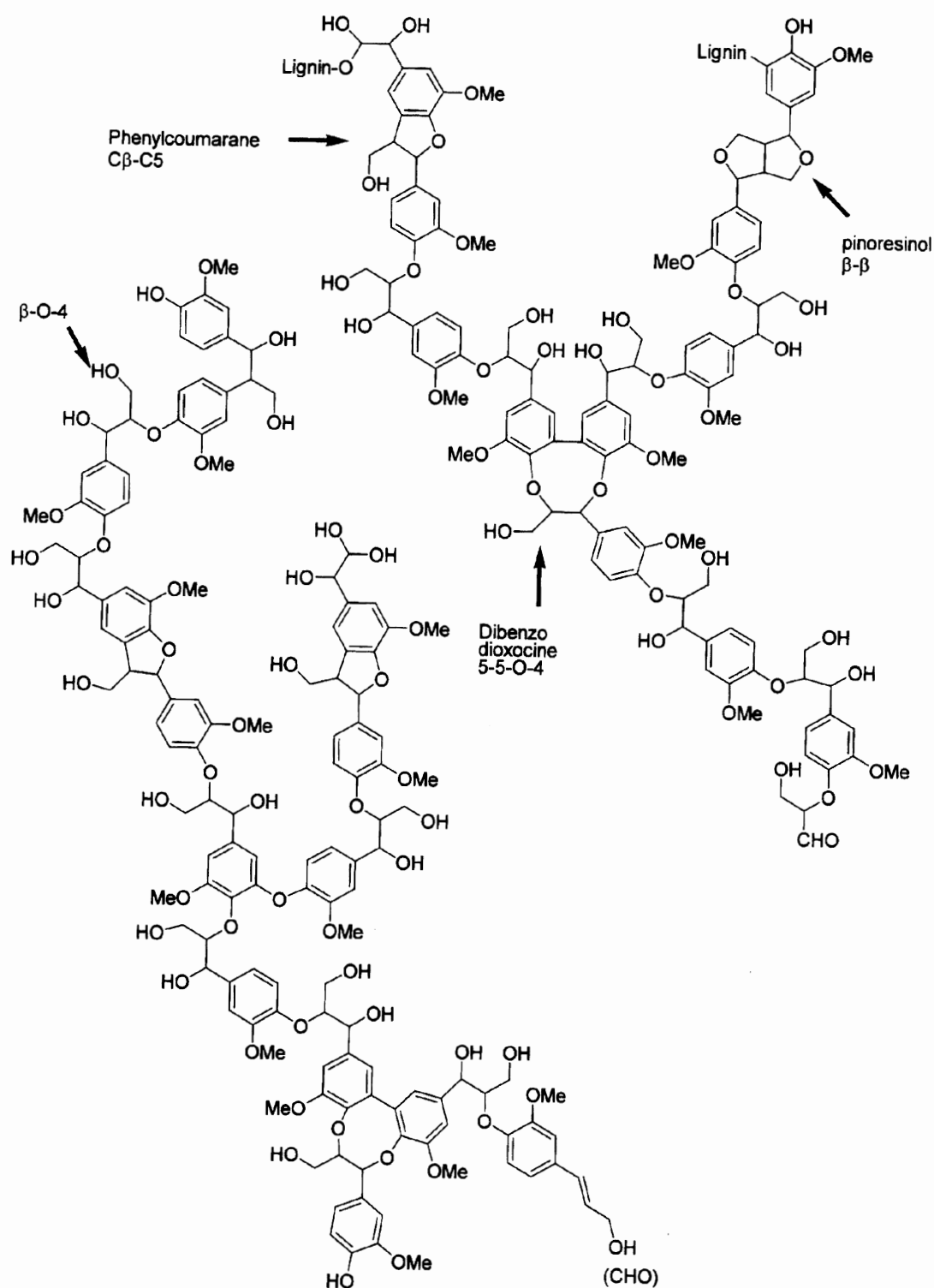


Figure 3. Schematic representation of the lignification process in the plant cell.

accelerate the depolymerization of lignin, and to minimize the loss of polysaccharides.<sup>34</sup> Lignin reacts with alkali and oxygen (air), or photochemically (daylight) causing the yellowing of paper. This process is initiated by the absorption of UV light by  $\alpha$ -carbonyl

groups present in lignin in low amount. The excited state of the lignin leads to the formation of phenoxy radicals which react with oxygen to form quinonoid chromophores.<sup>35,36</sup> In the lignin-degrading bleaching of pulp, bleaching chemicals (e.g., chlorine, hypochlorous acid,

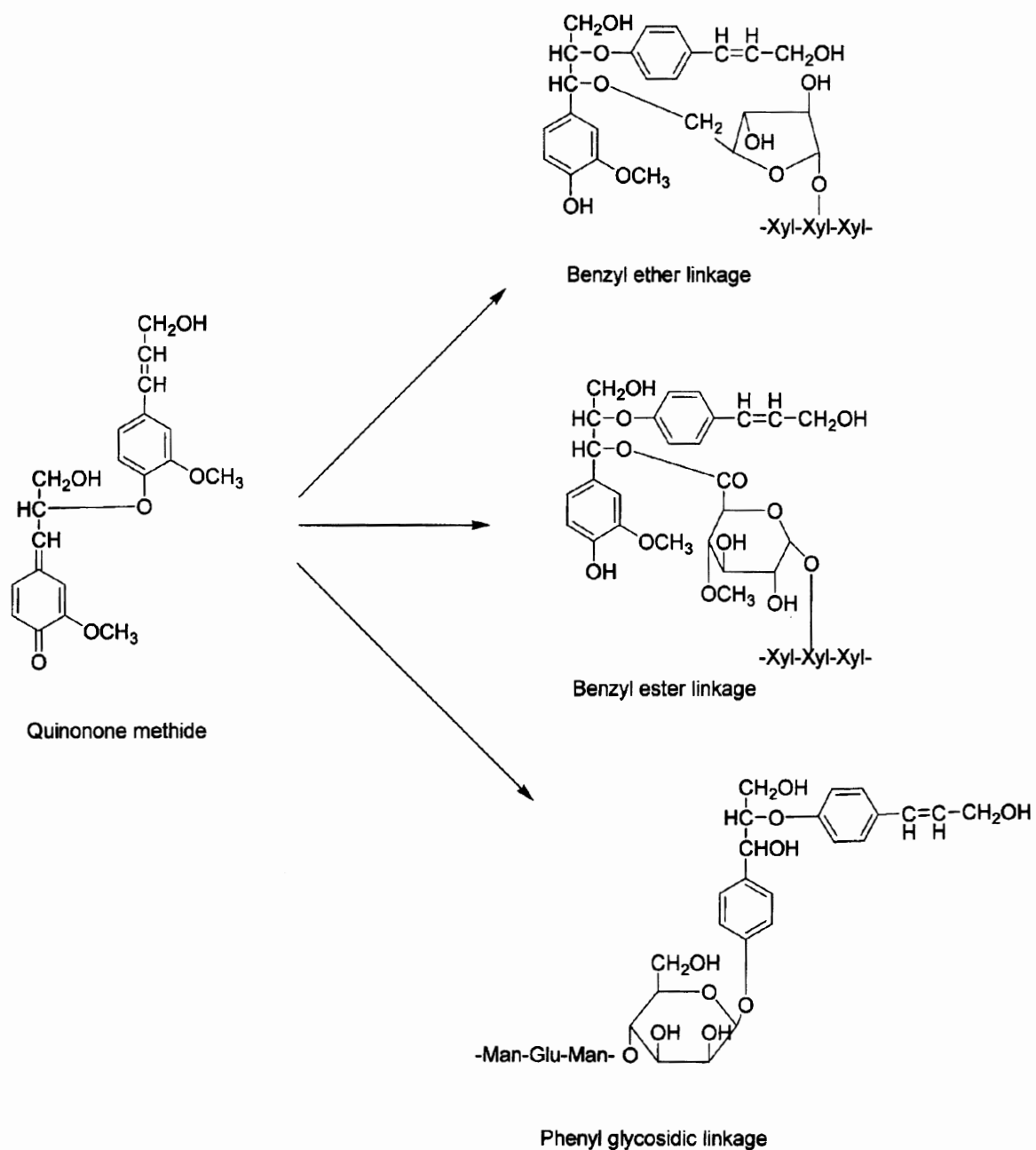


**Figure 4.** Schematic representation of the lignin structure proposed by Brunow *et al.* Reprinted with permission of the American Chemical Society.<sup>22</sup>

chlorine dioxide, oxygen, ozone, and peroxyacetic acid) cause the oxidative degradation of the lignin polymer.<sup>37</sup> The oxidative action of oxygen and peroxides on lignin in alkaline media is the basis for modern nonpolluting

pulp-bleaching processes.<sup>38</sup> Oxygen tends to form chromophoric structures during lignin degradation, while hydrogen peroxide preferentially destroys the chromophores. During the last years, despite the





**Figure 5.** Schematic representation of lignin carbohydrate bonds.

**Table 1.** Frequency of the Major Linkages in Softwood and Hardwood Lignins

Type of linkage	% of Total phenylpropane units	
	In softwoods	In hardwoods
$\beta$ -Aryl ether ( $\beta$ -O-4)	45–48	60
Biphenyl (5–5)	9.5–17	4.5
Phenylcoumaran ( $\beta$ -5)	9–12	6
$\beta$ -1	7–10	8
$\alpha$ -Aryl ether ( $\alpha$ -O-4)	6–8	6–8
Diphenyl ether (4-O-5)	3.5–8	6.5

higher yields obtained with the use of chlorinated reagents, environmental and economical concerns have prompted to the use of alternative oxidation processes. From this point of view, the use of low environmental impact reagents such as dioxygen or hydrogen peroxide is highly recommended. For this reason, hydrogen peroxide is widely used in the paper industry as a lignin-preserving bleaching agent for high yield pulps.<sup>39</sup> However, the continuous effort to improve the efficiency of processes and to lower costs led to the investigation of different oxidative systems that could show a high

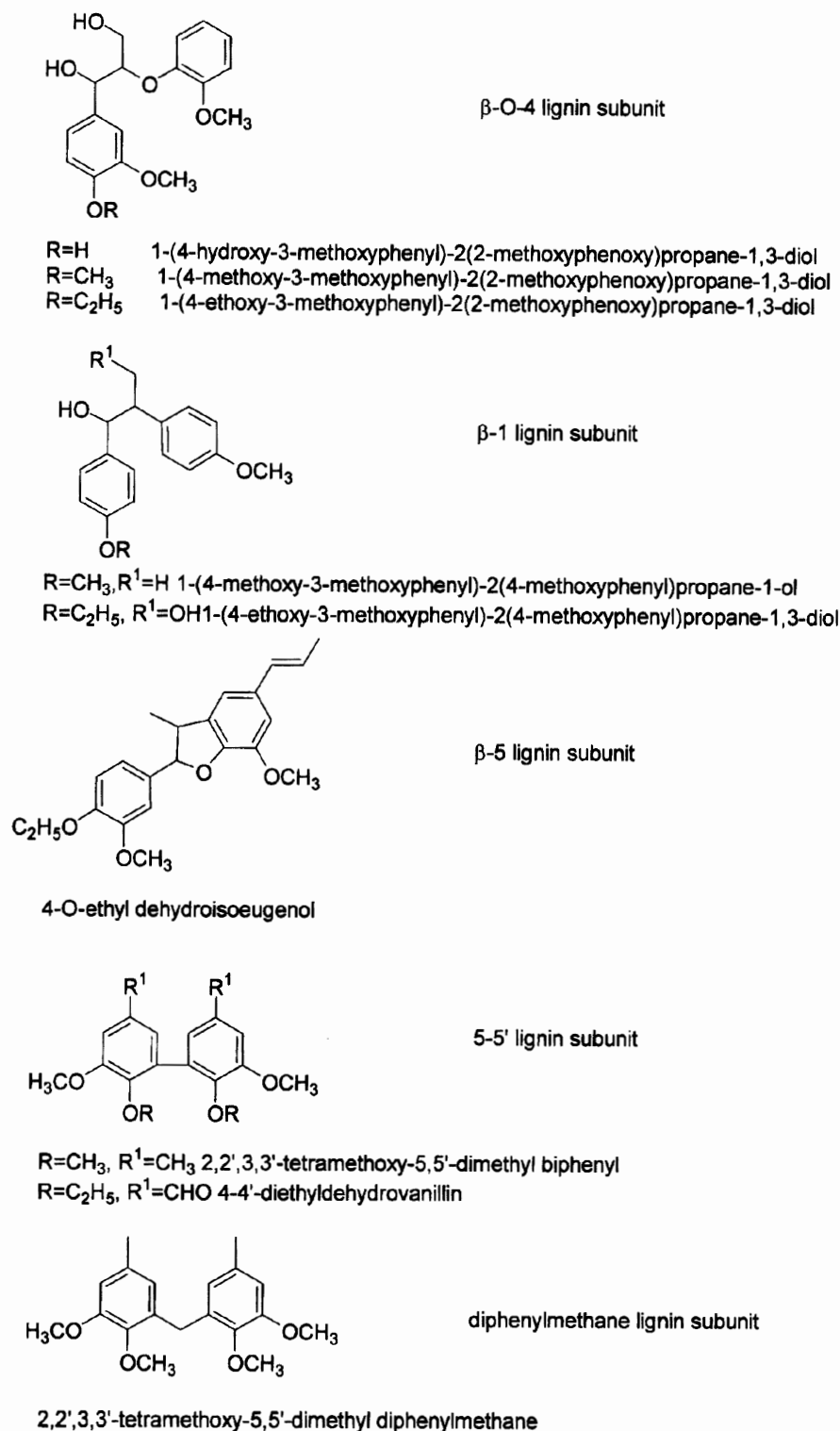


Figure 6. Dimeric lignin model compounds (non exhaustive list)

degree of selectivity, be environmentally safe and require mild reaction conditions. A possible approach to the development of alternative pulping and bleaching processes can be developed starting from the study of the natural processes of wood degradation.

### III. Lignin Degradation Enzymes Containing Porphyrins Prosthetic Group

In Nature, the removal of lignin in wood is accomplished by the white-rot basidiomycetes fungi. Such

microorganisms are able to selectively degrade lignin in wood with respect to cellulose and hemicellulose.<sup>40,41</sup> Several studies have been carried out in order to identify and isolate the pool of enzymes responsible for lignin degradation and to elucidate their action mechanisms.<sup>42</sup> White-rot fungi are able to produce three classes of ligninolytic enzymes: laccases, lignin peroxidases (LiP), and manganese dependent peroxidases (MnP). The former are oxygenases with an active site containing four copper atoms.<sup>43</sup> The oxidation of phenolic lignin subunits is performed, in the presence of oxygen, by the generation of phenoxy radicals.<sup>44,45</sup> LiP and MnP are enzymes that can perform the heterolytic oxygen transfer from hydrogen peroxide to the active center. MnP is able to oxidize only phenolic lignin substructures, while LiP, due to its higher redox potential, can oxidize phenolic and nonphenolic substrates.

### A. LIGNIN PEROXIDASE (LiP)

The best characterized lignin degrading fungus is the basidiomycete *Phanerochaete chrisosporium*. In 1983, an extracellular lignin peroxidase (ligninase, LiP) was isolated from ligninolytic cultures of this microorganism.<sup>4,5</sup> Lignin peroxidases are glycoproteins with a molecular weight of about 42,000 Da. Despite the low homology degree with cytochrome *c* peroxidase (only 20%), the crystal structure of LiP presents some similarities and all of the tested isozymes have a single iron protoporphyrin IX as prosthetic group. The heme is in a high-spin ferric state and has a histidine as a proximal ligand.<sup>46,47</sup> In the presence of hydrogen peroxide, the active center of LiP performs a one-electron oxidation of the lignin aromatic moieties.<sup>48</sup> The catalytic cycle consists in a two-electron oxidation of Fe(III) protoporphyrin IX (high-spin) to give a highly reactive oxo-iron(IV) protoporphyrin IX  $\Pi$ -cation radical, the LiP I complex (LiP compound I).<sup>49,50</sup> The LiP compound I is then reduced to the initial state by two different one-electron reductions by the substrates (Figure 7).<sup>51</sup> LiP is a fragile enzyme. When exposed to an excess of hydrogen peroxide (more than 20 equivalents), it is subject to inactivation by overoxidation, and gives the inactive form, LiP III.<sup>52,53</sup>

The protein scaffold around the active center provides stabilization of the metal complex, from possible overoxidation processes, and water solubility. In fact, the heterolytic cleavage of the peroxidic bond is subject to acid catalysis. The proximal His residue activates the complex to heterolytic cleavage by enhancing the electrophilic character of the oxygen atom, and

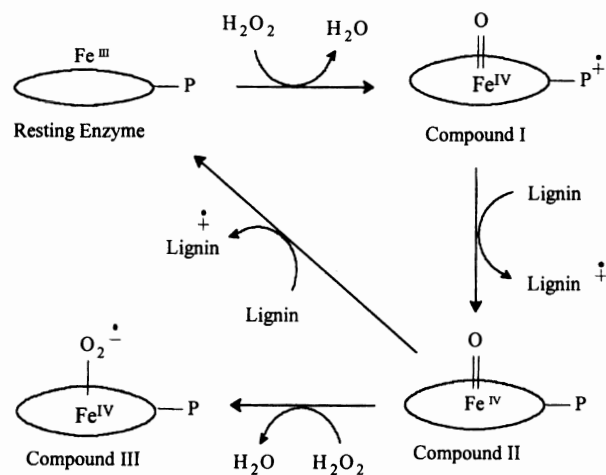
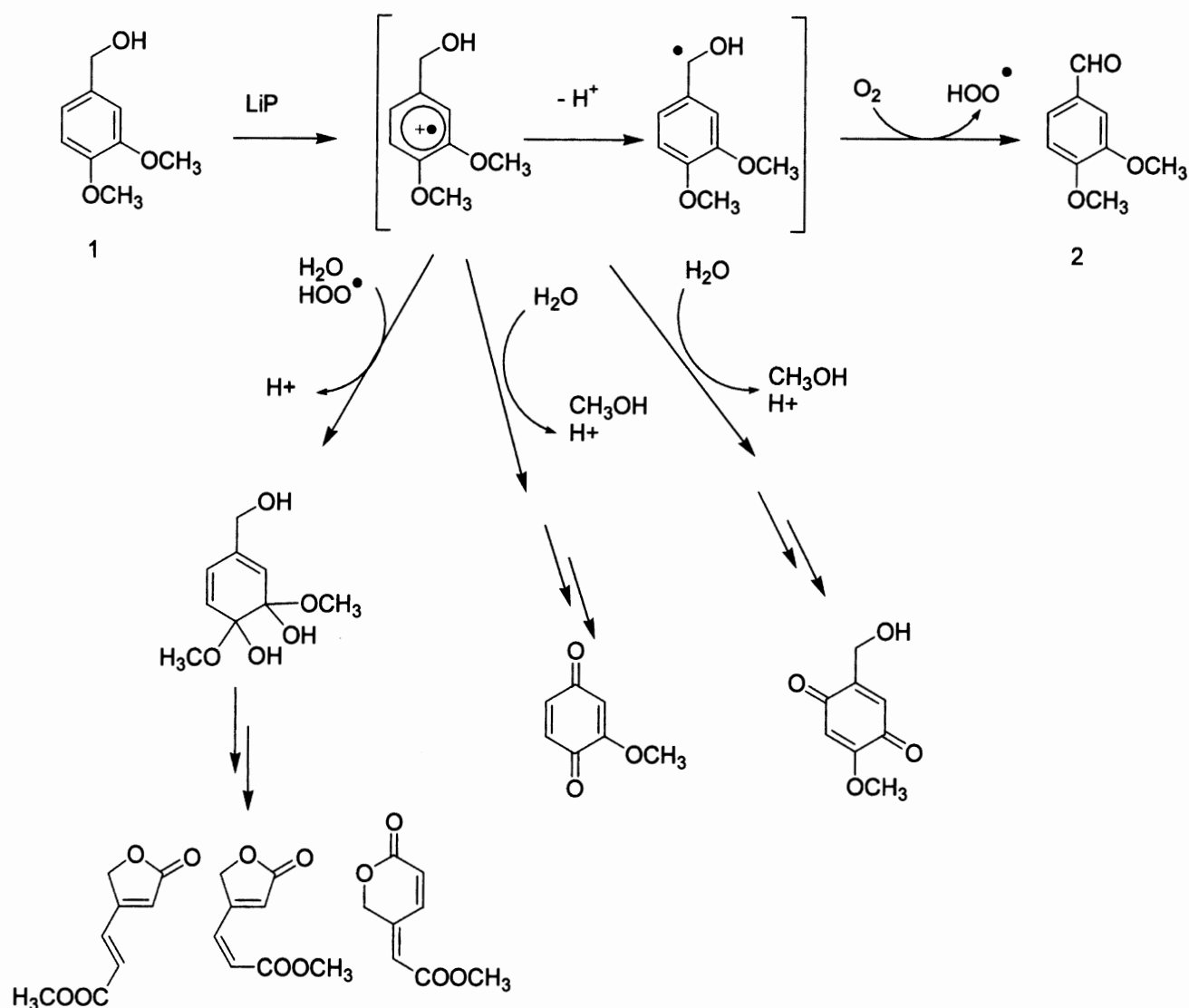


Figure 7. Catalytic cycle of Lignin peroxidase (LiP).

reducing the strength of the metal–oxygen bond.<sup>7</sup> Due to its high redox potential with respect to other ligninolytic enzymes, LiP is able to oxidize the nonphenolic lignin subunits. Several studies have been carried out on the most significant lignin model compounds. Veratryl alcohol 1 (Scheme 1) is readily oxidized by LiP in the presence of hydrogen peroxide, to yield veratraldehyde, a product of side-chain oxidation.<sup>54,55</sup> Experimental evidence showed that the reaction proceeds through the one-electron oxidation to veratryl alcohol radical cation and, after proton loss, to the corresponding veratryl alcohol radical (Scheme 1).

In the presence of oxygen (air), ring opening and quinone formation occur, thus indicating the formation of activated oxygen species such as superoxide anion radical. Syringyl models were also found oxidized to the corresponding benzaldehyde and *p*-quinone.  $\beta$ -O-4 lignin model compounds were found oxidized upon treatment with LiP in the presence of limiting amounts of hydrogen peroxide.<sup>56–58</sup> The oxidation proceeds through the formation of cation radicals at the  $C\beta$  oxygen followed by  $C\alpha$ – $C\beta$  cleavage leading to the formation of a benzylic radical in the  $C\alpha$  moiety and a positive charge on the  $C\beta$ . The final products found were aromatic ring cleavage, aldehyde, *p*-quinones derivatives. Other intermediate products were also characterized as reported in Scheme 2.

5–5' Biphenyl model compounds can also be degraded by LiP yielding to various side-chain oxidation products and to products of aromatic ring cleavage.<sup>59</sup> Lignin itself can be oxidized by LiP in the presence of limiting amounts of hydrogen peroxide with different degrees of success.<sup>60–63</sup> The lignin content in  $\beta$ -O-4-linked guaiacyl monomers and dimeric structures decreased after oxidation by the two enzymes, indicating



Scheme 1. Lignin peroxidase oxidation of veratryl alcohol.

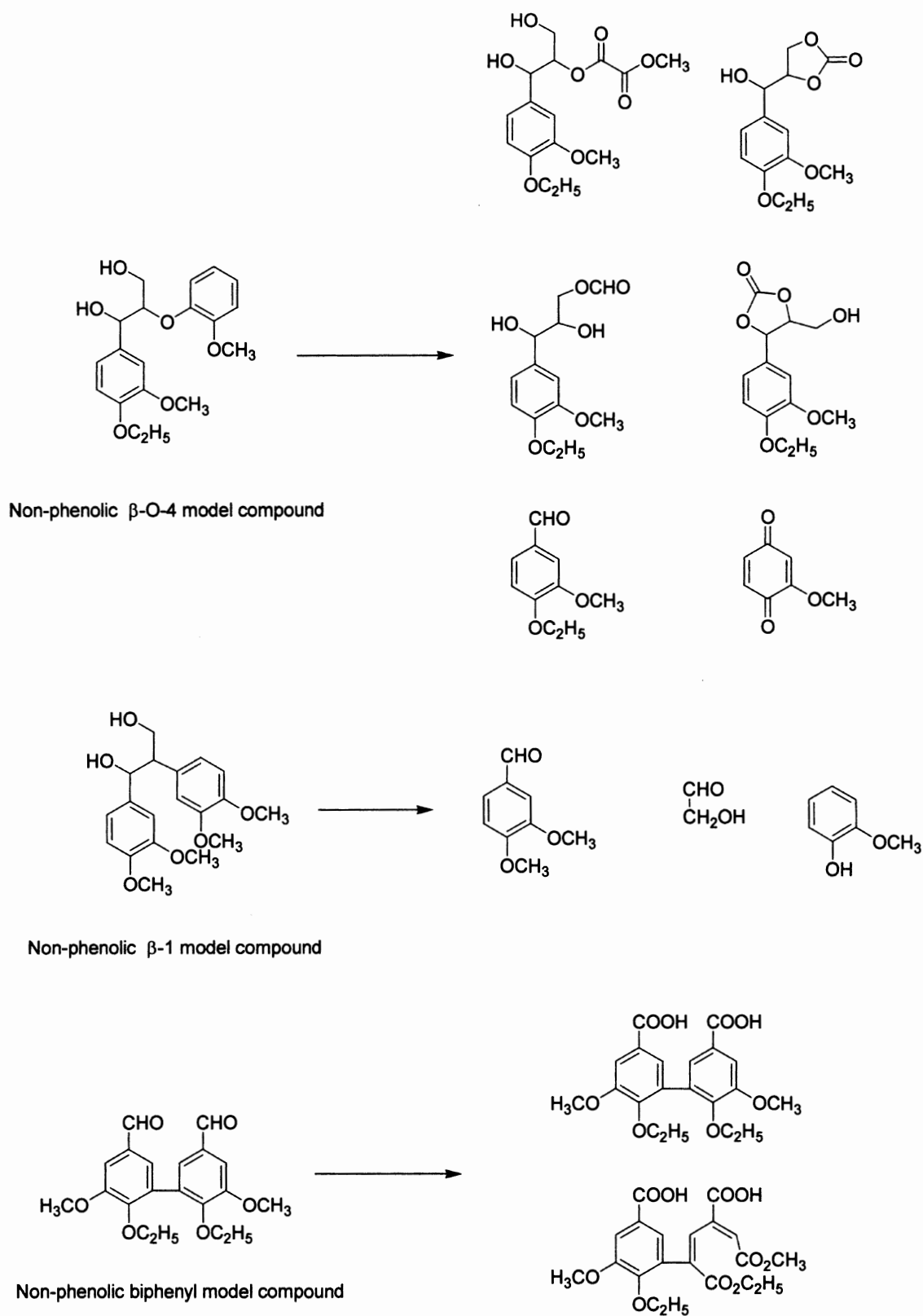
large structural changes in the polymer. Preferential degradation of  $\beta$ -5 and  $\beta$ -1 lignin dimeric units was also observed. This suggests a greater susceptibility to enzyme oxidation, as compared to the 5-5' and 4-O-5 lignin substructures. LiP activity can be enhanced by the presence of glyoxal oxidase, an enzyme produced by the same fungus, that is able to oxidize the glyoxal released in the LiP catalyzed reaction with controlled regeneration of hydrogen peroxide.<sup>64</sup>

Veratryl alcohol is a secondary metabolite produced by *Phanerochaete chrysosporium*. This compound plays a pivotal role in the LiP oxidation of lignin. In fact, in the presence of veratryl alcohol both the oxidation degree of lignin and of lignin model compounds is significantly enhanced.<sup>65-67</sup> Veratryl alcohol, when present in the reaction mixture, is a more favorable substrate for

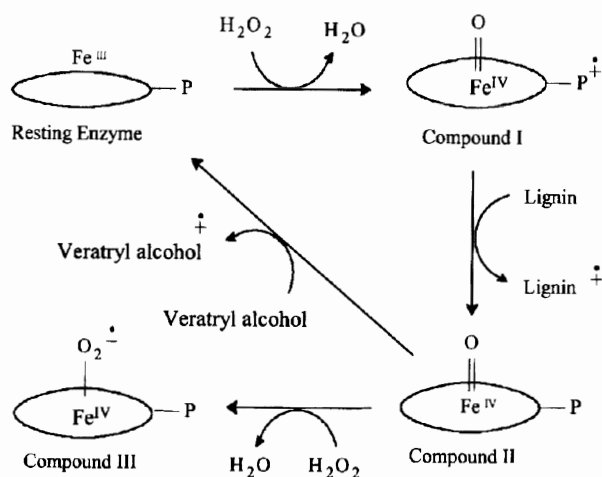
compound II, and functions to convert it to the resting enzyme, completing the catalytic cycle. Veratryl alcohol therefore recycles the enzyme and prevents its inactivation by the excess of H<sub>2</sub>O<sub>2</sub> (Figure 8). It has also been proposed an alternative role for veratryl alcohol in the degradation of lignin. In this hypothesis, veratryl alcohol acts as a diffusible mediator in the LiP catalyzed oxidation of lignin. In the latter case, the oxidative potential could be transferred from the enzyme to the bulk of the polymer avoiding kinetic barrier for the reaction.

## B. MANGANESE PEROXIDASE (MnP)

Manganese peroxidase constitutes with lignin peroxidase a synergistic system devoted to the degradation of lignin. While LiP is able to oxidize nonphenolic lignin



Scheme 2. Products of degradation of lignin model compounds by LiP



**Figure 8.** Possible role of veratryl alcohol in the catalytic cycle of lignin peroxidase.

subunits, MnP is able to carry out the oxidation of phenolic systems. More specifically  $\alpha$ -oxo- and  $\alpha$ -hydroxy lignin subunits are the targets of this enzyme (Figure 9).<sup>68,69</sup>

MnP contains a Mn(II) that seems to interact with one of the heme propionates, as suggested by its crystal structure.<sup>70</sup> Genetic studies performed by selective site-directed mutagenesis (site-directed studies) showed that Mn(II) is bound to the enzyme by residues of aspartic acid 179, glutamic acid 3 and 39, and by an heme propionate derivative. The one-electron transfer from Mn(II) center to the porphyrin occurs through the intermediate heme propionate ligand.<sup>71,72</sup> Site-directed studies to phenylalanine 190 showed that the heme center is stabilized by this amino acid.<sup>73</sup> The oxidation of lignin occurs by direct reaction with free diffusible Mn(III) chelates that act as mediators of the oxidation. Such species react efficiently with phenolic lignin subunits.<sup>74</sup> The Mn(III) chelating systems are  $\alpha$ -hydroxy or dicarboxylic acids such as lactate, succinate, malonate, and oxalate. They play the double role of enhancing the catalytic activity by allowing the dissociation of Mn(III) from the enzyme, and of stabilizing the oxidation state of manganese. Notably, oxalate is a secondary metabolite of several wood rotting fungi. In the absence of hydrogen peroxide, it can react with molecular dioxygen by autoxidation with the formation of superoxide anion radical, that in turn can generate the hydrogen peroxide necessary to the enzyme by dismutation.<sup>75,76</sup>

The MnP catalytic cycle is similar to the ligninase one. The oxidized intermediate MnP I, a Fe(IV) oxoporphyrin radical cation is generated upon hydrogen peroxide oxidation. MnP I is reduced to MnP II,

a Fe(IV) oxoporphyrin complex, by either Mn(II) chelates or phenolic substrates. In turn, compound MnP II can be reduced to the MnP resting state to close the catalytic cycle, only by Mn(II) chelates. Mn(III) chelates formed are able to oxidize phenolic lignin subunits.<sup>77</sup> The catalytic cycle of MnP is shown in Figure 10.

## IV. Models of Lignin Degradation Enzymes

### A. LiP MODELS

In principle, the use of an enzymatic system for delignification is not economically convenient with respect to simpler catalysts, due to the costs of purification. Moreover, since LiP is sensitive to hydrogen peroxide excess, its practical utilization in pulp and paper is difficult to develop. Hence, the need for the design of suitable ligninase models resistant to peroxide inactivation. These biomimetic systems are also helpful for understanding the mechanisms of complex lignin degradation. Early attempts at developing such models started from the use of the metal complex present as the enzyme active site: hemin (protoporphyrin IX iron(III) chloride).<sup>78-80</sup> Hemin is an iron complex easily deactivated by hydrogen peroxide by overoxidation. It lacks the polypeptidic envelope that in the natural enzyme provides stabilization and steric protection to the active site. More specifically, the  $\beta$  positions of the porphyrin ring are easily oxidized. For this reason, such a catalyst was used in the presence of *t*-butyl hydroperoxide (*t*-BuOOH) as oxygen donor rather than H<sub>2</sub>O<sub>2</sub>. Shimada *et al.*<sup>81</sup> reported that iron-PPIX catalyzes the oxidation of  $\beta$ -1,  $\beta$ -O-4, and  $\beta$ -5 lignin model compounds thus mimicking ligninase. Moreover, the regiospecificity found in iron-PPIX oxidation of veratryl alcohol was the same observed in LiP; this showed that the regiospecificity of oxygenation is not necessarily governed by the protein backbone of ligninase (Figure 11).

The oxidation of a diaryl propanediol lignin model compound, 1,2-*bis*(*p*-methoxyphenyl)propane-1,3-diol, yielded, in agreement with the reaction pattern of LiP, to the formation of *p*-anisaldehyde as the major product.<sup>82</sup> However, simple metalloporphyrins suffer from the major disadvantage of being unstable in the presence of excess oxidants. Their lability is due either to self-destruction or to the formation of inactive  $\mu$ -oxo complexes.<sup>7,8</sup> The study of biomimetic systems has thus focused toward the development of nonnatural iron porphyrins more resistant to degradation. Ligninase

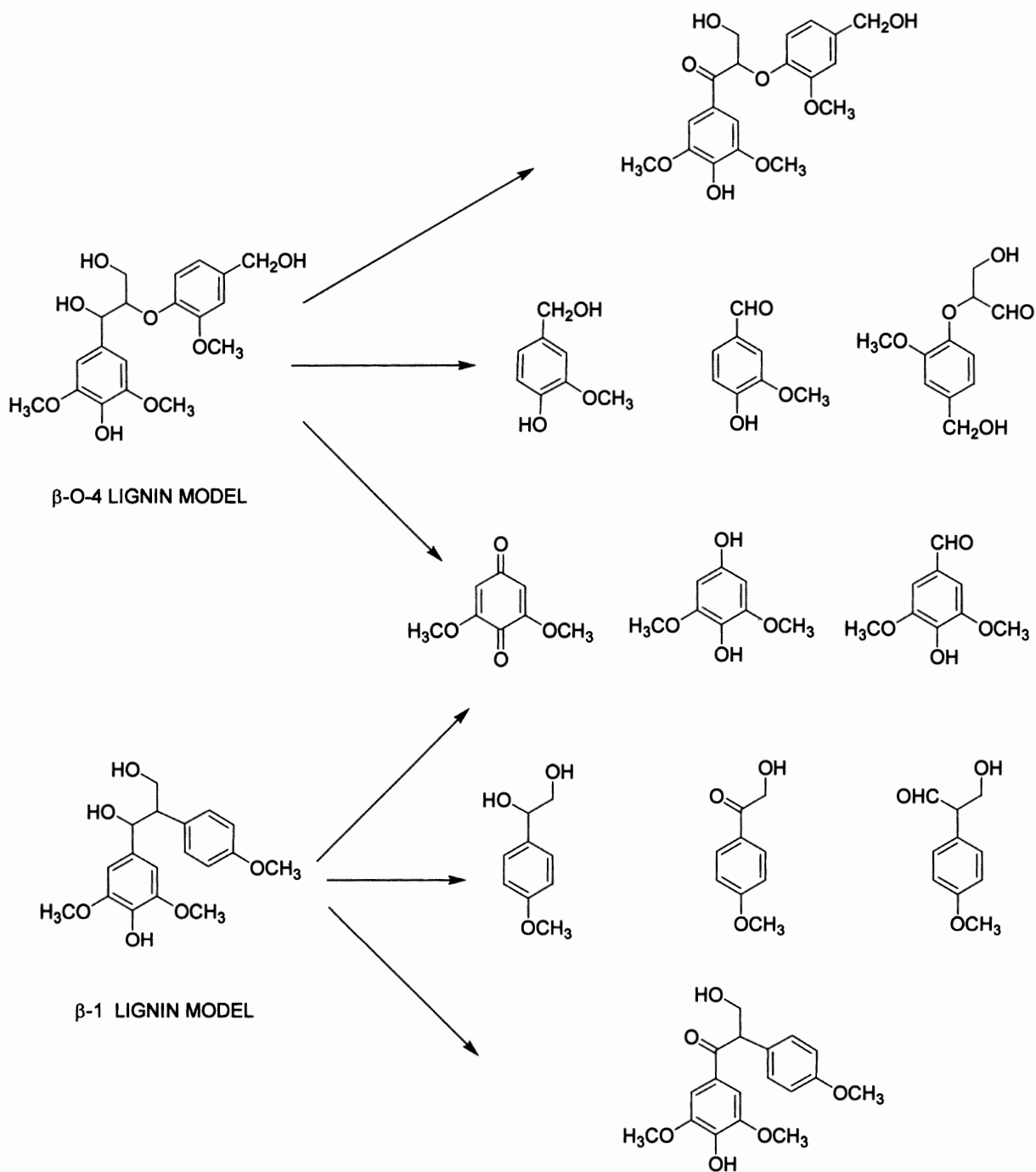


Figure 9. Oxidation of phenolic lignin model compounds by manganese peroxidase (MnP).

models have been studied also in the degradation of aromatic halides pollutants that are stable to usual microbiological treatment.

### B. MnP MODELS

The development of biomimetic systems for manganese peroxidase requires the selective oxidation of Mn(II) in the presence of chelating agents and phenolic

compounds. However, from the pulp and paper making point of view it is not the main target since it allows only the oxidation of phenolic lignin subunits while leaving unchanged the more recalcitrant non-phenolic ether linked bulk of lignin. The reactivity of Fe(TDCPPS)Cl in the presence of *m*-CPBA in the decolorization of dyes is actually improved by addition of manganese sulfate. The effect of manganese sulfate probably consists in preventing the iron catalyst from

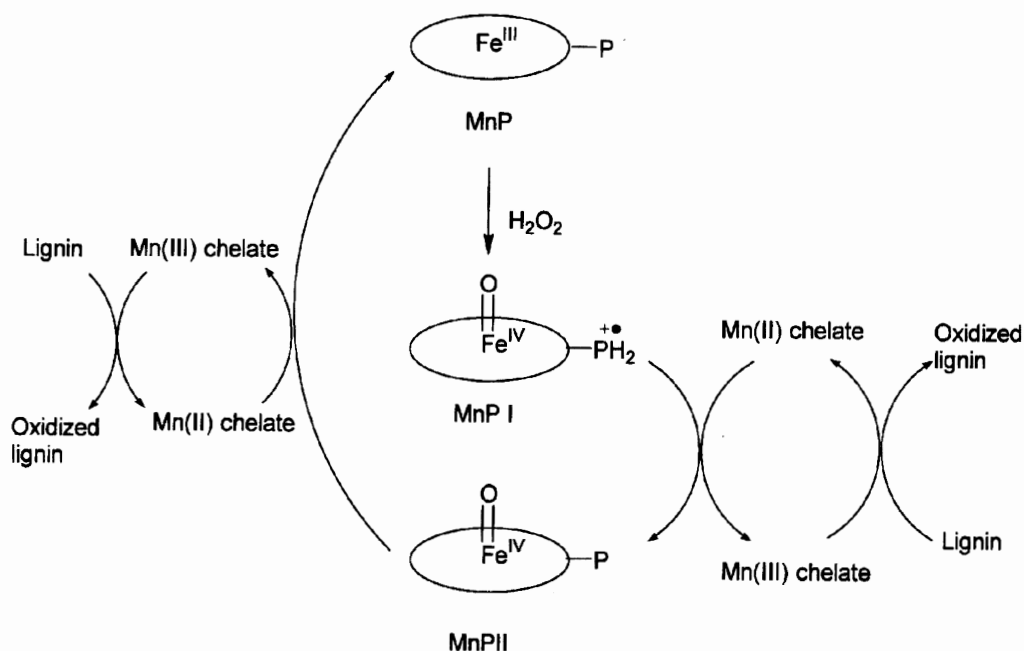


Figure 10. Catalytic cycle of manganese peroxidase (MnP).

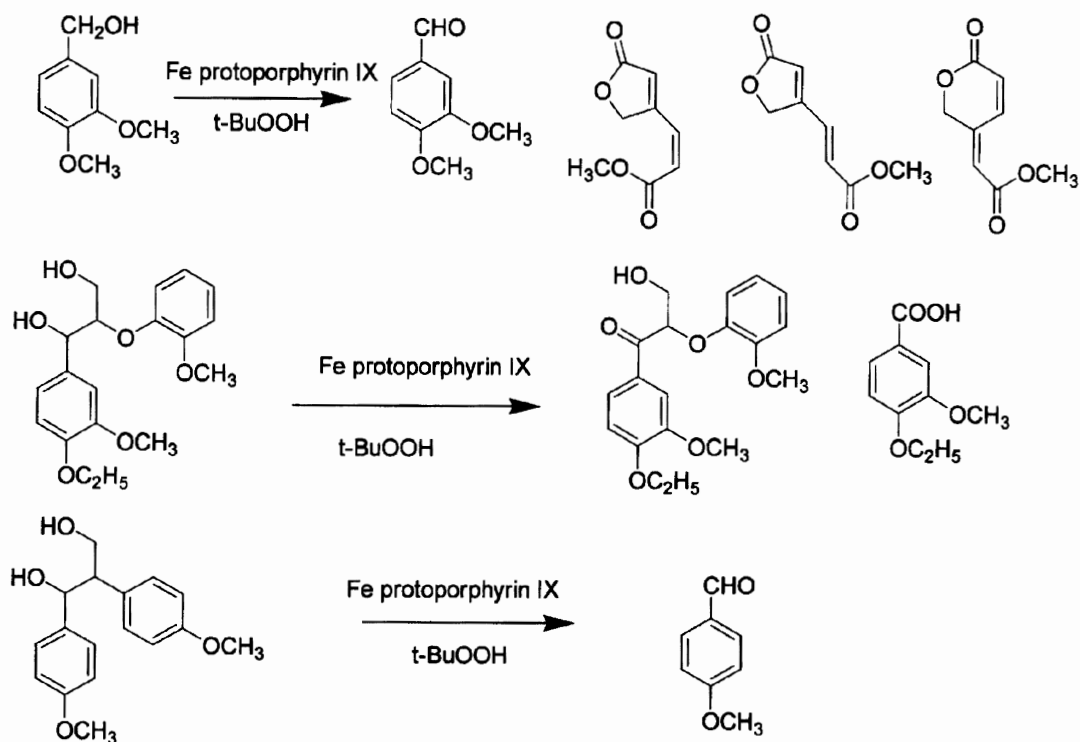


Figure 11. Iron PP IX catalyzed oxidation of veratryl alcohol,  $\beta$ -O-4 and  $\beta$ -1 lignin model compounds.

undesired bleaching.<sup>83,64</sup> Sulfonated iron porphyrin complexes (Fe(TMPS)Cl, Fe(TDCPPS)Cl, Fe(Br<sub>8</sub>-TMPS)Cl, Fe(Cl<sub>12</sub>TMPS)Cl) in the presence of potassium monopersulfate, KHSO<sub>5</sub> have been studied as manganese peroxidase biomimetic systems. More specifically they perform the oxidation of Mn(II) chelates,

but the activity is lower than MnP under similar experimental conditions.<sup>84</sup> The catalytic activity was improved by the addition of low amounts of methoxybenzene derivatives. They act as diffusible redox mediators or as cosubstrate, in analogy with the role of low molecular weight secondary metabolites produced



by with-rot fungi that are believed to play an important role as diffusible oxidizing agents.

A further improvement in the mimicking of the two metallic centers of MnP, the Mn and the iron porphyrin has been attempted by the synthesis of a binuclear  $[\text{Mn}^{\text{II}}(\text{bipy})-\text{Fe}^{\text{III}}(\text{porphyrin})]$  complex. This dimer catalyzes efficiently the formation of Mn(III) in the presence of iodosyl benzene ( $\text{C}_6\text{H}_5\text{IO}$ ) as primary oxidant, thus mimicking the second step of the MnP catalytic cycle.<sup>85</sup>

## V. Metalloporphyrins as Biomimetic Systems for Lignin and Lignin Model Compounds Degradation

Synthetic metalloporphyrins are biomimetic catalysts that can yield highly oxidized metallo-oxo species. They have been used as lignin peroxidase models, and their potentiality for lignin degradation has been a subject of several studies.<sup>7,8</sup> When synthetic metalloporphyrins are used as biomimetic catalysts in the presence of hydrogen

peroxide, several side reactions can occur. The peroxidic bond can undergo homolytic scission to yield  $\text{Fe}^{\text{IV}}\text{-OH}$  and hydroxyl radical in a Fenton like fashion. This reactivity is more significant in the presence of iron complexes and hydrogen peroxide as oxygen donor. A second molecule of peroxide may react with the metal oxo complex in a catalase-like fashion to yield the formation of  $\text{H}_2\text{O}$  and  $\text{O}_2$ , and ultimately the degradation of the active oxidant species (Figure 12). The metal oxo complex may react to yield  $\mu$ -oxo dimers.<sup>7</sup>

In Nature, the polypeptidic envelope of the enzyme protects the active site from side reactions, and activates it. As mentioned above, the proximal His residue activates the complex to heterolytic cleavage by enhancing the electrophilic character of the oxygen atom, and reducing the strength of the metal-oxygen bond. The addition of a nitrogen base such as pyridine or imidazole to the oxidizing solution can mimic this situation. The manganese porphyrins are not strictly biomimetic systems of LiP, since the natural enzyme active site is an iron complex. However, the use of manganese

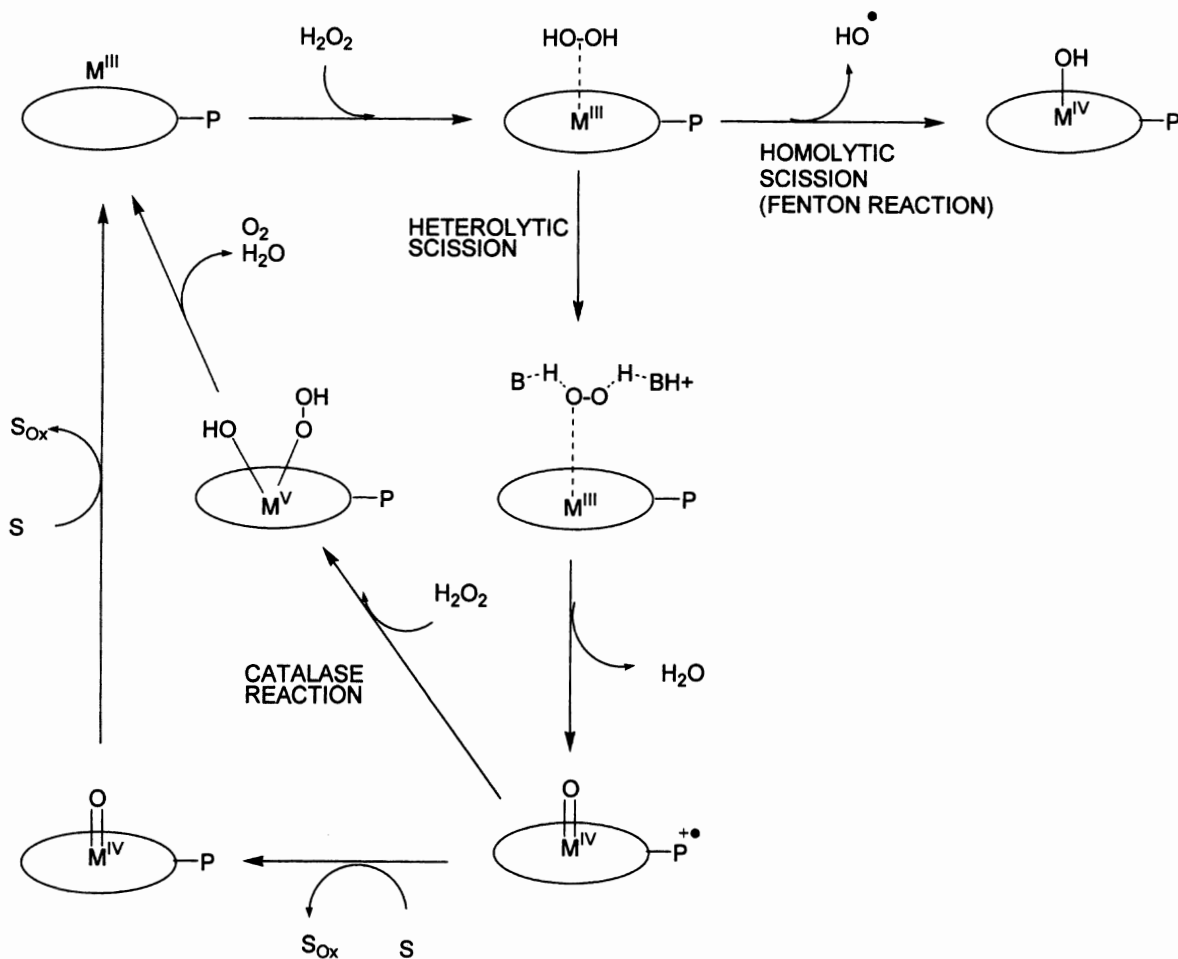


Figure 12. Possible reactions of metalloporphyrins with hydrogen peroxide.

complexes could override many reactivity problems. More specifically, manganese porphyrins form single adducts with nitrogen bases and in this way can be easily activated. Moreover, manganese shows a smaller tendency than iron to undergo homolytic cleavage of the peroxidic bond (Figure 12). Metalloporphyrins have been considered as possible biomimetic systems for lignin peroxidase. Studies on the oxidation of lignin model compounds and lignin have been partially reviewed in the past.<sup>86–89</sup> The design of such biomimetic systems aims to the availability of a catalyst both highly reactive and environmentally friendly. In order to meet such requirements, a metalloporphyrin should be highly reactive and robust to oxidation, that is show a high turnover number. The ideal solvent, for both environmental and economical concerns should be water, and the oxygen donor hydrogen peroxide rather than  $\text{KHSO}_5$ ,  $t\text{-BuOOH}$ ,  $\text{PhOI}$ ,  $\text{MMP}$  (magnesium mono-peroxy phthalate),  $\text{NaClO}$ , and  $m\text{-CPBA}$ .

The catalyst reactivity can be tuned at different levels, and more specifically by changing:

*The metal center.* The presence of manganese rather than iron can limit the extent of homolytic reactions.

*The substitution pattern on the porphyrin ring.* The introduction of electron withdrawing substituents in the *meso* positions increases both the porphyrin redox potential and the resistance to overoxidation. According to the substituents, the solubility in water and organic solvents can be tuned.

*The axial ligand.* Addition of suitable nitrogen bases or possible oxygen ligands can increase the reactivity of the catalyst.

*The pH value and solvent.* Metalloporphyrins reactivities depend also on pH values and hydrophobicity of the reaction medium.

*The catalyst support.* It is possible to mimic the enzyme scaffold of lignin peroxidase by immobilization of the metallo porphyrin onto a suitable support. This introduces the possibility to recycle the catalyst and to tune its reactivity by the choice of supports with different immobilization characteristics.

In Figure 13 are reported the metalloporphyrins which have been used in these experiments.

## A. OXIDATION OF LIGNIN MODEL COMPOUNDS

In the next sections are reported the most representative examples of oxidation of lignin and lignin model compounds by metalloporphyrins. The experiments are classified on the basis of the structure of the substrate: monomeric models, dimeric models, lignin models,

lignins, and pulps. The study of the reactivity of simple models is preliminary to the understanding of the general reactivity of lignin systems and is fundamental in order to rationalize the behavior of the more complex polymer. In turn, the knowledge of the reactivity of lignin is important in order to verify the possibility of selective lignin oxidation in lignocellulosic systems as pulps.

### 1. Oxidation of Monomeric Lignin Model Compounds

Labat and Meunier<sup>90,91</sup> reported a study of the oxidation of veratryl alcohol **1** with the free water-soluble iron and manganese derivatives of tetrasodium *meso-tetrakis*(*p*-sulfonatophenyl)porphyrin ( $\text{Fe}(\text{TPPS})\text{Cl}$  and  $\text{Mn}(\text{TPPS})\text{Cl}$ ) and the same two metalloporphyrins immobilized onto an ion-exchange resin, Amberlite (namely  $\text{Fe}(\text{TPPS})\text{Cl-Ad}$  and  $\text{Mn}(\text{TPPS})\text{Cl-Ad}$ ).<sup>90</sup> Three different factors were investigated: (i) the comparative efficiency of  $\text{KHSO}_5$  and  $\text{H}_2\text{O}_2$  as primary oxidants, (ii) the influence of pH of the buffer solution associated with acetonitrile ( $\text{CH}_3\text{CN}$ ), and (iii) the influence of the hydrophobicity of the reaction medium on the selectivity of the transformation. The reactions were performed in  $\text{CH}_3\text{CN}$ , in the presence of the appropriate catalyst (10% of catalyst vs. substrate in the homogeneous system, or 100 mg of loaded Amberlite IRA 900 in the heterogeneous system), and in the presence of citrate–phosphate buffer or acetate buffer. Both soluble catalysts,  $\text{Fe}(\text{TPPS})\text{Cl}$  and  $\text{Mn}(\text{TPPS})\text{Cl}$  gave with  $\text{H}_2\text{O}_2$  in  $\text{CH}_3\text{CN}$  and citrate–phosphate buffer low conversion of **1** (5% and 2% conversion, respectively). The conversion was not improved by the addition of imidazole as axial ligand (7% conversion in both cases). On the other hand, high conversions were observed with  $\text{KHSO}_5$ , in which case 67% conversions were obtained with  $\text{Fe}(\text{TPPS})\text{Cl}$  and  $\text{Mn}(\text{TPPS})\text{Cl}$ .<sup>90</sup> Noteworthy, similar results were obtained with the heterogeneous systems  $\text{Fe}(\text{TPPS})\text{Cl-Ad}$  and  $\text{Mn}(\text{TPPS})\text{Cl-Ad}$  (50% and 61%, respectively). In the latter cases, the catalysts maintained 95% of their catalytic activity after recycling experiments. The influence of the pH on the  $\text{KHSO}_5$  oxidation of **1** in the presence of  $\text{M}(\text{TPPS})\text{Cl}$  or  $\text{M}(\text{TPPS})\text{-Ad}$  ( $\text{M} = \text{Fe}$  or  $\text{Mn}$ ) was also described by the authors for a reaction time of 1 min at six different pH values (pH value: 2, 3, 4, 5, 7, and 8). Different results were observed depending on the nature of the metal bonded to the porphyrin ring. With iron porphyrins ( $\text{Fe}(\text{TPPS})\text{Cl}$  and  $\text{Fe}(\text{TPPS})\text{Cl-Ad}$ ), high conversions were obtained at low value of pH, the optimum value being  $\text{pH}=3$ . On the basis of these

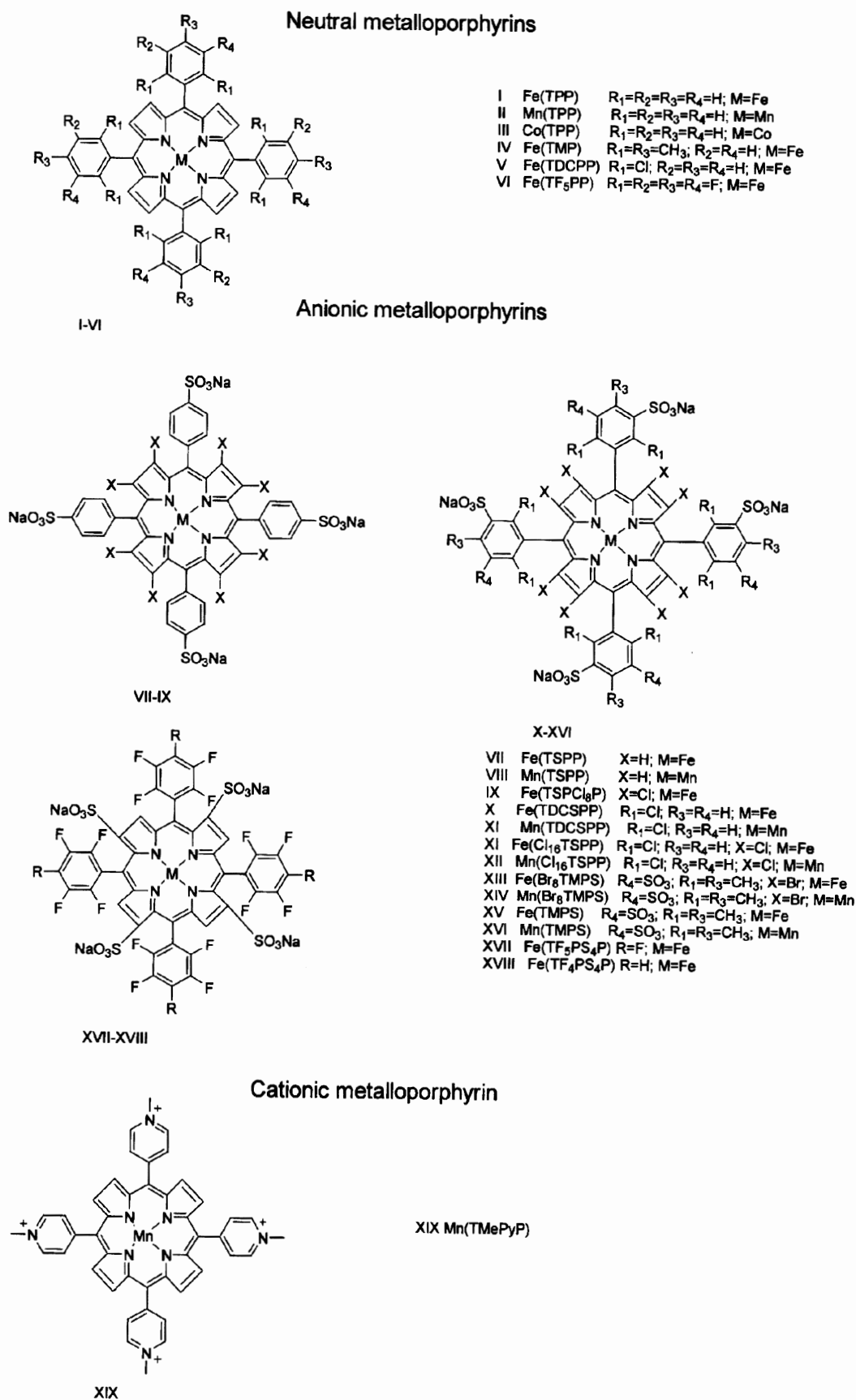


Figure 13. Structure of metalloporphyrins used in lignin and lignin model compound oxidations.

data, the authors suggest that low pH values “favor the cleavage of inactive  $\mu$ -oxo iron porphyrin dimers known to be formed in the oxidation of water-soluble porphyrin complexes.” Instead, an opposite pH effect was reported for manganese porphyrins, Mn(TPPS)Cl and Mn(TPPS)Cl-Ad. In the latter cases, the optimum was reached between pH 4.5 and 6.0, whereas low pH values considerably slow down the conversion of **1**. Thus, the activity maxima of the iron and manganese porphyrins are not reached in the same pH range. Probably a different reaction mechanism occurred. Moreover, in a direct comparison, the homogeneous Fe(TPPS)Cl system is more reactive than Mn(TPPS)Cl. For heterogeneous catalysts, the Mn(TPPS)Cl-Ad is more reactive than Fe(TPPS)Cl-Ad.

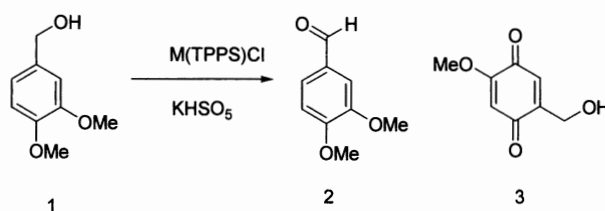
The same authors studied the influence of the hydrophobicity of the reaction medium on the  $\text{KHSO}_5$  oxidation of **1** catalyzed with M(TPPS)Cl and M(TPPS)-Ad, by variation of the ratio of the  $\text{CH}_3\text{CN}$ /buffer reaction mixture. For the iron based systems Fe(TPPS)Cl, the conversion of **1** at pH 3 decreased when the hydrophobicity of the medium increased. However, the influence of the hydrophobicity was not the same for Fe(TPPS)Cl-Ad, and acceptable conversion of **1** were obtained even in the presence of high amount of  $\text{CH}_3\text{CN}$  (25% of  $\text{CH}_3\text{CN}$ ). With the manganese based systems, Mn(TPPS) and Mn(TPPS)Cl-Ad, the maximum catalytic activity was obtained again with 25% of  $\text{CH}_3\text{CN}$ . Veratraldehyde **2**, and 2-methoxy-5-(hydroxymethyl)-1,4-benzoquinone **3** were recovered in appreciable amounts. Notably, these two products were obtained also by the oxidation of **1** with lignin peroxidase itself (Scheme 3). Even if no mechanistic

hypothesis are suggested, on the basis of the isolated products it is reasonable to hypothesize either a benzylic oxidation, and an initial C-5 hydroxylation with subsequent C-3 demethoxylation and oxidation to the quinonoid derivative **3**.

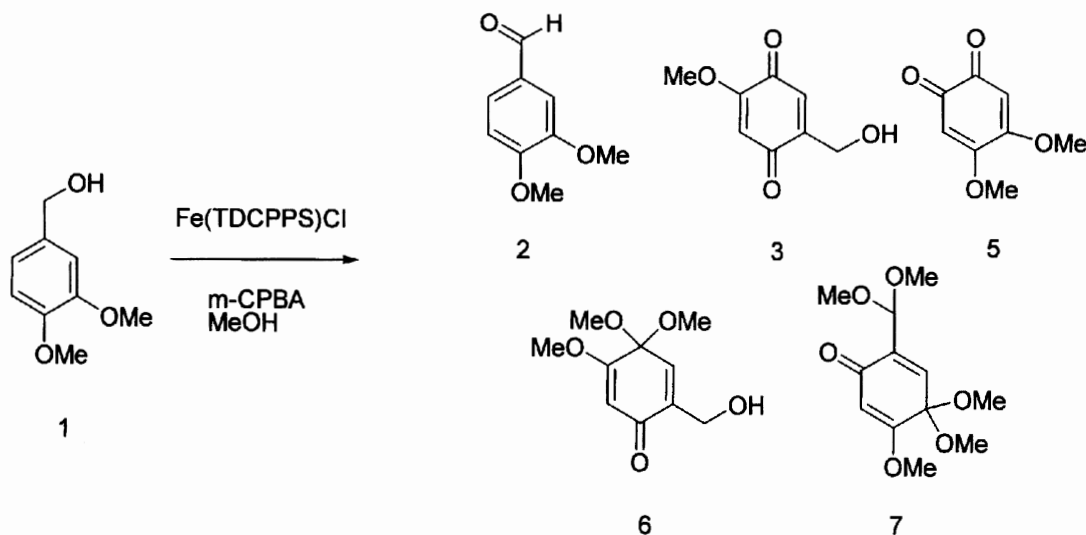
A higher amount of reaction products was characterized by Cui and Dolphin during their studies on the oxidation of **1** and veratryl acetate **4** with *meso*-tetra(2,6-dichloro-3-sulfonatophenyl)porphyrin iron chloride Fe(TDCPPS)Cl in the presence of *m*-chloroperbenzoic acid (*m*-CPBA) as oxidant in both aqueous and organic solvent.<sup>92</sup>

The reaction performed in MeOH at room temperature afforded veratraldehyde **2**, and the *p*-quinone derivative **3**, as the main products, beside to 4,5-dimethoxy-3,5-cyclohexadien-1,2-dione **5** (*ortho*-quinone derivative), 2-hydroxymethyl-4,4,5-trimethoxy-2,5-cyclohexadien-1-one **6**, and 2-dimethoxymethyl-4,4,5-trimethoxy-2,5-cyclohexadien-1-one **7**, as side products (Scheme 4).

Compound **6** is clearly formed by selective addition of two molecules of the solvent to **3**. Moreover, compound **7** is obtained from **3** by a multistep pathway that requires the oxidation of the primary alcohol to the corresponding



**Scheme 3.** Oxidative degradation of lignin model compound **1** by MTPPS and  $\text{KHSO}_5$



**Scheme 4.** Oxidation of veratryl alcohol with *meso*-tetra(2,6-dichloro-3-sulfonatophenyl)porphyrin iron chloride Fe(TDCPPS)Cl and *m*-CPBA in MeOH at room temperature.

aldehyde (not isolated by the authors) and the successive formation of the acetal derivative. This hypothesis is confirmed by the high yields of **6** and **7** obtained under forced reaction conditions (open to air and vigorous stirring) and by the recovery of **8** when the reaction was performed in ethanol as solvent (Figure 14).

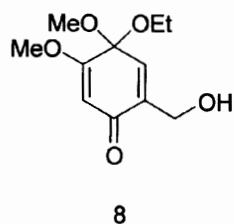
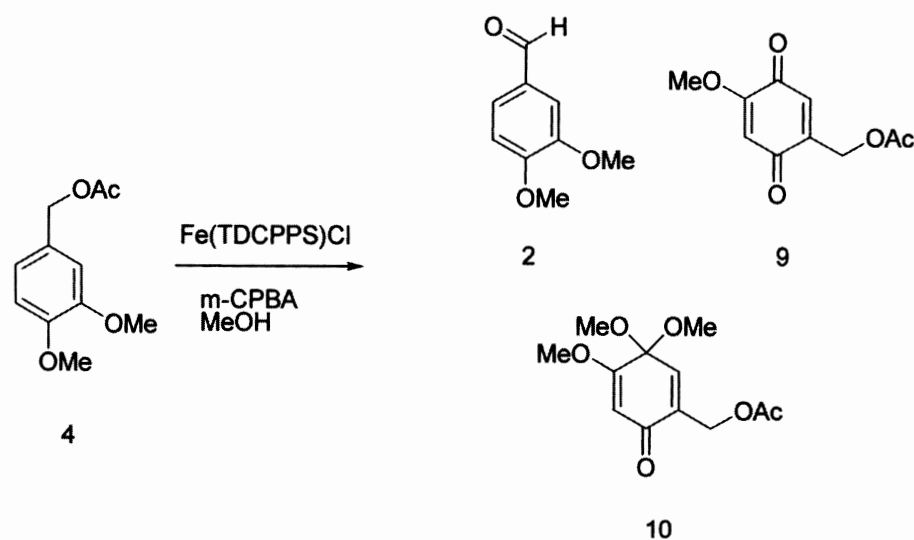


Figure 14. Compound **8**.

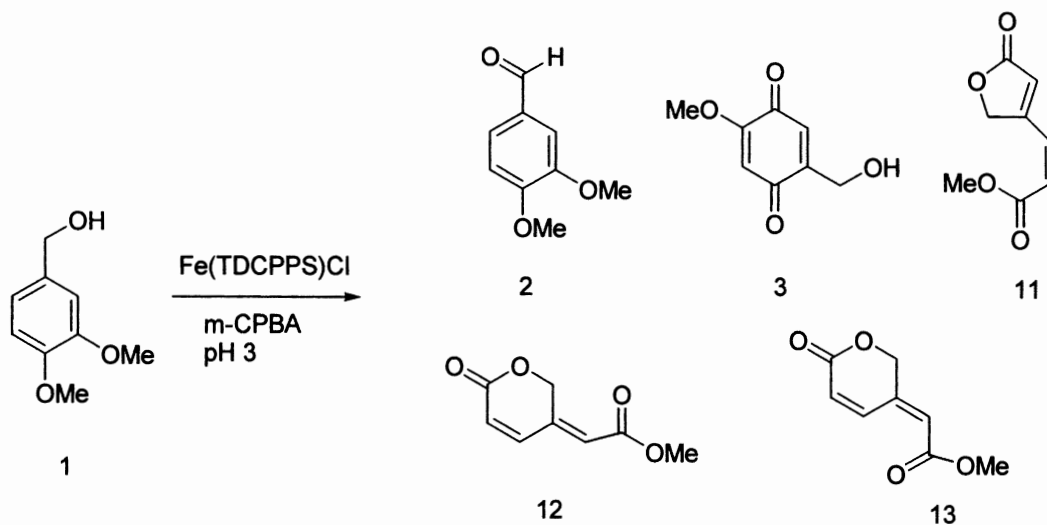
Veratryl acetate **4** showed a lower reactivity and only small amount of **2**, of the *p*-quinone derivative **9**, and of the ketal derivative **10** were obtained beside to unreacted substrate (Scheme 5). Notably, when the oxidation of **1** was performed in phosphate buffer (pH 3) beside to expected compounds **2** and **3**, products of oxidative ring cleavage, namely **11–13**, were also obtained (Scheme 6).

In a similar way, when the oxidation of veratryl acetate **4** was performed in similar experimental conditions, beside to the expected derivative **9**, one product of side-chain degradation, the 3,4-dimethoxy phenol **14**, and one product of oxidative ring opening, the ester **15**, were recovered in appreciable amounts (Scheme 7).

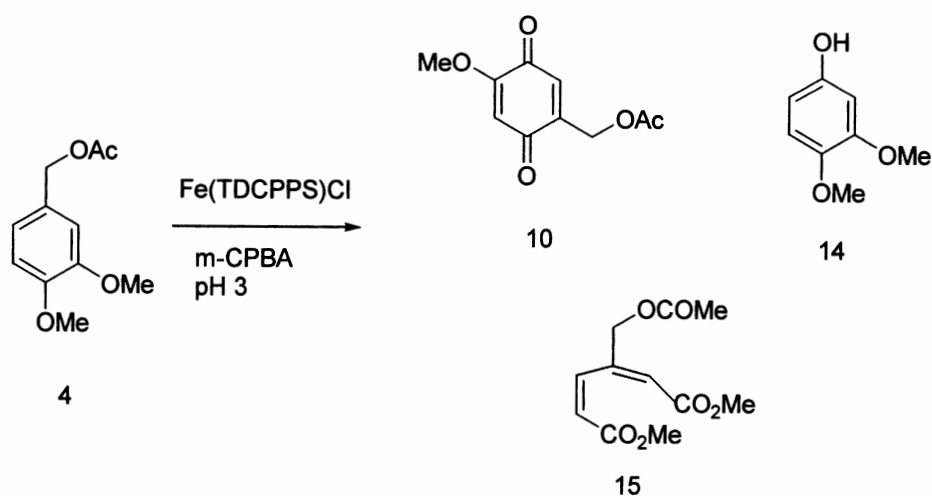
The authors proposed a mechanism to explain the presence of the phenol derivative **14**.<sup>93</sup> In this



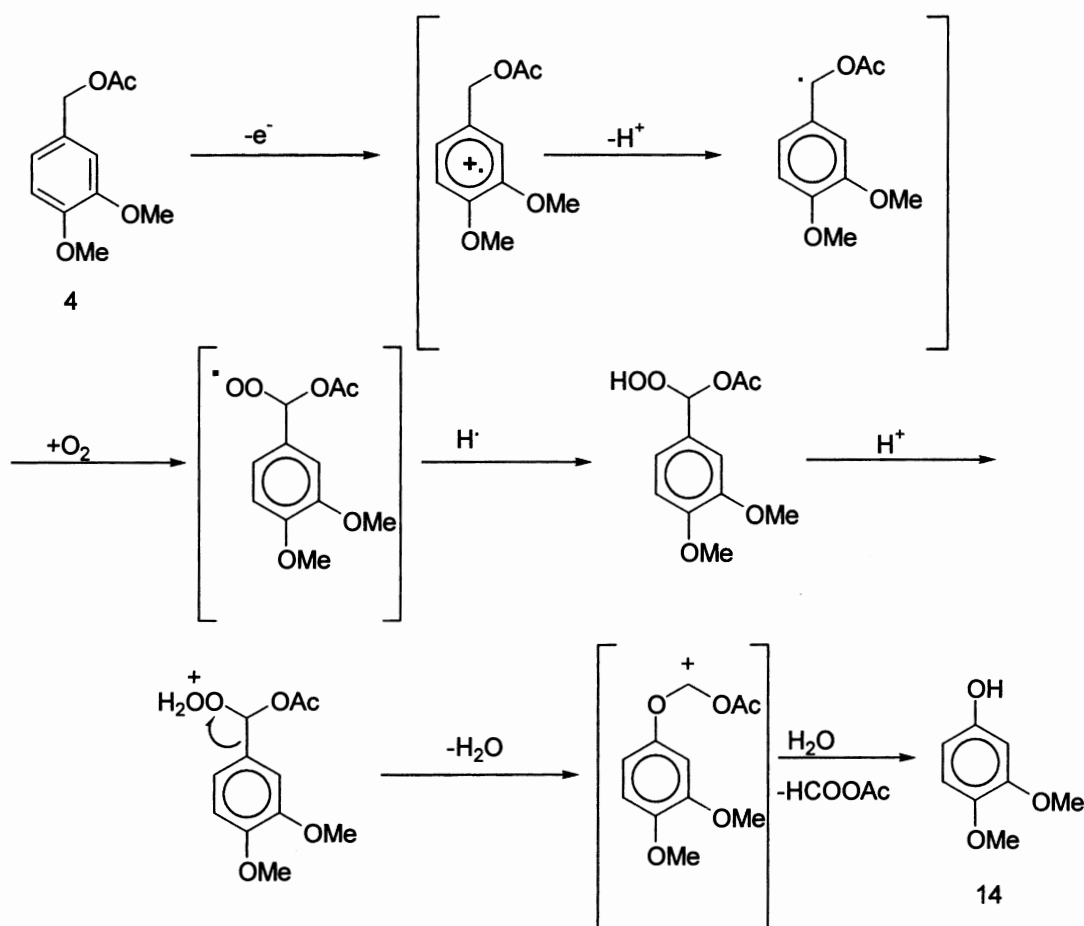
Scheme 5. Oxidation of veratryl acetate **4** with *meso*-tetra(2,6-dichloro-3-sulfonatophenyl)porphyrin iron chloride Fe(TDCPPS)Cl and *m*-CPBA acid in MeOH at room temperature.



Scheme 6. Oxidation of veratryl alcohol **1** with *meso*-tetra(2,6-dichloro-3-sulfonatophenyl)porphyrin iron chloride Fe(TDCPPS)Cl and *m*-CPBA acid in phosphate buffer at pH 3.



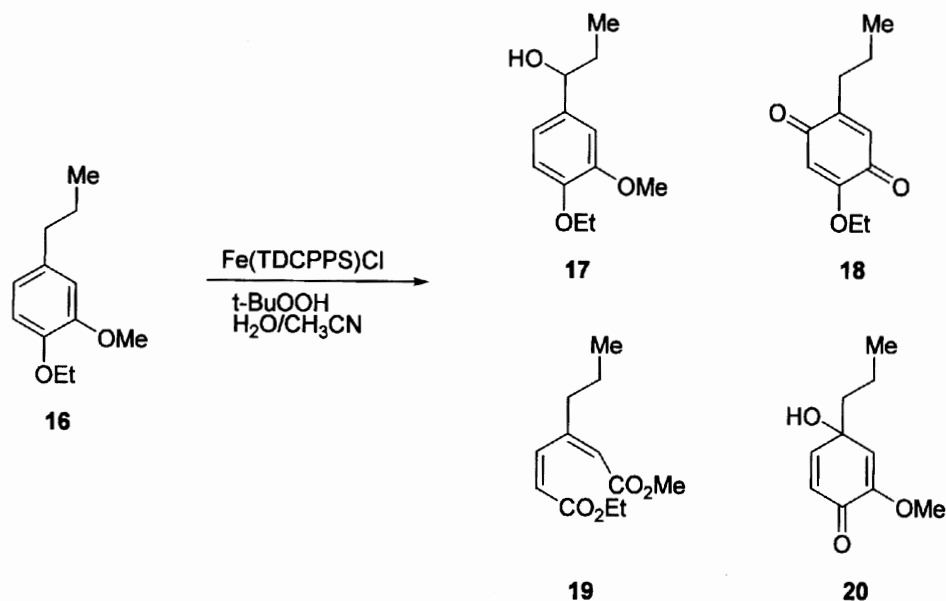
**Scheme 7.** Oxidation of veratryl acetate **4** with *meso*-tetra(2,6-dichloro-3-sulfonatophenyl)porphyrin iron chloride Fe(TDCPPS)Cl and *m*-CPBA phosphate buffer at pH 3.



**Scheme 8.** Hypothesis of formation of the phenol derivative **14**.

hypothesis, after the initial formation of the radical cation intermediate the loss of a proton may produce a benzylic radical which in turn can react with dioxygen to give a radical peroxide and successively the hydrogen peroxide intermediate (Scheme 8). After protonation of

this latter intermediate, a rearrangement of the phenyl moiety can occur with concomitant loss of one water molecule and generation of an alkoxy cation. Finally, the hydrolysis of ether linkage on the cation intermediate may produce the observed phenol derivative **14**.



**Scheme 9.** Products of oxidation of 1-(4-ethoxy-3-methoxyphenyl)propane **16** by  $\text{Fe}(\text{TDCPPS})\text{Cl}/t\text{-BuOOH}$  in aqueous acetonitrile at pH 3.

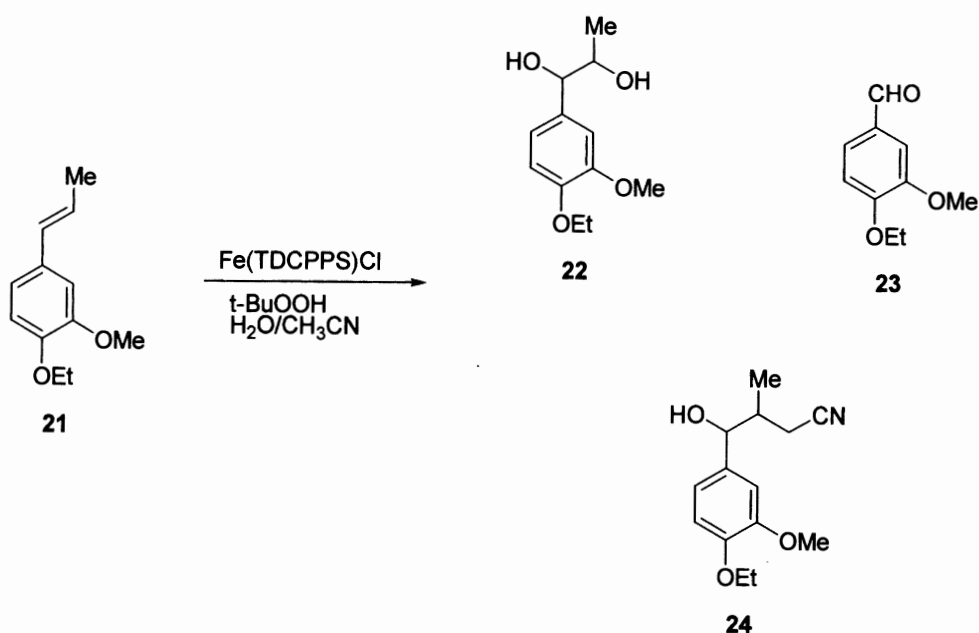
The authors successively reported the oxidation of 1-(4-ethoxy-3-methoxyphenyl)propane **16** under similar experimental conditions using  $t\text{-BuOOH}$  as oxygen atom donor (Scheme 9). In this case, a product of benzylic hydroxylation, namely compound **17**, the *p*-benzoquinone derivative **18**, the muconic acid methyl ethyl ester **19**, and the ketone **20** were recovered. Compound **20** can be considered as a “trapped” intermediate for the C–C cleavage of lignin phenolic model compounds and its presence in the reaction mixture is in accord with the mechanism of degradation previously proposed by Numba *et al.*<sup>94</sup>

$\text{Fe}(\text{TDCPPS})\text{Cl}$  was able to oxidize also a monomeric lignin model compound bearing a C=C double bond as in the case of **21**. In this case, a product of dihydroxylation, compound **22**, was obtained beside to the 4-ethoxy-3-methoxybenzaldehyde **23**. An addition product characterized by the presence of a molecule of the solvent, namely compound **24**, was also obtained. Isotope labeling experiments suggest the possibility of a cation radical intermediate also for the dihydroxylation process.<sup>95</sup> The presence of compound **24** is probably due to the formation of a C $\beta$ -centered radical intermediate, a data that provides an additional support to the cation radical hypothesis (Scheme 10).

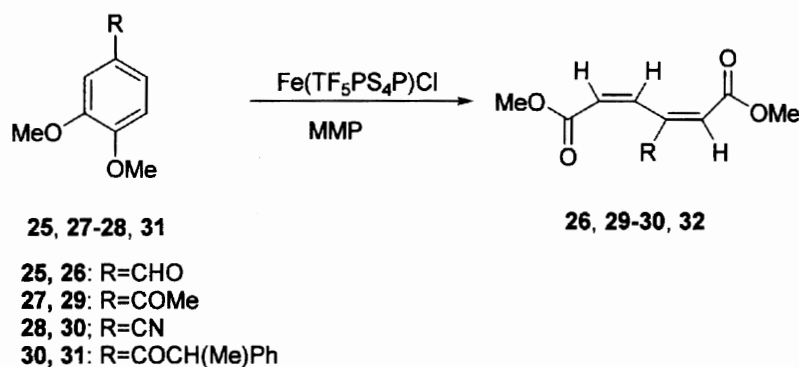
Several studies have been performed to obtain informations about the oxidative ring opening of substituted arenes to the corresponding muconic acids or muconic esters derivatives.<sup>96</sup> In this context, iron *meso-tetrakis*(pentafluorophenyl)- $\beta$ -tetrasulfonatoporphyrin chloride,  $\text{Fe}(\text{TF}_5\text{PS}_4\text{P})\text{Cl}$ , and magnesium

monoperoxyphthalate (MMP) or  $\text{H}_2\text{O}_2$  are able to oxidize 1,2-dimethoxy arenes bearing electron-withdrawing groups to muconic dimethyl esters functionalized in the  $\beta$ -position.<sup>97</sup> In a typical experiment, dimethoxy arene derivative **25** dissolved in a 1:4 mixture of MeCN and tartrate buffer (pH 3) was added to MMP at 0°C in the presence of catalytic amount of  $\text{Fe}(\text{TF}_5\text{PS}_4\text{P})\text{Cl}$  (substrate:catalyst molar ratio = 250). After work up of the reaction the muconic dimethyl ester **26** was obtained as the only recovered product (Scheme 11).

Similar reactions performed on 3,4-dimethoxy benzonitrile **27**, or 3,4-dimethoxy aceto phenone **28**, gave the corresponding muconic dimethylester derivatives **29**, and **30**, in 30 and 40%, yields, respectively (Scheme 11). Similar results were obtained in the oxidation of **31** to obtain the muconic ester derivative **32**. The catalyst was able to oxidize the substrate to muconic ester with 100 turnovers without important degradation. All products obtained from these reactions were fully characterized by mass spectrometry and nuclear magnetic resonance, and exhibited the characteristic pattern of the three vinylic hydrogens of (*2E*, *4Z*)-3-substituted-muconic diesters (that is: three doublets at *ca.* 6.1, 7.1, and 6.5; *J ca.* 12.1 and 2 Hz).<sup>98</sup> When  $\text{H}_2\text{O}_2$  was used as oxygen atom donor under similar experimental conditions the muconic dimethyl ester derivatives were again obtained but in lower yields. Other porphyrins, such as iron *meso-tetrakis*(4-sulfonatophenyl)porphyrin chloride  $\text{Fe}(\text{TPPS})\text{Cl}$ , and iron *meso-tetrakis*(2,6-dichloro-3-sulfonatophenyl)porphyrin



**Scheme 10.** Oxidation of 1-(4-ethoxy-3-methoxyphenyl)propene by the catalytic system Fe(TDCPPS)Cl/*t*-BuOOH in aqueous acetonitrile at pH 3.



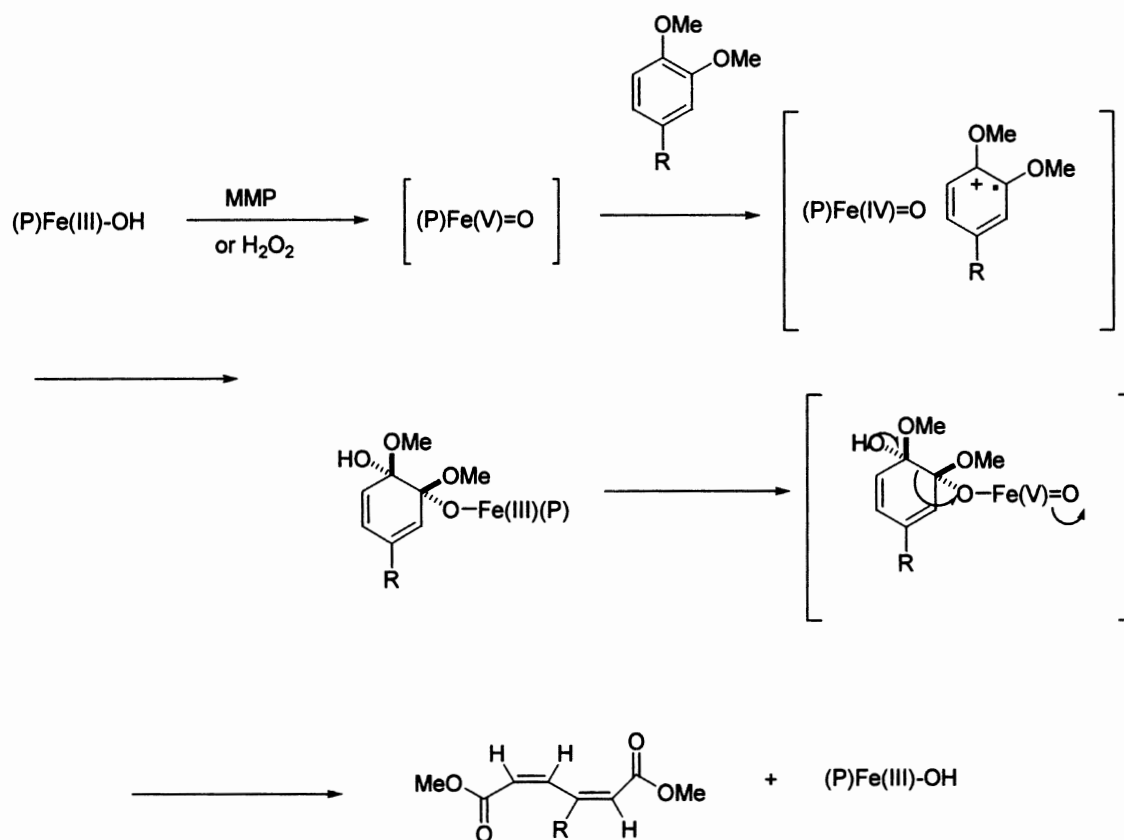
**Scheme 11.** Oxidation of dimethoxy arene derivatives by the catalytic system Fe(TF<sub>5</sub>PS<sub>4</sub>P)Cl/MMP or H<sub>2</sub>O<sub>2</sub>.

chloride Fe(TDCPPS)Cl failed to give muconic ester derivatives.<sup>99,100</sup> The former was completely bleached after addition of the primary oxidant, the latter led to partial consumption of the substrate without formation of the desired products. It is interesting to note that this cleavage reaction has very few precedents in the literature.<sup>101</sup> According to the known properties of such porphyrin, the authors hypothesize for the reaction mechanism reported in Scheme 12. This mechanism is characterized by the formation of the radical cation of the substrate, the addition of water at the cation center and of Fe<sup>IV</sup>=O at the radical site leading to the intermediate formation of a Fe(III)-cyclohexanedienolate, and the oxidation of the Fe(III) of this intermediate with concomitant cleavage of the C–C bond.

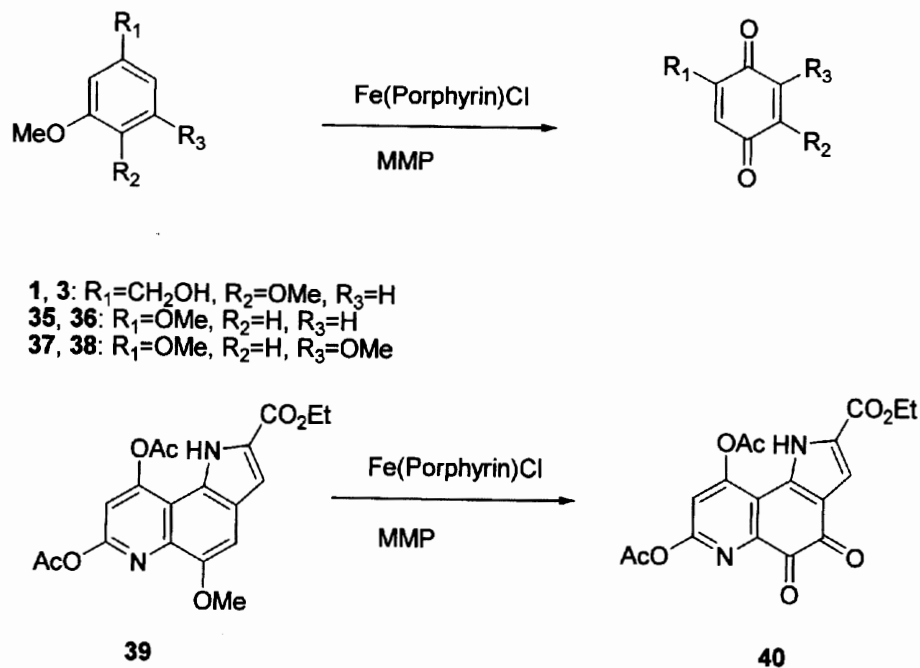
A different selectivity was observed in the oxidation of methoxy arenes bearing electron donating substituents.

As an example, the oxidation of veratryl alcohol **1**, 1,3-dimethoxy benzene **35**, and 1,3,5-trimethoxy benzene **37** with iron *meso-tetrakis*(2,3,5,6-tetrafluorophenyl)-tetrasulphonatoporphyrin chloride, and iron *meso-tetrakis*(pentafluorophenyl) tetrasulphonatoporphyrin chloride, in a mixture of MeCN and 0.1 mol dm<sup>-3</sup> tartrate, using MMP as oxygen atom donor, afforded the corresponding quinones **3**, **36**, and **38**, respectively, in satisfactory yields in the presence of trace of veratraldehyde as by-product (Scheme 13).<sup>102</sup> The reaction is operative also with iron *meso-tetrakis*(4-sulfonatophenyl)porphyrin chloride and iron *meso-tetrakis*(3-sulfonato-2,6-dichlorophenyl)porphyrin chloride, but, in the latter cases larger amounts of veratraldehyde as secondary product were obtained. The reaction was applied also to a methoxyarene for which the formation of a *p*-quinone was impossible, compound **39**, which is





**Scheme 12.** Mechanism of oxidation of arene derivatives to corresponding muconic ester derivatives by the catalytic system  $Fe(TF_5PS_4P)Cl/MMP$  or  $H_2O_2$  amounts of veratraldehyde were recovered from the reaction mixtures.



**Scheme 13.** Products of oxidation of veratryl alcohol **1**, of 1,3-dimethoxy benzene **35** and 1,3,5-trimethoxy benzene **37** with iron *meso-tetrakis*(2,3,5,6-tetrafluorophenyl) tetrasulphonatoporphyrin  $Fe(TF_4PS_4P)Cl$ , and iron *meso-tetrakis*(pentafluorophenyl) tetrasulphonatoporphyrin  $Fe(TF_5PS_4P)Cl$  and MMP.

an intermediate in the Corey synthesis of methoxatin.<sup>103</sup> The quinone **40** was obtained in good yield.

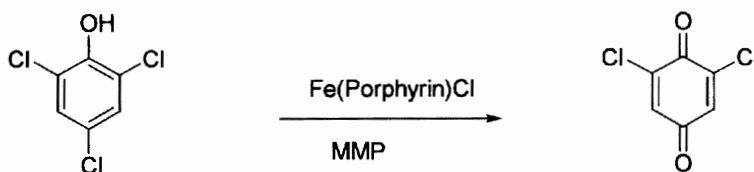
As an extension of studies on degradation of monomeric lignin model compounds, Meunier and coworkers reported the use of water-soluble iron porphyrins and of some supported porphyrins for the degradation of chloro phenols.<sup>104</sup> Organohalide pollutants resist microbial destruction and are subject to biomagnification and accumulation in the tissues of plants and animals.<sup>105,106</sup> The porphyrins used in this study were the Fe(TPPS)Cl, Fe(TMPS)Cl, and Fe(TDCPPS)Cl. Moreover, two new heterogeneous catalysts were prepared supporting Fe(TPPS)Cl, and Fe(TMPS)Cl on Amberlite® (these catalysts are named Fe(TPPS)Cl-Ad and Fe(TMPS)Cl-Ad, respectively). These catalytic systems were used in the oxidation of 2,4,6-trichloro phenol as reported in Scheme 14.

In all cases, 2,4,6-trichloro phenol was oxidized to 2,6-dichloro-1,4-benzoquinone as the only recovered product. The reaction was performed in citrate-phosphate buffer solution at pH 3 using KHSO<sub>5</sub> as oxygen atom donor. At higher pH (pH 6.0) the quinone polymerizes. Fe(TPPS)Cl, Fe(TMPS)Cl, and Fe(TDCPPS)Cl were the most active catalytic systems, affording the quinone in 95 and 92% yields, respectively. The corresponding heterogeneous systems, Fe(TPPS)Cl-Ad and Fe(TMPS)Cl-Ad were found less active, yielding the quinone in 30 and 36% yields, respectively, after a longer reaction time. The authors did not report examples of recycling experiments, thus it is not clear if the heterogeneous systems could be employed for more transformations. H<sub>2</sub>O<sub>2</sub> was also an effective

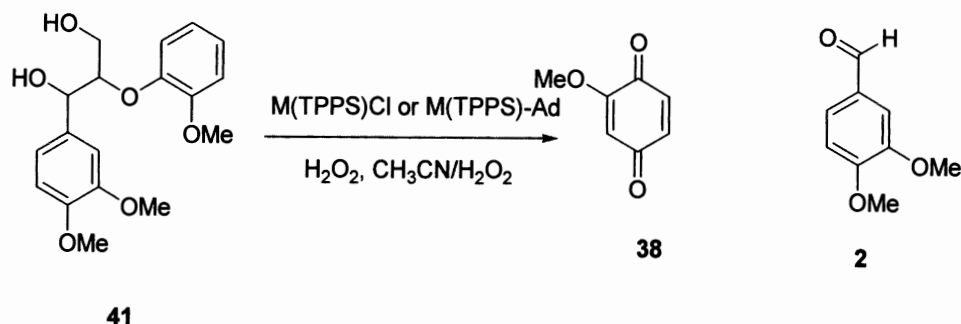
oxidant in the reactions with the homogeneous systems, but longer reaction time was again required to obtain the quinone in only 68% yield. Thus, the authors conclude that the “Fe-porphyrin/KHSO<sub>5</sub>” systems based on sulfonated porphyrin ligands are able to catalyze the oxidative dechlorination of phenols.

## 2. Oxidation of Dimeric Lignin Model Compounds

In a continuation of their studies on the ligninase models based on water-soluble manganese and iron-porphyrins complexes, Meunier and coworkers reported the degradation of 1-(3,4-dimethoxyphenyl)-2-(2-methoxyphenoxy)propane-1,3-diol **41** with KHSO<sub>5</sub> in the presence of catalytic amount of the iron and manganese derivatives of tetrasodium *meso-tetrakis*(*p*-sulfonatophenyl)porphyrin (Fe(TPPS)Cl and Mn(TPPS)Cl) and of the same two metalloporphyrins immobilized onto Amberlite IRA 900 (Fe(TPPS)Cl-Ad and Mn(TPPS)Cl-Ad).<sup>107</sup> Compound **41** is a useful model to study the efficiency of the oxidative system to break the C $\alpha$ -C $\beta$  bonds of the arylglycerol- $\beta$ -arylether linkages, the major type of linkage present into the lignin. The reaction was performed in CH<sub>3</sub>CN and a buffered water solution to obtain a single phase solution. Fe(TPPS)Cl, Fe(TPPS)Cl-Ad, and Mn(TPPS)Cl give full conversion of **41**, while Mn(TPPS)Cl-Ad gives a lower conversion (65%) under similar experimental conditions. Two main products were isolated and characterized from the reaction mixtures, 2-methoxy-1,4-benzoquinone **38**, and veratraldehyde **2** (Scheme 15), in yields ranging



**Scheme 14.** Oxidation of 2,4,6-trichloro phenol with Fe(TPPS)Cl, Fe(TMPS)Cl, Fe(TDCPPS)Cl, Fe(TPPS)Cl-Ad, and Fe(TMPS)-Ad.



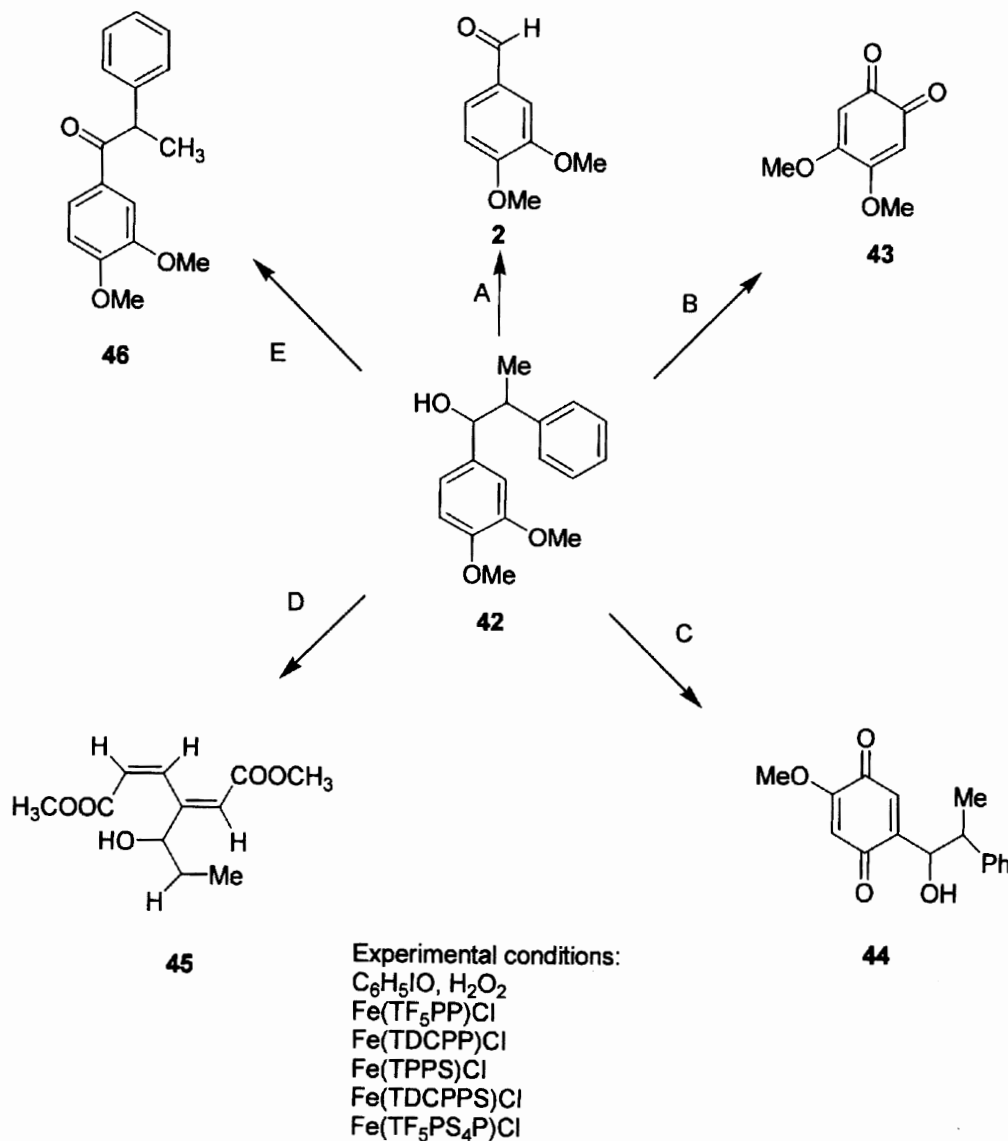
**Scheme 15.** Oxidative degradation of lignin model compound **41**.

from 15 to 30%. Thus, under these experimental conditions, only two reaction pathways were observed, the expected  $C\alpha-C\beta$  cleavage to **2**, and the  $C1-C\alpha$  cleavage to *p*-quinone **38**.

A detailed study of the mechanism of oxidation of a lignin dimeric model compound by different iron porphyrins was reported by Mansuy *et al.*<sup>108</sup> The oxidation of the nonphenolic  $\beta$ -1 dimeric lignin model **42** was performed using five different iron-porphyrins, namely iron(III) *meso-tetrakis*(pentafluorophenyl)porphyrin chloride  $Fe(TF_5PP)Cl$ , iron(III) *meso-tetrakis*-(2,6-dichlorophenyl) porphyrin chloride  $Fe(TDCPP)Cl$ , iron(III) *meso-tetrakis*(4-sulphonatophenyl) porphyrin chloride  $Fe(TSPP)Cl$ , iron(III) *meso-tetrakis*(2,6-dichloro-3-sulfonatophenyl)porphyrin

chloride  $Fe(TDCSPP)Cl$ , and iron(III) *meso-tetrakis*(pentafluorophenyl) $\beta$ -tetrasulfonatoporphyrin chloride  $Fe(TF_5PS_4P)Cl$ , in the presence of  $H_2O_2$  and  $C_6H_5IO$  as oxygen atom donors in organic solvents, or  $H_2O_2$  and magnesium monoperoxy phthalate (MMP) in water. As a general reaction pattern, four main transformations were observed which are reported in Scheme 16.

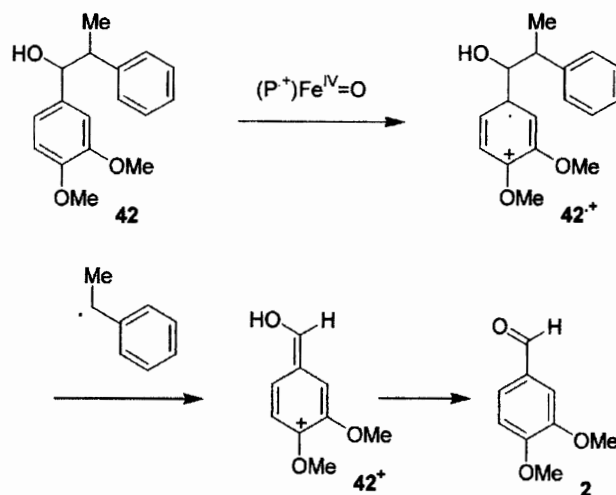
$C\alpha-C\beta$  cleavage leading to veratraldehyde **2** (route A), and the  $C1-C\alpha$  cleavage leading to *ortho*-quinone **43** (route B), the formation of the *p*-quinone **44** (route C), and of the muconic dimethyl ester **45** (route D) were detected. The relative importance of these transformations was found to be correlated on the structure of the catalyst and of the nature of the reaction solvent and of



**Scheme 16.** Reaction products observed in the oxidation of the nonphenolic  $\beta$ -1 dimeric lignin model **42** with the different iron(III) porphyrins.

the oxygen atom donor. As for example, with the  $\text{Fe}(\text{TDCPP})\text{Cl}/\text{H}_2\text{O}_2$  and  $\text{Fe}(\text{TF}_5\text{PP})\text{Cl}/\text{H}_2\text{O}_2$  catalytic systems in  $\text{CH}_2\text{Cl}_2/\text{CH}_3\text{CN}$  mixture, veratraldehyde **2** was recovered as the main reaction product. The same reaction performed with  $\text{Fe}(\text{TF}_5\text{PP})\text{Cl}/\text{H}_2\text{O}_2$  in a protic medium ( $\text{CH}_2\text{Cl}_2/\text{CH}_3\text{OH}$  mixture) afforded the *p*-quinone **44** as the main product, low amount of the muconic dimethyl ester **45**, and traces of compound **43**. When the reaction was performed in an aqueous medium (tartrate/ $\text{CH}_3\text{CN}$ ) with the water-soluble  $\text{Fe}(\text{TF}_5\text{PS}_4\text{P})\text{Cl}$ , a different selectivity was observed depending on the nature of the oxygen atom donor. In the latter case, veratraldehyde **2** was obtained as the main product with  $\text{H}_2\text{O}_2$  while the *p*-quinone **44** became the main product in the presence of MMP.  $\text{Fe}(\text{TSP})\text{Cl}$  and  $\text{Fe}(\text{TDCSPP})\text{Cl}$  were characterized by an intermediate behavior. Small amount of the ketone derivative **46** were also recovered from the reaction mixture (route E). To obtain information about the mechanism of these reactions, the oxidation of several 1,2-dimethoxyarenes bearing either an electron-releasing or an electron-withdrawing substituent in the *para*-position were performed in tartrate buffer and  $\text{CH}_3\text{CN}$ .<sup>97</sup> The oxidation of dimethoxyarenes bearing an electron-donating substituent gave almost exclusively *p*-quinones, while the oxidation of dimethoxyarenes bearing an electron-withdrawing group led to the corresponding muconic dimethyl esters. On the basis of these data, different hypotheses of the reaction mechanism were proposed for the different reaction products obtained. A common feature of these hypotheses was the initial reaction of the substrate with the radical cation species  $(\text{P}^+)\text{Fe}^{\text{IV}}=\text{O}$  formed after activation of the porphyrins by the primary oxidant. As a consequence of this first reactive event, a stabilized radical cation of the substrate (**42<sup>+</sup>**) and an iron(IV) oxo complex  $(\text{P})\text{Fe}^{\text{IV}}=\text{O}$  could be formed. The selectivity of the next reactive step depends on the stability of **42<sup>+</sup>** and on the reactivity of the  $(\text{P})\text{Fe}^{\text{IV}}=\text{O}$  intermediate. When  $(\text{P})\text{Fe}^{\text{IV}}=\text{O}$  shows low reactivity, as for example in the case of  $\text{Fe}(\text{TDCPP})\text{Cl}$  and  $\text{Fe}(\text{TF}_5\text{PP})\text{Cl}$  in organic aprotic medium, or  $\text{Fe}(\text{TF}_5\text{PS}_4\text{P})\text{Cl}/\text{MMP}$  in aqueous solution, the radical cation **42<sup>+</sup>** may undergo a  $\beta$ -scission with cleavage of the  $\text{C}\alpha\text{-C}\beta$  bond and formation of veratraldehyde and an aryl radical (Scheme 17).

The muconic dimethyl ester derivatives could now be formed by overoxidation of the aldehyde in accord with the results previously obtained for the oxidation of dimethoxyarenes bearing electron-withdrawing groups. In the latter case, a mesomeric form in which the location of the free radical is at the C3 position should

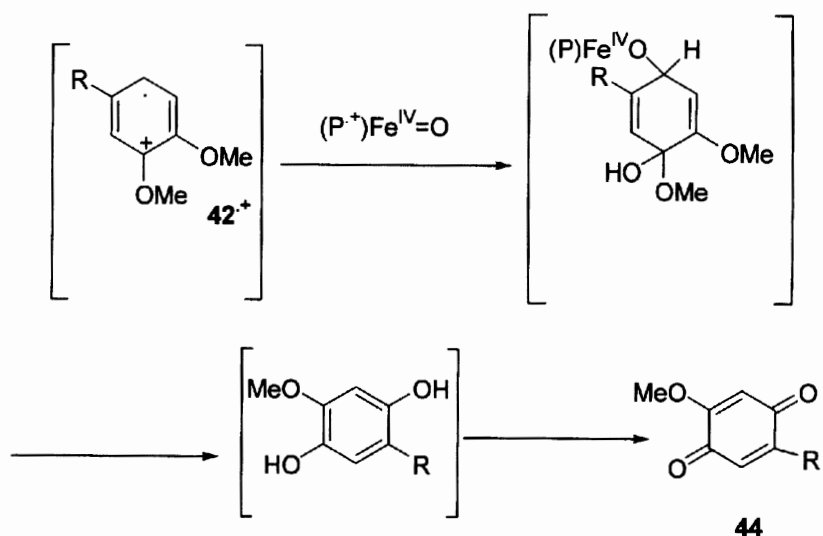
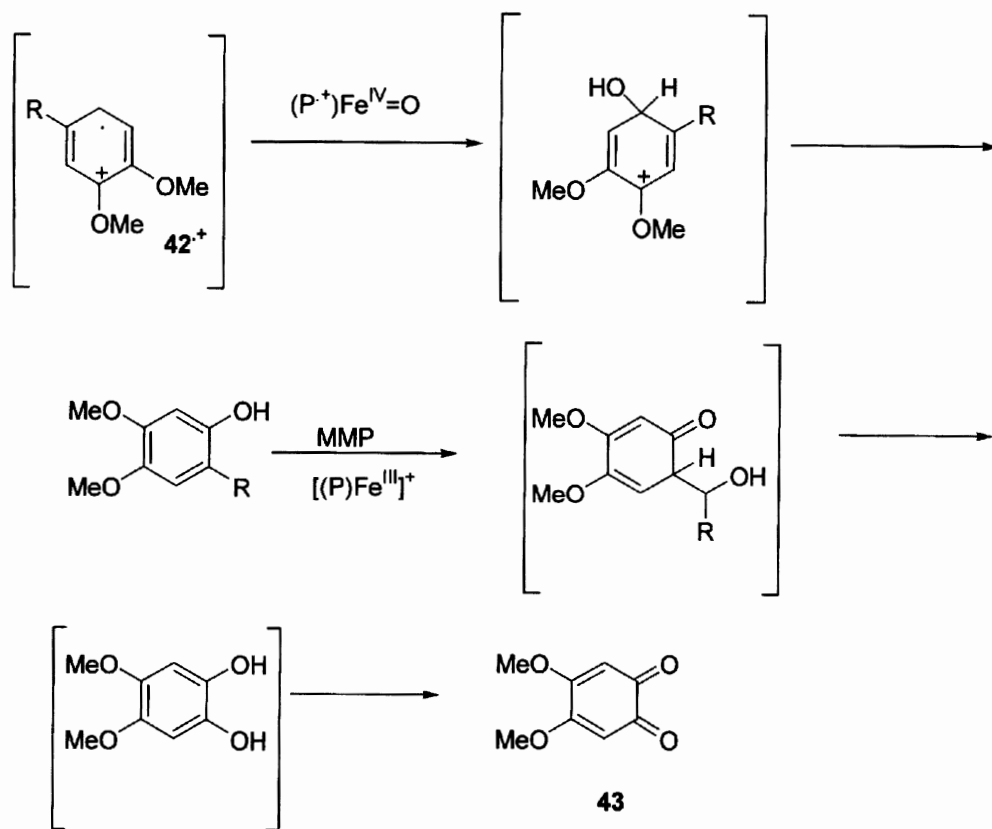


Scheme 17. Mechanism of cleavage of the  $\text{C}\alpha\text{-C}\beta$  bond.

be favored since in this position the radical is stabilized by a captodative effect.<sup>109</sup> In all of the cases in which the  $(\text{P})\text{Fe}^{\text{IV}}=\text{O}$  intermediate is highly reactive, it may react with the radical cation **42<sup>+</sup>** to give the other observed products. Thus, the formation of the *p*-quinone **44** is hypothesized to be due to transfer of the oxygen atom of  $(\text{P})\text{Fe}^{\text{IV}}=\text{O}$  to the C6 radical site of the mesomeric form of **42<sup>+</sup>** and contemporary addition of water to the cationic center. The elimination of methanol and of the regenerate catalyst from this intermediate lead to an hydroquinone that may be easily further oxidized to the observed *p*-quinone (Scheme 18).

On the other hand, if after the oxygen atom transfer from  $\text{Fe}^{\text{IV}}=\text{O}$  to the C6 radical site is possible the loss of a proton to give an hydroxyarene intermediate, a further oxidation of this intermediate could lead to a 1,2-diol at C1 and  $\text{C}\alpha$  that can produce the C1- $\text{C}\alpha$  cleavage with formation of the *ortho*-quinone **43** (Scheme 19). Thus, the selectivity of the reaction could be the result of the degree of the reactivity of the radical cation **42<sup>+</sup>** with the  $\text{Fe}^{\text{IV}}=\text{O}$  intermediate.<sup>110</sup>

The reactivity of *meso*-tetra(2,6-dichloro-3-sulfonato-phenyl)porphyrin iron chloride  $\text{Fe}(\text{TDCPPS})\text{Cl}$  toward four dimeric lignin model compounds has been reported by Cui and Dolphin.<sup>111</sup> Treatment of the  $\beta$ -O-4 dimer, 4-ethoxy-3-methoxy phenyl glycerol  $\beta$ -guaiacyl ether **47**, with  $\text{Fe}(\text{TDCPPS})\text{Cl}$  and *t*-BuOOH give 4-ethoxy-3-methoxy benzaldehyde **48**, and guaiacol **49**. Other products were present in minor amount in the reaction mixture but were not isolated and identified. In accord with data previously reported on the oxidation of monomeric lignin model compounds, the  $\text{C}\alpha\text{-C}\beta$  cleavage appears to be the main degradative reaction pattern (Scheme 20). Thus, the  $\text{Fe}(\text{TDCPPS})\text{Cl}$  porphyrin is not

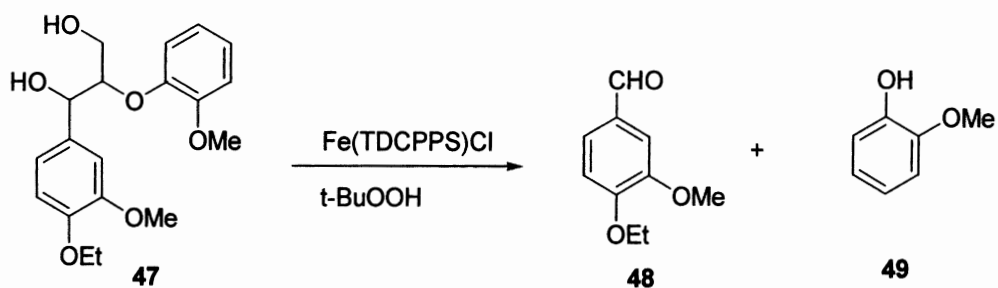
Scheme 18. Mechanism of formation of the *p*-quinone 44.Scheme 19. Mechanism of formation of the *ortho*-quinone 43.

able enough to stabilize the intermediate radical cation of **41** toward the formation of benzoquinone derivatives.

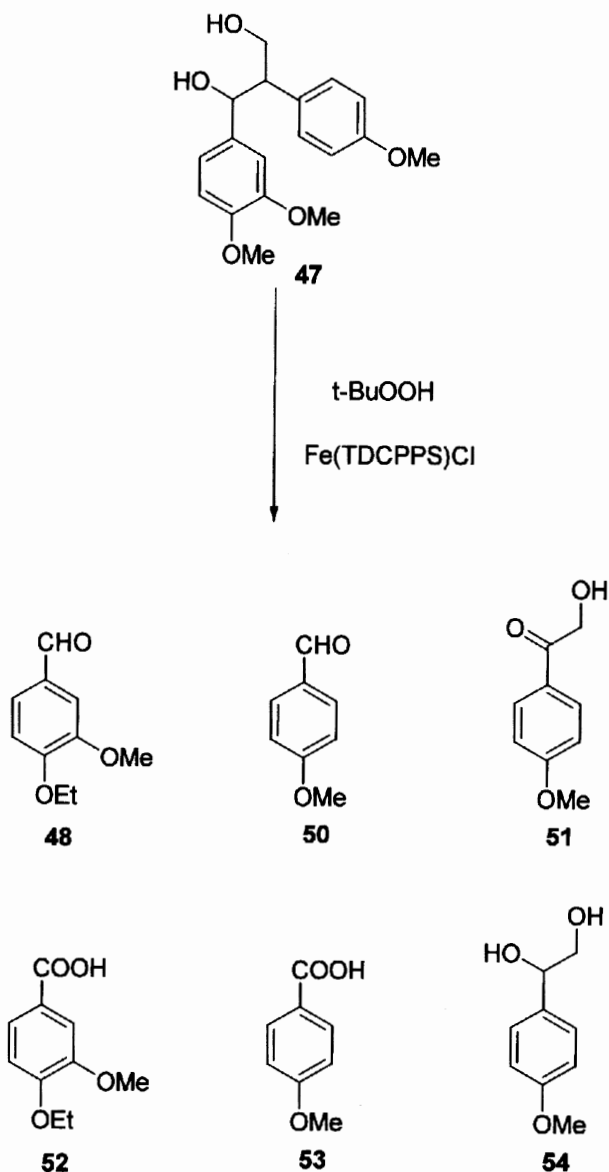
The oxidation of the  $\beta$ -1 dimer, 1-(4-ethoxy-3-methoxyphenyl)-2-(4-methoxyphenyl)-1,3-propanediol **47**, was successively studied under similar experimental conditions. In this case, 4-ethoxy-3-methoxybenzaldehyde **48**, 4-methoxybenzaldehyde **50**, and

4'-methoxy- $\alpha$ -hydroxyacetophenone **51** were obtained as the major products. Small amounts of 4-ethoxy-3-methoxybenzoic acid **52**, 4-methoxybenzoic acid **53**, and 4-methoxyglycol **54**, were detected after GC GC-MS analyses (Scheme 21).

In the oxidation of **47** by lignin peroxidase, compounds **48**, **50**, and **54** were recovered as the main



**Scheme 20.** Oxidation of the dimeric lignin model compound 4-ethoxy-3-methoxyphenylglycerol- $\beta$ -guaiacyl ether **47**, with  $\text{Fe}(\text{TDCPPS})\text{Cl}$  and  $t\text{-BuOOH}$ .



**Scheme 21.** Oxidation of the  $\beta$ -1 dimer, 1-(4-ethoxy-3-methoxyphenyl)-2-(4-methoxyphenyl)-1,3-propanediol **47**.

reaction products under aerobic conditions.<sup>112</sup> The small amount of **54** obtained by oxidation with  $\text{Fe}(\text{TDCPPS})\text{Cl}$  and  $t\text{-BuOOH}$  may be due to the high oxidizing power of the electronically activated catalyst.

Successively the same authors described the first example of porphyrin mediated degradation of  $\beta$ -5 lignin dimeric model compounds, as for example the oxidation of the easily available  $\beta$ -5 dimer, ethyl

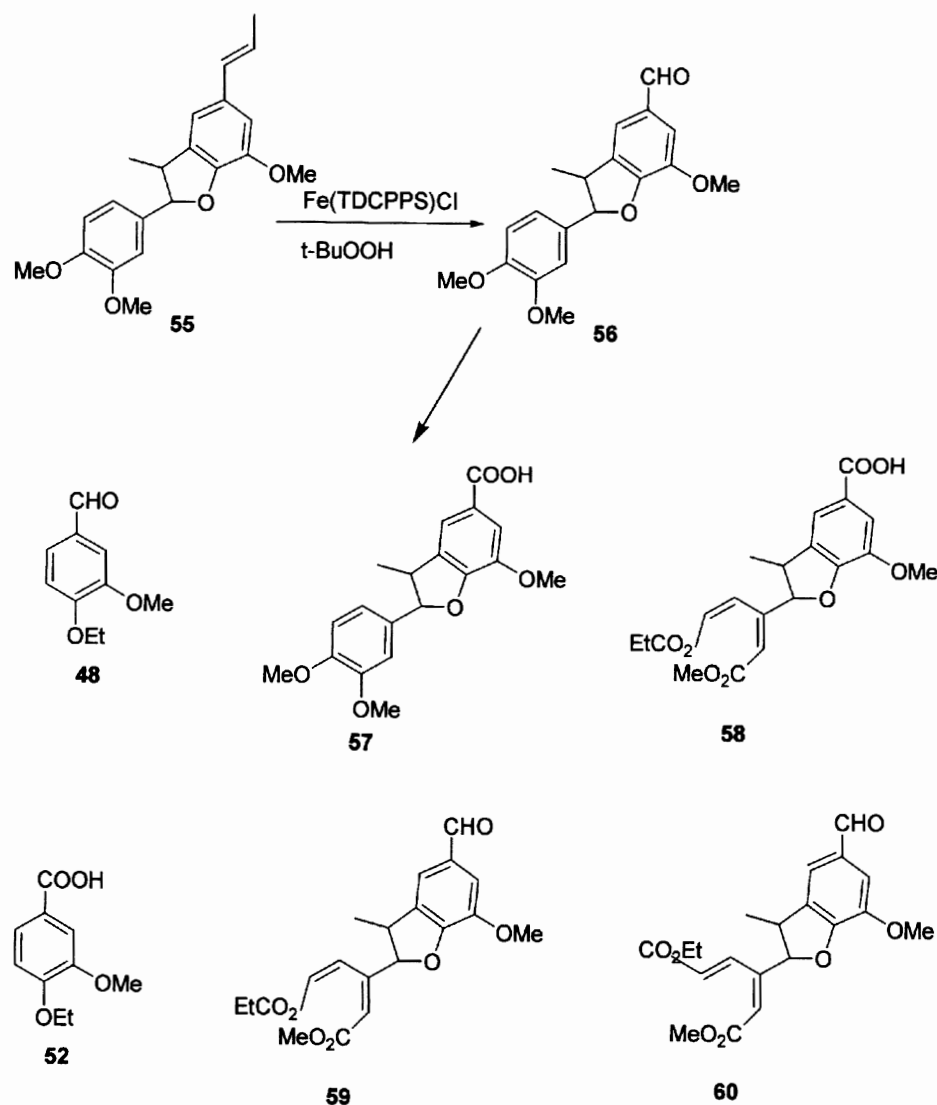
dehydrodiisogenol **55**. When compound **55** was treated with Fe(TDCPPS)Cl and *t*-BuOOH under similar experimental conditions, product **56**, obtained by cleavage on the side chain, was initially recovered (Scheme 22). Further oxidation afforded aldehyde **48** by the C $\alpha$ -C $\beta$  cleavage, the corresponding acid **52**, acids **57** and **58**, and products of aromatic ring cleavage, such as compounds **59** and **60**.

Notably, in the case of the reaction of ring cleavage of the aryl moiety present in the  $\beta$ -O-4 dimers, only the  $\beta$ -phenoxy ring is modified, while the same reaction was not found for the phenylglycerol ring.<sup>56,57</sup> This reaction pattern may be explained by the hypothesis that the C $\alpha$ -C $\beta$  cleavage occurs so rapidly and the phenylglycerol ring cation radical is too short-lived to be attacked by the (porphyrin) Fe<sup>IV</sup>=O intermediate or by the dioxygen to obtain the ring opening of the aromatic

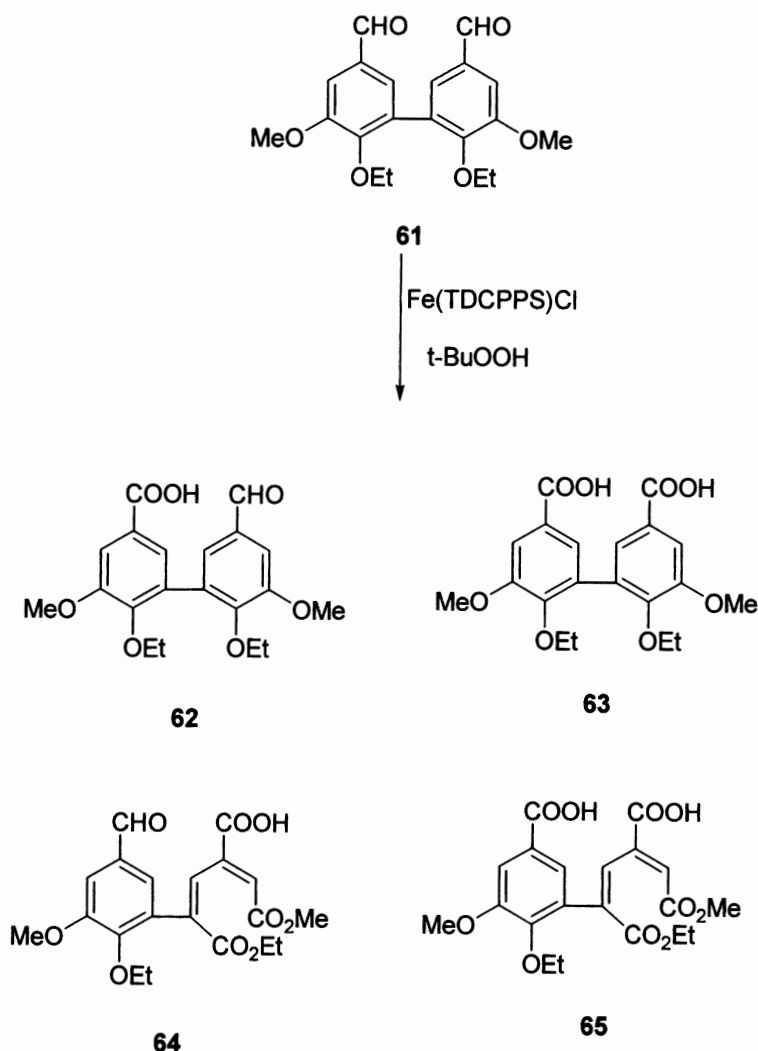
ring. This hypothesis is in accord with the detection by ESR of the cation radical of methoxybenzene derivatives<sup>113</sup> and of the  $\beta$ -phenoxy ring of an  $\alpha$ -oxo  $\beta$ -O-4 dimer.<sup>114</sup> On the other hand, the detection of the cation radical of the phenylglycerol ring has not been reported.

Guaiacyl substructures of lignin are easily condensed by enzymatic reactions to give 5,5'-biphenyl structures.<sup>115</sup> These units are stable to biodegradation, thus their oxidation is important. When 4,4'-diethyldehydrodivanillin **61** was treated with Fe(TDCPPS)Cl and *t*-BuOOH, products of side-chain oxidation, compounds **62** and **63**, and products of aromatic ring cleavage **64** and **65**, were recovered from the reaction mixture (Scheme 23).

As reported by the authors, the recovery of **64** and **65** shows that the aromatic ring of 5,5'-biphenyl structures is cleaved directly without initial demethoxylation, most



Scheme 22. Products of oxidation of ethyl dehydrodiisogenol **55** with Fe(TDCPPS)Cl and *t*-BuOOH.



**Scheme 23.** Products of oxidation of 4,4'-diethylhydrodivanillin **61** with Fe(TDCPPS)Cl and *t*-BuOOH.

probably by the same one-electron mechanism found for the degradation of other lignin model compounds. The aromatic ring cleavage of these substructures is one of the first and most critical steps for their complete degradation.

A further advance in the metalloporphyrins degradation of lignin model compounds derives from the “proximal ligand” concept, a proximal porphyrin ligand, that modeling the active site of cytochrome P-450, influences the rate, and the selectivity of the oxygen atom transfer to substrate.<sup>116–120</sup> A first possibility to apply this concept concerns the complexation of a pre-formed metalloporphyrin with an excess of the ligand, usually a nitrogenous base such as pyridine and imidazole.<sup>121–124</sup> A second approach is to synthesize porphyrins with the proximal ligand as substituent.<sup>125,126</sup> In this case, there is no excess of proximal ligand but the availability of these catalysts is limited by a multistep synthesis of the tetrapyrrolic macrocycle.

As an extension of the “proximal ligand” concept, the transition from heterogeneous to homogeneous systems is of paramount importance. In nature, the polypeptidic envelope around the active center of lignin peroxidase constitutes a pocket that provides protection of the active site from possible overoxidation processes. In order to mimic the biological system, the cationic catalyst can be immobilized on a suitable inorganic support. In this case, the simplest approach is the heterogenation of the metalloporphyrin on a stable support, using the proximal ligand as anchorage site.

Labat and Meunier reported the oxidation of veratryl alcohol and a  $\beta$ -O-4 model dimer with Fe(TPPS)Cl and Mn(TPPS)Cl immobilized on the exchange resin Amberlite IRA 900 EGA using H<sub>2</sub>O<sub>2</sub> or KHSO<sub>5</sub> as oxygen donor.<sup>90</sup> The system immobilized-Mn(TPPS) KHSO<sub>5</sub> showed to be the most active. The reactivity is strongly dependent on the pH value and on the presence of a nitrogen base as axial ligand. More specifically,



manganese porphyrins, that form five coordinate complexes, in the presence of pyridine or imidazole as external ligands increase their reactivity. On the other hand, iron porphyrins, that form primarily six-coordinate complexes or *bis*-adducts did not show an increase of reactivity.

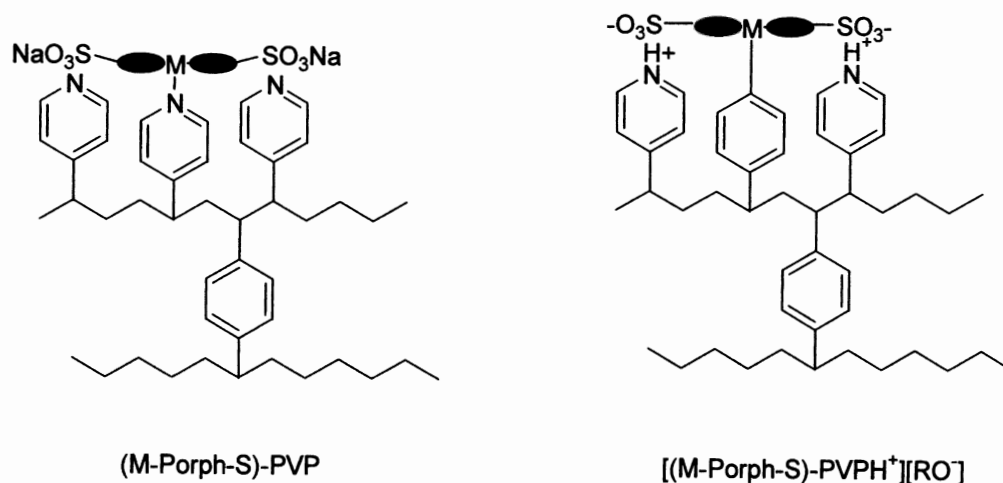
Meunier and coworkers<sup>127</sup> proposed the heterogenation of different sulfonated metalloporphyrins, namely Mn(TPPS)Cl, Mn(TMPS)Cl, Mn(TDCPPS)Cl, Fe(TMPS)Cl, and Fe(TDCPPS)Cl, on 4-polyvinylpyridine 2% cross-linked with divinylbenzene derivative. Two interactions were used for the anchorage: The axial coordination of the metal with the pyridine nitrogen atom, and the electrostatic interactions between the sulfonate moiety and the pyridinium base. As a general example of this procedure, the sulfonated metalloporphyrin complexes were immobilized on an excess of 4-polyvinylpyridine derivative to give the (M-Porph-S)PVP system, and the remaining pyridine units are protonated or methylated ( $[(M-Porph-S)-PVPH^+][TsO^-]$ ; Figure 15).

Manganese porphyrins supported on 4-polyvinylpyridine showed a blueshift of 6–7 nm for the Soret band.<sup>128,129</sup> These supported metalloporphyrins were used for the oxidations of two common lignin model compounds, 1-(3,4-dimethoxyphenyl)-2-(2-methoxyphenoxy)propane-1,2-diol **41** and veratryl alcohol **1**. The oxidations of **41** were performed in a buffered solution (pH 6.0) using  $KHSO_5$  as oxygen atom donor at room temperature. The supported metalloporphyrin systems showed a higher reactivity than the corresponding homogeneous systems under similar experimental conditions. The  $[MnTPPS-PVPH^+][AcO^-]$  catalyst was slightly more reactive than  $[MnTMPS-PVPH^+][AcO^-]$

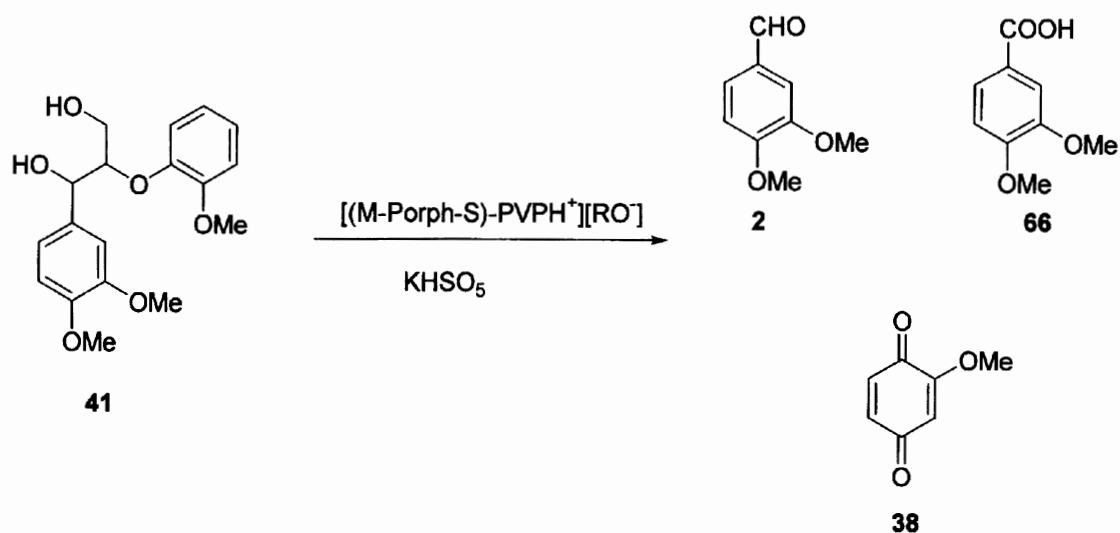
and  $[MnTDCPPS-PVPH^+][AcO^-]$  systems, even if it was completely bleached during the oxidation. There is thus an obvious advantage in using more robust catalysts, like Mn(TMPS)Cl and Mn(TDCPPS)Cl. The iron supported porphyrins were found less reactive with respect to the manganese counterparts, probably because of a possible coordination of the iron atom to two nitrogen atoms of the support giving rise to a low reactive *bis*-pyridine adduct. In Scheme 24 are reported the products isolated from the reaction mixture. These were characterized as 2-methoxy-1,4-benzoquinone **38**, veratraldehyde **2**, and 3,4-dimethoxybenzoic acid **66**, the 2-methoxy-1,4-benzoquinone **38** being the main isolated product in all the experimental conditions tested.

The presence of monomeric products in the reaction mixture clearly suggests that the  $C\alpha-C\beta$  bond of **41** was broken during the oxidation of this lignin model compound. In the oxidation of **1**, veratraldehyde **2** was the major recovered product in the presence of 3,4-dimethoxybenzoic acid **66** and 2-hydroxymethyl-5-methoxy-1,4-benzoquinone **3** as side products (Scheme 25).

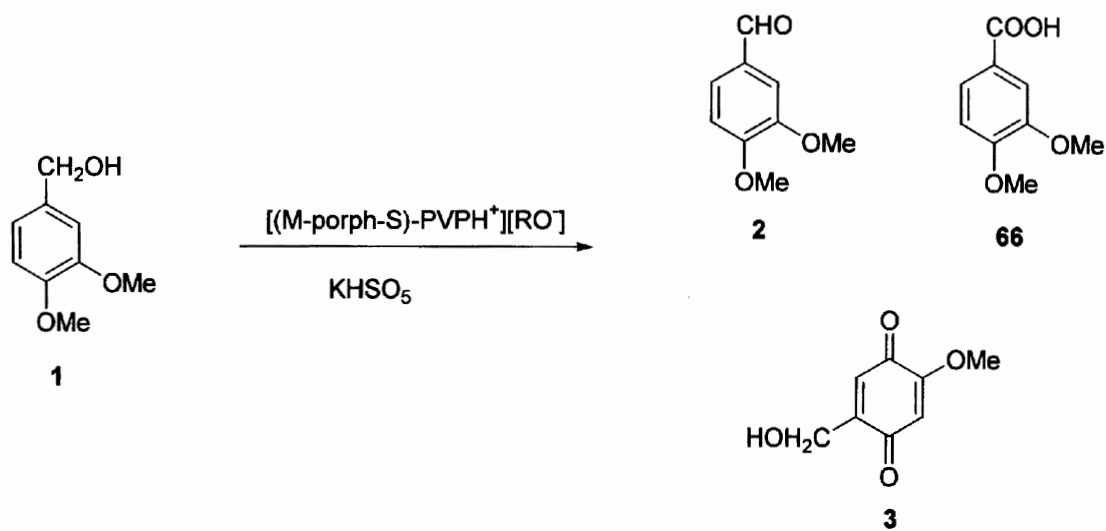
Notably, the reactivity of the homogeneous counterparts was found different showing that each supported metalloporphyrin is a unique catalyst. The catalysts retain their activity after several cycles of reaction. Supported iron porphyrins were found to be more active against phenolic lignin model compounds, as in the case of 1-(3-methoxy-4-hydroxyphenyl)-2-(2-methoxyphenoxy)propane-1,2-diol **67**. The oxidation of **67** performed with  $[FeTMPS-PVPMe^+][TsO^-]$  in acetate buffer using peracetic acid or  $KHSO_5$  as primary oxidants, give 100% and 75% conversion of substrate, respectively (Scheme 26).



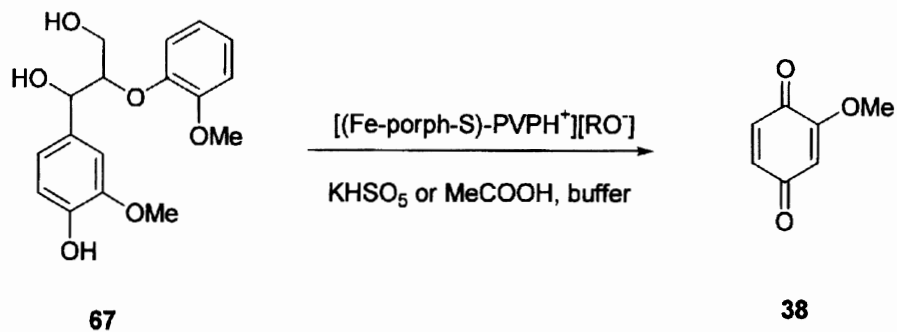
**Figure 15.** Schematic representation of (M-Porph-S)PVP and  $[(M-Porph-S)-PVPH^+][TsO^-]$  systems. M=Mn or Fe. Porph= (TPPS)Cl, (TMPS)Cl, (TDCPPS)Cl, (TMPS)Cl, (TDCPPS)Cl.



**Scheme 24.** Oxidation of 1-(3,4-dimethoxyphenyl)-2-(2-methoxyphenoxy)propane-1,2-diol **41** with supported metalloporphyrins and  $\text{KHSO}_5$ .



**Scheme 25.** Oxidation products of veratryl alcohol **1** with supported metalloporphyrins and  $\text{KHSO}_5$ .



**Scheme 26.** Oxidation products of 1-(3-methoxy-4-hydroxyphenyl)-2-(2-methoxyphenoxy)propane-1,2-diol **67** with supported metalloporphyrins and peracetic acid or  $\text{KHSO}_5$ .

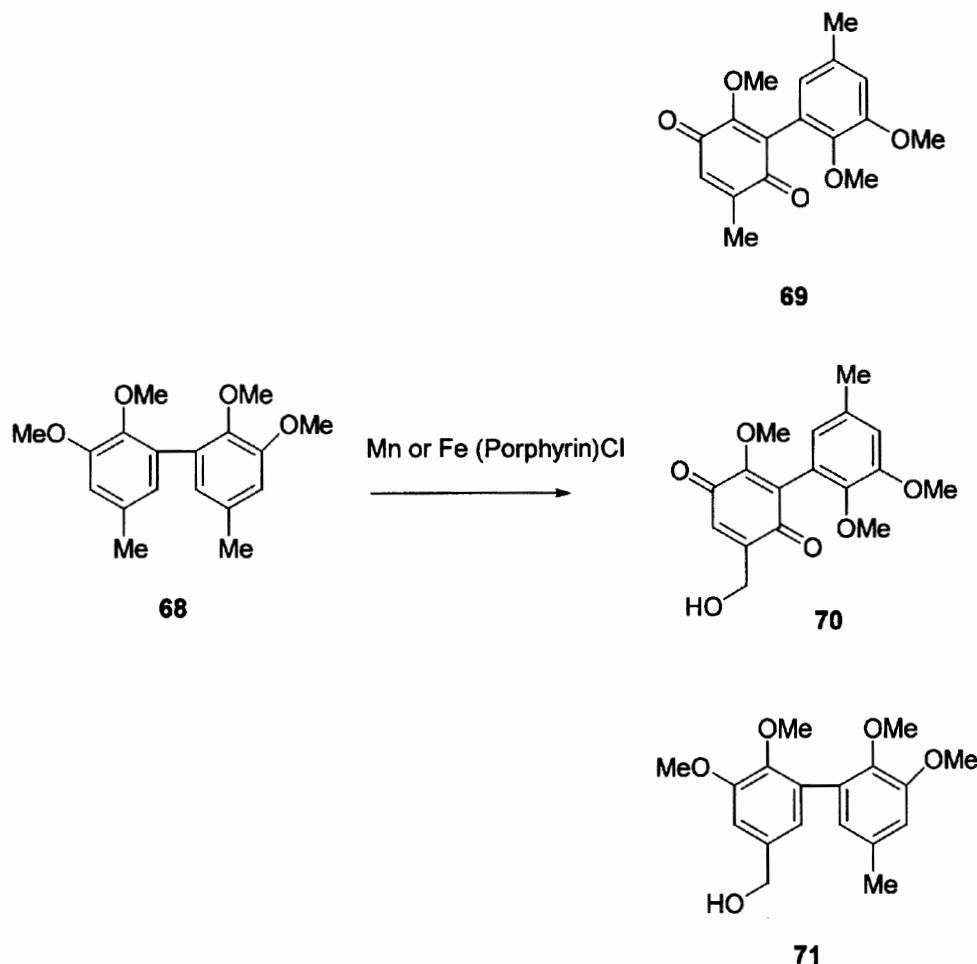
Only traces of 2-methoxy-*p*-benzoquinone **38** were detected in the reaction mixture, showing a high degree of degradation of the substrate. The authors performed a molecular modeling study to obtain information about structure of the porphyrin linked to support. The calculations suggested that after the anchorage both manganese and iron porphyrins have conformations that optimize strong electrostatic interactions between sulfonate groups of the porphyrin and pyridinium group of the polymer.

Residual Kraft lignin contains significant amounts of 5,5' and diphenylmethane substructure.<sup>130</sup> Crestini *et al.*<sup>131</sup> reported the first detailed study of oxidative degradation of 5,5' and diphenylmethane substructures and Kraft lignin comparing anionic and cationic water-soluble manganese and iron porphyrins. The porphyrins used in this study were manganese and iron *meso*-tetra(2,6-dichloro-3-sulfonatophenyl)porphyrin chloride M(TDCSPP)Cl (M= Fe or Mn), manganese *meso*-tetra-4-sulfonatophenylporphyrin chloride Mn(TSPP)Cl,

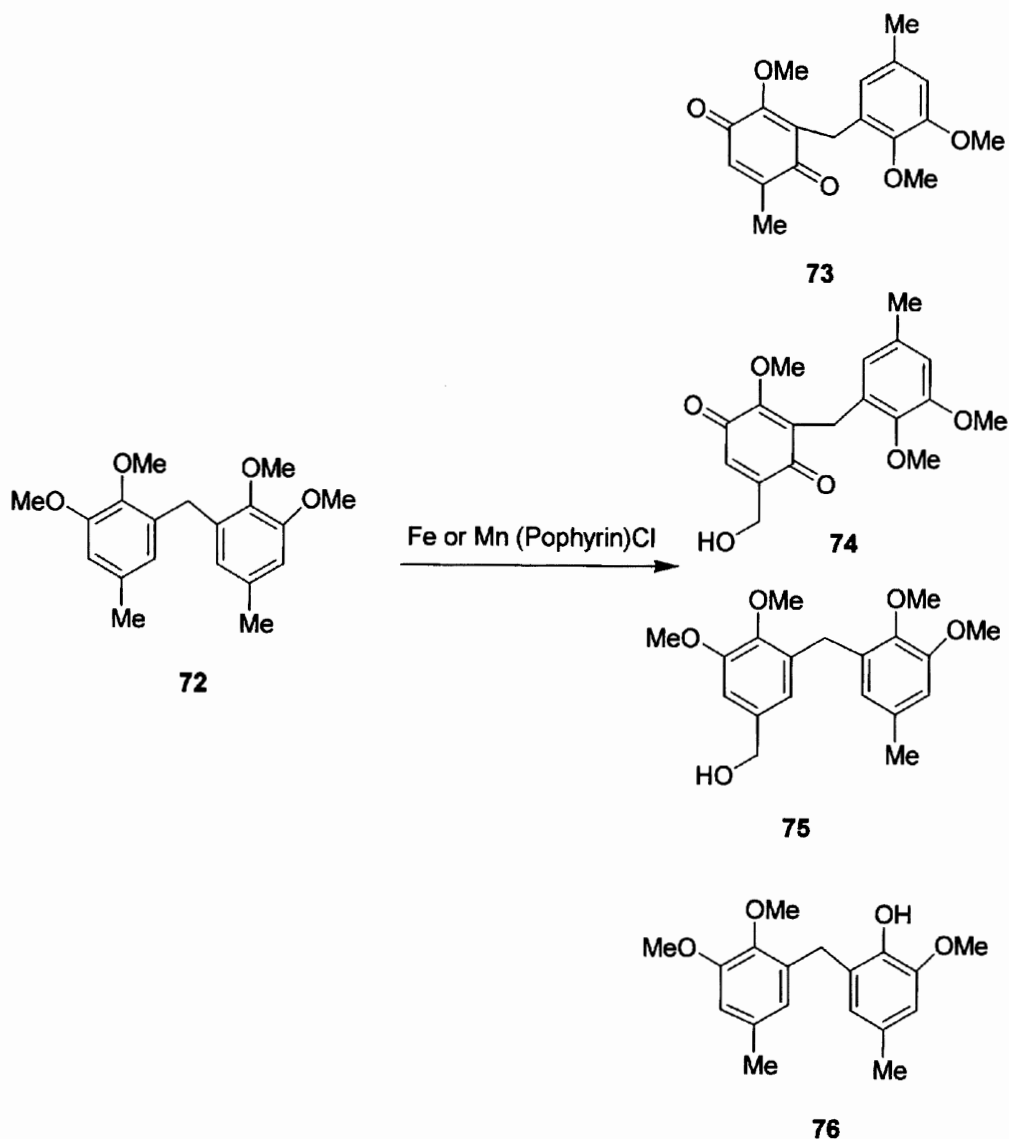
and manganese *meso*-tetra(*N*-methylpyridinio)porphyrin pentaacetate (TPyMeP)Mn(CH<sub>3</sub>COO)<sub>5</sub>. Products of degradation of dimeric lignin models were characterized by usual nuclear magnetic resonance analyses and by GC-MS spectrometry.

The oxidation of the 5,5'-condensed model 2,2',3,3'-tetramethoxy-5,5'-dimethyl biphenyl **68**, with the different porphyrins was performed at pH 3 or 6 in accordance with the maximum activity pH previously reported.<sup>93</sup> In all experiments the main reaction products observed were the *p*-quinones **69** and **70**, in addition to a product of side-chain oxidation, the alcohol **71** (Scheme 27).

The oxidation of the diphenylmethane model compound 2,2',3,3'-tetramethoxy-5,5'-dimethyl diphenylmethane **72** gives the *p*-quinone **73** as the main reaction product (Scheme 28). Beside quinone **73**, the other quinone **74**, and products of side-chain oxidation and demethoxylation, compounds **75** and **76**, were also recovered as side products.



**Scheme 27.** Products obtained from the oxidation of 5,5'-condensed model 2,2',3,3'-tetramethoxy-5,5'-dimethyl biphenyl **68**.



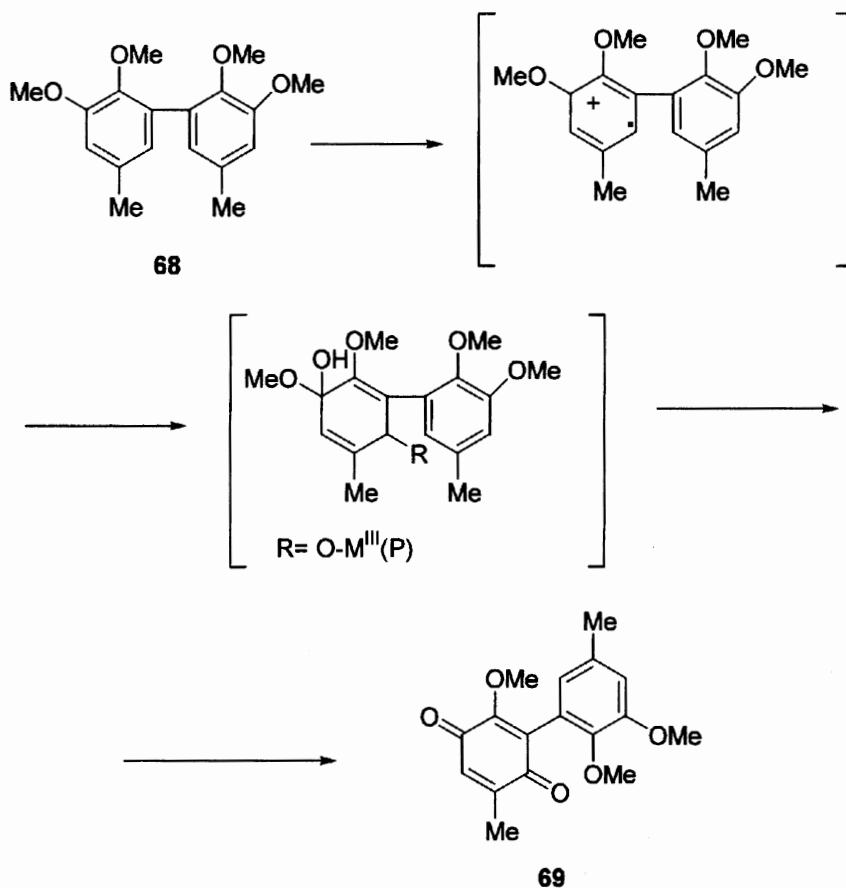
Scheme 28. Products obtained from the oxidation of 2,2',3,3'-tetramethoxy-5,5'-dimethyl diphenylmethane 72.

On the basis of the general oxidative mechanism previously described by Mansuy and coworkers, the formation of *p*-quinones, may be rationalized as reported in Scheme 29. The intermediate radical cation generated during the first one-electron oxidation step, could be further oxidized by the electrophilic species  $(P)M^{IV}=O$ . The site of this latter oxidation is determined by the distribution of the electron density of the aromatic ring, which is in turn modulated by the electronic effect of the substituent in the C-5 position. The electron donating effect of the methyl moiety probably directs the second oxidation to the C-6 position to yield the observed quinones. *para*-Quinones were successively formed by over-oxidation side-chain processes.

## B. AEROBIC OXIDATIONS

Oxidation reactions catalyzed by iron and manganese porphyrin complexes have been used as biomimetic systems for cytochrome P450.<sup>132-134</sup> Its catalytic cycle (Figure 16) requires the presence of a sacrificial reductant (NADPH) and the active oxidant is dioxygen.

Enzyme-like reactions by the catalysis of metalloporphyrin complexes by using molecular oxygen as oxygen atom source have been reported. The sacrificial reductant used were sodium ascorbate,<sup>135</sup> sodium tetrahydroborate,<sup>136,137</sup> hydrogen on platinum,<sup>138,139</sup> flavinmononucleotide/1-methyl-3-carbomolyl-1,4-1,4-dihydropyridine (FMN/MNAH),<sup>140</sup> and electrochemical reduction.<sup>141</sup> It is evident that the possibility to oxidize lignin by the use of dioxygen as oxygen atom



Scheme 29. Proposed reaction pathway for the formation of *p*-quinones.

donor represents an important target for the pulp and paper industry. However, such systems are to date complicated, and no studies have been performed in this direction. Only Okamoto and coworkers, described the cleavage of the C–C bond of 1,2-diols catalyzed by iron porphyrins using dioxygen as primary oxidant.<sup>142</sup> As an example, 1,2-*bis*(*p*-methoxyphenyl)-1,2-ethanediol **77** was converted to *p*-methoxybenzaldehyde **78** in a quantitative yield in the presence of low amount of (tetraarylporphyrinato)iron(III) and 1-benzyl-3-carbamoyl-1,4-dihydropyridine (BNAH) in CH<sub>2</sub>Cl<sub>2</sub> under dry air at room temperature (Scheme 30). A number of iron(III)-porphyrins were effective catalysts for the reaction, such as Fe(TPP)Cl, Fe(TPP)ClO<sub>4</sub>, Fe(TPP)Cl, Fe(TMP)Cl. Fe(TPP)Cl was the most reactive catalyst examined, while sterically crowded Fe(TMP)Cl was less reactive. Manganese and cobalt porphyrins were found also less reactive. Thus, Mn(TPP)(CH<sub>3</sub>COO) showed low reactivity, and Co(TPP)Cl gave only negligible amounts of ketones or aldehydes with concomitant formation of the dehydrogenation product, *p,p'*-dimethoxybenzoin, as the major product. The  $\mu$ -oxo dimer, [Fe(TPP)]<sub>2</sub>O, does not show

any detectable catalytic activity. In the cleavage reactions dichloromethane was the most suitable solvent in both reactivity and selectivity, while polar solvents, such as DMSO or DMF as well as pyridine were less effective.

Kinetic studies indicated that the reaction proceeds through the reversible binding of the diol to the iron catalyst, forming an iron–diol intermediate complex. The breakdown of this complex to the product is the rate-determining step of the catalytic cycle. The study of the binding constants using the Lineweaver–Burk plot, revealed that the former binding process is accelerated by electronegative substituents and is influenced by steric hindrance. On the contrary, the latter product-forming step is not affected by the steric effect and is slightly accelerated by electropositive substituents. The authors evidenced that this system closely resembles that proposed by Collman and coworkers for the epoxidation of olefins with hypochlorite and the Mn(TPP)Cl catalyst.<sup>143,144</sup> Thus, the aerobic C–C bond cleavage of 1,2-diols, and the epoxidation of olefins with hypochlorite, catalyzed by iron porphyrins, may proceed, at least in part, by similar mechanism.

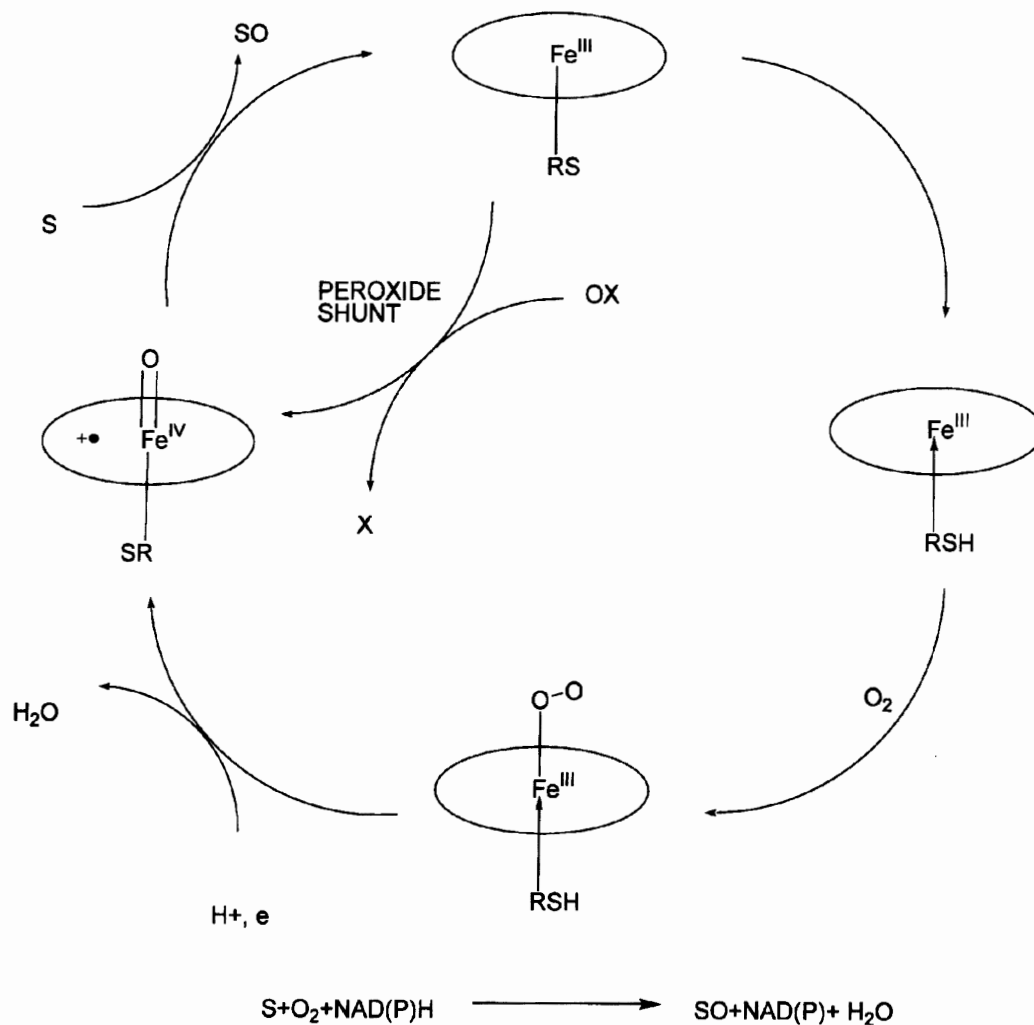
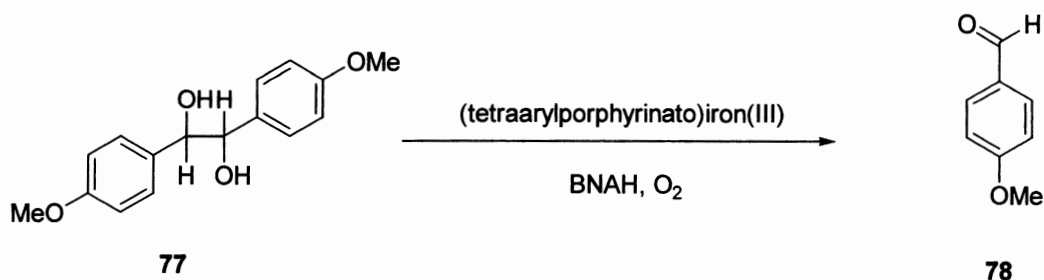


Figure 16. Mechanism of reaction of cytochrome P450-catalyzed oxidations



Scheme 30. Carbon-carbon bond cleavage of *p*-methoxybenzaldehyde **77** with (tetraarylporphyrinato)iron(III) and 1-benzyl-3-carbamoyl-1,4-dihydropyridine (BNAH).

### C. OXIDATION OF LIGNIN

The ability of the Fe(TDCSPP)Cl to oxidize Lignin Indulin AT sample was reported by Dolphin and coworkers.<sup>93</sup> Thus, gel permeation analyses performed on sample of Lignin Indulin AT treated with Fe(TDCSPP)Cl and peracetic acid showed an efficient degradation. The same reaction was also performed with

porphyrin Mn[TDCP(Cl<sub>8</sub>)S<sub>4</sub>P]Cl at either pH 2 and pH 10 caused substantial changes of the UV-vis difference spectra and reduced-difference spectra suggesting extensive degradation and structural modification of lignin.

The oxidative behavior of porphyrins on isolated lignins and residual Kraft lignins has not been much

explored. Kurek *et al.*<sup>145</sup> reported a study on the structural modification induced on spruce milled wood lignin (MWL) and extractive free wood (EFW) by Fe(TF<sub>5</sub>PS<sub>4</sub>P)Cl in water or water/dioxane mixture (9/1 v/v) using hydrogen peroxide as primary oxidant. The stability of the catalyst was first evaluated. It was noticed that in the presence of water as solvent, the bleaching of the catalyst occurred upon addition of 10–15 equiv of hydrogen peroxide, while in the presence of dioxane–water the catalyst was bleached upon addition of 400 equiv of hydrogen peroxide. <sup>1</sup>H-NMR analysis of the oxidized MWL showed a severe decrease of the signals attributed to aromatic rings and methoxy groups, indicating the occurrence of aromatic ring cleavage and demethylation reactions, respectively. Moreover, IR analysis showed the increase of the carbonyl band at 1720 cm<sup>-1</sup>, suggesting the formation of carboxylic acids, such as muconic acids, by oxidative aromatic ring cleavage. Muconic acid derivatives were not detected in the reaction mixture probably because of overoxidation processes to low molecular weight water soluble derivatives. The thioacidolysis analysis of the oxidized MWL and EFW polymers allowed to unambiguously establish that side-chain cleavage of guaiacyl units occurred upon oxidation. In the first case, HP-SEC studies showed that the oxidation proceeds through two main steps.

In the initial phase a partial repolymerization with formation of condensed units was observed, in accord with the higher amounts of molecules corresponding to C–C linked dimers, trimers, and oligomers (MW > 700) qualitatively observed respect to control experiments. Then, in a second stage, the degradation and depolymerization occurred, mainly by aromatic ring cleavage and demethylation reactions, affording molecules with low hydrodynamic volumes. Noteworthy, reactions carried out on EFW in water showed an analogous tendency to lignin oxidation by the penetration of the Fe(TF<sub>5</sub>PS<sub>4</sub>P)Cl/H<sub>2</sub>O<sub>2</sub> system into the wood fibers.<sup>145</sup> In the latter case, the HP-SEC experiments did not show the initial phase of repolymerization. The absence of the secondary C–C coupling is probably due to immobilization of lignin radicals within the cell wall structure. This absence of repolymerization during catalysis was never obtained either with fungal LiP or with Fe(TF<sub>5</sub>PS<sub>4</sub>P)Cl acting on isolated lignins. Therefore, the possibility to oxidize lignin *in situ* within extractive free spruce wood is of high importance in view of the industrial applications in the pulp and paper process.

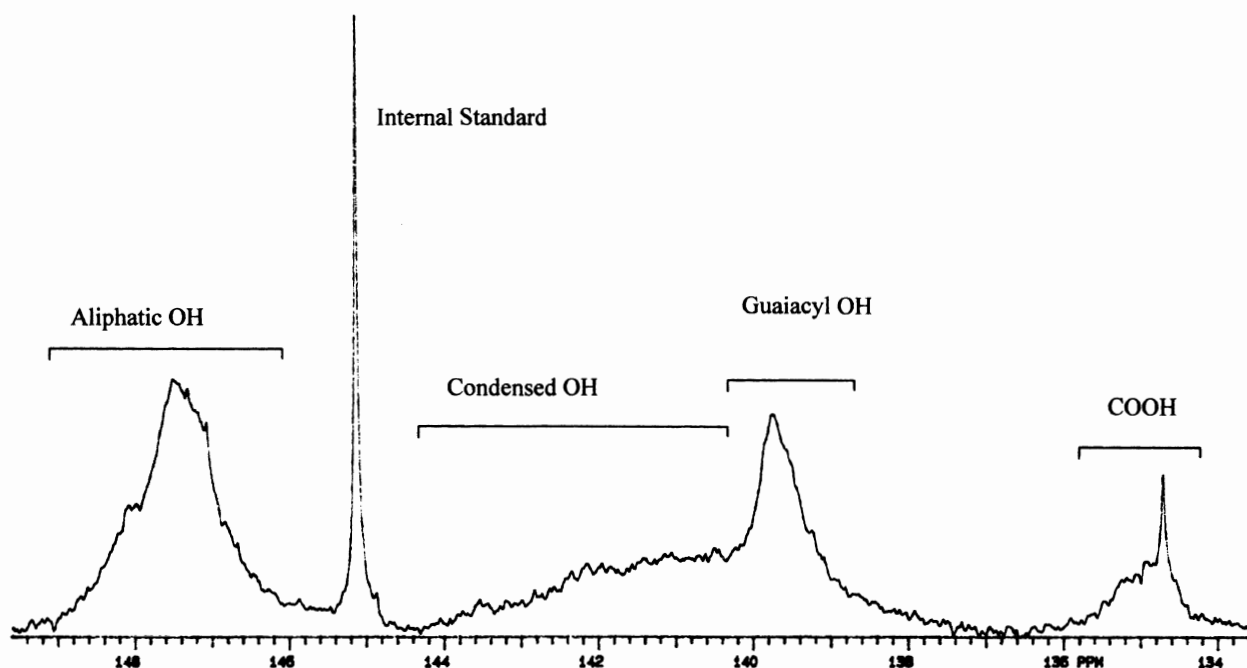
Crestini *et al.*<sup>131</sup> reported the oxidation of residual Kraft lignin with Mn(TDCPPS)Cl, Mn(TPPS)Cl,

Fe(TDCPPS)Cl, and (TPyMeP)Mn(CH<sub>3</sub>COO)<sub>5</sub> porphyrins. In the experiments with Mn(TDCPPS)Cl and Mn(TPPS)Cl the reactions were carried out at pH 6, while the oxidation with Fe(TDCPPS)Cl at pH 3 according to the previously reported data for the maximum of activity of these catalyst systems. Finally, the oxidations with Mn(TPyMeP)(CH<sub>3</sub>COO)<sub>5</sub> were performed both at pH 3 and 6. The degradation of the lignin was monitored by <sup>31</sup>P NMR. In particular, the degradation extent of samples of Kraft lignin was monitored by <sup>31</sup>P NMR spectroscopy, after phosphitylation, as described in the literature by Argyropoulos and coworkers.<sup>146–149</sup> This analysis allows the detection and quantitative determination of all functional groups in lignin possessing reactive hydroxyl groups, that is, aliphatic OH, the various forms of phenolic OH and carboxylic acids. In Figure 17 is reported a typical <sup>31</sup>P NMR spectrum of a lignin sample together with the detailed signal assignments based on the study of lignin model compounds as references.

In Table 2 are reported the results of the oxidation of the residual Kraft lignin with the anionic porphyrins Mn(TDCPPS)Cl and Fe(TDCPPS)Cl with H<sub>2</sub>O<sub>2</sub> as oxygen atom donor. The overall oxidation was found more extended with the manganese porphyrin than with the iron porphyrin. In particular, both porphyrins decrease the amount of the aliphatic OH with respect to no treated sample at either pH values of the reaction medium. The increase of the COOH units further confirms this behavior.

Moreover, the amount of COOH units observed after treatment of the lignin sample with Mn(TDCPPS)Cl is too high to be explained only by means of the oxidation of the aliphatic OH. Thus, a contribute to COOH units derived from ring-opening reactions of the aromatic moieties cannot be completely ruled out. On the other hand, Mn(TDCPPS)Cl oxidizes selectively the guaiacyl OH groups while in the case of Fe(TDCPPS)Cl an increase of the condensed phenolic OH (that is β-5, 4-O-5, and 5-5' condensed units) is also observed. The cationic porphyrin Mn(TPyMeP)(CH<sub>3</sub>COO)<sub>5</sub> was more active at pH 6 than pH 3 (see Table 2), in which case an increase of the COOH units was observed probably due to the oxidation of the aliphatic OH groups and to formation of muconic acid derivatives by aromatic ring-cleavage processes.

In the comparison between anionic and cationic porphyrins (Table 2), the Mn(TPyMeP)(CH<sub>3</sub>COO)<sub>5</sub>, never used before in lignin oxidation, was the best catalyst. It is interesting to note that the increase of the amount of the condensed phenolic OH units



**Figure 17.**  $^{31}\text{P}$  NMR spectrum of softwood residual Kraft lignin phosphitylated with 2-chloro-4,4,5,5-tetramethyl-1,3,2-dioxaphospholane in the presence of a known amount of cyclohexanol as internal standard. Peaks due to aliphatic, phenolic condensed, and guaiacyl hydroxy groups and carboxylic acids are clearly resolved.

**Table 2.** Distribution of Aliphatic, Phenolic, and Carboxylic Hydroxy Groups in Residual Kraft Lignins Before and After Porphyrin Catalyzed Oxidations

Lignin/treatment	Aliphatic OH	Condensed phenolic OH	Guaiacyl OH	COOH
(TPyMeP)Mn(CH <sub>3</sub> COO) <sub>5</sub> (pH 3)	1.78	0.97	1.04	0.35
(TPyMeP)Mn(CH <sub>3</sub> COO) <sub>5</sub> (pH 6)	1.64	0.91	1.09	0.65
Mn(TPPS)Cl (pH 6)	1.79	0.93	1.07	0.30
Mn(TDCPPS)MCl (pH 6)	1.76	0.90	0.98	0.48
Fe(TDCPPS)Cl (pH 3)	1.75	1.01	1.14	0.41
Kraft lignin <sup>a</sup>	1.94	0.92	1.27	0.27
H <sub>2</sub> O <sub>2</sub> (pH 3) <sup>b</sup>	1.78	0.94	1.02	0.36
H <sub>2</sub> O <sub>2</sub> (pH 6) <sup>c</sup>	1.80	0.89	1.08	0.34

observed in the oxidation with iron porphyrin suggests that the overall lignin oxidation by H<sub>2</sub>O<sub>2</sub> in the presence of Fe or Mn catalytic systems follows two different reaction pathways. This different behavior can be due to the formation of hydroxyl radicals by the homolytic cleavage of the peroxidic bond of hydrogen peroxide which, especially in the case of the iron porphyrins, can be in competition with the heterolytic one.

#### D. OXIDATION OF PULPS

Paszczynski *et al.*<sup>80</sup> studied the treatment of Kraft pulps in the presence of *t*BuOOH with a variety of natural and synthetic porphyrins. The biomimetic system was able to

effectively bleach the pulps. After treatment, the pulps were found essentially lignin free, although a little loss occurred in the cellulose content. Extensive delignification was obtained using the water-soluble catalysts Fe(TDCSPP)Cl, iron *meso-tetrakis*(2,6-dichloro-3-sulfonatophenyl)- $\beta$ -octachloroporphyrin Fe[TDCP(Cl<sub>8</sub>)S<sub>4</sub>P]Cl, and iron *meso-tetrakis*(4-sulfonatophenyl)- $\beta$ -octachloroporphyrin Fe[TSP(Cl<sub>8</sub>)P]Cl. The use of the corresponding manganese porphyrins did not significantly alter the lignin degradation extent (K number). However, a decrease in the viscosity of pulps, due to cellulose degradation, was evident in all the experiments. Possible technological applications require a better control of the oxidative reactions and



milder reaction conditions. From this viewpoint, the elucidation of the oxidation mechanism on lignin is of pivotal importance.

The iron porphyrin  $\text{Mn}[\text{TDCP}(\text{Cl}_8)\text{S}_4\text{P}]\text{Cl}$  showed to be effective for pulp bleaching and when it was used with *t*-BuOOH as oxygen atom donor, it reduced the Kappa Number of a Kraft pulp sample by over 40% in 15 min.<sup>150</sup> Other authors have studied both natural hemes and synthetic porphyrins in Kraft pulp bleaching.<sup>80,151</sup> As an example, the treatment of wood chips and Kraft pulp with a variety of natural hemes and synthetic porphyrins in the presence of *t*-BuOOH produced an appreciable bleaching of the pulp with very little loss in cellulose content. In a similar way, Petterson *et al.*<sup>151</sup> focused on the bleaching of Kraft pulps using hemoglobin, other heme-containing proteins, and natural hemins. In a continuation of this study, Dolphin and coworkers reported data on the bleaching of Kraft pulp with different iron porphyrins and *t*-BuOOH as oxygen atom donor.<sup>150</sup> The porphyrins used in these experiments were the iron(III) *meso*-tetra(2,6-dichloro-3-sulfonatophenyl)- $\beta$ -octachloroporphyrin chloride,  $\text{Fe}[\text{TPPS}(\text{Cl}_{16})]\text{Cl}$  that is chlorinated on both the porphyrin and the phenyl rings, the iron(III) *meso*-tetra(4-sulfonatophenyl)- $\beta$ -octachloroporphyrin chloride,  $\text{Fe}[\text{TPPS}(\text{Cl}_8)]\text{Cl}$  chlorinated only on the porphyrin ring, and the iron(III) *meso*-tetra(2,6-dichloro-3-sulfonatophenyl)- $\beta$ -porphyrin chloride,  $\text{Fe}(\text{TDCSPP})\text{Cl}$  chlorinated on the phenyl ring only. Both the chloro- and sulfonato moieties are electron withdrawing groups and make the porphyrin electron deficient and thus more difficult to oxidize. When samples of softwood Kraft pulp were treated with different concentrations of porphyrins for 18 h at 60°C, in 50 mM sodium citrate buffer (pH 4.8), using *t*-BuOOH as primary oxidant, appreciable reduction of the Kappa Number (that is an indication of the amount of lignin in the pulp) was observed. In particular,  $\text{Fe}[\text{TDCP}(\text{Cl}_8)\text{S}_4\text{P}]\text{Cl}$  was the most active catalyst, producing the 45% bleaching at a concentration of 0.0012% (w/v).  $\text{Fe}[\text{TPPS}(\text{Cl}_8)]\text{Cl}$  and  $\text{Fe}(\text{TDCSPP})\text{Cl}$  were less effective producing a delignification in the range from 8 to 21%, respectively.  $\text{Fe}[\text{TDCP}(\text{Cl}_8)\text{S}_4\text{P}]\text{Cl}$  was then selected to study the effect of several experimental variables, such as bleaching temperature, type of peroxide, peroxide concentration, porphyrin concentration, on the bleaching efficiency. These experiments indicate that increasing the porphyrin concentration and the peroxide concentration will produce better results. As the peroxide concentration decreased to 0.1%, and lower, the lignin removal became insignificant. Other peroxides were

also studied but better results were obtained with *t*-BuOOH. Notably, initial results indicated that pulp viscosity was seriously effected by porphyrin bleaching even in the presence of  $\text{MgSO}_4$ , that is usually employed in oxygen bleaching to protect the carbohydrate. Manganese porphyrins, as for example the  $\text{Mn}[\text{TPPS}(\text{Cl}_{16})]\text{Cl}$  behave in a similar way.

## E. DEVELOPMENT OF PORPHYRIN-MEDIATOR SYSTEMS

Despite the progress achieved in the synthesis of porphyrins resistant to oxidation and in the selection of better conditions suitable for bleaching processes a major drawback is still present to their applicability. Porphyrins are to date expensive catalysts. The potential use of metalloporphyrins in lignin oxidation is bound to the possibility of a further increase of their stability toward hydrogen peroxide, and of a possible recovery and recycle of the catalyst after its use. A possible approach to the development of such new catalysts has been attempted taking into consideration that these two aims could be reached by immobilization of the catalyst onto a suitable support. Several approaches of this kind are possible ranging from organic synthetic polymers to biopolymers or to inorganic matrices. Several procedures for their immobilization onto inert matrices have been developed.<sup>90</sup> Smectite clays minerals such as Montmorillonite have layer lattice structures in which two-dimensional oxyanions are separated by layers of hydrated cations. The hydrated cations on the interlamellar surfaces of the native minerals can be replaced with almost any desired cation by utilizing simple ion exchange methods.<sup>152</sup> Thus, immobilization onto clays would prevent from the formation of  $\mu$ -oxo dimers. In this case, a cationic metalloporphyrin can be immobilized by axial ligation of the metal center with the oxyanions layers, electrostatic interaction between the cationic centers of the porphyrin and the oxyanion moieties, and by physical encapsulation.<sup>153</sup>

The cationic manganese *meso*-tetra(4-*N*-methylpyridinio)porphyrin supported on Montmorillonite revealed to be an efficient catalyst in hydrogen peroxide oxidation reactions.<sup>153</sup> In this context, design of delignification procedure in which a heterogeneous metalloporphyrin system is used in the presence of a mediator of the oxidation to mimic the natural oxidative mechanism of lignin peroxidase, the mediator concept, is of paramount importance.

Since the discovery of the stimulating role of veratryl alcohol in LiP oxidation of lignin,<sup>154,155</sup> several

hypotheses were developed on its reaction mechanism. In 1986, Harvey *et al.* proposed that veratryl alcohol could function as diffusible redox mediator in lignin oxidation.<sup>156</sup> However, the mediating role of veratryl alcohol is still inconclusive.<sup>157,48</sup> It was also reported that veratryl alcohol could stimulate lignin oxidation by preventing the formation of the inactive form of the enzyme, Compound III. The mediating role of VA on the oxidation of lignin models such as anisyl alcohol, can be directly investigated using metalloporphyrins as biomimetic systems. Cui and Dolphin performed the oxidation of anisyl alcohol in the presence of Fe(TDCSPP)Cl and *m*-CPBA. In this case the presence of VA inhibited the reaction yielding lower anisaldehyde yields. It seems that the stimulating effect of veratryl alcohol on the LiP oxidation of anisyl alcohol could be mainly due to the prevention of the formation of Compound III (that is not formed during Fe(TDCSPP)Cl oxidation) rather than to a diffusible mediation effect. A biomimetic system that can efficiently mimic the bulk of natural enzymes involves the oxidation of lignin by use of electrodes.<sup>158,159</sup> The interaction between lignin and the electrode is sterically constrained. This system can be used to study the occurrence of mediation effects. More specifically, Cui and Dolphin selected a polymeric lignin model: Poly B-411.<sup>64</sup> This soluble polymeric dye has been used as lignin model, and its oxidation can be easily spectrally followed. In a second set of experiments, the authors submitted Poly B-411 to electrochemical oxidation, in the presence or absence of veratryl alcohol in order to further clarify its possible mediation role.<sup>160</sup> They showed that veratryl alcohol is able to accelerate the decolorization of Poly B-411 both in homogeneous (water) and heterogeneous (methylene chloride) conditions. However, the veratryl alcohol cation radical is so short-lived that oxidation to veratraldehyde and other reactions also occur. This finding opens the way to further studies on the oxidation of lignin by immobilized porphyrin systems in the presence of radical mediators. The first example of application of the mediator concept to heterogeneous porphyrin systems has been reported by Crestini and Tagliatesta.<sup>161</sup> In this study, the authors performed the immobilization of manganese tetramethylpyridinio porphyrin on Montmorillonite according to literature procedures, and used this system for the oxidation of veratryl alcohol and milled wood lignin in the presence of the mediator, using environmentally friendly hydrogen peroxide as oxygen atom donor. Veratryl alcohol was submitted to oxidation in the presence of hydrogen peroxide, hydrogen peroxide and

manganese tetramethylpyridinio porphyrin, hydrogen peroxide and manganese tetramethylpyridinio porphyrin immobilized on Montmorillonite in buffer citrate phosphate 100 mM at pH 6. In Table 3 are reported the conversion yields under the different experimental conditions. In the presence of clay immobilized porphyrin, the conversion extent of veratryl alcohol was found higher than in the presence of the soluble porphyrin. The main oxidation product recovered was found to be veratraldehyde. Thus, veratryl alcohol diffusion from the solution to the solid catalyst was an effective process under these experimental conditions.

Once clarified the capability of oxidation of such low molecular weight compound by soluble and immobilized porphyrin, the attention was focused on lignin. Black spruce milled wood lignin was submitted to oxidation in the presence of catalytic amount of manganese tetramethylpyridinio porphyrin pentaacetate and hydrogen peroxide. The structural modifications induced on the polymer were quantitatively determined by <sup>31</sup>P-NMR spectroscopy. The lignin samples were phosphitylated with 2-chloro-4,4,5,5-tetramethyl-1,3,2-dioxaphospholane in the presence of a known amount of cyclohexanol as internal standard and then submitted to quantitative <sup>31</sup>P-NMR spectroscopy. In Table 4 are reported the results of the oxidation.

The manganese porphyrin effectively catalyzed the oxidation of lignin. In fact, a decrease in aliphatic OH groups and phenolic guaiacyl groups was evident (Table 4). The amount of carboxylic units was found increased after treatment as expected from oxidation processes. When the experiment was performed in the presence of veratryl alcohol as oxidation mediator, the reactivity was not heavily affected and was found comparable as in its absence. In a second experiment, lignin was submitted to oxidation in the presence of the same catalyst immobilized onto Montmorillonite. In this case, the reactivity was found to be depressed with respect to the soluble catalyst. More specifically, the decrease in the aliphatic OH groups was the only apparent modification (Table 4). This decrease in the reactivity upon immobilization onto Montmorillonite

**Table 3.** Oxidation Extent of Veratryl Alcohol

Treatment	% Conversion of veratryl alcohol
Blank <sup>a</sup>	19
(TPyMeP)Mn(CH <sub>3</sub> COO) <sub>5</sub> immobilized on Clay	29
(TPyMeP)Mn(CH <sub>3</sub> COO) <sub>5</sub>	26

a: sample treatment in the presence of hydrogen peroxide.

**Table 4.** Distribution of Aliphatic, Phenolic, and Carboxylic Hydroxy Groups in Milled Wood Lignin Before and After Porphyrin Catalyzed Oxidations as Obtained from Quantitative  $^{31}\text{P}$ -NMR Spectroscopy

Sample/treatment	Aliphatic OH	Condensed OH	Guaiacyl OH	COOH
	(mmol/g)			
MWL <sup>a</sup>	4.59	0.054	0.749	0.154
MWL <sup>a</sup> +H <sub>2</sub> O <sub>2</sub>	4.55	0.069	0.667	0.156
MWL <sup>a</sup> +(TPyMeP)Mn(CH <sub>3</sub> COO) <sub>5</sub> + H <sub>2</sub> O <sub>2</sub>	4.57	0.055	0.630	0.160
MWL+(TPyMeP)Mn(CH <sub>3</sub> COO) <sub>5</sub> +VER <sup>b</sup> +H <sub>2</sub> O <sub>2</sub>	4.27	0.039	0.666	0.159
MWL <sup>a</sup> +CLAY <sup>c</sup> +H <sub>2</sub> O <sub>2</sub>	4.55	0.050	0.654	0.125
MWL <sup>a</sup> +CLAY <sup>c</sup> +VER+H <sub>2</sub> O <sub>2</sub>	4.14	0.038	0.729	0.187

a: milled wood lignin; b: veratryl alcohol; c: (TPyMeP)Mn(CH<sub>3</sub>COO)<sub>5</sub> immobilized on montmorillonite.

can be due to a steric difficulty of approach of lignin to the active site into the clay. In fact the lamellar structure of Montmorillonite allows only little room to the reactant. However, the complexation of oxygen atoms of Montmorillonite with the cationic porphyrin provides a strong stabilization of the catalyst itself similar and more intense than the axial stabilization by the proximal His residue in LiP. In Nature, the oxidation of lignin by the lignin peroxidase is performed despite a similar sterical difficulty of approach. In fact an oxidation mediator, veratryl alcohol, is the active species to be oxidized, and in turn performs the one-electron oxidation of lignin. Notably, when the oxidation of lignin with manganese tetramethylpyridinio porphyrin immobilized onto Montmorillonite was performed under similar experimental conditions in the presence of veratryl alcohol, a different reactivity was evident. In particular, the decrease in aliphatic OH groups was found more pronounced than in the presence of the soluble porphyrin. The carboxylic acids were also found highly increased. This results show that the “mediator” concept is of pivotal importance for the design of new porphyrin immobilized systems active in the hydrogen peroxide oxidation of lignin.

## VI. Conclusions

Metalloporphyrins are promising catalysts for the effective degradation of lignin in the paper and pulp processes. Monomeric, dimeric, and oligomeric lignin model compounds were extensively degraded by metalloporphyrins both in water and in organic solvents. In these transformations, environmentally friendly oxidants such as hydrogen peroxide or oxygen have been used, even if other primary oxidants, *t*-BuOOH or KHSO<sub>5</sub>, are, in some cases, more efficient. Studies on the oxidation of lignins with porphyrins showed that the reaction proceeds through different mechanisms; the side-chain oxidation, the

formation of *ortho*- and *para*-benzoquinones, and the aromatic ring cleavage to muconic acid derivatives being the main observed transformations. Thus, the lignin backbone is not only depolymerized, but the recalcitrant aromatic units are actively degraded. In general, robust water-soluble metalloporphyrins were found the most active systems. However, data obtained from the pulp treatment with representative examples of these porphyrins show that cellulose is also degraded at some extent. This means that the new target for the synthesis of metalloporphyrins to be applied in this field is the design of catalyst with high activity and high selectivity. From this view point, manganese porphyrins were found more selective in the degradation of lignins than the corresponding iron porphyrins. Probably, these latter systems give unselective Fenton reactions as relevant side-processes. A second crucial point for their industrial application is the design of heterogeneous porphyrin systems that might be used in several cycles of transformations. In this case, the use of the heterogenation technique based on the anchorage of the active catalyst on appropriate inert and low cost supports appears to be highly promising. In the use of such systems, the application of the “mediator” concept avoids kinetic problems due to the solid nature of the substrate and of the heterogeneous catalyst, and opens the way to advanced biomimetic ligninase mediator systems (porphyrin mediator systems, P.M. systems). In the P.M. systems the enzyme active center is mimicked by a water-soluble metalloporphyrin for which reactivity and selectivity can be tuned by the nature of the metal atom and by the substituents on the porphyrin ring. Moreover, the role of the enzyme proteic scaffold may be solved by the organic or inorganic support, which can also furnish the axial ligand to enhance the reactivity of the high valent metal oxo intermediate obtaining the “proximal ligand effect.” Next, this high oxidative potential may be transferred to the backbone of the substrate

by the mediator without steric difficulty. The P.M. systems represent the last step in the development of a "synthetic enzyme" for the pulp and paper transformations.

## REFERENCES

1. *Biotechnology in the Pulp and Paper Industry*, Kuwahara, M., Shimada, M., Eds.; Unipublishers: Tokyo, **1992**.
2. Gierer, J. *Holzforshung* **1997**, *51*, 34.
3. Reinhammer, B.; Malstrom, B. In *Copper Proteins*; Spiro, T. G., Ed.; Wiley-Interscience: New York, **1981**; pp. 109–149.
4. Tien, M.; Kirk, T. K. *Science* **1983**, *221*, 661.
5. Glenn, J. K.; Morgan, M. A.; Mayfield, M. B.; Kuwahara, M.; Gold, M. H. *Biochem. Biophys. Res. Commun.* **1983**, *114*, 1077.
6. Glenn, J. K.; Akileswaran, L.; Gold, M. H. *Arch. Biochem. Biophys.* **1986**, *251*, 688.
7. *Metalloporphyrins in Catalytic Oxidations*. Sheldon, R. A., Ed.; Marcel Dekker Inc.: New York, **1994**.
8. Meunier, B. In *Metalloporphyrins Catalyzed Oxidations*. Montanari, F., Casella, L., Eds.; Kluwer Academic Publishers: Dordrecht, **1994**; pp. 11–19.
9. Skerer, P. S.; Farrell, R. L.; Dolphin, D.; Cui, F.; Wijesekera, T. In *Biotechnology in Pulp and Paper Manufacture*. Kirk, T. K., Chang, H. M., Eds.; Butterworth-Heinemann: Stoneham, MA, **1990**, pp. 203–210.
10. *Lignin: Properties and Materials*. Wolfgang, G., Sarkanen, S., Eds.; ACS Symposium Series 397, Washington, DC, **1989**.
11. Neish, A. C. *Monomeric Intermediates in the Biosynthesis of Lignin*, In *Constitution and Biosynthesis of Lignin*. Freudenberg, K., Neish, A. C., Eds.; Springer-Verlag: Berlin, **1968**; pp. 5–43.
12. Sarkanen, K. V.; Hergert, H. L. In *Lignins, Occurrence, Formation, Structure and Reactions*. Sarkanen, K. V., Ludwig, C. H., Eds.; Wiley-Interscience: New York, **1971**; pp. 43–94.
13. Krüger, G. *Chem. Unserer Zeit* **1976**, *10*, 21–29.
14. Klein, R. J.; Meng, T. Y.; Jameel, H.; Sundaram, V. S. M. *Tappi Pulping Conference Proceedings* **1990**, *2*, 829–835.
15. Parthasarathy, V. R.; Klein, R.; Sundaram, V. S. M.; Jammel, H.; Gratzl, J. S. *Tappi J.* **1990**, *73(7)*, 177–185; and references cited therein.
16. Gross, G. G. In *Recent Adv. In Phytochem. 11*; Loewus, F. A., Runexkles, V. C., Eds.; Plenum Press: New York, **1977**; pp. 141–184.
17. Gross, G. G. In *Biochemistry of Plant Phenolics; Recent Adv. In Phytochem. 12*. Swain, T., Harborne, J. B., Van Sumere, C. F., Eds.; Plenum Press: New York, **1978**; pp. 177–220.
18. Glasser, W. G. In *Pulp and Paper Chemistry and Chemical Technology*. Casey, J. P., Ed.; Vol. 1, 3rd Ed. Wiley-Interscience: New York, **1980**; pp. 39–111.
19. Fengel, D.; Wegener, G. *Wood: Chemistry, Ultrastructure, Reactions*. Fengel, D., Wegener, G., Eds.; DeGruyter: Berlin, **1983**.
20. Nimz, H. H. *Wood Sci. Technol.* **1981**, *15*, 311–316.
21. Erickson, M.; Miksche, G. E. *Phytochemistry* **1974**, *13*, 2295–2299.
22. Brunow, G.; Kilpeläinen, Sipilä, J.; Syrjänen, K.; Karhunen, P.; Setälä, H.; Rummakko, P. In *Lignin and Lignans Biosynthesis*. Norman G. L., Sarkanen, S., Eds.; ACS Symposium Series: Washington DC, **1996**; pp. 131–147.
23. Katayama, Y.; Morohoshi, N.; Haraguchi, T. *Mozukai Gakkaishi* **1980**, *26*, 358–362.
24. Leary, G. J.; Sawtell, D. A.; Wong, H. *Int. Symp. Wood Pulp Chem. Stockholm* **1981**, Vol. 1, pp. 63–66.
25. Sarkanen, K. V. In *Lignins, Occurrence, Formation, Structure, and Reactions*. Sarkanen, K. V., Ludwig, C. H., Eds.; Wiley Interscience, **1971**; 95.
26. Adler, E. *Wood Sci. Technol.* **1977**, *11*, 169.
27. Katayama, T.; Nakatsubo, F.; Higuchi, T. *Mokuzai Gakkaishi* **1981**, *27*, 223.
28. Nakatsubo, F.; Higuchi, T. *Holzforshung* **1975**, *29*, 193.
29. Leopold, B. *Acta Chem. Scand.* **1950**, *4*, 1523.
30. Elbs, K.; Lerch, H. J. *Prakt. Chemie* **1916**, *93*, 1.
31. Pew, J. C. *Nature* **1962**, *193*, 25.
32. Pew, J. C. *J. Org. Chem.* **1963**, *28*, 1048.
33. a) Gierer, J. *Holzforshung* **1982**, *36*, 43–51, b) Gierer, J. *Holzforshung* **1982**, *36*, 55–64.
34. Gierer, J. *Holzforshung* **1979**, *33*, 213–214.
35. Kringstad, K. P.; Lin, S. Y. *Tappi* **1970**, *53*, 2296.
36. Gierer, J.; Lin, S. Y. *Sven. Papperstidn.* **1972**, *75*, 233.
37. Gierer, J.; Imsgard, F. *Sven. Papperstidn.* **1977**, *80*, 510–518.
38. Odermatt, J.; Patt, R.; Kordasachia, O.; Troughton, N. *Tappi Pulp Bleaching Conference Proceedings* **1994**, 77–85.
39. *Oxidative Delignification Chemistry: Fundamentals and Catalysis*. Argyropoulos D. S., Ed.; ACS Symposium Series 785, Washington DC, **2001**.
40. Leonowicz, A.; Mattuszewska, A.; Luterek, J.; Zieghagen, D.; Wojtas-Wasilewska, M.; Hofrichter, M.; Rogalski, J. *Fungal. Gen. Biol.* **1999**, *27*, 175–185.
41. Eriksson, K.-E. L.; Blanchette, R. A.; Ander, P. *Microbial and Enzymatic Degradation of Wood and Wood Components*. ISBN: 3-540-51600-X Springer Verlag: Berlin, Heidelberg, Germany, **1990**.
42. Viikari, L.; Kantelinen, A.; Sundquist, J.; Linko, M. *FEMS Microbiol. Rev.* **1994**, *13*, 335–350.
43. Call, H. P.; Mücke, I. J. *Biotechnol.* **1997**, *53*, 163–202.
44. Reinhammer, B.; Malstrom, B. In *Copper Proteins*. Spiro, T. G., Ed.; Wiley-Interscience: New York, **1981**; 109–149.
45. Call, H. P.; Mücke, I. J. *Biotechnol.* **1997**, *53*, 163–202.
46. Andersson, L. A.; Renganathan, V.; Chiu, A. A.; Loehr, T. M.; Gold, M. H. *J. Biol. Chem.* **1985**, *260*, 6080–6087.
47. Kuila, D.; Tien, M.; Fee, J. A.; Ondrias, M. *Biochemistry* **1985**, *24*, 3394–3397.
48. Kirk, T. K.; Farrell, R. L. *Annu. Rev. Microbiol.* **1987**, *41*, 465–505.
49. Chance, B. *Arch. Biochem. Biophys.* **1952**, *41*, 416–424.
50. Khindaria, A.; Aust, S. D. *Biochemistry* **1996**, *35*, 13107–13111.
51. Koduri, R. S.; Tien, M. *Biochemistry* **1994**, *33*, 4225–4230; and references cited therein.
52. Wariishi, H.; Gold, M. H. *FEBS Lett.* **1989**, *243*, 165–168.
53. Wariishi, H.; Gold, M. H. *J. Biol. Chem.* **1990**, *265*, 2070–2077.
54. Leisola, M. S. A.; Schimdt, B.; Thanei-Wyss, U.; Fiechter, A. *J. Biol. Chem.* **1985**, *3*, 97–107.
55. Haemmerli, S. D.; Schoemaker, H. E.; Schmidt, H. W. H.; Leisola, M. S. A. *FEBS. Lett.* **1987**, *220*, 149–154.
56. Umezawa, T.; Higuchi, T. *FEBS Lett.* **1986**, *205*, 293–298.
57. Umezawa, T.; Shimada, M.; Higuchi, T.; Kusai, K. *FEBS Lett.* **1986**, *205*, 287–292.
58. Miki, K.; Renganathan, V.; Mayfield, M. B.; Gold, M. H. *FEBS Lett.* **1987**, *210*, 199–203.
59. Hattori, T.; Higuchi, T. *Mokuzai Gakkaishi* **1991**, *37*, 542–547.
60. Kurek, B.; Monties, B. *Enzyme Microb. Technol.* **1994**, *16*, 125–130.
61. Hammel, K. E.; Moen, M. A. *Enzyme Microb. Technol.* **1991**, *13*, 15–18.
62. Wariishi, H.; Valli, K.; Gold, M. H. *Biochem. Biophys. Res. Commun.* **1991**, *176*, 269–275.
63. Hammel, K. E.; Jensen, K. A.; Mozuch, M. D.; Landucci, L. L.; Tien, M.; Pease, E. A. *J. Biol. Chem.* **1993**, *268*, 12274–12281.
64. Cui, F.; Dolphin, D. *Holzforshung* **1991**, *45*, 31–35.
65. Ulmer, D. C.; Leisola, M. S. A.; Fiechter, A. *J. Biotechnol.* **1984**, *1*, 13–24.
66. Harvey, P. J.; Schoemaker, H. E.; Palmer, J. M. *FEBS Lett.* **1986**, *195*, 242–246.

67. Tien, M.; Kirk, T. K.; Bull, C.; Fee, J. A. *J. Biol. Chem.* **1986**, *261*, 1687–1693.
68. Tuor, U.; Wariishi, H.; Shoemaker, H. E.; Gold, M. H. *Biochemistry* **1992**, *31*, 4986–4995.
69. Wariishi, H.; Valli, K.; Gold, H. *Biochem. Biophys. Res. Comm.* **1991**, *176*, 269–275.
70. Sundaramoorthy, M.; Kishi, K.; Gold, M. H.; Poulos, T. L. *J. Biol. Chem.* **1994**, *269*, 32759–32767.
71. Kusters-van Someren, M.; Kishi, K.; Lundell, T.; Gold, M. H. *Biochemistry* **1995**, *34*, 10620–10627.
72. Kishi, H.; Kusters-van Someren, M.; Mayfield, M. B.; Sun, J.; Loehr, T. M.; Gold, M. H. *Biochemistry* **1996**, *35*, 8986–8994.
73. Kishi, H.; Hildebrand, D. P.; Kusters-van Someren, M.; Gettemy, J.; Mauk, A. G.; Gold, M. H. *Biochemistry* **1997**, *36*, 4268–4277.
74. Tuor, U.; Wariishi, H.; Shoemaker, H. E.; Gold, M. H. *Biochemistry* **1992**, *31*, 10009–10017. Wariishi, H., Valli, K., Gold, M. H. *Biochemistry* **1989**, *28*, 6017–6023.
75. Kuan, I. C.; Tien, M. *Proc. Natl. Acad. Sci. USA* **1993**, *90*, 1242–1246.
76. Khindaria, A.; Grover, T. A.; Aust, S. D. *Arch. Biochem. Biophys.* **1994**, *314*, 301–306.
77. Kishi, K.; Wariishi, H.; Marquez, L.; Dunford, H. B.; Gold, M. H. *Biochemistry* **1994**, *33*, 8694–8701.
78. Hattori, T.; Shimada, M.; Umezawa, T.; Higuchi, T.; Leisola, M. S. A.; Fiechter, A. *Agric. Biol. Chem.* **1988**, *52*, 879–889.
79. Habe, T.; Shimada, M.; Okamoto, T.; Panijpan, B.; Higuchi, T. *J. Chem. Soc., Chem. Commun.* **1985**, 1323.
80. Paszczynski, A.; Crawford, R. L.; Blanchette, R. A. *Appl. Environ. Microbiol.* **1988**, *54*, 62.
81. Shimada, M.; Habe, T.; Higuchi, T.; Okamoto, T.; Panijpan, B. *Holzforshung* **1987**, *41*, 277.
82. Kersten, P. J.; Tien, B.; Kalyanaraman, B.; Kirk, T. K. *J. Biol. Chem.* **1985**, *260*, 2609.
83. Cui, F.; Dolphin, D. *Holzforshung* **1990**, *44*, 279–283.
84. Rance, S.; Meunier, B.; Séris, J. *New J. Chem.* **1992**, *16*, 1015–1016.
85. Policar, H.; Artaud, I.; Mansuy, D. *Inorg. Chem.* **1996**, *35*, 210–216.
86. Meunier, B. In *Metalloporphyrins in Catalytic Oxidations*. Sheldon, R. A., Ed.; Marcel Dekker Inc.: New York, **1994**; pp. 133–156.
87. Meunier, B.; Robert, A.; Pratiel, G.; Bernadou, J. In *The Porphyrin Handbook*. Kadish, K. M., Smith, K. M., Guillard, R., Ed.; Academic Press: Boston, **2000**; Vol 4, pp. 119–188.
88. Crestini, C.; Tagliatesta, P.; Saladino, R. In *Oxidative Delignification Chemistry; Fundamentals and Catalysis*. Argyropoulos, D. S., Ed.; ACS Symposium Series 785, **2000**; pp. 212–225.
89. Meunier, B. *Chem. Rev.* **1992**, 1411–1456.
90. Labat, G.; Meunier, B. *J. Org. Chem.* **1989**, *54*, 5008–5011.
91. Labat, G.; Meunier, B. *New J. Chem.* **1989**, *13*, 801–804.
92. Cui, F.; Dolphin, D. *Can. J. Chem.* **1992**, *70*, 2314.
93. Cui, F.; Wijesekera, T.; Dolphin, D.; Farrell, F.; Skerker, P. J. *Biotechnology* **1993**, *30*, 15–26.
94. Numba, H.; Nakatsubo, F.; Higuchi, T. *Wood Res.* **1983**, *69*, 52–60.
95. Anderson, L. A.; Renganathan, V.; Chiu, A. A.; Loehr, T. M.; Gold, M. H. *J. Biol. Chem.* **1985**, *260*, 6080–6087.
96. Que, L. *Adv. Inorg. Chem.* **1983**, *5*, 167.
97. Artaud, I.; Grennberg, H.; Mansuy, D. *J. Chem. Soc., Chem. Commun.* **1992**, 1036–1038.
98. Jaruszewski, J. M.; Etlinger, M. G. *J. Org. Chem.* **1989**, *54*, 1506.
99. Dolphin, D.; Nakanu, T.; Kirk, T. K.; Maione, T. E.; Farrell, R. L.; Wijesekera, T. P. Patent PCT Int. Appl. WO 88/07988, **1988**.
100. Panicucci, R.; Bruce, T. C. *J. Am. Chem. Soc.* **1990**, *112*, 6063.
101. Schmidt, H. W.; Haemmerli, S. D.; Schoemaker, H. E.; Leisola, M. S. A. *Biochemistry* **1989**, *28*, 1776.
102. Artaud, I.; Aziza, K. B.; Chopard, C.; Mansuy, D. *J. Chem. Soc., Chem. Commun.* **1991**, 31–33.
103. Corey, E. J.; Tramontano, A. *J. Am. Chem. Soc.* **1981**, *103*, 5599.
104. Labat, G.; Seris, J. L.; Meunier, B. *Angew. Chem., Int. Ed. Engl.* **1990**, *29*, 1471–1472.
105. Alexander, M. *Science* **1981**, *211*, 132.
106. Reineke, W. In *Microbial Degradation of Aromatic Compounds*. Gibson, D. T. Ed.; Dekker: New York, **1984**; pp. 319–360.
107. Meunier, B.; Belal, R.; Robert, A.; Momenteau, M.; Labat, G. *La Chimica & L'industria* **1990**, *72*, 433–440.
108. Artaud, I.; Ben-Aziza, K.; Mansuy, D. *J. Org. Chem.* **1993**, *58*, 3373–3380.
109. Viehe, H. G.; Janousek, Z.; Merenyi, R. *Acc. Chem. Res.* **1985**, *18*, 148–154.
110. Latrignano, L.; Goldstein, B. D.; Witz, G. *Proc. Natl. Acad. Sci. USA* **1986**, *83*, 8356.
111. Cui, F.; Dolphin, D. *Bioorg. and Med. Chem.* **1994**, *2*, 735–742.
112. Gold, M. H.; Kuwahara, M.; Chiu, A. A.; Glenn, J. H. *Arch. Biochem. Biophys.* **1984**, *234*, 353.
113. Kirk, T. K.; Tien, M.; Kersten, P. J.; Mozuch, M. J.; Kalyanaraman, B. *Biochem. J.* **1986**, *236*, 279.
114. Kirk, T. K.; Harkin, J. M.; Cowling, E. B. *Biochim. Biophys. Acta* **1968**, *165*, 134.
115. Kamaya, Y.; Higuchi, T. *Mozukai Gakkaishi* **1983**, *29*, 789.
116. Meunier, B.; de Carvalho, M. E.; Guilmet, E.; Poiblan, R. *J. Am. Chem. Soc.* **1984**, *106*, 755–764.
117. Traylor, T. G.; Lee, W.; Stynes, D. W. *J. Am. Chem. Soc.* **1984**, *106*, 755–764.
118. Meunier, B.; de Carvalho, M. E.; Bortolini, O.; Momenteau, M. *Inorg. Chem.* **1988**, *27*, 161–164.
119. Groves, J. T.; Stern, M. K. *J. Am. Chem. Soc.* **1988**, *110*, 8668–8638.
120. Battistoni, P.; Renaud, J. P.; Bartoli, J. F.; Reina-Artiles, M.; Fort, M.; Mansuy, D. *J. Am. Chem. Soc.* **1988**, *110*, 8462–8470.
121. Guilmet, E.; Meunier, B. *Nouv. J. Chim.* **1982**, *6*, 511–513.
122. Collman, J. P.; Kodadek, T.; Raybuck, S. A.; Meunier, B. *Proc. Natl. Acad. Sci. USA* **1983**, *80*, 7039–7041.
123. Mansuy, D.; Battistoni, P.; Renaud, J. P. *J. Chem. Soc., Chem. Commun.* **1984**, 1255–1257.
124. Naruta, Y.; Tani, F.; Maruyama, K. *Tetrahedron Lett.* **1992**, *33*, 6323–6326.
125. Belal, R.; Momenteau, M.; Meunier, B. *J. Chem. Soc., Chem. Commun.* **1989**, 412–414.
126. Anelli, L.; Banfi, S.; Montanari, F.; Quici, S. *J. Chem. Soc., Chem. Commun.* **1989**, 779–780.
127. Pattou, D.; Labat, G.; Defrance, S.; Séris, J. L.; Meunier, B. *Bull. Soc. Chim. Fr.* **1994**, *131*, 78–88.
128. Campestrini, B. Meunier, *Inorg. Chem.* **1992**, *31*, 1999–2006.
129. Cooke, P. R.; Lindsay Smith, J. R. *Tetrahedron Lett.* **1992**, *33*, 2737–2740.
130. Eriksson, T.; Gierer, J. *J. Wood Chem. Technol.* **1985**, *5*, 53.
131. Crestini, C.; Saladino, R.; Tagliatesta, P.; Boschi, T. *Bioorganic Med. Chem.* **1999**, *7*, 1897–1905.
132. Traylor, T. G.; Nakano, T.; Mikszta, A. R.; Dunlap, B. E. *J. Am. Chem. Soc.* **1987**, *109*, 3625–3632.
133. Bruce, T. C.; Dickeu, M. C.; Balasubramanian, P. N.; Woon, T. C. *J. Am. Chem. Soc.* **1987**, *109*, 3436–3443.
134. Ostovic, D.; Knololer, C. B.; Bruce, T. C. *J. Am. Chem. Soc.* **1987**, *109*, 3444–3451.
135. Mansuy, D.; Laclaire, J.; Fontecave, M.; Momenteau, M. *Tetrahedron* **1984**, *40*, 4297–4311.
136. Tabushi, I.; Koga, N. *J. Am. Chem. Soc.* **1979**, *101*, 6456–6458.
137. Perree-Fauvet, M.; Gaudemer, A. *J. Chem. Soc., Chem. Commun.* **1981**, 874–875.

138. Tabushi, I.; Yazoki, A. *J. Am. Chem. Soc.* **1981**, *103*, 7371–7373.
139. Tabushi, I.; Morimite, K. *J. Am. Chem. Soc.* **1984**, *106*, 6871–6872.
140. Tabushi, I.; Kodera, M. *J. Am. Chem. Soc.* **1986**, *108*, 1101–1103.
141. Creager, S. E.; Raybuck, S. A.; Murray, R. W. *J. Am. Chem. Soc.* **1986**, *108*, 4225–4227.
142. Okamoto, T.; Sasaki, K.; Oka, S. *J. Am. Chem. Soc.* **1988**, *110*, 1187–1196.
143. Collman, J. P.; Brauman, J. I.; Meunier, B.; Raybuck, S. A.; Kodadek, T. *Proc. Natl. Acad. Sci. USA* **1984**, *81*, 3245–3248.
144. Collman, J. P.; Brauman, J. I.; Meunier, B.; Hayashi, T.; Kodadek, T.; Raybuck, S. A. *J. Am. Chem. Soc.* **1985**, *107*, 2000–2005.
145. Kurek, B.; Artaud, I.; Pollet, B.; Lapierre, C.; Monties, B. *J. Agric. Food Chem.* **1996**, 1953.
146. Crestini, C.; Argyropoulos, D. S. *J. Agr. Food Chem.* **1997**, *49*, 1212.
147. Granata, A.; Argyropoulos, D. S. *J. Agr. Food Chem.* **1995**, *33*, 375.
148. Argyropoulos, D. S. *Res. Chem. Intermed.* **1995**, *21*, 373.
149. Crestini, C.; Giovannozzi Sermanni, G.; Argyropoulos, D. S. *Bioorg. Med. Chem.* **1998**, *6*, 967.
150. Skerker, P. S.; Farrell, R. L.; Dolphin, D.; Cui, F.; Wijesekera, T. In *Biotechnology in Pulp and Paper Manufacture: Application and Fundamental Investigations*. Kirk, T. K., Chang, H.-M., Eds.; Butterworth-Heinemann, Boston, MA, **1990**; pp. 203–210.
151. Pettersson, B.; Yang, J.-I.; Eriksson, K. E. *Nordic Pulp and Paper Research Journal* **1988**, *4*, 198.
152. Pinnavia, T. *J. Science* **1983**, *220*, 3659.
153. Barloy, L.; Battioni, P.; Mansuy, D. *J. Chem. Soc., Chem. Comm.* **1990**, 1365.
154. Leisola, M. S. A.; Ulmer, D. C.; Waldner, R.; Fiechter, A. *J. Biotechnol.* **1984**, *1*, 331–339.
155. Ulmer, D. C.; Leisola, M. S. A.; Fiechter, A. *J. Biotechnol.* **1984**, *1*, 13–24.
156. Harvey, P. J.; Shoemaker, H. E.; Palmer, J. M. *FEBS Lett.* **1986**, *195*, 242–246.
157. Tien, M.; Kirk, T. K.; Bull, C.; Fee, J. A. *J. Biol. Chem.* **1986**, *261*, 1687–1693.
158. Sundholm, F.; Sundholm, G. *Holzforshung* **1982**, *36*, 277–285.
159. Limosin, D.; Pierre, G.; Cauquis, G. *Holzforshung.* **1985**, *39*, 91–98.
160. Glenn, J. K.; Gold, M. H. *Appl. Environ. Microbiol.* **1983**, *45*(6), 1741–1747.
161. Crestini, C.; Tagliatesta, P. Proceedings of the Sixth European Workshop on Lignocellulosics and Pulps, Bordeaux, september 3–6 2000 pp. 37–60.

# Biochemistry of Methyl-CoM Reductase and Coenzyme F<sub>430</sub>

67

STEPHEN W. RAGSDALE

Department of Biochemistry, Beadle Center, 19th and Vine Streets, University of Nebraska, Lincoln, Nebraska 68588-0664, USA

I. Introduction	205
A. Introducing Methanogens and Factor F <sub>430</sub>	205
B. Introducing MCR	206
C. The Genes Encoding MCR	206
D. Discovery of the Nickel Coenzyme F <sub>430</sub>	207
E. Structure and Biosynthesis of F <sub>430</sub>	208
F. Properties of the MCR Substrates – Methyl-Coenzyme M (Methyl-SCoM) and Coenzyme B	208
II. Isolation and Activation of MCR	209
III. Structure of F <sub>430</sub> and MCR	210
IV. Spectroscopic Studies of MCR	212
A. EPR Spectroscopy	212
B. ENDOR Studies	215
C. Cryoreduction of MCR	215
D. X-ray Absorption Studies	217
E. Resonance Raman (RR) Spectroscopy of MCR	218
F. Spectroscopy of MCR <sub>ox1</sub> versus MCR <sub>red1</sub>	220
G. Other Red States of MCR	221
V. Mechanism of Methane Formation by MCR	221
A. Steady State and Presteady-State Kinetic Studies	221
1. Steady-State Kinetics	221
B. Presteady-State Kinetic Studies	222
C. Mechanisms of Methane Formation	222
1. Mechanisms Involving a Methyl-Ni Intermediate	222
2. A Mechanism Lacking Methyl-Ni Based on Density Functional Theory Calculations	224
3. Other Possible Mechanisms and Mechanistic Considerations	225
VI. Summary and Perspectives for the Future	226
References	226

## I. Introduction

### A. INTRODUCING METHANOGENS AND FACTOR F<sub>430</sub>

Söhnngen was first to define the reactions of methanogenesis in 1910 and showed that 4 mol of H<sub>2</sub> could reduce 1 mol of CO<sub>2</sub> to methane.<sup>1</sup> It was many years before, scientists learned how to work with these strictly anaerobic microbes in pure culture.<sup>2-4</sup> Working with cell-free extracts of methanogens was accomplished with the isolation of the first thermophilic methanogen, *Methanobacterium thermoautotrophicum*, which could be mass cultured and its enzyme fractionated.<sup>5</sup> These advances were essential before the biochemistry of methanogenesis could be addressed.

F<sub>430</sub> is a coenzyme in one enzyme, methyl-coenzyme M reductase (MCR), which catalyzes the ultimate step in the biological synthesis of methane. Methane formation or methanogenesis is catalyzed by a unique group of microbes, called methanogens, which are members of the so-called third kingdom of life, the archaea, the other two kingdoms being Eukarya and Bacteria. Despite the evolutionary distance between bacteria and archaea, the metabolism of methanogens resembles that of many strictly anaerobic bacteria that survive on very simple growth substrates including H<sub>2</sub>/CO<sub>2</sub>, methanol, CO, methylamines, acetic acid, and methyl mercaptans (Figure 1a).

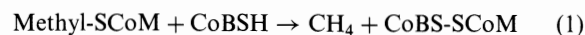
Methanogens are found in diverse anaerobic environments, which include gastrointestinal tracts like

the animal large intestine, the cecum, and the rumen; rice paddies; the termite hindgut; large water masses (seas and anaerobic oceans), marshes, and freshwater sediments; and landfills and sewage sludge digesters. Many methanogens associate with protozoa in such environments. The beneficial effects of methanogenesis include the removal of H<sub>2</sub> formed during the oxidative metabolism of biomass, thus enhancing the biodegradation of complex organics. This is because elevated H<sub>2</sub> levels inhibit biodegradation. However, there are several negative aspects of ruminant methanogenesis. Methane is a potent greenhouse gas that is 21 times more effective at trapping heat in the atmosphere than carbon dioxide.<sup>6</sup> Furthermore, the atmospheric methane concentration has doubled over the past two centuries, reaching a current global emission rate of 560 million metric tons per year and a 2002 level of 1.75 ppm. The increase is due primarily to increased livestock domestication and expanded rice cultivation. The largest source of anthropogenic methane emissions is by domesticated ruminant livestock. Reducing anthropogenic methane emissions is one strategy for mitigating global warming, particularly in the near term, because the atmospheric lifetime of methane is only about 9 years, while that of carbon dioxide is between 50 and 200 years. Besides the environmental impact of increasing methane levels, livestock methane production results in loss of between 3 and 12% of energy available in the feed; thus, inhibition of methanogenesis has long been considered as a strategy to improve agricultural productivity.<sup>7</sup> Redirection of reducing equivalents in the rumen as a result of inhibiting methanogenesis can enhance production of nutrients that are useful to the host.<sup>8</sup> Among other strategies, bromoethanesulfonate, a specific potent inhibitor of MCR,<sup>9</sup> the subject of this review, has been tested as a possible antidote to methane production in sheep.<sup>8</sup>

### B. INTRODUCING MCR

Regardless of the source of carbon and energy, all biologically produced methane is the result of MCR activity (Figure 1b). MCR catalyzes the final step in methane formation from methyl-coenzyme M (methyl-SCoM) and N-7-mercaptoheptanoylthreonine phosphate (CoBSH) (Eq. 1),<sup>10</sup> which serves as the electron donor<sup>11</sup> and, the mixed disulfide CoBS-SCoM is the product of the oxidative half-reaction. At the active site of MCR is Coenzyme F<sub>430</sub>, which is a nickel hydrocorphin.<sup>12-14</sup> The structure of F<sub>430</sub> is shown in Figure 1b. X-ray crystallographic studies of MCR reveal that F<sub>430</sub>

forms the base of a narrow well that accommodates the two substrates and shields the reaction from solvent.<sup>15</sup> The phosphate group of CoBSH binds at the upper lip of the well with its thiol group located 6 Å from the central Ni atom of F<sub>430</sub>.

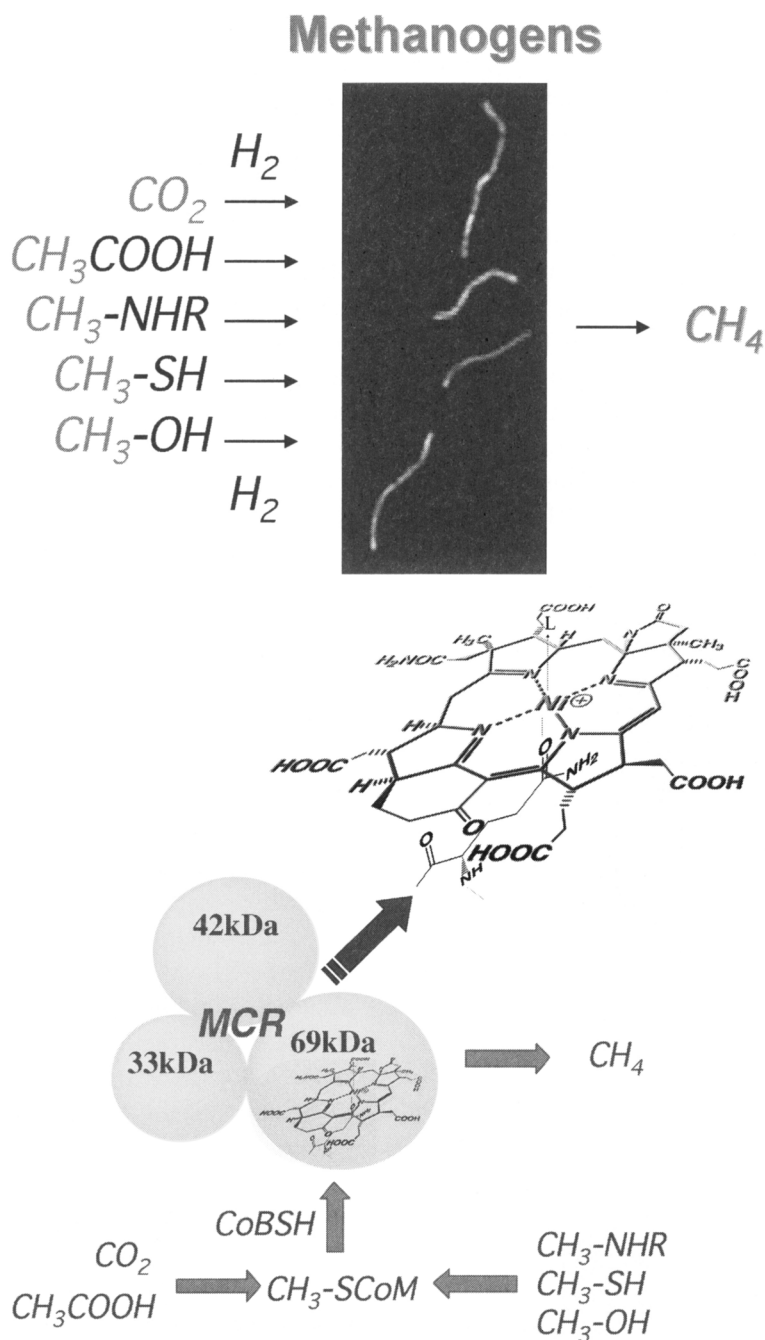


### C. THE GENES ENCODING MCR

As was first shown in *M. thermoautotrophicum* and *M. marburgensis*,<sup>16</sup> most methanogens apparently contain two MCR isozymes (MCR I and MCR II). Both gene clusters contain the structural genes (ABG) in the catalytically active protein ( $\alpha\beta\gamma$ ). MCR I is encoded by the *mcrBCDGA* operon, while MCR II is encoded by the *mrtBDGA* operon. The *mcr* operon is immediately upstream from the *mtr* operon that encodes N5-methyltetrahydromethanopterin:coenzyme M methyltransferase, which catalyzes the preceding step in methanogenesis.<sup>17</sup> When H<sub>2</sub> and CO<sub>2</sub> are sufficient and the cells are growing exponentially, essentially only MCR II is present, while under H<sub>2</sub>-limiting conditions, MCR I predominates.<sup>16</sup> Reeve has shown that the level of H<sub>2</sub> in the *M. thermoautotrophicum* growth medium regulates transcription of these two gene clusters as well as growth rate, methanogenesis, and growth yield.<sup>18</sup> When H<sub>2</sub> is present in excess, growth and methanogenesis increase exponentially and the *mrt* genes are expressed. Conversely, when the percentage of H<sub>2</sub> in the gas mixture is decreased or the speed of the fermenter impeller is decreased, H<sub>2</sub> becomes limiting and the growth rate and methanogenesis decrease, and the *mcr* genes are transcribed.<sup>18</sup> Other methanogenesis genes are under similar H<sub>2</sub>-regulation.<sup>19</sup> There is evidence that a coenzyme, called F<sub>390</sub> acts a response regulator that senses the levels of H<sub>2</sub> and signals changes in these levels, ultimately regulating methanogenic metabolism at the transcriptional level.<sup>20,21</sup> Coenzyme F<sub>390</sub> is the 8-hydroxyadenylylated form of the redox Coenzyme F<sub>420</sub> (a deazaflavin); correspondingly, the relative levels of F<sub>390</sub>/F<sub>420</sub> are controlled by Coenzyme F<sub>390</sub> synthetase and hydrolyase, whose activities depend on the redox state of the cell.<sup>22</sup>

The genes encoding MCR have been cloned and sequenced from a variety of methanogens, including *M. thermoautotrophicum* Marburg and  $\Delta$ H, *M. fervidus*, *M. kandleri*, *M. barkeri*, *M. vannielii*, and *M. voltae*.<sup>19</sup> The *mrt* operons contain the *mrtD* and *mrtC* genes of unknown function.<sup>23</sup> The *Methanococcus vannielii* MCR was shown to associate with the three-subunit MCR but





**Figure 1.** Introduction to MCR and methanogenesis. (a) Growth substrates for methanogenesis. *M. marburgensis* is shown under UV illumination, which results from Coenzyme F<sub>420</sub> fluorescence. (b) Cartoon of MCR showing the three subunits and Coenzyme F<sub>430</sub>.

was present at a molar ratio of 15-fold lower in the purified enzyme.<sup>24</sup> It now appears possible to use site-directed mutagenesis of methanogenic enzymes.<sup>25,26</sup>

#### D. DISCOVERY OF THE NICKEL COENZYME F<sub>430</sub>

The active site of MCR contains a nickel tetrapyrrole Coenzyme F<sub>430</sub>, which has a maximum absorption at ~430 nm, making it bright yellow. It is alternatively

called Factor F<sub>430</sub>, F<sub>430</sub>, or Coenzyme F<sub>430</sub>. Given its well-defined structure and requirement for MCR, “coenzyme” is a more appropriate term and will be used here. F<sub>430</sub> was discovered in cell extracts of *M. thermoautotrophicum* in 1978.<sup>27</sup> The first link between nickel and F<sub>430</sub> was established in 1980 based on the isolation of radioactive <sup>63</sup>Ni-F<sub>430</sub> from methanogenic cell extracts grown in media supplemented with this Ni isotope<sup>12</sup> and based on neutron activation analysis of F<sub>430</sub>.<sup>14</sup>

Recognition that  $F_{430}$  is a component of MCR came two years later when Wolfe and coworkers released and isolated  $^{63}\text{Ni}-F_{430}$  from the purified enzyme.<sup>28</sup> All methanogens contain  $F_{430}$ ,<sup>29</sup> which so far has only been found to be associated with MCR.

An explosion of discoveries related to nickel in the late 1970s and early 1980s accompanied the finding of  $\text{Ni}-F_{430}$  in MCR. The first report of a nickel enzyme was in 1975 with jack bean urease,<sup>30</sup> which in 1926 became the first crystalline enzyme and the basis for Sumner's controversial proof that enzymes are proteins. Nickel was shown to be required for hydrogenase activity<sup>31</sup> and then identified as a component of hydrogenases.<sup>32,33</sup> Similarly, Ni was shown to be required for CO dehydrogenase activity<sup>34</sup> and then was identified as a component of this enzyme.<sup>35</sup>

### E. STRUCTURE AND BIOSYNTHESIS OF $F_{430}$

The structure of  $F_{430}$  (Figure 2), which was elucidated by X-ray and NMR methods,<sup>36,37</sup> insinuates its evolutionary and biosynthetic relationship to porphyrin, chlorophyll, and vitamin  $\text{B}_{12}$ <sup>38</sup> (Figure 3) (see Chapter 68 by Kräutler and Ostermann and Chapter 76 by Scott et al. in this Handbook). All these compounds are tetrapyrroles derived from 5-aminolevulinic acid (see Chapter 70 by Shoolingin-Jordan in this Handbook). The common precursor of  $F_{430}$ , sirohaem, and vitamin  $\text{B}_{12}$  is dihydrosirohydrochlorin (Precorrin II).<sup>39,40</sup> While the macrocycles of heme and chlorophyll are completely conjugated, the ring system of  $\text{B}_{12}$  consists of six extended double bonds, whereas,  $F_{430}$  has one isolated double bond in Ring A and four conjugated double bonds linking Rings B, C, and D. Evidence suggests that formation of active  $F_{430}$  involves reduction of one of the four conjugated double bonds.<sup>41</sup> The Ni site is ligated by

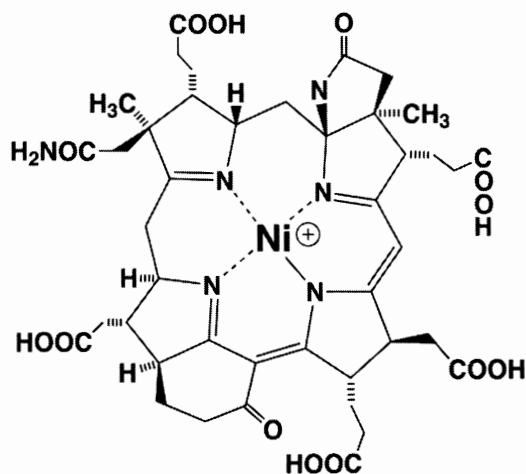


Figure 2. Structure of  $F_{430}$ .

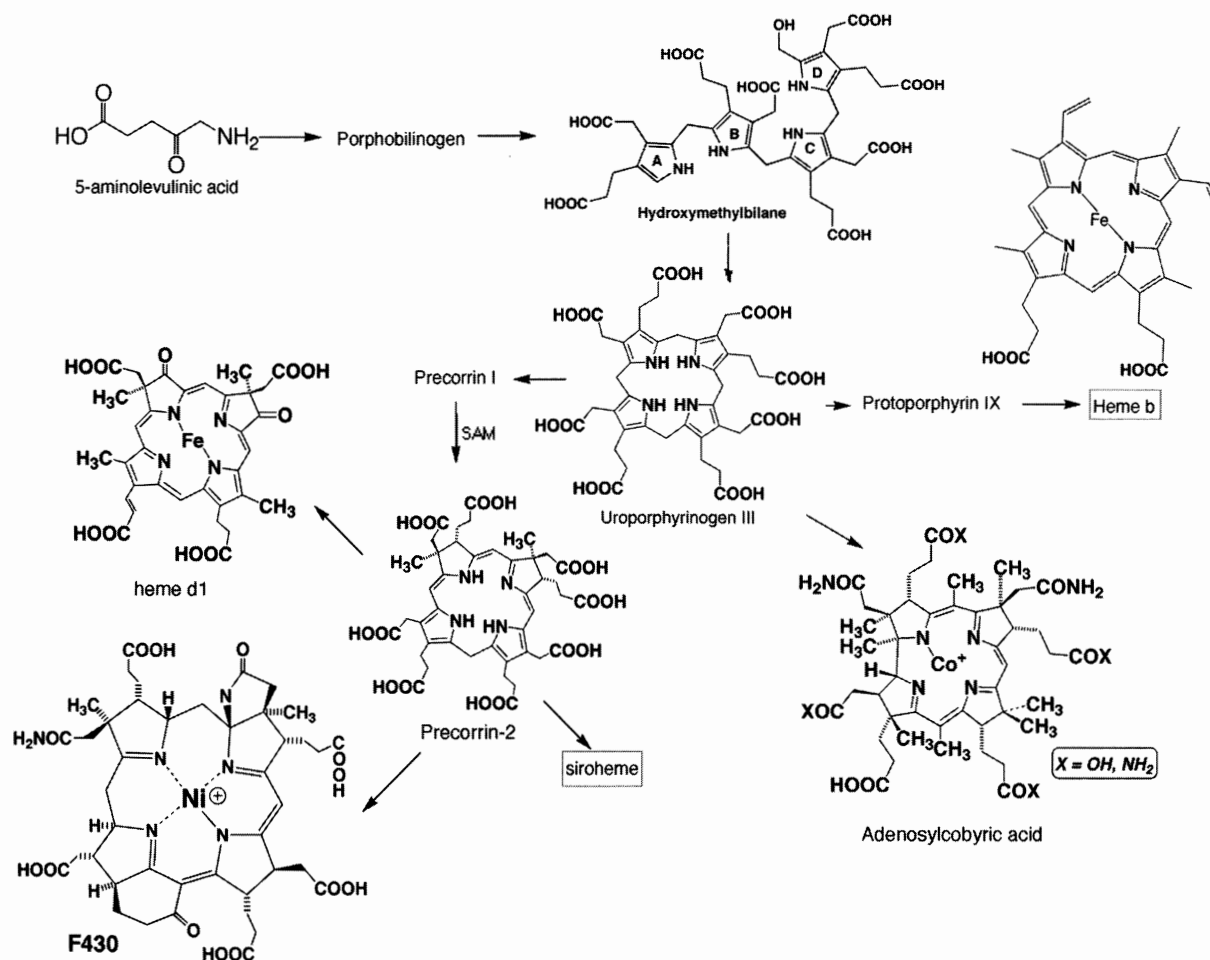
the four tetrapyrrole N atoms, a glutamine residue, and a sixth ligand that differs with the state of the enzyme.

### F. PROPERTIES OF THE MCR SUBSTRATES – METHYL-COENZYME M (METHYL-SCoM) AND COENZYME B

MCR is highly selective for methyl-SCoM ( $K_m = 0.1$  mM), the smallest known coenzyme. Wolfe and coworkers discovered Coenzyme M in 1971<sup>42</sup> and determined its structure<sup>43</sup> and its essentiality for growth of methanogens<sup>44</sup> in 1974. Until 1999, CoM was considered to only occur in methanogens; it has been identified as a coenzyme for aliphatic epoxide carboxylation in the Gram-negative bacterium *Xanthobacter* strain *Py2*.<sup>45</sup> In *Xanthobacter*, CoM biosynthesis is encoded by a linear megaplasmid which also harbors the genes for the alkene oxidation and epoxide carboxylation enzymes.<sup>46</sup> The Michaelis constants for a variety of substrates and inhibitors of the MCR reaction are listed in Table 1 and discussed in Section VA,B.

The other required substrate for methanogenesis is Coenzyme B or mercaptoheptanoylthreonine phosphate, which was discovered in 1980 to be “an oxygen-labile, heat-resistant, dialyzable cofactor with a size of about 1,000 daltons and with no apparent absorption in the visible range.”<sup>47</sup> CoB was used for six years as an uncharacterized cofactor. There were several key discoveries in 1986–87. Wolfe and coworkers isolated, elucidated its structure,<sup>48</sup> and extracted it from MCR.<sup>49</sup> In the following year, Wolfe and coworkers synthesized CoB and demonstrated its activity in the MCR reaction<sup>50</sup> and showed that the heterodisulfide, CoBS-S-CoM is the product of the MCR reaction.<sup>51</sup> These findings were complemented by experiments by Thauer and coworkers who showed that methyl-SCoB is an inhibitor, not a substrate, of MCR and proposed that CoB is the electron donor for methyl-SCoM reduction to methane.<sup>11</sup>

The heterodisulfide product of the MCR reaction is regenerated by  $F_{420}$ -dependent heterodisulfide reductase (HDR), which was discovered in 1988.<sup>52</sup> This reaction is coupled to proton translocation, which leads to ATP synthesis.<sup>53</sup> There are two forms of this enzyme, one containing flavin and iron-sulfur clusters<sup>54</sup> and the other containing heme and iron-sulfur clusters.<sup>55</sup> The *Ms. thermophila* HDR consists of a 53 kDa subunit containing two distinct  $[\text{Fe}_4\text{S}_4]$  clusters and a 27 kDa subunit with two *b*-type hemes.<sup>56</sup> A new membrane-bound cofactor, methanophenazine, which has a 25-carbon isoprenoid chain attached to position 2 of phenazine via



**Figure 3.** Biosynthesis of F<sub>430</sub>: Enzymes: A, Glutamyl tRNA reductase; B, Glutamate semialdehyde aminomutase; C, 5-Aminolaevulinic acid synthase; D, Porphobilinogen synthase (ALA dehydratase); E, Hydroxymethylbilane synthase (PBG deaminase). F, Uroporphyrinogen III synthase (cosynthetase); In the precorrin part: Enzymes: A, S-Adenosylmethionine-uroporphyrinogen III methyl transferase (SUMT) or CysG (in *E. coli*); B, S-Adenosylmethionine-precorrin-2 methyl transferase (SP2MT); C, CysG (in *E. coli*). Modified from <http://www-leeper.ch.cam.ac.uk/TetrapyrroleBiosynth/HaemBiosynth.html>

an ether bond, mediates electron transfer between F<sub>420</sub> and the heme containing HDR.<sup>57</sup> Rapid kinetic and spectroscopic studies indicate that electrons are transferred from reduced F<sub>420</sub> to methanophenazine to a high potential 4Fe cluster to a low potential heme and finally to CoB-S-S-CoM.<sup>58</sup>

The biosynthetic pathways leading to CoM<sup>59</sup> and CoB (Figure 4) have been extensively studied by White.<sup>60</sup> The final step in CoM biosynthesis, addition of SH, is speculative since the involved enzyme(s) has not been characterized.

## II. Isolation and Activation of MCR

It is quite easy to isolate large amounts of inactive MCR because MCR is present in high concentrations in the methanogenic cell; in fact, in many methanogens there

are several isozymes.<sup>16</sup> In addition, MCR has a large molecular mass and a low pI. However, it has been extremely difficult to isolate and maintain this enzyme in an active state. Early studies were with the MCR from the ΔH strain of *M. thermoautotrophicum* and required three components for activity, including H<sub>2</sub>, Component A (which was actually three components including hydrogenase), Component B (Coenzyme B), and ATP.<sup>47</sup> To quote from a Wolfe paper describing a simplification! of an earlier MCR preparation, “When titanium(III) citrate was used as electron donor... component A1 was no longer required. The simpler system thus obtained required components A2, A3, and C as well as catalytic amounts of ATP, vitamin B<sub>12</sub>, and the disulfide of 7-mercaptoheptanoylthreonine phosphate.”<sup>61</sup> This paper demonstrated that activation of MCR required reduction, yet it was still far from “simple” and orders of magnitude from fully active.

**Table 1.** Michaelis Parameters for MCR Substrates and Inhibitors

	$K_m/K_i$	Reference
<i>Substrates</i>		
methyl-ScoM	0.6 to 5.4 mM	62,104,105
CoBSH	0.1 to 0.3 mM	62,104
hydroxocobalamin	0.2 mM	105
2-(methylthio)propionate	1.3 mM	117
ethyl-ScoM	1.3 mM	117
methyl-SeCoM	0.3 mM	117
difluoromethyl-ScoM	2.5 mM	117
<i>Inhibitors</i>		
CoBS-ScoM	0.6 mM	62
mercaptooctanoyl-threoninephosphate	0.015 mM	118
7-(methylthio)hexanoyl-threoninephosphate	0.009 mM	118
7-(methylthio)heptanoyl-threoninephosphate	0.007 mM	62
7-bromoheptanoyl-threoninephosphate	0.005 mM	62
mercaptohexanoyl-threoninephosphate	100 nM	118
2-chloroethanesulfonate	0.07 mM	9
cyano-ScoM	0.03 mM	117
allyl-ScoM	0.02 mM	117
2-bromoethanesulfonate	0.008 mM	9
4-bromobutanesulfonate	0.006 mM	119
2-azidoethanesulfonate	0.001 mM	119
bromomethanesulfonate	0.0015	118
3-bromopropanesulfonate	50 nM	119
$V_{max}$	100 U mg <sup>-1</sup> , 60°C	65
$k_{cat}$	250 s <sup>-1</sup> , 60°C	65
$k_{cat}/K_m$ for methyl-ScoM	40 mM <sup>-1</sup> s <sup>-1</sup>	105

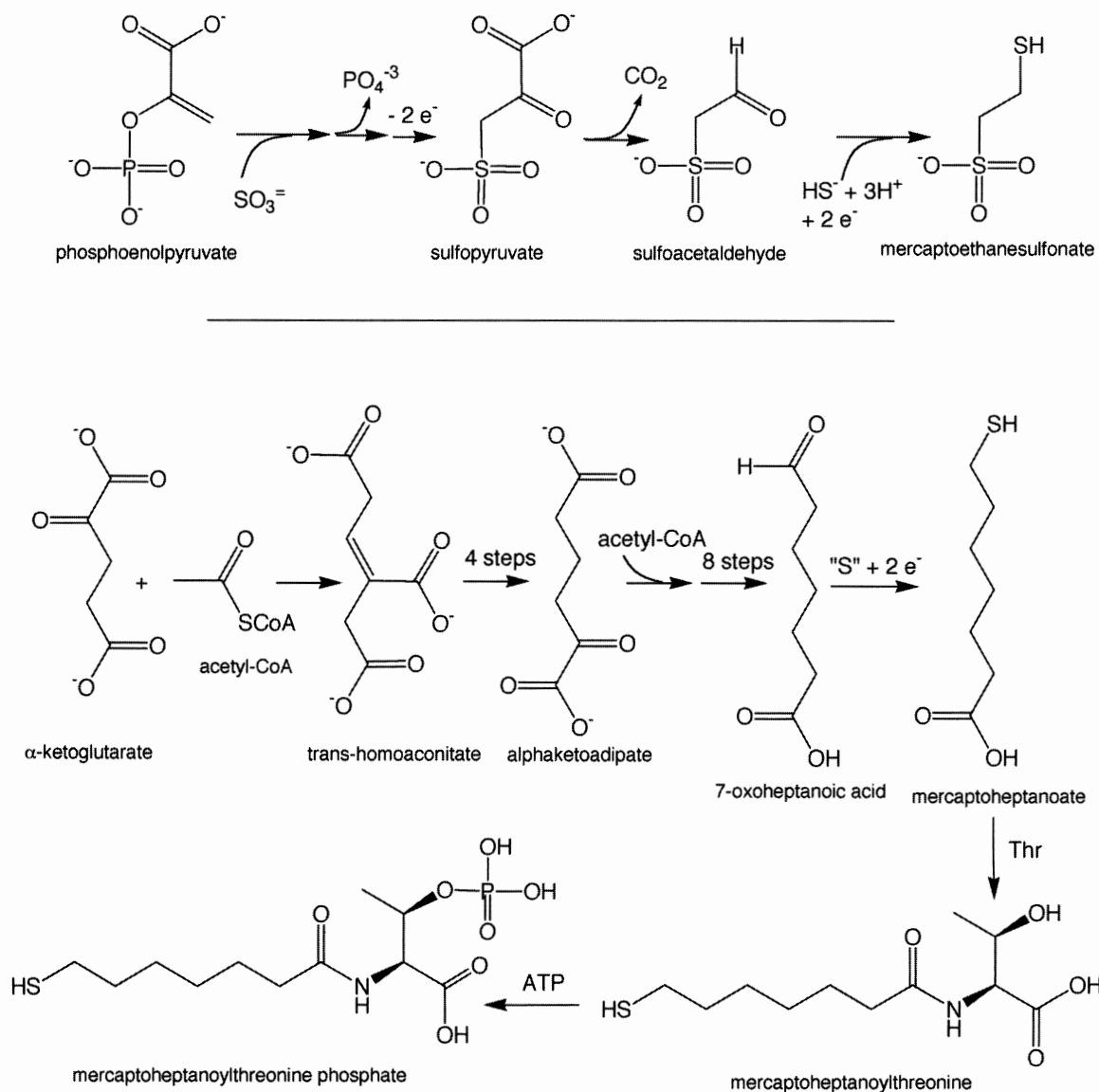
The MCR from *Methanobacter marburgensis* (formerly, *M. thermoautotrophicum*, strain Marburg) was found to only require Ti(III) citrate, Coenzyme B, and Component C (the yellow MCR).<sup>62</sup> However, even with this system and with the design of a rapid purification protocol, the achievement of activities up to 2  $\mu\text{mol min}^{-1} \text{mg}^{-1}$ , which was much higher than shown ever before, amounted to only 5% of the activity present in the microbial cells. Ninety-five percent of the MCR activity was lost upon lysis. Another important advancement was to assess MCR by EPR spectroscopy. The various states of MCR are discussed below and interconversion among the various important states is diagrammed in Figure 5. Thauer and coworkers showed that when *M. thermoautotrophicum* cells were preincubated with 100% H<sub>2</sub> and methyl-S-CoM before lysis, the MCR activity reached 20 U/mg in the presence of methyl-coenzyme M, which stabilized both the activity and the EPR signal MCR<sub>red1</sub>.<sup>63</sup> These and other studies strongly indicated that the MCR<sub>red1</sub> form of the enzyme is required to initiate catalysis.<sup>63-65</sup> Then, Thauer informed the author that he had discovered a way to

isolate MCR is an inactive, but “ready,” state called MCR<sub>ox1</sub> that can be reduced *in vitro* by titanium(III) citrate.<sup>65</sup> This was important because the ox1-state decays much more slowly than does active MCR<sub>red1</sub>. Don Becker, in the author’s laboratory then focused on identifying conditions to achieve the highest possible amount of MCR<sub>ox1</sub>.

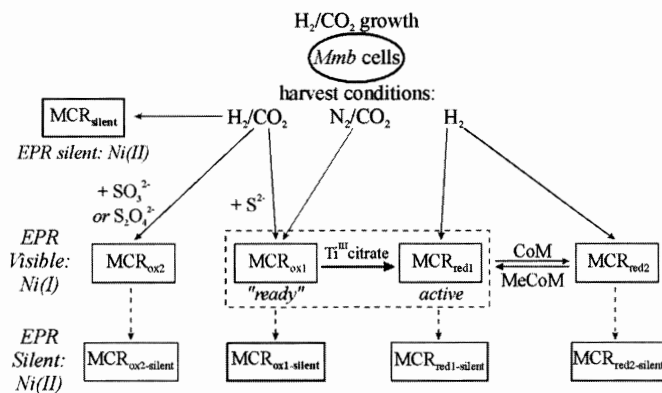
Based on some of the results described above, it seemed possible that some addition to the growth medium could enhance ox1 formation. We hypothesized that the key to optimizing ox1 formation was to find a suitable nickel ligand that would be able to stabilize Ni(I) and undergo replacement during the conversion of ox1 to red1 (which we incorrectly expected would be 4-coordinate Ni(I)). Thus, a number of potential Ni ligands were added to the cell culture and whole cell EPR was used to assess success or failure. Although many of the treatments led to complete inactivation of MCR, sodium sulfide addition before harvesting the cells produced a whole-cell MCR<sub>ox1</sub> EPR spectrum as strong as any preparation of pure enzyme we had ever examined (Figure 6). The sulfide-treated enzyme could be purified to homogeneity and highly reproducibly converted quantitatively to the MCR<sub>red1</sub> state.<sup>66</sup> Furthermore, this treatment could be used with the MCR from *Methanosarcina thermophila* and, thus, presumably any MCR.<sup>66</sup> Goubeaud and Thauer were successful in generating high yields of ox1 (that could be converted to red1) by replacing the H<sub>2</sub>/CO<sub>2</sub> gas phase used during growth with N<sub>2</sub>/CO<sub>2</sub>.<sup>65</sup> Importantly, a protocol(s) to generate highly active MCR<sub>red1</sub> suitable for mechanistic studies had been achieved.

### III. Structure of F<sub>430</sub> and MCR

The structure of F<sub>430</sub>, shown in Figure 2, including the complete stereochemical assignment of the configuration of the pendant groups from the macrocycle has been defined by X-ray crystallography and NMR studies.<sup>37</sup> The crystal structures of the MCR-substrate and the MCR-product complexes in the inactive Ni(II) oxidation state have been resolved.<sup>15</sup> The structures of the inactive Ni(II) enzyme in complex with CoM and CoB (MCR<sub>ox1-silent</sub>) and in complex with the heterodisulfide CoM-S-S-CoB product (MCR<sub>silent</sub>) have been resolved at 1.16 Å and 1.8 Å resolution, respectively.<sup>67</sup> The resolution is sufficient to confirm the stereochemical assignment determined for the free coenzyme. What seems unusual is that the accepted structure, shown here, appears to not have a continuous pattern of



**Figure 4.** The biosynthetic pathways for CoM and CoB. Modified from Figure 1 of Graupner et al.<sup>59</sup> for CoM and from Figure 1 of Howell et al.<sup>121</sup> for CoBSH biosynthesis.



**Figure 5.** Interconversion among various MCR species. The dashed arrows indicate the conversion over time, even under anaerobic conditions, of EPR-visible forms of MCR to EPR-silent forms. From Telser et al.<sup>122</sup>

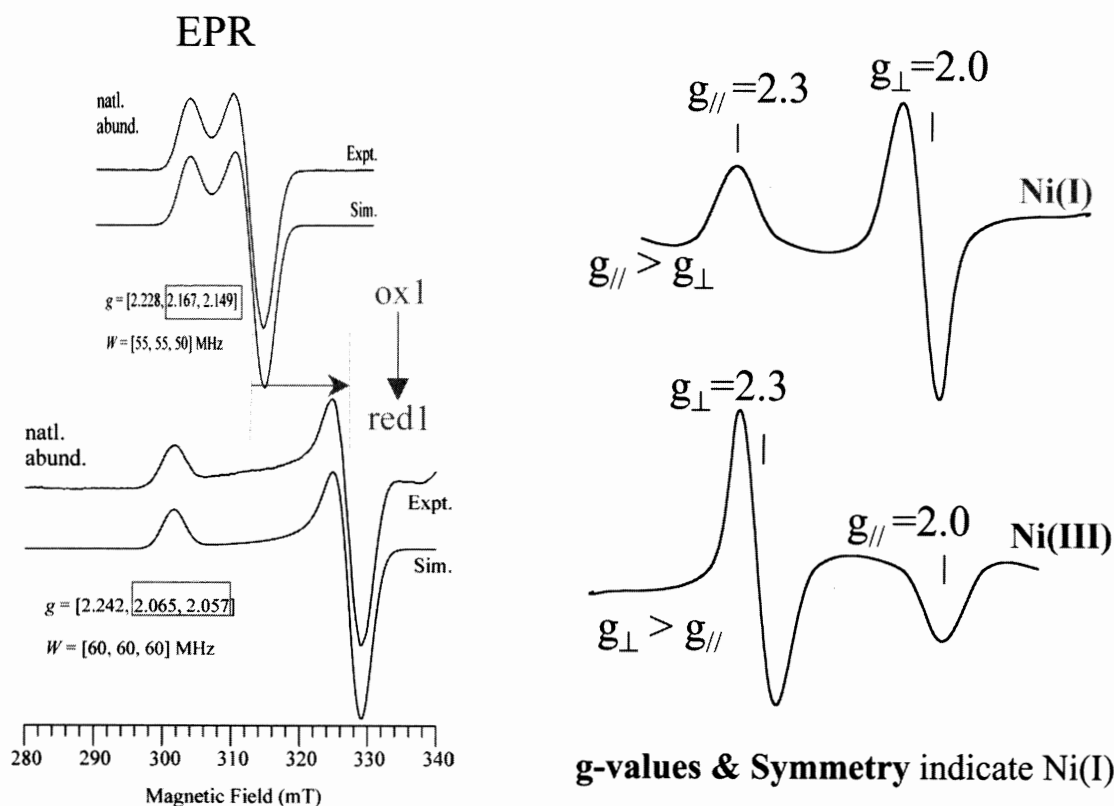


Figure 6. EPR spectra of MCR forms ox1 and red1.

delocalized double bonds. If the optical spectrum is due primarily to  $\pi$  to  $\pi^*$  transitions, one would expect a large proportion of another isomeric state in which the four double bonds in rings B, C, and D have undergone isomerization. This is described in the Section IV, E. The two  $F_{430}$ 's are separated from each other by roughly 50 Å. MCR is predominantly composed of helices forming an overall ellipsoidal shape (Figure 7a) of about  $120 \times 85 \times 80$  Å. There is an extensive interaction between subunits of the adjacent dimer.

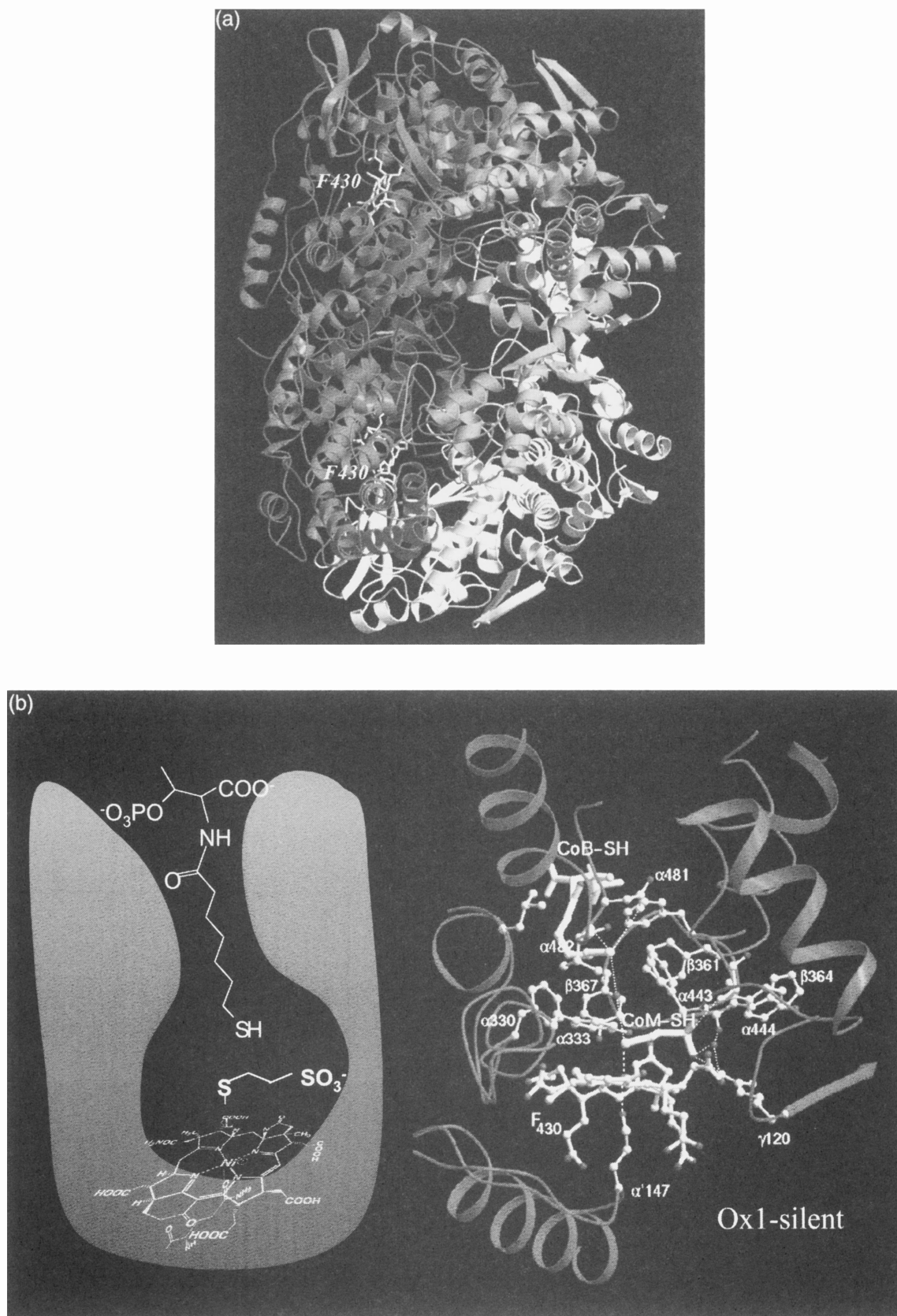
As illustrated for MCR<sub>ox1-silent</sub>,  $F_{430}$  is located at the bottom of a 50 Å long narrow channel, which forms a hydrophobic binding site for the two substrates, methyl-CoM and CoB (Figure 7b). From the crystal structure, it is clear that only CoM (and methyl-SCoM), but not CoB, can directly interact with the Ni(I) center in bound  $F_{430}$  since the thiol group of CoB is 8 Å away from the Ni ion. The channel contains a number of modified amino acid residues located in the  $\alpha$  subunits near the  $F_{430}$  binding site, including 1-*N*-methylhistidine ( $\alpha 257$ ), 5-*(S)*-methylarginine ( $\alpha 271$ ), 2-methylglutamine ( $\alpha 400$ ), *S*-methylcysteine ( $\alpha 452$ ), and, thioglycine ( $\alpha 445$ ), in which the carbonyl oxygen is substituted by sulfur. It appears that the methyl groups are introduced by *S*-adenosylmethionine dependent methylation reactions.<sup>68</sup>

#### IV. Spectroscopic Studies of MCR

What are the coordination and oxidation states of the active state of MCR? How can one generate the active enzyme? Where do substrates and inhibitors bind? Is activation a metal- or ligand-centered redox process? These and other key questions have been addressed by spectroscopy. Metalloenzymes like MCR are often rich in spectroscopic signals. As in all metalloenzymes, X-ray absorption studies can be performed since Ni is at the active site. The active states are EPR-active allowing a number of advanced magnetic resonance studies to be performed, including ESEEM, ENDOR, and MCD.  $F_{430}$ , which is at the heart of MCR, is a chromophore with a strong absorption spectrum in the visible region, allowing Resonance Raman and MCD studies.

##### A. EPR SPECTROSCOPY

A key question addressed by EPR studies of MCR is, do the various EPR-detectable forms of MCR contain Ni(I) or Ni(III)? Only Ni(I) ( $d^9$ ) and Ni(III) ( $d^7$ ) are EPR-active. Typical Ni(I) complexes differ from Ni(III) complexes by the symmetry of the EPR spectra. Because the unpaired electron in tetragonally elongated or square planar complexes of Ni(I) (like Cu(II)) is in



the  $d(x^2-y^2)$  orbital, the absorption feature is to the low field (high  $g$ -value) side of the S-shaped feature. In this case,  $g_{\parallel}$  (2.2–2.3)  $>$   $g_{\text{perp}}$  (2.05)  $>$   $g_e$  (2.0).<sup>69</sup> The opposite symmetry is observed for Ni(III) (like Co(II)) with its unpaired electron in the  $d(z^2)$  orbital. The literature on Ni(I) is fairly sparse and there are especially very few reports of EPR spectra for Ni(I)-tetraazamacrocycles.<sup>70–73</sup> There are also a few examples of <sup>61</sup>Ni-enriched complexes of Ni(III),<sup>74</sup> and some of Ni(I).<sup>75–77</sup> However, because of the similar electronic structures, one can compare Ni(I) with Cu(II) and Ni(III) with Co(II).

EPR spectra for ox1 and red1 are summarized in Figure 6 and the  $g$ -values of the distinct EPR-active states that have been identified are summarized in Table 2. Albracht spearheaded the early EPR work on MCR and several states were identified.<sup>78</sup> There are apparently two active, reduced (red) states, MCR<sub>red1</sub> and MCR<sub>red2</sub>. The assignment of Ni(I) to MCR<sub>red1</sub> is well accepted.<sup>79</sup> Depending upon which ligands were added to generate or stabilize the red1 state, Thauer further classified red1 as MCR<sub>red1m</sub> (methyl-CoM), MCR<sub>red1c</sub> (CoM), MCR<sub>red1a</sub> (absence of substrates). A distinct axial EPR signal, designated MCR<sub>BPS</sub>, is obtained upon incubating the ox1 or red1 states with 3-bromopropanesulfonate (BPS).<sup>78</sup> The Br ( $I=3/2$ ) of BPS can be replaced with F ( $I=1/2$ ) or I ( $I=5/2$ ) without altering the EPR signal, indicating that the halogen must not be close to the Ni.

MCR<sub>red1</sub> has been unambiguously assigned to Ni(I) based on the similarity of its UV-visible and EPR spectra with isolated Ni<sup>I</sup>F<sub>430</sub>.<sup>79–81</sup> MCR<sub>ox1</sub> and MCR<sub>ox2</sub> retain the overall symmetry of the Ni(I) complexes, however, they exhibit an unusually large S-shaped feature with its  $g_{\perp}$  at 2.15, not 2.05. However, none of the EPR spectra described in Table 2 resemble that of

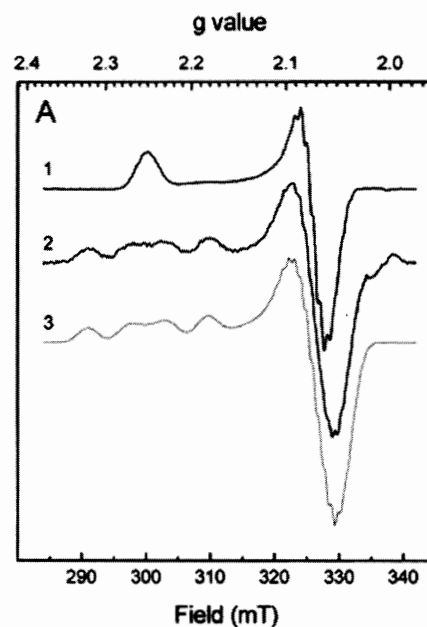
isolated Ni<sup>III</sup>F<sub>430</sub>Me<sub>5</sub>.<sup>82</sup> On the basis of the EPR spectra and ENDOR (described below) spectra of the ox1 and ox2 states, we proposed that all EPR-visible forms of MCR contain Ni(I).<sup>83</sup>

This assignment is consistent with EPR studies of isotopically labeled MCR. The ox1 and red1 states exhibit marked splittings when cells are grown in a medium containing Ni-61, a nuclear isotope of Ni with  $I=3/2$ <sup>84</sup> (Figure 8). These are the first published examples of resolved <sup>61</sup>Ni hyperfine splitting for a Ni(I)-tetraazamacrocycle. These spectra show that significant spin density resides on Ni. Importantly, the largest splittings are in the low field spectral component ( $g \sim 2.3$ ) for the ox and red1 states, which is consistent for a Ni(I) and not a Ni(III) assignment. The X-band spectra of ox1 and red1 also show resolved <sup>14</sup>N hyperfine couplings indicating that there are interactions between the unpaired spin and four nearly equivalent nitrogen ligands and that there is significant spin density on the nitrogen ligands.<sup>64,78,81</sup> EPR spectra of <sup>15</sup>N-enriched MCR samples agree with this interpretation.<sup>85</sup> The <sup>15</sup>N data are quite definitive since there are fewer lines with large spacings for <sup>15</sup>N versus <sup>14</sup>N. The major nitrogen hyperfine splittings are about 30 MHz and are very similar among the different EPR-active states, strongly indicating a Ni(I) assignment.

On the basis of <sup>61</sup>Ni and <sup>14</sup>N hyperfine coupling values obtained by ENDOR and EPR studies,<sup>85</sup> it is estimated

**Table 2.** EPR Parameters of Various States of MCR

EPR signal	$g$ Values	Reference
MCR <sub>red1</sub>	2.249, 2.070, 2.060	83
MCR <sub>red1c</sub>	2.250, 2.071, 2.061	84
MCR <sub>red1m</sub>	2.252, 2.073, 2.064	84
MCR <sub>red2</sub>	2.288, 2.235, 2.179	84
MCR <sub>ox1</sub>	2.229, 2.166, 2.148	83
MCR <sub>ox2</sub>	2.227, 2.140, 2.125	83
MCR <sub>dark</sub>	2.23, 2.128	64
MCR <sub>light</sub>	2.29, 2.25, 2.20	64
MCR <sub>ox1-BPS</sub>	2.222, 2.113	120
MCR <sub>red1-BPS</sub>	2.223, 2.115	120
MCR <sub>BrHpoThrP</sub>	2.210, 2.113	78
MCR <sub>red1-MOPS</sub>	2.223, 2.115	120
Ni <sup>I</sup> F <sub>430</sub>	2.244, 2.063, 2.063	83



**Figure 8.** EPR spectra of <sup>61</sup>Ni-MCR<sub>red1</sub>. (1) MCR<sub>red1c</sub> from cells grown in medium containing the natural isotopes of nickel; (2) MCR<sub>red1c</sub> isolated from cells grown in <sup>61</sup>Ni-enriched medium; (3) Simulation of 2 using a <sup>61</sup>Ni content of 82%. From Mählert et al.<sup>84</sup>



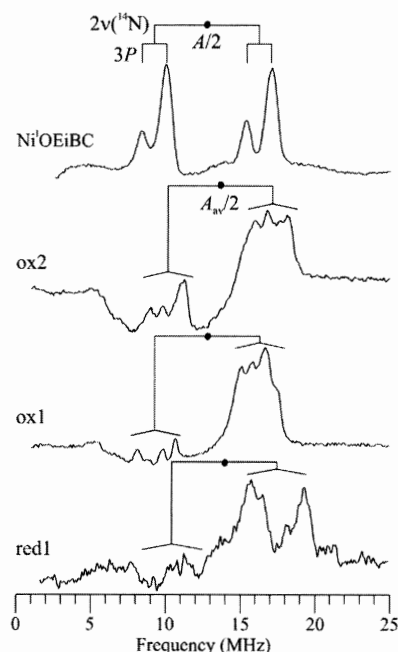
that approximately 80–90% of the unpaired spin density is on nickel in the MCR<sub>red1</sub> and the various Ni(I) states of F<sub>430</sub>. This would leave 10–20% of spin density on the nitrogens of the F<sub>430</sub> macrocycle. In the case of MCR<sub>ox1</sub>, the spin density on nitrogen is similar to the other states (based on the N-hyperfine splitting values); however there is approximately 60% spin density on Ni. This indicates that the missing spin density in ox1 relative to the other states is on sulfur (in ox1, the thiol of CoM is ligated to Ni, see below). By comparison, with CuTPP, also a d<sup>9</sup> tetraazamacrocycle, approximately 70% spin density resides on Cu.

Thus, the combined EPR spectra indicate that all the EPR-active states of MCR contain Ni in the 1+ oxidation state. This assignment was in some cases contrary to prior expectations, as indicated by the “ox” label based on biochemical studies that switching the cells from a reducing H<sub>2</sub> to a less reducing N<sub>2</sub> gas phase elicits the ox1 EPR signal.

## B. ENDOR STUDIES

ENDOR studies have been reported for isolated F<sub>430</sub> and of a model compound, Ni(I)OEiBC (octaethylisobacteriochlorin).<sup>86</sup> In addition, <sup>14</sup>N-ENDOR studies were performed at 35 GHz for MCR forms red1, ox1, and ox2<sup>83</sup> (Figure 9). The spectra are strikingly similar. The hyperfine couplings to the pyrrole-like <sup>14</sup>N at *g*<sub>max</sub> have the value *A*(<sup>14</sup>N) of 26 MHz. This large, roughly isotropic <sup>14</sup>N coupling are characteristic of a system with the unpaired electron in the d(*x*<sup>2</sup>−*y*<sup>2</sup>) orbital, indicating that these EPR-active forms of MCR are d<sup>9</sup> complexes, like Ni<sup>I</sup>F<sub>430</sub> and Cu<sup>II</sup>(TPP). In contrast, a d(*z*<sup>2</sup>) ground state, with low-spin d<sup>7</sup> complexes, exhibits very weak couplings to the equatorial ligands. For example, for Co<sup>II</sup>(TPP), the N coupling to the equatorial ligands has a value of 3.1 MHz for the pyrrole nitrogens and exhibits strong couplings to the axial ligands.<sup>70,87–90</sup>

Thus, the ENDOR and EPR spectra strongly indicate that the unpaired electron is in the d(*x*<sup>2</sup>−*y*<sup>2</sup>) orbital. Could the energy levels be inverted in MCR such that the unpaired electron is in this orbital? This could be true for a trigonal bipyramidal geometry, and molecular mechanics calculations suggest that such a distortion is possible for the *free* Ni<sup>II</sup>F<sub>430</sub> ligand.<sup>91</sup> However, given that the known structure of bound F<sub>430</sub> shows a tetragonal distortion, it is highly unlikely that such a strong geometric distortion can occur; furthermore, there are no examples of trigonal bipyramidal geometry with tetraazamacrocyclic ligands, which require tripodal



**Figure 9.** 35 GHz CW <sup>14</sup>N ENDOR spectra (2°K) at *g*<sub>1</sub> for (top to bottom): Ni(I)-OEiBC (top), MCR<sub>ox2</sub>, MCR<sub>ox1</sub>, and MCR<sub>red1</sub> (bottom). The closed circle indicates *A*/2, the line passing through the circle indicates twice the <sup>14</sup>N Larmor frequency (7 MHz), and the “goalposts” indicate the quadrupole splitting (3*P*). From Telsler et al.<sup>83</sup>

ligands. A strong tetragonal compression can also generate a d(*x*<sup>2</sup>−*y*<sup>2</sup>) ground state for Ni(III)-F<sub>430</sub>. This has been observed for Ni(III)(CN)<sub>2</sub>, with two *trans*-cyano ligands.<sup>92</sup> However, the potential axial ligands for the Ni in MCR are N, O, or S, which are too weak to invert the d(*z*<sup>2</sup>) and d(*x*<sup>2</sup>−*y*<sup>2</sup>) levels. That MCR<sub>ox1</sub> and ox2 have about the same <sup>14</sup>N isotropic coupling value as the Ni(I) in red1<sup>80</sup> negates an alternative description for the MCR<sub>ox1</sub> and ox2 states, that they arise from a radical coupled to a high-spin Ni(II).

In conclusion, EPR and ENDOR studies of MCR indicate that both ox1 and red1 are Ni(I) states. This presents an apparent discrepancy with the requirement for a low potential reductant (Ti(III)) for the activation of ox1 to red1.

## C. CRYOREDUCTION OF MCR

As described above, the structurally characterized forms of MCR are Ni(II) states, which are catalytically inactive. How can one bridge the high resolution structural data with the active Ni(I) states? One way is to freeze MCR in structurally defined states (MCR<sub>ox1-silent</sub> and MCR<sub>silent</sub>, for example) and perform reduction at 77 K, a temperature at which ligands cannot rearrange and reduced states decay extremely slowly. Roman Davydov (Northwestern University, Chicago, IL) has developed this method and, in

collaboration with Brian Hoffman, has interfaced it with advanced EPR methods. Electrons are produced by  $^{60}\text{Co}$  gamma rays which irradiate the solvent and produce mobile electrons.

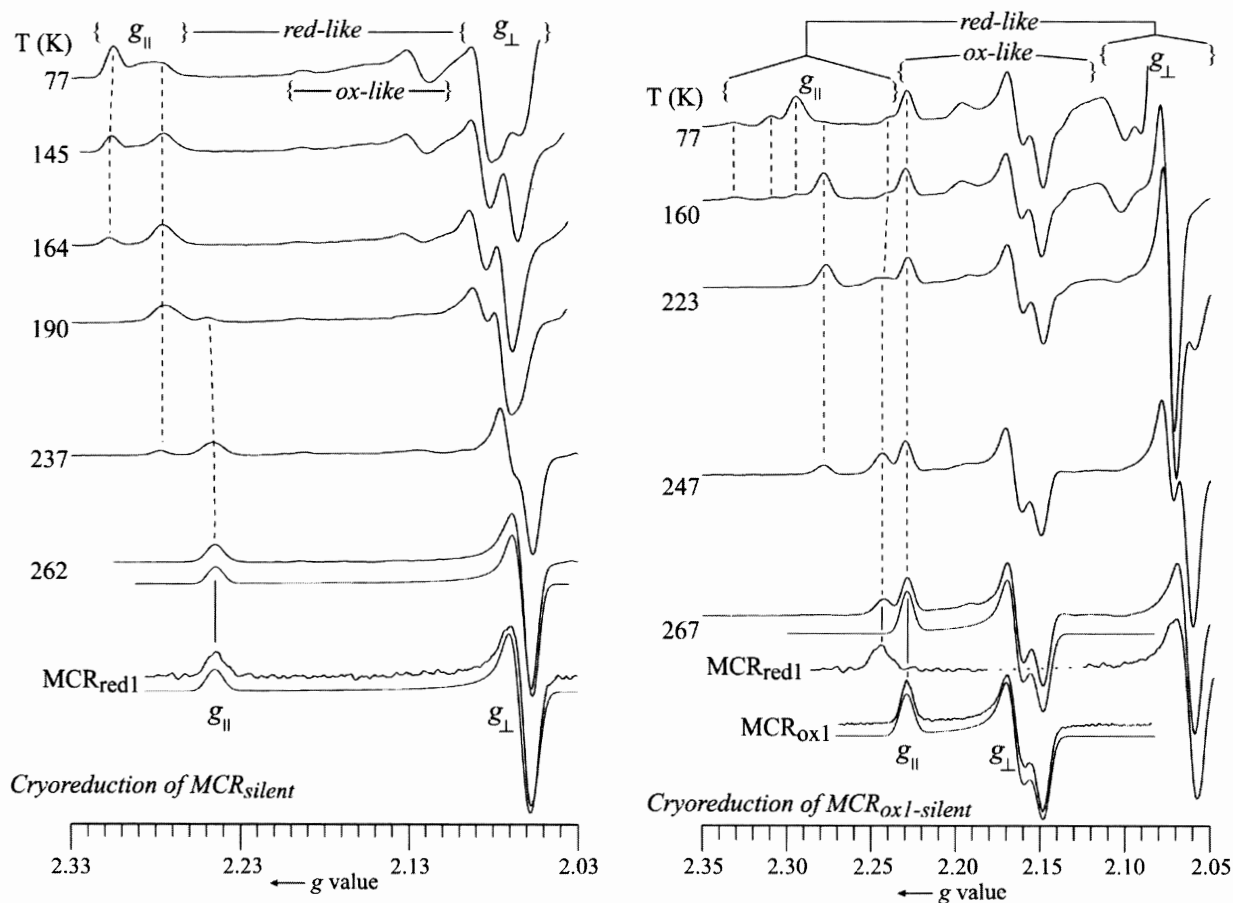
The most obvious question that can be answered again relates to oxidation state. If ox1 is a Ni(I) state, then cryoreduction of the related Ni(II) state should elicit an EPR spectrum identical to that of ox1. As shown in Figure 10 (left panel), the major species observed upon cryoreduction at 77 K is indistinguishable from ox1. This observation suggests that the coordination environment of ox1 is very similar, if not identical, to that of crystallographically characterized ox1-silent (Figure 7B). There is a small amount of a red1-like component, but we surmise that this is formed from some proportion of "red1-silent" in the solution before irradiation. Upon annealing, more ox1 is formed and red1 appears. Electrons are still present in the sample, so further reduction is possible, but the fact that very little red1 is formed at 77 K from ox1-silent

indicates that there is a thermodynamic or kinetic barrier, perhaps ligand rearrangement or isomerization of the tetrapyrrole, that must be overcome to form red1.

When the  $\text{MCR}_{\text{silent}}$  state is irradiated at 77 K, red1 is the major species observed. Upon annealing, the red1 state is the only one remaining. These results indicate that the coordination environment of Ni(II)-silent is similar to that of Ni(I)-red1.

In both the ox1-silent and silent states of MCR, the 77 K irradiation produces a species called "red-like," with  $g$  values greater than those of red1. It is likely that this state is a high-energy state that could be described as "Ni(I) in Ni(II) clothes." That is the Ni-ligand bond distances are optimized for Ni(II) and reduction generates an unstable intermediate that is trapped by the low temperatures. Annealing results in conversion of these "high-energy" states to the stable Ni(I) states.

In summary, the cryoreduction results strongly support the proposal that ox1, like red1, is a Ni(I)



**Figure 10.** Q-Band EPR spectra of 77 K cryoreduced 1 mM samples of MCR as a function of annealing temperature. The annealing temperature is given for each spectrum. The abscissa is in  $g$  value and the spectra are presented as digital first derivatives. Simulations are shown for samples annealed at 267 K. Included are spectra of conventionally (biochemically) prepared  $\text{MCR}_{\text{ox1}}$  and red1 with the simulations. The left panel shows the results of cryoreduction of ox1-silent and the right panel, Ni(II)-silent. From Telser et al.<sup>122</sup>

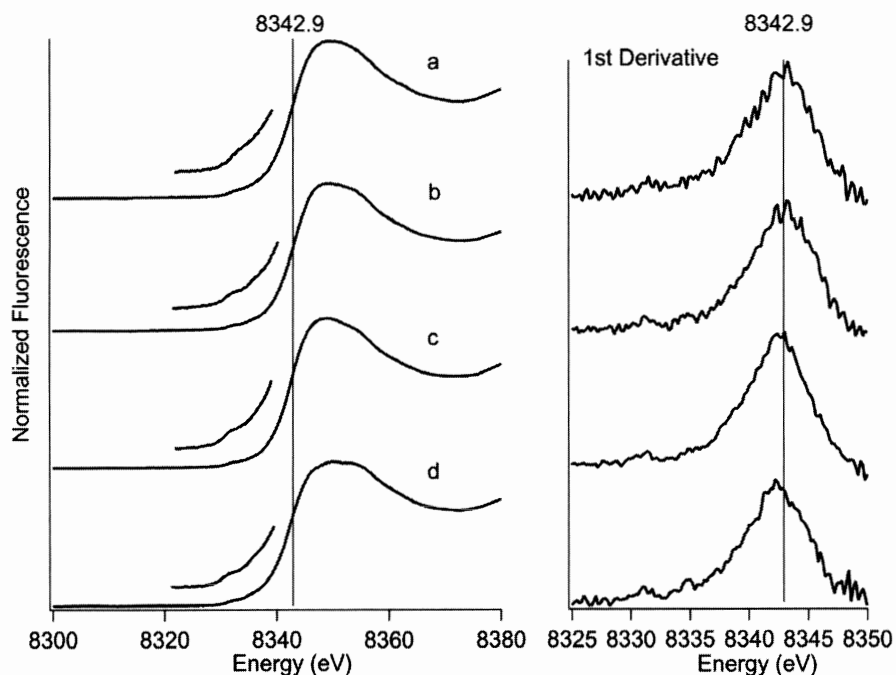
state. Since the 77 K *gamma* irradiation process *reduces* metalloproteins,<sup>93</sup> the generation of MCR<sub>red1</sub> and MCR<sub>ox1</sub> by irradiation of EPR-silent Ni(II) forms of MCR demonstrates that the red1 and ox1 forms must be assigned as Ni(I) states. However, the puzzle remains—why is reduction of the enzyme required to generate Ni(I)-red1 from Ni(I)-ox1?

#### D. X-RAY ABSORPTION STUDIES

X-ray absorption studies are particularly useful in deducing structural information about catalytically important forms of the enzyme. XANES (X-ray absorption near edge spectra) can provide information about the oxidation state of the metal ion and the coordination number, while EXAFS (extended X-ray absorption fine structure spectroscopy) reveals the type of ligand and the interatomic distances between the metal ion and its first and second coordination sphere ligands. An advantage of X-ray absorption experiments is that, once a defined state of MCR is generated, it can be frozen and studied at liquid nitrogen temperatures where the state can be maintained throughout the experiment and for many months thereafter. Furthermore, the distances obtained from EXAFS are considered to be of higher precision than X-ray diffraction data.

Ni-XANES spectra of the Ni(II) states are nearly identical, as are those of the ox1 and red1 states (Figure 11). The Ni K-edge energy for the ox1 and red1 states is 0.5 eV lower than that for the Ni(II) states, which is consistent with a lower oxidation state for the ox1 and red1 states. However, the edge shift is only about 25% of the expected edge energy shift for a full one-electron reduction. This apparent discrepancy is partly explained by the fact that the MCR<sub>ox1</sub> and MCR<sub>red1</sub> samples contain a ~50/50 mixture of EPR-silent Ni(II) with the EPR-active state. Unfortunately, no one has yet learned how to completely convert to the EPR-active states. In addition, the electron density changes associated with reduction to the Ni(I) state appear to be delocalized onto the ligands and not primarily localized on the Ni center.

The XANES spectra also indicate that the ox1, ox1-silent, Ni(II)-silent, and red1 states are six-coordinate. This agrees with the conclusions from the ENDOR experiments described above. None of them are four-coordinate, on the basis that they all lack preedge peaks near 8338 eV that correspond to a 1s → 4p<sub>z</sub> electronic transition (with shakedown contributions).<sup>94–96</sup> They also do not appear to be five-coordinate because the feature near 8332 eV is much weaker and outside the window of values



**Figure 11.** Left: XANES of (a) MCR<sub>silent</sub>, (b) MCR<sub>ox1silent</sub>, (c) MCR<sub>ox1</sub>, (d) MCR<sub>red1</sub> species from *M. marburgensis*. Inset plots are an expansion of the region around 8332 eV showing peaks assigned to 1s to 3d transitions. Right: First derivative of the XANES spectra. The center of the peak (first inflection point) is taken as the Ni K-edge edge energy ( $E_k$ ) for each species. As a basis of comparison, the vertical line (8342.9 eV) indicates the Ni K-edge for the MCR<sub>silent</sub> species. From Tang et al.<sup>41</sup>

previously observed for a five-coordinate complex. This feature, which results from a  $1s \rightarrow 3d$  electronic transition is in the range expected for six-coordinate complexes, which have a much weaker pre-edge feature.<sup>94</sup> These results rule out a long-cherished hypothesis of SWR that activation of MCR generated a four- or five-coordinate Ni center with an empty upper axial ligation site poised to react with the methyl group of methyl-SCoM and generate a methyl-Ni intermediate. Thus, if such a coordination environment is part of the MCR mechanism, it must appear in the transition state of the reaction, not in the ground state.

EXAFS studies of the Ni(II) states (Figure 12) reinforce the X-ray crystallographic results. Given that all states are six-coordinate, we presume that all MCR states apparently contain the lower axial glutamine oxygen ligand. The results also indicate that both the Ni(I)ox1 and Ni(II)-ox1-silent states appear to contain a sulfur ligand and the red1 states contains only N/O ligands. Thus, it was proposed that during activation of MCR, the thiolate sulfur of CoM is replaced by a O/N ligand, which is probably the CoM sulfonate or a water ligand.<sup>41</sup>

### E. RESONANCE RAMAN (RR) SPECTROSCOPY OF MCR

The spectroscopic results described above indicate that activation of MCR involves reduction of six-coordinate Ni(I) ox1 to six-coordinate Ni(I) red1 and replacement of the upper axial thiolate ligand with a N/O ligand. These conclusions still do not explain the requirement for a low potential reductant for the activation. First, Resonance Raman (RR) studies of the coenzyme will be described, then the spectra of the enzyme in several of

its important states. RR studies are key in providing a rationale for the puzzling redox requirement for the ox1 to red1 conversion.

In RR spectroscopy, vibrational spectra are obtained for modes that are coupled to an electronic excitation. RR spectroscopy has been extensively used to characterize the conformation and the axial-ligation state of tetrapyrrolic macrocycles.<sup>97,98</sup>  $F_{430}$  is an ideal candidate for RR studies since the  $\sim 400$  nm absorption band has such a high extinction coefficient and during the 1980s, several RR studies examined the Ni(II)-silent form of MCR and Ni(II)- $F_{430}$ .<sup>99-103</sup> For Ni<sup>II</sup> $F_{430}$ , the major vibrational bands observed upon excitation at  $\sim 430$  nm are at 1630, 1614, 1560, and 1384  $\text{cm}^{-1}$ , which are assigned to a six-coordinate complex, and at 1532, which is the only unambiguous signature for the four-coordinate complex.<sup>99-103</sup> Thus, it appears that Ni<sup>II</sup> $F_{430}$  equilibrates between four- and six-coordinate complexes in aqueous solution, although under certain conditions, only the six-coordinate complex is formed.<sup>99,100,103</sup> This ability to switch between four- and six-coordinate geometry for  $F_{430}$  in solution gives rise to temperature-dependent resonance Raman, optical, and X-ray absorption spectra. At temperatures below 250 K, in aqueous solution (or in methanol or ethanol) and without coordinating ligands, the six-coordinate *bis*-aquo form of the coenzyme predominates; whereas, at higher temperatures, solutions contain both four- and six-coordinate species in a dynamic equilibrium.<sup>100</sup> In solvents with strong electron-withdrawing substituents such as 2,2,2-trifluoroethanol and 2-mercaptoethanol, the four-coordinate form is the major form. Scott called attention to what he termed a facile ligand exchange and considered this to be important for the MCR mechanism.<sup>100</sup> In the presence of excess cyanide,

Distance (Å)	Ni(II) MCR-sil Crystal	Ni(II) MCR-ox1sil Crystal	Ni(II) MCR-sil EXAFS	Red1 EXAFS	Ox1 EXAFS	Ox1-sil EXAFS
4 Ni-N	2.08	2.08	2.076	2.062	2.060	2.054
Axial Ni-N/O	1 @ 2.1 (Gln) 1 @ 2.1 (R-SO <sub>3</sub> )	1 @ 2.1 (Gln) -	2 @ 2.158	1 @ 2.252	-	1 @ 2.277
Axial Ni-S	-	2.4 (CoM)	-	-	1 @ 2.381	1 @ 2.338
BVA	1.9	1.8	1.8	1.4	1.4	1.9

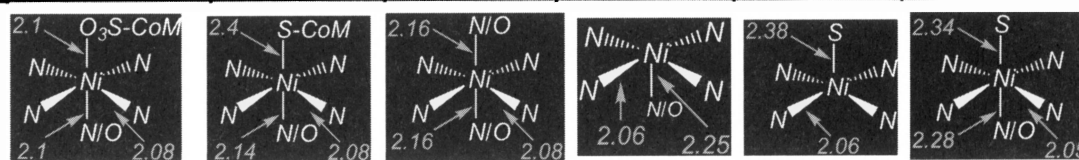


Figure 12. Summary of EXAFS results for MCR states.

pyridine, or 1-methylimidazole, these strong ligands coordinate to both axial positions, eliciting a 5–10 nm red shift in the 430 nm optical absorption band and approximately 30 cm<sup>-1</sup> shifts in the high-frequency Raman lines.<sup>99</sup> It is interesting that generation of a di-cyano-F<sub>430</sub> complex elicits a maximum of a 10 nm shift in the optical absorption band whereas, as discussed below, conversion of ox1 to red1 results in a 40 nm shift.

RR studies have been performed of F<sub>430</sub> in the Ni(I), Ni(II), and Ni(III) states and of MCR in several states (Figure 13). Each of these states exhibits similar RR features; however, the relative intensities of certain RR bands vary and there are oxidation-state shifts, especially in the region above 1350 cm<sup>-1</sup>. As described above, the six-coordinate Ni<sup>II</sup>F<sub>430</sub> complex displays bands at 1630, 1614, \*1560, \*1532 (four-coordination marker), and \*1384 cm<sup>-1</sup>. The asterisks indicate bands that exhibit <sup>15</sup>N shifts, indicating that these modes have C=N character. The RR spectrum of Ni<sup>III</sup>F<sub>430</sub> exhibits bands that exhibit a 1/1 correspondence with those of Ni(II) at 1646, 1624, 1567, 1539, and 1403 cm<sup>-1</sup>, with no observable bands in the 1350–1390 cm<sup>-1</sup> region. Thus, oxidation of Ni-F<sub>430</sub> *upshifts* the highest-frequency Raman bands. Accordingly, reduction *downshifts* these bands. For Ni<sup>I</sup>F<sub>430</sub>, the first two bands are assigned at 1616 and 1593 cm<sup>-1</sup>. In the Ni(I) complex, there also is a band at 1375 cm<sup>-1</sup>, which appears to be analogous to the 1384 cm<sup>-1</sup> band of the Ni(II) complex. There also are bands at 1483 and 1462 cm<sup>-1</sup> that do not match with either the 1560 or 1532 bands of the Ni(II) complex, and hence would require a huge downshift of 80 to 100 cm<sup>-1</sup>, respectively. It seems likely that the 1483 and 1462 cm<sup>-1</sup> bands of Ni<sup>I</sup>F<sub>430</sub> are new features that gain resonance enhancement only in the Ni(I) complex. If this is correct, then 1560 cm<sup>-1</sup>

band of Ni<sup>II</sup>F<sub>430</sub> (1567 for Ni(III)) is absent from the spectrum of the Ni(I) complex. The absence of this band is of significant interest, especially in relation to the enzyme.

With the MCR<sub>silent</sub> form of the enzyme in the 1350–1700 cm<sup>-1</sup> region, there are bands at 1654, 1634, \*1574, \*1547, and \*1383 cm<sup>-1</sup>. It is interesting that most of these bands are shifted by ~15–20 cm<sup>-1</sup> relative to the Ni(II) coenzyme. The origin of this shift is not known, however, similar results are observed for the Ni(I) states. For MCR<sub>red1</sub>, bands are observed at 1631, 1604, 1493, and 1467 cm<sup>-1</sup>, which correspond to the bands at 1616, 1593, 1483, 1462 cm<sup>-1</sup> bands of Ni<sup>I</sup>F<sub>430</sub>. Both MCR<sub>red1</sub> and Ni<sup>I</sup>F<sub>430</sub> exhibit a band at 1375 cm<sup>-1</sup>. Again, the four highest-frequency bands of the enzyme are at higher frequencies than those of the coenzyme. For MCR<sub>ox1</sub>, bands are observed at 1633, 1613 cm<sup>-1</sup>, 1560, 1547 cm<sup>-1</sup>, a broad feature near 1464 cm<sup>-1</sup>, and weak band at 1384 cm<sup>-1</sup>. Thus, the RR spectra of MCR<sub>red1</sub> (and Ni<sup>I</sup>F<sub>430</sub>) differ significantly from those of MCR<sub>ox1</sub> and MCR<sub>silent</sub> (and Ni(II) and Ni(III) states of F<sub>430</sub>); the \*1574 and \*1547 cm<sup>-1</sup> bands in the RR spectrum of MCR<sub>red1</sub> (and isolated Ni<sup>I</sup>F<sub>430</sub>) do not exhibit clear analogs for the modes that are observed for both MCR<sub>ox1</sub> and MCR<sub>silent</sub>.

It was proposed that the marked differences in the spectra of Ni<sup>I</sup>F<sub>430</sub> and Ni<sup>I</sup>MCR<sub>red1</sub> results from two-electron reduction of an imino bond in ring B or D of the coenzyme, which would decrease the conjugation of the coenzyme by one double bond (Figure 14). This explanation also rationalizes the previously puzzling blue shift in the absorption maximum of MCR<sub>red1</sub> (and Ni<sup>I</sup>F<sub>430</sub>) by nearly 40 nm relative to that of MCR<sub>ox1</sub> or the Ni(II) states (see Figure 15). Thus, the blue shift appears to be derived from ligand, not metal-centered, chemistry.

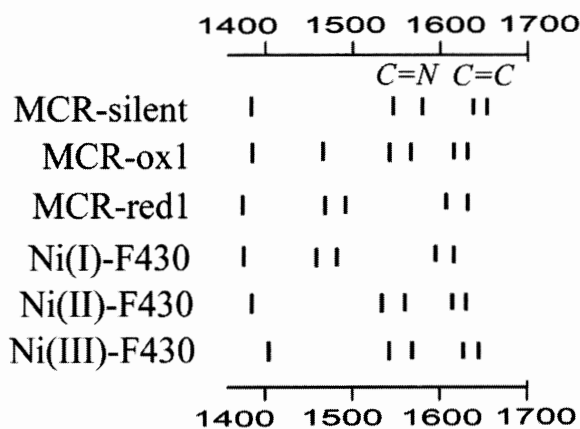


Figure 13. RR studies of F<sub>430</sub> in the Ni(I), Ni(II), and Ni(III) states.

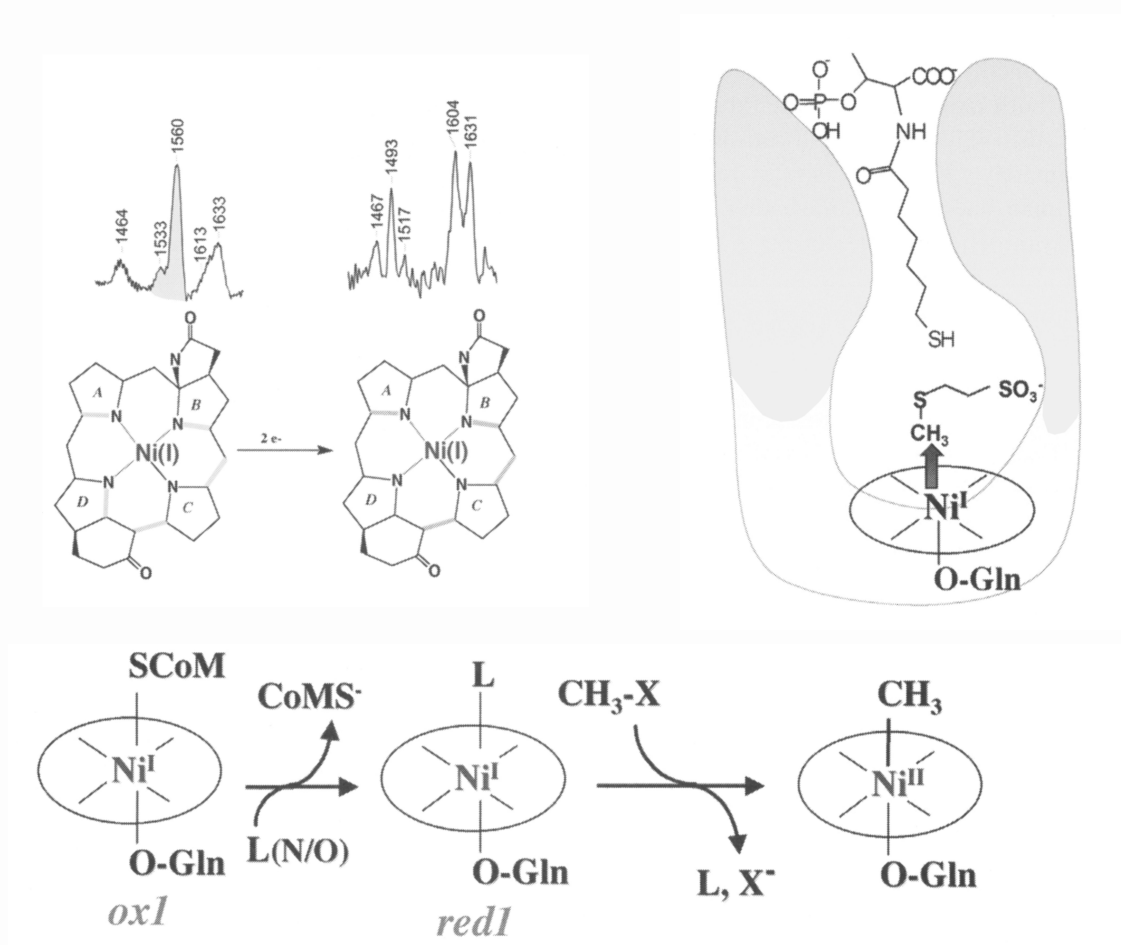


Figure 14. Proposed Activation Mechanism includes ligand switch and ring reduction.

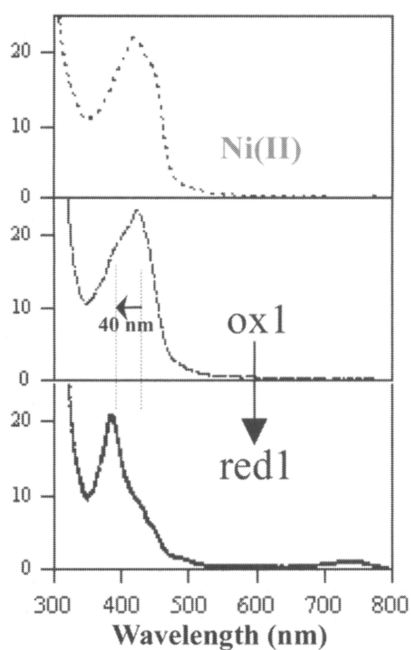


Figure 15. UV-visible spectra of MCR in various states. Modified from Becker and Ragsdale.<sup>66</sup>

### F. SPECTROSCOPY OF $MCR_{ox1}$ VERSUS $MCR_{red1}$

A variety of spectroscopic bullets have been aimed at various states of MCR, especially those that are important in catalysis—namely,  $ox1$  and  $red1$ . It is clear that these two states contain Ni(I) and that reduction by a low potential electron donor is required to convert the “ready”  $ox1$  to the “active”  $red1$  state. Thus, this cannot be a metal-centered reduction. XAS studies indicate that both states (and also the Ni(II)-silent state) are six-coordinate and that there is a provocative ligand switch from a thiolate (in  $ox1$ ) to a N/O in  $red1$ . Presumably, this switch places an exchange labile ligand in position which is to be removed during catalysis, perhaps in the transition state of the reaction as the putative methyl-Ni intermediate is formed. UV-visible and RR studies provided the shocking revelation that the tetrapyrrole ring of  $F_{430}$ , already the most reduced tetrapyrrole known in nature, likely undergoes a two-electron reduction.

What poises MCR<sub>ox1</sub> in particular toward reductive activation? Perhaps the upper axial thiolate ligand at the base of a highly protected cavity in the protein, with its propensity to delocalize the electron density into the metal center, is uniquely qualified to direct the electrons to the terminal bond of the extended pi-network. In solution, the coenzyme is freely accessible and would not require the participation of the thiolate. We speculated that catalysis may not even be metal centered, but that the macrocycle may itself participate in catalysis.<sup>41</sup> If the reduction of the macrocycle is reversible, the two electrons from the ring could be directed to the methyl group during the formation of methane. On the other hand, we have not observed a 30 nm red shift during transient kinetic analysis of methane formation, which may indicate that ring reduction–oxidation is not part of the catalytic cycle, but is only necessary for activation of the enzyme. Another possibility is that the oxidized ring (ox1-like) is a transient intermediate that is rapidly re-reduced to MCR<sub>red1</sub>, which would be the predominant state during catalysis. These questions will be addressed with the following sections on the reaction mechanism of MCR.

### G. OTHER RED STATES OF MCR

Thauer has defined several states of MCR; and MCR<sub>red1a</sub> is most probably the active enzyme without substrates and products bound, while MCR<sub>red1m</sub> is defined as the enzyme-methyl-CoM complex and MCR<sub>red1c</sub> (and another distinct state called red2) is the enzyme-CoM complex. Thauer noted that MCR<sub>red1c</sub> and MCR<sub>red2</sub> do not participate in the catalytic cycle since coenzyme M, which induces the red1c and red2 signals is not a substrate or a product of the MCR-catalyzed reaction.

### V. Mechanism of Methane Formation by MCR

MCR catalyzes methane formation from methyl-SCoM and CoBSH (Eq. 1, above). In this reaction, CoBSH is the electron donor<sup>11</sup> and has been proposed to be the proton donor.<sup>79</sup> Methane and the mixed disulfide CoBS-SCoM are the products of the reaction. The requirement for the Ni(I)-MCR<sub>red1</sub> form of Factor F<sub>430</sub> for catalysis<sup>65</sup> has been explained by the involvement of a methyl-Ni intermediate as the direct precursor of methane. It is

proposed that the methyl group of methyl-SCoM, possibly complexed with CoBSH (see below), suffers nucleophilic attack by Ni(I) to form a methyl-Ni species, which undergoes protonolysis to form methane.<sup>79</sup>

## A. STEADY STATE AND PRESTEADY-STATE KINETIC STUDIES

### 1. Steady-State Kinetics

Steady-state kinetic<sup>62,104,105</sup> and crystallographic studies<sup>15</sup> support an ordered mechanism in which first methyl-SCoM and then CoBSH must bind before methane is formed (see<sup>79</sup> for review) (Figure 16). F<sub>430</sub> forms the base of a narrow well (30 Å long × 6 Å diameter) that neatly accommodates the two substrates (Figure 17). CoBSH binds at the top of the well with its phosphate group at the upper lip and thiol about 9 Å from the Ni site. The ternary complex mechanism shown in Figure 16 is also supported by steady-state experiments in which the integrated form is the Michaelis-Menten equation is used.<sup>105</sup>

The Michaelis parameters for a variety of substrates and inhibitors of MCR are given in Table 1. Methyl-CoM, the simplest coenzyme known, has a  $K_m$  value ranging from 0.6 to 5.4 mM.<sup>62,104,105</sup> The higher values are in accord with transient kinetics studies.<sup>105</sup> The  $K_m$  value for CoBSH is much lower, from 0.1 to 0.3 mM.<sup>62,104</sup> The  $k_{cat}$  value, correcting to 1.0 spin/mol enzyme, is 250 s<sup>-1</sup> (100 U mg<sup>-1</sup>) at 60 °C.<sup>65</sup> The value of  $k_{cat}/K_m$  for methyl-SCoM has been independently determined to be 40 mM<sup>-1</sup> s<sup>-1</sup>,<sup>105</sup> which agrees with the  $K_m$  and  $V_{max}$  values.

Addition of or subtraction of even a single methylene group to CoBSH causes a 100-fold loss of activity;<sup>62</sup> however, these compounds serve as strong inhibitors. CoBS-SCoM is a strong product inhibitor, with an apparent inhibition constant of 0.6 mM.<sup>62</sup> Therefore, the MCR reaction is enhanced by including hydroxocobalamin plus Ti(III)citrate in the reaction mixture, which forms cob(I)alamin, a catalyst for reducing the disulfide bonds of CoBS-SCoB, CoBS-SCoM, and CoMS-SCoM.<sup>52,61</sup> The  $K_m$  for hydroxocobalamin is 0.2 mM.<sup>105</sup> At low concentrations of hydroxocobalamin, the reaction is limited by dissociation of the heterodisulfide from the active site.<sup>105</sup> It is clear that the

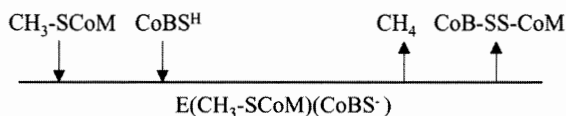
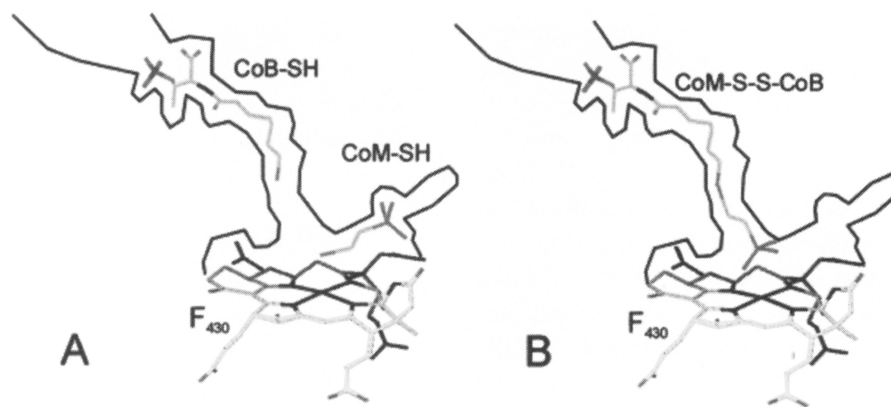


Figure 16. Cleland nomenclature for the ordered ternary complex mechanism of MCR.



**Figure 17.** Schematic of the ternary substrate and product complexes based on structures of the  $MCR_{ox1}$  and red1 states (from Mahler et al.<sup>84</sup>).

effect of hydroxocobalamin is simply to catalyze heterodisulfide reduction and that there is no direct stimulatory effect on MCR itself.

## B. PRESTEADY-STATE KINETIC STUDIES

Only one transient kinetic study of MCR has been reported.<sup>105</sup> The author wished to narrow the choices to Class I or Class II mechanisms (Figure 18), which can be distinguished by the role of CoBSH in the reaction mechanism. In the Class II mechanism, CoBSH is required for the cleavage of the C–S bond of methyl-SCoM; however, in the class I mechanism, it is not. The question can be most easily answered by single turnover kinetic studies using the chemical quench technique with radioactive  $^{14}C$ -methyl-SCoM as the substrate. In this method, a highly concentrated solution of MCR is reacted with limiting amounts of one substrate, CoBSH in this case, the reaction is quenched with acid, and the loss of radioactivity from the solution is followed.

In the Class II mechanism, a single turnover of methane formation requires CoBSH; in contrast, the class I mechanism predicts that the first turnover of methane can occur in the absence of CoBSH. Our results demonstrate that absolutely no methane is formed in the absence of CoBSH. Performing the proper experiment was compromised because MCR always has CoBSH bound. Thus, the amount of bound CoBSH was determined and it was found that the amount of acid-labile methyl groups equals the amount of bound CoBSH. Thus, CoBSH is required for even a single turnover of methane formation, suggesting that CoBSH is integrally involved in the steps leading up to C–S bond cleavage. This is inconsistent with the Class II mechanism and supports the Class I mechanism.

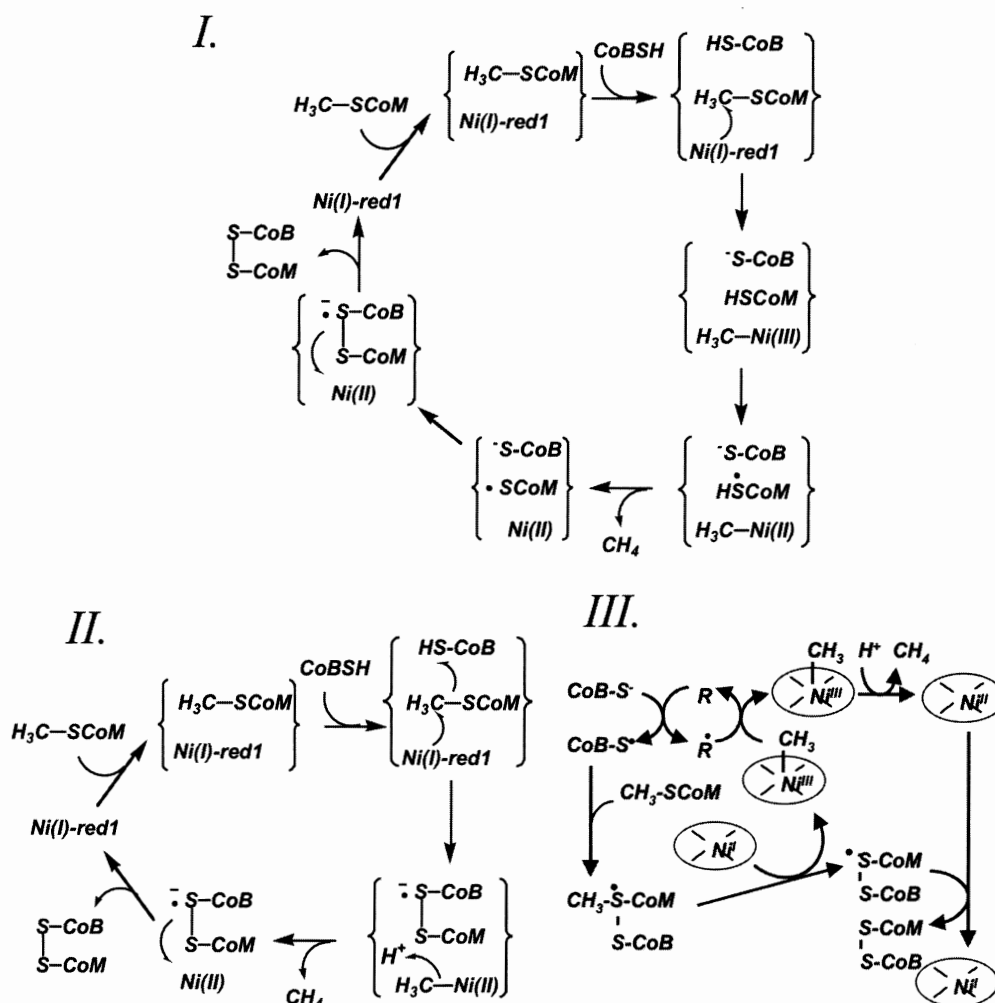
## C. MECHANISMS OF METHANE FORMATION

### 1. Mechanisms Involving a Methyl-Ni Intermediate

Figure 18 describes a proposed mechanism for methane formation.<sup>79</sup> In Mechanism I, Ni(I)-red1 binds both substrates and catalyzes an  $S_N2$ -type displacement of the methyl group of methyl-CoM to form a methyl-Ni(III) intermediate. C–S bond cleavage is assumed to accompany proton transfer, perhaps from CoBSH, to CoM. Thauer has proposed that methyl-Ni(III), a highly oxidizing species, reacts with the immediate product of this reaction to generate a cationic thiy radical on CoM and methyl-Ni(II). Protonolysis of the methyl-Ni species generates methane and Ni(II). The next step is proposed to be reaction between the thiy radical and the  $CoBS^-$  anion, which generates a disulfide anion radical, which is a strong reductant that can reduce Ni(II) back to the active Ni(I)-red1 state and generate the heterodisulfide  $CoBS-S-CoM$ . A concerted reaction (Mechanism II) can also be considered, which omits several uncharacterized radical species.

A different type of mechanism (Mechanism III) can be considered in which a methylsulfuranyl radical species is the direct precursor of the methyl-Ni intermediate, as proposed by Berkessel.<sup>106</sup> For this to be feasible, a one electron oxidant must be present to generate the  $CoBS^{\bullet}$  radical intermediate. Perhaps a thioglycine residue in the active site accomplishes this oxidation. According to this scenario, reduction of the thioglycine would generate a thioketyl radical, which has been suggested to play a role in the MCR reaction.<sup>67</sup> Thus, in this mechanism, generation of the “R $^{\bullet}$ ” radical is linked to generating  $CoB-S^{\bullet}$ . In this alternative mechanism, the redox potential for the R/R $^{\bullet}$  couple should be fairly positive since the redox potentials for





**Figure 18.** Mechanistic classes for the MCR reaction. In Mechanistic Class I, the C–S bond of methyl-S-CoM is cleaved after CoBSH binds, but before it reacts. Also in this class would be mechanism in which CoBSH binds after C–S bond cleavage. In Mechanisms II and III, CoBSH is involved directly in C–S bond cleavage, similar to the Berkessel mechanism.<sup>106</sup> Mechanism II is a concerted reaction, otherwise similar to mechanism I. Mechanism III involves attack of CoBSH on methyl-S-CoM to activate the methyl group before the methyl-S bond is cleaved. “R” is a possible radical species that is responsible for oxidation of CoBSH to a radical; possibly this is the thioglycine/thioethyl radical couple. In the Class II Mechanism,

the methyl-Ni(III)/methyl-Ni(II) and the thiol radical/thiol couples are above +0.5 V.

Mechanism III is supported by several studies. Jaun<sup>82</sup> and Berkessel<sup>106</sup> suggested similar mechanism, in which a methyl donors (e.g., methyl iodide, methyl tosylate, methyl dialkyl sulfonium)methyl sulfuranyl radical intermediate precedes the methylnickel species, because methyl thioethers related to and including the natural substrate, methyl-S-CoM, do not react directly with Ni<sup>I</sup>F<sub>430</sub>.<sup>82</sup> Additionally, a radical pair, consisting of the Ni(I) state of F<sub>430</sub> and a thiol radical, reacts with a methyl thioether to yield methane and the corresponding disulfide,<sup>107</sup> which establishes an important chemical precedent for this class of mechanisms. A third line of investigation that supports this type of mechanism is

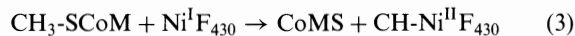
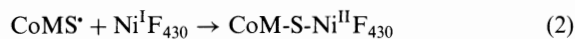
based on presteady-state studies, described below. Chemical quench studies demonstrate that a single turnover of methyl-S-CoM to methane requires CoBSH.<sup>105</sup> Since an acid quench that denatures the enzyme was used in the single turnover studies, all forms of bound and acid-labile methyl groups should be released as methane, which indicates that cleavage of the C–S bond of methyl-S-CoM requires CoBSH. Furthermore, when MCR was reacted under single turnover conditions with “homo-CoBSH” (mercaptoHEXanoylthreonine phosphate), a substrate analog, called CoB<sub>6</sub>SH, which is a very slow substrate in steady-state turnover, a single exponential decay was observed with a rate constant for methane formation that is 440-fold slower than with CoBSH. Presuming

that the acid quench supplies the proton required for generation of methane from its bound precursor, these results are inconsistent with Mechanism I, which predicts that the first turnover of methane formation should occur at the same rate with CoBSH or CoB<sub>6</sub>SH. In agreement with Mechanisms II and III, MCR absolutely requires the slow substrate analog to form methane, even when the rate of methanogenesis is decreased by 10<sup>3</sup>-fold.

All three mechanisms are consistent with stereochemical studies in which a net inversion of configuration is observed when ethyl-SCoM is reduced to ethane.<sup>108</sup> The inversion is expected to occur when the methyl-Ni intermediate is formed; whereas, the subsequent protonolysis should proceed with retention of configuration, resulting in net inversion.

## 2. A Mechanism Lacking Methyl-Ni Based on Density Functional Theory Calculations

All the above mechanisms include a hypothetical methylnickel intermediate. There is chemical evidence for this hypothesis. The Ni(I) form of the pentamethyl ester of F<sub>430</sub> reacts with activated methyl donors (e.g., methyl sulfonium ions and methyl iodide) to yield methane through protonation of a methylnickel intermediate.<sup>109–111</sup> It was proposed, on the basis of density functional theory calculations, that there is no methylnickel intermediate in the MCR mechanism.<sup>112</sup> Instead, it is proposed that Ni(I) can induce formation of a CH<sub>3</sub><sup>•</sup> radical from methyl-SCoM that is quenched by H-atom transfer from CoBSH. The reason for excluding the methylnickel intermediate is that the C–S bond strength of methyl-SCoM was calculated to be 70 kcal/mol, while the C(methyl)-Ni bond is calculated to be 25 kcal/mol. Therefore, conversion of methyl-SR to methyl-Ni would be endothermic by 45 kcal/mol. Furthermore, they assume that the starting state contains a Ni–S bond (which is true actually only for the inactive ox1 state). The Ni–S bond strength in reaction 2 is 46 kcal/mol. The basis of the argument is that for methyl transfer from S to Ni to occur, reaction 3 must be at least as endothermic as the difference between the bond strengths of methyl-S and methyl-Ni. For the calculation, the F<sub>430</sub> structure was truncated to omit all the pendant groups, the lower axial glutamine ligand was replaced with acetamide, CoBSH was simplified to methanethiol, and the only amino acids included in the active site were the two tyrosines residues (which were replaced with methanol).



The proposed mechanism (Figure 19) based on these theoretical studies begins with methyl-CoM bound near a square planar Ni(I)-F<sub>430</sub> near two tyrosine residues. As described above, spectroscopic studies indicate that active red1 state is six-coordinate. *Step 1* involves cleavage of the C–S bond of methyl-CoM to generate a methyl radical and a thiyl radical on CoM, which is proposed to accept an electron from Ni(I) to generate Ni(II) and the CoM-S<sup>−</sup> anion. The influence of CoBSH in the active site with a 6.2 Å S–S bond distance is proposed to lower the C–S bond dissociation energy from 70 to 32.5 kcal/mol. An additional H bonding interaction from two tyrosine residues to neutralize and stabilize the negative charge on the CoM thiolate once the methyl radical is released is proposed to lower this energy barrier by an additional 6.6 kcal/mol. Thus, in this environment, the energy barrier for cleavage of the C–S bond is estimated to be 19.5 kcal/mol, which should make Step 1 the rate limiting step in methane formation. A strong (39 kcal/mol) Ni(II)-SCoM bond is expected to occur during this reaction. *Step 2* involves H atom abstraction from CoBSH to form methane and a thiyl radical on CoB. This step was calculated to have a very small energy barrier and thus, to occur quite rapidly relative to Step 1. This step is expected to lead to inversion of stereochemistry at carbon. If so, the H-atom transfer to the methyl radical must occur before the methyl group has a chance to rotate in the active site. Steps 3 and 4 are barely discussed in.<sup>112</sup> *Step 3* involves formation of a S–S bond between CoBS<sup>•</sup> and CoMS<sup>−</sup>, which would form a disulfide anion radical and *Step 4* involves reduction of Ni(II) back to the active Ni(I) state, release of products, and binding of substrates.

The major stated objection to the methyl-Ni intermediate is the high thermodynamic barrier to C–S bond cleavage relative to the low barrier to formation of the methyl-Ni bond.<sup>112</sup> However, there are similar barriers to the formation of well-established methyl-Co(III) intermediates in the mechanisms of cobalamin-dependent methyltransferases such as methionine synthase, methyl-CoM methyltransferase, and a corrinoid iron-sulfur protein methyltransferase.<sup>113</sup> The situation with methionine synthase and the methyl-CoM methyltransferase is particularly instructive. Similar to MCR, these reactions involve cleavage of high energy methyl-N and methyl-S bonds. In the methyltransferases, the key is to activate the methyl group through coordination to zinc or by protonation.

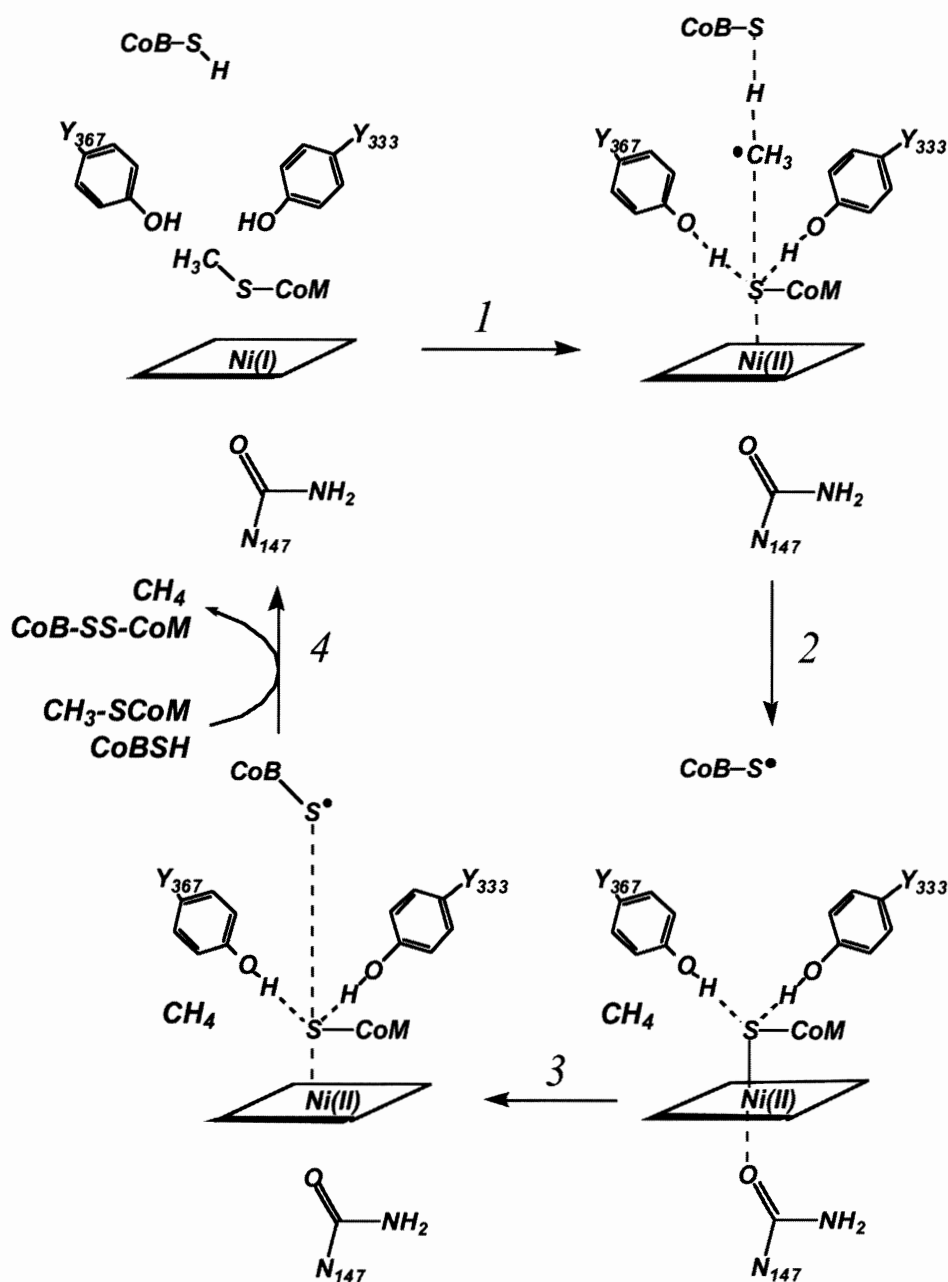


Figure 19. Proposed mechanism of methane formation based on Figure 9 of Pelmenchikov et al.<sup>112</sup>

### 3. Other Possible Mechanisms and Mechanistic Considerations

Two aspects of MCR<sub>red1</sub> may be important for catalysis. The additional two electrons in the ring might allow greater flexibility of Coenzyme F<sub>430</sub> and could even serve as a transient electron source for the two-electron reduction of methyl-S-CoM to methane. Furthermore, the upper axial "oxo/nitrogen" Ni(I) ligand may be relatively exchange labile, which would poise the Ni ion for interaction with the methyl group and for formation of the proposed methyl-Ni

intermediate. Preliminary results indicate this to be the case (Singh, Horng, & Ragsdale, in preparation). There are several possible mechanisms by which this intermediate could be formed. A dissociative transition state in which the upper axial ligand is removed before Ni(I) and the methyl group interact is feasible. Work by Meyerstein and coworkers suggests the possibility of an associative mechanism in which both the upper axial O/N ligand remains as the methyl-Ni bond is formed.<sup>114-116</sup> In the latter scenario, methyl transfer could be viewed as a ligand exchange reaction.

## VI. Summary and Perspectives for the Future

MCR contains a nickel macrocycle at its active center, which is the most highly reduced tetrapyrrole known. It catalyzes a reaction between two novel coenzymes to make methane, a widely used energy source and a potent greenhouse gas. Biochemical research has uncovered previously unknown post-translational modifications of amino acids in the MCR active site; however, the rationale for these unusual alterations is not yet clear. X-ray crystallographic studies have provided snapshots of the enzyme and its interactions with substrates and products. Complementing these atomic level insights with spectroscopic studies of the catalytically important forms of the enzyme have exposed some puzzling enigmas. For example, why is reduction of one Ni(I) state of the enzyme to another Ni(I) state necessary for catalysis and what is actually being reduced? Spectroscopic studies indicate that we must broaden our outlook beyond a "nickel-centric" view of activation and perhaps of catalysis. Spectroscopic and theoretical studies suggest that the Ni(I) ion may be a bystander in at least part of the reaction and activation mechanisms. Although MCR remains one of the most challenging enzymes because of its extreme lability and oxygen sensitivity, new doors are opening. Scientists have learned how to generate enzyme with sufficient activity to pursue mechanistic studies. It is now possible to perform site-directed mutagenesis of methanogenic enzymes.<sup>25,26</sup> Application of these techniques to MCR will greatly influence future mechanistic studies.

Many mechanistic questions remain unanswered. What are the elementary steps in the MCR catalytic cycle? Are sulfur radicals involved in the mechanism? How is the very stable C-S bond of methyl-SCoM labilized and the methyl group activated? What is the immediate precursor of methane? Is it the organometallic methyl-Ni intermediate, a free radical poised between the thiol groups of the two substrates, or does the tetrapyrrole itself participate in the reduction? The use of Ti(III)citrate to activate MCR is a useful tool, however, it is important to determine how the cell generates the active form of MCR. To answer this question, we will need to readdress the complex system studied by Ralph Wolfe which includes H<sub>2</sub>/hydrogenase and ATP.

### ACKNOWLEDGMENTS

Donald Becker, Yih-Chern Horng, and Kuljeet Singh performed the work on MCR in SWR's laboratory that is described here. I thank them for their dedication and

for their insights, which have made studying methanogenesis extremely stimulating. I have enjoyed the many productive and delightful interactions with my collaborators, David Bocian, Brian Hoffman, Mike Maroney, and Josh Telser on this project. I am grateful to Rolf Thauer for the many stimulating discussions, which have influenced my thinking about the MCR mechanism, and for his willingness to share unpublished information from his laboratory. I thank the Department of Energy for supporting our studies of methanogenesis.

This review is dedicated to Ralph S. Wolfe, who has made seminal contributions to the microbiology and biochemistry of methanogenesis and to the study of methyl-CoM reductase and its coenzyme F<sub>430</sub>. His aphorisms and scholarship have guided and inspired the next generation of "methanogen-ists." I acted on his recommendation about 10 years ago to enter this field and have no regrets.

### REFERENCES

1. Söhngen, N. L. *Recl. Trav. Chim. Pays Bas.* **1910**, *29*, 238-250.
2. Hungate, R. E. In *Methods in Microbiology*. Norris, J. R., Ribbons, D. W., Eds.; Academic Press, Inc.: New York, **1969**; Vol. 3B, Chapter IV; p. 117.
3. Barker, H. A. *Bacterial Fermentations*; Wiley: New York, N.Y., **1956**.
4. Balch, W. E.; Fox, G. E.; Magrum, L. J.; Woese, C. R.; Wolfe, R. S. *Microbiol. Rev.* **1979**, *43*, 260-296.
5. Zeikus, J. G.; Wolfe, R. S. *J. Bacteriol.* **1972**, *109*, 707-715.
6. Schimel, J. *Nature* **2000**, *403*, 375, 377.
7. Wolin, M. J. *Science* **1981**, *213*, 1463-1468.
8. Immig, I.; Demeyer, D.; Fiedler, D.; Van Nevel, C.; Mbanzamihigo, L. *Arch. Tierernähr.* **1996**, *49*, 363-370.
9. Gunsalus, R. P.; Romesser, J. A.; Wolfe, R. S. *Biochem.* **1978**, *17*, 2374-2377.
10. DiMarco, A. A.; Bobik, T. A.; Wolfe, R. S. *Ann. Rev. Biochem.* **1990**, *59*, 355.
11. Ellermann, J.; Kobelt, A.; Pfaltz, A.; Thauer, R. K. *FEBS Lett.* **1987**, *220*, 358-362.
12. Diekert, G.; Klee, B.; Thauer, R. K. *Arch. Microbiol.* **1980**, *124*, 103-106.
13. Diekert, G.; Jaenchen, R.; Thauer, R. K. *FEBS Lett.* **1980**, *119*, 118-120.
14. Whitman, W. B.; Wolfe, R. S. *Biochem. Biophys. Res. Commun.* **1980**, *92*, 1196-1201.
15. Ermler, U.; Grabarse, W.; Shima, S.; Goubeaud, M.; Thauer, R. K. *Science* **1997**, *278*, 1457-1462.
16. Rospert, S.; Linder, D.; Ellermann, J.; Thauer, R. K. *Eur. J. Biochem.* **1990**, *194*, 871-877.
17. Pihl, T. D.; Sharma, S.; Reeve, J. N. *J. Bacteriol.* **1994**, *176*, 6384-6391.
18. Morgan, R. M.; Pihl, T. D.; Nolling, J.; Reeve, J. N. *J. Bacteriol.* **1997**, *179*, 889-898.
19. Reeve, J. N.; Nolling, J.; Morgan, R. M.; Smith, D. R. *J. Bacteriol.* **1997**, *179*, 5975-5986.
20. Vermeij, P.; Pennings, J. L. A.; Maassen, S. M.; Keltjens, J. T.; Vogels, G. D. *J. Bacteriol.* **1997**, *179*, 6640-6648.

21. Pennings, J. L.; Keltjens, J. T.; Vogels, G. D. *J. Bacteriol.* **1998**, *180*, 2676–2681.
22. Vermeij, P.; van der Steen, R. J.; Keltjens, J. T.; Vogels, G. D.; Leisinger, T. *J. Bacteriol.* **1996**, *178*, 505–510.
23. Bokranz, M.; Bäumner, G.; Allmansberger, R.; Ankel-Fuchs, D.; Klein, A. *J. Bacteriol.* **1988**, *170*, 568.
24. Stroup, D.; Reeve, J. N. *Biochim. Biophys. Acta* **1993**, *1203*, 175–183.
25. Meuer, J.; Kuettner, H. C.; Zhang, J. K.; Hedderich, R.; Metcalf, W. W. *Proc. Natl. Acad. Sci. U.S.A.* **2002**.
26. Zhang, J. K.; White, A. K.; Kuettner, H. C.; Boccuzzi, P.; Metcalf, W. W. *J. Bacteriol.* **2002**, *184*, 1449–1454.
27. Gunsalus, R. P.; Wolfe, R. S. *FEMS Microbiol. Lett.* **1978**, *3*, 191–193.
28. Ellefson, W. L.; Whitman, W. B.; Wolfe, R. S. *Proc. Natl. Acad. Sci. U.S.A.* **1982**, *79*, 3707–3710.
29. Diekert, G.; Konheiser, U.; Piechulla, K.; Thauer, R. K. *J. Bacteriol.* **1981**, *148*, 459–464.
30. Dixon, N. E.; Gazzola, C.; Blakeley, R. L.; Zerner, B. *J. Am. Chem. Soc.* **1975**, *97*, 4131–4133.
31. Friedrich, B.; Heine, E.; Finck, A.; Friedrich, C. G. *J. Bacteriol.* **1981**, *145*, 1144–1149.
32. Kruger, H. J.; Huynh, B. H.; Ljungdahl, P. O.; Xavier, A. V.; Der Vartanian, D. V.; Moura, I.; Peck, H. D., Jr.; Teixeira, M.; Moura, J. J.; LeGall, J. *J. Biol. Chem.* **1982**, *257*, 14620–14623.
33. Friedrich, C. G.; Schneider, K.; Friedrich, B. *J. Bacteriol.* **1982**, *152*, 42–48.
34. Diekert, G. B.; Graf, E. G.; Thauer, R. K. *Arch. Microbiol.* **1979**, *122*, 117–120.
35. Drake, H. L.; Hu, S.-I.; Wood, H. G. *J. Biol. Chem.* **1980**, *255*, 7174–7180.
36. Pfaltz, A.; Juan, B.; Fassler, A.; Eschenmoser, A.; Jaenchen, R.; Gilles, H. H.; Diekert, G.; Thauer, R. K. *Helv. Chim. Acta* **1982**, *65*, 828–865.
37. Färber, G.; Keller, W.; Kratky, C.; Jaun, B.; Pfaltz, A.; Spinner, C.; Kobelt, A.; Eschenmoser, A. *Helv. Chim. Acta* **1991**, *74*, 697–716.
38. Friedmann, H. C.; Klein, A.; Thauer, R. K. In *Biosynthesis of Tetrapyrroles*. Jordan, P. M., Ed.; Elsevier Science Publishers: Amsterdam, **1991**; Chapter 4; pp. 139–154.
39. Thauer, R. K.; Bonacker, L. G. *Ciba Found Symp* **1994**, *180*, 210–222.
40. Hengerer, C.; Weiss, D. S.; Thauer, R. K.; Jahn, D. *Bioorg. Med. Chem.* **1996**, *4*, 1089–1095.
41. Tang, Q.; Carrington, P. E.; Horng, Y.-C.; Maroney, M. J.; Ragsdale, S. W.; Bocian, D. F. *J. Am. Chem. Soc.* **2002**, in press.
42. McBride, B. C.; Wolfe, R. S. *Biochem.* **1971**, *10*, 2317–2324.
43. Taylor, C. D.; Wolfe, R. S. *J. Biol. Chem.* **1974**, *249*, 4879–4885.
44. Taylor, C. D.; McBride, B. C.; Wolfe, R. S.; Bryant, M. P. *J. Bacteriol.* **1974**, *120*, 974–975.
45. Allen, J. R.; Clark, D. D.; Krum, J. G.; Ensign, S. A. *Proc. Nat. Acad. Sci. USA* **1999**, *96*, 8432–8437.
46. Krum, J. G.; Ensign, S. A. *J. Bacteriol.* **2001**, *183*, 2172–2177.
47. Gunsalus, R. P.; Wolfe, R. S. *J. Biol. Chem.* **1980**, *255*, 1891–1895.
48. Noll, K. M.; Rinehart, K. L., Jr.; Tanner, R. S.; Wolfe, R. S. *Proc. Nat. Acad. Sci. USA* **1986**, *83*, 4238–4242.
49. Noll, K. M.; Wolfe, R. S. *Biochem. Biophys. Res. Commun.* **1986**, *139*, 889–895.
50. Noll, K. M.; Donnelly, M. I.; Wolfe, R. S. *J. Biol. Chem.* **1987**, *262*, 513–515.
51. Bobik, T. A.; Olson, K. D.; Noll, K. M.; Wolfe, R. S. *Biochem. Biophys. Res. Commun.* **1987**, *149*, 455–460.
52. Hedderich, R.; Thauer, R. K. *FEBS Lett.* **1988**, *234*, 223–227.
53. Deppenmeier, U.; Blaut, M.; Mahlmann, A.; Gottschalk, G. *Proc. Natl. Acad. Sci., USA* **1990**, *87*, 9449–9453.
54. Hedderich, R.; Berkessel, A.; Thauer, R. K. *Eur. J. Biochem.* **1990**, *193*, 255–261.
55. Heiden, S.; Hedderich, R.; Setzke, E.; Thauer, R. K. *Eur. J. Biochem.* **1993**, *213*, 529–535.
56. Simianu, M.; Murakami, E.; Brewer, J. M.; Ragsdale, S. W. *Biochem.* **1998**, *37*, 10027–10039.
57. Abken, H. J.; Tietze, M.; Brodersen, J.; Bäumer, S.; Beifuss, U.; Deppenmeier, U. *J. Bacteriol.* **1998**, *180*, 2027–2032.
58. Murakami, E.; Deppenmeier, U.; Ragsdale, S. W. *J. Biol. Chem.* **2001**, *276*, 2432–2439.
59. Graupner, M.; Xu, H.; White, R. H. *Biochem.* **2002**, *41*, 3754–3761.
60. White, R. H. *Vitam. Horm.* **2001**, *61*, 299–337.
61. Rouviere, P. E.; Bobik, T. A.; Wolfe, R. S. *J. Bacteriol.* **1988**, *170*, 3946–3952.
62. Ellermann, J.; Hedderich, R.; Böcher, R.; Thauer, R. K. *Eur. J. Biochem.* **1988**, *172*, 669–677.
63. Rospert, S.; Böcher, R.; Albracht, S. P. J.; Thauer, R. K. *FEBS Lett.* **1991**, *291*, 371–375.
64. Albracht, S. P. J.; Ankel-Fuchs, D.; Böcher, R.; Ellermann, J.; Moll, J.; van der Zwann, J. W.; Thauer, R. K. *Biochim. Biophys. Acta* **1988**, *941*, 86–102.
65. Goubeaud, M.; Schreiner, G.; Thauer, R. K. *Eur. J. Biochem.* **1997**, *243*, 110–114.
66. Becker, D. F.; Ragsdale, S. W. *Biochem.* **1998**, *37*, 2639–2647.
67. Grabarse, W. G.; Mahler, F.; Duin, E. C.; Goubeaud, M.; Shima, S.; Thauer, R. K.; Lamzin, V.; Ermler, U. *J. Mol. Biol.* **2001**, *309*, 315–330.
68. Selmer, T.; Kahnt, J.; Goubeaud, M.; Shima, S.; Grabarse, W.; Ermler, U.; Thauer, R. K. *J. Biol. Chem.* **2000**, *275*, 3755–3760.
69. Maki, A. H.; Edelstein, N.; Davison, A.; Holm, R. H. *J. Am. Chem. Soc.* **1964**, *86*, 4580–4587.
70. Lovecchio, F. V.; Gore, E. S.; Busch, D. H. *J. Am. Chem. Soc.* **1974**, *96*, 3109–3118.
71. Renner, M. W.; Furenlid, L. R.; Stolzenberg, A. M. *J. Am. Chem. Soc.* **1995**, *117*, 293–300.
72. Stolzenberg, A. M.; Stershic, M. T. *J. Am. Chem. Soc.* **1988**, *110*, 5397–5403.
73. Stolzenberg, A. M.; Stershic, M. T. *J. Am. Chem. Soc.* **1988**, *110*, 6391–6402.
74. Wang, J.-F.; Kumar, K.; Margerum, D. W. *Inorg. Chem.* **1989**, *28*, 3481–3484.
75. Pilbrow, J. R. *Transition Ion Electron Paramagnetic Resonance*. Clarendon Press: Oxford, **1990**.
76. Bowmaker, G. A.; Boyd, P. D. W.; Campbell, G. K.; Hope, J. M.; Martin, R. L. *Inorg. Chem.* **1982**, *21*, 1152–1159.
77. Symons, M. C. R.; West, D. X. *J. Chem. Soc., Dalton Trans.* **1985**, 379–381.
78. Rospert, S.; Voges, M.; Berkessel, A.; Albracht, S. P. J.; Thauer, R. K. *Eur. J. Biochem.* **1992**, *210*, 101–107.
79. Thauer, R. K. *Microbiology Uk* **1998**, *144*, 2377–2406.
80. Holliger, C.; Pierik, A. J.; Reijerse, E. J.; Hagen, W. R. *J. Am. Chem. Soc.* **1993**, *115*, 5651–5656.
81. Telser, J. In *Structure and Bonding*. Williams, R. J. P., Ed.; Springer Verlag: Heidelberg, **1998**, Vol. 91; pp. 32–63.
82. Jaun, B. *Helvetica Chimica Acta* **1990**, *73*, 2209–2217.
83. Telser, J.; Horng, Y.-C.; Becker, D.; Hoffman, B.; Ragsdale, S. W. *J. Am. Chem. Soc.* **2000**, *122*, 182–183.
84. Mahler, F.; Grabarse, W.; Kahnt, J.; Thauer, R. K.; Duin, E. C. *J. Biol. Inorg. Chem.* **2002**, *7*, 101–112.
85. Telser, J.; Horng, Y. C.; Ragsdale, S. W.; Hoffman, B. M. unpublished.
86. Telser, J.; Fann, Y. C.; Renner, M. W.; Fajer, J.; Wang, S. K.; Zhang, H.; Scott, R. A.; Hoffman, B. M. *J. Am. Chem. Soc.* **1997**, *119*, 733–743.
87. Ragsdale, S. W.; Lindahl, P. A.; Münck, E. *J. Biol. Chem.* **1987**, *262*, 14289–14297.
88. Lappin, A. G.; Murray, C. K.; Margerum, D. W. *Inorg. Chem.* **1978**, *17*, 1630–1634.

89. Haines, R. I.; McAuley, A. *Inorg. Chem.* **1980**, *19*, 719–723.
90. Gore, E. S.; Busch, D. H. *Inorg. Chem.* **1973**, *12*, 1–3.
91. Zimmer, M.; Crabtree, R. H. *J. Am. Chem. Soc.* **1990**, *112*, 1062–1066.
92. Wang, Y. L.; Beach, M. W.; Pappenhagen, T. L.; Margerum, D. W. *Inorg. Chem.* **1988**, *27*, 4474–4472.
93. Davydov, R.; Valentine, A. M.; Komar-Panicucci, S.; Hoffman, B. M.; Lippard, S. J. *Biochem.* **1999**, *38*, 4188–4197.
94. Colpas, G. J.; Maroney, M. J.; Bagyinka, C.; Kumar, M.; Willis, W. S.; Suib, S. L.; Mascharak, P. K.; Baidya, N. *Inorg. Chem.* **1991**, *30*, 920–928.
95. Furenid, L. R.; Renner, M. W.; Smith, K. M.; Fajer, J. *J. Am. Chem. Soc.* **1990**, *112*, 1634–1635.
96. Furenid, L. R.; Renner, M. W.; Fajer, J. *J. Am. Chem. Soc.* **1990**, *112*, 8987–8989.
97. Spiro, T. G.; Li, X.-Y. In *Biological Applications of Raman Spectroscopy*. Spiro, T. G., Ed.; Wiley Interscience: New York, **1988**; Vol. III; pp. 1–38.
98. Procyk, A. D.; Bocian, D. F. *Annu. Rev. Phys. Chem.* **1992**, *43*, 465–496.
99. Shiemke, A. K.; Kaplan, W. A.; Hamilton, C. L.; Shelnut, J. A.; Scott, R. A. *J. Biol. Chem.* **1989**, *264*, 7276–7284.
100. Shiemke, A. K.; Shelnut, J. A.; Scott, R. A. *J. Biol. Chem.* **1989**, *264*, 11236–11245.
101. Shiemke, A. K.; Eirich, L. D.; Loehr, T. M. *Biochim. Biophys. Acta* **1983**, *748*, 143.
102. Shiemke, A. K.; Shelnut, J. A.; Scott, R. A. *J. Am. Chem. Soc.* **1988**, *110*, 1645.
103. Li, M. In *Chemistry*. University of Georgia: Athens, GA, **1993**.
104. Bonacker, L. G.; Baudner, S.; Mörschel, E.; Böcher, R.; Thauer, R. K. *Eur. J. Biochem.* **1993**, *217*, 587–595.
105. Horng, Y.-C.; Becker, D. F.; Ragsdale, S. W. *Biochem.* **2001**, *40*, 12875–12885.
106. Berkessel, A. *Biorganic Chem.* **1991**, *19*, 101–115.
107. Signor, L.; Knuppe, C.; Hug, R.; Schweizer, B.; Pfaltz, A.; Jaun, B. *Chemistry. A European Journal* **2000**, *6*, 3508–3516.
108. Ahn, Y.; Krzycki, J. A.; Floss, H. G. *J. Am. Chem. Soc.* **1991**, *113*, 4700–4701.
109. Lin, S.-K.; Jaun, B. *Helvetica Chimica Acta* **1991**, *74*, 1725–1738.
110. Lin, S.-K.; Jaun, B. *Helv. Chim. Acta* **1992**, *75*.
111. Jaun, B.; Pfaltz, A. *J. Chem. Soc. Chem. Commun.* **1988**, 1327, 293–294.
112. Pelmenschikov, V.; Blomberg, M. R. A.; Siegbahn, P. E. M.; Crabtree, R. H. *J. Am. Chem. Soc.* **2002**, *124*, 4039–4049.
113. Matthews, R. G. *Acc. Chem. Res.* **2001**, *34*, 681–689.
114. Goldstein, S.; Czapski, G.; van Eldik, R.; Shaham, N.; Cohen, H.; Meyerstein, D. *Inorg. Chem.* **2001**, *40*, 4966–4970.
115. Van Eldik, R.; Meyerstein, D. *Acc. Chem. Res.* **2000**, *33*, 207–214.
116. Shaham, N.; Cohen, H.; van Eldik, R.; Meyerstein, D. *J. Chem. Soc. Dalton* **2000**, 3356–3359.
117. Wackett, L. P.; Honeck, J. F.; Begley, T. P.; Wallace, V.; Orme-Johnson, W. H.; Walsh, C. T. *Biochem.* **1987**, *26*.
118. Olson, K. D.; Chmurkowska-Cichowlas, L.; McMahon, C. W.; Wolfe, R. S. *J. Bacteriol.* **1992**, *174*, 1007–1012.
119. Ellermann, J.; Rospert, S.; Thauer, R. K.; Bokranz, M.; Klein, A.; Voges, M.; Berkessel, A. *Eur. J. Biochem.* **1989**, *184*, 63–68.
120. Horng, Y. C.; Ragsdale, S. W. unpublished.
121. Howell, D. M.; Graupner, M.; Xu, H.; White, R. H. *J. Bacteriol.* **2000**, *182*, 5013–5016.
122. Telser, J.; Davydov, R.; Horng, Y. C.; Ragsdale, S. W.; Hoffman, B. M. *J. Am. Chem. Soc.* **2001**, *123*, 5853–5860.

# Structure, Reactions, and Functions of B<sub>12</sub> and B<sub>12</sub>-Proteins

68

BERNHARD KRÄUTLER AND SIGRID OSTERMANN

Institute of Organic Chemistry, University of Innsbruck, Innrain 52a, A-6020 Innsbruck, Austria

I. Introduction	229
II. B <sub>12</sub> : Structure and Reactivity	231
A. Crystallographic Structural Studies	231
1. Co(III)-Cobamides with Inorganic $\beta$ -Ligands	231
2. Incomplete Cobamides	233
3. Reduced B <sub>12</sub> -Derivatives	233
4. Organometallic B <sub>12</sub> -Derivatives	234
5. Trans-Effects	236
6. The "Upwards Folding" of the Corrin Ligand	237
B. Structural Studies of B <sub>12</sub> -Derivatives by Nuclear Magnetic Resonance (NMR) Spectroscopy	238
1. Early Studies with Cyano-Co(III)-Cobyrinates	238
2. Multidimensional NMR-Studies of B <sub>12</sub> -Structures in Solution	238
C. Other Methods Used for Structural Studies of B <sub>12</sub> -Derivatives	240
III. B <sub>12</sub> -Electrochemistry	241
A. Thermodynamic Redox Properties of Cobamides	241
B. Kinetic Redox Properties of Cobamides	244
C. Organometallic Electrochemical Synthesis	244
IV. Reactivity of B <sub>12</sub> -Derivatives in Organometallic Reactions	245
V. B <sub>12</sub> -Cofactors in Enzymatic Reactions	250
A. Occurrence and Structure of Natural Corrinoids	250
B. B <sub>12</sub> -Dependent Methyl Transferases	251
1. Methionine Synthase	253
2. B <sub>12</sub> -Cofactors in Enzymatic Methyl-Group Transfer	254
C. Coenzyme B <sub>12</sub> -Dependent Enzymes	255
1. Carbon Skeleton Mutases	258
2. Diol Dehydratases, Glycerol Dehydratase, and Ethanolamine Ammonia Lyase	262
3. B <sub>12</sub> -Dependent Amino Mutases	264
4. B <sub>12</sub> -Dependent Ribonucleotide Reductase	264
5. B <sub>12</sub> -Coenzymes in Enzymatic Radical Reactions	266
D. Other B <sub>12</sub> -Dependent Enzymatic Reactions	268
E. Metabolism Using an Adenosyl Radical not Derived from Coenzyme B <sub>12</sub>	269
VI. B <sub>12</sub> : Medical Aspects	269
References	270

## I. Introduction

The B<sub>12</sub>-coenzymes perhaps are the most complex and physiologically relevant organometallic cofactors and are known to undergo unique organometallic enzymatic reactions that directly depend upon the reactivity of metal coordinated organic ligands. Accordingly, B<sub>12</sub>-derivatives hold a key position in the area of

bio-organometallic chemistry and have attracted broad interest from physical, biological and chemical sciences. With the exception of the higher plants, the metabolism of most living organisms depends on catalysis by B<sub>12</sub>-dependent enzymes.<sup>1</sup>

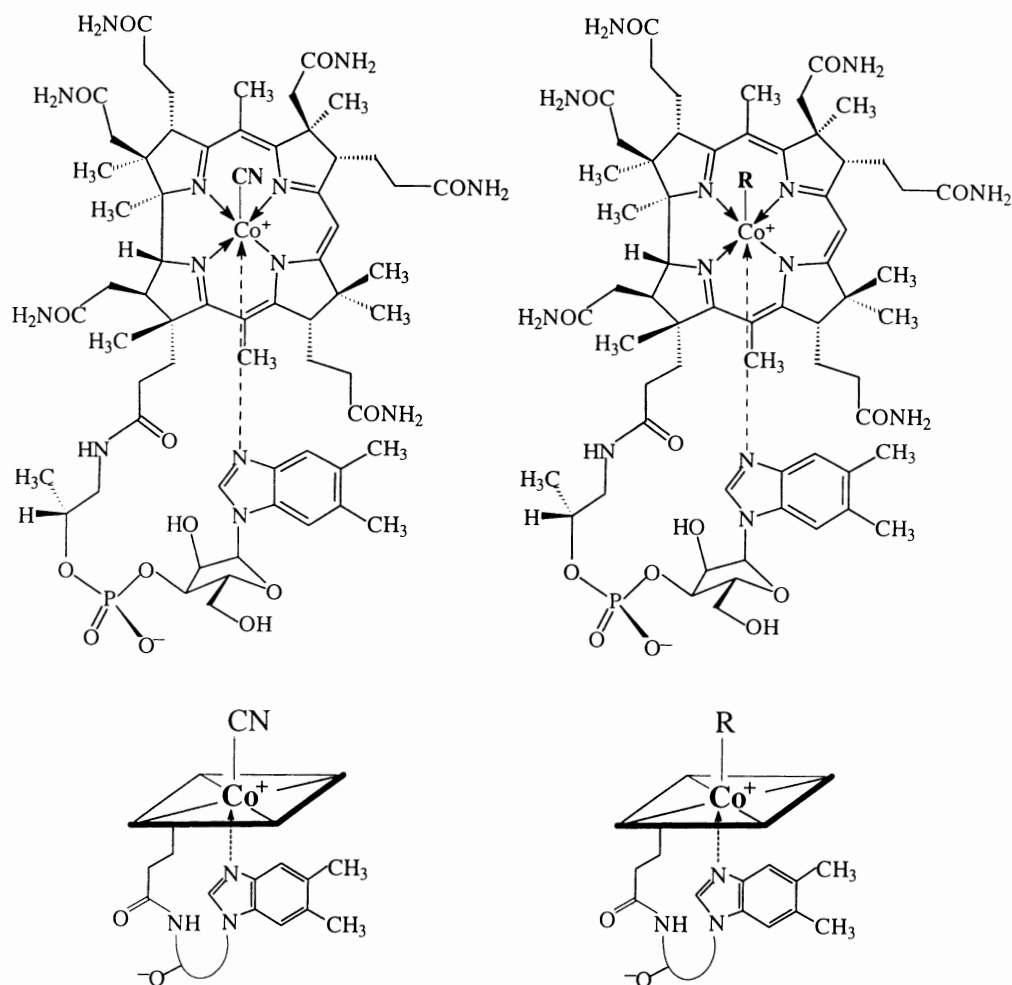
Nearly 60 years ago, the red cyanide-containing cobalt-complex vitamin B<sub>12</sub> (**1**, cyanocob(III)alamin, CNCbl) was discovered and isolated as the (extrinsic)

anti-pernicious anemia factor.<sup>2,3</sup> Vitamin B<sub>12</sub> (**1**, CNCbl) crystallizes readily and is a relatively inert Co(III)-complex. CNCbl is the most important commercially available form of the naturally occurring B<sub>12</sub>-derivatives, but appears not to have a physiological function itself.<sup>4</sup> Other pharmaceutically relevant vitamin B<sub>12</sub>-derivatives are the highly light-sensitive and chemically more labile organometallic coenzyme forms, coenzyme B<sub>12</sub> (**2**, 5'-deoxy-5'-adenosylcobalamin, AdoCbl) and methylcobalamin (**3**, MeCbl), as well as the "inorganic" B<sub>12</sub>-derivatives aquocob(III)alamin (H<sub>2</sub>Ocbl, as chloride 4<sup>+</sup>-Cl) and hydroxocob(III)-alamin (**5**, HOCbl) (see Figure 1).

Over the years, the remarkable scientific advances towards the solution of some of the major "B<sub>12</sub>-mysteries" were reported in a series of European Symposia on "Vitamin B<sub>12</sub> and B<sub>12</sub>-Proteins," beginning

in 1956 in Hamburg (Germany),<sup>5</sup> to be continued in Hamburg (1961),<sup>6</sup> in Zürich (Switzerland, 1979),<sup>7</sup> in Innsbruck (Austria, 1996)<sup>8</sup> and in Marburg (Germany, 2000). Two of the top achievements in this field concern the elucidation of the biosynthetic pathways to B<sub>12</sub>,<sup>9-12</sup> and the synthetic conquest of the vitamin B<sub>12</sub> structure,<sup>13-15</sup> which are reviewed in more detail in the chapters by Scott et al.<sup>16</sup> elsewhere in the present Handbook, and by Stevens.<sup>17</sup>

Several concise books, two earlier ones written by Pratt<sup>18</sup> and by Friedrich,<sup>19</sup> and the more recent ones on "B<sub>12</sub>," edited by Dolphin<sup>20</sup> and on "Chemistry and Biochemistry of B<sub>12</sub>" (edited by Banerjee),<sup>21</sup> all provide more systematic information on a broad range of topics around "B<sub>12</sub>," such as (i) on the elucidation of the enigmatic structures of vitamin B<sub>12</sub><sup>22,23</sup> and of coenzyme B<sub>12</sub> (**2**),<sup>24</sup> as well as on the exciting first



**Figure 1.** Top, left: Structural formula of vitamin B<sub>12</sub> (**1**, CNCbl); top, right: Structural formulae of coenzyme B<sub>12</sub> (**2**, R = 5'-deoxy-5'-adenosyl, AdoCbl), methylcobalamin (**3**, R = methyl, MeCbl), aquocobalamin cation (**4**<sup>+</sup>, R = H<sub>2</sub>O<sup>+</sup>, H<sub>2</sub>Ocbl), hydroxocobalamin (**5**, R = HO, HOCbl), chlorocobalamin (**12**, R = Cl), superoxocobalamin (**13**, R = O-O),  $\gamma$ -glutamylcysteinyl-cobalamin (**14**, R =  $\gamma$ -glutamylcysteinate). Bottom: Symbols used for vitamin B<sub>12</sub> (**1**, CNCbl) (left) and for other cobalamins (right).



X-ray crystal structures of B<sub>12</sub>-binding proteins,<sup>25–30</sup> (ii) on the physiological roles of vitamin B<sub>12</sub>-derivatives, which are intimately connected with their function as cofactors in enzymatic reactions, as well as, (iii) with the ways in which vitamin B<sub>12</sub>-forms are made available to living organisms by their own biosynthesis<sup>9–12</sup> or else, via uptake, transport and storage.<sup>31</sup>

## II. B<sub>12</sub>: Structure and Reactivity

### A. CRYSTALLOGRAPHIC STRUCTURAL STUDIES

The structures of vitamin B<sub>12</sub> (**1**) and of coenzyme B<sub>12</sub> (**2**) were established by pioneering X-ray crystallographic studies from the laboratory of Hodgkin,<sup>22–24</sup> by which the structure of the corrin ligand of **1** and the organometallic nature of **2** were also discovered (see Figure 5). In the more recent crystallographic investigations the primary attention has turned away from constitutional and stereochemical questions concerning B<sub>12</sub>-molecules, but to studies of specific conformational aspects and to the collection of more accurate structural data of a range of B<sub>12</sub>-derivatives, as detailed in more recent reviews.<sup>33,34</sup>

#### 1. Co(III)-Cobamides with Inorganic β-Ligands

Vitamin B<sub>12</sub> (**1**, CNCbl) and other cobalamins, which have the cyanide ligand of **1** replaced by another “upper” β-ligand (see Figure 1) are 5',6'-dimethylbenzimidazolyl-cobamides (DMB-Cba) and are the most commonly discussed “complete” B<sub>12</sub>-derivatives. So far, only “base-on” cobalamins, in which the nucleotide function coordinates in an intramolecular mode, have been analyzed by X-ray crystallography.<sup>33,34</sup> The systematic atomic numbering used here for vitamin B<sub>12</sub>-derivatives (Figure 2),<sup>32</sup> builds on the convention that atom numbers of the heavy atoms of a substituent reflect the number of the points of attachment to the corrin ligand and are indexed consecutively.<sup>35</sup> The axial ligands at cobalt are numbered internally according to these rules and labeled with an additional letter to denote the structural segment (nucleotide function: “R” for ribose, “N” for nucleotide base; “L” for β-ligand). This system can be used consistently for the numbering of heavy atoms in X-ray and in NMR structural work.

Two structure analyses of vitamin B<sub>12</sub> (**1**) were originally reported for “air-dried” and “wet” B<sub>12</sub>-crystals.<sup>22,23,33,34</sup> The molecular geometry of the B<sub>12</sub> moiety of Hodgkin's original structure determination

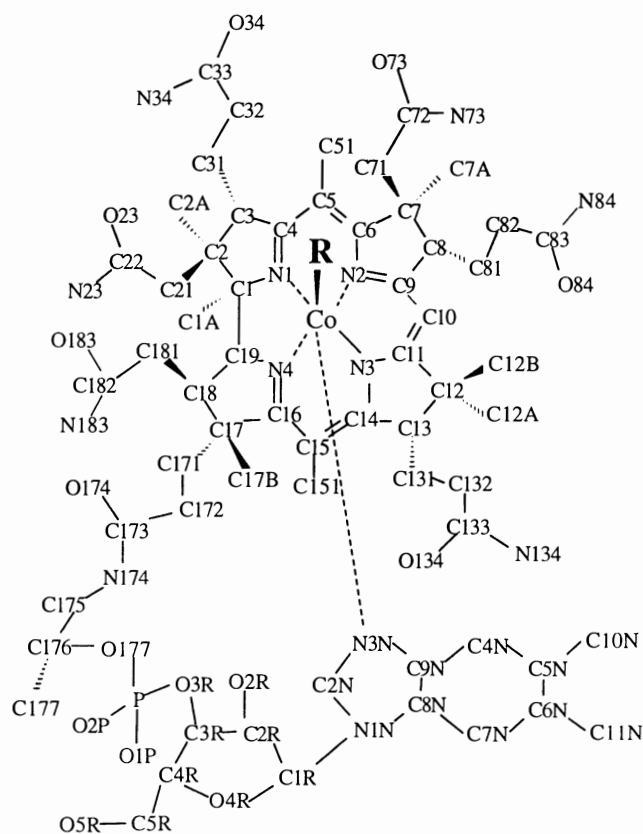
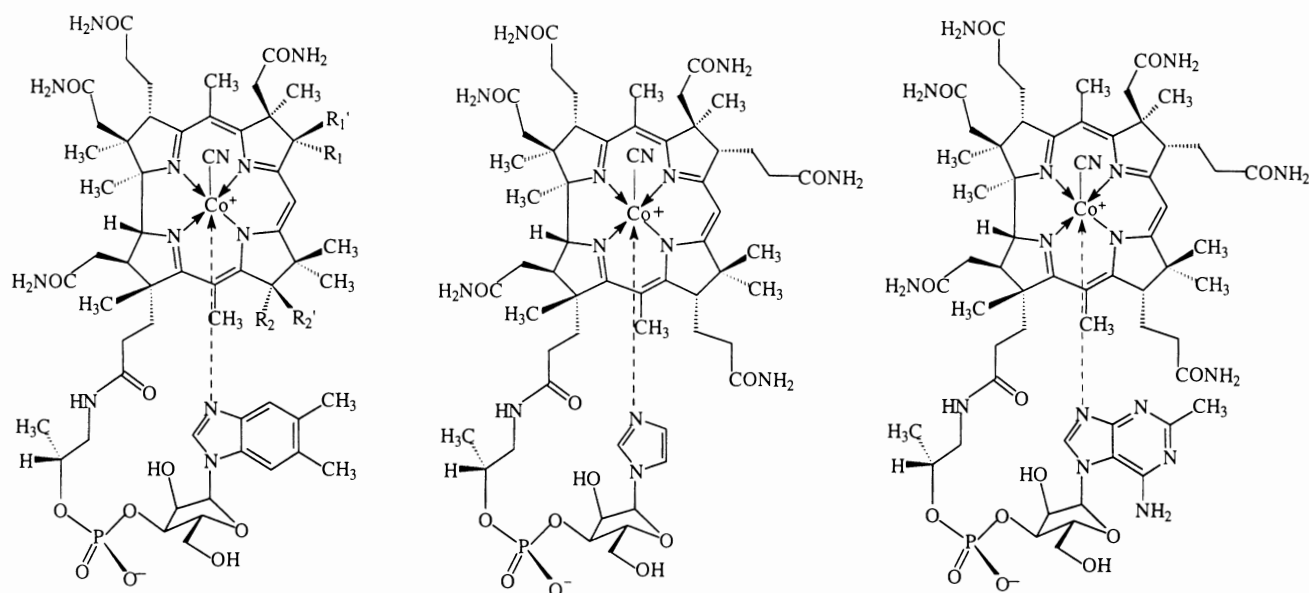


Figure 2. Atom numbering for vitamin B<sub>12</sub>-derivatives.<sup>32</sup>

and that obtained by more recent and modern cryo-crystallography (at 88 K)<sup>36</sup> agreed within experimental error. The crystal structure of neovitamin B<sub>12</sub> (**6**, cyano-13-epicobalamin), the vitamin B<sub>12</sub>-derivative with the propionamide side chain at C13 in β-configuration, was studied twice.<sup>37,38</sup> The 6° larger fold-angle for **6** than for **1** (23.7° vs. 17.9°, see below, Section II.A.6) represents a notable distinctiveness of the two structures. In the crystal structure of cyano-8-epi-cobalamin (**7**), the C8 epimer of CNCbl (**1**),<sup>39</sup> an even larger fold angle of the corrin ring was observed (23.8°). The structure of cyano-10-chlorocobalamin (**8**) again was found to be very similar to that of vitamin B<sub>12</sub> (**1**).<sup>40</sup>

Co<sub>β</sub>-cyano-imidazolylcobamide (**9**) is the analogue of vitamin B<sub>12</sub>, in which the cobalt-coordinating DMB-base is replaced by imidazole (see Figure 3). Comparison of the crystal structures of **9** and of vitamin B<sub>12</sub> (**1**) revealed a number of structural differences, which allowed a first quantitative assessment of the effect of an exchange of the sterically demanding DMB-base by the less bulky and more nucleophilic imidazole base of **9**.<sup>36</sup> The corrin ring fold angle decreased to 11.3° in Co<sub>β</sub>-cyano-imidazolylcobamide (**9**) and the axial Co–N bond shortened



**Figure 3.** Structural formulae of cyano-DMB-cobamides (at left): neovitamin B<sub>12</sub> (**6**, cyano-13-epicobalamin, R<sub>1</sub>' = R<sub>2</sub> = H, R<sub>1</sub> = R<sub>2</sub>' = propionamide), cyano-8-epi-cobalamin (**7**, R<sub>1</sub> = R<sub>2</sub>' = H, R<sub>1</sub>' = R<sub>2</sub> = propionamide), of Co<sub>β</sub>-cyano-imidazolylcobamide (**9**, middle) and of factor A (Co<sub>β</sub>-cyano-2'-methyladeninylcobamide, **10**, right).

(from 2.011 Å in **1** to 1.968 Å in **9**), both effects consistent with the smaller size and the more nucleophilic nature of the imidazole base. In addition, the “base tilt” of **9** (i.e. half the difference between the two Co–N–C angles to the coordinating base) decreased to about zero. In all cobalamin crystal structures a “tilt” of about 5° is found,<sup>41</sup> which appears to be an inherent property of cobalt-coordinated DMB, as it has also been observed in model complexes with an axial DMB ligand.<sup>42,43</sup> The crystal structure of **9** was the first structure analysis of a “complete” corrinoid with an imidazole base. In view of the discovery of a replacement of the cobalt-coordinated DMB base by a protein-derived imidazole in several B<sub>12</sub>-dependent enzymes (see below), this analysis was of particular interest.

The analysis of the crystal structure of factor A (Co<sub>β</sub>-cyano-2'-methyladeninylcobamide, **10**, see Figure 3) constituted another crystallographic study of a natural B<sub>12</sub>-derivative with a nucleotide base different from DMB.<sup>44</sup> The structure of **10** turned out to be similar to that of vitamin B<sub>12</sub> (**1**) and – as expected – the purine base was found to coordinate to the cobalt center *via* its nitrogen in the 9-position. However, the axial (Co<sub>α</sub>–N)-bond to the base was longer than the corresponding bond of **1** (2.12 Å vs. 2.01 Å).<sup>36</sup> Both, the longer axial (Co<sub>α</sub>–N)-bond and the lesser steric bulk of the purine base of **10** are compatible with the observed, smaller upwards folding of the corrin ring (15.7° vs. 17.9° for **1**).<sup>36</sup>

In the crystal structure analysis of aquocobalamin perchlorate (**4**<sup>+</sup>-ClO<sub>4</sub>)<sup>45</sup> the length of the axial (Co<sub>α</sub>–N)-bond was 1.925 Å, making it the shortest axial (Co<sub>α</sub>–N)-bond observed in a B<sub>12</sub>-derivative. The structure also showed a large upwards folding angle of 18.7°, which led to the conclusion that the steric repulsion between DMB-base and corrin ring existed, but that it did not lead to a stretching of the bond length, but to a flexing of the corrin ring (see Ref. 41). The crystallographically observed short axial (Co<sub>α</sub>–N)-bond for the **4**<sup>+</sup>-ion was consistent with the weak donor ability of the trans-axial aquo ligand. In an independent analysis of the crystal structure of **4**<sup>+</sup>-ClO<sub>4</sub> Brown et al. obtained virtually identical results.<sup>38</sup> However, EXAFS experiments apparently yielded an axial Co–N distance of 2.14 Å, much longer even than that observed in CNCbl (2.01 Å).<sup>46</sup> In the structure of **4**<sup>+</sup>-ClO<sub>4</sub> the cobalt-coordinated water molecule on the β-side is at a distance of 1.952 Å. The diffraction data permitted the location of its two hydrogen atoms, one of which was seen to form an intramolecular H-bond to the carbonyl oxygen of the c-acetamide (as was also shown by NMR spectroscopy in aqueous solution, see below). The analogue aquo-10-chlorocobalamin perchlorate (**11**<sup>+</sup>-ClO<sub>4</sub>, see Figure 6)<sup>40</sup> again was indicated to have a Co–O bond of similar length as that found in **4**<sup>+</sup>-ClO<sub>4</sub> (1.943 Å). Crystallization of aquocobalamin chloride from water/acetone gave crystals of chlorocobalamin (**12**), whose structure was reported in preliminary form.<sup>41</sup> From crystallization of

aquocobalamin chloride with lithium chloride, crystals of **12** with the composition  $12 \cdot 2\text{LiCl} \cdot n\text{H}_2\text{O}$  were obtained.<sup>47</sup> The structure of **12** was found to exhibit an axial (Co<sub>ax</sub>-N)-bond of 1.999 Å length, a corrin ring fold angle of 16.7° and an intramolecular H-bond to the β-axial chloride ligand. The structures of several other “inorganic” B<sub>12</sub>-derivatives were solved, as reviewed elsewhere.<sup>34</sup>

At low temperature, molecular oxygen binds reversibly to cob(II)alamin (B<sub>12r</sub>, see below), to form a species termed “superoxocobalamin” (**13**, B<sub>12r</sub>-O<sub>2</sub>), which is rapidly oxidized to aquocobalamin at room temperature in solution. A solid-state synthesis of **13** by diffusion of molecular oxygen into single crystals of B<sub>12r</sub> was achieved by exposure of a single crystal of B<sub>12r</sub> to 10 bar of gaseous O<sub>2</sub>, flash-cooling to 100 K. Data collection at cryo-temperature provided a crystal structure, in which the dioxygen molecule was attached to the cobalt center in a bent end-on fashion, inclined toward the meso-carbon C10.<sup>48</sup> This conformation appears to be favored by steric factors and was predicted from the analysis of EPR spectra.<sup>49</sup> Two hydrogen bonds connect the metal-coordinated dioxygen to the water network within the solvent channel. All features of the crystal structure of **13** are consistent with the description as superoxocob(III)alamin.

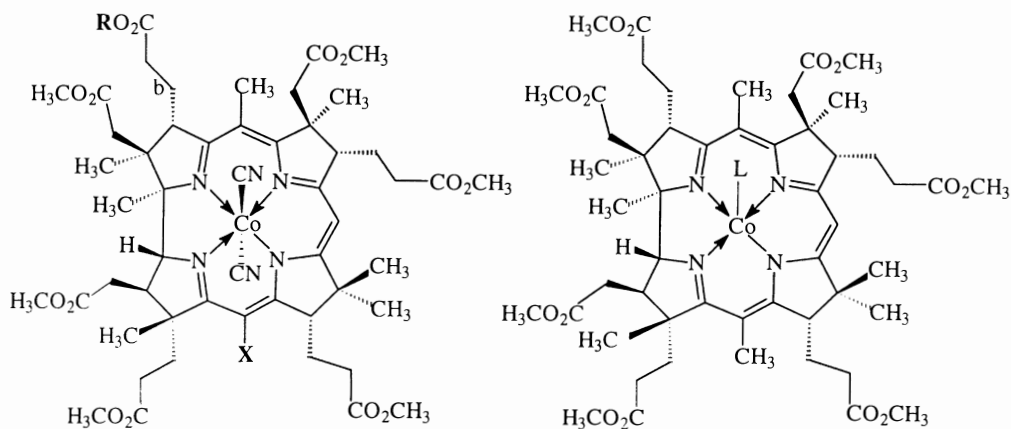
As an interesting case of a cob(III)alamin with a cobalt-coordinated thiolate ligand γ-glutamylcysteinylcob(III)alamin (**14**) was prepared and its crystal structure was studied.<sup>50</sup> In **14** a “normal” (Co-S)-bond was found (2.267 Å), but the largest fold angle of a corrin ligand known in a B<sub>12</sub>-derivative (24.2°), slightly larger than that in cyano-8-epicobalamin (**7**).

## 2. Incomplete Cobamides

In the earlier X-ray analytical investigations, several crystal structures of “incomplete” cobamides were characterized, as reviewed by Glusker.<sup>33</sup> More recently, attention has turned to dicyano-heptamethylcobyrinate (**15**, “cobester”, see Figure 4), which was originally prepared and studied in the context of the total synthesis of vitamin B<sub>12</sub><sup>13,51</sup> and of biosynthetic studies.<sup>10,12</sup> The crystal structure analyses of **15** yielded detailed information on the basic conformational properties of this “incomplete” Co(III)-corrin.<sup>52–54</sup> Notably, the folding angles of the corrin ligand of **15**, as well as that of cobester-b-monoacid (**15b**),<sup>55</sup> were observed to be as small as 7.5°,<sup>53</sup> considerably less than in CNCbl (17.9°<sup>36</sup>). In an investigation of the effect of methyl groups at the meso-positions C5 and C15 of cobyrinic acid derivatives, which are introduced in the late stages in B<sub>12</sub> biosynthesis,<sup>10,12</sup> the structure of 15-norcobester (**16**)<sup>56,57</sup> was analyzed and was found to differ only insignificantly from that of cobester (**15**).<sup>58</sup>

## 3. Reduced B<sub>12</sub>-Derivatives

A dimeric iodide-bridged heptamethylcobyrinate<sup>59</sup> was the first crystallizable and structurally characterized (diamagnetic) Co(II)cobyrinate.<sup>33</sup> The crystal structure of the monomeric and paramagnetic heptamethylcob(II)yrinate (**17**) revealed a preference of “incomplete” Co(II)-corrins to coordinate an axial ligand at their sterically less hindered “upper” β-face, contrasting with the “complete” Co(II)corrin cob(II)alamin (**18**), where axial coordination occurs at the “lower” α-side (see below). The Co(II)-complex **17** exhibited a five-coordinate Co(II)-center, to which a perchlorate ligand was



**Figure 4.** Structural formulae, left of cobester (**15**, R = CH<sub>3</sub>, X = CH<sub>3</sub>), cobester-b-monoacid (**15b**, R = H, X = CH<sub>3</sub>), 15-norcobester (**16**, R = CH<sub>3</sub>, X = H) and (right) of perchlorato-heptamethylcob(II)yrinate (**17**, L = ClO<sub>4</sub>), and of the Co(I)-heptamethylcobyrinate (**27**, L = absent, see Section B.2).

coordinating at the  $\beta$ -face and via a long axial (Co–O)-bond (2.31 Å), and a 6° folding of the corrin ligand.<sup>60</sup>

Cob(II)alamin (**18**, B<sub>12r</sub>) is the corrinoid product of (Co–C)-bond homolysis of coenzyme B<sub>12</sub> (**2**), which occurs during the catalytic cycle of coenzyme B<sub>12</sub>-dependent enzymes, and knowledge of the 3D structure of **18** was of particular interest (see below). The crystal structure of cob(II)alamin (**18**) showed the corrin moiety of coenzyme B<sub>12</sub> (**2**) and **18** to have a very similar structure (see Figure 5):<sup>61</sup> (i) the “folding” of the corrin ring is similar in the two compounds (16.3° in **18**, 13.3° in **2**); (ii) the axial cobalt–nitrogen bond is slightly shorter in the five-coordinated **18** (2.13 Å) than in the six-coordinated coenzyme B<sub>12</sub> (2.24 Å), but the distance between the coordinating DMB-base and the corrin ring is almost the same in **2** and **18**, as a result of a “downward” displacement of the cobalt atom from the plane of the corrin ligand in **18**. The length of the axial (Co–N)-bond in **18** was surprising, as one would expect a longer bond for the reduced Co(II) species, compared to a Co(III) species. Accordingly, in AdoCbl (**2**) and related organocobalamins, the “structural trans effect” of the organic ligand appears to lengthen the axial (Co(III)–N)-bond and to compensate for the inherently larger covalent radius of Co(II) compared to Co(III) (see below). These observations led to the conclusion that “the interactions (apoenzyme/coenzyme) at the corrin moiety of the coenzyme appear insufficient to provide by themselves the major means for a protein-induced activation of the bound coenzyme toward homolysis of its (Co–C)-bond. Instead, the organometallic bond may be labilized largely by way of apoenzyme

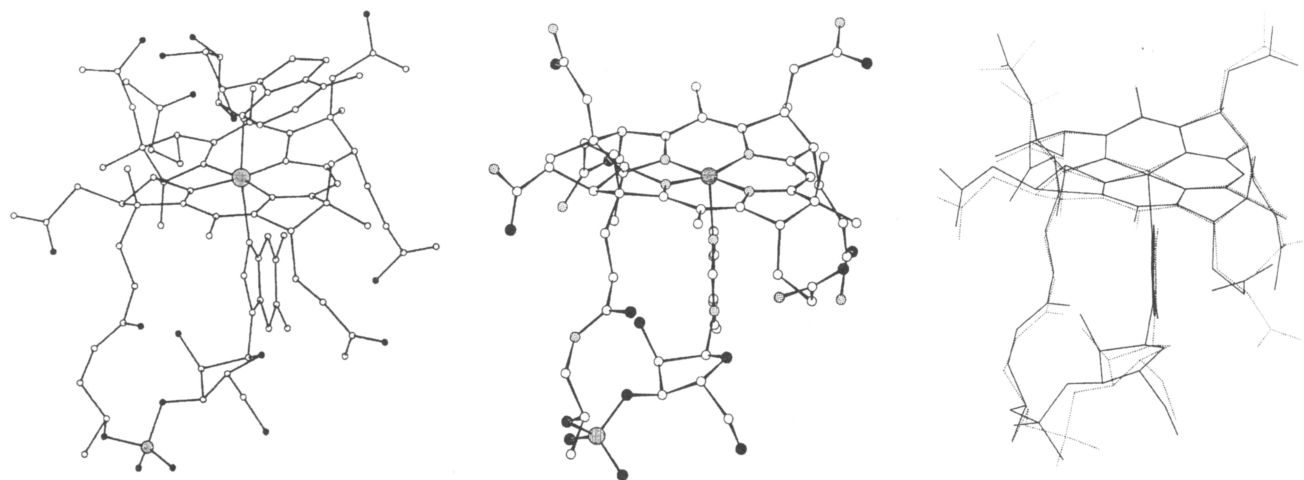
(and substrate) induced separation of the homolysis fragments, made possible by strong binding of both separated fragments to the protein.”<sup>61</sup>

#### 4. Organometallic B<sub>12</sub>-Derivatives

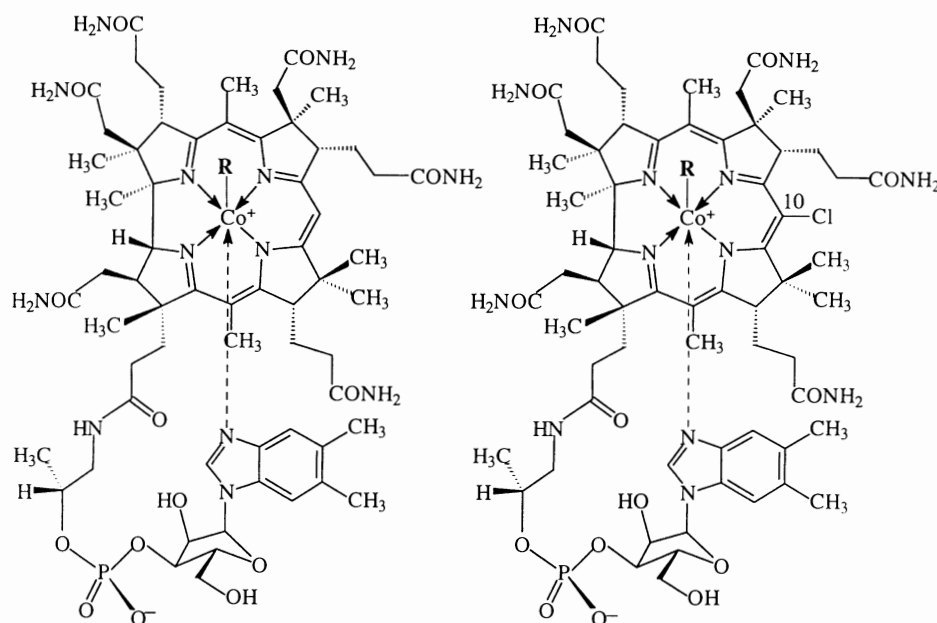
The classical crystal structure analysis of coenzyme B<sub>12</sub> (**2**, AdoCbl)<sup>24,62</sup> (see Figure 5) and their basic results were fully confirmed by more recent extensive studies by X-ray and neutron crystallography.<sup>63,64</sup> Accordingly, in AdoCbl both axial (Co–C)- and (Co–N)-bonds are relatively long: 2.03 Å (Co–C) and 2.24 Å (Co–N).<sup>33,34</sup> The organometallic adenosyl moiety is bound in an anti-conformation and with the adenine ring placed above the south-eastern quadrant (ring C) of the corrin ligand. In the crystal of **2** a notably large Co–C–C bond angle of 125° is observed for the organometallic group.<sup>62</sup>

In  $\alpha$ -adenosylcobalamin (**19**) the adenine base of the organometallic ligand is attached at the ribose moiety with an  $\alpha$ -configuration (see Figure 6) and **19** is a stereoisomer of AdoCbl (**2**). The crystal structure of **19** revealed the corrin ring to be flatter (fold angle = 11.7°) than in **2**, but the lengths of the axial (Co–N)- and (Co–C)-bonds (of 2.24 Å and 2.02 Å, respectively) to be similar.<sup>65</sup> In crystals of **19**, the adenosyl ligand was found to lie over the south-eastern quadrant, as in **2**, but the position of the adenine moiety relative to the ribose unit of the organometallic ligand was disordered, with significantly different conformations of the adenine heterocycle. Analysis of the solution structure of **19** by NMR (see below) also supported a flexible attachment of the adenine ring at the ribose unit.

In adeninyllalkylcobalamins a methylene chain connects the adenine residue with the cobalt center



**Figure 5.** Crystal structures of coenzyme B<sub>12</sub> (AdoCbl, **2**) (left), of cob(II)alamin (**18**) (center), and superposition (right) of the structure of **18** (—) with that of the cobalt-corrin part of **2** (....).



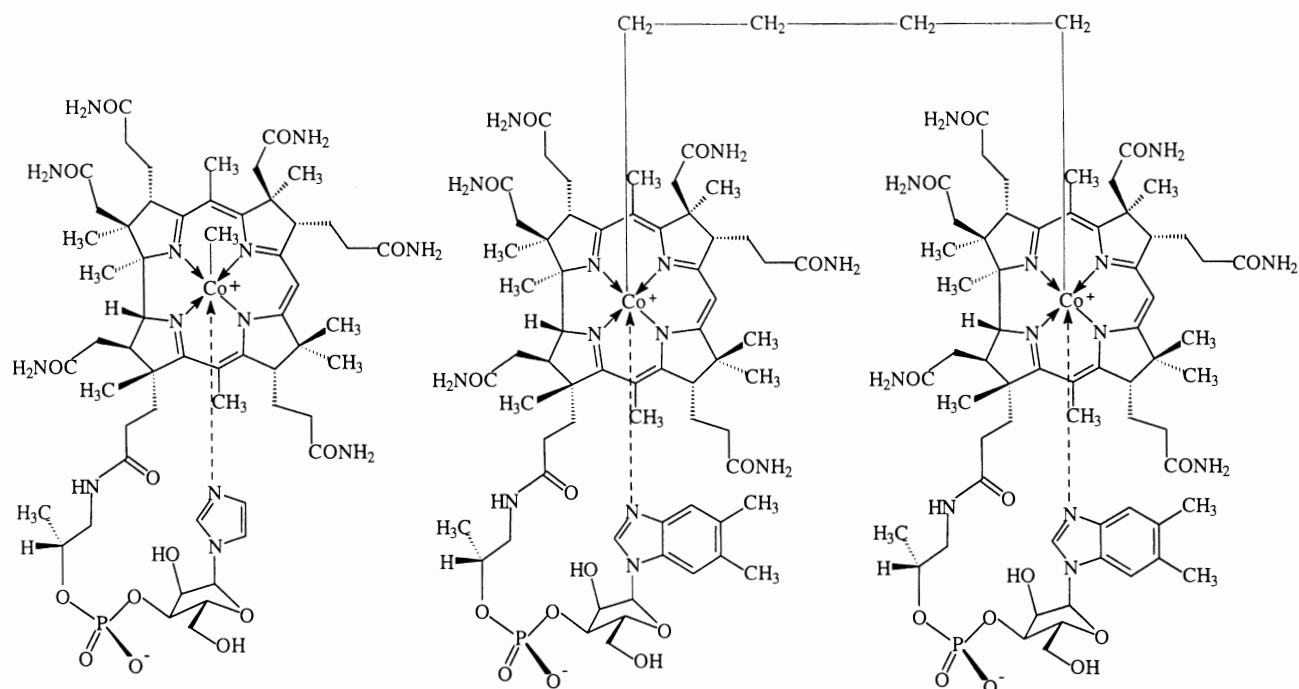
**Figure 6.** Structural formulae. Left:  $\alpha$ -adenosylcobalamin (**19**, R =  $\alpha$ -adenosyl), adeninylpropylcobalamin (**20**, R = 3'-adeninyl-propyl) and the diastereomeric 2,3-dihydroxypropylcobalamins **21R** (R = (2R)-2,3-dihydroxypropyl) and **21S** (R = (2S)-2,3-dihydroxypropyl), trifluoromethylcobalamin (**23**, R = CF<sub>3</sub>), difluoromethylcobalamin (**24**, R = CHF<sub>2</sub>). Right: aquo-10-chloro-cobalamin perchlorate (**11**<sup>+</sup>-ClO<sub>4</sub>, R = H<sub>2</sub>O<sup>+</sup>), 10-chloro-methylcobalamin (**22**, R = CH<sub>3</sub>).

(see Figure 6).<sup>66</sup> Adeninyllalkylcobalamins may inhibit a variety of AdoCbl-dependent enzymes, depending upon the length of the methylene chain.<sup>67,68</sup> The structure of adeninylpropylcobalamin (**20**) was analyzed in the crystal, as well as in solution.<sup>69</sup> The structure of **20** in the crystal was found to resemble that of **2** as concerns the corrin ring and the lower nucleotide loop. However, the adenine group, which is oriented almost parallel to the corrin plane in **20**, is positioned over ring D of the corrin ligand at about 120° clockwise from its position in coenzyme B<sub>12</sub> (see Figure 5). Again the 3'-adeninylpropyl function in **20** is indicated to be dynamic with several orientations of the adenine heterocycle.

The crystal structures of the 2,3-dihydroxypropylcobalamins (the diastereomeric *R*- and *S*-isomers **21R** and **21S**) were studied, in order to examine, whether the large Co–C<sub>1</sub>–C<sub>2</sub> angle observed in **2** is typical for organocobalamins.<sup>70</sup> While the observed Co–C distances (2.00 and 2.08 Å for **21R** and **21S**, respectively, were similar to the value for AdoCbl (2.03 Å),<sup>62</sup> the bond angles were smaller (119.6° and 113.6°). The lower of the two values (113.6° for **21S**) should be considered the “normal” angle, with minor interactions between the corrin ring and the  $\beta$ -substituent. However, the angles observed in **21R**, as well as that observed in AdoCbl are to be considered to be increased due to steric interactions.

The crystal structure of methylcobalamin (**3**, MeCbl), the simplest of the organometallic B<sub>12</sub>-derivatives and an important methyl transfer catalyst in enzymatic methylation reactions,<sup>71</sup> was reported as recently as 1985.<sup>72</sup> It confirmed the folding of the corrin ligand of **3** (and other conformational properties of the cobalamin moiety) to be similar to that of coenzyme B<sub>12</sub> (fold angle in **3**: 15.8°), as well as the earlier derived “base-on” constitution of **3**. The bulkiness of the 5'-deoxyadenosyl ligand in **2** was concluded not to be a main contributor to the conformation of the corrin ligand of **2**. The lengths of the axial (Co–N)- and (Co–C)-bonds of MeCbl with values of 2.19 Å and 1.99 Å, respectively, are each shorter by about 0.05 Å when compared to AdoCbl.<sup>33,62,63</sup> The axial bond to the DMB-base in **3** is shorter than in **2**, consistent with the stronger nucleotide coordination in **3**. The phosphate group of **3** is associated with specifically bound water molecules, and the conformation of **3** is indicated by NMR studies to differ in the crystal and in aqueous solution.<sup>73</sup> More recently, the crystal structures of MeCbl (**3**), of 10-chloro-methylcobalamin (**22**), of trifluoromethylcobalamin (**23**)<sup>40</sup> and of difluoromethylcobalamin (**24**) were compared.<sup>74</sup>

Co $\beta$ -methyl-imidazolylcobamide (**25**, see Figure 7) was prepared as a first model for organometallic B<sub>12</sub>-cofactors bound in a “base-off/His-on” form and its crystal structure was analyzed.<sup>75</sup> The structure of **25**



**Figure 7.** Structural formulae of  $\text{Co}_\beta$ -methyl-imidazolylcobamide (**25**, left) and of tetramethylene-1,4-biscobalamin (**26**, right).

showed the axial (Co–C)- and (Co–N)-bonds to be shorter by 0.01 Å and 0.1 Å, respectively, than in MeCbl (**3**), and the fold angle of the corrin ligand amounted to 12.5°, i.e. about 2° less than in **3**. Thus, the substitution of the DMB-base of **3** by the less bulky and more nucleophilic imidazole base in **25** had structural effects, as expected in a qualitative way.

Alkylation of cob(I)alamin with 1,ω-dibromoalkanes provided a preparative entry to tetramethylene-1,4-biscobalamin (**26**, see Figure 7) and to its homologues, in which two cobalamin moieties are bridged via oligomethylene chains bound to both of the “upper” faces of the two cobalt centers. As expected on the basis of geometric considerations, only dimers with bridges having four or more methylene units could be prepared.<sup>76</sup> In the crystal structure of the dimer **26**, the tetramethylene bridge is attached to the cobalt centers of the two  $\text{B}_{12}$ -units and is seen to adopt a synclinal conformation. The two  $\text{B}_{12}$ -units pack rather tightly, but are not significantly strained and exhibit a ligand folding of 16.5°. The conformational properties of **26** in solution are indicated by 2D-NMR to be similar to those in the crystal.

## 5. Trans-Effects

The classic “trans-effect” is a kinetic effect of a metal-coordinated group on the rates of exchange reactions

of ligands trans to it.<sup>77</sup> “Thermodynamic” and “structural” trans-effects (or “trans-influences”)<sup>78</sup> have been studied with  $\text{B}_{12}$ -derivatives. The effect of one cobalt-coordinated axial ligand on chemical equilibria<sup>18,79,80</sup> and on coordination properties of an axial ligand trans to the first one were analyzed in Co(III)-corrins.<sup>33,34,45,78</sup> An increasing  $\sigma$ -donor power of the  $\text{Co}_\beta$ -ligands X was found to correlate with the size of the thermodynamic trans-effect in  $\text{B}_{12}$ -derivatives<sup>18</sup> and the length of the axial (Co $_\alpha$ –N)-bond to the DMB-base in cobalamins generally increases with the  $\sigma$ -donor property of the  $\text{Co}_\beta$ -ligand.<sup>33,34</sup> In the same sequence, the  $\sigma$ -ligand influences the base-on/base-off equilibria. A linear correlation thus exists between the free enthalpy of the base-on/base-off equilibria in aqueous solution and the length of the axial (Co–N)-bond.<sup>38</sup> However, in  $\text{B}_{12}$ -derivatives (and in  $\text{B}_{12}$  models), both axial bonds lengthen simultaneously with increasing  $\sigma$ -donor character of the axial-ligands.<sup>78</sup> This “anomalous” trans-influence in  $\text{B}_{12}$  models and in  $\text{B}_{12}$ -derivatives may best be compared with the heterolytic fragmentation of alkyl-Co(III)-complexes into Co(I)-complexes.<sup>78,81</sup> Both axial bonds are shorter in  $\text{Co}_\beta$ -methyl-imidazolylcobamide (**25**: (Co–C)=1.97 Å, (Co–N)=2.09 Å) than in MeCbl (**3**: (Co–C)=1.99 Å, (Co–N)=2.19 Å) and in AdoCbl (**2**: (Co–C)=2.04 Å, (Co–N)=2.24 Å).<sup>34,41,75,78</sup>

## 6. The “Upwards Folding” of the Corrin Ligand

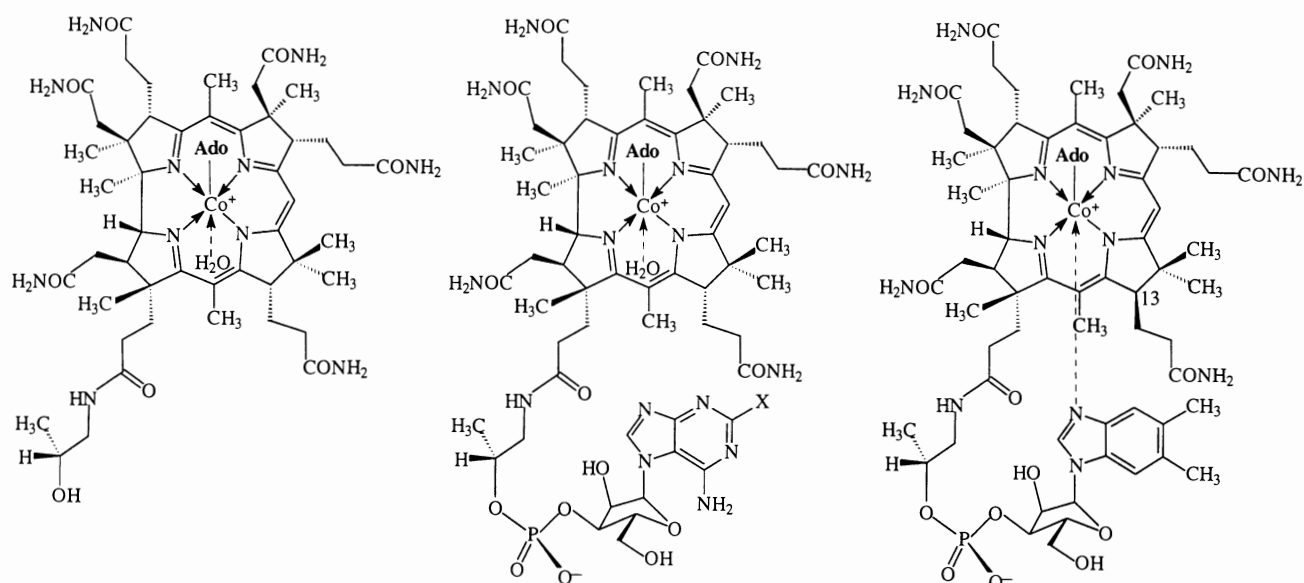
The nonplanar nature of the corrin ligand is due, mainly, to the saturated and direct trans-junction between two of its four five-membered rings. The characteristic “ligand-folding” is a main contributor to the conformational variability of the corrin ligand.<sup>82</sup> The “folding” of the corrin ligand has always been found as “upwards” (towards the  $\beta$ -face) and the “fold” angle is defined as the angle between the best planes through atoms N1-C4-C5-C6-N2-C9-C10 and C10-C11-N3-C14-C15-C16-N4 (see e.g. Ref. 33). The nonplanar five-rings may also contribute to the “folding” of the corrin ligand. Conformational coupling with the corrin ligand may put the hydropyrrolic rings “in tune” (or not) with the overall fold of the corrin ligand.<sup>14,83</sup> In the fully substituted cobyric acid derivatives, such as vitamin B<sub>12</sub>, five-ring conformations are observed that allow for a crucial staggering of the tightly interacting peripheral substituents along the “northern and southern” rims<sup>51</sup> and including the pivotal methyl substituents at positions 5 and 15. Several other structural elements were analyzed with respect to their “electronic” and “steric” effects on the “upwards folding” of the corrin ligand.<sup>33,34,41,82</sup> “Fold” angles are typically smaller in “incomplete” corrinoids (with a minimal observed value of 1.9° in Co $_{\alpha}$ -aquo-Co $_{\beta}$ -cyano-8-dehydro-cob(III)yrinic acid *c*-lactone<sup>33</sup>), than in “complete” corrinoids, where values up to 23.8° are found, as in cyano-8-epicobalamin (**7**).<sup>39</sup> The value of 7.5°, as found in the dicyanocobyrinate **15**,<sup>53</sup> may be characteristic for the corrin ligand in (intact) cob(III)yrinates. The five-coordinate Co(II)-center of the “incomplete” Co(II)-corrin **17** carries its axial ligand on the “upper”  $\beta$ -side and the fold angle is only 6°.<sup>60</sup>

Indeed, the bulky DMB-base was suggested by Lenhart<sup>62</sup> to be a relevant contributor to the “upwards folding” of corrins.<sup>33</sup> The possible effect of the intramolecular coordination of the DMB-base on the “folding” of the corrin ligand in cob(III)alamins was examined more recently.<sup>36,41,45</sup> The comparison of the structures of a series of “inorganic” and “organometallic” cob(III)alamins correlates long (Co $_{\alpha}$ -N)-bonds with smaller “fold” angles (and vice versa), exemplified by aquocobalamin (**4**<sup>+</sup>, (Co $_{\alpha}$ -N)=1.925 Å, fold angle=18.7°) and by coenzyme B<sub>12</sub> (**2**, (Co $_{\alpha}$ -N)=2.24 Å, fold angle=13.3°). In contrast, the folding of the corrin ligand in cyano-imidazolylcobamide **9** (11.3°) is considerably less than that of vitamin B<sub>12</sub> (**1**), in spite of a shorter (Co $_{\alpha}$ -N)-bond (1.97 Å vs. 2.01 Å).<sup>36</sup>

A correlation between the “folding” of the corrin ligand and the length of the axial (Co $_{\alpha}$ -N)-bond to the DMB-base in cobalamins thus is apparent. The bulky DMB-base, which “sterically” interacts with the corrin ligand, when “pulled” towards it by a short and strong axial bond is indicated to induce a mechanical deformation of the corrin ligand,<sup>34,41,45,84</sup> similar to the situation in “cobaloximes” and other B<sub>12</sub>-models<sup>84</sup> with an axial DMB-base.<sup>42</sup> Accordingly, “upwards folding” is most manifest in cob(III)alamins with short (Co $_{\alpha}$ -N)-bonds (near 2.0 Å or less), to which the known “inorganic” B<sub>12</sub>-derivatives belong. On the other hand, in the typical organocobalamins (such as coenzyme B<sub>12</sub>) the length of the crucial (Co $_{\alpha}$ -N)-bond is close to or greater than 2.2 Å, so that the steric interaction of the nucleotide base with the corrin ligand is considerably reduced.

From analysis of the crystal structures of B<sub>12</sub>-derivatives a steric effect of bulky organometallic groups on the “folding” of the corrin ring has been suggested to counterbalance the “upwards folding”.<sup>79,85</sup> However, the dynamic nature of organic ligands, as observed by NMR and as deduced from molecular dynamics simulations,<sup>86</sup> is also not compatible with significant repulsive nonbonded interactions with the corrin ligand.<sup>69,87</sup> The mentioned qualitative correlation between the nature of the organometallic ligand and the “upwards folding” of the corrin ligand may also be ascribed to an indirect effect: the  $\sigma$ -ligand exerts a structural trans effect (see above) and influences in this way, the crucial length of the trans-axial (Co $_{\alpha}$ -N)-bond.

The “ligand-folding” of the corrin macro-ring has been suggested by Halpern to be its biologically crucial property: an “upwards conformational distortion” was proposed to represent the means of the enigmatic enzymatic activation of the bound coenzyme B<sub>12</sub>.<sup>88,89</sup> However, all available structural information on B<sub>12</sub>-derivatives (see e.g. Refs. 34,41,61) has not provided support for the relevance of this hypothesis: Cob(II)alamin (**18**, B<sub>12r</sub>) was found by X-ray analysis to have a rather similar structure to the corrinoid moiety of the coenzyme itself (see Figure 5).<sup>61</sup> In particular, the “folding” of the corrin ligand is only slightly larger (16.3°) than in **2**, but falls within the range indicated by the correlation between the length of the (Co $_{\alpha}$ -N)-bond and fold angles in cob(III)alamins. In fact, the structure of the corrin ligand and the position of the DMB-base with respect to the corrin ring do not differ significantly in the Co(II)-homolysis fragment **18** and in the organometallic coenzyme B<sub>12</sub> (**2**).



**Figure 8.** Structural formulae of  $\text{Co}_\beta$ -5'-deoxy-5'-adenosylcobinamide (**28**, left), of pseudocoenzyme  $\text{B}_{12}$  (**29**,  $\text{Co}_\beta$ -adenosyl-adeninyl-cobamide,  $\text{X} = \text{H}$ ) and  $\text{Co}_\beta$ -adenosyl-factor A (**30**,  $\text{Co}_\beta$ -adenosyl-2'-methyladeninyl-cobamide,  $\text{X} = \text{CH}_3$ , center) and neocoenzyme  $\text{B}_{12}$  (**31**,  $\text{Co}_\beta$ -adenosyl-13-epi-cobalamin, right); Ado = 5'-deoxy-5'-adenosyl.

## B. STRUCTURAL STUDIES OF $\text{B}_{12}$ -DERIVATIVES BY NUCLEAR MAGNETIC RESONANCE (NMR) SPECTROSCOPY

### 1. Early Studies with Cyano-Co(III)-Cobyrinates

Nuclear magnetic resonance spectroscopy (NMR) has contributed strongly to the development of the  $\text{B}_{12}$ -field. The earlier NMR-spectroscopic investigations mainly depended on one-dimensional analyses and served the purpose of establishing the nature of many non-crystalline  $\text{B}_{12}$ -derivatives, in their  $\text{Co}_\beta$ -cyano forms mostly (see e.g. Ref. 90). These analyses were typically based on comparisons of tabulated  $^1\text{H}$ - and  $^{13}\text{C}$ -chemical shift values from spectra of several well-characterized  $\text{B}_{12}$ -derivatives and helped to identify and describe the structure of a range of synthetic derivatives of vitamin  $\text{B}_{12}$  (**1**),<sup>90,91</sup> of the dicyanoheptamethylcobyrinate **15**,<sup>92–95</sup> reviewed in,<sup>96</sup> and of natural analogues of **1**. In this way the natural corrinoids from a range of methanogenic, sulfur-metabolizing and acetogenic bacteria were characterized in their  $\text{Co}_\beta$ -cyano-Co(III)-form.<sup>81,97–99</sup>

### 2. Multidimensional NMR-Studies of $\text{B}_{12}$ -Structures in Solution

The means of heteronuclear NMR-spectroscopy in aqueous or nonaqueous solutions have eliminated all of the earlier assignment problems (see e.g. Refs. 87,96). Pioneered by contributions concerning the solution structure of the diamagnetic, Co(I)-heptamethylcobyrinate **27** (see Figure 4),<sup>100</sup> of coenzyme  $\text{B}_{12}$  (**2**)<sup>101,102</sup> and of the noncrystalline  $\text{B}_{12}$ -derivative

$\text{Co}_\beta$ -5'-deoxy-5'-adenosylcobinamide (**28**, AdoCbi, see Figure 8),<sup>103</sup> the newer NMR-studies have begun to rival (in certain aspects) and complement (in others) X-ray analytical studies of structures of  $\text{B}_{12}$ -derivatives in the solid state (see below).

The methodological developments of heteronuclear two- and multidimensional (2D and  $n\text{D}$ ) NMR-spectroscopy (as reviewed in Refs. 87,96) nowadays have provided the means to obtain detailed insights into structure and dynamics of diamagnetic  $\text{B}_{12}$ -derivatives in aqueous and nonaqueous solutions. Based on a selection of well-established homo- and heteronuclear 2D-experiments, assignment of signals in  $^1\text{H}$ -,  $^{13}\text{C}$ - and  $^{15}\text{N}$ -spectra typically is unambiguous and provides a reliable basis for the exploration of detailed structural information. Techniques for suppression of solvent (water) signals allow for the recording of spectra from aqueous solutions of  $\text{B}_{12}$ -derivatives with little loss of spectral information. The  $^1\text{H}$ -,  $^{13}\text{C}$ - and  $^{15}\text{N}$ -spectra of the diamagnetic  $\text{B}_{12}$ -derivatives (**1–16**, **19–26**) mentioned earlier in this review have been recorded in the context of their routine characterization (see e.g. Refs. 87,96), as are nowadays typically the  $^1\text{H}$ - and  $^{13}\text{C}$ -NMR-spectra of newly prepared  $\text{B}_{12}$ -derivatives.

Characteristic  $^1\text{H}$ -,  $^{13}\text{C}$ -,  $^{15}\text{N}$ - and  $^{31}\text{P}$ -chemical shift values provide important diagnostic information on the constitution and conformation of "complete"  $\text{B}_{12}$ -derivatives. The coordination of the DMB-base (in a "base-on" form) induces characteristic high-field shifts of the  $^1\text{H}$ -NMR signals of the unique singlet of HC10, due mainly to an increased electron density in the corrin



ligand from axial coordination of the base, which has been used extensively to characterize (the temperature dependence of) “base-on/base-off” equilibria in aqueous solution (e.g. of methylcobalamin (**3**)).<sup>96</sup> In the <sup>1</sup>H-NMR spectrum of e.g. **3**, the anisotropic shielding effect of the coordinated DMB-base also induces characteristic high-field shifts of protons, which are located nearby, such as those of the methyl group H<sub>3</sub>C1A, as well as those of the methylene groups H<sub>2</sub>C81 and H<sub>2</sub>C82 (see Figure 2).<sup>73</sup> Shielding by the cobalt-corrin in the axial direction leads to high-field shifts of HC2N and HC4N in the coordinated DMB-base, two DMB-protons close to the cobalt-corrin, resulting in, for example, unusual high-field positions for these protons in the <sup>1</sup>H-NMR spectra of aquocobalamin perchlorate (**4**<sup>+</sup>-ClO<sub>4</sub>).<sup>45</sup> Likewise, shielding by the cobalt-corrin in the axial direction leads to characteristic up-field shifts of the signals of protons attached to the organometallic ligand, as seen e.g. in the <sup>1</sup>H-NMR spectrum of the alkyl bridged B<sub>12</sub>-dimer tetramethylene-1,4-biscobalamin (**26**, see Figure 7).<sup>76</sup>

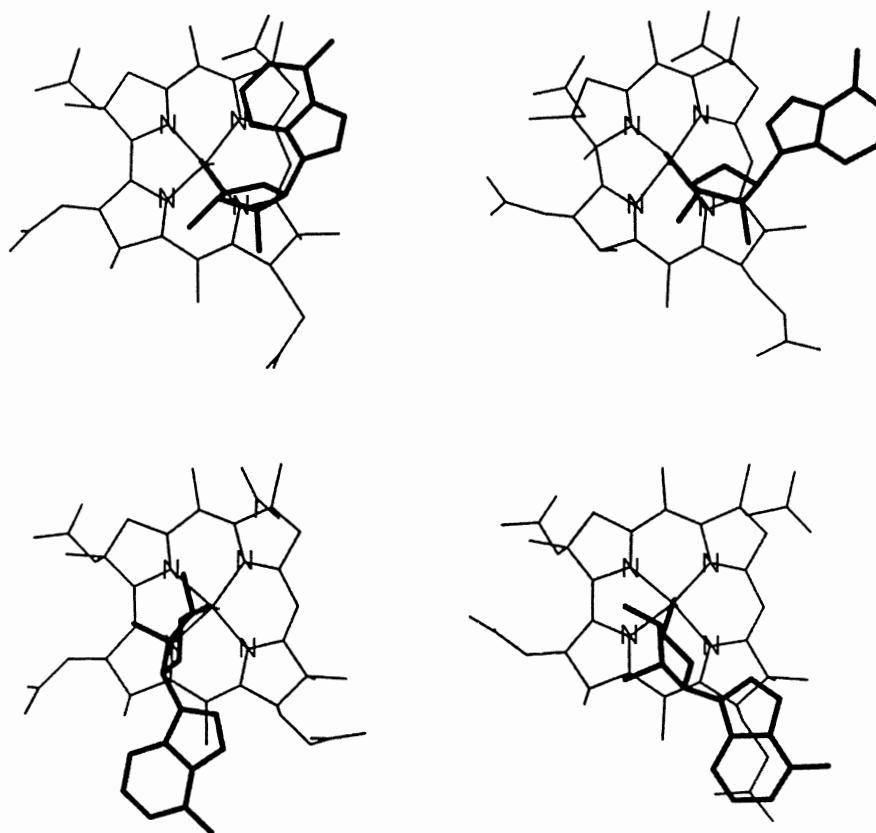
Rather complete sets of <sup>1</sup>H-, <sup>13</sup>C-, <sup>15</sup>N- and <sup>31</sup>P-chemical shift values have been obtained from NMR-analyses, e.g. of vitamin B<sub>12</sub> (**1**),<sup>36,104</sup> coenzyme B<sub>12</sub> (**2**),<sup>101,102</sup> aquocobalamin perchlorate (**4**<sup>+</sup>-ClO<sub>4</sub>),<sup>45</sup> factor A (Co<sub>β</sub>-cyano-2'-methyladeninyl-cobamide, **10**) and pseudovitamin B<sub>12</sub> (Co<sub>β</sub>-cyano-adeninyl-cobamide),<sup>105</sup> Co<sub>β</sub>-cyano-imidazolylcobamide (**9**)<sup>36</sup> and methylcobalamin.<sup>106</sup> Extensive tabulations of the dependencies of the chemical shift values upon structural variations of the axial ligands in these and other B<sub>12</sub>-derivatives have provided interesting structural correlations, as reviewed by Brown.<sup>96</sup> When in parallel studies the NMR-derived solution structures of diamagnetic Co(III)-cobamides could be compared with the crystal structures, relevant conformational differences between the solution and crystal structures were noted, such as in studies with coenzyme B<sub>12</sub> (**2**)<sup>101</sup> and with methylcobalamin (**3**).<sup>73</sup>

Nowadays heteronuclear NMR spectroscopy provides the means to characterize extensively the solution structures of “incomplete” B<sub>12</sub>-derivatives and other noncrystalline corrinoids. A first example in this direction was the natural “complete” but “base-off” B<sub>12</sub>-derivative, the protonated base-off form of coenzyme B<sub>12</sub> (**2**-H<sup>+</sup>).<sup>102</sup> More recently, the solution structures of pseudocoenzyme B<sub>12</sub> (**29**, Co<sub>β</sub>-adenosyl-adeninyl-cobamide), Co<sub>β</sub>-adenosyl-factor A (**30**, Co<sub>β</sub>-adenosyl-2'-methyladeninyl-cobamide),<sup>107</sup> the phenolyl-cobamides<sup>99</sup> and of neocoenzyme B<sub>12</sub> (**31**, Co<sub>β</sub>-adenosyl-13-epi-cobalamin)<sup>108</sup> could be analyzed in

detail. The structures and the “base-off”/“base-on” equilibria of a range of protonated “base-off” cobamides could also be investigated in aqueous solution.<sup>87,96</sup>

NOE-measurements have provided the first reliable basis for the assignment of the position (“upper” or Co<sub>β</sub> vs. “lower” or Co<sub>α</sub>) of the cobalt-bound methyl group in noncrystalline methyl-cob(III)yrinates<sup>95</sup> (for later examples of NMR-spectroscopic studies of such isomerism, see Ref. 96). The analysis of NOE data and of three-bond coupling constants was used to extract detailed and important information on conformational properties of the (ribose part of the) nucleotide moiety, of the (ribose and base parts of the) organometallic group and of the other peripheral side chains.<sup>87</sup> Accordingly, among the most noteworthy findings from the more recent NMR studies are investigations of important conformational effects on B<sub>12</sub>-structures in aqueous. From such studies the detection of relevant conformational dynamics of the organometallic 5'-deoxy-5'-adenosyl moiety has resulted in the pioneering study of AdoCbl (**2**).<sup>102</sup> In a related context, extensive conformational dynamics of organometallic adenosyl ligand and the unusual (syn)-orientations of its adenine heterocycle were discovered in a series of coenzyme B<sub>12</sub> analogues, such as pseudocoenzyme B<sub>12</sub> (**29**),<sup>107</sup> neocoenzyme B<sub>12</sub> (**31**)<sup>108</sup> (see Figure 9) and other adenosyl-cobamides.<sup>87</sup> As noted above, extensive conformational flexibility of the organometallic ligand was also observed in the solution structures of adeninyl-alkyl-cobamides, such as adeninylpropylcobalamin (**20**)<sup>69</sup> and in α-adenosylcobalamin (**19**).<sup>65</sup>

2D-NMR spectroscopy was explored and proved to be a versatile method as a means to detect intra- and intermolecular H-bonding. The axially coordinating water-ligand of aquocobalamin perchlorate (**4**<sup>+</sup>-ClO<sub>4</sub>),<sup>45</sup> which forms an H-bond to an acetamide side chain in the crystal, could also be shown by NMR to still form a similar H-bond in aqueous solution. Pseudo-intramolecular H-bonding of a specific “external” water molecule to the nucleotide portion of methylcobalamin (**3**)<sup>73</sup> and some other organometallic cobamides, which is accompanied by a remarkable adjustment of the conformation of the nucleotide moiety, was characterized by NMR-spectroscopy.<sup>87</sup> In this way, first contributions have been made to characterize the hydration behavior of B<sub>12</sub>-derivatives in aqueous solution. Indeed, further exploratory studies have been undertaken recently to investigate in more detail the solvent environment of B<sub>12</sub>-derivatives in aqueous solution<sup>87</sup> and to complement other recent results from studies on the structure



**Figure 9.** Representative models of the structure of neocoenzyme  $B_{12}$  (**31**,  $Co_{\beta}$ -adenosyl-13-epi-cobalamin) in aqueous solution,<sup>108</sup> as obtained from NMR-restrained simulated annealing and minimization.

of the water networks in crystals of  $B_{12}$ -derivatives.<sup>47,63,64</sup> By way of measurements of NOE's between the solvent and methylcobalamin (MeCbl, **3**) the aqueous solution environment of **3** was investigated recently. As one result of these studies, a water molecule could also be detected to be the  $Co_{\alpha}$ -axial ligand in the protonated "base-off" form of MeCbl ( $3-H^+$ ), providing a first experimental example, where the (solution) structure of an organometallic "yellow" cobyrinic acid derivative was observed as a hexa-coordinated cobalt-corrin.<sup>109</sup>

Multidimensional NMR spectroscopy promises to provide not only an increasingly sophisticated means for the structural characterization of noncrystallizable  $B_{12}$ -derivatives with high resolution, but also to describe the dynamics of these complex molecules and their solution environment in a broad range of time domains.

### C. OTHER METHODS USED FOR STRUCTURAL STUDIES OF $B_{12}$ -DERIVATIVES

For structural analysis of the colored and chiral  $B_{12}$  molecules, UV-Vis-spectroscopy and circular

dichroism (CD) spectroscopy clearly were among the classical spectroscopic techniques.<sup>18,110</sup> The paramagnetic  $Co(II)$ -forms have attracted attention in structural investigations by electron spin resonance (ESR) spectroscopy,<sup>111</sup> a technique that has become of increasing importance for the characterization of paramagnetic intermediates in coenzyme  $B_{12}$ -catalyzed enzymatic reactions.<sup>112</sup> More recently, the development of soft ionization techniques in mass spectrometry has opened the  $B_{12}$ -field to the important bioanalytical techniques of fast atom bombardment (FAB) and electron spray ionization (ESI) mass spectrometry.<sup>113,114</sup> All of these spectroscopic techniques are well established as means of obtaining information on the constitution of  $B_{12}$ -derivatives, and can be combined routinely with chromatographic methods in order to rapidly analyze the  $B_{12}$ -content of samples from natural (bacterial, etc.) sources.<sup>105</sup> Applications of infrared (IR), Raman and resonance Raman spectroscopy, as well as the newly evolving branches FT-IR and FT-Raman spectroscopy have been powerful in helping to characterize the strengths of organometallic bonds in organometallic  $B_{12}$ -derivatives

and in other organo-Co(III)-complexes.<sup>115</sup> The latter techniques again are of particular use also for the characterization of protein-bound B<sub>12</sub>-derivatives.

### III. B<sub>12</sub>-Electrochemistry

Under physiological conditions vitamin B<sub>12</sub>-derivatives have been observed in three different oxidation states – Co(III), Co(II) or Co(I) – each possessing different coordination properties and qualitatively differing reactivities.<sup>18,70,81</sup> Oxidation–reduction processes therefore are of key importance for the chemistry and biology of B<sub>12</sub>. Electrochemical methods appear particularly valuable for controlled generation of reduced vitamin B<sub>12</sub>-derivatives<sup>116,117</sup> and have been applied for the purpose of synthetic transformations using B<sub>12</sub> as substrate<sup>118</sup> or as catalyst,<sup>119,120</sup> as well as for the purpose of the generation of reduced forms of protein-bound B<sub>12</sub>-derivatives<sup>121</sup> and electrode-bound B<sub>12</sub>-derivatives for analytical applications.<sup>122</sup> The combined use of electrochemical (potentiostatic) and spectroscopic (UV–Vis- or ESR-spectroscopic) techniques has provided significant information on redox processes involving homogeneously dissolved<sup>123</sup> or enzyme-bound<sup>121</sup> corrinoids.

Axial coordination to the corrin-bound cobalt center characteristically depends on the formal oxidation state of the cobalt ion<sup>34</sup> and, as a rule, the number of axial ligands decreases in parallel with the cobalt oxidation state: In the thermodynamically predominating forms of cobalt corrins, two axial ligands are bound to the diamagnetic Co(III)-center (coordination number 6), one axial ligand is bound to the paramagnetic (low spin) Co(II)-center (coordination number 5) and axial ligands are absent or only very weakly bound to the diamagnetic Co(I)-center (coordination number 4).<sup>18,79,116</sup> Electron transfer reactions involving B<sub>12</sub>-derivatives accordingly are accompanied by changes in the number of axial ligands. Thermodynamic and kinetic features of the electrochemistry of cobalt corrins therefore depend heavily upon the nature of (potential) axial ligands.<sup>116,117</sup>

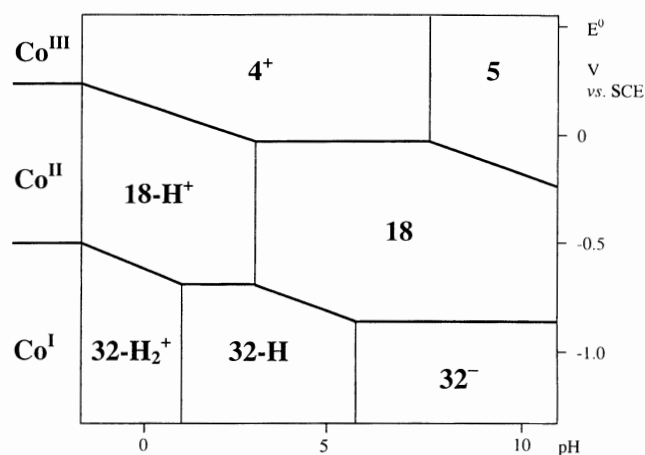
In Co(III)-corrins, such as the cob(III)alamins vitamin B<sub>12</sub> (**1**, CNCbl), aquocobalamin (**4**<sup>+</sup>, B<sub>12a</sub>), hydroxocobalamin (**5**, HOCbl), methylcobalamin (**3**, MeCbl) and coenzyme B<sub>12</sub> (**2**, AdoCbl) (see Figure 1) the corrin-bound metal center binds two axial ligands kinetically rather labile and has (variable) electrophilic properties. In the “base-on” cobalamins, one of the axial ligands is the DMB-base. In contrast, the metal center in

Co(I)-corrins, such as in cob(I)alamin (**32**<sup>−</sup>, B<sub>12s</sub>), represents a highly nucleophilic center<sup>124</sup> with very low basicity.<sup>116,125</sup> The intermediate oxidation state, that of Co(II)-corrins, such as in cob(II)alamin (**18**, B<sub>12r</sub>), provides a highly reactive metal-centered radicaloid species.<sup>79,126</sup> Electrochemistry thus provides an excellent means for generating B<sub>12</sub>-derivatives with specific reactivities as well as for investigating redox processes interconverting them. A review article by Lexa and Savéant<sup>116</sup> on the groundbreaking work on the electrochemistry of B<sub>12</sub>-derivatives, covers their own, now classic contributions<sup>123,127–137</sup> and earlier work from other laboratories up to about 1982 (e.g. Refs. 138,139).

#### A. THERMODYNAMIC REDOX PROPERTIES OF COBAMIDES

The electrochemistry of the B<sub>12</sub>-derivative aquocobalamin (**4**<sup>+</sup>) was particularly well studied.<sup>116,123,127,129,134–137</sup> The one-electron reduction of **4**<sup>+</sup> gives B<sub>12r</sub> (**18**) first and then B<sub>12s</sub> (**32**<sup>−</sup>). In contrast to the well-known structures of HOCbl,<sup>41</sup> of **4**<sup>+</sup>,<sup>45,96</sup> and of B<sub>12r</sub> (**18**),<sup>61,112</sup> pertinent structural data of a Co(I)-corrin are unavailable, such as of B<sub>12s</sub> (**32**<sup>−</sup>).<sup>34</sup>

Typically, electrochemical studies with aquocobalamin (**4**<sup>+</sup>) were carried out in aqueous solution. A diagram that correlates standard potentials (referenced to the saturated aqueous calomel electrode (SCE), whose potential is 0.242 V vs. normal hydrogen electrode (NHE))<sup>140</sup> and pH values in aqueous solution for measurements with the system aquocobalamin (**4**<sup>+</sup>)–B<sub>12r</sub> (**18**)–B<sub>12s</sub> (**32**<sup>−</sup>) is depicted in Figure 10.



**Figure 10.** Diagram showing the dependence of standard potentials of the redox system Co(III)/Co(II)/Co(I)-corrin (B<sub>12a</sub>, **4**<sup>+</sup>/B<sub>12r</sub>, **18**/B<sub>12s</sub>, **32**<sup>−</sup>), upon pH in aqueous solution (at 22°C), adapted from Lexa and Savéant;<sup>116</sup> electrochemical potentials are referenced to the saturated aqueous calomel electrode (SCE), which is at 0.242 V vs. normal hydrogen electrode (NHE).<sup>140</sup>

The interconversions between the different oxidation states of  $B_{12}$ -derivatives usually can be monitored well by UV-Vis-spectroscopy<sup>141</sup> and the data in Figure 10 were obtained from potentiostatic measurements, which were followed by UV-Vis-spectroscopy.<sup>116,123</sup> Within the ranges from pH -1 to 11 and of applied potentials between  $E=0.5$  V and  $-1.2$  V vs. SCE seven solution cobalamins are predominant thermodynamically,<sup>116</sup> spanning a range of the three formal oxidation states of  $B_{12}$ .

Aquocob(III)alamin ( $4^+$ ) and HOCbl (**5**) differ by the state of protonation of the “upper” axial ligand, with  $pK_a(4^+)=7.8$ .<sup>116</sup> The Co(II)-corrin **18** represents the “base-on” form of the Co(II)-oxidation level (i.e. having the nucleotide moiety coordinated intramolecularly), which is transformed into the “base-off” form (**18-H<sup>+</sup>**) by the protonation of the DMB-base, with  $pK_a(18-H^+)=2.9$ .<sup>116</sup> At the Co(I)-level, cob(I)alamin (**32<sup>-</sup>**) is protonated first at the nucleotide base to **32-H**, and then at the Co(I)-center, to give the “Co(III)-hydride”<sup>125</sup> **32-H<sub>2</sub><sup>+</sup>**, with a  $pK_a(32-H_2^+)$  of about 1<sup>116,125,142</sup> (see Figure 11). For **32-H** the  $pK_a$  has been estimated as 5.6 more recently,<sup>143,144</sup> which differs from the value (4.7) determined originally.<sup>116,123,129</sup>

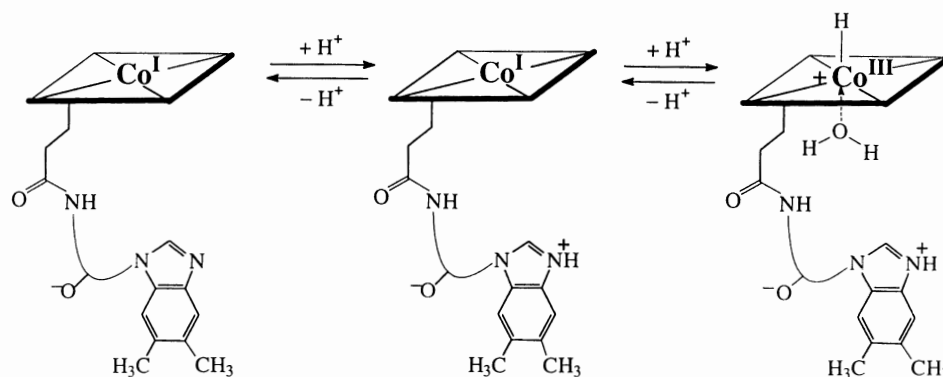
In the pH range from 2.9 to 7.8,  $4^+$  and (base-on)  $B_{12r}$  (**18**) represent the predominant Co(III)-/Co(II)-redox couple, with a standard potential of  $-0.04$  V (see Figure 10). For the Co(II)-/Co(I)-redox system there are two pH-independent standard potentials:<sup>116</sup> below pH 5.6 the Co(II)-/Co(I)-couple (base-off) **18-H<sup>+</sup>**/**32-H** predominate at a standard potential of  $-0.74$  V, but for the redox couple (base-on)  $B_{12r}$  (**18**)/ $B_{12s}$  (**32<sup>-</sup>**) the standard potential is more negative, at  $-0.85$  V<sup>116</sup> ( $-0.88$  V<sup>144</sup>).

A shift by about 120–140 mV to more negative potentials therefore is indicated for the reduction of (the base-on form of)  $B_{12r}$  (**18**), when compared to that of the protonated base-off form **18-H<sup>+</sup>**. This reflects the

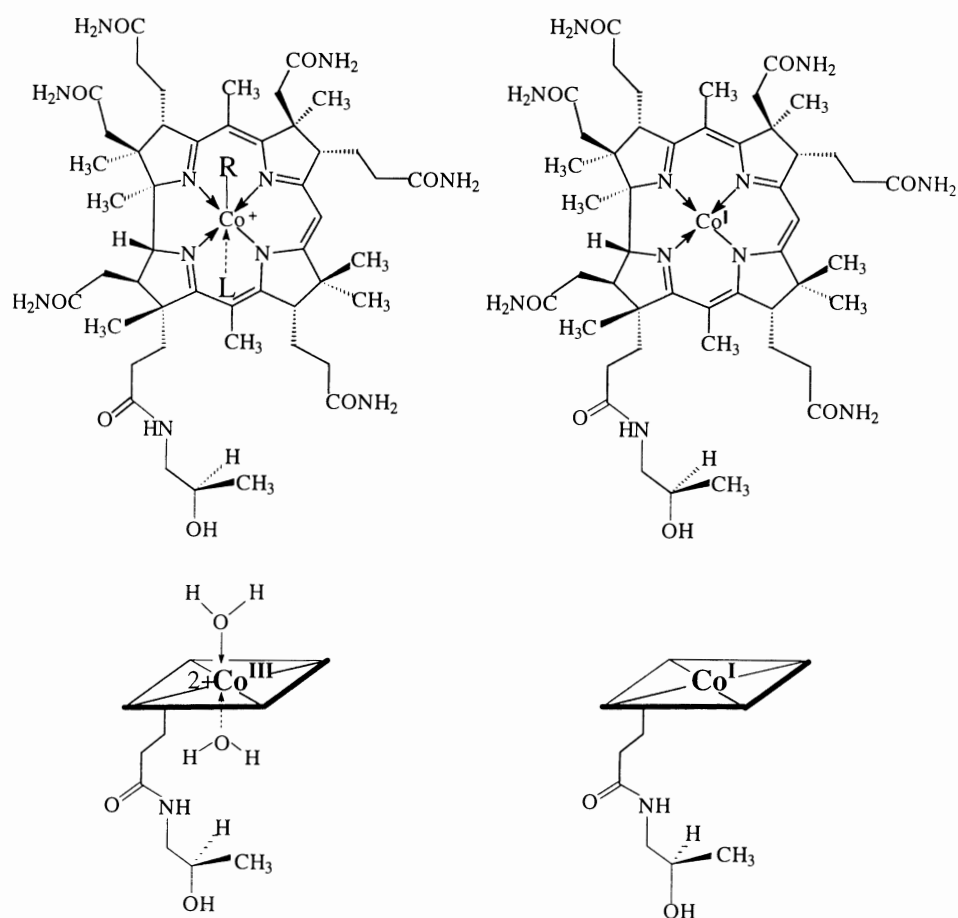
selective stabilization of the Co(II)-corrin **18** by intramolecular nucleotide coordination.<sup>81,116</sup> A dependence of the standard potentials of the Co(III)-/Co(II)-redox couples of roughly 60 mV per pH unit, at pH > 7.8 for HOCbl (**5**)/ $B_{12r}$  (**18**) and at pH < 2.9 for  $4^+$ /protonated base-off Co(II)-corrin (**18-H<sup>+</sup>**) reflects the effect of the removal by protonation of one axial ligand. Likewise, the Co(II)-/Co(I)-redox couple  $B_{12r}$  (**18**)/protonated (base-off) Co(I)-corrin (**32-H**) exhibits an analogous dependence of the potential between pH 2.9 and ca. 5.6, as well as, below pH 1, that of the Co(II)-/Co(I)-redox couple **18-H<sup>+</sup>** and **32-H<sub>2</sub><sup>+</sup>**. At all pH-values the disproportionation of Co(II)-corrins to Co(I)- and Co(III)-corrins is thermodynamically disfavored (with a disproportionation equilibrium constant below about  $10^{-10}$ ).<sup>116</sup>

The analogous electrochemical studies with vitamin  $B_{12}$  (**1**) reflect a complex interplay between thermodynamic and kinetic aspects of electron transfer reactions due to the involvement of the strongly coordinating cyano ligand (reviewed in<sup>116,117</sup>). Cyanide ion transforms vitamin  $B_{12}$  (**1**) into (base-off) dicyanocob(III)alamin (**1-CN<sup>-</sup>**) with an equilibrium constant of about  $10^4$  M<sup>-1</sup>.<sup>18,132</sup> Coordination of (one or two) cyanide ions to the Co(III)-center stabilizes it against reduction and shifts the Co(III)-/Co(II)-standard potentials to more negative values.<sup>116,132</sup>

Electrochemical studies with the “incomplete” diaquocobinamide (**33-H<sup>2+</sup>**) (see Figure 12) positioned the standard electrochemical potential of the diaquocob(III)inamide (**33-H<sup>2+</sup>**)/aquo-cob(II)inamide (**34<sup>+</sup>**) couple at  $+0.270$  V.<sup>116,133</sup> The potential of the corresponding aquo-cob(II)inamide (**34<sup>+</sup>**)/cob(I)inamide (**35**) couple was determined as  $-0.73$  V.<sup>116</sup> The standard potential of the redox couple of the “incomplete” corrins **34<sup>+</sup>** and **35** thus is indistinguishable from that of the Co(II)-/Co(I)-couple of the base-off cobalamins



**Figure 11.** Acid/base equilibria involving the Co(I)corrin  $B_{12s}$  (**32<sup>-</sup>**): Protonation of  $B_{12s}$  in water occurs at the DMB-base first to give **32-H**. At pH < 1, the second protonation gives diprotonated **32-H<sub>2</sub><sup>+</sup>**, a “Co(III)-hydride”.<sup>125</sup>



**Figure 12.** Top: Left: Structural formulae of diaquocob(III)inamide (**33-H<sup>2+</sup>**, R = H<sub>2</sub>O<sup>+</sup>, L = H<sub>2</sub>O) and methylcob(III)inamide (**36<sup>+</sup>**, R = CH<sub>3</sub>; L = H<sub>2</sub>O). Right: structural formula of cob(I)inamide (**35**); Bottom: corresponding symbols for diaquocob(III)inamide (**33-H<sup>2+</sup>**) and cob(I)inamide (**35**).

**18-H<sup>+</sup>/32-H.**<sup>116</sup> The standard potential of the diaquocob(III)inamide (**33-H<sup>2+</sup>**)/aquocob(II)inamide (**34<sup>+</sup>**) couple at +0.27 V corresponds to the value extrapolated for the very acidic protonated base-off form (**4-H<sup>2+</sup>**) of aquocob(III)alamin (**4<sup>+</sup>**), with pK<sub>a</sub> (**4-H<sup>2+</sup>**) = ca. -2.4.

Electrochemical studies with organometallic B<sub>12</sub>-derivatives are complicated due to rapid and irreversible loss of the organic ligand upon reduction of organometallic B<sub>12</sub>-derivatives<sup>116,128,143,144</sup> and low temperature conditions are used to obtain pertinent thermodynamic information.<sup>128</sup> The standard potential (at -30°C) for the Co(III)-/Co(II)-redox couple methylcob(III)alamin (**3**)/methylcob(II)alamin (**37<sup>-</sup>**) was estimated as -1.60 V vs. SCE,<sup>116,128,131</sup> similar to the pair coenzyme B<sub>12</sub>/5'-deoxy-5'-adenosyl-cob(II)alamin.<sup>144</sup> One-electron reduction of methylcob(III)alamin (**3**) occurs with decoordination of the nucleotide base and gives the methylcob(II)alamin anion **37<sup>-</sup>**, which rapidly decomposes into cob(I)alamin (**32<sup>-</sup>**) and a methyl radical (see below). The standard potential of the typical

Co(III)-/Co(II)-redox couple of organometallic B<sub>12</sub>-derivatives is significantly more negative than that of B<sub>12r</sub> (**18**)/B<sub>12s</sub> (**32<sup>-</sup>**) and out of the reach of biological reductants. For the data on the redox-couple methylcob(III)inamide (**36<sup>+</sup>**)/methylcob(II)inamide (**38**) see below.<sup>128</sup>

The thermodynamic trends of the B<sub>12</sub>-redox systems can be summarized as:

- (i) Intramolecular coordination of the nucleotide base stabilizes the corrin-bound cobalt center against one-electron reduction.
- (ii) Aquo-Co(III)-corrinoids are rather strong oxidizing agents and are unstable toward reduction at the intracellular redox potential of most living cells.<sup>121</sup>
- (iii) Strongly coordinating or nucleophilic ligands (such as cyanide ions) shift the Co(III)-/Co(II)-redox couples to more negative potentials.
- (iv) The one-electron reduction of alkyl-Co(III)corrins typically occurs at potentials more negative than the Co(II)-/Co(I)-redox couple B<sub>12r</sub>/B<sub>12s</sub>.<sup>116,128,144</sup> Exceptions to the last correlation are provided by some organometallic B<sub>12</sub>-derivatives with

electron withdrawing substituents on the organo-metallic group, such as methoxycarbonylmethylcob(III)alamin.<sup>145,146</sup>

## B. KINETIC REDOX PROPERTIES OF COBAMIDES

One-electron transfer reactions with corrinoid cobalt complexes are intimately coupled to cleavage or formation of bonds to axial ligands. A reduction is accompanied by expulsion (and oxidation by the coordination) of an axial ligand.<sup>116</sup> The electron transfer steps accordingly take place either in a concerted fashion or in a rapid associated step with dissociation or coordination of an axial ligand.

Electron transfer in the protonated Co(II)/Co(I)-couple  $18\text{-H}^+ / 32\text{-H}$  is fast in aqueous solution ( $k_S^{\text{app}} > 0.1 \text{ cm s}^{-1}$ ) as the presumed axial water ligand is only weakly bound kinetically in the base-off Co(II)-corrin  $18\text{-H}^+$ .<sup>116,127</sup> As soon as the aquo ligand in  $18\text{-H}^+$  is substituted by a stronger axial ligand, e.g. by the nucleotide base, as in base-on  $B_{12r}$ , electron transfer is slowed down sufficiently, so that its kinetics can conveniently be measured by cyclic voltammetry.<sup>116,135,136</sup> For the Co(II)/Co(I)-redox couple  $B_{12r} / B_{12s}$   $k_S^{\text{app}} = 0.0002 \text{ cm s}^{-1}$ ,<sup>116</sup> i.e. electron transfer is at least a thousand times slower than in the base-off forms  $18\text{-H}^+ / 32\text{-H}$ .

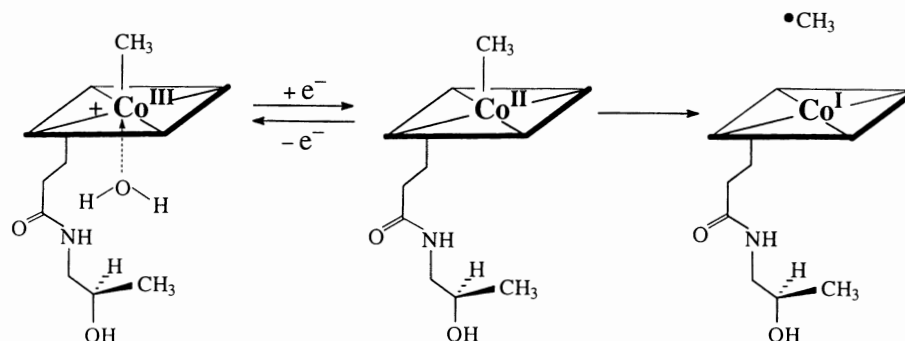
The electron transfer interconverting the Co(III)/Co(II)-couple aquocob(III)alamin ( $4^+$ )/ $B_{12r}$  ( $18$ ) is rather slow, with an apparent rate constant  $k_S^{\text{app}}$  for heterogeneous electron transfer of about  $10^{-5} \text{ cm s}^{-1}$ .<sup>116</sup> The electron transfer steps for the cyano-cob(III)- and cyano-cob(II)alamins  $1\text{-CN}^-$  and  $18\text{-CN}^-$  are slower still.<sup>116,132,134</sup> The trend in the kinetics is similar for Co(III)/Co(II)-couples as for the corresponding Co(II)/Co(I)-couples. There is an approximately linear correlation between the equilibrium constant for coordination by the axial ligand and the standard apparent rate

constant for electron transfer.<sup>116</sup> This correlation has been rationalized by a model, in which stretching of the bond between the corrin-bound cobalt ion and the axial ligand represents the main parameter of the kinetics of the electron transfer reaction. As a consequence, kinetic and thermodynamic dependence of the electron transfer on the strength of the complexation of axial ligands both add up, resulting in a rapid shift of the effective reduction potentials as the strength of the ligand increases.

Organocobalamins, such as coenzyme  $B_{12}$  ( $2$ ) and MeCbl ( $3$ ), exhibit a different kinetic behavior from CNCbl and other Co(III)-corrins bearing strong axial ligands. While the Co(III)/Co(II)-reduction potentials are quite negative (see above) kinetics of electron transfer is fast.<sup>116</sup> The intermediate Co(II)-complex  $38$  formed upon one-electron reduction of methylcobinamide ( $36^+$ ) (see Figure 13) has a half life of only about 0.1 s (even) at  $-20^\circ \text{C}$ . An Arrhenius plot of the kinetics of the decomposition of  $38$  gave 19 kcal/mol as activation energy and a pre-exponential factor  $A = 10^{17.6} \text{ s}^{-1}$ .<sup>116,128,131</sup> The one-electron reduction product of MeCbl ( $3$ ) has electrochemical properties of the even more unstable base-off Co(II)-intermediate ( $37^-$ ), which was estimated to decompose to a methyl radical and cob(I)alamin ( $32^-$ ) with a rate constant of about  $1200 \text{ s}^{-1}$  at  $-30^\circ \text{C}$ . From the corresponding value (37 kcal/mol) of the (Co-C)-bond dissociation energy in MeCbl ( $3$ ),<sup>147,148</sup> and the kinetics of the decomposition of the reduction intermediate  $37^-$ , the one-electron reduction thus is suggested to reduce the strength of the (Co-C)-bond of MeCbl (by about 12 kcal/mol) to "half" of its value.<sup>116,128</sup>

## C. ORGANOMETALLIC ELECTROCHEMICAL SYNTHESIS

Electrochemistry provides a convenient method for the selective production of reduced  $B_{12}$  forms under



**Figure 13.** One-electron reduction of methylcob(III)inamide ( $36^+$ ) presumably occurs with loss of a water ligand and gives methylcob(II)inamide ( $38$ ), which rapidly decomposes into cob(I)inamide ( $35$ ) and a methyl radical.

potentiostatic control. Alkyl halides or alkyl tosylates react quickly and with high efficiency with the highly nucleophilic Co(I)-corrins.<sup>18,124</sup> As Co(I)-corrins may be generated cleanly at controlled electrode potentials near that of the Co(II)/Co(I)-couples, electrochemistry provides an excellent means for the synthesis of organometallic B<sub>12</sub>-derivatives on a preparative scale (see Figure 14).<sup>76,80</sup> In one approach, the Co(III)cobamide is first reduced electrochemically to its Co(I)-form, followed by addition of the alkylating agent to the reduced solution of the Co(I)-corrinoid with strict protection from air (see e.g. Ref. 118). Alternatively, electrochemical two-electron reduction of the Co(III)cobamide to its Co(I)-form is carried out in the presence of the alkylating agent and direct formation of the organometallic Co(III)cobamide occurs (see e.g. Refs. 80,149). Both approaches benefit from the resistance of most organometallic B<sub>12</sub>-derivatives to heterogeneous or homogeneous reduction under conditions, where Co(I)-corrins are present.

Using electrolysis at a controlled potential of  $-1.1$  V vs. SCE, coenzyme B<sub>12</sub> (**2**) was prepared in 95% yield from vitamin B<sub>12</sub> (**1**) or from aquocobalamin (**4**<sup>+</sup>).<sup>150</sup> Other organometallic B<sub>12</sub>-derivatives prepared similarly were e.g. pseudocoenzyme B<sub>12</sub> (**29**: 78% yield, from pseudovitamin B<sub>12</sub>,<sup>107</sup> 2',3'-dideoxycoenzyme B<sub>12</sub> (**39**: 83% yield from aquocobalamin (**4**<sup>+</sup>) and 2',3',5'-trideoxy-5'-tosyladenosine,<sup>118</sup> and the alkyl bridged, photochemically labile dimeric B<sub>12</sub>-derivative **26**.<sup>76</sup>

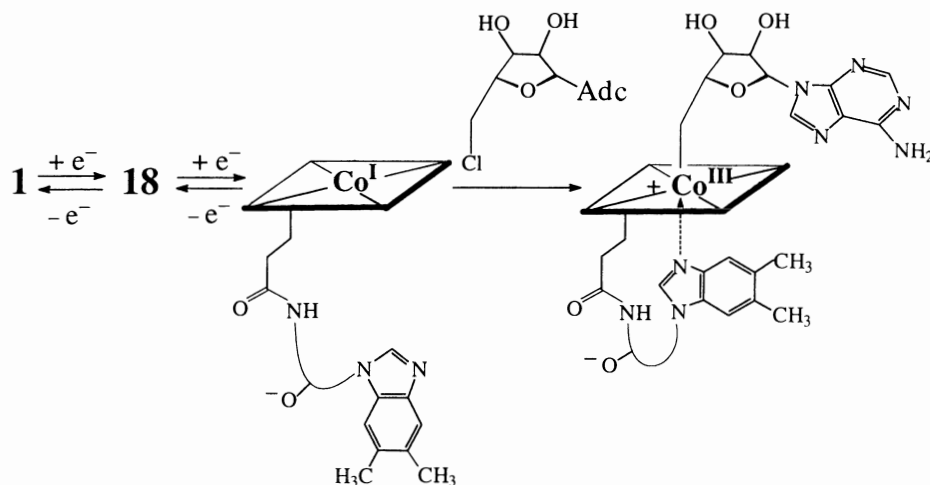
Commercial vitamin B<sub>12</sub> (**1**) and aquocobalamin (**4**<sup>+</sup>) could be made useful as catalysts in electrochemical devices:<sup>119,151,152</sup> dehalogenation reactions of various alkylhalides to the corresponding alkyl-derivatives were carried out cleanly,<sup>151-153</sup> vicinal dihaloalkanes were

reduced to alkenes<sup>154</sup> and electrocatalysis with B<sub>12</sub> was developed as a mild method for (C-C)-bond formation in organic synthesis.<sup>119,152,153</sup> Exploiting the well-known photolability of the intensely colored organometallic B<sub>12</sub>-derivatives, visible light was used in addition to the electrochemical system, to drive the catalytic cycle, leading to the development of new photo-electrocatalysis with B<sub>12</sub>.<sup>119,152,153,155</sup> A variety of interesting problems in natural products synthesis could be tackled with good success, providing new synthetic entries to some terpenes,<sup>156</sup> prostaglandins,<sup>157</sup> jasmonates<sup>158</sup> and carbohydrate derivatives.<sup>155</sup> In related studies, but using the more lipophilic heptamethylcobyrinate "cobester" (**15**) and analogous heptaalkylcobyrinates, electrochemical reactions have been explored to mediate radical reactions in organic solvents.<sup>159</sup>

The knowledge concerning the redox chemistry of B<sub>12</sub>-derivatives provides a basis for their application in (electro)synthesis and electrocatalysis in aqueous solution, as well as in analytical electrochemical devices. In this way, the natural cofactor and vitamin, B<sub>12</sub> contributes to today's developments in "green" synthetic chemistry.<sup>160</sup>

#### IV. Reactivity of B<sub>12</sub>-Derivatives in Organometallic Reactions

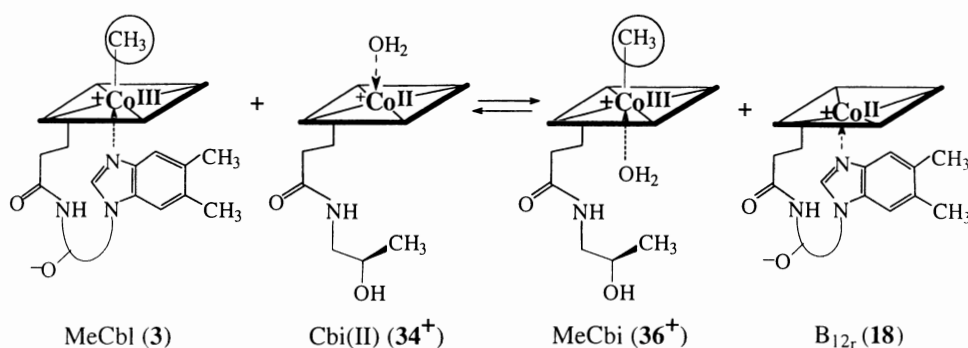
The chemistry of vitamin B<sub>12</sub>-derivatives has many interesting facets, many of which are relevant for the biological roles of the corrinoids.<sup>18,20,81,161-165</sup> The (biological) formation and cleavage of the (Co-C)-bond in the (organometallic) B<sub>12</sub>-cofactors are essential steps of the reactions catalyzed by B<sub>12</sub>-dependent enzymes



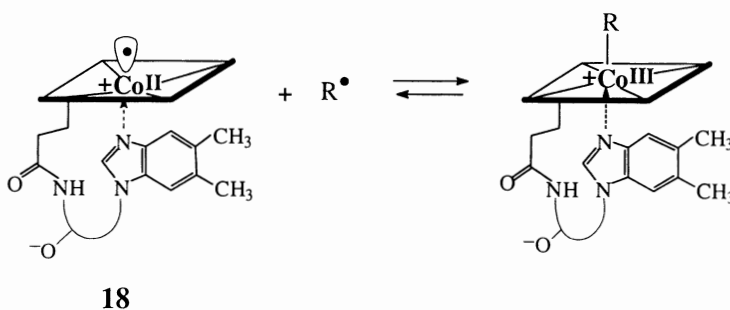
**Figure 14.** Preparation of coenzyme B<sub>12</sub> (**2**) from CNCbl (**1**) by electrochemical reduction to cob(I)alamin (**32**<sup>-</sup>) and alkylation with 5'-deoxy-5'-chloroadenine.







**Figure 15.** Methyl-transfer reaction involving MeCbl (3) and MeCbi (36<sup>+</sup>) as methyl group donors and B<sub>12r</sub> (18) and Cbi(II) (34<sup>+</sup>) as methyl-group acceptors.



**Figure 16.** Cob(II)alamin (18), a “radical trap” specific for combination on the “upper”  $\beta$ -face.

of 18. The DMB-coordination in cob(II)alamin controls the ( $\alpha/\beta$ )-diastereoface selectivity (in a kinetic and a thermodynamic sense) in alkylation reactions at the corrin-bound Co(II) center (see Figure 16).

In “incomplete” corrins (such as cob(II)ester (17) or “base-off”-forms of “complete” corrins, the stereochemical situation is considerably more complex: the (often hypothetical) axial ligand at the corrin-bound Co(II) center is also expected to direct the recombination reaction of such Co(II)-corrins with alkyl radicals to the unligated face of the metal center; in this way, kinetic control may lead with high efficiency to the “rare”  $\alpha$ -alkyl-Co(III)-corrins.<sup>95,173</sup> Accordingly, in such radical recombination reactions the axial ligand at the ( $\alpha$ - or  $\beta$ -side) of the Co(II)-center will not only steer the diastereoselectivity of the alkylation at the Co(II)-center, but it may also contribute significantly to altering the cage effects.<sup>168,169</sup> The observation of considerable cage effects in homolytic reactions of organocobalamins (such as AdoCbl, 2) and organocobinamides (such as Co $_{\beta}$ -5'-deoxy-5'-adenosyl-cobinamide, AdoCbi, 28)<sup>169,173</sup> is consistent with the finding of magnetic field effects on homolytic reactions (in homogeneous solution and in B<sub>12</sub>-dependent enzymes) of AdoCbl.<sup>175,176</sup>

The second biologically important type of organometallic reactivity of the B<sub>12</sub>-derivatives is provided by

the highly nucleophilic/nucleofugal character of Co(I)-corrins.<sup>81,124,177</sup> It is the basis for a heterolytic mode of formation/cleavage of the (Co–C)-bond in methyl-corrinoids in enzyme-catalyzed methyl-transfer reactions.<sup>170–172</sup> This mode is represented by the reaction of Co(I)-corrins with alkylating agents and by the nucleophile-induced demethylation of methyl-Co(III)-corrins and formally corresponds to an oxidative trans addition/reductive trans elimination at the corrin-bound metal center.<sup>161,178</sup>

Alkylation at the corrin-bound Co(I) center may accordingly proceed via the “classical” bimolecular nucleophilic substitution (S<sub>N</sub>2) mechanism (involving Co(I)-corrins as “supernucleophiles”).<sup>124,177</sup> However, in specific cases, it may occur via a two-step one-electron transfer path (involving Co(I)-corrins as strong one-electron reducing agents and progressing via Co(II)-corrin intermediates).<sup>95</sup> In nucleotide-containing “complete” corrins, such as B<sub>12s</sub> (32<sup>-</sup>), either pathway will result, for thermodynamic and for kinetic reasons<sup>80,178</sup> in preferential  $\beta$ -methylation (see Figure 17), allowing the nucleotide to coordinate intramolecularly at the  $\alpha$ -face in methylcobalamin (3) (and in the intermediate cob(II)alamin (18)). The exchange of the nucleotide base from a DMB-base to imidazole, as similarly observed in methionine synthase, has little effect on the thermodynamics of the methyl-transfer reaction.<sup>75</sup>

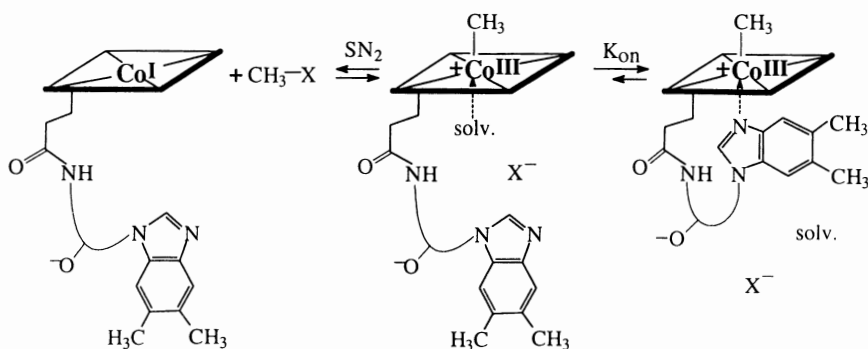


Figure 17. Methylation of the DMB-containing cob(I)alamin B<sub>12s</sub> (32<sup>-</sup>) is directed to the "upper" β-face.

Studies with Co(I)-corrins in solution, such as B<sub>12s</sub> (32<sup>-</sup>), have provided the following reactivity patterns relevant for the S<sub>N</sub>2-alkylation path:

- the nucleophilicity of Co(I)-corrins in solution is practically independent of the presence of an appended nucleotide, "complete" or "incomplete" Co(I)-corrins preferentially react at their β-face with electrophiles, i.e. their β-face is inherently more nucleophilic;<sup>124,177,178</sup>
- the immediate product of the β-alkylation accordingly may be a pentacoordinate (or already solvated and effectively hexacoordinate) Co<sub>β</sub>-alkyl-Co(III)-corrin;
- in aqueous solution and at room temperature the "base-on" (hexacoordinate) methyl-cob(III)alamin (3) is more stable by about 4 kcal/mol than the "base-off" Co<sub>α</sub>-aquo-Co<sub>β</sub>-methylcob(III)alamin (3a)<sup>179</sup> (i.e. in Figure 17,  $K_{ON} \approx 1000$ ). From NMR studies, the latter can be estimated to still be more stable in water by about 7 kcal/mol than the corresponding ("base-off" and dehydrated form of) Co<sub>β</sub>-methylcob(III)alamin (3b), carrying a penta-coordinate Co<sub>β</sub>-methyl-Co(III)-center.<sup>180</sup> Indeed, convincing structural evidence for the existence of pentacoordinate alkyl-Co(III)-corrins<sup>181</sup> is (still) lacking, while indications for hexacoordinate "base-off" Co<sub>α</sub>-aquo-Co<sub>β</sub>-methylcob(III)alamin (3a) recently could be obtained from NOE-studies in water.<sup>109</sup>

Corresponding considerations from solution chemistry on the less well studied one-electron transfer pathway of alkylation at the corrin-bound Co(I)-center in "complete" corrins, such as cob(I)alamin,<sup>182</sup> would arrive at the same overall structural result (see Scheme 9 in Ref. 81).

The situation is, once again, more complex in the nucleotide devoid (i.e. "incomplete") cobalt-corrins, where two diastereoisomeric alkylation products are

often found.<sup>96,178</sup> In specific cases, under suitable kinetic control, one of the two diastereoisomeric alkyl-Co(III)-corrins may form with high selectivity: as shown with the lipophilic Co(I)-heptamethylcobyrinate,<sup>95</sup> the S<sub>N</sub>2-pathway can provide β-methylation with high diastereoselectivity (>95%), while the one-electron transfer mechanism may actually permit the formation of the Co<sub>α</sub>-methylation product, with high diastereoselectivity (up to >98%).<sup>81,95</sup> In these investigations and in related ones, methyl-group transfer reactions (involving Co(I)-, Co(II)- and unalkylated Co(III)-corrins as methyl-group acceptors) may often provide a complication by allowing for rapid equilibration.<sup>178</sup>

The less well investigated reverse processes, the nucleophile-induced dealkylations of methyl-Co(III)-corrins, are impeded by the intramolecular coordination of the nucleotide base, both for thermodynamic and kinetic reasons.<sup>178,183</sup> Indeed, thiolates demethylate methyl-cobinamide to cob(I)inamide roughly 1000 times faster than MeCbl (3) to B<sub>12s</sub> (32<sup>-</sup>),<sup>183</sup> reflecting the stabilizing effect of the nucleotide coordination in 3.<sup>80,178</sup> This is of relevance for enzymatic methyl-group transfer reactions involving protein bound Co(I)- and methyl-Co(III)-corrins, where considerable axial base effects are therefore to be expected, as actually observed in methionine synthase (see below).<sup>170,184</sup>

The two elementary modes of formation and cleavage of the (Co-C)-bond at the corrin-bound cobalt center differ critically in their structural requirements:

- the heterolytic mode of cleavage and of formation (e.g.) of the (Co-CH<sub>3</sub>)-bond of methylcobalamin is subject to extensive reorganization at both faces of the corrin-bound cobalt center and is induced by attack of a nucleophile (either an external nucleophile or the Co(I)-center) at the easily accessible methyl-group carbon;
- the homolytic mode of cleavage and of formation (e.g.) of the (Co-C)-bond of coenzyme B<sub>12</sub> on the

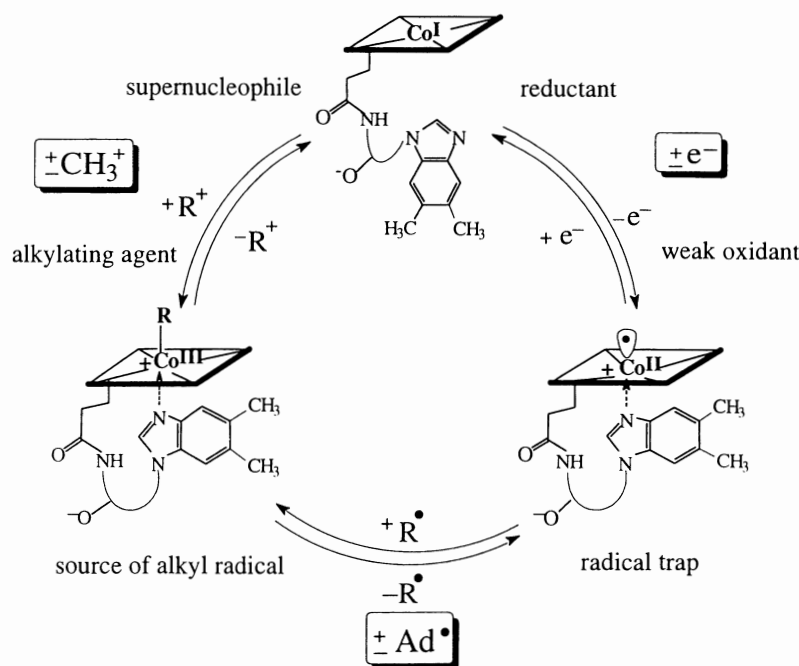
other hand, can hardly experience electronic stabilization from interaction of the radical center with the (proteinic) environment and the accompanying structural reorganization concerns largely the separation of the homolysis fragments, but is indicated to be insignificant in the Co(III)-corrin portion (of **2**) itself (see Figure 18).

Further basic modes of formation/cleavage of the (Co–C)-bond of alkyl-Co(III)-corrins involve nucleophilic alkylating agents and the electrophilic reactivity of Co(III)-corrins.<sup>162–165</sup> The persistence of alkyl-Co(III)-corrins against proteolytic cleavage of the (Co–C)-bond is an important property, crucial for the cofactor role of the organometallic B<sub>12</sub>-coenzymes under physiological conditions (and surprising at first sight for organometallic compounds). Here also, the intramolecular nucleotide coordination modifies the reactivity of the metal center: it enhances the ease of abstraction of the cobalt-bound alkyl group by an electrophile, both in a kinetic and a thermodynamic sense.<sup>81,185</sup> In addition, acid-induced heterolytic cleavage of the (Co–C)-bond of organocobamides has been found to be highly dependent upon the substituents on the metal-bound organic group: coenzyme B<sub>12</sub> (**2**) proved to be less sensitive to this mode of heterolytic cleavage of the (Co–C)-bond, than e.g. 2'-deoxycoenzyme B<sub>12</sub> and 2',3'-di-deoxycoenzyme B<sub>12</sub> (2',5'-dideoxy-5'-adenosylcobalamin and 2',3',5'-trideoxy-5'-adenosylcobalamin).<sup>118,186</sup> This (significant) reactivity difference with respect to

acid-induced dealkylation can be traced back to the combined effect of ease of protonation of the metal-bound organic group and conformational control of eliminative fragmentation.<sup>118</sup> These latter factors contribute to the surprising insensitivity for proton-induced heterolytic cleavage of the (Co–C)-bond of the coenzyme **2**.

A still little recognized mode of cleavage of the carbon–cobalt bond of organocobamides, may be represented by the thermodynamically (and presumably also kinetically) favorable radical-induced substitution at the cobalt-bound carbon center.<sup>76,187</sup> This type of reactivity may be of interest in the context of some unusual (C–C)-bond forming reactions at seemingly unactivated carbon centers.<sup>188</sup> On the other hand, further interesting, mechanistically complex (but potentially biologically relevant) modes of formation of the (Co–C)-bond in methyl-Co(III)-corrins involve the alkylation of Co(II)-corrins by highly reactive and easily reduced alkylating agents (such as methyl iodide).<sup>106,189</sup>

Organometallic B<sub>12</sub>-derivatives have long been known to be very sensitive to visible light,<sup>179</sup> which induces the (homolytic) cleavage of the organometallic bond with a quantum yield of about 0.3.<sup>190,191</sup> One-electron reduction of organyl-Co(III)-corrins has also been found to weaken the (Co–C)-bond dramatically, rendering organo-cob(III)amides labile to strong one-electron reducing agents (see Section III<sup>146</sup>). This latter



**Figure 18.** Formal analysis of elementary reaction steps of "complete" corrinoids characterizing their patterns of reactivity relevant for their cofactor function in B<sub>12</sub>-dependent enzymes.

aspect may render it difficult to prepare those organo-cob(III)amides via alkylation of the corresponding (strongly reducing) cob(I)amides that bear electron-withdrawing substituents.<sup>146</sup> Occasionally, such organometallic B<sub>12</sub>-derivatives may be made by the alternative way of alkylating via Co(II)-corrins.<sup>106</sup>

## V. B<sub>12</sub>-Cofactors in Enzymatic Reactions

### A. OCCURRENCE AND STRUCTURE OF NATURAL CORRINOIDS

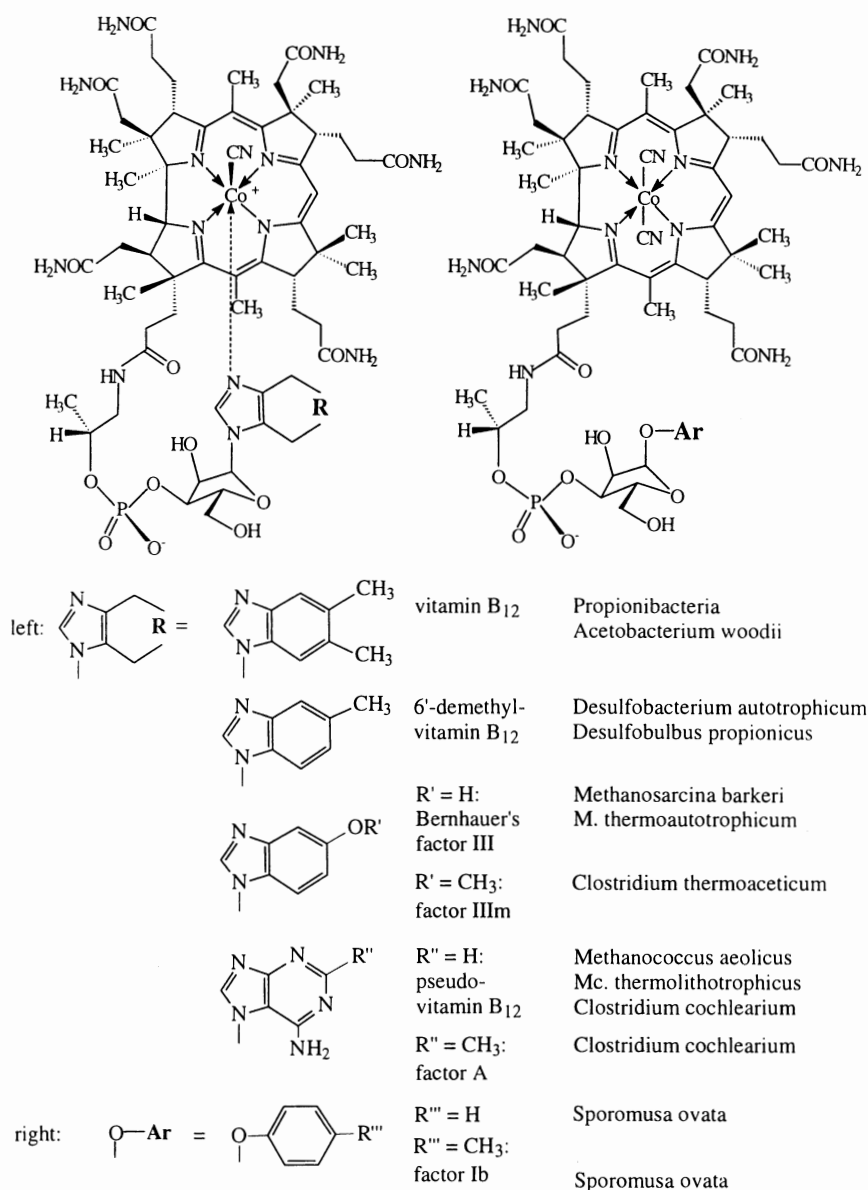
The natural B<sub>12</sub>-derivatives occur as “complete” corrinooids, which, are cobamides carrying a nucleotide function as an appendage of the propionic acid substituent at C17, or as “incomplete” corrinooids, i.e. cobyrinic acid derivatives lacking a nucleotide function and generally representing biosynthetic intermediates on the way to the “complete” corrinooids<sup>19,32</sup> (see e.g. Figures 1, 2 and 12). As a rule, the natural “complete” corrinooids may vary by the constitution of the “nucleotide base,” as well as of their (functional)  $\beta$ -axial ligand (see Section IV). For the purpose of the characterization of the corrinoid moiety, natural samples are routinely transformed into their stable cyano-Co(III)-forms. Sewage sludge is a particular rich, classical source of corrinooids.<sup>19</sup>

In vitamin B<sub>12</sub> (**1**, CNCbl) and in natural B<sub>12</sub>-analogues, benzimidazoles are found as the “nucleotide base,” such as the 5,6-dimethylbenzimidazole (DMB) of the cobalamins, purines, such as adenine and 2-methyladenine are found in pseudovitamin B<sub>12</sub> (**40**) and in factor A (**10**), respectively, and phenols, such as *p*-cresol in dicyano-*p*-cresolylcobamide (**41**)<sup>192</sup> (see Figure 19). The purine bases known to be present in “complete” corrinooids are mostly adenine derivatives or related heterocycles, as also found in RNA.<sup>193</sup> More recent studies on the corrinooids from anaerobic microorganisms have shown a spectrum of purine bases,<sup>81,105</sup> as well as selected benzimidazoles (see Figure 20).<sup>194</sup> In a variety of anaerobes, the nucleotide moiety of “complete” corrinooids is subject to rapid biosynthetic exchange, and exogenous heterocycles could be incorporated by the strategy of “guided biosynthesis”.<sup>192</sup> The latter method was used for the preparation of B<sub>12</sub>-derivatives with “unnatural” bases, such as Co $\beta$ -cyano-imidazolylcobamide (**9**), in which imidazole is the  $\alpha$ -axial ligand.<sup>36</sup> The benzimidazoles and DMB are available from an anaerobic biosynthetic sequence, while the aerobes have evolved a second, different path for the biosynthesis of DMB.<sup>194</sup> The nucleotide portion

is attached to the B<sub>12</sub>-moiety in the later phases of the biosynthesis of “complete” cobamides.<sup>195</sup>

The functional B<sub>12</sub>-cofactors are unique due to their unusual  $\alpha$ -nucleotide function and all known “complete” corrinooids adhere to this common stereochemical feature, even with the non-coordinating phenolic (pseudo)nucleotides.<sup>18,19,192,194</sup> The unusual  $\alpha$ -configuration of the (pseudo)nucleotide appendage of “complete” corrinooids, first of all, enables the heterocyclic base to coordinate to the “lower”  $\alpha$ -axial coordination site of the corrin-bound cobalt center in an intramolecular fashion,<sup>22</sup> but may also be relevant for the discriminative recognition and binding of B<sub>12</sub>-derivatives by the B<sub>12</sub>-binding apoenzymes. The selective tight binding of complete corrinooids by human (and other) B<sub>12</sub>-binding proteins points to the importance of the structure of the nucleotide function for B<sub>12</sub>-uptake and B<sub>12</sub>-transport there as well (but the binding mode is not yet experimentally characterized).<sup>31,196</sup>

In solution, the intramolecular coordination to the “lower”  $\alpha$ -axial coordination site of the corrin-bound cobalt center of the nucleotide function of “complete” corrins occurs with little build-up of strain.<sup>51</sup> In this way, the (coordinating) nucleotide function steers the reactivity, as well as the face-selectivity, of certain organometallic reactions involving the corrin-bound cobalt center (see Section IV<sup>81</sup>). The finding that cobalamins can self-constitute in solution from the B<sub>12</sub>-nucleotide portion and incomplete cobyrinic acid derivatives has pointed to a remarkable kinetic and thermodynamic preference for the specific formation of the particular B<sub>12</sub> structure and to a pre-enzymatic origin of the basic structural elements of the complete corrins.<sup>51</sup> The structural variety of the unique (pseudo)-nucleotide unit of the “complete” corrinooids (the cobamides, see Figures 19 and 20) appears to be largely the consequence of the particular biosynthetic availability in the various (micro)organisms. For a functional “rationalization,” the differing coordination properties of the “complete” corrinooids may be considered, as reflected by the tendency of their biologically relevant organometallic forms (methyl-, 5'-deoxy-5'-adenosyl or other) to be “base-off” or “base-on” in aqueous solution.<sup>105</sup> Clearly, the phenolyl-cobamides are “complete” corrinooids with “base-off” structure, helpful for binding in a “base-off/His-on” form to B<sub>12</sub>-binding apoenzymes.<sup>197</sup> As revealed by the X-ray structure analysis of the B<sub>12</sub>-binding domain of methionine synthase,<sup>25</sup> the “base-off” form of the B<sub>12</sub>-cofactor MeCbl (**3**) presents a molecular surface to the protein, which is considerably larger than that of the “base-on” form **3**. Indeed, the



**Figure 19.** Structural formulae of representative CN-Co(III)-forms of "complete" corrinoids containing different nucleotide functionalities, as isolated from specific bacterial sources.<sup>81,105</sup>

unique nucleotide function of B<sub>12</sub>-cofactors thus is a specific structural attribute of the "complete" corrinoids, but, in the "dinucleotides" MeCbl (3), B<sub>12r</sub> (18) and B<sub>12s</sub> (32<sup>-</sup>), it also represents a moiety that is a general and essential feature of (dinucleotide)-cofactors, as well.<sup>81</sup>

### B. B<sub>12</sub>-DEPENDENT METHYL TRANSFERASES

B<sub>12</sub>-dependent enzymatic methyl-group transfer is broadly relevant in metabolism of microorganisms, and higher organisms as well. The particular ability of Co(I)- and methyl-Co(III)-corrins to function as the catalytically relevant cofactor-intermediates in such enzymatic

methyl-group transfer reactions appears explicable, considering the reactivity in solution of B<sub>12</sub>-derivatives<sup>18,79,81,165</sup> such as the "supernucleophilic" character of Co(I)-corrins<sup>124,177</sup> and the associated reactivity as exceptional entering and leaving groups in nucleophilic displacement reactions. B<sub>12</sub>-dependent methionine synthesis is well studied (see e.g. Ref. 170), as are methyl transferases in anaerobic acetogenesis (see e.g. Refs. 198,199), in methanogenesis (see e.g. Ref. 171), and in anaerobic catabolism of acetic acid to methane and carbon dioxide (see e.g. Ref. 200). Various substrates act as sources of methyl groups for B<sub>12</sub>-catalyzed methyl-group transfer: methanol, aromatic methyl ethers, methyl amines or N<sup>5</sup>-methyltetrahydropterins

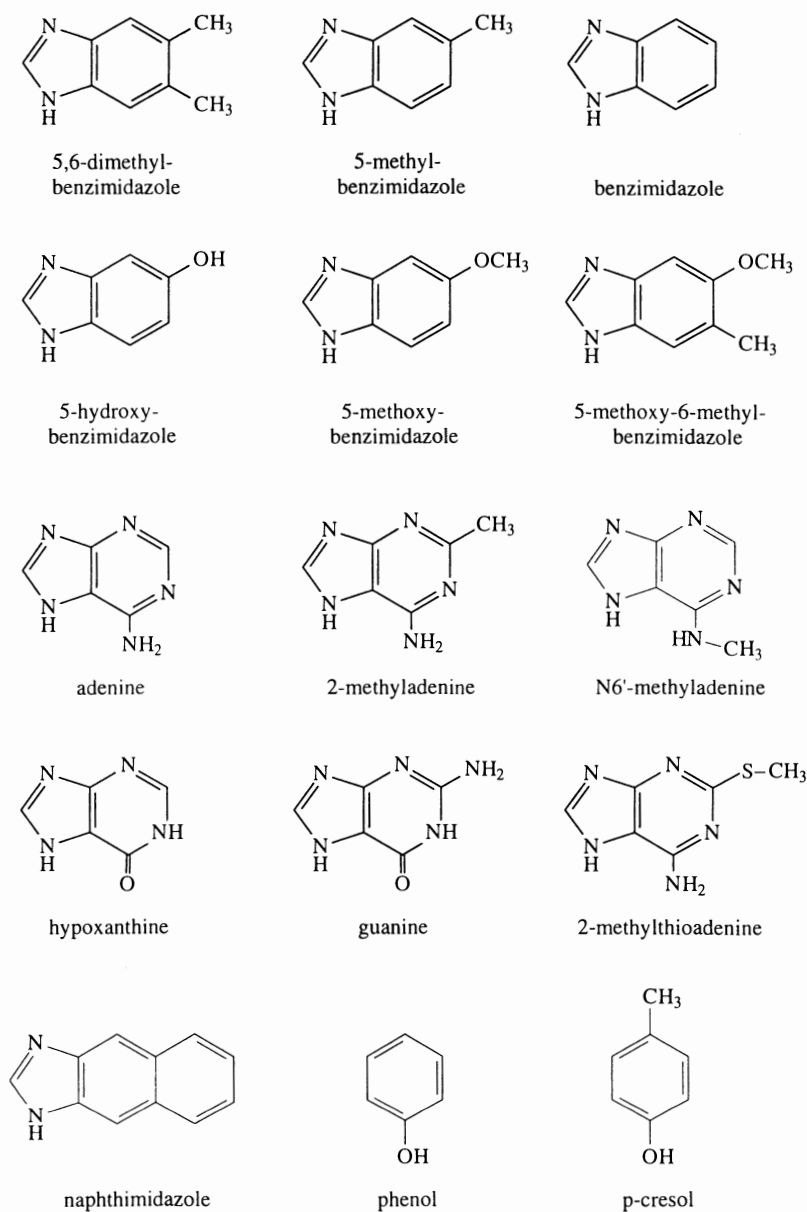


Figure 20. Representative benzimidazoles, purines, naphthimidazole and phenols found in natural B<sub>12</sub>-derivatives.

(such as N<sup>5</sup>-methyltetrahydromethanopterin or N<sup>5</sup>-methyltetrahydrofolate).<sup>192</sup> More specifically, with N<sup>5</sup>-methyltetrahydrofolate as source of the methyl group, the methyl-group donor has been made likely to be the protonated form of N<sup>5</sup>-methyltetrahydrofolate.<sup>201</sup> In the anaerobic biosynthesis of acetyl-coenzyme A from one-carbon precursors in *Clostridium thermoaceticum*, the methyl-group acceptor has been suggested to be the nickel-center of an Fe/Ni-cluster of the carbon monoxide dehydrogenase/acetyl-CoA-synthase complex,<sup>199</sup> while it is a (deprotonated) thiol in methanogenesis (coenzyme M)<sup>171</sup> and in methionine synthesis (homocysteine).<sup>170</sup>

The methyl-group transfers catalyzed by B<sub>12</sub>-dependent methyl transferases are indicated to occur with an

overall retention of configuration (i.e. consistent with two nucleophilic displacement steps, each with inversion of configuration). This has been studied with methionine synthase from *E. coli*,<sup>202,203</sup> in methanogenesis with cell-free extracts of *Methanosarcina barkeri*<sup>204</sup> and in the assembly of the two-carbon unit of acetyl coenzyme A by the acetogens *C. thermoaceticum*<sup>205</sup> and *Sporomusa ovata*.<sup>192</sup> These stereochemical findings exclude free methyl cations (or methyl radicals) as intermediates. However, in a formal sense, the methyl-transfer reactions catalyzed by B<sub>12</sub>-enzymes involve (nucleophile-bound) methyl "cations" and heterolytic cleavage/formation of the (Co-CH<sub>3</sub>)-bond. Correspondingly, methyl-group transfer relies on the catalytic properties

of enzyme-bound Co(I)-corrins and methyl-Co(III)-corrins<sup>203</sup> and, in turn, is amenable to considerable control by the protein environment,<sup>206</sup> due to the large structural changes expected to accompany the transitions from (tetra-coordinate) Co(I)-corrins to (hexacoordinate) methyl-Co(III)-corrins.<sup>81</sup>

### 1. Methionine Synthase

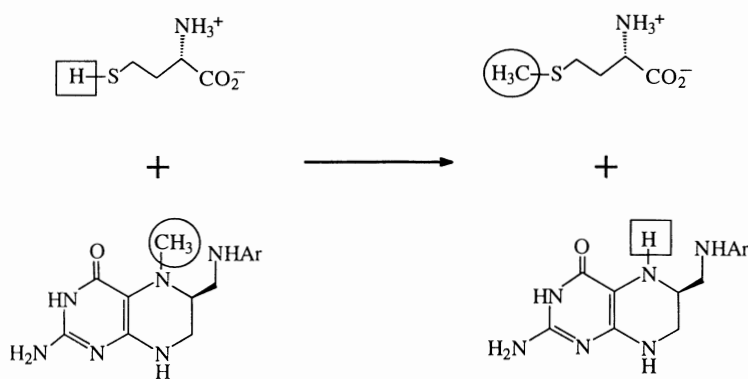
Methionine synthase (MetH) of *Escherichia coli* probably represents the most thoroughly studied B<sub>12</sub>-dependent methyl transferase. B<sub>12</sub>-dependent methionine synthesis is one of the essential roles of B<sub>12</sub> in mammalian metabolism.<sup>170</sup> Methyl transfer catalyzed by MetH in *E. coli* involves a sequential mechanism, in which tetrahydrofolate and methionine are formed and homocysteine and N<sup>5</sup>-methyltetrahydrofolate act as methyl-group acceptors and donors, respectively (see Figure 21).<sup>71,170,203</sup> MetH is a modular protein, in which the B<sub>12</sub>-binding domain is surrounded by an N<sup>5</sup>-methyltetrahydrofolate-binding module, the homocysteine-binding module and an activating module (that binds S-adenosyl-methionine, SAM).<sup>71,207</sup>

MetH catalyzes the methylation of the bound and reduced cob(I)alamin (B<sub>12s</sub>, **32**<sup>-</sup>) cofactor by (N<sup>5</sup>-protonated) N<sup>5</sup>-methyltetrahydrofolate to give enzyme-bound methylcobalamin (MeCbl, **3**) in a “base-off/His-on” form (see below).<sup>170</sup> The methyl-Co(III)-corrinoid is demethylated by homocysteine, whose sulfur is activated and deprotonated due to coordination to a zinc ion (held by three cysteine residues) of the homocysteine binding domain.<sup>208</sup> The two methyl-transfer steps occur in a sequential mechanism (see Figure 22). Occasionally, the bound B<sub>12s</sub> is oxidized to enzymatically inactive cob(II)alamin (B<sub>12r</sub>, **18**) and requires a reactivation by reductive

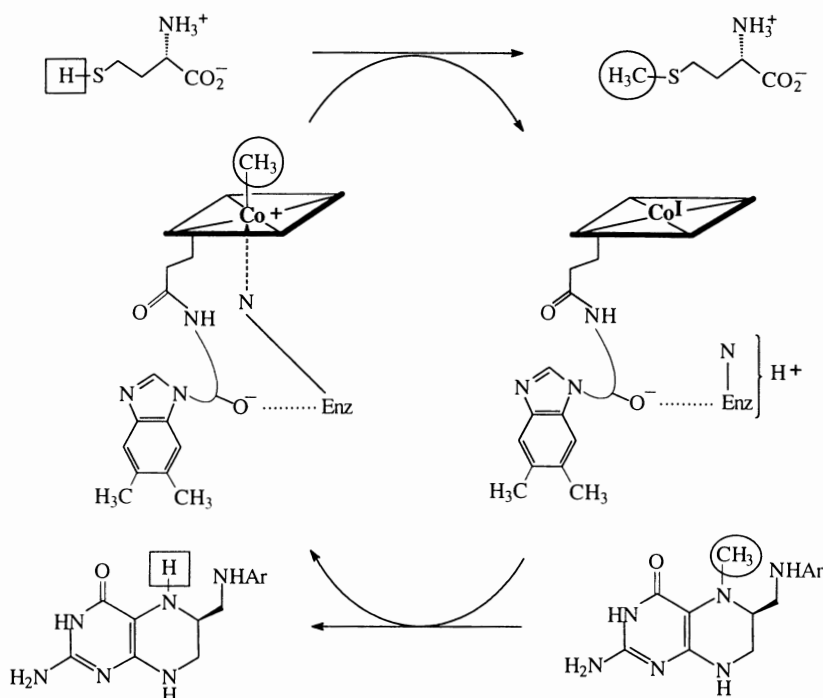
methylation with SAM and a flavodoxin as a reducing agents.<sup>170,207</sup>

X-ray crystal analysis of the B<sub>12</sub>-binding domain of MetH by Drennan et al. provided the first insight into the three-dimensional structure of a B<sub>12</sub>-binding protein.<sup>25,26,184,206</sup> It contradicted the earlier established views concerning B<sub>12</sub>-proteins, based on the known structure of vitamin B<sub>12</sub>-derivatives (see e.g. Ref. 209): This work revealed the cobalt-coordinating DMB-nucleotide tail of the protein-bound cofactor MeCbl (**3**) to be displaced by a histidine imidazole and to be anchored in a pocket of the protein, an  $\alpha/\beta$ -domain that exhibits structural characteristics of the “Rossmann fold” of nucleotide-binding proteins.<sup>25,184,206</sup> Accordingly, in methionine synthase the corrinoid cofactor is bound by histidine ligation to the metal center and in a “base-off”-constitution, i.e. bound in a “base-off/His-on” mode. The crucial cobamide-ligating histidine residue<sup>25</sup> is part of a Gly-X-X-His-X-Asp-sequence, which was noticed earlier as a conserved sequence in some B<sub>12</sub>-binding proteins.<sup>210</sup> The B<sub>12</sub>-binding domain of MetH thus provides both an anchoring site for the nucleotide tail and cobalt-ligation via the conserved residues of the His-Asp-Ser triad (the “regulatory” unit).<sup>25,184,206</sup> It holds the corrinoid cofactor with its “catalytic”  $\beta$ -side exposed at an interdomain interface.

The pioneering work on the X-ray crystal structure of the B<sub>12</sub>-binding domain of MetH by C. L. Drennan, M. Ludwig, R. G. Matthews and coworkers<sup>25,184,211</sup> was followed by the crystal structure analysis of the C-terminal “(re)activating” domain.<sup>26,206</sup> More recently the whole C-terminal fragment that spans the B<sub>12</sub>- and the SAM-binding domains of the enzymologically already well-studied MetH (see Ref. 170) could be solved to high resolution.<sup>207</sup> These studies have revealed the structures of two domains of the remarkable



**Figure 21.** The formation of methionine by methylation of homocysteine (and demethylation of N<sup>5</sup>-methyltetrahydrofolate to tetrahydrofolate) in a methyl-group transfer catalyzed by methionine synthase (MetH).<sup>71,81</sup>



**Figure 22.** Illustration of methionine formation catalyzed by MetH (Enz signifies the MetH-apoenzyme), where the bound corrinoid shuttles between MeCbl (3), in a “base-off/His-on” form, and cob(I)alamin ( $B_{12s}$ , **32**<sup>-</sup>).<sup>170</sup>

modular and multifunctional MetH, the enzymatic functions of which concern not only the catalysis of the two crucial methyl-group transfers (estimated acceleration  $> 10^5$ -fold<sup>170,212</sup>), but also the mentioned reductive (re)activation reaction for the protein-bound cofactor. Reductive cofactor (re)activation, cofactor cycling and the synchronized alternating positioning for methyl-group transfer via  $S_N2$ -steps of the enzyme-bound and activated deprotonated methyl-group acceptor, homocysteine, or the (protonated?) methyl-group donor,  $N^5$ -methyltetrahydrofolate, have been suggested earlier to be achieved by intriguing “molecular juggling acts.”<sup>184</sup> The recent crystallographic work on the complete C-terminal domain has confirmed the suspected domain alternation as a means of control of the two ways of methylation of the bound corrinoid.<sup>207</sup>

The crystallographic revelations on the structure of MetH and the finding of the “base-off/His-on” mode of cofactor binding in a  $B_{12}$ -dependent methyl-transferase were consistent with earlier ESR-spectroscopic evidence for histidine binding to the cobalt center of the corrinoid cofactor (*p*-cresoyl-cobamide) in the acetogen *Sporomusa ovata*.<sup>192,213</sup> Several other  $B_{12}$ -dependent methyltransferases are indicated to carry a “base-off/His-on”-form of the bound methyl-Co(III)-corrinoid, such as the methyltransferases of *S. ovata*<sup>192</sup> and of the methanogen *M. thermoautotrophicum*.<sup>171</sup> The carbon monoxide dehydrogenase/acetyl-CoA-synthase complex

of *Cl. thermoaceticum* contains its methyl-corrinoid cofactor in “base-off” form, but His-coordination is absent.<sup>198</sup>

## 2. $B_{12}$ -Cofactors in Enzymatic Methyl-Group Transfer

In a catalytic cycle of MetH and of other  $B_{12}$ -dependent methyl transferases, the corrinoid cofactor is indicated to cycle between the states of a methyl-Co(III)-corrin and of a Co(I)-corrin.<sup>170,171</sup> The shuttling between hexacoordinate methyl-Co(III)-form and (presumably) tetracoordinate Co(I)-form of the protein-bound corrinoid cofactor is accompanied by constitutional/conformational changes, which, in turn, are likely to provide a means of controlling the organometallic reactivity of the bound cofactor,<sup>214</sup> subject to modulation by  $H^+$ -uptake or  $H^+$ -release. In response, a  $H^+$ -mediated switch mechanism may result, mediated via the “regulatory” His-Asp-Ser-triad, which provides the crucial conformational changes associated with the enzyme’s multifunctional tasks.<sup>170,184,209</sup> Indeed, nucleophile-induced methyl-group transfers, involving heterolytic modes of cleavage and formation of the organometallic (Co- $CH_3$ )-bond at the corrin-bound cobalt center are expected to be in-line attacks (incoming nucleophile/ $CH_3$ -group/leaving group) and to be subject to stringent geometric control: a key role of the His-Asp-Ser-triad in assuring



the proper function of MetH as a methyl transferase appears to be its participation in maintaining conformational control of the mutual placement of the corrinoid cofactors and the enzyme-bound substrates.<sup>170,203</sup>

An important second role of the His-Asp-Ser triad for such heterolytic organometallic reactions can be associated with the thermodynamic effect of the  $\alpha$ -axial base-coordination on the strength of the (Co $\beta$ -CH<sub>3</sub>)-bond. From studies in solution, a significant thermodynamic trans-effect of the DMB-coordination in methylcobalamin (**3**)<sup>80,81</sup> and of the imidazole-coordination in Co $\beta$ -CH<sub>3</sub>-imidazolyl-cobamide (**25**, see Figure 7)<sup>75</sup> on methyl-group transfer reactions of methyl-Co(III)- and Co(I)-corrins could be determined. Accordingly, a strongly coordinating (nitrogen-)ligand stabilizes the methyl-Co(III)-form against abstraction of the methyl group (formally as a methyl cation) by a nucleophile, and by about 4 kcal/mol in **3**.<sup>80</sup> This may be seen mainly as an “electronic” effect,<sup>81</sup> consistent with the observation of anomalous structural trans-effects in other methyl-Co(III)-complexes.<sup>78</sup> The more recent model studies with Co $\beta$ -CH<sub>3</sub>-imidazolyl-cobamide (**25**, see Figure 7) indicated the imidazole base to exert similar “electronic effects” as the DMB-base in MeCbl (**3**), but to be more basic and, therefore, imidazolyl-coordinated Co $\beta$ -CH<sub>3</sub>-imidazolyl-cobamides (**25** or the “base-off/His-on” form of MeCbl) to be more readily protonated near neutral pH.<sup>75</sup>

A third role of the His-Asp-Ser triad concerns the ease of reduction of the Co(II)-cofactor in methionine synthase<sup>170</sup> (and in other B<sub>12</sub>-dependent methyl transferases<sup>171</sup>). When compared to data of the Co(II)/Co(I)-redox pair **18/32**<sup>-</sup> in aqueous solution,<sup>116</sup> a more positive Co(II)/Co(I)-redox potential of the bound corrinoid appears to be crucial for the access to the Co(I)-state under physiological conditions. Consistent with the dependence of the potentials on axial ligation in cobalamins,<sup>116</sup> coordination of an N-ligand to the ESR-active Co(II)-form of the bound cofactor is either absent or is weakened, “stabilizing” the reduced Co(I)-form.<sup>198</sup> Electrochemical reduction of Co(II)- to Co(I)-form of methionine synthase is accompanied by H<sup>+</sup>-uptake, consistent with a higher basicity associated with the noncoordinated His-Asp-Ser triad. This triad may be the “relay” in H<sup>+</sup>-release/uptake, which is presumed to operate also in the enzymatic methylation/demethylation cycles.<sup>212</sup>

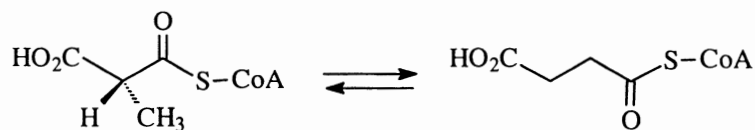
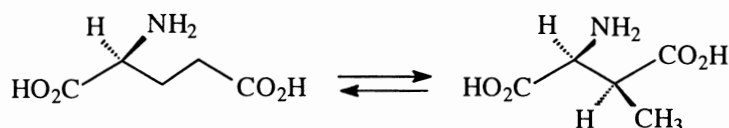
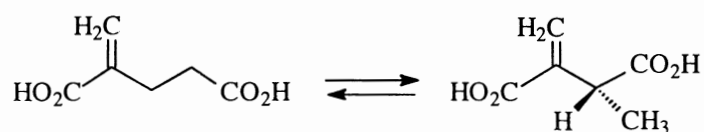
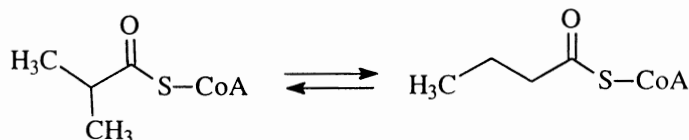
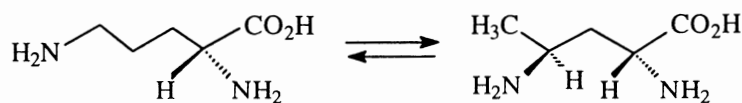
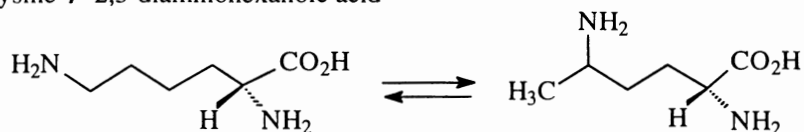
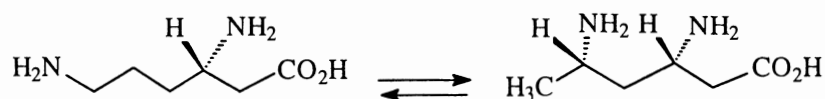
The axial (Co-N<sub>ax</sub>)-bond in the methyl-Co(III)-form of the protein-bound cofactor of MetH (and other B<sub>12</sub>-dependent methyl transferases) thus has three important

consequences. Weakening it activates both (i) the methyl group for heterolytic abstraction by a nucleophile and (ii) the Co(II)-form for reduction to the Co(I)-form and (iii) it helps to position the methyl-cob(III)amide cofactor for methyl-group transfer. Protonation/deprotonation of the “regulatory” triad (His-Asp-Ser) then represents a means of “tuning” the heterolytic strength of the (Co-C $\beta$ )-bond,<sup>170,184</sup> by (i) modulating the nucleophilicity of the histidine ligand and (ii) by controlling its position with respect to the cobalt-center.<sup>170,184,209</sup> Point mutations involving the “regulatory” triad (His-Asp-Ser) of MetH indeed confirmed the essential control of the reactivity of the bound corrinoid cofactor by this section of the protein environment. Replacement of the histidine of the “regulatory” triad (His-Asp-Ser) by a nonligating residue crippled the catalytic cycle.<sup>170,212</sup>

### C. COENZYME B<sub>12</sub>-DEPENDENT ENZYMES

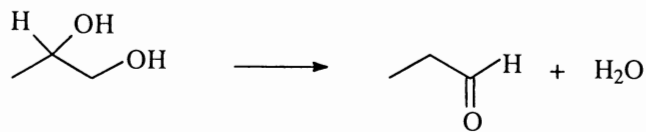
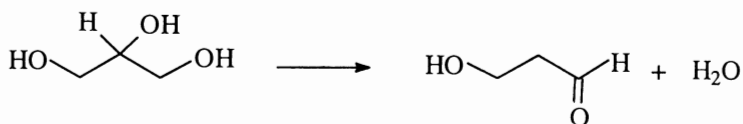
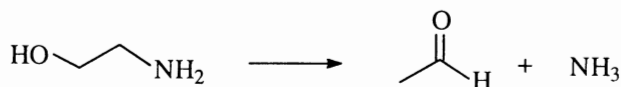
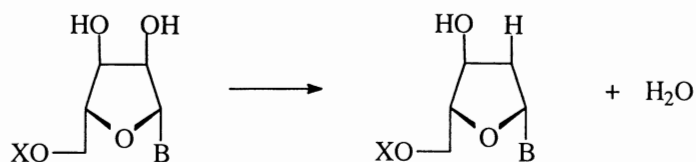
About ten coenzyme B<sub>12</sub>-dependent enzymes are now known (reviewed in Refs. 8,21,215, see Tables 1 and 2 and Section VD for less well established roles). These ten enzymes are the carbon skeleton mutases (methylmalonyl-CoA mutase,<sup>216</sup> glutamate mutase,<sup>217,218</sup> methyleneglutarate mutase,<sup>217</sup> isobutyryl-CoA mutase,<sup>219</sup> diol dehydratase,<sup>220</sup> glycerol dehydratase,<sup>220</sup> ethanalamine ammonia lyase,<sup>221</sup> two amino mutases<sup>222,223</sup> and B<sub>12</sub>-dependent ribonucleotide reductase.<sup>224</sup>

The known coenzyme B<sub>12</sub>-dependent enzymes all perform chemical transformations that are difficult to achieve by typical “organic” reactions. Early biochemical studies (reviewed e.g. in Ref. 225) had indicated the nonstereospecific exchange of hydrogen atoms at the 5'-position of 5'-adenosylcobalamin in coenzyme B<sub>12</sub>-catalyzed enzymatic rearrangements to accompany the pseudointramolecular H-migration. Homolytic cleavage of the (Co-C)-bond of the protein-bound coenzyme B<sub>12</sub> (**2**) to a 5'-deoxy-5'-adenosyl radical (**42**) and cob(II)alamin (**18**) was suggested as an entry to reversible H-abstraction reactions involving the 5'-position of the radical **42** (see e.g. Ref. 225). Therefore, homolysis of the (Co-C)-bond of coenzyme B<sub>12</sub> (**2**), which is indeed the thermally most easily achieved reaction of **2** in solution (homolytic (Co-C)-BDE of about 30 kcal/mol<sup>89,169</sup>), also appeared to be its biologically most relevant reactivity: coenzyme B<sub>12</sub> then is, according to Halpern, a “reversible free radical carrier.”<sup>89</sup> However, to be relevant for the observed rates of catalysis by the coenzyme B<sub>12</sub>-dependent enzymes, the homolysis of the (Co-C)-bond of the protein-bound

**Table 1.** List of Enzyme Reactions Involving Natural Substrates and Cobamide-Dependent Mutases*(R)*-methylmalonyl-CoA / succinyl CoA<sup>166,216</sup>*(S)*-glutamic acid / *(2S,3S)*-methylaspartic acid<sup>215,217,218</sup>2-methyleneglutarate / *(R)*-3-methylitaconate<sup>217</sup>isobutyryl-CoA / n-butyryl-CoA<sup>219</sup>D-ornithine / *(2R,4S)*-2,4-diaminovaleric acid<sup>222</sup>D-( $\alpha$ )-lysine / 2,5-diaminohexanoic acid<sup>222</sup>L-( $\beta$ )-lysine / *(3S,5S)*-3,5-diaminohexanoic acid<sup>222</sup>

coenzyme 2 needs to be accelerated by a factor of about  $10^{12}$ , in the presence of substrate.<sup>89,169</sup> Therefore, the major tasks of the enzyme should concern not only the catalysis of its proper reactions

but also the reversible generation of the radical intermediates and the protection of the proteinic environment from nonspecific radical chemistry, dubbed "negative catalysis".<sup>225,226</sup>

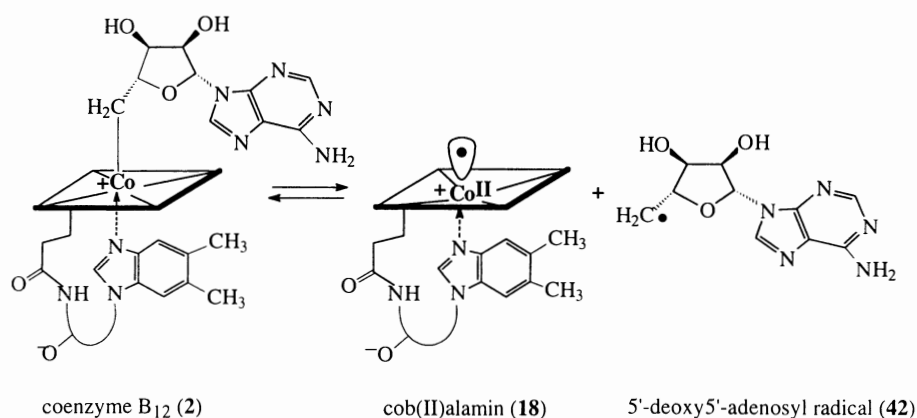
**Table 2.** List of Reactions Involving Natural Substrates and Cobamide-Dependent Dehydratases, Deaminase and Ribonucleotide Reductase1,2-propanediol / propanal<sup>220</sup>glycerol / 3-hydroxypropanal<sup>220</sup>ethanolamine / acetaldehyde<sup>221</sup>ribonucleotide / 2'-deoxyribonucleotide<sup>224</sup>

B = nucleotide base, X = diphosphate or triphosphate group

The coenzyme B<sub>12</sub>-dependent enzymes accordingly all appear to rely upon the reactivity of bound organic radicals, which are formed (directly or indirectly) by a H-atom abstraction by the 5'-deoxy-5'-adenosyl radical (**42**), that originates from the homolysis of the (Co–C)-bond of coenzyme B<sub>12</sub> (**2**, AdoCbl). In these enzymatic reactions, the radical **42** is the established reactive partner in the proper enzymatic radical reaction, so that AdoCbl (**2**) should be looked at as a “pre-catalyst” (or catalyst precursor<sup>81</sup>). Tight control of the reactivity of **42** must be of advantage and correct mutual orientation of **42** and of the substrate for H-atom transfer as well,<sup>226</sup> but means of (further) activation of the catalyst **42** by the protein environment can hardly be recognized. A similar situation presumably also prevails in other enzymatic radical reactions involving protein-bound **42** not derived from AdoCbl (**2**),<sup>222</sup> or peptidic

radicals.<sup>224,227</sup> Coenzyme B<sub>12</sub> (**2**) might then be considered, first of all, to be a structurally sophisticated, reversible source for an alkyl radical, whose (Co–C)-bond is labilized in the protein-bound state<sup>89</sup> (see Figure 23). Organometallic B<sub>12</sub>-species, in which (the putative) organic radicals are bound to the corrin-bound cobalt center via a (Co–C<sub>β</sub>)-bond are now considered unlikely as (kinetically competent) intermediates in the rearrangements catalyzed by B<sub>12</sub>-dependent enzymes.<sup>228</sup>

Coenzyme B<sub>12</sub>-dependent enzymes are unevenly distributed in the living world. Only one of the coenzyme B<sub>12</sub>-dependent enzymes (Methylmalonyl-CoA mutase) is indispensable also in human metabolism.<sup>216</sup> In methanogens a functional role of coenzyme B<sub>12</sub>-dependent enzymes is also suspected, but has not (yet) been revealed clearly.<sup>171</sup> With the exception of the enzymatic ribonucleotide reduction,<sup>224</sup>



**Figure 23.** Coenzyme B<sub>12</sub> (AdoCbl, **2**) a reversible source of the 5'-deoxy-5'-adenosyl radical (**42**) and of cob(II)alamin (B<sub>12r</sub>, **18**).

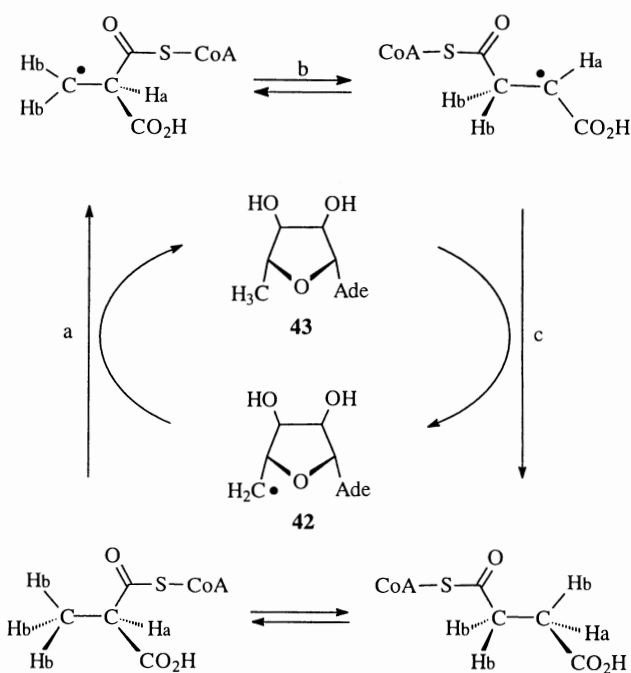
the results of the known coenzyme B<sub>12</sub>-catalyzed enzymatic reactions formally correspond to isomerizations with mutual vicinal exchange of the positions of a hydrogen atom and of a group with heavy atom centers, that occur, in general, with stringent stereochemical control.<sup>231,233</sup>

### 1. Carbon Skeleton Mutases

In the four known carbon skeleton rearrangement reactions catalyzed by coenzyme B<sub>12</sub>-dependent mutases, two vicinal groups (a hydrogen atom and an organic substituent) exchange their positions in a (pseudo)intramolecular fashion.<sup>215</sup> The B<sub>12</sub>-cofactor is bound in a “base-off/His-on” constitution (as found in MetH originally<sup>25</sup>) and at an interface between two modules, called the B<sub>12</sub>-binding and the substrate-activating domains (or subunits). The crystal structures of methylmalonyl-CoA mutase (MMCM)<sup>28</sup> and glutamate mutase (GM)<sup>29</sup> have been analyzed. The B<sub>12</sub>-binding motif (Gly-X-X-His-X-Asp)<sup>210</sup> occurs in MMCM and in GM, as well as in the other two (C–C)-bond rearranging enzymes, 2-methyleneglutarate mutase (MGM)<sup>233,234</sup> and (in an unusual part of) isobutyryl-CoA mutase (ICM).<sup>219</sup> Indeed, the B<sub>12</sub>-binding domains (in MMCM and MGM) and the B<sub>12</sub>-binding subunits (in GM and ICM) exhibit considerable sequence homology, that includes even the B<sub>12</sub>-binding domain of MetH. Such a homology does not extend to the other coenzyme B<sub>12</sub>-depending enzymes or even to the substrate-binding domains (subunits) of the carbon skeleton mutases.<sup>219,245</sup>

#### a. Methylmalonyl-CoA Mutase

Methylmalonyl-CoA mutase (MMCM) interconverts *R*-methylmalonyl-CoA and succinyl-CoA in a carbon



**Figure 24.** Methylmalonyl-CoA mutase (MMCM) interconverts (*R*-methylmalonyl-CoA and succinyl-CoA. Proposed reaction mechanism of the carbon skeleton rearrangement, catalyzed by MMCM involving H-atom abstraction (step a), radical rearrangement (step b) and back transfer of H-atom (step c). (The experimentally supported substrate triggered formation of the 5'-deoxy-5'-adenosyl radical (**42**) and of cob(II)alamin (**18**, B<sub>12r</sub>) by homolysis of protein bound AdoCbl (**2**) is omitted here, see Figure 23.)<sup>166,215,231</sup>

skeleton rearrangement reaction.<sup>166,216</sup> According to the generally accepted scheme (see Figure 24), binding of the substrate triggers the homolysis of the (Co–C)-bond of the bound adenosyl-corrinoid. The radical **42** then prepares the substrate for the rearrangement reaction by abstracting an H-atom from the methyl group of enzyme-bound methylmalonyl-CoA. A large deuterium isotope effect of the (substrate) H-atoms to be abstracted on the apparent rate of homolysis of the (Co–C)-bond of AdoCbl (**2**) was observed. H-atom

abstraction accordingly, has been suggested to occur by tunneling and to be coupled kinetically to the homolysis step.<sup>229</sup> Labilization of the (Co–C)-bond towards homolysis is largely due to a decrease of the enthalpy of activation by about 16 kcal/mol.<sup>230</sup> H-atom abstraction gives the 2-methylmalon-2'-yl-CoA radical which rearranges rapidly to the succin-3-yl-CoA radical.<sup>216,231</sup> An intramolecular rearrangement has been suggested, involving a transition through the stage of (formally a substituted) cyclopropyloxy radical, as no evidence for a fragmentation mechanism in model experiments was seen.<sup>232</sup> More recent experimental and theoretical evidence fully supports a mechanism in which (i) the succin-3-yl-CoA radical arises from an intramolecular radical rearrangement and (ii) which occurs without noticeable participation of the bound cob(II)alamin (i.e. the corrinoid is merely a “spectator”).<sup>231</sup> The radical rearrangement step appears to be critically controlled by the interactions with the apoenzyme<sup>235</sup> and is assisted by an H-bond to His244 in the substrate-activating domain of the enzyme, as indeed suggested to be helpful by theoretical studies.<sup>236</sup> Mutation of His244 of MMCM reduced the rate of the rearrangement reaction by about 10<sup>3</sup>-fold.<sup>237</sup> The succin-3-yl-CoA radical (resulting from the rearrangement) is suggested to re-abtract an H-atom from 5'-deoxyadenosine (**43**) to give succinyl-CoA, and the 5'-deoxyadenosyl radical (**42**), that recombines with cob(II)alamin to give enzyme-bound coenzyme B<sub>12</sub> (**2**).

The X-ray analysis of methylmalonyl-CoA mutase (MMCM) gave the first crystal structure of a coenzyme B<sub>12</sub>-dependent enzyme and was reported by Evans et al.<sup>27,28,206,238</sup> This study concerned the 150 kDa heterodimeric MMCM from *P. shermanii* and showed the B<sub>12</sub>-cofactor to be bound “base-off/His-on” again. The  $\alpha$ -side of the corrin-bound cobalt center was coordinated to the histidine of a His-Asp-Lys triad as the “regulatory” unit. The nucleotide tail of the bound corrinoid was tightly inserted into the protein, similar to the situation in MetH. The crystal structure revealed a rather “flat” corrin ligand with a “ligand-folding” comparable to that in the imidazolyl-cobamides<sup>36,75</sup> and that showed no indication of a significant “upwards conformational distortion.” Similar to MetH, in MMCM the corrinoid was bound at an interface between two domains (of the  $\alpha$ -chain of the heterodimer, whose  $\beta$ -chain essentially made no contact to the bound corrin and substrate molecules). However, the remains of the  $\beta$ -ligand (the 5'-deoxyadenosyl group) of the bound AdoCbl (**2**) were absent in the first structure and the major fraction of the corrinoid cofactor

appeared to be bound as (“base-off/His-on”) cob(II)alamin<sup>28</sup> and the “catalytic”  $\beta$ -face of the pentacoordinate cobalt center was exposed to the substrate-binding domain.<sup>206</sup> The pseudosubstrate used, a dethiacoenzyme A, was bound tightly in a funnel provided by the “substrate-binding” domain of the  $\alpha$ -chain. It was positioned in such a way, that the methylmalonyl- and succinyl-moieties, respectively, of the proper enzyme substrates would approach the corrinoid cofactor. However, a significant direct interaction between the rearranging substrate's reactive centers and the corrinoid cofactor was made unlikely by the crystal structure.<sup>28,206,238</sup>

In more recent crystallographic work, MMCM was investigated in a substrate-free form, which revealed considerable opening of the substrate-binding TIM-barrel, indicating an intriguing conformational reorganization by the substrate binding.<sup>239</sup> In this crystal, coenzyme B<sub>12</sub> (**2**) was found to be bound “base-off/His-on” again and to be largely intact, with the adenosine still bound to cobalt, but rotated away from its position in the crystal structure of **2** (above ring C of the corrin ligand, see Section IIA) and towards a position above ring B. In a further crystal analysis of MMCM, this time with pseudosubstrates bound, the adenosyl group of the bound coenzyme AdoCbl (**2**) was again found to be repositioned (presumably with the help of the bound substrate), indicating the organometallic group to be particularly strained or to be detached from the cobalt center.<sup>238,240</sup> The data suggest substrate binding to assist the labilization of the (Co–C)-bond by squeezing the adenosyl group off from the cobalt-corrin.<sup>206,240</sup>

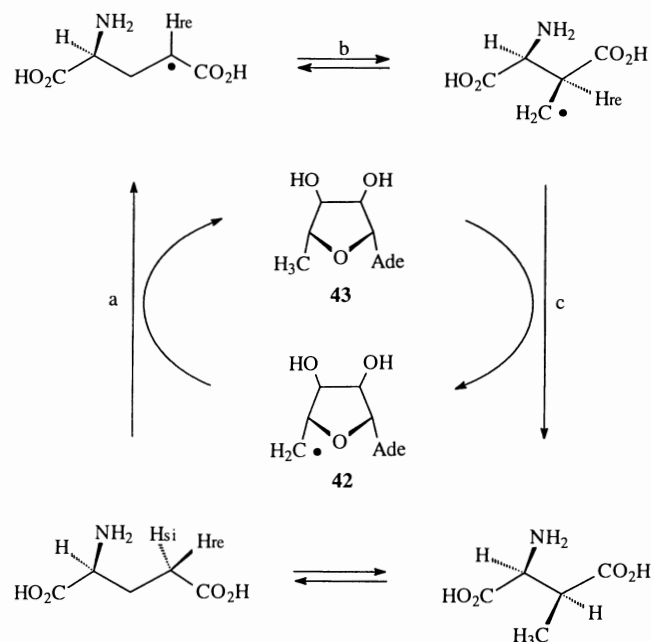
An intriguing and much discussed observation of the MMCM crystal structures concerned the length (observed at 2.5–2.7 Å) of the axial (Co–N <sub>$\alpha$</sub> )-bond between the cobalt center and the coordinating histidine.<sup>28,206,238</sup> Compared to all reference values known from crystal structures of corrinoids (see Section II and Ref. 34), such as e.g. of cob(II)alamin (2.13 Å),<sup>61</sup> of coenzyme B<sub>12</sub> (2.24 Å)<sup>63</sup> and of Co $\beta$ -methyl-imidazolylcobamide<sup>75</sup> (**25**, 2.09 Å) significant lengthening of the axial (Co–N <sub>$\alpha$</sub> )-bond was implied, which was interpreted as an indication of a mode of activation of the protein-bound coenzyme towards homolysis.<sup>28,206</sup> However, judged on the basis of the listed reference values and specifically of the observed length in the homolysis product cob(II)alamin,<sup>61</sup> the “long” bond also indicates a “lengthened” axial (Co–N <sub>$\alpha$</sub> )-bond in the product of homolysis (**18**), rather than just in the B<sub>12</sub>-coenzyme (**2**). Accordingly, the “long” axial (Co–N)-bond was suggested to be an

unlikely factor directly indicating a (potential) activating effect on the homolysis of the (Co–C)-bond of the bound cofactor AdoCbl (**2**).<sup>81</sup> Indeed, the “long” (Co–N)-bond may be an artifact of the crystal structure analysis.<sup>238,241</sup> It was shown, that under irradiation with strong X-ray beams adventitious reduction of the Co(III)-centers of bound B<sub>12</sub>-cofactors to Co(II)corrins with a hexacoordinate cobalt center does occur.

### b. Glutamate Mutase

Glutamate mutase (GM) from *Clostridium tetanomorphum* was the first enzyme discovered (around 1960) to be dependent upon a B<sub>12</sub>-coenzyme.<sup>242</sup> This finding eventually also led to the discovery of the organometallic nature of coenzyme B<sub>12</sub> (AdoCbl, **2**). Glutamate mutase (GM) from *Cl. tetanomorphum* and (more recently) also from *Cl. cochlearium* has been studied extensively, but other microorganisms are suspected to have enzymes with GM-activity as well.<sup>217</sup> GM catalyzes the reversible rearrangement between (*S*)-glutamate and (2*S*,3*S*)-3-methylaspartate, where equilibrium favors glutamate (by about 10) (see Figure 25).<sup>217,243–245</sup>

The GM proteins from *Cl. tetanomorphum* and from *Cl. cochlearium* are heterotetramers ( $\epsilon\sigma$ ), consisting of



**Figure 25.** Glutamate mutase (GM) interconverts (*S*)-glutamate and (2*S*,3*S*)-3-methylaspartate. Proposed reaction mechanism of the carbon skeleton rearrangement, catalyzed by GM involving H-atom abstraction (step a), radical rearrangement (step b) and back transfer of H-atom (step c). (The experimentally supported substrate triggered formation of the 5'-deoxy-5'-adenosyl radical (**42**) and of cob(II)alamin (**18**, B<sub>12</sub>) by homolysis of protein bound AdoCbl (**2**) is omitted here, see Figure 23.)<sup>215,217,218</sup>

a pair of smaller B<sub>12</sub>-binding subunits ( $\sigma$ ) and larger substrate-binding subunits ( $\epsilon$ ), and share a high sequence homology.<sup>244,246</sup> Functional GM is a protein of about 140 kDa and contains two molecules of adenosyl-cobamide. The cofactors from the two clostridia were identified as pseudocoenzyme B<sub>12</sub> (**29**, Co $\beta$ -adenosyl-adeninyl-cobamide)<sup>247</sup> and adenosyl-factor A (**30**, Co $\beta$ -adenosyl-2'-methyladeninyl-cobamide),<sup>105</sup> but the cobalamin coenzyme B<sub>12</sub> (AdoCbl, **2**) also functions as cofactor.<sup>217,244</sup> Binding of the substrate triggers homolysis of the (Co–C)-bond of the adenosyl-cobamide cofactor. Similar to the situation with MMC<sup>229</sup> H-atom abstraction and homolysis of bound AdoCbl to give the radical **42** are kinetically coupled processes and a pre-steady-state D-isotope effect of about 30 is observed.<sup>215,248</sup> The rearrangement reaction catalyzed by GM is initiated by the abstraction of an H-atom from the bound substrate, i.e. (in the “reverse” direction) from the methyl group of enzyme-bound methyl aspartate, followed by a rearrangement of the 3-methylaspart-3'-yl radical to the glutam-4-yl radical.<sup>217,245</sup> Experiments by Golding, Buckel and coworkers suggested this step in the radical rearrangement of GM to possibly take place via a fragmentation/recombination mechanism involving acrylate as a fragment.<sup>243</sup> Nowadays, the intriguing fragmentation/recombination mode for the radical rearrangement catalyzed by GM is supported by the available experimental<sup>249</sup> and theoretical evidence.<sup>215,250,251</sup> The glutam-4-yl radical then is suggested to re-abstract an H-atom from 5'-deoxyadenosine to give the rearrangement product, (*S*)-glutamate, and the 5'-deoxyadenosyl radical, that recombines with cob(II)alamin to give enzyme-bound **2**. The radicals are indicated to be bound to the protein via several H-bonds and the rearrangement step to be critically controlled by the interactions with the apoenzyme (see Figure 25).<sup>218,251</sup> Over all, the glutamate/methylaspartate rearrangement is pseudo-intermolecular and occurs without noticeable participation of the bound cob(II)alamin (i.e. the corrinoid is merely a “spectator” again).<sup>231</sup>

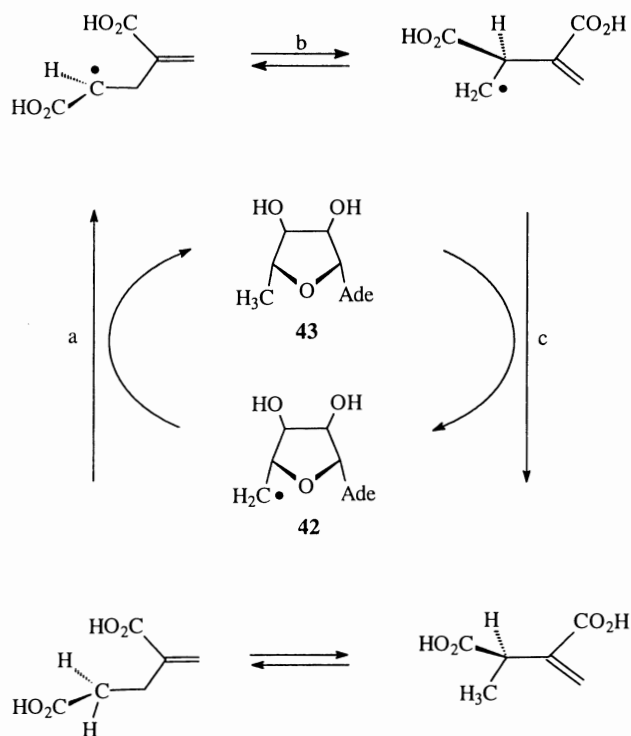
Crystallographic studies with GM from *Cl. cochlearium* have provided a detailed structural picture of the enzyme, in which the corrinoid cofactor is bound “base-off/His-on” again and at the interface between the subunits  $\sigma$  and  $\epsilon$ .<sup>29</sup> In these studies an (*S,S*)-tartrate molecule acts as pseudosubstrate and occupies the presumed site of (2*S*,3*S*)-3-methylaspartate. The cobalt-coordinating histidine is part of an H-bonded “regulatory” His-Asp-Ser triad. Detailed analysis of GM with bound coenzyme B<sub>12</sub> (**2**) revealed the position

of the ribose part of the 5'-deoxyadenosyl moiety to be disordered and to be present in two conformations, related to each other by a pseudorotation of the furanose ring.<sup>252</sup> One of these structures places the 5'-methylene group of the adenosine close to the position of the corrin-bound cobalt center, but at a distance of about 3.1 Å, and thus appears to have features expected for the direct product of the homolysis of the (Co–C)-bond of the bound cofactor **2**. In the other conformation the 5'-methylene carbon is at a distance of about 4.5 Å from the metal center and is displaced towards the substrate-binding site, as if in van der Waals contact with the bound substrate. In this way, GM achieves a controlled and energetically facile transposition of the 5'-radical center from cobalt to the substrate.<sup>218,252</sup>

The solution structures of the (roughly 15 kDa) B<sub>12</sub>-binding  $\sigma$ -subunits of GM from *Cl. tetanomorphum*<sup>253,254</sup> and of *Cl. cochlearium* were analyzed by heteronuclear NMR-spectroscopy<sup>255</sup> and provided the first structure of a cofactor-free B<sub>12</sub>-binding protein. These studies indicated the  $\sigma$ -subunit to be structured similar in solution as in the crystal of the holo-enzyme, and to be largely preorganized for B<sub>12</sub>-binding. However, the apo-protein was seen to contain a flexible loop and a “nascent” helix, which both were suggested to structure only upon binding of the corrinoid.<sup>256</sup> A model for the events in binding of the “base-off/His-on” form of the B<sub>12</sub>-cofactor by the  $\sigma$ -subunit could be derived. According to this model, the nucleotide tail of the “base-off” form of the adenosyl-corrinoid is trapped first and the attached nucleotide moiety stabilizes the (“nascent” helix) of the protein. In aqueous solution AdoCbl (**2**) prefers to be in the “base-on” form (with only about 1% of the “base-off”-form).<sup>38</sup> However, the natural cobamide cofactors of the two clostridia are adeninyl-cobamides, such as pseudocoenzyme B<sub>12</sub> (**29**, Co <sub>$\beta$</sub> -adenosyl-adeninyl-cobamide), for which the “base-off” form predominates in aqueous solution.<sup>107</sup> Binding of the nucleotide part of the cofactor favors conformations of the  $\sigma$ -subunit which resemble those in the crystal of the holo-protein. Indeed, calorimetric investigations have shown B<sub>12</sub>-binding to be entropy driven.<sup>257</sup>

### c. Other B<sub>12</sub>-Dependent Carbon Skeleton Mutases

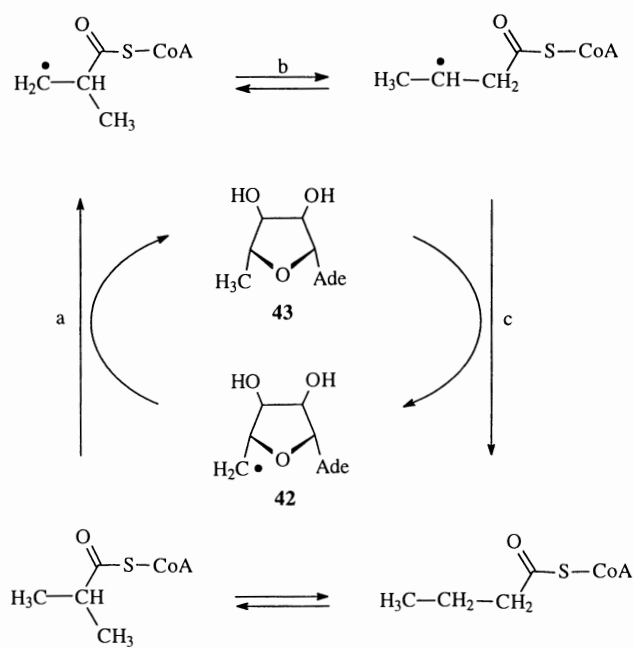
Besides MMCM and GM two other B<sub>12</sub>-dependent carbon skeleton mutases are known. These are (i) methylene glutarate mutase (MGM), which catalyzes the reversible interconversion of 2-methylene-glutarate and R-3-methylitaconate (see Figure 26) as part of a degradative path of nicotinic acid in *Clostridium*



**Figure 26.** Methylene-glutarate mutase (MGM) interconverts 2-methylene-glutarate and R-3-methylitaconate. Proposed reaction mechanism of the carbon skeleton rearrangement, catalyzed by MGM involving H-atom abstraction (step a), radical rearrangement (step b) and back transfer of H-atom (step c). (The substrate triggered formation of the 5'-deoxy-5'-adenosyl radical (**42**) and of cob(II)alamin (**18**, B<sub>12</sub>) by homolysis of protein bound AdoCbl (**2**) is not represented in the figure for clarity, but see Figure 23.)<sup>217</sup>

*barkeri*<sup>217,243</sup> and (ii) isobutyryl-CoA mutase (ICM), which is observed in species of the Gram-positive bacteria *Streptomyces*.<sup>219</sup>

Coenzyme B<sub>12</sub> (**2**) is the authentic cofactor of MGM, where it is bound strongly and in presumably a “base-off/His-on” form, as made likely by the presence of the “B<sub>12</sub>-binding motif” in the sequence of the C-terminal (B<sub>12</sub>-binding) domain and mutation studies.<sup>217</sup> All available experimental information points to a radical rearrangement again, induced by H-atom abstraction (as similarly described above for MMCM and GM). The mechanism of the proper rearrangement step is not well established yet, as MGM is inhibited even by acrylate alone (with a square dependence on its concentration), but not by any of the four stereoisomeric 1-methylcyclopropyl-1,2-di-carboxylates (one of which is likely to have roughly similar spatial requirements for binding, as the putative cyclopropylmethyl radical intermediate of the intramolecular rearrangement pathway). Both of these findings support a fragmentation/recombination mechanism, but the mechanistic issue is far from being settled, since solution studies give precedence for intramolecular rearrangements with radicals having functional groups



**Figure 27.** Isobutyryl-CoA mutase (ICM) interconverts isobutyryl-CoA and n-butyryl-CoA. Proposed reaction mechanism of the carbon skeleton rearrangement, catalyzed by ICM involving H-atom abstraction (step a), radical rearrangement (step b) and back transfer of H-atom (step c). (The presumed substrate triggered homolysis of protein-bound AdoCbl (**2**) to 5'-deoxy-5'-adenosyl radical (**42**) and cob(II)alamin (**18**, B<sub>12r</sub>) is omitted here, see Figure 23.)<sup>219,259</sup>

similar to those of methyleneglutarate<sup>232</sup> and theoretical work also classifies the intramolecular rearrangement to be proceeding with smaller activation barriers.<sup>217</sup>

Isobutyryl-CoA mutase (ICM) catalyzes the reversible rearrangement of iso-butyryl-CoA and n-butyryl-CoA, an isomerization that is relevant in the course of the biosynthesis of polyketide antibiotics (see Figure 27,<sup>219</sup>). This coenzyme B<sub>12</sub>-dependent isomerase appears to be distributed over a wide range of microorganisms, but, so far, is the least well investigated of the four carbon skeleton mutases. The enzyme seems to be organized in a similar way as glutamate mutase (GM) and consists of large and small subunits. The two subunits of ICM are indicated from sequence comparison to activate and bind the substrate (larger subunit) or to bind the B<sub>12</sub>-cofactor (smaller subunit) in a “base-off/His-on” form.<sup>258</sup> The rearrangement reaction is indicated to be a rather (but not strictly) stereoselective radical reaction.<sup>259</sup>

## 2. Diol Dehydratases, Glycerol Dehydratase, and Ethanolamine Ammonia Lyase

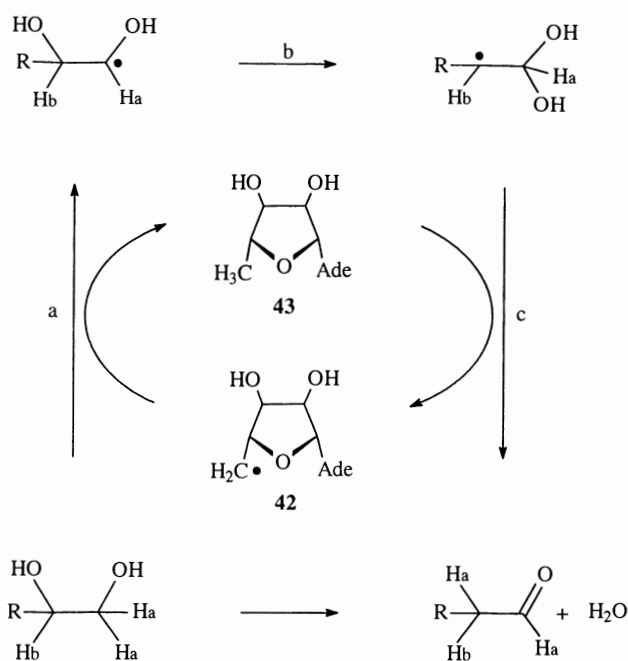
### a. Diol Dehydratases and Glycerol Dehydratase

Diol dehydratase and glycerol dehydratase are isofunctional enzymes that catalyze the dehydration of

propane-1,2-diol, ethane-1,2-diol, glycerol to propanal, acetaldehyde and 3-hydroxypropanal, respectively (other glycols can be dehydrated in analogous fashion).<sup>220</sup> Diol dehydratase has about a two-fold preference for conversion of propane-1,2-diol (rather than glycerol), whereas the sequence of conversion is reversed in glycerol dehydratase (preference for glycerol). Conversion of glycerol (or even diols) brings about an irreversible deactivation of the enzymes, which can be repaired with the assistance of a reactivating enzyme.<sup>220</sup>

The diol dehydratases are B<sub>12</sub>-dependent and use adenosyl-cobamides (such as AdoCbl, **2**) as cofactors. They catalyze the dehydration via a (pseudo)intramolecular H-transfer involving the 5'-position of the organometallic cofactor (for reviews see Refs. 220,260,261). In contrast to the B<sub>12</sub>-dependent carbon skeleton mutases (previous section), the cofactor in these dehydratases is bound in a (conventional) “base-on” form. This was made likely first by analysis of the protein sequence of diol dehydratase, which lacks the diagnostic “B<sub>12</sub>-binding” (Gly-X-X-His-X-Asp)-sequence motif.<sup>262</sup> B<sub>12</sub>-binding in a “base-on” form was made likely by ESR-investigations of diol dehydratase<sup>263,264</sup> and was finally confirmed by X-ray analysis.<sup>30,220</sup> In addition, in the active site of diol dehydratase of *Klebsiella oxytoca* (DD) a potassium ion is bound (together with the substrate propane-1,2-diol) to which a role as Lewis acid in the radical rearrangement reaction has been ascribed.<sup>30,265</sup> The AdoCbl-catalyzed reaction again is based on a substrate-assisted homolysis of the (Co–C)-bond of the corrinoid cofactor and formation of the 5'-deoxy-5'-adenosyl radical (**42**) and cob(II)alamin (B<sub>12r</sub>, **18**), as indicated by rapid kinetic studies by ESR- and UV-Vis-spectroscopic means.<sup>261,266</sup> In diol dehydratase the radical **42** then abstracts a H-atom from the (C-1)-position of propane-1,2-diol, followed by 1,2-migration of the hydroxyl group vicinal to the radical site (see Figure 28). The migration of the hydroxyl-group is suggested to be assisted by the potassium ion and by H-bonding with protic residues of the protein.<sup>261,265</sup> A “partial protonation” and/or complexation by the K<sup>+</sup>-ion have been calculated to lower the activation barrier for the 1,2-migration of the hydroxyl group.<sup>265,267</sup> The (formal) product of the isomerization is a 1,1-diol (or the hydrate of the aldehyde propanal). The propanal isolated from <sup>18</sup>O-labeled (*S*)-propane-1,2-diol still is <sup>18</sup>O-labeled, while unlabeled propanal is obtained from <sup>18</sup>O-labeled (*R*)-propane-1,2-diol.<sup>220,268</sup> In view of the more detailed structural and kinetic data available nowadays (see below), protein-based radicals





**Figure 28.** Diol dehydratase and glycerol dehydratase isomerize vicinal diols – via 1,2-migration of a hydroxyl group – to geminal diols (such as 1,2-propane-diol to 1,1-propane-diol, which loses water to give propanal). Possible reaction mechanism of the hydroxyl group migration, catalyzed by DD (or GD) and involving H-atom abstraction (step a), radical rearrangement (step b) and back transfer of H-atom (step c); substrates for diol dehydratase: propane-1,2-diol ( $R = \text{CH}_3$ ) or ethane-1,2-diol ( $R = \text{H}$ ); for glycerol dehydratase: glycerol ( $R = \text{CH}_2\text{-OH}$ ). (The experimentally supported substrate triggered formation of the 5'-deoxy-5'-adenosyl radical (**42**) and of cob(II)alamin (**18**, B<sub>12</sub>) by homolysis of protein bound AdoCbl (**2**) is omitted here, see Figure 23.)<sup>220,260</sup>

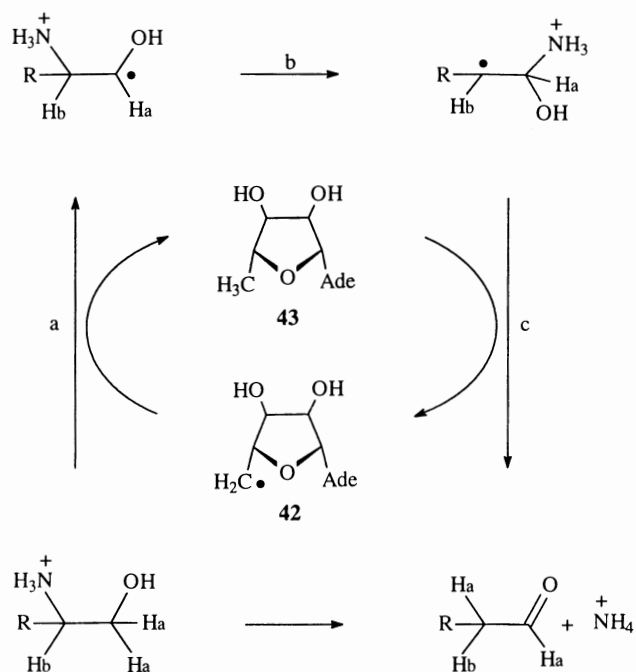
in a radical chain type mechanism in the diol dehydratase reaction<sup>269</sup> are not given consideration any longer.<sup>261</sup>

The crystal structure of DD (from *Klebsiella oxytoca*) was solved recently as the complex with vitamin B<sub>12</sub> (**1**) and (*S*)-propane-1,2-diol.<sup>30,220</sup> It showed the corrinoid to be bound (again) at an interdomain-interface (of the B<sub>12</sub>-binding  $\beta$ -subunit and of the substrate-binding  $\alpha$ -subunit) and confirmed the “base-on” nature of the bound corrinoid (from CNCbl, **1**), which (however) is not active as cofactor. The crystal structure showed the corrin-bound cobalt ion to be (largely) pentacoordinated, with an axial (Co–N<sub>ax</sub>)-bond with 2.5 Å length, and the diol substrate to be ligating the potassium ion, which is situated at a distance of 11.7 Å from the cobalt center of the corrinoid.<sup>30</sup> The diol substrate is also bound via a tight net of H-bonds to polar protein residues and at an observed distance of more than 7 Å from the corrin-bound cobalt ion.<sup>30</sup> These observations excluded direct contacts of reaction intermediates with the cobalt center of the cofactor.

More recently an analysis of the crystal structure of DD reconstituted with the coenzyme B<sub>12</sub> analogue 5-adeninyl-pentyl-cobalamin was reported.<sup>270</sup> In this study the binding of an analogue of AdoCbl (**2**) to DD was examined, in which a flexible pentamethylene unit links an adenine function to the cobalt center, similar to the ribose in the adenosyl-ligand. Together with earlier structure–function studies of a variety of other analogues of coenzyme B<sub>12</sub> (**2**)<sup>262</sup> this study supported the view of an effective adenine-binding pocket in the “substrate-binding”  $\alpha$ -subunit. The observed binding of the adenine moiety of 5-adeninyl-pentyl-cobalamin, when compared to the still unobserved situation with bound AdoCbl (**2**), would indicate build up of strain in the adenosyl-cobamide cofactor and activation towards homolysis of its (Co–C)-bond. Modeling of the available crystallographic data also suggested a rotation of the ribose ring of the 5'-deoxy-5'-adenosyl radical (**42**) to represent a possible path for relocating the radical center of **42** close to the (C-1)-position of the substrate.<sup>270</sup>

### b. Ethanolamine Ammonia Lyase

Ethanolamine ammonia lyase converts ethanolamine (and homologous vicinal aminoalcohols) to acetaldehyde (and homologues of it), with loss of ammonia and has been identified in a variety of microorganisms. Historically, ethanolamine ammonia lyase was studied in *E. coli* or in clostridia.<sup>221,271</sup> Its activity depends upon adenosyl-cobamides, such as coenzyme B<sub>12</sub> (AdoCbl, **2**), but a range of other adenosyl-cobamides are also accepted as cofactors, while cobalamins with  $\beta$ -ligands other than the 5'-deoxy-5'-adenosyl group (of AdoCbl) are inhibitors. More recently ethanolamine ammonia lyase from *Salmonella typhimurium* (EAL) was successfully overexpressed from *E. coli*.<sup>272</sup> Before addition of substrate, the UV–Vis-spectrum of EAL resembles that of the intact “base-on” AdoCbl, but during steady-state turnover of the enzyme with excess of propanolamine, the spectrum has features of cob(II)alamin (**18**), indicating effective homolysis of the bound AdoCbl. The active enzyme is multimeric, has an apparent molecular mass of about 560–600 kDa, but further studies are much less advanced with EAL than those with the AdoCbl-dependent enzymes described above. Similar to the mechanism of diol dehydratase, a radical mechanism is proposed for the isomerization of the vicinal aminoalcohol substrates (ethanolamine, (*R*)- and (*S*)-aminopropanol), starting with the abstraction of an H-atom from the (C-1)-position of the substrates



**Figure 29.** Ethanolamine ammonia lyase (EAL) isomerizes vicinal aminoalcohols – via 1,2-migration of an amine group – to semiaminals (such as 2-aminopropan-1-ol to 1-aminopropan-1-ol, which loses ammonia to give propanal). Possible reaction mechanism of the migration of the amino group, catalyzed by EAL and involving H-atom abstraction (step a), radical rearrangement (step b) and back transfer of H-atom (step c); substrates for EAL: 2-aminopropan-1-ol ( $R = \text{CH}_3$ ) or ethanolamine ( $R = \text{H}$ ). (The experimentally supported substrate triggered formation of the 5'-deoxy-5'-adenosyl radical (**42**) and of cob(II)alamin (**18**,  $\text{B}_{12}$ ) by homolysis of protein bound AdoCbl (**2**) is omitted here, see Figure 23.)<sup>221,271</sup>

(see Figure 29). Rearrangement to a geminal 1-amino-1-hydroxy-propan-2-yl (or loss of ammonia to a propanal-2-yl) radical are the subsequent steps,<sup>221</sup> but recent ESR-spectroscopic studies were not able to distinguish between the two rearrangement paths.<sup>273</sup>

### 3. $\text{B}_{12}$ -Dependent Amino Mutases

Two coenzyme  $\text{B}_{12}$ -dependent amino mutases have been characterized, both of which catalyze the mechanistically less well investigated migration of  $\omega$ -amino groups to the ( $\omega$ -1)-position in diamino-acids with the help of coenzyme  $\text{B}_{12}$  (AdoCbl, **2**) and pyridoxal-phosphate as cofactors.<sup>222,223</sup> One of them, ornithine-4,5-aminomutase, catalyzes the migration of the terminal amino group of D-ornithine to the 4-position, to give (2*R*,4*S*)-diaminovaleric acid (see Table 1). The migration of the amino group is achieved in a radical reaction, which is initiated by abstraction of a H-atom from the pyridoxal-conjugate of the substrate by the 5'-deoxy-5'-adenosyl radical (**42**) that originates from enzyme induced homolysis of the (Co–C)-bond of AdoCbl (**2**). The pyridoxal cofactor (PLP), required by this enzyme,

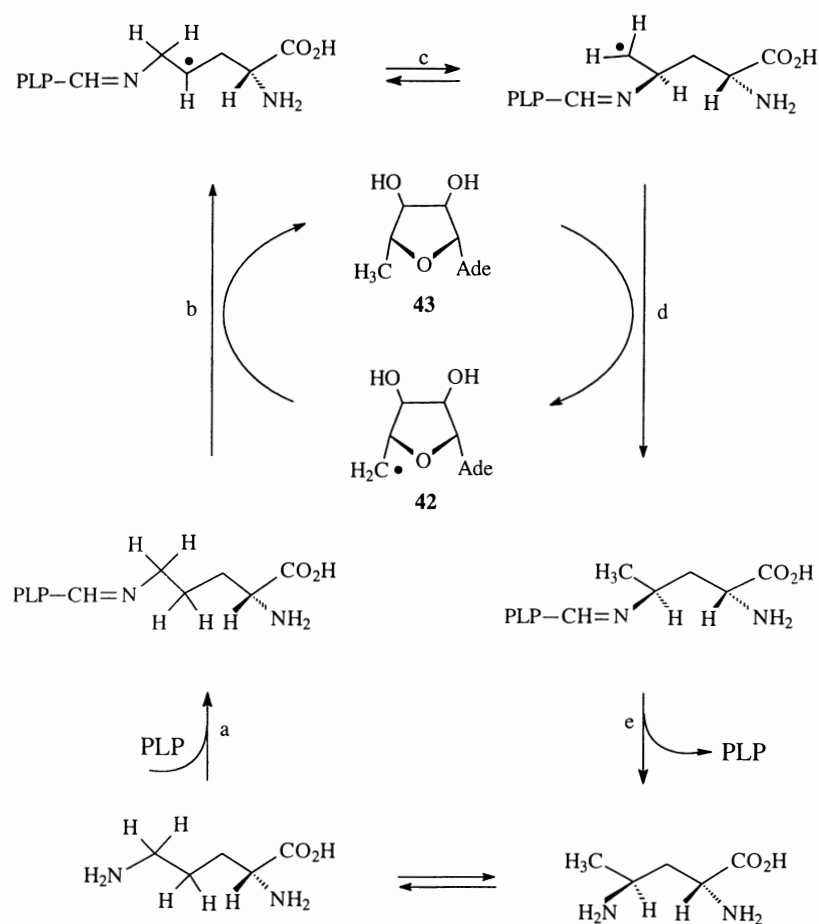
assists the migration by forming a Schiff's base involving the migrating amino function (see Figure 30).

The situation is more complex with the so called D-lysine/L- $\beta$ -lysine 5,6-aminomutase, which catalyzes the isomerization of D-lysine to 2,5-diaminohexanoic acid and of L- $\beta$ -lysine to (3*S*,5*S*)-3,5-diaminohexanoic acid.<sup>222,223</sup> The mechanism of the migration of the amino group is suggested to be similar to that of D-ornithine amino mutase (see Figure 30). A related isomerization of L- $\alpha$ -lysine to L- $\beta$ -lysine is catalyzed by lysine-2,3-aminomutase, which, however, is an amino mutase that is independent of coenzyme  $\text{B}_{12}$  (**2**) (see Section VE).<sup>222</sup>

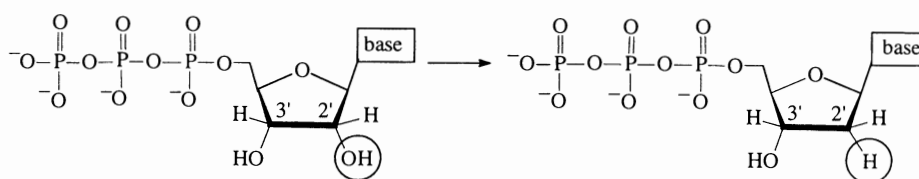
### 4. $\text{B}_{12}$ -Dependent Ribonucleotide Reductase

In all organisms, the ribonucleotide reductases (RNRs) play essential roles in the biosynthesis of DNA by catalyzing the reduction of all four nucleoside di- or triphosphates to the corresponding 2'-deoxynucleotides.<sup>224,274</sup> Despite their central role in primary metabolism, the RNRs have evolved to use a diverse array of metal cofactors to initiate the radical reaction that eventually leads to the nucleotide reduction (see Figure 31).<sup>275,276</sup>

The reductase from *Lactobacillus leichmanii* (RNR-*Ll*) belongs to the class II RNRs which make use of adenosyl-cobamides, such as coenzyme  $\text{B}_{12}$  (**2**), to initiate the radical reaction. RNR-*Ll* is the best studied of the group of RNRs that depend upon adenosyl-cobamides, representatives of which are also known from a range of other microorganisms.<sup>274</sup> The reductase RNR-*Ll* uses nucleoside triphosphates (NTPs) as substrates and 2'-deoxynucleoside triphosphates (dNTPs) as allosteric effectors.<sup>224</sup> Work from the Stubbe laboratories in particular has enlarged quite significantly the state of knowledge concerning the amazing  $\text{B}_{12}$ -dependent ribonucleotide reductase (RNR-*Ll*) from *L. leichmanii*.<sup>224</sup> In RNR-*Ll* the “ $\text{B}_{12}$ -binding motif”, the (Gly-X-X-His-X-Asp)-sequence, was not found and, indeed, by ESR-spectroscopy, “base-on” binding of the corrinoid cofactor was made likely.<sup>277</sup> In RNR-*Ll* a protein-centered thiyl-radical is generated from the homolysis of the (Co–C)-bond of the bound coenzyme **2**, which induces the radical reactions that formally lead to the reductive substitution by hydrogen of the 2'-hydroxyl group of the ribonucleotide (see Figure 32). Homolytic (Co–C)-bond cleavage of AdoCbl (**2**) is known to be accelerated by about  $10^{11}$ -fold in RNR.<sup>278</sup> The free enthalpy of activation of AdoCbl, when bound to GTP-activated but



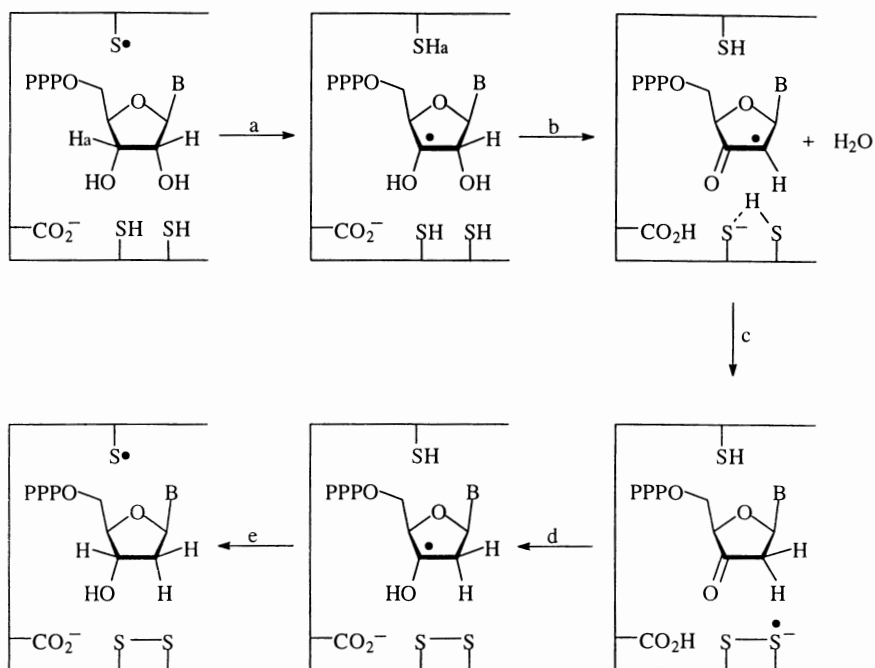
**Figure 30.** D-ornithine-4,5-aminomutase isomerizes D-ornithine to (2*R*,4*S*)-diaminovalerate – via a  $\omega$ ,( $\omega$ -1)-migration of an amino group. Possible reaction mechanism of the migration of the amino group, catalyzed by D-ornithine-4,5-aminomutase and involving formation of a Schiff's base with the pyridoxal-phosphate cofactor (step a), H-atom abstraction by the 5'-deoxy-5'-adenosyl radical (**42**) (step b), radical rearrangement (step c), back transfer of H-atom with regeneration of the 5'-deoxy-5'-adenosyl radical (**42**) (step d), and hydrolysis of the imine, with liberation of the pyridoxal-phosphate cofactor (step e). (The experimentally supported formation of the 5'-deoxy-5'-adenosyl radical (**42**) and of cob(II)alamin (**18**, B<sub>12</sub>) by homolysis of protein bound AdoCbl (**2**) (see Figure 23) is omitted here.)<sup>222,223</sup>



**Figure 31.** Schematic illustration of the reduction of ribonucleoside triphosphates to 2'-deoxyribonucleoside triphosphates, as catalyzed by ribonucleotide reductase from *L. leichmanii* (RNR-*Ll*).<sup>224</sup>

substrate-free RNR-*Ll*, was determined to be lowered in the enzyme by about 13–15 kcal/mol compared to the value for the homolysis of AdoCbl in aqueous solution.<sup>278,279</sup> The origin of this enhancement of the rate of homolysis by the protein was interpreted differently, as to result mainly from lowering of the bond-dissociation energy,<sup>279</sup> or from favorable entropic contributions.<sup>278</sup> The presence of the cysteine residue C-408 of the apoenzyme has been shown to be required

for the cleavage of the organometallic bond of **2** to be effective: the cleavage of the (Co–C)-bond of **2** and formation of 5'-deoxyadenosine (**43**) and of the thiyl radical are indicated to be kinetically coupled.<sup>279,280</sup> The thiyl radical at C-408 then abstracts the H-atom at C-3' of the bound substrate to induce the reductive dehydration of the bound NTP to a dNTP (see Figure 32 for a proposed mechanism), which involves the oxidation of the thiol groups of two



**Figure 32.** Adenosyl-cobamide-dependent ribonucleotide reductase catalyzes the reduction of ribonucleotides to 2'-deoxyribonucleotides. Proposed mechanism involving H-atom abstraction by the protein thiyl radical (step a), loss of water (step b), two successive one-electron reduction steps (steps c and d) and back transfer of the H-atom (step e). (The experimentally supported substrate triggered formation of the 5'-deoxy-5'-adenosyl radical (**42**) and of cob(II)alamin (**18**,  $B_{12}$ ) by homolysis of protein bound AdoCbl (**2**) (see Figure 23), as well as the H-atom abstraction by **42** from the cysteine residue are omitted here.)<sup>224,276</sup> (Adapted with permission of Wiley-VCH from ref. 224.)

cysteines (suggested to be C-119 and C-419) to a disulfide bridge.

The crystal structures of dGTP-free AdoCbl-dependent RNR-*Ll* in the apo-form and complexed with  $Co_{\beta}$ -adeninylpentyl-cobalamin (see e.g. Ref. 270), a structural analog of AdoCbl (**2**), were solved recently.<sup>281</sup> The crystal structure confirmed, first of all, the “base-on” nature of the bound corrinoid, deduced from ESR-data earlier<sup>277</sup> of which, the position of the organometallic ligand was strongly disordered. The global fold of all crystal structures of class I, II and III RNRs thus are rather similar. In crystalline RNR-*Ll* the crucial cysteine, C-408, is at a distance of about 10 Å from the cobalt(II)-center of the bound corrinoid and in a region of space that is also well conserved in the three classes of RNRs. In many regards, the AdoCbl-dependent RNR-*Ll* appears to represent the least complex form of the three classes of RNRs now known.<sup>281</sup>

### 5. $B_{12}$ -Coenzymes in Enzymatic Radical Reactions

Until about two decades ago, the coenzyme  $B_{12}$ -catalyzed enzymatic reactions had no experimental counterpart from (nonenzymatic) solution chemistry (see e.g. Refs. 164,167,231,243 and references therein).

Today the relevance of radical mechanisms for the coenzyme  $B_{12}$ -catalyzed enzymatic rearrangements is hardly questioned, based on a broad spectrum of spectroscopic, structural, and kinetic findings.<sup>228,231,243</sup> The homolytic cleavage of the (Co–C)-bond of the protein-bound organometallic cofactor **2** is the initial step of the coenzyme  $B_{12}$ -catalyzed enzymatic reactions (see Figure 23). As coined by Halpern<sup>89</sup> adenosyl-cobamides, such as coenzyme  $B_{12}$  (**2**), can indeed be considered as being “reversibly functioning sources for organic radicals.” Coenzyme  $B_{12}$  (**2**) therefore is a “pre-catalyst”<sup>282</sup> for the enzymatic radical reactions and is well suited for this task by its inherent chemical reactivity. Neutral aqueous solutions of the coenzyme **2** are remarkably stable with an estimated half life of **2** of about  $10^{10}$  s (in the dark and at room temperature), but decompose at higher temperatures with homolysis of the (Co–C)-bond mainly.<sup>89,169</sup> The coenzyme  $B_{12}$ -catalyzed enzyme reactions occur with typical maximal rates of roughly  $100 \text{ s}^{-1}$ .<sup>215,280</sup> Rapid formation of paramagnetic species and/or of Co(II)corrins only occurs upon mixing solutions of holoenzyme (or of apoenzymes and coenzyme  $B_{12}$ ) with substrate, as could be demonstrated in most of the known coenzyme  $B_{12}$ -dependent enzymes, e.g. in methyl-malonyl-CoA mutase (MMCM),<sup>167</sup> glutamate mutase (GM)<sup>248</sup> and

class II ribonucleotide reductase from *Lactobacillus leichmanii* (RNR-*Ll*).<sup>280</sup>

An intriguing feature of the coenzyme B<sub>12</sub>-dependent enzymes thus is the implied dramatic (> 10<sup>12</sup>-fold) labilization of the bound organometallic cofactor towards homolysis of its (Co–C)-bond.<sup>89,169,215</sup> The mechanism of the enzyme- (and substrate-induced) labilization of the (Co–C)-bond of the coenzyme **2** is still a key problem and a major dispute in B<sub>12</sub>-chemistry. Evidence for covalent restructuring of the bound organometallic cofactor (except for the formation of the “base-off/His-on”-form in the carbon skeleton mutases) is not available.<sup>27,81,89,169,215</sup> Furthermore, protein and solvent molecules are able to stabilize a radical center only weakly,<sup>283</sup> such as the one of the 5'-deoxy-5'-adenosyl radical (**42**) from (Co–C)-bond homolysis of coenzyme B<sub>12</sub>. Steric distortions of the protein-bound coenzyme **2** are discussed as a means for the observed enhanced rate of (Co–C)-bond homolysis.<sup>61,89,206,270</sup> Halpern's hypothesis of an “upwards-conformational distortion” of the corrin ligand of **2** by the proteinic environment<sup>89</sup> and the related suggestion of a sterically induced conformational distortion of the corrin ring of **2** by movement towards (of it) the bulky dimethylbenzimidazole (DMB) base (e.g. Ref. 284) have been particularly attractive. However, in view of available crystal structures of cob(II)alamin (**18**)<sup>61</sup> of the enzymes methylmalonyl-CoA mutase (MMCM),<sup>240</sup> glutamate mutase (GM),<sup>251</sup> diol dehydratase (DD)<sup>270</sup> and ribonucleotide reductase (RNR-*Ll*)<sup>281</sup> an “upwards conformational distortion” of the cobalt-corrin part of **2** are not considered of major relevance any longer. In fact, it appears that the labilization may come about largely by way of a protein- and substrate-induced strain on the organometallic group, separation of the largely nonstrained homolysis fragments and strong binding by the protein of the separated pair, the 5'-deoxy-5'-adenosyl radical (**42**) and cob(II)alamin in “base-on”<sup>61,261</sup> or in “base-off/His-on” form.<sup>206,251</sup> Consistent with this structure-based view, that the support of the mere spatial separation of the homolysis fragments by increased binding to the protein would stabilize the homolized state of the coenzyme **2**, “post-homolysis” analogues of **2** (“stretched” homologues of AdoCbl) were found to be bound better than the coenzyme **2** itself.<sup>197,285</sup>

Chemical reactions in solution as well as theoretical studies have provided chemical models for the coenzyme B<sub>12</sub>-dependent enzymatic rearrangements, mostly based on the reactivity of free radicals (see e.g. Refs. 89,225,228,231,236,243,250,267). In general, it is

assumed nowadays, that the rearrangement steps are accomplished by tightly protein-bound radicals that are controlled in their reaction space,<sup>218,226,243,261</sup> but (practically) unassisted by the Co(II)-corrin fragment of the coenzyme (which has the role of a “spectator”).<sup>226,243</sup> Clearly, the problems of how in the presence of bound substrate the protein environment succeeds in unleashing quickly the radical **42** by homolysis of the coenzyme **2**, how the enzyme-bound radical **42** (and also the Co(II)-corrin fragment **18**) are controlled by the apoenzyme to achieve the mechanistically complex rearrangement reactions (see e.g. Ref. 252) and how 5'-deoxyadenosine (**43**) finally is brought back as the organometallic ligand of **2** are still fascinating aspects of the coenzyme B<sub>12</sub>-dependent enzymatic reactions, which invite further fundamental experimental work.

The presence of “base-off/His-on” binding in the coenzyme B<sub>12</sub>-dependent carbon skeleton mutases, is (happens to be) similar to the situation in the methionine synthase B<sub>12</sub>-binding domain,<sup>206</sup> but contrasts with most of the other investigated types of coenzyme B<sub>12</sub>-dependent enzymes, and appears as strikingly “unsystematic.” These findings have renewed interest in the “axial base problem.”<sup>36,75,169,206</sup> When giving thought to potential benefits of the nucleotide part of the “complete” corrinoids (or of related nitrogen bases) for their cofactor roles, the basically different tasks of methyl transferases and of mutases catalyzing radical rearrangements need to be considered separately. In the methyl-group transferases, the H<sup>+</sup>-dependent coordination of the His-residue (as part of a His-Asp-Ser-triad) may lead to a better accommodation by the holo-enzyme of the constitutional and conformational changes accompanying and regulating the nucleophile-induced methyl transfer steps (“molecular juggling acts”<sup>26</sup>) which are accompanied by coordinative changes at both faces of the corrin-bound cobalt center.<sup>81,206</sup>

In the coenzyme B<sub>12</sub>-dependent mutases, the main requirement for the bound corrinoid cofactor is “only” the production and controlled presentation of the 5'-deoxy-5'-adenosyl radical (**42**) from homolysis of the (Co–C)-bond of **2**, but little structural reorganization elsewhere in its cobalt-corrin part.<sup>81</sup> Labilization of the (Co–C)-bond of the bound **2** during catalysis appears to be the consequence of strain produced in the substrate-binding/activating domain (or subunit).<sup>240,261</sup> Firm placement of the corrin moiety at the interfaces of B<sub>12</sub>-binding and substrate-binding/activating domains appears to be crucial and movements of the corrin moieties may not be required. Indeed, as reviewed above, with coenzyme B<sub>12</sub>-dependent enzymes the

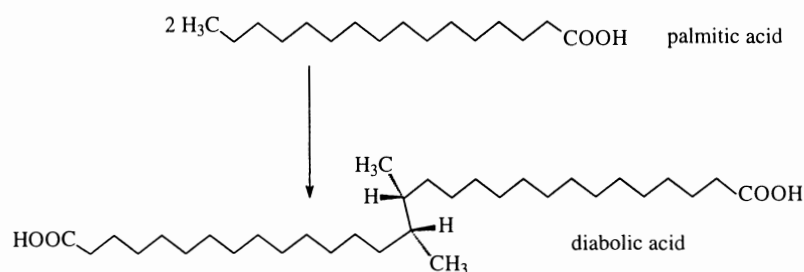


Figure 33. Schematic illustration of the (oxidative) dimerization of palmitic acid to diabolic acid.<sup>188</sup>

“base-off/His-on” mode of cofactor binding is not the general situation, even though it appears to be the characteristic motif of carbon skeleton mutases. The “regulatory triads” (such as His-Asp-Lys in MMCM) logically appears not to be involved in proton-transfer steps and accordingly may conserve its structure largely during enzymatic turnover. “Electronic effects” of the axial trans ligand on the homolytic (Co–C)-bond dissociation energy in MeCbl (**3**) and AdoCbl (**2**) are seen to be less important.<sup>80,103</sup> The existence of two (or more) basic B<sub>12</sub>-binding motifs may be a consequence (again) of two (or more) “protein ancestors” (see e.g. Ref. 261).

#### D. OTHER B<sub>12</sub>-DEPENDENT ENZYMATIC REACTIONS

Recent experiments involving isotopic labeling and stereochemical studies have indicated a range of novel metabolic (C–C)-bond forming reactions at seemingly unactivated (saturated) positions, such as in unusual core lipids from several archaea and (e.g.) the formation of diabolic acid from palmitic acid in the eubacterium *Butyrivibrio fibrisolvens* (see Figure 33). As candidates for the crucial (C–C)-bond forming steps in these transformations, enzymatic reactions involving organometallic B<sub>12</sub>-chemistry were suggested by Arigoni et al.<sup>188</sup> All findings are consistent with the operation of stereochemically controlled “radical” abstraction reactions of a weakly bound, organometallic moiety, potentially that of a corresponding alkyl-corrinoid.<sup>188</sup>

Chemical experiments providing precedence for such a type of a reaction involving an organometallic B<sub>12</sub>-dimer<sup>76</sup> or methylcobalamin (MeCbl, **3**)<sup>187</sup> have been presented lately. Indeed, in the latter work, MeCbl (**3**) was shown to function as a rather good methylating agent, not only in nucleophilic displacement reactions (see Section VB), but also in intermolecular radical reactions, such as the homolytic methylation of 2,2-dimethyl-diethyl-malonate (see Figure 34). The radical methylation reaction (as well as other radical alkylation reactions) with direct homolytic abstraction

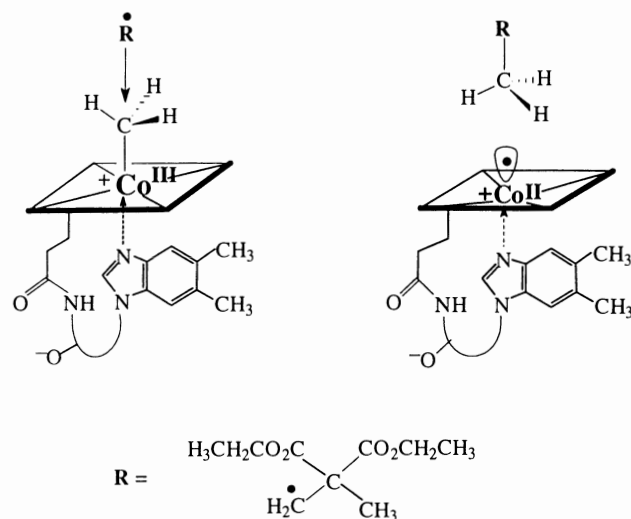
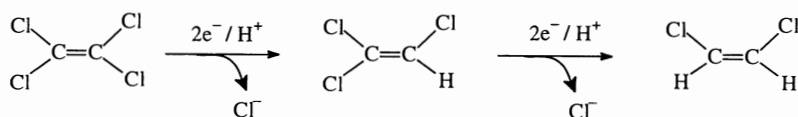


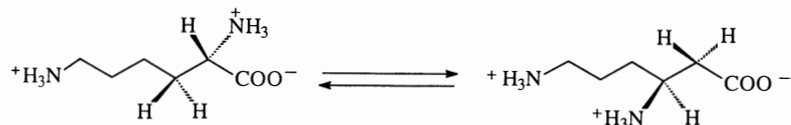
Figure 34. Methylcobalamin (**3**) as a methylating agent for an organic radical.<sup>187</sup>

of a cobalt-bound organic group, clearly are very favorable thermodynamically, as a strong (C–C)-bond is made and a weak (Co–C)-bond is cleaved in such reactions.<sup>187,286</sup>

The ability of methanogens and acetogens to dechlorinate reductively chloromethanes was studied in the last two decades and was proposed to involve reduced metal cofactors, such as reduced corrinoids, in particular (see e.g. Ref. 287). Attention was also given lately to several environmentally relevant microbiological dehalogenation reactions of chloroethenes.<sup>288–291</sup> In the anaerobic bacterium *Dehalospirillum multivorans* tetrachloroethene functions as the terminal electron acceptor and is dechlorinated by the B<sub>12</sub>-dependent tetrachloroethene reductive dehalogenase (TCED).<sup>291,292</sup> The dehalogenase TCED uses a novel corrinoid cofactor, that enables the redox reaction to occur at potentials that are significantly less negative than those of the corresponding cobalamin redox-couples.<sup>293</sup> TCED reduces tetrachloroethene to trichloroethene (first) and (then) to *cis*-dichloroethene (see Figure 35).<sup>291</sup> Model chemistry in the case of reductive dechlorination reactions is little developed, than it is for



**Figure 35.** Schematic illustration of the reductive dechlorination of tetrachloroethene (to trichloroethene and to cis-dichloroethene) by tetrachloroethene reductive dehalogenase.



**Figure 36.** Schematic illustration of the isomerization of L- $\alpha$ -lysine to L- $\beta$ -lysine by lysine-2,3-aminomutase.<sup>222,296</sup>

other reduction reactions, but organometallic B<sub>12</sub>-derivatives are presumed to be intermediates.<sup>288,291,294</sup>

An interesting new twist of the involvement of coenzyme B<sub>12</sub> in metabolism was presented recently with the proposal, that AdoCbl (**2**) could be involved in the biosynthetic build-up of the “extra” cyclopentanone-unit of (bacterio)chlorophylls in the photosynthetic bacterium *Rhodobacter capsulatus*.<sup>295</sup>

### E. METABOLISM USING AN ADENOSYL RADICAL NOT DERIVED FROM COENZYME B<sub>12</sub>

The enzyme lysine-2,3-aminomutase catalyzes the interconversion of L-( $\alpha$ )-lysine and L- $\beta$ -lysine (Figure 36), a reaction typical of those normally associated with coenzyme B<sub>12</sub>-catalyzed enzymatic reactions and indeed appearing similar to related reactions involving the B<sub>12</sub>-coenzyme **2**. Lysine-2,3-aminomutase from *Clostridium subterminale* requires the participation of three cofactors, S-adenosylmethionine (SAM), pyridoxalphosphate (PLP) and an iron–sulfur cluster [4Fe–4S], but not a B<sub>12</sub>-derivative.<sup>222,296</sup>

SAM is the source of the 5'-deoxy-5'-adenosyl radical (**42**) in lysine 2,3-aminomutase from *C. subterminale*. According to the work by Frey et al.,<sup>222,296,297</sup> enzyme-bound SAM is reduced by the [4Fe–4S]-cluster to give methionine and the radical **42**. The latter, in turn, abstracts a hydrogen atom from the aldimine between the substrate and PLP, inducing a radical rearrangement, seemingly related to those of coenzyme B<sub>12</sub>-dependent amino mutases. Even though a (single) molecule of SAM engages in many enzymatic turnovers, it gradually decomposes into 5'-deoxyadenosine and methionine.

However, SAM is of central importance as source of the 5'-deoxy-5'-adenosyl radical (**42**) in a broad range of other radical enzymes, such as class III ribonucleotide reductase,<sup>276</sup> pyruvate-formiat lyase<sup>227</sup> and which are now recognized to be members of a whole new “radical

SAM” protein superfamily.<sup>298</sup> The metabolic use of SAM (“poor man’s B<sub>12</sub>”) accordingly has several parallels with that of the vitamin B<sub>12</sub>-derivatives: SAM is a structurally simpler source of an 5'-deoxy-5'-adenosyl radical (**42**) than coenzyme B<sub>12</sub> (**2**) and a simpler methylating agent than methylcobalamin (MeCbl, **3**). So far, corrinoids have not been found in (higher) plants.<sup>299</sup> In their metabolism, SAM also appears to have both of the two roles known from other organisms, i.e. its function as source of the radical **42** and as methylating agent. SAM was established as the source of the 5'-deoxy-5'-adenosyl radical (**42**) in the last step of the biosynthesis of biotin in *Arabidopsis thaliana*,<sup>300</sup> and has been suggested, as well, to catalyze a 1,2-radical rearrangement in the biosynthesis of the tropane alkaloid hyoscyamine.<sup>301</sup>

## VI. B<sub>12</sub>: Medical Aspects

B<sub>12</sub>-deficiency was recognized in the first half of last century to be the cause for “pernicious” anemia, considered then to be a relatively rare disease (see e.g. Ref. 31). Within the last decade it was realized, that B<sub>12</sub>-deficiency is a common condition, especially with older persons, of whom 10–15% suffer from it.<sup>302,303</sup> In rare cases cobalamin deficiency can be traced back to lack of the vitamin in the diet,<sup>304</sup> but it is generally the consequence of the impaired uptake from the ingested food or to deficient transport in the body.<sup>31,303</sup> An average dose of about 2–3 nmol/day (about 3–4  $\mu$ g/day) of vitamin B<sub>12</sub> are considered necessary for sustained physical well being, which need to be supplied externally, e.g. with the food.<sup>31</sup>

Three soluble B<sub>12</sub>-binding proteins are known to be involved in the uptake and transport of cobalamins in humans: intrinsic factor (IF), transcobalamin (TC) and haptocorrin (HC).<sup>31,305</sup> These three proteins ensure that the needed amounts of cobalamins reach the two

intracellular enzymes, methionine synthase (in the cytosol) and methylmalonyl-CoA mutase (in the mitochondria).<sup>31,306</sup> In the small intestine, IF, which itself is synthesized in the stomach, binds the cobalamins (from food) and the IF-cobalamin complex is then absorbed by specific receptors on the brush borders of the epithelial cells of the small intestines. After absorption there, the cobalamins are bound to TC or to HC, to be internalized with these B<sub>12</sub>-binders. In the cytosol, B<sub>12</sub> mostly is metabolically active as methylcobalamin (**3**), in the mitochondria as coenzyme B<sub>12</sub> (**2**). Vitamin B<sub>12</sub> (cyanocobalamin, **1**) appears to have no physiological role by itself<sup>4</sup> and most B<sub>12</sub> in human metabolism is actually present in the form of coenzyme B<sub>12</sub> (**2**) and methylcobalamin (**3**).<sup>306</sup>

IF, TC and HC are all strong B<sub>12</sub>-binders (apparent binding constants of roughly 10<sup>12</sup> l/mol), genetically related and built-up of about 400 amino acid residues. TC (45 kDa) contains no carbohydrates, whereas IF (50 kDa) and HC (about 70 kDa) are both heavily glycosylated (HC to a varying degree).<sup>31,305</sup> For tight binding to these (glyco)proteins the presence of a nucleotide function is critical, that is able to coordinate to the cobalt center, and they are thus indicated to recognize the "lower"  $\alpha$ -side of the intact cobalamins.<sup>196</sup>

Intracellular B<sub>12</sub>-trafficking appears to depend upon a complex interplay between the B<sub>12</sub>-binders and cellular surface receptors that recognize (as one of their functions) complexes between B<sub>12</sub> and B<sub>12</sub>-binding proteins, such as the B<sub>12</sub>-complexes of IF, TC and HC.<sup>307</sup> IF-B<sub>12</sub> receptors are broadly distributed and appear to mediate endocytosis of the IF-B<sub>12</sub>-complex. One of them is the protein gp280 with a molecular weight of about 460 kDa.<sup>308,309</sup> Megalin (gp330), another multiligand binding and endocytosis-mediating membrane protein, has a molecular weight of about 600 kDa and binds TC-B<sub>12</sub> complexes.<sup>307</sup> The multifunctional asialo-glycoprotein receptor recognizes glycoproteins with free galactose residues and binds the B<sub>12</sub>-complex of the heavily glycosylated B<sub>12</sub>-binder HC.<sup>31,305,309</sup>

The capacity of the B<sub>12</sub>-binding proteins to recognize and transport a range of cobalamins<sup>31</sup> has been exploited for the uptake and transport of B<sub>12</sub>-based radioactive imaging agents: covalent peripheral attachment of chelating units for various radionuclides leads to radioactive B<sub>12</sub>-conjugates, which appear to be promising diagnostic agents in nuclear medicine and in magnetic resonance imaging.<sup>310,311</sup>

Lack of IF is a relatively common disorder, lack of TC is a rare inborn disorder, both resulting in

B<sub>12</sub>-deficiency.<sup>31,312</sup> Disbalanced values for the pairs of methyl-group homologues, methionine/homocysteine and N<sup>5</sup>-methyltetrahydrofolate/tetrahydrofolate, respectively, may result from B<sub>12</sub>-deficiency, reduced activity of methionine synthase or from exposure to nitrous oxide (laughing gas), and is associated with megaloblastic anemia.<sup>303,313</sup> Methyl-malonic aciduria is a syndrome that is often fatal in infants and is another consequence of cobalamin-deficiency associated with the impairment of the function of human methyl-malonyl-CoA mutase.

## ACKNOWLEDGEMENTS

We would like to thank Paula Enders, Robert Konrat, Christian Eichmüller, Mario Fasching, Wolfgang Fieber, Renate Hannak, Bernd Hofmann, Michael Oberhuber, Karl-Hans-Ongania, Alexander Rieder and Martin Tollinger for their important recent contributions to our work, Christoph Kratky, Bernard Golding, Wolfgang Buckel, János Rétey and Erhard Stupperich and their groups for fruitful cooperations within a European network. We are grateful to Hoffmann La-Roche, Basel, Switzerland, for a generous gift of vitamin B<sub>12</sub>. Our work has been supported financially by the Austrian Science Foundation (FWF, project No. 13595) and by the European Commission. The acquisition of major instrumentation was made possible by the University of Innsbruck and by the Ministerium für Wissenschaft & Forschung.

## REFERENCES

1. Fraústo da Silva, J. J. R.; Williams, R. J. P. *The Biological Chemistry of the Elements*; Clarendon Press: Oxford, **1991**.
2. Rickes, E. L.; Brink, N. G.; Koniuszy, F. R.; Wood, T. R.; Folkers, K. *Science* **1948**, *107*, 396–397.
3. Smith, E. L.; Parker, L. F. J. *Biochem.* **1948**, *43*, VIII.
4. Ellenbogen, L.; Cooper, B. A. In *Handbook of Vitamins*. Machlin, L. J., Ed.; Marcel Dekker: New York & Basel, **1991**, pp. 491.
5. Heinrich, H. C., Ed.; *Vitamin B<sub>12</sub> and Intrinsic Factor* (1st European Symposium), Enke Verlag: Hamburg **1956**, Stuttgart, **1957**.
6. Heinrich, H. C., Ed.; *Vitamin B<sub>12</sub> and Intrinsic Factor* (2nd European Symposium), Enke Verlag: Hamburg **1961**, Stuttgart, **1962**.
7. Zagalak, B.; Friedrich, W., Eds.; *Vitamin B<sub>12</sub>*, (Proceedings of the 3rd European Symposium on Vitamin B<sub>12</sub> and Intrinsic Factor), Walter de Gruyter: Berlin, New York, **1979**.
8. Kräutler, B.; Arigoni, D.; Golding, B. T., Eds.; *Vitamin B<sub>12</sub> and B<sub>12</sub>-Proteins*, Wiley-VCH: Weinheim, Germany, **1998**.
9. Battersby, A. R. In *Vitamin B<sub>12</sub> and B<sub>12</sub>-Proteins*. Kräutler, B.; Arigoni, D.; Golding, B. T., Eds.; Wiley-VCH: Weinheim, Germany, **1998**, pp. 47–61.
10. Blanche, F.; Cameron, B.; Crouzet, J.; Debussche, L.; Thibaut, D.; Vuilhorgne, M.; Leeper, F. J.; Battersby, A. R. *Angew. Chem. Int. Ed. Engl.* **1995**, *34*, 383–411.



11. Thibaut, D.; Blanche, F.; Cameron, B.; Crouzet, J.; Debussche, L.; Rémy, E.; Vuilhorgne, M. In *Vitamin B<sub>12</sub> and B<sub>12</sub>-Proteins*. Kräutler, B.; Arigoni, D.; Golding, B. T., Eds.; Wiley-VCH: Weinheim, Germany, **1998**, pp. 63–79.
12. Scott, A. I. In *Vitamin B<sub>12</sub> and B<sub>12</sub>-Proteins*. Kräutler, B.; Arigoni, D.; Golding, B. T., Eds.; Wiley-VCH: Weinheim, Germany, **1998**, pp. 81–100.
13. Eschenmoser, A.; Wintner, C. *Science* **1977**, *196*, 1410–1420.
14. Eschenmoser, A. In *Nova Acta Leopoldina*. Neue Folge/Bd. 55, Deutsche Akademie der Naturforscher: Halle, Germany **1982**, pp. 5–47.
15. Woodward, R. B. In *Vitamin B<sub>12</sub>* (Proceedings of the 3rd European Symposium on Vitamin B<sub>12</sub> and Intrinsic Factor). Zagalak, B.; Friedrich, W., Eds.; Walter de Gruyter: Berlin, New York, **1979**, pp. 37–87.
16. Scott A. I.; Roessner, C. A.; Santander, P. J. In *The Porphyrin Handbook*. Kadish, K. M.; Smith K. M.; Guillard, R. Eds.; Elsevier Science: Amsterdam, **2003**; Chapter 76.
17. Stevens, R.V. In Dolphin, D., Ed.; *B<sub>12</sub>*, Vol I, John Wiley & Sons: New York, Chichester, **1982**, pp. 169–200.
18. Pratt, J. M. *Inorganic Chemistry of B<sub>12</sub>*, Academic Press: New York, London, **1972**.
19. Friedrich, W. Vitamin B<sub>12</sub> und verwandte Corrinoiden. In *Fermente, Hormone und Vitamine*. Ammon, R.; Dirscherl, W. Eds.; Vol III/2, Georg Thieme Verlag: Stuttgart, **1975**.
20. Dolphin, D. *B<sub>12</sub>*, John Wiley & Sons: New York, Chichester, **1982**, Vol I; Dolphin, D. *B<sub>12</sub>*, John Wiley & Sons: New York, Chichester, **1982**, Vol II.
21. Banerjee, R. *Chemistry and Biochemistry of B<sub>12</sub>*, John Wiley & Sons: New York, Chichester, **1999**.
22. Hodgkin, D. C.; Pickworth, J.; Robertson, J. H.; Trueblood, K. N.; Prosen, R. J.; White, J. G. *Nature (London)* **1955**, *176*, 325–328.
23. Hodgkin, D. C.; Kamper, J.; Mackay, M.; Pickworth, J.; Trueblood, K. N.; White, J. G. *Nature (London)* **1956**, *178*, 64–66.
24. Lenhert, P. G.; Hodgkin, D. C. *Nature* **1961**, *192*, 937–938.
25. Drennan, C. L.; Huang, S.; Drummond, J. T.; Matthews, R. G.; Ludwig, M. L. *Science* **1994**, *266*, 1669–1674.
26. Drennan, C. L.; Dixon, M. M.; Hoover, D. M.; Jarrett, J. T.; Goulding, C. W.; Matthews, R. G.; Ludwig, M. L. In *Vitamin B<sub>12</sub> and B<sub>12</sub>-Proteins*. Kräutler, B.; Arigoni, D.; Golding, B. T., Eds.; Wiley-VCH: Weinheim, Germany, **1998**, pp. 133–155.
27. Evans, P. R.; Mancina, F. In *Vitamin B<sub>12</sub> and B<sub>12</sub>-Proteins*. Kräutler, B.; Arigoni, D.; Golding, B. T., Eds.; Wiley-VCH: Weinheim, Germany, **1998**, pp. 217–226.
28. Mancina, F.; Keep, N. H.; Nakagawa, A.; Leadlay, P. F.; McSweeney, S.; Rasmussen, B.; Bösecke, P.; Diat, O.; Evans, P. R. *Structure* **1996**, *4*, 339–350.
29. Reitzer, R.; Gruber, K.; Jogl, G.; Wagner, U. G.; Bothe, H.; Buckel, W.; Kratky, C. *Structure* **1999**, *7*, 891–902.
30. Shibata, N.; Masuda, J.; Tobimatsu, T.; Toraya, T.; Suto, K.; Morimoto, Y.; Yasuoka, N. *Structure* **1999**, *7*, 997–1008.
31. Nexø, E. In *Vitamin B<sub>12</sub> and B<sub>12</sub>-Proteins*. Kräutler, B.; Arigoni, D.; Golding, B. T., Eds.; Wiley-VCH: Weinheim, Germany, **1998**, pp. 461–475.
32. Kräutler, B. In *Vitamin B<sub>12</sub> and B<sub>12</sub>-Proteins*. Kräutler, B.; Arigoni, D.; Golding, B. T., Eds.; Wiley-VCH: Weinheim, Germany, **1998**, pp. 517–522.
33. Glusker, J. P. In *B<sub>12</sub>*. Dolphin, D., Ed.; John Wiley & Sons: New York, Chichester, **1982**, Vol I, pp. 23–106.
34. Kratky, C.; Kräutler, B. In *Chemistry and Biochemistry of B<sub>12</sub>*. Banerjee R., Ed.; John Wiley & Sons: New York, Chichester, **1999**, pp. 9–41.
35. Moss, G. P. *Pure Appl. Chem.* **1987**, *6*, 779–832.
36. Kräutler, B.; Konrat, R.; Stupperich, E.; Färber, G.; Gruber, K.; Kratky, C. *Inorg. Chem.* **1994**, *33*, 4128–4139.
37. Stoeckli-Evans, H.; Edmond, E.; Crowfoot Hodgkin, D. *J. Chem. Soc. Perkin II* **1972**, 605–614.
38. Brown, K. L.; Evans, D. R.; Zubkowsky, J. D.; Valente, E. J. *Inorg. Chem.* **1996**, *35*, 415–423.
39. Brown, K. L.; Zou, X.; Wu, G. Z.; Zubkowsky, J. D.; Valente, E. J. *Polyhedron* **1995**, *14*, 1621–1639.
40. Brown, K. L.; Cheng, S. F.; Zou, X.; Zubkowsky, J. D.; Valente, E. J.; Knapton, L.; Marques, H. M. *Inorg. Chem.* **1997**, *36*, 3666–3675.
41. Gruber, K.; Jogl, G.; Klintschar, G.; Kratky, C. In *Vitamin B<sub>12</sub> and B<sub>12</sub>-Proteins*. Kräutler, B.; Arigoni, D.; Golding, B. T., Eds.; Wiley-VCH: Weinheim, Germany, **1998**, pp. 335–347.
42. Charland, J.-P.; Zangrando, E.; Bresciani-Pahor, N.; Randaccio, L.; Marzilli, L. G. *Inorg. Chem.* **1993**, *32*, 4256–4267.
43. Parker, W. O.; Zangrando, E.; Bresciani-Pahor, N.; Marzilli, P. A.; Randaccio, L.; Marzilli, L. G. *Inorg. Chem.* **1988**, *27*, 2170–2180.
44. Kopf, J.; Bieganski, R.; Friedrich, W.; Vondeuten, K. Z. *Naturforsch.* **1981**, *C36*, 506–515.
45. Kratky, C.; Färber, G.; Gruber, K.; Wilson, K.; Dauter, Z.; Nolting, H.-F.; Konrat, R.; Kräutler, B. *J. Am. Chem. Soc.* **1995**, *117*, 4654–4670.
46. Sagi, I.; Chance, M. R. *J. Am. Chem. Soc.* **1992**, *114*, 8061–8066.
47. Randaccio, L.; Furlan, M.; Geremia, S.; Slouf, M. *Inorg. Chem.* **1998**, *37*, 5390–5393.
48. Hohenester, E.; Kratky, C.; Kräutler, B. *J. Am. Chem. Soc.* **1991**, *113*, 4523–4530.
49. Jörin, E.; Schweiger, A.; Günthard, H. H. *J. Am. Chem. Soc.* **1983**, *105*, 4277–4286.
50. Suto, R. K.; Brasch, N. E.; Anderson, O. P.; Finke, R. G. *Inorg. Chem.* **2001**, *40*, 2686–2692.
51. Eschenmoser, A. *Angew. Chem.* **1988**, *100*, 5–40; *Angew. Chem. Int. Ed. Engl.* **1988**, *27*, 5–40.
52. Fischli, A.; Daly, J. J. *Helv. Chim. Acta* **1980**, *63*, 1628–1643.
53. Kamiya, K.; Kennard, O. *J. Chem. Soc., Perkin Trans I* **1982**, 2279–2288.
54. Markwell, A. J.; Pratt, J. M.; Shaikjee, M. S.; Toerien, J. G. *J. Chem. Soc., Dalton Trans.* **1987**, 1349–1357.
55. Kräutler, B.; Caderas, C.; Konrat, R.; Puchberger, M.; Kratky, C. *Helv. Chim. Acta* **1995**, *78*, 581–599.
56. Lewis, N. J.; Eschenmoser, A.; Kräutler, B.; Nussberger, R. *Angew. Chem. Int. Ed. Engl.* **1983**, *22*, 736–737.
57. Nussbaumer, C.; Arigoni, D. *Angew. Chem. Int. Ed. Engl.* **1983**, *22*, 737–738.
58. Battersby, A. R.; Harms, K.; Sheldrick, G. M.; Grgurina, I.; Egert, E.; Raithby, P. R. *Acta Crystallogr.* **1989**, *C45*, 1589–1593.
59. Werthemann, L. Dissertation No. 4097 ETH Zürich, Juris Druck + Verlag: Zürich, 1968.
60. Kräutler, B.; Keller, W.; Hughes, M.; Caderas, C.; Kratky, C. *J. Chem. Soc., Chem. Commun.* **1987**, 1678–1680.
61. Kräutler, B.; Keller, W.; Kratky, C. *J. Am. Chem. Soc.* **1989**, *111*, 8936–8938.
62. Lenhert, P. G. *Proc. Roy. Soc. (London)* **1968**, *A303*, 45–84.
63. Savage, H. F. J.; Lindley, P. F.; Finney, J. L. *Acta Cryst.* **1987**, *B43*, 280–295.
64. Bouquiere, J. P.; Finney, J. L.; Lehmann, M. S.; Lindley, P. F.; Savage, H. F. J. *Acta Crystallogr.* **1993**, *B49*, 79–89.
65. Brown, K. L.; Cheng, S.; Zou, X.; Li, J.; Chen, G.; Valente, E. J.; Zubkowsky, J. D.; Marques, H. M. *Biochemistry* **1998**, *37*, 9704–9715.
66. Sando, G. N.; Blakley, R. L.; Hogenkamp, H. P.; Hoffmann, P. J. *J. Biol. Chem.* **1975**, *250*, 8774–8779.
67. Krouwer, J. S.; Holmquist, B.; Kipnes, R. S.; Babior, B. M. *Biochim. Biophys. Acta* **1980**, *612*, 153–159.
68. Babior, B. M. In *Vitamin B<sub>12</sub>*. Zagalak, B.; Friedrich, W., Eds.; Walter de Gruyter: Berlin, **1979**, pp. 461–470.

69. Pagano, T. G.; Marzilli, L. G.; Flocco, M. M.; Tsai, C.; Carrell, H. L.; Glusker, J. P. *J. Am. Chem. Soc.* **1991**, *113*, 531–542.
70. Alcock, N. W.; Dixon, R. M.; Golding, B. T. *J. Chem. Soc., Chem. Commun.* **1985**, 603–605.
71. Matthews, R. G.; Banerjee, R. V.; Ragsdale, S. W. *BioFactors* **1990**, *2*, 147–152.
72. Rossi, M.; Summers, M. F.; Randaccio, L.; Toscano, P. J.; Glusker, J. P.; Marzilli, L. G. *J. Am. Chem. Soc.* **1985**, *107*, 1729–1738.
73. Tollinger, M.; Konrat, R.; Kräutler, B. *Helv. Chim. Acta* **1999**, *82*, 1596–1609.
74. Wagner, T.; Afshar, C. E.; Carrell, H. L.; Glusker, J. P. *Inorg. Chem.* **1999**, *38*, 1785–1794.
75. Fasching, M.; Schmidt, W.; Kräutler, B.; Stupperich, E.; Schmidt, A.; Kratky, C. *Helv. Chim. Acta* **2000**, *83*, 2295–2316.
76. Kräutler, B.; Dérer, T.; Liu, P.; Mühlecker, W.; Puchberger, M.; Gruber, K.; Kratky, C. *Angew. Chem. Int. Ed. Engl.* **1995**, *34*, 84–86.
77. Purcell, K. F.; Kotz, J. C. *Inorg. Chem.* **1977**, Holt-Saunders Edition, Philadelphia.
78. De Ridder, D. J. A.; Zangrando, E.; Bürgi, H.-B. *J. Mol. Struct.* **1996**, *374*, 63–93.
79. Pratt, J. M. In *B<sub>12</sub>. Dolphin, D.*, Ed.; John Wiley & Sons: New York, Chichester, **1982**, Vol. I, pp. 325–392.
80. Kräutler, B. *Helv. Chim. Acta* **1987**, *70*, 1268–1278.
81. Kräutler, B. In *Vitamin B<sub>12</sub> and B<sub>12</sub>-Proteins*. Kräutler, B.; Arigoni, D.; Golding, B. T., Eds.; Wiley-VCH: Weinheim, Germany, **1998**, pp. 3–44.
82. Pett, V. B.; Liebman, M. N.; Murray-Rust, P.; Prasad, K.; Glusker, J. P. *J. Am. Chem. Soc.* **1987**, *109*, 3207–3215.
83. Eschenmoser, A. *Annals New York Acad. Sci.* **1986**, *471*, 108–129.
84. Randaccio, L.; Bresciani-Pahor, N.; Zangrando, E.; Marzilli, L. G. *Chem. Soc. Rev.* **1989**, *18*, 225–250.
85. Grate, J. H.; Schrauzer, G. N. *J. Am. Chem. Soc.* **1979**, *101*, 4601–4611.
86. Marques, H. In *Chemistry and Biochemistry of B<sub>12</sub>*. Banerjee R., Ed.; John Wiley & Sons: New York, Chichester, **1999**, pp. 289–314.
87. Konrat, R.; Tollinger, M.; Kräutler, B. In *Vitamin B<sub>12</sub> and B<sub>12</sub>-Proteins*. Kräutler, B.; Arigoni, D.; Golding, B. T., Eds.; Wiley-VCH: Weinheim, Germany, **1998**, pp. 349–368.
88. Geno, M. K.; Halpern, J. *J. Am. Chem. Soc.* **1987**, *109*, 1238–1240.
89. Halpern, J. *Science*, **1985**, *227*, 869–875.
90. Hensens, O. D.; Hill, H. A. O.; McClelland, C. E.; Williams, R. J. P. In *B<sub>12</sub>. Dolphin, D.*, Ed.; John Wiley & Sons: New York, Chichester, Vol. I, **1982**, pp. 463–500.
91. Anton, D. L.; Hogenkamp, H. P. C.; Walker, T. E.; Matwiyoff, N. A. *Biochemistry* **1982**, *21*, 2372–2378.
92. Ernst, L. *Liebigs Ann. Chem.* **1981**, 376–386.
93. Ernst, L. *J. Chem. Soc., Perkin Trans. 1* **1984**, 2267–2270.
94. Battersby, A. R.; Edington, C.; Fookes, C. J. R.; Hook, J. M. *J. Chem. Soc., Chem. Commun.* **1982**, 181–182.
95. Kräutler, B.; Caderas, C. *Helv. Chim. Acta* **1984**, *67*, 1891–1896.
96. Brown, K. L. In *Chemistry and Biochemistry of B<sub>12</sub>*. Banerjee, R., Ed.; John Wiley & Sons: New York, Chichester, **1999**, pp. 197–237.
97. Stupperich, E.; Kräutler, B. *Arch. Microbiol.* **1988**, *149*, 268–271.
98. Kräutler, B.; Kohler, H.-P. E.; Stupperich, E. *Eur. J. Biochem.* **1988**, *176*, 461–469.
99. Stupperich, E.; Eisinger, H. J.; Kräutler, B. *Eur. J. Biochem.* **1988**, *172*, 459–464.
100. Benn, R.; Mynott, R. *Angew. Chem. Int. Ed. Engl.* **1985**, *24*, 333–335.
101. Summers, M. F.; Marzilli, L. G.; Bax, A. *J. Am. Chem. Soc.* **1986**, *108*, 4285–4294.
102. Bax, A.; Marzilli, L. G.; Summers, M. F. *J. Am. Chem. Soc.* **1987**, *109*, 566–574.
103. Pagano, T. G.; Yohannes, P. G.; Hay, B. P.; Scott, J. R.; Finke, R. G.; Marzilli, L. G. *J. Am. Chem. Soc.* **1989**, *111*, 1484–1491.
104. Calafat, A. M.; Marzilli, L. G. *J. Am. Chem. Soc.* **1993**, *115*, 9182–9191.
105. Hoffmann, B.; Oberhuber, M.; Stupperich, E.; Bothe, H.; Buckel, W.; Konrat, R.; Kräutler, B. *J. Bacteriol.* **2000**, *182*, 4773–4782.
106. Tollinger, M.; Dérer, T.; Konrat, R.; Kräutler, B. *J. Mol. Cat. A (Chemical)* **1997**, *116*, 147–155.
107. Fieber, W.; Hoffmann, B.; Schmidt, W.; Stupperich, E.; Konrat, R.; Kräutler, B. *Helv. Chim. Acta* **2002**, *85*, 927–944.
108. Kontaxis, G.; Riether, D.; Hannak, R.; Tollinger, M.; Kräutler, B. *Helv. Chim. Acta* **1999**, *82*, 848–869.
109. Fieber, W.; Konrat, R.; Kräutler, B., manuscript in preparation.
110. Gianotti, C. In *B<sub>12</sub>. Dolphin, D.*, Ed.; John Wiley & Sons: New York, Chichester, Vol. I, **1982**, pp. 393–430.
111. Pilbrow, J. R. In *B<sub>12</sub>. Dolphin, D.*, Ed.; John Wiley & Sons: New York, Chichester, Vol. I, **1982**, pp. 431–462.
112. Gerfen, G. J. In *Chemistry and Biochemistry of B<sub>12</sub>*. Banerjee R., Ed.; John Wiley & Sons: New York, Chichester, **1999**, pp. 165–195.
113. Watson, J. T. In *Biological Mass Spectrometry*. Matsuo, T.; Caprioli, R. M.; Gross, M. L.; Seyama, Y., Eds.; John Wiley & Sons: New York, Chichester, **1994**, pp. 23–40.
114. Smith, R. D.; Light-Wahl, K. J.; Winger, B. E.; Goodlett, D. R. In *Biological Mass Spectrometry*. Matsuo, T.; Caprioli, R. M.; Gross, M. L.; Seyama, Y., Eds.; John Wiley & Sons: New York, Chichester, **1994**, pp. 41–74.
115. Hirota, S.; Marzilli, L. G. In *Chemistry and Biochemistry of B<sub>12</sub>*. Banerjee, R., Ed.; John Wiley & Sons: New York, Chichester, **1999**, pp. 239–260.
116. Lexa, D.; Savéant, J. M. *Acc. Chem. Res.* **1983**, *16*, 235–243.
117. Kräutler, B. In *Chemistry and Biochemistry of B<sub>12</sub>*. Banerjee R., Ed.; John Wiley & Sons: New York, Chichester, **1999**, pp. 315–339.
118. Kräutler, B. In *Organic Reactivity: Physical and Biological Aspects*. Golding, B. T.; Griffin, R. J.; Maskill, H., Eds.; Royal Soc. Chem.: London, **1995**, pp. 209–222.
119. Scheffold, R.; Abrecht, S.; Orłinski, R.; Ruf, H.-R.; Stamouli, P.; Tinembart, O.; Waldner, L.; Weymuth, C. *Pure & Appl. Chem.* **1987**, *59*, 363–372.
120. Murakami, Y.; Hisaeda, Y. *Pure & Appl. Chem.* **1988**, *60*, 1363–1368.
121. Ragsdale, S. W. *Crit. Rev. Biochem. Mol. Biol.* **1991**, *26*, 261–300.
122. Steiger, B.; Ruhe, A.; Walder, L. *Anal. Chem.* **1990**, *62*, 759–766.
123. Lexa, D.; Savéant, J. M.; Zickler, J. *J. Am. Chem. Soc.* **1977**, *99*, 2786–2790.
124. Schrauzer, G. N.; Deutsch, E.; Windgassen, R. *J. Am. Chem. Soc.* **1968**, *90*, 2441–2442.
125. Chemaly, S. M.; Pratt, J. M. *J. Chem. Soc. Dalton Trans.* **1984**, 595–599.
126. Endicott, J. F.; Netzel, T. L. *J. Am. Chem. Soc.* **1979**, *101*, 4000–4002.
127. Lexa, D.; Savéant, J. M. *J. Am. Chem. Soc.* **1976**, *98*, 2652–2658.
128. Lexa, D.; Savéant, J. M. *J. Am. Chem. Soc.* **1978**, *100*, 3220–3222.
129. de Tacconi, N. R.; Lexa, D.; Savéant, J. M. *J. Am. Chem. Soc.* **1979**, *101*, 469–473.
130. Savéant, J. M.; de Tacconi, N.; Lexa, D.; Zickler, J. In *Vitamin B<sub>12</sub>. Zagalak, B.; Friedrich, W.*, Eds.; Walter de Gruyter: Germany, **1979**, pp. 203–212.
131. Lexa, D.; Savéant, J. M.; Soufflet, J. P. In *Vitamin B<sub>12</sub>. Zagalak, B.; Friedrich, W.*, Eds.; Walter de Gruyter: Germany, **1979**, pp. 213–216.

132. Lexa, D.; Savéant, J. M.; Zickler, J. *J. Am. Chem. Soc.* **1980**, *102*, 2654–2663.
133. Lexa, D.; Savéant, J. M.; Zickler, J. *J. Am. Chem. Soc.* **1980**, *102*, 4851–4852.
134. Amatore, C.; Lexa, D.; Savéant, J. M. *J. Electroanal. Chem.* **1980**, *111*, 81–89.
135. Faure, D.; Lexa, D.; Savéant, J. M. *J. Electroanal. Chem.* **1982**, *140*, 269–284.
136. Faure, D.; Lexa, D.; Savéant, J. M. *J. Electroanal. Chem.* **1982**, *140*, 285–295.
137. Faure, D.; Lexa, D.; Savéant, J. M. *J. Electroanal. Chem.* **1982**, *140*, 297–309.
138. Hogenkamp, H. P. C.; Holmes, S. *Biochemistry* **1970**, *9*, 1886–1892.
139. Swetik, P.-G.; Brown, D. G. *J. Electroanal. Chem.* **1974**, *54*, 433–439.
140. Bard, A. J.; Faulkner, L. R. *Electrochemical Methods*; John Wiley & Sons: New York, **1980**.
141. Pratt, J. In *Chemistry and Biochemistry of B<sub>12</sub>*. Banerjee R., Ed.; John Wiley & Sons: New York, Chichester, **1999**, pp. 113–164.
142. Lexa, D.; Savéant, J. M. *J. Chem. Soc., Chem. Commun.* **1975**, 872–874.
143. Rubinson, K. A.; Itabashi, E.; Mark, H. B., Jr. *Inorg. Chem.* **1982**, *21*, 3571–3573.
144. Rubinson, K. A.; Parekh, H. V.; Itabashi, E.; Mark, H. B., Jr. *Inorg. Chem.* **1983**, *22*, 458–463.
145. Zhiu, D.-L.; Tinembart, O.; Scheffold, R.; Walder, L. *Helv. Chim. Acta* **1990**, *73*, 2225–2241.
146. Tinembart, O.; Walder, L.; Scheffold, R. *Ber. Bunsenges. Phys. Chem.* **1988**, *92*, 1225–1231.
147. Martin, B. D.; Finke, R. G. *J. Am. Chem. Soc.* **1992**, *114*, 585–592.
148. Waddington, M. D.; Finke, R. G. *J. Am. Chem. Soc.* **1993**, *115*, 4629–4640.
149. Hannak, R. B.; Färber, G.; Konrat, R.; Kräutler, B. *J. Am. Chem. Soc.* **1997**, *119*, 2313–2314.
150. Hannak, R.; Kräutler, B., unpublished results.
151. Lexa, D.; Savéant, J. M.; Soufflet, J. P. *J. Electroanal. Chem.* **1979**, *100*, 159–172.
152. Scheffold, R.; Rytz, G.; Walder, L. In *Modern Synthetic Methods. Transition Metals in Organic Synthesis*. Scheffold, R., Ed.; Salle & Sauerländer: Frankfurt/Main, **1983**, pp. 335–440.
153. Scheffold, R.; Rytz, G.; Walder, L.; Orlinski, R.; Chilmonczyk, Z. *Pure & Appl. Chem.* **1983**, *55*, 1791–1797.
154. Rusling, J. F.; Miaw, C.-L.; Couture, E. C. *Inorg. Chem.* **1990**, *29*, 2025–2027.
155. Scheffold, R. *Nachr. Chem. Tech. Lab.* **1988**, *36*, 261–267.
156. Auer, L.; Weymuth, C.; Scheffold, R. *Helv. Chim. Acta* **1993**, *76*, 810–818.
157. Busato, S.; Tinembart, O.; Zhang, Z.-D.; Scheffold, R. *Tetrahedron* **1990**, *46*, 3155–3166.
158. Busato, S.; Scheffold, R. *Helv. Chim. Acta* **1994**, *77*, 92–99.
159. Hisaeda, Y.; Nishioka, T.; Inoue, Y.; Asada, K.; Hayashi, T. *Coord. Chem. Rev.* **2000**, *198*, 21–37.
160. Steiger, B.; Walder, L.; Scheffold, R. *Chimia* **1986**, *40*, 93–97.
161. Bonnett, R. In *B<sub>12</sub>*. Dolphin, D., Ed.; John Wiley & Sons: New York, Chichester, **1982**, Vol. I, pp. 201–244.
162. Brown, K. L. In *B<sub>12</sub>*. Dolphin, D.; Ed.; John Wiley & Sons: New York, Chichester, **1982**, Vol. I, pp. 245–294.
163. Hogenkamp, H. P. C. In *B<sub>12</sub>*. Dolphin, D., Ed.; John Wiley & Sons: New York, Chichester, **1982**, Vol. I, pp. 295–324.
164. Halpern, J. In *B<sub>12</sub>*. Dolphin, D., Ed.; John Wiley & Sons: New York, Chichester, 1982, Vol. I, pp. 501–542.
165. Golding, B. T. In *B<sub>12</sub>*. Dolphin, D., Ed.; John Wiley & Sons: New York, Chichester, 1982, Vol. I, pp. 543–582.
166. Rétey, J. In *B<sub>12</sub>*. Dolphin, D., Ed.; John Wiley & Sons: New York, Chichester, 1982, Vol. II, pp. 357–380.
167. Rétey, J. In *Vitamin B<sub>12</sub> and B<sub>12</sub>-Proteins*. Kräutler, B.; Arigoni, D.; Golding, B. T., Ed.; Wiley-VCH: Weinheim, Germany, **1998**, pp. 273–288.
168. Hay, B. P.; Finke, R. G. *J. Am. Chem. Soc.* **1986**, *108*, 4820–4829.
169. Finke, R. G. In *Vitamin B<sub>12</sub> and B<sub>12</sub>-Proteins*. Kräutler, B.; Arigoni, D.; Golding, B. T., Ed.; Wiley-VCH: Weinheim, Germany, **1998**, pp. 383–402.
170. Matthews, R. In *Chemistry and Biochemistry of B<sub>12</sub>*. Banerjee, R., Ed.; John Wiley & Sons: New York, Chichester, **1999**, pp. 681–706.
171. Sauer, K.; Thauer, R. K. In *Chemistry and Biochemistry of B<sub>12</sub>*. Banerjee, R. Ed.; John Wiley & Sons: New York, Chichester, **1999**, pp. 655–679.
172. Harms, U.; Thauer, R. K. In *Vitamin B<sub>12</sub> and B<sub>12</sub>-Proteins*. Kräutler, B.; Arigoni, D.; Golding, B. T., Ed.; Wiley-VCH: Weinheim, Germany, **1998**, pp. 157–165.
173. Brown, K. L.; Zhou, L.; Zhao, D.; Cheng, S.; Zou, X. In *Vitamin B<sub>12</sub> and B<sub>12</sub>-Proteins*. Kräutler, B.; Arigoni, D.; Golding, B. T., Ed.; Wiley-VCH: Weinheim, Germany, **1998**, pp. 417–432.
174. Chemaly, S. M.; Pratt, J. M. *J. Chem. Soc., Dalton Trans.* **1980**, 2259–2266.
175. Natarajan, E.; Grissom, C. B. In *Vitamin B<sub>12</sub> and B<sub>12</sub>-Proteins*. Kräutler, B.; Arigoni, D.; Golding, B. T., Ed.; Wiley-VCH: Weinheim, Germany, **1998**, pp. 403–416.
176. Grissom, C. B. In *Chemistry and Biochemistry of B<sub>12</sub>*. Banerjee, R., Ed.; John Wiley & Sons: New York, Chichester, **1999**, pp. 261–269.
177. Schrauzer, G. N.; Deutsch, E. *J. Am. Chem. Soc.* **1969**, *91*, 3341–3350.
178. Kräutler, B. In *The Biological Alkylation of Heavy Elements*. Craig, P. J.; Glockling, F., Ed.; Roy. Soc. Chem.: London, **1988**, pp. 31–45.
179. Pailles, W. H.; Hogenkamp, H. P. C. *Biochemistry* **1968**, *7*, 4160–4166.
180. Milton, P.; Brown, T. L. *J. Am. Chem. Soc.* **1977**, *99*, 1390–1396.
181. Pratt, J. M. In *Chemistry and Biochemistry of B<sub>12</sub>*. Banerjee, R., Ed.; John Wiley & Sons: New York, Chichester, **1999**, pp. 73–112.
182. Breslow, R.; Khanna, P. L. *J. Am. Chem. Soc.* **1976**, *98*, 1297–1299.
183. Hogenkamp, H. P. C.; Bratt, G. T.; Sun, S. *Biochemistry*, **1985**, *24*, 6428–6432.
184. Drennan, C. L.; Matthews, R. G.; Ludwig, M. L. *Curr. Opin. Struct. Biol.* **1994**, *4*, 919–929.
185. Fanchiang, Y. T.; Bratt, G. T.; Hogenkamp, H. P. C. *Proc. Natl. Acad. Sci USA*, **1984**, *81*, 2698–2702.
186. Jensen M.P.; Halpern, J. *J. Am. Chem. Soc.* **1999**, *121*, 2181–2192.
187. Mosimann, H.; Kräutler, B. *Angew. Chem. Int. Ed. Engl.* **2000**, *39*, 393–395.
188. Galliker, P.; Gräther, O.; Rümmler, M.; Fitz, W.; Arigoni, D. In *Vitamin B<sub>12</sub> and B<sub>12</sub>-Proteins*. Kräutler, B.; Arigoni, D.; Golding, B. T., Ed.; Wiley-VCH: Weinheim, Germany, 1998, pp. 447–458.
189. Blaser, H.; Halpern, J. *J. Am. Chem. Soc.* **1980**, *102*, 1684–1689.
190. Walker, L. A. II; Jarrett, J. T.; Anderson, N. A.; Pullen, S. H.; Matthews, R. G.; Sension, R. J. *J. Am. Chem. Soc.* **1998**, *120*, 3597–3603.
191. Cole, A. G.; Yoder, L. M.; Shiang, J. J.; Anderson, N. A.; Walker, L. A. II; Banaszak Holl, M. M.; Sension, R. J. *J. Am. Chem. Soc.* **2002**, *124*, 434–441.
192. Stupperich, E.; Konle, R.; Lehle, M. In *Vitamin B<sub>12</sub> and B<sub>12</sub>-Proteins*. Kräutler, B.; Arigoni, D.; Golding, B. T., Ed.; Wiley-VCH: Weinheim, Germany, **1998**, pp. 179–187.

193. Limbach, P. A.; Crain, P. F.; McCloskey, J. A. *Nucleic Acids Res.* **1994**, *22*, 2183–2196.
194. Renz, P. In *Chemistry and Biochemistry of B<sub>12</sub>*. Banerjee, R., Ed.; John Wiley & Sons: New York, Chichester, **1999**, pp. 557–576.
195. Escalante Semerena, J. C. In *Chemistry and Biochemistry of B<sub>12</sub>*. Banerjee, R., Ed.; John Wiley & Sons: New York, Chichester, **1999**, pp. 577–594.
196. Stupperich, E.; Nexø, E. *Eur. J. Biochem.* **1991**, *199*, 299–303.
197. Poppe, L.; Hull, W. E.; Nitsche, R.; Graf, T.; Stupperich, E.; Rétey, J. *Helv. Chim. Acta* **1999**, *82*, 1250–1265.
198. Ragsdale, S. W.; Kumar, M.; Zhao, S.; Menon, S.; Seravalli, J.; Doukov, T. In *Vitamin B<sub>12</sub> and B<sub>12</sub>-Proteins*. Kräutler, B.; Arigoni, D.; Golding, B. T., Ed.; Wiley-VCH: Weinheim, Germany, **1998**, pp. 167–178.
199. Ragsdale, S. W.; Kumar, M. *Chem. Rev.* **1996**, *96*, 2515–2539.
200. Ferry, J. G. *Annu. Rev. Microbiol.* **1995**, *49*, 305–333.
201. Doukov, T.; Seravalli, J.; Stezowski, J. J.; Ragsdale, S. W. *Structure* **2000**, *8*, 817–830.
202. Zydowsky, T. M.; Courtney, L. F.; Frasca, V.; Kobayashi, K.; Shimizu, H.; Yuen, L. D.; Matthews, R. G.; Benkovic, S. J.; Floss, H. G. *J. Am. Chem. Soc.* **1986**, *108*, 3152–3153.
203. Matthews, R. G. *Acc. Chem. Res.* **2001**, *34*, 681–689.
204. Zydowsky, L. D.; Zydowsky, T. M.; Haas, E. S.; Brown, J. W.; Reeve, J. N.; Floss, H. G. *J. Am. Chem. Soc.* **1987**, *109*, 7922–7923.
205. Lebertz, H.; Simon, H.; Courtney, L. F.; Benkovic, S. J.; Zydowsky, L. D.; Lee, K.; Floss, H. G. *J. Am. Chem. Soc.* **1987**, *109*, 3173–3174.
206. Ludwig, M. L.; Evans, P. R. In *Chemistry and Biochemistry of B<sub>12</sub>*. Banerjee, R., Ed.; John Wiley & Sons: New York, Chichester, **1999**, pp. 595–632.
207. Bandarian, V.; Patridge, K. A.; Lennon, B. W.; Huddler, D. P.; Matthews, R. G.; Ludwig, M. L. *Nature Struct. Biol.* **2002**, *9*, 53–56.
208. Goulding, C. W.; Postigo, D.; Matthews, R. G. *Biochemistry*, **1997**, *36*, 8082–8091.
209. Kräutler, B.; Kratky, C. *Angew. Chem. Int. Ed. Engl.* **1996**, *35*, 167–170.
210. Marsh, E. N. G.; Holloway, D. E. *FEBS Lett.* **1992**, *310*, 167–170.
211. Gruber, K.; Kratky, C. In *Handbook of Metalloproteins*. Messerschmidt, A.; Huber, R.; Poulos T.; Wieghardt, K. Eds.; John Wiley & Sons: Chichester, **2001**, pp. 1010–1022.
212. Jarrett, J. T.; Amatarunga, M.; Drennan, C. L.; Scholten, J. D.; Sands, R. H.; Ludwig, M. L.; Matthews, R. G. *Biochemistry* **1996**, *35*, 2464–2475.
213. Stupperich, E.; Eisinger, H.-J.; Albracht, S. P. J. *Eur. J. Biochem.* **1990**, *193*, 105–109.
214. Kräutler, B. In *Carbon Dioxide Fixation and Reduction in Biological and Model Systems*. Brändén, C.-I.; Schneider, G., Ed.; Proceedings of the Royal Swedish Academy of Sciences Noble Symposium 1991, Oxford University Press **1994**, pp. 83–92.
215. Marsh, E. N. G.; Drennan, C. L. *Curr. Opin. Chem. Biol.* **2001**, *5*, 499–505.
216. Banerjee, R.; Chowdhury, S. In *Chemistry and Biochemistry of B<sub>12</sub>*. Banerjee, R., Ed.; John Wiley & Sons: New York, Chichester, **1999**, pp. 707–730.
217. Buckel, W.; Bröker, G.; Bothe, H.; Pierik, A. J.; Golding, B. T. In *Chemistry and Biochemistry of B<sub>12</sub>*. Banerjee, R., Ed.; John Wiley & Sons: New York, Chichester, **1999**, pp. 757–782.
218. Kratky, C.; Gruber, K. *Curr. Opin. Chem. Biol.*, in press.
219. Zerbe-Burckhardt, K.; Ratnatilleke, A.; Vrijbloed, J. W.; Robinson, J. A. In *Chemistry and Biochemistry of B<sub>12</sub>*. Banerjee, R., Ed.; John Wiley & Sons: New York, Chichester, **1999**, pp. 859–870.
220. Toraya, T. In *Chemistry and Biochemistry of B<sub>12</sub>*. Banerjee, R., Ed.; John Wiley & Sons: New York, Chichester, **1999**, pp. 783–810.
221. Bandarian, V.; Reed, G. H. In *Chemistry and Biochemistry of B<sub>12</sub>*. Banerjee, R., Ed.; John Wiley & Sons: New York, Chichester, **1999**, pp. 811–834.
222. Frey, P. A.; Chang, C. H. In *Chemistry and Biochemistry of B<sub>12</sub>*. Banerjee, R., Ed.; John Wiley & Sons: New York, Chichester, **1999**, pp. 835–858.
223. Baker J. J.; Stadtman, T. C. In *B<sub>12</sub>*. Dolphin, D., Ed.; John Wiley & Sons: New York, Chichester, **1982**, Vol. II, pp. 203–232.
224. Stubbe, J.; Licht, S.; Gerfen, G.; Silva, D.; Booker, S. In *Vitamin B<sub>12</sub> and B<sub>12</sub>-Proteins*. Kräutler, B.; Arigoni, D.; Golding, B. T., Ed.; Wiley-VCH: Weinheim, Germany, **1998**, pp. 321–332.
225. Reatey, J. In *Chemistry and Biochemistry of B<sub>12</sub>*. Banerjee, R., Ed.; John Wiley & Sons: New York, Chichester, **1999**, pp. 271–288.
226. Reatey, J., *Angew. Chem. Int. Ed. Engl.* **1990**, *29*, 355–352.
227. Wagner, A. F. V.; Frey, M.; Neugebauer, F. A.; Schäfer, W.; Knappe, J. *Proc. Natl. Acad. Sci. USA* **1992**, *89*, 996–1000.
228. Dowd, P.; Wilk, B.; Wilk, B. K. *J. Am. Chem. Soc.* **1992**, *114*, 7949–7951.
229. Chowdhury, S.; Banerjee, R. *J. Am. Chem. Soc.* **2000**, *122*, 5417–5418.
230. Chowdhury, S.; Banerjee, R. *Biochemistry* **2000**, *39*, 7998–8006.
231. Golding, B. T.; Anderson, R. J.; Ashwell, S.; Edwards, C. H.; Garnett, I.; Kroll, F.; Buckel, W. In *Vitamin B<sub>12</sub> and B<sub>12</sub>-Proteins*. Kräutler, B.; Arigoni, D.; Golding, B. T., Ed.; Wiley-VCH: Weinheim, Germany, **1998**, pp. 201–216.
232. Wollowitz, S.; Halpern, J. *J. Am. Chem. Soc.* **1988**, *110*, 3112–3120.
233. Bothe, H.; Bröker, G.; Müller, U.; Schall, I.; Textor, S.; Golding, B. T.; Buckel, W. In *Vitamin B<sub>12</sub> and B<sub>12</sub>-Proteins*. Kräutler, B.; Arigoni, D.; Golding, B. T., Ed.; Wiley-VCH: Weinheim, Germany, **1998**, pp. 237–251.
234. Beatrix, B.; Zelder, O.; Linder, D.; Buckel, W. *Eur. J. Biochem.* **1994**, *221*, 101–109.
235. Thomä, N. H.; Meier, T. W.; Leadley, P. F. In *Vitamin B<sub>12</sub> and B<sub>12</sub>-Proteins*. Kräutler, B.; Arigoni, D.; Golding, B. T., Ed.; Wiley-VCH: Weinheim, Germany, **1998**, pp. 227–236.
236. Smith, D. M.; Golding, B. T.; Radom, L. *J. Am. Chem. Soc.* **1999**, *121*, 9388–9399.
237. Thomä, N. H.; Evans, P. R.; Leadley, P. F. *Biochemistry* **2000**, *39*, 9213–9221.
238. Gruber, K.; Kratky, C. *Handbook of Metalloproteins*; Messerschmidt, A.; Huber, R.; Poulos, T.; Wieghardt, K. Eds.; John Wiley & Sons: Chichester, **2001**, pp. 995–1009.
239. Mancia, F.; Evans, P. R. *Structure* **1998**, *6*, 711–720.
240. Mancia, F.; Smith, G. A.; Evans, P. R. *Biochemistry*, **1999**, *38*, 7999–8005.
241. Champloy, F.; Jogl, G.; Reitzer, R.; Buckel, W.; Bothe, H.; Michalowicz, A.; Meyer-Klaucke, W.; Kratky, C. *J. Am. Chem. Soc.* **1999**, *121*, 11780–11789.
242. Barker, H. A.; Rooze, V.; Suzuki, F.; Iodice, A. A. *J. Biol. Chem.* **1964**, *239*, 3260–3266.
243. Buckel, W.; Golding, B. T. *Chem. Soc. Rev. (London)* **1996**, *25*, 329–338.
244. Holloway, D. E.; Marsh, E. N. G. *J. Biol. Chem.* **1994**, *269*, 20425–20430.
245. Marsh, E. N. G. *Bioorg. Chem.* **2000**, *28*, 176–189.
246. Zelder, O.; Beatrix, B.; Leutbecher, U.; Buckel, W. *Eur. J. Biochem.* **1994**, *226*, 577–585.
247. Barker, H. A.; Weissbach, H.; Smyth, R. D. *Proc. Natl. Acad. Sci. USA* **1958**, *44*, 1093–1097.
248. Marsh, E. N. G.; Ballou, D. P. *Biochemistry*, **1998**, *37*, 11864–11872.

249. Chih, H.-W.; Marsh, E. N. G. *J. Am. Chem. Soc.* **2000**, *122*, 10732–10733.
250. Wetmore, S. D.; Smith, D. M.; Golding, B. T.; Radom, L. *J. Am. Chem. Soc.* **2001**, *123*, 7963–7972.
251. Kratky, C.; Gruber, K. In *Handbook of Metalloproteins*. Messerschmidt, A.; Huber, R.; Poulos, T.; Wieghart, K. Eds.; John Wiley & Sons: Chichester, **2001**, pp. 983–994.
252. Gruber, K.; Reitzer, R.; Kratky, C. *Angew. Chem. Int. Ed. Engl.* **2001**, *40*, 3377–3380.
253. Tollinger, M.; Konrat, R.; Hilbert, B. H.; Marsh, E. N. G.; Kräutler, B. *Structure* **1998**, *6*, 1021–1033.
254. Hoffmann, B.; Tollinger, M.; Konrat, R.; Huhta, M.; Marsh, E. N. G.; Kräutler, B. *Chem. Bio. Chem.* **2001**, *2*, 643–655.
255. Hoffmann, B.; Konrat, R.; Bothe, H.; Buckel, W.; Kräutler, B. *Eur. J. Biochem.* **1999**, *263*, 178–188.
256. Tollinger, M.; Eichmüller, C.; Konrat, R.; Huhta, M. S.; Marsh, E. N. G.; Kräutler, B. *J. Mol. Biol.* **2001**, *309*, 777–791.
257. Huhta, M. S.; Chen, H.-P.; Hemann, C.; Hille, C. R.; Marsh, E. N. G. *Biochem. J.* **2001**, *355*, 131–137.
258. Zerbe-Burckhardt, K.; Ratnatilleke, A.; Philippon, N.; Birch, A.; Leiser, A.; Vrijbloed, J. W.; Hess, D.; Hunziker, P.; Robinson, J. A. *J. Biol. Chem.* **1998**, *273*, 6508–6517.
259. Moore, B. S.; Eisenberg, R.; Weber, C.; Bridges, A.; Nanz, D.; Robinson, J. A. *J. Am. Chem. Soc.* **1995**, *117*, 11285–11291.
260. Toraya, T.; Fukui, S. In *B<sub>12</sub>*. Dolphin, D., Ed.; John Wiley & Sons: New York, Chichester, **1982**, Vol. II, pp. 233–262.
261. Toraya, T. *Cell. Mol. Life Sci.* **2000**, *57*, 106–127.
262. Toraya T. In *Vitamin B<sub>12</sub> and B<sub>12</sub>-Proteins*. Kräutler, B.; Arigoni, D.; Golding, B. T., Ed.; Wiley-VCH: Weinheim, Germany, **1998**, pp. 303–320.
263. Abend, A.; Nitsche, R.; Bandarian, V.; Stupperich, E.; Rétey, J. *Angew. Chem. Int. Ed. Engl.* **1998**, *37*, 625–627.
264. Yamashita, M.; Yamada, S.; Muguruma, H.; Murakami, Y.; Tobimatsu, T.; Ishida, A.; Toraya, T. *Biochemistry* **1998**, *37*, 4799–4803.
265. Toraya, T.; Yoshizawa, K.; Eda, M.; Yamabe, T. *J. Biochem.* **1999**, *126*, 650–654.
266. Abeles, R. In *Vitamin B<sub>12</sub>*. (Proceedings of the 3rd European Symposium on Vitamin B<sub>12</sub> and Intrinsic Factor); Zagalak, B.; Friedrich, W., Ed.; Walter de Gruyter: Berlin, New York, **1979**, p. 373–388.
267. Smith, D. M.; Golding, B. T.; Radom, L. *J. Am. Chem. Soc.* **2001**, *123*, 1664–1675.
268. Rétey, J.; Umani-Rouchi, A.; Seibl, J.; Arigoni, D. *Experientia* **1966**, *22*, 502–503.
269. Finke, R. G. In *Molecular Mechanisms in Bioorganic Processes*. Bleasdale, C.; Golding, B. T., Ed.; Roy. Soc. Chem.: London, **1990**, pp. 244–280.
270. Masuda, J.; Shibata, N.; Morimoto, Y.; Toraya, T.; Yasuoka, N. *Structure*, **2000**, *8*, 775–788.
271. Babior, B. M. In *B<sub>12</sub>*. Dolphin, D., Ed.; John Wiley & Sons: New York, Chichester, **1982**, Vol. II, pp. 263–288.
272. Faust, L. P.; Babior, B. M. *Arch. Biochem. Biophys.*, **1992**, *294*, 50–54.
273. Warncke, K.; Schmidt, J. C.; Ke, S.-C. *J. Am. Chem. Soc.* **1999**, *121*, 10522–10528.
274. Blakley, R.L. In *B<sub>12</sub>*. Dolphin, D. Ed.; John Wiley & Sons: New York, Chichester, **1982**, Vol. II, pp. 381–418.
275. Stubbe, J., van der Donk, W. A. *Chem. Rev.* **1998**, *98*, 705–762.
276. Stubbe, J. *Curr. Opin. Struct. Biol.* **2000**, *10*, 1373–1377.
277. Lawrence, C. C.; Gerfen, G. J.; Samano, V.; Nitsche R.; Robins, M. J.; Rétey, J.; Stubbe, J. *J. Biol. Chem.* **1999**, *274*, 7039–7042.
278. Licht, S. S.; Lawrence, C. C.; Stubbe, J. *Biochemistry*, **1999**, *38*, 1234–1242.
279. Brown, K. L.; Li, J. *J. Am. Chem. Soc.* **1998**, *120*, 9466–9474.
280. Licht, S. S.; Booker, S.; Stubbe, J. *Biochemistry*, **1999**, *38*, 1221–1233.
281. Sintchak, M. D.; Arjara, G.; Kellogg, B. A.; Stubbe, J.; Drennan, C. D. *Nature Struct. Biol.* **2002**, *9*, 293–300.
282. Gates, B. C. *Catalytic Chemistry*, John Wiley & Sons: New York, **1992**.
283. Griller, D.; Wayner, D. D. M. *Pure & Appl. Chem.* **1989**, *61*, 717–724.
284. Bresciani-Pahor, N.; Forcolin, M.; Marzilli, L. G.; Randaccio, L.; Summers, M. F.; Toscano, P. J. *Coord. Chem. Rev.* **1985**, *63*, 1–125.
285. Hannak, R.; Ostermann, S.; Gruber, K.; Kratky, C.; Kräutler, B.; unpublished.
286. Glasenapp-Breiling, M.; Montforts, F.-P. *Angew. Chem. Int. Ed. Engl.* **2000**, *39*, 721–723.
287. Ensley, B. D. *Ann. Rev. Microbiol.* **1991**, *45*, 283–299.
288. Schumacher, W.; Holliger, C. *J. Bacteriol.* **1996**, *178*, 2328–2333.
289. Neumann, A.; Wohlfahrt, G.; Diekert, G. *J. Biol. Chem.* **1996**, *271*, 16515–16519.
290. Maymó-Gatell, X.; Chien, Y.-T.; Gossett, J. M.; Zinder, S. H. *Science* **1997**, *276*, 1568–1571.
291. Wohlfarth, G.; Diekert, G. In *Chemistry and Biochemistry of B<sub>12</sub>*. Banerjee, R., Ed.; John Wiley & Sons: New York, Chichester, **1999**, pp. 871–893.
292. Neumann, A.; Siebert, A.; Trescher, T.; Reinhard, S.; Wohlfarth, G.; Diekert, G. *Arch. Microbiol.* **2002**, *163*, 420–426.
293. Kräutler, B.; Fieber, W.; Ostermann, S.; Ongania, K.-H.; Siebert, A.; Diekert, G.; publication in preparation.
294. Shey, J.; van der Donk, W. A. *J. Am. Chem. Soc.* **2000**, *122*, 12403–12404.
295. Gough, S. P.; Petersen, B. O.; Duus, J. O. *Proc. Natl. Acad. Sci. USA* **2000**, *97*, 6908–6913.
296. Frey, P. A.; Reed, G. H.; Ballinger, M. D.; Lieder, K. W.; Wu, W.; Chang, C. H.; Bandarian, V.; Ruzicka, F. J.; LoBrutto, R.; Beinert, H. In *Vitamin B<sub>12</sub> and B<sub>12</sub>-Proteins*. Kräutler, B.; Arigoni, D.; Golding, B. T., Ed.; Wiley-VCH: Weinheim, Germany, **1998**, pp. 435–446.
297. Magnusson, O. T.; Reed, G. H.; Frey, P. A. *Biochemistry*, **2001**, *40*, 7773–7782.
298. Sofia, H. J.; Chen, G.; Hetzler, B. G.; Reyes-Spindola, J. F.; Miller, N. E. *Nucleic Acids Res.* **2001**, *29*, 1097–1106.
299. Leete, E. *Planta Med.* **1990**, *56*, 339–352.
300. Baldet, P.; Alban, C.; Douce, R. *FEBS Lett.* **1997**, *419*, 206–210.
301. Ollagnier, S.; Kervio, E.; Rétey, J. *FEBS Lett.* **1998**, *437*, 309–312.
302. Lindenbaum, J.; Rosenberg, I. H.; Wilson, P. W.; Stabler, S. P.; Allen, R. H. *Am. J. Clin. Nutr.* **1994**, *60*, 2–11.
303. Stabler, S. P. In *Chemistry and Biochemistry of B<sub>12</sub>*. Banerjee, R., Ed.; John Wiley & Sons: New York, Chichester, **1999**, pp. 343–365.
304. Lau, K. S. *Pathology* **1981**, *13*, 189–195.
305. Alpers, D. H.; Russel-Jones, G. J. In *Chemistry and Biochemistry of B<sub>12</sub>*. Banerjee, R., Ed.; John Wiley & Sons: New York, Chichester, **1999**, pp. 411–440.
306. Rosenblatt, D. S.; Fenton, W. A. In *Chemistry and Biochemistry of B<sub>12</sub>*. Banerjee, R., Ed.; John Wiley & Sons: New York, Chichester, **1999**, pp. 367–384.
307. Moestrup, S. K. In *Vitamin B<sub>12</sub> and B<sub>12</sub>-Proteins*. Kräutler, B.; Arigoni, D.; Golding, B. T., Ed.; Wiley-VCH: Weinheim, Germany, **1998**, pp. 477–489.
308. Verroust, P.; Christensen, E. I.; Moestrup, S. K.; Hammond, T. G.; Seetharam, B. In *Vitamin B<sub>12</sub> and B<sub>12</sub>-Proteins*. Kräutler, B.; Arigoni, D.; Golding, B. T., Ed.; Wiley-VCH: Weinheim, Germany, **1998**, pp. 491–504.
309. Moestrup, S. K.; Verroust, P. J. In *Chemistry and Biochemistry of B<sub>12</sub>*. Banerjee, R., Ed.; John Wiley & Sons: New York, Chichester, **1999**, pp. 475–488.

310. Hogenkamp, H. P. C.; Collins, D. A. In *Vitamin B<sub>12</sub> and B<sub>12</sub>-Proteins*. Kräutler, B.; Arigoni, D.; Golding, B. T., Ed.; Wiley-VCH: Weinheim, Germany, **1998**, pp. 505–514.
311. Hogenkamp, H. P. C.; Collins, D. A.; Grissom, C. B.; West, F. G. In *Chemistry and Biochemistry of B<sub>12</sub>*. Banerjee, R., Ed.; John Wiley & Sons: New York, Chichester, **1999**, pp. 343–365.
312. Chanarian, I. *The Megaloblastic Anemias*, Blackwell Scientific Publications: London, **1990**.
313. Gulati, S.; Baker, P.; Li, Y. N.; Fowler, B.; Kruger, W.; Brody, L. C.; Banerjee, R. *Human Molecular Genetics* **1996**, *5*, 1859–1865 (and references therein).

# Index to Volume 11

Page numbers in italics, e.g. 125, refer to figures. Page numbers in bold, e.g. 111, indicate entries in tables.

- A**  
Absolute configurations 98, 104  
Acetogenesis 251  
Active centers of enzymes 168  
*S*-Adenosyl methionine (SAM) 246, 253, 269  
Adenosyl radicals 269  
Aerobic oxidation 187  
  by metalloporphyrins 193–195  
Alanine 85, 100, 123, 125  
Alkoxy cations 179  
Alkyl–iron complexes 136  
Alkyl–iron(III) porphyrins 142  
Alkyl radicals 246  
*N*-Alkylporphyrins 76, 146  
Allyl amines 151  
Allyl sulfides 151  
 $\alpha$ -helix 56, 57–58  
Amberlite 176  
Amino mutases 255, 256, 264, 265  
2-Aminobutanol 99, 121  
5-Aminolevulinic acid 208  
2-Aminopropanol 99, 121  
Antibodies 110  
Apocytochrome *b562* 109  
Aquacob(III)alamin 230, 242  
Aromatic halide pollutants 172  
Aromatic ring cleavage 189, 196  
Associative mechanisms 226  
Asymmetric cyclopropanation 147, 150
- B**  
 $B_{12}$ -binding motif 261, 264  
 $B_{12}$ -binding proteins 231  
 $B_{12}$ -cofactors, structure of natural corrinoids 250–251, 251  
 $B_{12}$ -dependent enzymes 229, 234, 245–246, 247  
  methyl transferases 251–253  
  methionine synthase 253–254  
  methyl-group transfer 254–255  
  reactivity 249  
 $B_{12}$ -derivatives 252  
 $B_{12}$ -trafficking 270  
Bacterial cytochrome P450 153, 155  
Bacteriochlorin zinc derivatives 148  
Base-off cobalamins 242, 231, 242  
Base-on/base-off equilibrium 239, 246, 250  
Basidiomycetes (white rot fungus) 162, 167–168  
Basket-handled porphyrins 78, 86  
1,3-Benzodioxole 154  
Benzodioxole-derived cytochrome P450 140, 140  
Benzylic radicals 179  
 $\beta$ -sheets 56–58  
BINAP phosphines 104  
Binap-capped porphyrins 82  
Binaphthyl-strapped porphyrins 82  
Binuclear ligand systems 6  
Biocartol 111, **111**  
Biochemical applications of chiral metalloporphyrins 110, 110  
  glycosylated porphyrins 109–110  
  helical porphyrin-containing peptides 108–109  
Biomagnification 183  
Biomimetic catalysts 162  
Biomimetic oxidation of lignin 161–162, 171, 172, 173, 200–201  
  by metalloporphyrins 174–175  
  dimeric model compounds 183–193, 184, 187, 188, 189, 190, 191, 192, 193  
  metalloporphyrin structures 176  
  monomeric model compounds 175–183, 177, 178, 179, 180, 181, 182, 183  
Biopolymers 162  
Biscarbene complexes 143, 144  
  *trans*- forms 145, 145  
Bovine serum albumin (BSA) 86, 103  
Brevetoxin B 107  
Bridled chiroporphyrins 113, 114  
Bromoethanesulfonate 206  
3-Bromopropanesulfonate 214  
2-Butanol 120  
*t*-Butyl hydroperoxide 171
- C**  
Captodative effect 185  
Carbene transfer 149  
Carbenes  
  biscarbene complexes 143, 144  
  *trans*- forms 145, 145  
  bridged 141, 141  
  catalysts for carbene transfer  
  cyclopropanation 148–150  
  insertion 150–151  
  olefination of aldehydes 152  
  sigmatropic rearrangements 151–152  
  cationic derivatives 147  
  electrochemistry of iron complexes 142  
  five-coordinate carbenes 144  
  geometries 146  
  intermediates 155  
  ligands for heme proteins  
  cytochrome P450 152–155  
  myoglobin and hemoglobin 155–156  
  metal–carbene binding 134  
  M–N inserted complexes **135**  
  photocarbenes 155  
  photochemical generation of free carbenes 142  
  structure and bonding  
  metal–carbene formalism 135  
  spectroscopic characterization 135, 136, **136**  
  X-ray methods 134–135, 134, **135**  
  synthesis of metal–carbene bonds in porphyrins 136  
  insertion of metals into *N,N'*-bridged porphyrins 138–139, 139  
  preparation from diazo compounds 137, 137  
  preparation from iodonium ylide 138  
  preparation from isonitrile complexes 137–138, 138  
  preparation from metalloporphyrin dianions 137, 138  
  preparation from polyhalogenated precursors 136–137, 137  
  synthetic metal–carbene porphyrins 139  
  cobalt 146  
  copper 148  
  iron 139–143, 141, 142

- Carbenes (*continued*)  
 synthetic metal-carbene porphyrins (*continued*)  
 manganese 139  
 nickel 148  
 osmium 145  
 rhodium 147–148  
 ruthenium 143–145  
 zinc 148
- Carbido dimeric complexes 140
- Carbon skeleton mutases 255, 258  
 glutamate mutase (GM) 260–261, 260, 266–267  
 isobutyryl-CoA mutase (ICM) 261, 262, 262  
 methylene glutarate mutase (MGM) 261–262  
 methylmalonyl-CoA mutase (MMCM) 258–260, 258, 266–267
- Carbon tetrachloride metabolism 152, 152
- Carbon-carbon bond cleavage 194, 195
- Carbon-carbon bond rearranging enzymes 258
- Catalysts  
 activated 187  
 soluble 176  
 supports for 175
- Catalytic systems 161–162
- Catechol formation 154
- Cellulose 162, 168, 197, 198
- Cellulosic fibers 162
- Chiral NMR shift reagent 121
- Chiral porphyrins  
 enantiocontrol 76  
 asymmetric catalytic oxidation 76–90  
 fortress porphyrins 76  
 strapped metalloporphyrins 78–84  
 synthesis 76  
 chiral aliphatic aldehydes 90  
 chiral aromatic aldehydes 87, 88–89  
 di- and tri-porphyrin arrays 76, 95–96  
 meso-substitution 76, 78, 79–82, 83–84, 85, 86, 87  
 nonclassical examples 91–94  
 terpene-derived D<sub>4</sub>-symmetric metalloporphyrins 78  
 wall porphyrins 76, 90
- Chiroporphyrins  
 bridled 113, 114  
 derivatizing agents 123–124
- Chlorin 148
- Chlorophenols 183, 183
- Chromophores 165
- Circular dichroism (CD) spectroscopy 103, 104, 105
- Clay minerals 198, 200
- Climate change 206
- CO dehydrogenase 208
- Cob(I)alamin 221, 236, 243, 244, 246, 248, 248, 253, 254  
 preparation of coenzyme B<sub>12</sub> 245
- Cob(II)alamin 233, 234, 243, 246, 247, 253, 255, 258, 258, 259  
 structure 234
- Cob(III)amides 250
- Cobalt  
 cobalt-carbene complexes 146  
 Co(II)-corrins 233  
 Co-C bonds 234, 235, 236, 237, 244, 245, 246, 255, 258–259, 260  
 homolytic cleavage 246, 247, 248–249, 255, 257, 264  
 Co-CH<sub>3</sub> bonds 252, 254, 255  
 Co-N bonds 234, 235, 236, 237, 255, 259–260  
 bond length 263  
 Co(II)-N versus Co(III)-N distance 234  
 irreversible binding of amines to Co(III) chiroporphyrins 121, 123  
 oxidation states 241  
 standard potentials 241, 242
- Cobamides 231–233, 232, 239, 253, 254, 255, 260, 261, 263, 266  
 dependent mutases 256  
 kinetic redox properties 244  
 redox properties 241–244  
 thermodynamic redox properties  
 UV-vis spectroscopy 242
- Cobesters 233, 233
- Cobyric acid 233, 240, 250
- Coenzyme (factor) F430 206  
 discovery 207–208  
 structure and biosynthesis 208, 208, 209, 210–212
- Coenzyme (factor) F430 synthetase 206
- Coenzyme B (CoB) 208, 211
- Coenzyme B<sub>12</sub> 230, 234, 237, 241, 258  
 base-off/His-on form 235, 253, 254, 254, 255, 258, 259, 260, 261, 262
- crystallographic studies 231
- dependent enzymes 255–258, 268–269  
 amino mutases 264, 265  
 carbon skeleton mutases 258–262  
 diol dehydratase (DD) 262–263, 263  
 ethanolamine ammonia lyase (EAL) 263–264, 264  
 glycerol dehydratase 262–263, 263  
 ribonucleotide reductase 264–266, 265, 266, 267  
 NMR spectroscopy 238, 239  
 preparation from cob(I)alamin 245, 246, 248–249  
 radical reactions 266–268  
 structure 230, 231–241, 234
- Coenzyme M (CoM) 208, 211
- Cofacial diporphyrins 35–36, 36  
 catalytic properties of  
 monocobaltdiporphyrins 43–44, 43  
 “pull” effect 43  
 electrocatalytic O<sub>2</sub> reduction 40–43, 41, 42  
 molecular structure and physicochemical properties 36–38, 37  
 nonaqueous dioxygen chemistry of group 2 biscobaltdiporphyrins 38–40, 38  
 π-stacking 36
- Condensed units 196
- Conformational effects 239
- Copper  
 (por)Fe(CO)Cu(LN) complexes  
 IR spectroscopy 18  
 NMR spectroscopy 18  
 X-ray studies 18  
 (por)Fe(μ-CN)Cu(LN) complexes  
 IR spectroscopy 15, 16  
 Mossbauer spectroscopy 14–15  
 NMR spectroscopy 15  
 X-ray studies 14, 14  
 (por)Fe(μ-O)Cu(LN) complexes  
 Currie-Weiss behavior 12  
 magnetic properties 12  
 Mossbauer spectroscopy 13  
 NMR spectroscopy 13  
 protonation 13  
 X-ray studies 11–12, 12  
 (por)Fe(μ-O<sub>2</sub>)Cu(LN) complexes  
 NMR spectroscopy 20, 21  
 Raman spectroscopy 21  
 redox titration 20, 23  
 copper-carbene complexes 148  
 heme/copper terminal oxidases 1–5, 3
- Corrin ligands 231, 233, 235, 236, 259  
 acid/base equilibria 242
- Co(I)-corrins 241, 242, 245, 246, 251, 253, 254  
 oxidation 246  
 reactivity 248  
 supernucleophiles 247
- Co(II)-corrins 241, 242, 244, 247  
 oxidation 246
- Co(III)-corrins 241, 243, 244, 245, 247, 249, 251, 253, 254  
 reduction 246  
 standard potentials of redox system 241  
 upwards folding 237
- Corrinoids, structure 250–251, 251
- Currie-Weiss behavior of (por)Fe(μ-O)Cu(LN) complexes 12
- Cyanide, inhibition of CcO analogs 34
- β-Cyclodextrin 85, 106
- Cyclopropanation  
 asymmetric 147, 150  
 intramolecular 150  
 metalloporphyrin catalysts for carbene transfer 148–150  
 olefins 147
- Cyclopropane carboxylate esters 149
- Cyclopropylmethyl radical intermediate 261
- Cyclopropyloxyl radical 259
- Cytochrome b562  
 denaturation by guanidine hydrochloride 64–65  
 redox-coupled folding 64–65, 65  
 structure 66
- Cytochrome bd 2
- Cytochrome c 2, 32, 45



- denaturation by guanidine hydrochloride 63, 63, 64  
redox-coupled folding 63–64  
Ru-modified 53–55, 54  
  driving force dependence of intramolecular transfer 54, 55  
zinc-substituted  
  denaturation by guanidine hydrochloride 68–69  
  ET quenching 68  
  redox-coupled folding 67–70, 70  
Cytochrome *c* oxidase (CcO) 2  
  binuclear model systems 9  
  bovine (BOX) 2–3, 2  
  CN– adduct 14, 15–16  
  EXAFS structure 12  
  heme a<sub>3</sub>/Cu<sub>B</sub> site 3, 4  
  metal sites 3  
  carbon monoxide adducts 17  
  chemical and spectroscopic properties 17–18  
  synthesis 17  
  carboxylate-bridged model systems 8, 16  
  solid state structural studies 17  
  synthesis 16–17  
  CuA cofactor 4, 27  
  Cu-free mutants 5, 18  
  cyanide-bridged model systems 7, 13  
  chemical and electronic properties 14–16, 15  
  solid state structural studies 14  
  synthesis 13–14  
  dioxygen adduct (compound A) 4, 5, 21, 44  
  EPR-silent resting state 10–11  
  “fast” form 16  
  formate-treated 16, 17  
  fully oxidized (compound O) 2–3, 4, 5, 27  
  peroxide bridging 3  
  fully reduced ferryl (compound F) 2, 4, 5, 27, 28  
  heme a cofactor 4, 27, 28  
  mixed valence form (compound P) 4, 5, 26–27, 44  
  O<sub>2</sub> reduction mechanism 4–5, 4  
  oxo- and hydroxo-bridged model systems 6, 11  
  chemical and electronic properties 12  
  solid state structural studies 11  
  synthesis 11  
  *P. denitrificans* (POX) 2–3  
  redox cooperativity 44–45  
  reduced (compound R) 4, 26–27  
  resting state 16  
  “slow” form 16, 17  
  steady state O<sub>2</sub> reduction 26  
  *T. thermophilus* (TOX) 3  
  CN– adduct 14  
  structure 12  
  Cytochrome *c*'  
  nonnative ligand binding 67  
  redox-coupled folding 65–67  
  heterogeneous kinetics 66, 66  
  structure 66  
  four-helix bundles 67  
  Cytochrome P450 152–155, 189, 193  
  bacterial 153, 155  
  carbene complexes 153  
  isozyme 154  
  liver 153  
  microsomal 152, 155, 155  
  oxidation mechanism 195
- D**  
Decolorization of dyes 172  
Delignification strategies 161–162, 171, 197  
Deltamethrin 111  
Demethoxylation 192  
Demethylation 196  
5'-Deoxy-5'-adenosyl radical 246, 255, 258, 258, 260, 262, 262, 263  
5'-Deoxyadenosine 259  
Deoxymyoglobin 155  
Depolymerization 196  
Deuteroporphyrin 10, 19  
Diaboloic acid 268  
Diaquocob(III)inamide 243, 244  
Diazo compounds 137, 137  
Diazoalkanes 143  
Diazoesters 143, 149  
Diazoketones 142  
Dichlorocarbene 152  
  complexes 142  
Diels–Alder reactions 102  
Diffusible redox mediators 173, 199  
Dihalogenated carbenes 139, 142  
1,2-Dihydronaphthalene 82, 118, 118  
Dihydrosirohydrochlorin 208  
Diisopropyl diazomethylphosphonate 151  
1,3-Dimetalla-allene systems 140  
Dimethoxy arene derivatives 181, 182  
Dinorbornabenzene tetraarylporphyrin 84  
Dinorbornabenzene-derived porphyrins 102  
Diol dehydratase (DD) 255, 257, 262–263, 263  
Disproportionation 242  
Distance decay constant 53, 55  
Drug metabolism 156
- E**  
Electron transfer 244, 244, 247  
Electron transfer, semiclassical theory 51–53  
  driving force 52  
  intramolecular transfer 54, 55  
  electron exchange between ferrous and ferric ions 53  
  electron tunneling 53  
  milestones of discovery 52  
  multistep tunneling 59  
  rate/distance dependence 56–57  
  tunneling pathways (TP) in proteins 56  
  tunneling timetables 57–59, 58, 58  
  electronic coupling 55  
  coupling across helices 58  
  distance decay constant 53, 55  
  rate/distance dependence 56–57  
  square potential barrier 55  
  superexchange coupling 55–56  
  tunneling pathways (TP) in proteins 56, 57  
  uniform barrier (UB) 56  
  electronic coupling matrix element 51, 52  
  nonadiabatic electron transfer 52  
  rate constant 52  
  reorganization energy 52  
  reorganization parameter 51  
  tunneling timetables 57  
  heme proteins 57–58, 58, 58, 59  
  water 58–59, 59  
  Electrostatic interactions 190, 192  
  Enantiocontrol by chiral metalloporphyrins 75, 76, 111, 112  
  applications 102, 103  
  biochemical applications 108–111, 110  
  catalysis of asymmetric reactions 102–103  
  chiral assemblies and chiral aggregates 104–106, 105  
  chirality probes 104  
  metal bisporphyrinate double-deckers 104  
  optical properties of chiral conjugates 106–108  
  stirring effects on supramolecular chirogenesis 110–111  
  tweezers 103  
  asymmetric catalytic aziridination 90, 97  
  asymmetric catalytic cyclopropanation 90–94  
  enantiopure carbenoid catalysis 94  
  asymmetric catalytic oxidation 76, 85–87, 97  
  amidation 90  
  epoxidation 76–84, 97  
  hydroxylation 84–85  
  chiral recognition 94–98, 98  
  alcohols 98–99  
  amines 98  
  amino acids 99  
  amino alcohols 99  
  amino esters 101  
  isocyanides 102  
  phosphines 101–102  
  memory systems 102, 102  
  stereochemistry  
  free bases 113–114  
  synthesis 111–113, 112  
  X-ray structure of nickel complex 113  
  Environmentally friendly processes 162  
  Enzymatic oxidation by lignin peroxidase 169  
  Epoxidation 76–78  
  olefins 194  
  other metalloporphyrins 84

- Epoxidation (*continued*)  
 strapped metalloporphyrins 78–84  
 terpene-derived  $D_4$ -symmetric metalloporphyrins 78
- Ethanolamine 263–264, 264
- Ethanolamine ammonia lyase (EAL) 255, 257, 263–264, 264
- 1-(4-Ethoxy-3-methoxyphenyl)propane 180, 181
- Ethyl diazoacetate 147, 151
- Exciton-coupled circular dichroism (CD) 107–108
- Extractive free wood (EFW) 196
- F**
- Factor A 232, 232, 250
- Factor (Coenzyme) F430 206  
 discovery 207–208  
 structure and biosynthesis 208, 208, 209, 210–212
- Fenton chemistry 32, 34, 174, 174, 200
- Ferryl porphyrins 19, 28, 29, 32
- Fluorescence 106, 106
- Formylcarbenes 146
- Fructose 98
- G**
- Galactose 98
- Gel permeation analysis 195
- Genetic studies 171
- Global warming 206
- Glucose 98
- (*S*)-Glutamate 260, 260
- Glutamate mutase (GM) 255, 256, 258, 260–261, 260, 266–267
- Glutamic acid 109, 123, 124, 126
- Glycerol 262
- Glycerol dehydratase 255, 257, 262–263, 263
- Glycosylated porphyrins 109–110
- Greenhouse gases 206
- Guanidine hydrochloride  
 denaturation of cytochrome *b562* 64–65  
 denaturation of cytochrome *c* 63, 63, 64  
 denaturation of Zn-cytochrome *c* 68–69
- H**
- Halogenated hydrocarbons 153
- Halomethyl-cobalt(III) porphyrins 146
- Halothane 153, 156
- Haptocorrin (HC) 269
- Heme 51
- Heme oxygenase 32
- Heme proteins  
 carbene ligands  
 cytochrome P450 152–155  
 myoglobin and hemoglobin 155–156  
 electron tunneling across  
 protein–protein interfaces 59–62, 60, 61  
 interprotein interactions in crystals 60–62  
 multistep tunneling 59  
 electron tunneling timetables 57–58, 58, 58, 59  
 redox-coupled folding 62–63  
 cytochrome *b562* 64–65, 65  
 cytochrome *c* 63–64  
 cytochrome *c'* 65–67  
 free-energy diagram 62  
 redox potentials 62  
 thermodynamic cycle 62  
 Zn-cytochrome *c* 67–70, 70  
 reorganization energies of  
 Ru-modified proteins 53  
 cytochrome *c* 53–55, 54
- Heme propionates 171
- Hemicellulose 168
- Hemoglobin 43, 155–156  
 CO adduct 18  
 human 156
- Heterodisulfide reductase 208
- Heterogeneous catalyst systems 162, 176, 183
- Heterogeneous porphyrin systems 199
- Heterolytic cleavage 168
- Hexachloroethane 155
- Histidine 100
- HIV protease inhibitors 156
- Homocysteine 252, 253, 253
- Homogeneous catalytic systems 190
- Homolytic cleavage 246, 249, 255, 266
- Hydrocorphin 206
- Hydrogen-atom abstraction 257, 258, 259, 260, 261, 262, 263, 264
- Hydrogen bonding 99, 100, 123  
 C–H...O bonds 113, 114, 120, 121, 124
- Hydrogen peroxide  
 electroreduction 29  
 intermediate in O<sub>2</sub> reduction 20, 27  
 oxidation by 162, 166, 168, 171  
 reactions with metalloporphyrins 174  
 role in porphyrin bleaching 32
- Hydroxides, bridging in synthetic CcO analogs 11
- Hydroxocobalamin 221–222
- p*-Hydroxycinnamyl alcohols 163
- Hydroxyl radicals 29, 32, 34
- Hyperporphyrin spectra 141
- I**
- Imidazolylcobamide 231, 237, 239, 250, 255
- Induced circular dichroism (CD) 98, 106–107
- Intrinsic factor (IF) 269
- Iodine ylide 138
- IR spectroscopy  
 cytochrome *c* oxidase (CcO) CN<sup>-</sup> adduct 15  
 (por)Fe(CO)Cu(LN) complexes 18  
 (por)Fe(μ-CN)Cu(LN) complexes 15–16, 16
- Iron**  
 alkyl iron(III) porphyrins 142  
 carbene derivatives 153  
 cyclopropanation catalysis 149  
 electron exchange between ferrous and ferric ions 53  
 iron porphyrins 152  
 (por)Fe(CO)Cu(LN) complexes  
 IR spectroscopy 18  
 NMR spectroscopy 18  
 X-ray studies 18  
 (por)Fe(μ-CN)Cu(LN) complexes  
 IR spectroscopy 15, 16  
 Mossbauer spectroscopy 14–15  
 NMR spectroscopy 15  
 X-ray studies 14, 14  
 (por)Fe(μ-O)Cu(LN) complexes  
 Currie-Weiss behavior 12  
 magnetic properties 12  
 Mossbauer spectroscopy 13  
 NMR spectroscopy 13  
 protonation 13  
 X-ray studies 11–12, 12  
 (por)Fe(μ-O<sub>2</sub>)Cu(LN) complexes  
 NMR spectroscopy 20, 21  
 Raman spectroscopy 21  
 redox titration 20, 23  
 [(por)Fe]<sub>2</sub>(μ-O) 11  
 reaction with O<sub>2</sub> 22  
 solid state structural studies 11–12, 12  
 synthesis 11  
 spin states of Fe(III) chiroporphyrins 114–116  
 synthetic iron–carbene porphyrins  
 reactivity 141–143, 142  
 synthesis 139–141, 141
- Isobutyryl-CoA mutase (ICM) 255, 256, 258, 261, 262, 262
- Isoleucine 123, 125
- Isonitrile complexes 137–138, 138
- Isotope labeling 180
- K**
- Ketocarbene-iron porphyrins 138
- Koutecky–Levich equation 24–25, 26
- Kraft lignin 192, 195–196, 197, 198
- L**
- Laccases 162, 168
- Langmuir–Blodgett (LB) films 105–106
- Leucine 99, 100
- Ligand folding 259
- Lignification of plant cells 162–163, 164
- Lignin 161–162, 200–201  
 biomimetic oxidation systems 174–175  
 dimeric model compounds 183–193, 184, 187, 188, 189, 190, 191, 192, 193  
 metalloporphyrin structures 176  
 monomeric model compounds 175–183, 177, 178, 179, 180, 181, 182, 183

- porphyrin–mediator systems  
 198–200  
 degradation 163, 165, 167–171, 169  
 enzyme models 171–174  
   Kappa number 197, 198  
   products of LiP degradation 170  
   products of MnP degradation 172  
 depolymerization 164  
 Kraft 192, 195–196, 197, 198  
 milled wood lignin (MWL) 196, 199, 200  
 model compounds 163, 167, 168, 171, 174–175, 199  
   biomimetic oxidation of dimeric compounds 183–193, 184, 187, 188, 189, 190, 191, 192, 193  
   biomimetic oxidation of monomeric compounds 175–183, 177, 178, 179, 180, 181, 182, 183  
   metalloporphyrin structures 176  
 occurrence and biological role 162–163  
   biosynthesis 162  
 oxidation 195–197  
   lignin peroxidase (LiP) 169  
 structure 163, 165, 166  
   carbohydrate bonds 163, 166  
   nonphenolic subunits 168, 171  
 Lignin peroxidase (LiP) 162, 168–169, 177, 189  
   catalytic cycle 168, 169  
   models 171–172  
   oxidation of veratryl alcohol 169, 171  
   products of lignin degradation 170  
 Ligninase models 171–172  
 Lignolytic enzymes 168  
 Lineweaver–Burk plot 194  
 Liver cytochrome P450 153  
 Lysine 106
- M**
- Magnetic properties  
   carboxylate-bridged CcO models 17  
   cofacial diporphyrins 38  
   (por)Fe( $\mu$ -O)Cu(LN) complexes 12  
 Mandelic acid 102  
 Manganese  
   asymmetric additions to olefins  
     catalyzed by Mn(III)  
     chiorporphyrins  
     aziridination 118, 119  
     epoxidation 116–118, 119  
   manganese-dependent peroxidases (MnP) 162, 168, 169–171  
     catalytic cycle 171, 173, 174  
     models 172–174  
     products of lignin degradation 172  
   Mn(III) chelates 171  
   synthetic manganese–carbene porphyrins 139  
 Mass spectrometry, biomimetic oxidation of lignin 180  
*mcr* operon 206  
 Mediators 162
- N*-7-Mercaptoheptanoylthreonine phosphate 206, 208  
 Metabolism of carbon tetrachloride 152, 152  
 Metabolism of drugs 156  
 Metalloporphyrin dianions 137, 138  
 Metal–oxygen bonds 174  
*Methanobacter marburgensis* 210  
*Methanobacterium thermoautotrophicum* 205, 207  
 Methanogenesis 251, 252  
 Methanogens 205–206, 207  
 Methanophenazine 208  
*Methanosarcina thermophila* 210  
 Methionine, B<sub>12</sub>-dependent synthesis 251, 253  
 Methionine synthase 224, 247, 248, 250, 252, 253–254, 253  
 Methyl radicals 243, 244, 252  
 Methyl transferase 252, 254  
 Methylamines 205  
 (2*S*,3*S*)-3-Methylaspartate 260, 260  
 Methylcobalamin 230, 235, 239, 240, 241, 244, 247, 253, 255, 268  
 Methylcob(III)inamide, one-electron reduction 244  
 Methyl-coenzyme M reductase (MCR) 205, 206, 207  
   future perspectives 226  
   genetic encoding 206–207  
   interconversion 211  
   isolation and activation 209–210  
   methane formation mechanism 221  
     mechanistic considerations 225–226  
     methyl–Ni intermediate 222–224, 223  
     pre-steady-state kinetics 222  
     steady-state kinetics 221–222  
     theoretical mechanism based upon functional theory calculations 224–225  
   Michaelis parameters 210, 221  
   properties 208–209  
   spectroscopic studies 212  
     cryoreduction 215–217, 216  
     electron–nuclear double resonance (ENDOR) studies 215, 215  
     EPR spectroscopy 210, 212–215, 212, 214, 214  
     oxidized versus reduced states 220–221  
     proposed activation mechanism 220  
     Resonance Raman (RR) studies 218–219, 219  
     UV-vis spectra 220  
     X-ray absorption 217–218, 217, 218  
   structure 210–212, 213  
 Methylene-glutarate mutase (MGM) 255, 256, 261–262  
 Methyl-imidazolylcobamide 235, 236  
 2'-Methylmalon-2'-yl-CoA radical 259  
 Methylmalonyl-CoA mutase (MMCM) 255, 256, 257, 258, 258–260, 258, 266–267  
 Methylsulfuranyl radical 222
- N*<sup>5</sup>-Methyltetrahydrofolate 252, 253, 253, 254  
 Methyl-transfer reaction 247, 247, 248, 251, 252, 253, 254, 254–255  
 Methyltransferases 224  
 Michael addition 103, 104  
 Microsomal cytochrome P450 152, 155, 155  
 Mid-spin state 117  
 Molecular modeling 192  
 Monooxygenase systems 152  
 Montmorillonite 198, 199, 200  
 Mossbauer spectroscopy  
   cytochrome c oxidase (CcO) CN– adduct 14  
   (por)Fe( $\mu$ -CN)Cu(LN) complexes 14–15  
   (por)Fe( $\mu$ -O)Cu(LN) complexes 13  
*mtr* operon 206  
 Myoglobin 39, 43, 155–156
- N**
- N,N'*-bridged porphyrins 138–139, 139  
 1-(1-Naphthyl)ethylamine 98  
 Nascent helix 261  
 Negative catalysis 256  
 Neovitamin B<sub>12</sub> 231, 232  
 Nickel  
   carbene nickel porphyrins 148  
   homoporphyrins 148  
   nickel–carbene complexes 148  
 NMR spectroscopy  
   biomimetic oxidation of lignin 180  
   chiral shift reagent 121  
   (por)Fe(CO)Cu(LN) complexes 18  
   (por)Fe( $\mu$ -CN)Cu(LN) complexes 15  
   (por)Fe( $\mu$ -O)Cu(LN) complexes 13  
   (por)Fe( $\mu$ -O<sub>2</sub>)Cu(LN) complexes 20  
   (por)Fe( $\mu$ -O<sub>2</sub>)Cu(LN) complexes 21  
   vitamin B<sub>12</sub>  
     early studies 238  
     multidimensional studies 238–240  
 Nonadiabatic electron transfer 52  
 Non-heme/copper oxidases 2, 35, 44  
 Nonnative ligand binding 67  
 Nonnatural iron porphyrins 171  
 Nopinone 78  
 Nucleic acids 106, 108  
 Nucleotide base 231, 232, 237, 243, 243, 244, 247, 248  
 Nucleotide function 231, 246, 250, 251, 270  
 Nucleotide moiety 239, 250, 261
- O**
- Octaethylporphyrin (OEP), oxidative degradation 32  
*ortho*-Octafluorotetraphenylporphyrin (H<sub>2</sub>F<sub>8</sub>TPP) as synthetic precursor 6  
 2-Octanol 120  
 Olefins, cyclopropanation 147  
 One-electron oxidation 168, 171, 193, 244, 244, 247, 248

- Optical properties of chiral metalloporphyrins  
 exciton-coupled circular dichroism (CD) 107–108  
 fluorescence 106  
 induced circular dichroism (CD) 106–107  
 photoinduced electron transfer 106  
 vibrational circular dichroism (VCD) 108
- Organocobalamins 244, 247
- Organometallic cofactors 229
- Organometallic enzymatic reactions 229
- Osmium  
 cyclopropanation catalysis 149, 150  
 osmium–carbene complexes 145  
 porphyrin carbene complexes 137  
 ylide complexes 145
- Oxidative degradation 161–162
- Oxidative ring opening 180, 188
- $\mu$ -Oxo complexes 171, 174, 177, 198  
 Fe/Cu bridged 11, 19–20, 23  
 chemical and electronic properties 12  
 chemical and spectroscopic parameters **20**  
 solid state structural studies 11–12, **12**  
 synthesis 11
- Oxygen  
 atom donors 180, 181, 184, 185, 189  
 electroreduction  
 electrocatalytic properties of heme  $a_3$ /Cu<sub>B</sub> analogs **33**  
 electrocatalytic properties of porphyrin Fe ligands **31**  
 structures and abbreviated names of porphyrin Fe ligands **30**  
 typical linear sweep voltammograms **31**  
 half-wave potentials of O<sub>2</sub> reduction  
 pH dependence 29, 33, 42  
 O–O bond heterolysis 27, 28, 43  
 oxidation by 162, 166  
 partially reduced intermediates 5  
 selectivity of O<sub>2</sub> reduction 25  
 pH dependence 29–30, 42
- Oxygenases 168
- P**
- Palmitic acid 268
- Paper  
 bleaching 163–167  
 non-polluting processes 165  
 pulping 163–167  
 yellowing 163, 164
- Partially reduced oxygen species (PROS) 25–26, 29, 34
- 1,3-Pentadiene 149
- Peptide-bridged porphyrins 106, 107
- Peptides 108–109, 110
- Peptidic radicals 257
- Pernicious anemia 230, 269
- Peroxides  
 bridging adducts in *biscobaltdiporphyrins* 39, 40  
 bridging adducts in synthetic CcO analogs 35, 44  
 bridging in synthetic CcO analogs 19–22  
 intermediate adducts of Fe porphyrins 27, 28, 29, 33  
*Phanerochaete chrysosporium* 168  
 Phenylalanine 99, 100, 107, 123  
 $\alpha$ -Phenylethylamine 86  
 Phenylglycerol ring 188  
 Philanthotoxin 107, 108  
 Phosphine oxidation 97  
 Phosphorane 152  
 Photocarbenes 155  
 Photochemical generation of free carbenes 142  
 Photodynamic therapy 109  
 Photoinduced electron transfer 106  
 $\pi$ -stacking 36  
 Picket-fence porphyrins 98, 108  
 Pillared diporphyrins 35, 37  
 $\alpha$ -Pinene 85, 97  
 Platinum electrode 25–26  
 Polyhalogenated precursors of metal–carbene complexes 136–137, 137  
 Polypeptidic envelopes 171, 174, 189  
 Polysaccharides 163  
 Porphyrinogen carboxylase 110
- Porphyrins  
 alkyl iron(III) 142  
*N*-alkylporphyrins 76  
 basket-handled 78, 86  
 binap-capped 82  
 binaphthyl-strapped 82  
 chiral *see* Chiral porphyrins  
 chiral fortress 76  
 chiral wall 76, 90  
 dinorbornabenzene-derived 102  
 glycosylated 109–110  
 ketocarbene-iron 138  
 lignin degradation enzymes 167–171  
*N,N'*-bridged 138–139, 139  
 peptide-bridged 106, 107  
 picket-fence 98, 108  
 ruffled 113  
 single-armed 76  
 strapped 76, 78–82  
 threitol-strapped 76, 82  
 tweezer 98, 99, 103  
 twin-coronet 76, 78–82, 87  
 vaulted 84, 86  
 Venus flytrap 114, 116  
 1,4-xylylene-strapped 87  
 $\alpha,\alpha'$ -xylylenediamide-strapped 101
- Pre-catalysts 257
- Precorrin II 208
- Prolinol 99, 121, 122
- Propanal-2-yl radical 264
- Propane-1,2-diol 262, 263, 263
- Protease inhibitors 154
- Protein dynamics 51  
 $\alpha$ -helix 56, 57–58  
 $\beta$ -sheet 56–58
- denaturation of cytochrome *b562* by guanidine hydrochloride 64–65  
 denaturation of cytochrome *c* by guanidine hydrochloride 63, 63, 64  
 electron tunneling across protein–protein interfaces 59–62, 60, 61  
 interprotein interactions in crystals 60–62  
 multistep tunneling 59  
 redox-coupled folding 62–63  
 cytochrome *b562* 64–65, 65  
 cytochrome *c* 63–64  
 cytochrome *c'* 65–67  
 free-energy diagram 62  
 redox potentials for heme proteins 62  
 thermodynamic cycle 62  
 Zn-cytochrome *c* 67–70, 70  
 tunneling pathways (TP) 56
- Protein folding 51
- Protein scaffold 168, 200
- Protein-based radicals 262–263
- Proton pump 2, 5, 45
- Protonation  
 (por)Fe( $\mu$ -O)Cu(LN) complexes 13  
 O<sub>2</sub>-/cofacial *biscobaltdiporphyrin* adducts 40
- Protoporphyrin IX 162, 162, 168  
 catalysis of oxidation 173
- Proximal ligands 189, 200
- Pseudovitamin B<sub>12</sub> 245, 250
- Q**
- o*-Quinones 186  
*p*-Quinones 186, 194
- R**
- Radical abstraction 246
- Radical carriers 255
- Radical cation intermediates 179, 180, 181, 185, 188, 193, 256  
 stabilized 185, 186
- Radical center 249
- Radical peroxides 179
- Radical rearrangement 258, 259, 260, 260, 261, 262, 263, 264
- Radical recombination reactions 247
- Radical traps 246, 247
- Radical-induced substitution 249
- Raman spectroscopy  
 O<sub>2</sub>-/cofacial *biscobaltdiporphyrin* adducts 40  
 (por)Fe( $\mu$ -O<sub>2</sub>)Cu(LN) complexes 21
- Reaction selectivity 185
- Redox titration of (por)Fe( $\mu$ -O<sub>2</sub>)Cu(LN) complexes 20, 23
- Regiospecificity of oxygenation 171
- Reorganization energy 52  
 Ru-modified heme proteins 53  
 cytochrome *c* 53–55, 54
- Reorganization parameter 51
- Repolymerization 196

- Resonance Raman (RR) spectroscopy 218–219, 219
- Rhodium  
dirhodium carboxylate catalysts 149  
rhodium porphyrins  
  diazoalkyl adduct 147  
  insertion of carbethoxycarbenes 150  
  synthesis from carbenes 147  
  rhodium–carbene complexes 147–148
- Ribonucleotide reductase 255, 257, 264–266, 265, 266, 267
- Ring-opening reactions 196
- Rotating disk electrode (RDE) 23
- Rotating ring-disk electrode (RRDE) 23, 25, 25, 45  
  collection efficiency 26
- Ruffled distortion 114, 118
- Ruffled porphyrins 113
- Ruthenium  
  asymmetric cyclopropanation 150  
  chiral ruthenium(II) porphyrins 149  
  ruthenium porphyrin carbene complexes 144  
  X-ray structure 143  
  ruthenium porphyrin complexes 149  
  dimers 143  
  insertion into N–H bonds 151, 151  
  insertion into S–H bonds 151, 151  
  zero-valent 143  
  ruthenium–carbene complexes 137, 143–145  
  chiral forms 144, 144  
  diphenyl complexes 144
- S**
- Saccharides 98, 103, 104
- Sacrificial reduction 193
- Selenocarbonyl complexes 140
- Self-assembled monolayers (SAMs) 45
- Self-assembled systems 6, 105
- Serine 100, 107
- Shikimic acid pathway 162
- Side-chain oxidation 168, 188, 192, 196
- Single-armed porphyrins 76
- Sirohaem 208
- Smectic clays 198
- SN<sub>2</sub>-alkylation 248
- Spectrophotometric O<sub>2</sub> titration 23
- Square potential barrier 55
- Stabilization of metal complexes 168
- Steroids 76, 98, 100, 107
- Stirring effects 110–111
- Strapped porphyrins 76, 78–82
- Styryl-cobalt(III) porphyrins 146
- Substitution patterns 175
- Succin-3-yl-CoA radical 259
- Succinyl-CoA 258, 258
- Superoxide anion 168
- Superoxides  
  cofacial *biscobaltdiporphyrins*  
  adducts 39, 39  
  Fe porphyrin adducts 20, 22, 28, 34, 44
- Supramolecular chirogenesis 102, 103, 110–111
- Supramolecular orbitals 37
- Syndones 142  
  metabolism 155, 155
- T**
- Terminal oxidases  
  cofacial diporphyrins 35–36, 36  
  catalytic properties of  
  monocobaltdiporphyrins 43–44, 43  
  electrocatalytic O<sub>2</sub> reduction 40–43, 41, 42  
  molecular structure and  
  physicochemical properties  
  36–38, 37  
  nonaqueous dioxygen chemistry of  
  group 2 *biscobaltdiporphyrins*  
  38–40, 38  
  π-stacking 36  
  functional analogs of the dioxygen  
  reduction site 23  
  electrocatalytic O<sub>2</sub> reduction by  
  simple Fe porphyrins 29–32  
  electrocatalytic O<sub>2</sub> reduction,  
  general mechanism 28–29, 28  
  heme a<sub>3</sub>/CuB analogs 32–35, 33  
  methodologies 23–28  
  selectivity of O<sub>2</sub> reduction 25  
  structures and abbreviated names  
  24, 30  
  heme/copper terminal oxidases 1–5, 3  
  isolated forms 3–4  
  non-heme/copper terminal oxidases  
  2  
  reactivity of heme a<sub>3</sub>/CuB analogs to  
  O<sub>2</sub> 18–19  
  characterization of peroxide-  
  bridged intermediates 19–22  
  reaction of FeIII/CuI centers with  
  O<sub>2</sub> 22–23  
  structural and spectroscopic models  
  of heme a<sub>3</sub>/CuB site  
  carbon monoxide adducts 17–18  
  carboxylate-bridged systems 16–17  
  model systems 8  
  cyanide-bridged systems 13–16  
  model systems 7  
  general synthetic methodologies  
  5–11  
  oxo- and hydroxo-bridged model  
  systems 6, 11–13
- Terpenes 78
- Tetrachloroethane dehalogenase  
  (TCED) 268–269, 269
- Tetrachloromethane  
  metabolism 152, 152
- Tetramethylchiroporphyrin (TMCP) 90,  
  98, 99, 118
- Tetra-*ortho*-aminophenylporphyrin  
  (TAPP) 7–8  
  atropisomers 8–9
- Tetrapyrrolic macromolecules 189
- Thiocarbonyl complexes 140
- Thioglycine 222
- Thioketyl radical 222–223
- Thiyl radical 224, 264, 265
- Threitol-strapped porphyrins 76, 82
- Threonine 101, 107, 123, 125
- Titanium(III) citrate 209, 210, 221,  
  226
- Totally chlorine free (TCF) processes  
  162
- Transcobalamin (TC) 269
- Trans*-effects 236, 255
- Transition metal chiroporphyrins 111,  
  112  
  asymmetric additions to olefins  
  catalyzed by Mn(III)  
  chiroporphyrins  
  aziridination 118, 119  
  epoxidation 117–118, 119  
  chiroporphyrin derivatizing agents  
  123–124  
  enantioselective binding 118–121, 120  
  irreversible binding of amines to  
  Co(III) chiroporphyrins 121, 123  
  perspectives 124  
  spin states of Fe(III) chiroporphyrins  
  114–117  
  stereochemistry  
  conformational switches 114  
  free bases 113–114, 114, 115  
  synthesis 111–113, 112  
  X-ray structure of nickel complex 113
- Trichloromethyl radical 156
- 2,4,6-Trichlorophenol 183
- Trifluoromethyl carbene 153
- Trimethylsilyldiazomethane 142
- Tröger's base 76, 100
- Tryptophan-2,3-dehydrogenase 85–86,  
  97
- Turnover number 175
- Tweezer porphyrins 98, 99, 103
- Twin-coronet porphyrins 76, 78–82, 87
- Tyrosine 123, 125
- U**
- Ubiquinol 2, 32
- Ubiquinol oxidase 2, 2  
  *B. subtilis*  
  EXAFS structure 12  
  *E. coli* (EOX) 3
- Uniform barrier (UB) 56
- Urease 208
- V**
- Valine 100, 101
- Vaulted porphyrins 84, 86
- Venus flytrap porphyrins 114, 116
- Veratryl acetate 178, 179
- Veratryl alcohol 169, 169, 171, 173, 177,  
  178, 199
- Vibrational circular dichroism (VCD)  
  108
- Vinyl-cobalt(III) porphyrins 146
- N*-Vinylprotoporphyrin IX 155
- Vitamin B<sub>12</sub> 208, 229–231  
  crystallographic studies 231

- Vitamin B<sub>12</sub> (*continued*)  
crystallographic studies (*continued*)  
cobamides 231–233, 232  
cobamides, incomplete 233  
organometallic B<sub>12</sub>-derivatives  
234–236  
reduced B<sub>12</sub>-derivatives 233–234  
*trans*-effects 236  
upwards folding of corrin ligands  
237  
electrochemistry 241  
kinetic redox properties of  
cobamides 244  
organometallic electrochemical  
synthesis 244–245  
thermodynamic redox properties of  
cobamides 241–244  
mass spectrometry 240  
medical aspects 269–270  
NMR spectroscopy  
early studies 238  
multidimensional studies 238–240  
organometallic derivatives 243, 245  
reactivity 245–250  
structure 230  
atom numbering 231  
Co–N distance 232, 234  
Co–O bond length 232  
conformational effects 239  
corrin ligands 231, 233, 235, 236,  
237  
fold angle 231, 234, 236, 237  
NMR spectroscopy 238–241  
other techniques 240–241  
solution structure 234  
upwards folding 232, 237  
X-ray crystallography 231–238  
UV-vis spectroscopy 240
- W**  
Water, electron tunneling timetables  
58–59, 59  
Water-soluble porphyrin complexes 175,  
177  
White rot fungus (basidiomycetes) 162,  
167–168  
Wood 162, 167–168  
extractive free wood (EFW) 196  
fibers 196  
milled wood lignin (MWL) 196, 199,  
**200**  
secondary metabolites of fungi 171,  
173–174  
Woodpulp  
bleaching 196, 198  
oxidation 197–198  
viscosity 197, 198
- X**  
X-ray studies  
crystallography of vitamin B<sub>12</sub> 231  
cobamides 231–233, 232  
cobamides, incomplete 233  
organometallic B<sub>12</sub>-derivatives  
234–236  
reduced B<sub>12</sub>-derivatives 233–234  
*trans*-effects 236  
upwards folding of corrin ligands  
237  
extended X-ray absorption fines  
structure spectroscopy (EXAFS)  
217–218, 218  
(por)Fe(CO)Cu(LN) complexes 18  
(por)Fe(μ-CN)Cu(LN) complexes 14  
bonding parameters **14**  
(por)Fe(μ-O)Cu(LN) complexes  
11–12, **12**  
X-ray absorption near edge spectra  
(XANES) 217–218, 217  
1,4-Xylylene-strapped porphyrins 87  
α,α'-Xylylenediamide-strapped  
porphyrins 101
- Z**  
Zinc  
cytochrome *c*, zinc-substituted 67–70,  
70  
denaturation by guanidine  
hydrochloride 68–69  
ET quenching 68  
porphyrin tweezers 98, 99  
zinc-carbene complexes 148